

IDENTIFICATION OF PROTEIN TARGETS AND QUANTIFICATION OF BIOCHEMICAL  
AND TOXICOGENOMIC EFFECTS OF INORGANIC AND ORGANIC MERCURY  
EXPOSURE IN *E. COLI*

by

STEPHEN PATRICK LAVOIE

(Under the Direction of Anne O. Summers)

ABSTRACT

Mercury is a ubiquitous environmental toxin that poses a risk to human health in all of its chemical forms, but toxicity mechanisms at the molecular level remain poorly understood. The ecological and health associated roles of microorganisms are increasingly being recognized, but there remains limited knowledge of how bacteria respond to mercury exposure. This dissertation details advancements in methodologies for studying mercury exposure and expands knowledge of toxicity mechanisms using the model prokaryotic organism, *Escherichia coli*. The combined results from three studies provide a system wide comparative view of the biochemical effects, *in vivo* protein targets, and transcriptional changes in response to varying concentrations of inorganic and organic mercury exposure. In one study, several biochemical methods were used to study the effects of acute exposure to different mercurials. Inorganic mercury was more effective in binding total and protein thiols than PMA or merthiolate and non-thiol ligands were observed as inorganic mercury depleted the cellular thiol pool. All mercurials disrupted the electrolyte balance of the cell and iron homeostasis with varying effectiveness. In another study, methodologies were developed to identify *in vivo* mercury binding proteins within a global

proteome. There were 307 proteins observed with mercury modifications distributed across all functional roles, but translation and cysteine rich metabolism categories were predominately affected. In addition, twenty-two proteins with highly conserved domains were identified that could serve as biomarkers. These results greatly expand current knowledge of mercury targets and methods could be implemented for studies in other organisms. The final study compares the transcriptional response over time for sub-acute exposure to inorganic and organic mercury using the RNA-Seq method for the first time. Exposure to either mercurial resulted in over 40% of all genes being differentially expressed ten minutes after exposure and subsequent time points reveal gene expression changes throughout recovery of growth. Inorganic and organic mercury displayed distinct transcriptional profiles, which suggests different toxicity mechanisms. The down-regulated gene response was highly conserved, while the up-regulated response was more unique to each compound. These findings provide the most comprehensive view of the effects of mercury exposure in any organism to date.

INDEX WORDS: Mercury, Organomercurials, Toxicity, Escherichia coli, Metals  
Homeostasis, EPR, ICP-MS, EXAFS, Proteomics, Transcriptomics, RNA-Seq, Gene Expression, Oxidative Stress

IDENTIFICATION OF PROTEIN TARGETS AND QUANTIFICATION OF BIOCHEMICAL  
AND TOXICOGENOMIC EFFECTS OF INORGANIC AND ORGANIC MERCURY  
EXPOSURE IN *E. COLI*

by

STEPHEN PATRICK LAVOIE

B.S., University of Georgia, 2006

A Dissertation Submitted to the Graduate Faculty of The University of Georgia in Partial  
Fulfillment of the Requirements for the Degree

DOCTOR OF PHILOSOPHY

ATHENS, GEORGIA

2016

© 2016

Stephen P. LaVoie

All Rights Reserved



IDENTIFICATION OF PROTEIN TARGETS AND QUANTIFICATION OF BIOCHEMICAL  
AND TOXICOGENOMIC EFFECTS OF INORGANIC AND ORGANIC MERCURY  
EXPOSURE IN *E. COLI*

by

STEPHEN PATRICK LAVOIE

Major Professor:	Anne O. Summers
Committee:	Harry A. Dailey Michael K. Johnson Mary Ann Moran

Electronic Version Approved:

Suzanne Barbour  
Dean of the Graduate School  
The University of Georgia  
August 2016

## DEDICATION

To my family and E.S.

## ACKNOWLEDGEMENTS

I would first like to thank my advisor, Dr. Anne O. Summers, for her patience, encouragement, and guidance since I joined the lab. I am grateful for all that she has done to help me mature as a scientist and opportunities she has provided for me to learn from others. I would also like to thank past and present members of the lab for their support and friendship. My work has afforded me the opportunity to collaborate with many people outside of the lab at UGA, UCSF, U. of Missouri, PNNL, and ORNL on various projects, and I am thankful for the assistance, feedback, and shared knowledge from all of these collaborators. I would also like to thank the members of my committee for all that they have done to help me through this process, as well as other microbiology faculty members that have provided support and guidance. Finally, I would like to thank my family, Erin Sanders, and my friends for their support and encouragement through the years.

## TABLE OF CONTENTS

	Page
ACKNOWLEDGEMENTS .....	v
CHAPTER	
1 INTRODUCTION AND LITERATURE REVIEW .....	1
2 ORGANIC AND INORGANIC MERCURIALS HAVE DISTINCT EFFECTS ON CELLULAR THIOLS, METAL HOMEOSTASIS, AND FE-BINDING PROTEINS IN <i>ESCHERICHIA COLI</i> .....	29
3 THE ORGANOMERCURY EXPOSOME OF <i>ESCHERICHIA COLI</i> .....	71
4 TRANSCRIPTIONAL RESPONSES OF <i>ESCHERICHIA COLI</i> DURING RECOVERY FROM INORGANIC OR ORGANIC MERCURY EXPOSURE .....	103
5 SUMMARY .....	167
APPENDICES	
A DISCOVERING MERCURY PROTEIN MODIFICATIONS IN WHOLE PROTEOMES USING NATURAL ISOTOPE DISTRIBUTIONS OBSERVED IN LIQUID CHROMATOGRAPHY-TANDEM MASS SPECTROMETRY .....	170

B	SUPPLEMENTAL INFORMATION FOR CHAPTER 2 .....	235
C	SUPPLEMENTAL INFORMATION FOR CHAPTER 3 .....	299
D	SUPPLEMENTAL INFORMATION FOR CHAPTER 4 .....	325

## **CHAPTER 1**

### **INTRODUCTION AND LITERATURE REVIEW**

Mercury is the 80<sup>th</sup> element of the periodic table and is categorized as a group 12 transition metal, along with zinc and cadmium. The unique properties of mercury have made it attractive for use in various applications since antiquity. However, its toxic effects have always presented a challenge that limit how it can be used. Limiting exposure to mercury remains a concern and it continually ranks third on the priorities list for the Agency of Toxic Substances and Disease Registry Superfund (<https://www.atsdr.cdc.gov/spl/>). Mercury toxicity mechanisms are still poorly understood and very few studies have used a system-wide approach to examine the effects of mercury exposure and how inorganic and organic compounds differ.

#### **Mercury's biogeochemical cycle**

Mercury exists in a variety of chemical forms, including inorganic and organic species, as part of a complex biogeochemical cycle that involves microbially mediated transformations (Barkay et al., 2003, Mason et al., 1994, Morel et al., 1998). Naturally occurring species include elemental mercury (liquid or vapor;  $\text{Hg}^0$ ), insoluble mercury-sulfide ( $\text{HgS}$ ; cinnabar) and mercuric oxide ( $\text{HgO}$ ), inorganic mercury salts of ionic mercury ( $\text{Hg}^{+2}$ ,  $\text{Hg}^{+1}$ , or  $(\text{Hg}_2)^{2+}$ ) of varying solubility, and organomercurial compounds ( $\text{RHg}^+$ ) which can be membrane-permeable, depending on available counterions. The zero valence state ( $\text{Hg}^0$ ) of mercury is stable as a liquid with a highly volatile monoatomic vapor at ambient temperature and pressure, which makes it unique among metallic elements.

The main ores of mercury are mercury-sulfide (HgS) compounds, cinnabar and metacinnabar; they serve as the major reservoir of mercury in the environment due to low solubility under non-acidic conditions (Mason et al., 2012, Rytuba, 2003). Mercury compounds are transformed by abiotic reactions including photodegradation of organomercurials, photooxidation of atmospheric mercury vapor, and photoreduction of inorganic mercury, which all contribute to atmospheric mercury emissions and deposits (Barkay et al., 2003). In addition to abiotic transformation mechanisms, microbes play an important role in transformations of all known inorganic and many organic mercury species. Bacteria can even enhance transformation of cinnabar and metacinnabar to Hg(II) and Hg(0) (Jew et al., 2014, Vazquez-Rodriguez et al., 2015). Some sulfate reducing bacteria have long been known to methylate Hg and many other bacteria have lately been discovered to have this property (Gilmour et al., 2013). Methylmercury is more readily absorbed than the ionized inorganic species (though not than Hg vapor) and biomagnifies in all animal species examined (Morel et al., 1998). Mercury resistant bacteria carrying the *mer* operon effect other transformation reactions (Barkay et al., 2003) including reduction of Hg(II) to Hg(0) by MerA (Ledwidge et al., 2005) and protonolysis of the carbon-mercury bond of organomercurial compounds to Hg(II) catalyzed by MerB (Pitts and Summers, 2002). These *mer* locus-mediated transformations have attracted attention for possible for bioremediation purposes. Their ability to reduce mercury to monoatomic vapor differs from defense mechanisms to other toxic metals that use efflux (Nies, 1999). Lastly, bacteria with catalase can oxidize Hg vapor to reactive ionic  $\text{Hg}^{2+}$  (Smith et al., 1998) just as animals and humans can (Magos et al., 1978).

Approximately one-third of Hg emissions are from natural sources (Driscoll et al., 2013, Mason et al., 2012, Mason et al., 1994, Pirrone et al., 2009), which include natural ore deposits

and terrestrial and oceanic volcanism (Pirrone et al., 2009). Of the two-thirds of present mercury emissions that are anthropogenic, the primary source is fossil fuel burning power plants (Pirrone et al., 2009). The second largest anthropogenic contributor is artisanal gold mining (Pirrone et al., 2009), whose contamination can spread well beyond their immediate locales, especially in the Amazon basin (Malm, 1998). Other major sources of anthropogenic mercury emissions include industrial applications, such as metal production, chlor-alkali production, cement production and vinyl chloride production (Pirrone et al., 2009).

### **Sources of exposure**

The primary routes of mercury exposure in humans are through ingestion of soluble mercury species and inhalation of mercury vapor. Artisanal gold mining is based on the fact that gold in ore is soluble in liquid Hg in a process called amalgamation. After sieving to remove rocks, dirt, etc, the liquid Hg-Au amalgam is boiled in open air to drive off the Hg(0), leaving nearly pure Au precipitated as a fine dust or flakes (Malm, 1998, Veiga et al., 2006). These refining processes expose mine workers directly to liquid mercury and inhalation of mercury vapor. Runoff from mining operations, as well as natural and other anthropogenic sources, leads to bioaccumulation of organic and inorganic mercury in fish and rice (Diez, 2009, Zhang et al., 2010), so ingestion of mercury containing foods also presents a direct risk to human health.

Dental amalgam fillings are a very immediate major source of mercury exposure in humans (Clarkson and Magos, 2006, Crinnion, 2000, Richardson et al., 2011). Mercury vapor is released during installation or removal of amalgam fillings, and also with chewing, brushing and even consumption of hot beverages (Crinnion, 2000). Mercury vapor is readily absorbed into circulation and quickly oxidized by blood catalase to reactive ionic mercury once in the blood



(Clarkson and Magos, 2006). This chronic iatrogenic source of inorganic Hg exposure not only affects human health directly (Hahn et al., 1989, Hultman et al., 1994, Lorscheider et al., 1995, Prochazkova et al., 2004), it also selects mercury resistant bacteria, resulting in co-selection and spread of genetically linked antibiotic resistance genes in commensals and pathogens (Pal et al., 2015, Summers et al., 1993).

Organomercurials, have historically been used as antiseptics in medicine or as preservative agents in agriculture or the pharmaceutical industry (Clarkson and Magos, 2006, Tchounwou et al., 2003). Phenylmercury has been used in medical products such as contact lens cleaning solution (Rietschel and Wilson, 1982, Tosti and Tosti, 1988), vaginal douches (Freed, 1948), skin disinfectants (Weed, 1931), and diaper rinse (Gotelli et al., 1985) and as a preservative in latex paint (Agocs et al., 1990). The major use of methylmercury in agriculture as a fungicide for crop seeds led to several devastating episodes of massive human exposure either from proximity to methylmercury manufacturing plants or from inadvertent human consumption of treated seed meant for planting (Hintelmann, 2010, Magos and Clarkson, 2006).

The compound ethylmercury thiosalicylate, under the trade names of thimerosal and merthiolate, has been used as a preservative in multi-dose vials containing vaccines since it was developed in the 1930's (Clarkson and Magos, 2006). This practice was not called into question as being hazardous to health until 2001 (Ball et al., 2001, WHO, 2002) and though it has been gradually removed from use in pediatric vaccines, it continues to be used in most other vaccines.

### **Routes of exposure and excretion**

Mercury exposure primarily occurs through ingestion or inhalation of mercury vapor. Elemental mercury in the liquid state was thought to be poorly absorbed, but up to ten times

normal levels were observed in blood after ingestion of several grams (Suzuki and Tanaka, 1971). Approximately 75% of mercury inhaled as monatomic vapor is retained within the body (Hursh et al., 1976). Mercury vapor is highly diffusible and lipid soluble, which results in around 10% of the inhaled mercury being deposited into the brain. Mercury vapor itself is relatively inert, but once it enters the blood it is oxidized by catalase to highly reactive ionic mercury, which builds up in the kidneys and to a lesser degree in the liver (Clarkson and Magos, 2006, Magos, 1997) although it is eliminated to some extent in feces and in urine.

Ionic mercuric mercury ( $\text{Hg}^{2+}$ ) that is ingested is poorly absorbed through the gastrointestinal tract. On average only 7% of mercuric mercury was absorbed in human subjects, with a range of 1 to 16% (Rahola et al., 1973). However, animal experiments suggested that  $\text{Hg}^{2+}$  absorption might be higher in infants, with up to 38% gastrointestinal absorption in newborn rats, compared to only 1% in adults (Kostial et al., 1983).  $\text{Hg}^{2+}$  is secreted in bile from the liver as a conjugate with glutathione into the lower intestinal tract from whence most Hg in any form is excreted. Approximately 10% of ingested Hg is eliminated through the kidneys, which tend to accumulate mercury 22-fold better than the liver (Hahn et al., 1990); i.e. the liver is better at mobilizing Hg out of the body than the kidney which acts like a Hg sponge to its own eventual detriment (Lorscheider et al., 1995). Dermal exposure absorption is not well studied, but believed to be negligible for mercuric salts.

Organomercurials are better absorbed than inorganic species, with as much as 95% of ingested methylmercury (MeHg) absorbed through the gastrointestinal tract (WHO, 1991). Distribution of MeHg through the body is completed in about four days with around 6% of the dose deposited in the brain, which is roughly six times greater than the concentration found in blood (WHO, 1991). Like inorganic mercury, methylmercury is bound by glutathione in the liver

before being excreted in bile (Clarkson and Magos, 2006). Once in the bile, methylmercury-glutathione can be broken down to methylmercury-cysteine, which is reabsorbed from the gastrointestinal tract and redistributed through the bloodstream (Clarkson and Magos, 2006). Up to 90% of methylmercury is excreted through feces and much of this is as inorganic mercury, which is formed by microbial mediated breakdown of methylmercury to mercuric mercury in the gastrointestinal tract (Clarkson and Magos, 2006). Dermal absorption of organomercurials varies by compound, but the deadly neurotoxin dimethylmercury is very easily absorbed through skin (Clarkson and Magos, 2006).

Mercury compounds are excreted through urine, feces, hair, and nails which are all used to measure exposure and retention. All mercury compounds manifest distinct multimodal excretion patterns indicating distinct but poorly defined anatomic and biochemical compartments. Inhaled mercury vapor has a half-life of around 58 days in the whole body and kidneys, and ingested mercuric mercury around 53 days in the liver (Clarkson and Magos, 2006). Inorganic mercury in the blood has a rapid half-life of 1-3 days, followed by a slower half-life of 1-3 weeks (Barregard et al., 1992, Clarkson and Magos, 2006, Sandborgh-Englund et al., 1998). Methylmercury has a half-life of around 44-50 days in the blood, with most elimination occurring through feces (Smith et al., 1994, Smith and Farris, 1996) and incorporation into growing hair, which can be used to measure accumulated dose (Cernichiari et al., 1995, Suzuki et al., 1993). Even though mercuric mercury is not well absorbed across the blood-brain barrier, elevated inorganic mercury has been observed in the brain. This may be due to oxidation of mercury vapor and/or protonolysis of organomercurials, which results in retention for many years due to poor mobilization of mercuric species in the brain (Clarkson and Magos, 2006, Vahter et al., 1995). Total body retention was also affected by the intestinal microbiota, which

decreased excretion of inorganic mercury and increased tissue organic mercury in antibiotic-treated mice consuming mercury-amended food (Rowland et al., 1984).

### **Pathophysiology of mercury exposure**

Since mercury vapor can enter the brain, disruption of the central nervous system and neurological disorders are most commonly associated with this type of exposure (Clarkson and Magos, 2006). Low-level Hg exposure can present nonspecific symptoms like fatigue, weight loss, and gastrointestinal disturbance (Bernhoft, 2012). Higher exposures are associated with motor skill disturbances, like tremors, severe mood changes, anxiety, memory loss, and hallucinations (Bernhoft, 2012), as well as gingivitis and excessive salivation (Goldwater, 1972) when the source is dental amalgams.

Inorganic mercury, from direct exposure, oxidation of mercury vapor, or degradation of organic mercury, primarily damages the gastrointestinal tract and kidneys (Clarkson and Magos, 2006). Mercuric salts, such as mercuric chloride, are corrosive and cause gastrointestinal damage (Magos and Clarkson, 2006). Inorganic mercury bound by glutathione primarily accumulates in the renal glomeruli causing nephrotic syndrome (Magos and Clarkson, 2006). Higher exposure can cause a complete collapse of kidney function, while lower level exposure is thought to damage the proximal tubules (Clarkson and Magos, 2006). Immune system and thyroid dysfunction have also been associated with chronic inorganic mercury exposure (Bernhoft, 2012, Clarkson and Magos, 2006).

There have been two prominent cases of large scale, severe organomercury poisoning. The best known was caused in the late 1960's by consumption of fish containing high levels of methylmercury from the Minamata Bay in Japan, as a result of an acetaldehyde manufacturing

plant that, for decades, discharged large amounts of mercury into the bay used by subsistence fishermen (Harada, 1995). The health effects associated with this event became known as Minamata Disease and resulted in hundreds of deaths and thousands of people affected, many permanently (Harada, 1995). This acute exposure caused visual and hearing impairment, olfactory disturbances, cerebral ataxia, somatosensory disturbances, psychiatric symptoms, and fetal poisoning that caused a number of birth defects (Ekino et al., 2007).

A similar tragedy occurred in Iraq in the 1970's when US surplus seed grain, routinely treated with ethylmercury and methylmercury fungicides, was donated to Iraq, which was beset by crop failures. As the labels specifying the grain was only for planting were in English, many recipients accidentally consumed the grain themselves and/or used it as animal feed (Bakir et al., 1973). Again, hundreds died and thousands were debilitated even though the acute exposure period was shorter than Minamata, (Myers et al., 2000). Phenylmercury has also been used in some instances as a fungicide to treat grains, but degrades to mercuric ion within a few days (Clarkson and Magos, 2006). Since organomercurials protonolyze to mercuric mercury in the body, it has been hypothesized that inorganic mercury is the ultimate toxic form responsible for chronic exposure health effects, while organomercurials are associated with short-term effects (Rooney, 2007).

More recently, there is growing concern that deleterious health effects of liquid Hg could occur in areas surrounding artisanal gold mining operations. Although such problems have not yet been reported (Veiga et al., 2006), this may in part be because the demographic involved is outside established health monitoring programs.

## Biochemical effects of exposure

The precise molecular basis for the differential toxicology of inorganic and organic mercury compounds is a surprisingly under examined area. Mercury, a soft metal, is expected to make nearly covalent bonds with cellular thiols and selenols due to its high affinity for the soft chalcogen elements, sulfur and selenium (Dyrssen and Wedborg, 1991, Sugiura et al., 1978). Notwithstanding bacteria and all eukaryotes have millimolar levels of low molecular weight monothiols such as glutathione that could protect key protein thiols from mercuriation, bacteria and eukaryotes are sensitive to micromolar levels of Hg compounds (Becker and Soliman, 2009, Satoh et al., 1997). Mercury reacts even more strongly with selenocysteine-containing proteins, which are found in all domains of life (Gladyshev and Kryukov, 2001, Romagne et al., 2014, Zhang et al., 2006), and evidence suggests these proteins may protect by sequestering mercury (Carvalho et al., 2011, Khan and Wang, 2009), albeit, by suffering protein-suicide in the process as the bound Hg cannot be removed. This high affinity for selenium ligands can also lead to deficiency of selenium-dependent enzymes, consistent with the protein-suicide basis of protection (Ralston et al., 2007, Watanabe et al., 1999) and likely contributes to long retention times of mercuric mercury in the brain.

X-ray absorption spectroscopy (XAS) identified elevated levels of mercuric selenide in brain tissue samples from humans severely poisoned with methylmercury, but brain tissue from individuals that consume fish daily showed lower levels of mercuric selenide and greater levels of methylmercury cysteineate (Korbas et al., 2010). X-ray fluorescence (XRF) mapping in zebrafish larvae found that methylmercury-cysteine and ethylmercury from thimerosal primarily accumulated in the lens epithelium, with lower levels localized to the brain, optic nerve, and other organs (Korbas et al., 2008). In contrast, mercuric chloride in zebrafish larvae accumulated

in the olfactory epithelium and kidney, and mercury added as a cysteine complex significantly decreased uptake to all organs. These studies emphasize the importance of distinguishing mercury species when determining toxicity mechanisms (Korbas et al., 2012).

Inorganic mercury induces oxidative stress, first, by inhibiting the respiratory enzyme, ATP synthase, leading to partial reduction of dioxygen to superoxide and, second, by direct formation of adducts with redox defense proteins and with the bulk cytosolic redox buffer, glutathione (Ercal et al., 2001, Valko et al., 2005). The thioredoxin and glutaredoxin systems are essential for intracellular redox homeostasis, but these systems are inhibited when mercury binds directly to these enzymes (Carvalho et al., 2008). Mercury compounds uncouple oxidative phosphorylation in bacterial cytosolic membranes and in eukaryotic mitochondria, leading to the production of reactive oxygen species (ROS) (Lund et al., 1991, Nath et al., 1996, Verity et al., 1975). Reactive oxygen species damage proteins, DNA, and lipids (D'Autreaux and Toledano, 2007, Imlay, 2013) and contribute to neurodegeneration (Uttara et al., 2009) and some types of cancer (Waris and Ahsan, 2006).

Approximately half of all enzymes in the six Enzyme Commission (EC) functional classes use metal cofactors (Andreini et al., 2008, Cvetkovic et al., 2010, Waldron et al., 2009). Transition metal cofactors are often bound by protein cysteine residues and are vulnerable to displacement by mercury with the consequent loss of protein function. Electron paramagnetic resonance (EPR) spectroscopy revealed that iron-sulfur clusters in redox enzymes are susceptible to damage from mercury exposure (Xu and Imlay, 2012), but apart from work reported here effects on the total iron pool and other transition metals have not been examined.

Homeostasis of the essential bulk alkaline earth element, calcium, is damaged by mercury exposure (Suzuki et al., 2004, Tan et al., 1993). Cellular calcium is critical for cell signaling

(Brini et al., 2013, Brini et al., 2014) and mitochondrial viability (InSug et al., 1997, Shenker et al., 1999). Inorganic and organic mercury affect calcium homeostasis in different ways. Both compounds increase calcium influx, but methylmercury is also thought to release intracellular calcium stores (Tan et al., 1993). With higher cytosolic calcium mitochondrial permeability increases resulting in loss of membrane potential, which leads to cell death by apoptosis (Jacobson and Duchon, 2004, Zoratti and Szabo, 1995).

Inorganic and organic mercury also disrupt microtubule structure and function (Bonacker et al., 2004, Philbert et al., 2000). Microtubules are critical for chromosome separation, cell division, and neural development (Conde and Caceres, 2009, Etienne-Manneville, 2013). Binding of mercury to thiol groups of immature tyrosinated microtubules resulted in catastrophic depolymerization (Philbert et al., 2000). Immunotoxicity also occurs *in vitro* upon sub-acute Hg exposure in human peripheral blood mononuclear cells. An increase in inflammatory cytokines was observed for mercuric chloride and methylmercury, but ethylmercury as thimerosal had the opposite effect (Gardner et al., 2010).

### **Proteomics studies**

Proteomics-based techniques are becoming more prevalent for studying global effects on protein expression and for identification of toxicology biomarkers (Kakkar and Jaffery, 2005, Luque-Garcia et al., 2011, Titz et al., 2014). Most mercury toxico-proteomics studies have used 2-D gel electrophoresis to identify mercury-induced differential protein expression, using trypsinolysis of an excised gel spot and mass spectrometry to identify the protein. Acute mercuric chloride exposure in medaka fish (*Oryzias melastigma*) altered expression of proteins in the liver and brain (Wang et al., 2011) that are involved in oxidative stress, cytoskeletal



assembly, signal transduction, protein modification, and metabolism. Chronic mercuric chloride exposure resulted in similar changes in the medaka liver and brain (Wang et al., 2013, Wang et al., 2015) with increased expression of glutathione-S-transferase and peroxiredoxin and decreased expression of mitochondrial flavoproteins and ATP-synthase subunits. Similar effects were observed after methylmercury exposure in Atlantic cod (*Gadus morhua*), but numerous neurotransmitter and axon related proteins were also up-regulated, that had not been previously identified (Berg et al., 2010). In the ameoba *Dictyostelium discoideum* (Marsano et al., 2010) and the bacterium *Corynebacterium glutamicum* (Fanous et al., 2008), oxidative stress response proteins were the most obvious responders to mercuric chloride exposure.

A few studies have combined synchrotron radiation X-ray fluorescence (SRXRF, a qualitative measure) to visualize mercury-bound proteins in gels, and mass spectrometry proteomics to identify such proteins excised from the gel. Both mercuric chloride and methylmercury exposure in rice roots (*Oryza sativa*) induced similar expression effects on oxidative stress response, sulfur and glutathione metabolism, carbohydrate and energy metabolism, and programmed cell death (Li et al., 2016). SRXRF revealed that both mercury compounds bind to proteins 15-25 kDa and identified three ribosomal proteins and six putative proteins.

An SRXRF study of *E. coli* grown in LB medium with 15  $\mu$ M HgCl<sub>2</sub> observed decreased expression of outer membrane protein W, and increased expression of the transcription termination factor Rho, cysteine synthase, transaldolase A, alkyl hydroperoxide reductase, and pyruvate kinase (Gao et al., 2013). More than 20 mercury-binding spots were observed by SRXRF analysis in the 2D gel. That so few proteins were observed in these SRXRF studies may owe to the fact that both used the reducing agent DTT during protein extraction and gel

electrophoresis, which could displace mercury from protein thiols and compromise detection of all *in vivo* binding (Benison et al., 2004).

There have been a few global proteomic studies of Hg exposure that used the newer global bottom-up technique where the entire crude protein extract is digested directly, followed by liquid chromatography separation coupled with tandem mass spectrometry (LC-MS/MS). Two different studies used serum from methylmercury and mercury sulfide treated mice (Kim et al., 2013) or from children of low-level ambient methylmercury exposure (Gump et al., 2012) and both showed an increase in the inflammatory response. Although fish consumption increased atheroprotective lipids in the children, it also increased the inflammatory response and decreased diurnal cortisol levels, which could negatively impact energy levels (Gump et al., 2012). Another proteome study of blood plasma and serum from children with ambient environmental exposure to mercury identified expression changes in a dozen proteins correlated to cardiovascular health (Birdsall et al., 2010). However, these studies only examined protein abundance changes and did not identify mercury bound peptides, so the proteins they found may not have actually been the ones that bound Hg. Rather, their fluctuations may have resulted from Hg-binding to some regulatory protein.

Several proteomics studies have attempted to map the cysteine proteome in humans (Jones and Go, 2011) or to identify reactive cysteines using iodoacetamide-linked mass tags (Weerapana et al., 2010). These studies did not focus on mercury, but they do provide a reference for potential mercury-binding protein sites that could be used as biomarkers of exposure. Mercury forms very stable bonds with thiols and its seven stable isotopes allow detection of modified proteins by mass spectrometry using its distinct isotopic profile (Krupp et al., 2008), even in a global proteome (Polacco et al., 2011). Mercury's distinctive stable isotope

profile has been used to identify reactive cysteine thiols in yeast, where reduced thiols were derivatized, *in vitro*, using *p*-hydroxymercury benzoate (PHMB) (Bakirdere et al., 2010, Rao et al., 2010). Thus, building upon Polacco et al, the work presented in this dissertation is the first in any organism to use global proteomics to identify proteins with high affinity for organic and/or inorganic mercury among all proteins following *in vivo* exposure, which could be used as biomarkers of exposure in other organisms.

### **Mercury effects on transcription**

There have been very few studies that have examined the effects of mercury on transcription and all have used microarray or RT-PCR techniques, which have limitations compared to RNA-Seq (Wang et al., 2009). In the yeast *Saccharomyces cerevisiae* microarray analysis of the transcriptional response to three-hour exposure to 19  $\mu$ M and 47  $\mu$ M mercuric chloride was examined and found altered expression of transport and ribosome synthesis genes, increase in sulfur metabolism and oxidative stress response, and decrease in glucose and carbohydrate metabolism (Jin et al., 2008). In human hepatoma cells microarrays revealed induction of the oxidative stress response following mercuric chloride exposure (Kawata et al., 2007). In zebrafish *Danio rerio* a liver microarray examination of transcription at 24, 48 and 96 hours after mercuric chloride exposure found roughly the same number of up- and down-regulated genes (Ung et al., 2010). However, the number of up-regulated genes increased as mercury accumulated, and down-regulated genes decreased. Gene expression of the electron transport chain was down at 24 hours and mitochondrial fatty acid beta-oxidation remained down for 48 hours. Not until 96 hours did the proteasome, immune response, DNA damage, apoptosis, and electron transport chain increase. In another study, a 25-day exposure to methylmercury in

zebrafish using a skeletal muscle found similar effects, but also observed altered expression of 14 ribosomal proteins using serial analysis of gene expression (SAGE) technique (Cambier et al., 2010).

There has been only one microarray study in the nematode *Caenorhabditis elegans* to directly compare the effects of mercuric chloride and methylmercury exposure (McElwee and Freedman, 2011, McElwee et al., 2013). For all concentrations tested, methylmercury exposure resulted in more than four-times as many differentially expressed genes than inorganic mercury exposure. Both compounds resulted in more up-regulated than down-regulated genes, but they also induced opposite effects on transcription of many genes, suggesting different toxicity mechanisms. Among the functional categories affected by mercurials were carbohydrate metabolism, lipid glycosylation, oxidative stress, proteolysis, cell morphogenesis, and locomotion.

Microarrays are limited to seeing the genes chosen to put on the microarray, as well as lower resolution and dynamic range, whereas state-of-the-art RNA-Seq methods do not have such limitations. The work reported here is the first RNA-Seq study that directly compares transcriptional effects of inorganic and organic mercury over time in any organism.

## **Objectives**

There has been little research done to examine how microorganisms respond to mercury exposure. Most mercury-related studies in microorganisms have focused on mercury resistance or methylation, but far less is known about the cellular response in non-resistant bacteria. The importance of commensal bacteria to health and viability of larger ecosystems is increasingly recognized. *Escherichia coli* strain MG1655 was chosen as the model organism for these studies

because this prototrophic K12 strain has become the universal standard for all *E. coli* 'omics work providing a great depth and breadth of physiological, biochemical, and genetic knowledge for assessing the effects of mercury on the cell.

The objectives of this dissertation have been to use a whole cell approach to identify the biochemical effects, *in vivo* protein damage, and transcriptional response to inorganic or organic mercury exposure in a model prokaryote. The information from this study will contribute to understanding of mercury toxicity mechanisms and provide methods and insight for future studies on how mercury exposure affects microbial communities, including the human intestinal microbiome. In Chapter 2, the bulk biochemical effects of acute inorganic and organic mercury exposure and differences between compounds were examined. *E. coli* cultures were briefly exposed to varying concentrations of mercury compounds during exponential phase growth and assessed by a number of methods. The effects of each mercury compound on the total thiols pool were examined using a standard colorimetric assay and effects on protein thiols were analyzed by a technique developed that uses a thiol specific fluorescence tag followed by SDS-PAGE separation to visualize proteins for densitometry analysis. The effects on the intracellular concentration of essential metals and mercury accumulation were studied using ICP-MS. Iron homeostasis was examined in detail using EPR. In addition, EXAFS was used to identify mercury ligand speciation within intact cells as the mercury concentration was increased to exceed the cellular thiol pool.

In Chapter 3, a global proteomics analysis was done to identify proteins especially vulnerable to modification by phenylmercury in growing cultures. *E. coli* cultures were grown aerobically in minimal medium and briefly exposed to an acute concentration of the organomercurial, phenylmercuric acetate. Sample preparation methods were developed to

preserve *in vivo* mercury adducts and enhance detection of cysteine peptides. Methods for data processing using computational filters were also developed to identify mercury bound peptides within a global proteome. In addition, the biological roles and functional distribution of mercury bound proteins were examined and compared to unexposed conditions. Mercury binding sites within proteins were also assessed for viability as biomarkers in other organisms by searching for conserved domains found in humans and their correlation to health effects.

In Chapter 4, a highly resolved view of the transcriptional effects of sub-acute mercuric chloride and phenylmercuric acetate exposure were compared over time. In order to examine the initial effects of exposure and throughout recovery, it was necessary to determine a concentration of mercurials that would inhibit growth rate, but allow for recovery of growth within one hour after exposure during exponential phase growth. Aliquots of each culture were collected at three time points following exposure and RNA was extracted for RNA-Seq analysis from three biological replicates. The data were analyzed for differentially expressed genes in the mercury exposed conditions compared to the unexposed condition. Differentially expressed genes for each mercury compound were then compared to identify toxicity mechanisms that are shared or unique to each. The results presented in this dissertation provide the most comprehensive view of the effects of mercury exposure in any organism to date.

## References

- AGOCs, M. M., ETZEL, R. A., PARRISH, R. G., PASCHAL, D. C., CAMPAGNA, P. R., COHEN, D. S., KILBOURNE, E. M. & HESSE, J. L. 1990. Mercury exposure from interior latex paint. *N Engl J Med*, 323, 1096-101.
- ANDREINI, C., BERTINI, I., CAVALLARO, G., HOLLIDAY, G. L. & THORNTON, J. M. 2008. Metal ions in biological catalysis: from enzyme databases to general principles. *J Biol Inorg Chem*, 13, 1205-18.
- BAKIR, F., DAMLUJI, S. F., AMIN-ZAKI, L., MURTADHA, M., KHALIDI, A., AL-RAWI, N. Y., TIKRITI, S., DAHAHIR, H. I., CLARKSON, T. W., SMITH, J. C. & DOHERTY, R. A. 1973. Methylmercury poisoning in Iraq. *Science*, 181, 230-41.
- BAKIRDERE, S., BRAMANTI, E., D'ULIVO, A., ATAMAN, O. Y. & MESTER, Z. 2010. Speciation and determination of thiols in biological samples using high performance liquid chromatography-inductively coupled plasma-mass spectrometry and high performance liquid chromatography-Orbitrap MS. *Anal Chim Acta*, 680, 41-7.
- BALL, L. K., BALL, R. & PRATT, R. D. 2001. An assessment of thimerosal use in childhood vaccines. *Pediatrics*, 107, 1147-54.
- BARKAY, T., MILLER, S. M. & SUMMERS, A. O. 2003. Bacterial mercury resistance from atoms to ecosystems. *FEMS Microbiol Rev*, 27, 355-84.
- BARREGARD, L., SALLSTEN, G., SCHUTZ, A., ATTEWELL, R., SKERFVING, S. & JARVHOLM, B. 1992. Kinetics of mercury in blood and urine after brief occupational exposure. *Arch Environ Health*, 47, 176-84.
- BECKER, A. & SOLIMAN, K. F. 2009. The role of intracellular glutathione in inorganic mercury-induced toxicity in neuroblastoma cells. *Neurochem Res*, 34, 1677-84.
- BENISON, G. C., DI LELLO, P., SHOKES, J. E., COSPER, N. J., SCOTT, R. A., LEGAULT, P. & OMICHINSKI, J. G. 2004. A stable mercury-containing complex of the organomercurial lyase MerB: catalysis, product release, and direct transfer to MerA. *Biochemistry*, 43, 8333-45.
- BERG, K., PUNTERVOLL, P., VALDERSNES, S. & GOKSOYR, A. 2010. Responses in the brain proteome of Atlantic cod (*Gadus morhua*) exposed to methylmercury. *Aquat Toxicol*, 100, 51-65.
- BERNHOF, R. A. 2012. Mercury toxicity and treatment: a review of the literature. *J Environ Public Health*, 2012, 460508.
- BIRDSALL, R. E., KILEY, M. P., SEGU, Z. M., PALMER, C. D., MADERA, M., GUMP, B. B., MACKENZIE, J. A., PARSONS, P. J., MECHREF, Y., NOVOTNY, M. V. &

- BENDINSKAS, K. G. 2010. Effects of lead and mercury on the blood proteome of children. *J Proteome Res*, 9, 4443-53.
- BONACKER, D., STOIBER, T., WANG, M., BOHM, K. J., PROTS, I., UNGER, E., THIER, R., BOLT, H. M. & DEGEN, G. H. 2004. Genotoxicity of inorganic mercury salts based on disturbed microtubule function. *Arch Toxicol*, 78, 575-83.
- BRINI, M., CALI, T., OTTOLINI, D. & CARAFOLI, E. 2013. Intracellular calcium homeostasis and signaling. *Met Ions Life Sci*, 12, 119-68.
- BRINI, M., CALI, T., OTTOLINI, D. & CARAFOLI, E. 2014. Neuronal calcium signaling: function and dysfunction. *Cell Mol Life Sci*, 71, 2787-814.
- CAMBIER, S., GONZALEZ, P., DURRIEU, G., MAURY-BRACHET, R., BOUDOU, A. & BOURDINEAUD, J. P. 2010. Serial analysis of gene expression in the skeletal muscles of zebrafish fed with a methylmercury-contaminated diet. *Environ Sci Technol*, 44, 469-75.
- CARVALHO, C. M., CHEW, E. H., HASHEMY, S. I., LU, J. & HOLMGREN, A. 2008. Inhibition of the human thioredoxin system. A molecular mechanism of mercury toxicity. *J Biol Chem*, 283, 11913-23.
- CARVALHO, C. M., LU, J., ZHANG, X., ARNER, E. S. & HOLMGREN, A. 2011. Effects of selenite and chelating agents on mammalian thioredoxin reductase inhibited by mercury: implications for treatment of mercury poisoning. *FASEB J*, 25, 370-81.
- CERNICHIARI, E., BREWER, R., MYERS, G. J., MARSH, D. O., LAPHAM, L. W., COX, C., SHAMLAYE, C. F., BERLIN, M., DAVIDSON, P. W. & CLARKSON, T. W. 1995. Monitoring methylmercury during pregnancy: maternal hair predicts fetal brain exposure. *Neurotoxicology*, 16, 705-10.
- CLARKSON, T. W. & MAGOS, L. 2006. The toxicology of mercury and its chemical compounds. *Crit Rev Toxicol*, 36, 609-62.
- CONDE, C. & CACERES, A. 2009. Microtubule assembly, organization and dynamics in axons and dendrites. *Nat Rev Neurosci*, 10, 319-32.
- CRINNION, W. J. 2000. Environmental medicine, part three: long-term effects of chronic low-dose mercury exposure. *Altern Med Rev*, 5, 209-23.
- CVETKOVIC, A., MENON, A. L., THORGERSEN, M. P., SCOTT, J. W., POOLE, F. L., II, JENNEY, F. E., JR, LANCASTER, W. A., PRAISSMAN, J. L., SHANMUKH, S., VACCARO, B. J., TRAUGER, S. A., KALISIAK, E., APON, J. V., SIUZDAK, G., YANNONE, S. M., TAINER, J. A. & ADAMS, M. W. 2010. Microbial metalloproteomes are largely uncharacterized. *Nature*, 466, 779-82.
- D'AUTREAU, B. & TOLEDANO, M. B. 2007. ROS as signalling molecules: mechanisms that generate specificity in ROS homeostasis. *Nat Rev Mol Cell Biol*, 8, 813-24.



- DIEZ, S. 2009. Human health effects of methylmercury exposure. *Rev Environ Contam Toxicol*, 198, 111-32.
- DRISCOLL, C. T., MASON, R. P., CHAN, H. M., JACOB, D. J. & PIRRONE, N. 2013. Mercury as a global pollutant: sources, pathways, and effects. *Environ Sci Technol*, 47, 4967-83.
- DYRSSEN, D. & WEDBORG, M. 1991. The sulphur-mercury(II) system in natural waters. *Water Air & Soil Pollution*, 56, 507-519.
- EKINO, S., SUSAKI, M., NINOMIYA, T., IMAMURA, K. & KITAMURA, T. 2007. Minamata disease revisited: an update on the acute and chronic manifestations of methyl mercury poisoning. *J Neurol Sci*, 262, 131-44.
- ERCAL, N., GURER-ORHAN, H. & AYKIN-BURNS, N. 2001. Toxic metals and oxidative stress part I: mechanisms involved in metal-induced oxidative damage. *Curr Top Med Chem*, 1, 529-39.
- ETIENNE-MANNEVILLE, S. 2013. Microtubules in cell migration. *Annu Rev Cell Dev Biol*, 29, 471-99.
- FANOUS, A., WEISS, W., GORG, A., JACOB, F. & PARLAR, H. 2008. A proteome analysis of the cadmium and mercury response in *Corynebacterium glutamicum*. *Proteomics*, 8, 4976-86.
- FREED, L. F. 1948. Trichomoniasis, the seventh venereal disease. *S Afr Med J*, 22, 223-9.
- GAO, Y., PENG, X., ZHANG, J., ZHAO, J., LI, Y., LI, Y., LI, B., HU, Y. & CHAI, Z. 2013. Cellular response of *E. coli* upon Hg<sup>2+</sup> exposure--a case study of advanced nuclear analytical approach to metalloproteomics. *Metallomics*, 5, 913-9.
- GARDNER, R. M., NYLAND, J. F. & SILBERGELD, E. K. 2010. Differential immunotoxic effects of inorganic and organic mercury species in vitro. *Toxicol Lett*, 198, 182-90.
- GILMOUR, C. C., PODAR, M., BULLOCK, A. L., GRAHAM, A. M., BROWN, S. D., SOMENAHALLY, A. C., JOHS, A., HURT, R. A., JR., BAILEY, K. L. & ELIAS, D. A. 2013. Mercury methylation by novel microorganisms from new environments. *Environ Sci Technol*, 47, 11810-20.
- GLADYSHEV, V. N. & KRYUKOV, G. V. 2001. Evolution of selenocysteine-containing proteins: significance of identification and functional characterization of selenoproteins. *Biofactors*, 14, 87-92.
- GOLDWATER, L. J. 1972. *Mercury; a history of quicksilver*, Baltimore,, York Press.
- GOTELLI, C. A., ASTOLFI, E., COX, C., CERNICHIARI, E. & CLARKSON, T. W. 1985. Early biochemical effects of an organic mercury fungicide on infants: "dose makes the poison". *Science*, 227, 638-40.

GUMP, B. B., MACKENZIE, J. A., DUMAS, A. K., PALMER, C. D., PARSONS, P. J., SEGU, Z. M., MECHREF, Y. S. & BENDINSKAS, K. G. 2012. Fish consumption, low-level mercury, lipids, and inflammatory markers in children. *Environ Res*, 112, 204-11.

HAHN, L. J., KLOIBER, R., LEININGER, R. W., VIMY, M. J. & LORSCHIEDER, F. L. 1990. Whole-body imaging of the distribution of mercury released from dental fillings into monkey tissues. *FASEB J.*, 4, 3256-3260.

HAHN, L. J., KLOIBER, R., VIMY, M. J., TAKAHASHI, Y. & LORSCHIEDER, F. L. 1989. Dental "silver" tooth fillings: a source of mercury exposure revealed by whole-body image scan and tissue analysis. *FASEB Journal*, 3, 2641-2646.

HARADA, M. 1995. Minamata disease: methylmercury poisoning in Japan caused by environmental pollution. *Crit Rev Toxicol*, 25, 1-24.

HINTELMANN, H. 2010. Organomercurials. Their formation and pathways in the environment. *Met Ions Life Sci*, 7, 365-401.

HULTMAN, P., JOHANSSON, U., TURLEY, S. J., LINDH, U., ENESTROM, S. & POLLARD, K. M. 1994. Adverse immunological effects and autoimmunity induced by dental amalgam and alloy in mice. *FASEB J.*, 8, 1183-1190.

HURSH, J. B., CHERIAN, M. G., CLARKSON, T. W., VOSTAL, J. J. & MALLIE, R. V. 1976. Clearance of mercury (HG-197, HG-203) vapor inhaled by human subjects. *Arch Environ Health*, 31, 302-9.

IMLAY, J. A. 2013. The molecular mechanisms and physiological consequences of oxidative stress: lessons from a model bacterium. *Nat Rev Microbiol*, 11, 443-54.

INSUG, O., DATAR, S., KOCH, C. J., SHAPIRO, I. M. & SHENKER, B. J. 1997. Mercuric compounds inhibit human monocyte function by inducing apoptosis: evidence for formation of reactive oxygen species, development of mitochondrial membrane permeability transition and loss of reductive reserve. *Toxicology*, 124, 211-24.

JACOBSON, J. & DUCHEN, M. R. 2004. Interplay between mitochondria and cellular calcium signalling. *Mol Cell Biochem*, 256-257, 209-18.

JEW, A. D., BEHRENS, S. F., RYTUBA, J. J., KAPPLER, A., SPORMANN, A. M. & BROWN, G. E., JR. 2014. Microbially enhanced dissolution of HgS in an acid mine drainage system in the California Coast Range. *Geobiology*, 12, 20-33.

JIN, Y. H., DUNLAP, P. E., MCBRIDE, S. J., AL-REFAI, H., BUSHEL, P. R. & FREEDMAN, J. H. 2008. Global transcriptome and deletome profiles of yeast exposed to transition metals. *PLoS Genet*, 4, e1000053.

- JONES, D. P. & GO, Y. M. 2011. Mapping the cysteine proteome: analysis of redox-sensing thiols. *Curr Opin Chem Biol*, 15, 103-12.
- KAKKAR, P. & JAFFERY, F. N. 2005. Biological markers for metal toxicity. *Environ Toxicol Pharmacol*, 19, 335-49.
- KAWATA, K., YOKOO, H., SHIMAZAKI, R. & OKABE, S. 2007. Classification of heavy-metal toxicity by human DNA microarray analysis. *Environ Sci Technol*, 41, 3769-74.
- KHAN, M. A. & WANG, F. 2009. Mercury-selenium compounds and their toxicological significance: toward a molecular understanding of the mercury-selenium antagonism. *Environ Toxicol Chem*, 28, 1567-77.
- KIM, B. H., MOON, P. G., LEE, J. E., LEE, S., KIM, S. K., LEE, J. K., KIM, S. H. & BAEK, M. C. 2013. Identification of potential serum biomarkers in mercury-treated mice using a glycoproteomic approach. *Int J Toxicol*, 32, 368-75.
- KORBAS, M., BLECHINGER, S. R., KRONE, P. H., PICKERING, I. J. & GEORGE, G. N. 2008. Localizing organomercury uptake and accumulation in zebrafish larvae at the tissue and cellular level. *Proc Natl Acad Sci U S A*, 105, 12108-12.
- KORBAS, M., MACDONALD, T. C., PICKERING, I. J., GEORGE, G. N. & KRONE, P. H. 2012. Chemical form matters: differential accumulation of mercury following inorganic and organic mercury exposures in zebrafish larvae. *ACS Chem Biol*, 7, 411-20.
- KORBAS, M., O'DONOGHUE, J. L., WATSON, G. E., PICKERING, I. J., SINGH, S. P., MYERS, G. J., CLARKSON, T. W. & GEORGE, G. N. 2010. The chemical nature of mercury in human brain following poisoning or environmental exposure. *ACS Chem Neurosci*, 1, 810-8.
- KOSTIAL, K., SIMONOVIC, I., RABAR, I., BLANUSA, M. & LANDEKA, M. 1983. Age and intestinal retention of mercury and cadmium in rats. *Environ Res*, 31, 111-5.
- KRUPP, E. M., MILNE, B. F., MESTROT, A., MEHARG, A. A. & FELDMANN, J. 2008. Investigation into mercury bound to biothiols: structural identification using ESI-ion-trap MS and introduction of a method for their HPLC separation with simultaneous detection by ICP-MS and ESI-MS. *Anal Bioanal Chem*, 390, 1753-64.
- LEDWIDGE, R., PATEL, B., DONG, A., FIEDLER, D., FALKOWSKI, M., ZELIKOVA, J., SUMMERS, A. O., PAI, E. F. & MILLER, S. M. 2005. NmerA, the metal binding domain of mercuric ion reductase, removes Hg<sup>2+</sup> from proteins, delivers it to the catalytic core, and protects cells under glutathione-depleted conditions. *Biochemistry*, 44, 11402-16.
- LI, Y., ZHAO, J., LI, Y. F., XU, X., ZHANG, B., LIU, Y., CUI, L., LI, B., GAO, Y. & CHAI, Z. 2016. Comparative metalloproteomic approaches for the investigation proteins involved in the toxicity of inorganic and organic forms of mercury in rice (*Oryza sativa* L.) roots. *Metallomics*.

- LORSCHIEDER, F. L., VIMY, M. J., SUMMERS, A. O. & ZWIERS, H. 1995. The dental amalgam mercury controversy--inorganic mercury and the CNS; genetic linkage of mercury and antibiotic resistances in intestinal bacteria. *Toxicology*, 97, 19-22.
- LUND, B. O., MILLER, D. M. & WOODS, J. S. 1991. Mercury-induced H<sub>2</sub>O<sub>2</sub> production and lipid peroxidation in vitro in rat kidney mitochondria. *Biochem Pharmacol*, 42 Suppl, S181-7.
- LUQUE-GARCIA, J. L., CABEZAS-SANCHEZ, P. & CAMARA, C. 2011. Proteomics as a tool for examining the toxicity of heavy metals. *TrAC Trends in Analytical Chemistry*, 30, 703-716.
- MAGOS, L. 1997. Physiology and toxicology of mercury. *Met Ions Biol Syst*, 34, 321-70.
- MAGOS, L. & CLARKSON, T. W. 2006. Overview of the clinical toxicity of mercury. *Ann Clin Biochem*, 43, 257-68.
- MAGOS, L., HALBACH, S. & CLARKSON, T. W. 1978. Role of catalase in the oxidation of mercury vapor. *Biochem Pharmacol*, 27, 1373-7.
- MALM, O. 1998. Gold mining as a source of mercury exposure in the Brazilian Amazon. *Environ Res*, 77, 73-8.
- MARSANO, F., BOATTI, L., RANZATO, E., CAVALETTO, M., MAGNELLI, V., DONDERO, F. & VIARENGO, A. 2010. Effects of mercury on Dictyostelium discoideum: proteomics reveals the molecular mechanisms of physiological adaptation and toxicity. *J Proteome Res*, 9, 2839-54.
- MASON, R. P., CHOI, A. L., FITZGERALD, W. F., HAMMERSCHMIDT, C. R., LAMBORG, C. H., SOERENSEN, A. L. & SUNDERLAND, E. M. 2012. Mercury biogeochemical cycling in the ocean and policy implications. *Environ Res*, 119, 101-17.
- MASON, R. P., FITZGERALD, W. F. & MOREL, F. M. M. 1994. The Biogeochemical Cycling of Elemental Mercury - Anthropogenic Influences. *Geochimica Et Cosmochimica Acta*, 58, 3191-3198.
- MCELWEE, M. K. & FREEDMAN, J. H. 2011. Comparative toxicology of mercurials in Caenorhabditis elegans. *Environ Toxicol Chem*, 30, 2135-41.
- MCELWEE, M. K., HO, L. A., CHOU, J. W., SMITH, M. V. & FREEDMAN, J. H. 2013. Comparative toxicogenomic responses of mercuric and methyl-mercury. *BMC Genomics*, 14, 698.
- MOREL, F. M. M., KRAEPIEL, A. M. L. & AMYOT, M. 1998. THE CHEMICAL CYCLE AND BIOACCUMULATION OF MERCURY. *Annual Review of Ecology and Systematics*, 29, 543-566.

- MYERS, G. J., DAVIDSON, P. W., COX, C., SHAMLAYE, C., CERNICHIARI, E. & CLARKSON, T. W. 2000. Twenty-seven years studying the human neurotoxicity of methylmercury exposure. *Environ Res*, 83, 275-85.
- NATH, K. A., CROATT, A. J., LIKELY, S., BEHRENS, T. W. & WARDEN, D. 1996. Renal oxidant injury and oxidant response induced by mercury. *Kidney Int*, 50, 1032-43.
- NIES, D. H. 1999. Microbial heavy-metal resistance. *Appl Microbiol Biotechnol*, 51, 730-50.
- PAL, C., BENGTSSON-PALME, J., KRISTIANSSON, E. & LARSSON, D. G. 2015. Co-occurrence of resistance genes to antibiotics, biocides and metals reveals novel insights into their co-selection potential. *BMC Genomics*, 16, 964.
- PHILBERT, M. A., BILLINGSLEY, M. L. & REUHL, K. R. 2000. Mechanisms of injury in the central nervous system. *Toxicol Pathol*, 28, 43-53.
- PIRRONE, N., CINNIRELLA, S., FENG, X., FINKELMAN, R. B., FRIEDLI, H. R., LEANER, J., MASON, R., MUKHERJEE, A. B., STRACHER, G., STREETS, D. G. & TELMER, K. 2009. Global Mercury Emissions to the Atmosphere from Natural and Anthropogenic Sources. In: MASON, R. & PIRRONE, N. (eds.) *Mercury Fate and Transport in the Global Atmosphere: Emissions, Measurements and Models*. Boston, MA: Springer US.
- PITTS, K. E. & SUMMERS, A. O. 2002. The roles of thiols in the bacterial organomercurial lyase (MerB). *Biochemistry*, 41, 10287-96.
- POLACCO, B. J., PURVINE, S. O., ZINK, E. M., LAVOIE, S. P., LIPTON, M. S., SUMMERS, A. O. & MILLER, S. M. 2011. Discovering mercury protein modifications in whole proteomes using natural isotope distributions observed in liquid chromatography-tandem mass spectrometry. *Mol Cell Proteomics*, 10, M110 004853.
- PROCHAZKOVA, J., STERZL, I., KUCEROVA, H., BARTOVA, J. & STEJSKAL, V. D. 2004. The beneficial effect of amalgam replacement on health in patients with autoimmunity. *Neuro Endocrinol Lett*, 25, 211-8.
- RAHOLA, T., HATTULA, T., KOROLAINEN, A. & MIETTINEN, J. K. 1973. Elimination of free and protein-bound ionic mercury ( $20\text{Hg}^{2+}$ ) in man. *Ann Clin Res*, 5, 214-9.
- RALSTON, N. V., BLACKWELL, J. L., 3RD & RAYMOND, L. J. 2007. Importance of molar ratios in selenium-dependent protection against methylmercury toxicity. *Biol Trace Elem Res*, 119, 255-68.
- RAO, Y., XIANG, B., BRAMANTI, E., D'ULIVO, A. & MESTER, Z. 2010. Determination of thiols in yeast by HPLC coupled with LTQ-orbitrap mass spectrometry after derivatization with p-(Hydroxymercuri)benzoate. *J Agric Food Chem*, 58, 1462-8.

- RICHARDSON, G. M., WILSON, R., ALLARD, D., PURTILL, C., DOUMA, S. & GRAVIERE, J. 2011. Mercury exposure and risks from dental amalgam in the US population, post-2000. *Sci Total Environ*, 409, 4257-68.
- RIETSCHEL, R. L. & WILSON, L. A. 1982. Ocular inflammation in patients using soft contact lenses. *Arch Dermatol*, 118, 147-9.
- ROMAGNE, F., SANTESMASSES, D., WHITE, L., SARANGI, G. K., MARIOTTI, M., HUBLER, R., WEIHMANN, A., PARRA, G., GLADYSHEV, V. N., GUIGO, R. & CASTELLANO, S. 2014. SelenoDB 2.0: annotation of selenoprotein genes in animals and their genetic diversity in humans. *Nucleic Acids Res*, 42, D437-43.
- ROONEY, J. P. 2007. The role of thiols, dithiols, nutritional factors and interacting ligands in the toxicology of mercury. *Toxicology*, 234, 145-56.
- ROWLAND, I. R., ROBINSON, R. D. & DOHERTY, R. A. 1984. Effects of diet on mercury metabolism and excretion in mice given methylmercury: role of gut flora. *Arch Environ Health*, 39, 401-8.
- RYTUBA, J. J. 2003. Mercury from mineral deposits and potential environmental impact. *Environmental Geology*, 43, 326-338.
- SANDBORGH-ENGLUND, G., ELINDER, C. G., LANGWORTH, S., SCHUTZ, A. & EKSTRAND, J. 1998. Mercury in biological fluids after amalgam removal. *J Dent Res*, 77, 615-24.
- SATOH, M., NISHIMURA, N., KANAYAMA, Y., NAGANUMA, A., SUZUKI, T. & TOHYAMA, C. 1997. Enhanced renal toxicity by inorganic mercury in metallothionein-null mice. *J Pharmacol Exp Ther*, 283, 1529-33.
- SHENKER, B. J., GUO, T. L., O, I. & SHAPIRO, I. M. 1999. Induction of apoptosis in human T-cells by methyl mercury: temporal relationship between mitochondrial dysfunction and loss of reductive reserve. *Toxicol Appl Pharmacol*, 157, 23-35.
- SMITH, J. C., ALLEN, P. V., TURNER, M. D., MOST, B., FISHER, H. L. & HALL, L. L. 1994. The kinetics of intravenously administered methyl mercury in man. *Toxicol Appl Pharmacol*, 128, 251-6.
- SMITH, J. C. & FARRIS, F. F. 1996. Methyl mercury pharmacokinetics in man: a reevaluation. *Toxicol Appl Pharmacol*, 137, 245-52.
- SMITH, T., PITTS, K., MCGARVEY, J. A. & SUMMERS, A. O. 1998. Bacterial oxidation of mercury metal vapor, Hg(0). *Appl Environ Microbiol*, 64, 1328-32.

SUGIURA, Y., TAMAI, Y. & TANAKA, H. 1978. Selenium protection against mercury toxicity: high binding affinity of methylmercury by selenium-containing ligands in comparison with sulfur-containing ligands. *Bioinorg Chem*, 9, 167-80.

SUMMERS, A. O., WIREMAN, J., VIMY, M. J., LORSCHIEDER, F. L., MARSHALL, B., LEVY, S. B., BENNETT, S. & BILLARD, L. 1993. Mercury released from dental "silver" fillings provokes an increase in mercury- and antibiotic-resistant bacteria in oral and intestinal floras of primates. *Antimicrob Agents Chemother*, 37, 825-34.

SUZUKI, N., YAMAMOTO, M., WATANABE, K., KAMBEGAWA, A. & HATTORI, A. 2004. Both mercury and cadmium directly influence calcium homeostasis resulting from the suppression of scale bone cells: the scale is a good model for the evaluation of heavy metals in bone metabolism. *J Bone Miner Metab*, 22, 439-46.

SUZUKI, T., HONGO, T., YOSHINAGA, J., IMAI, H., NAKAZAWA, M., MATSUO, N. & AKAGI, H. 1993. The hair-organ relationship in mercury concentration in contemporary Japanese. *Arch Environ Health*, 48, 221-9.

SUZUKI, T. & TANAKA, A. 1971. Absorption of metallic mercury from the intestine after rupture of Miller-Abbot Balloon. *Ind. Med*, 13, 52-53.

TAN, X. X., TANG, C., CASTOLDI, A. F., MANZO, L. & COSTA, L. G. 1993. Effects of inorganic and organic mercury on intracellular calcium levels in rat T lymphocytes. *J Toxicol Environ Health*, 38, 159-70.

TCHOUNWOU, P. B., AYENSU, W. K., NINASHVILI, N. & SUTTON, D. 2003. Environmental exposure to mercury and its toxicopathologic implications for public health. *Environ Toxicol*, 18, 149-75.

TITZ, B., ELAMIN, A., MARTIN, F., SCHNEIDER, T., DIJON, S., IVANOV, N. V., HOENG, J. & PEITSCH, M. C. 2014. Proteomics for systems toxicology. *Comput Struct Biotechnol J*, 11, 73-90.

TOSTI, A. & TOSTI, G. 1988. Thimerosal: a hidden allergen in ophthalmology. *Contact Dermatitis*, 18, 268-73.

UNG, C. Y., LAM, S. H., HLAING, M. M., WINATA, C. L., KORZH, S., MATHAVAN, S. & GONG, Z. 2010. Mercury-induced hepatotoxicity in zebrafish: in vivo mechanistic insights from transcriptome analysis, phenotype anchoring and targeted gene expression validation. *BMC Genomics*, 11, 212.

UTTARA, B., SINGH, A. V., ZAMBONI, P. & MAHAJAN, R. T. 2009. Oxidative stress and neurodegenerative diseases: a review of upstream and downstream antioxidant therapeutic options. *Curr Neuroparmacol*, 7, 65-74.

- VAHTER, M. E., MOTTET, N. K., FRIBERG, L. T., LIND, S. B., CHARLESTON, J. S. & BURBACHER, T. M. 1995. Demethylation of methyl mercury in different brain sites of *Macaca fascicularis* monkeys during long-term subclinical methyl mercury exposure. *Toxicol Appl Pharmacol*, 134, 273-84.
- VALKO, M., MORRIS, H. & CRONIN, M. T. 2005. Metals, toxicity and oxidative stress. *Curr Med Chem*, 12, 1161-208.
- VAZQUEZ-RODRIGUEZ, A. I., HANSEL, C. M., ZHANG, T., LAMBORG, C. H., SANTELLI, C. M., WEBB, S. M. & BROOKS, S. C. 2015. Microbial- and thiosulfate-mediated dissolution of mercury sulfide minerals and transformation to gaseous mercury. *Front Microbiol*, 6, 596.
- VEIGA, M. M., MAXSON, P. A. & HYLANDER, L. D. 2006. Origin and consumption of mercury in small-scale gold mining. *Journal of Cleaner Production*, 14, 436-447.
- VERITY, M. A., BROWN, W. J. & CHEUNG, M. 1975. Organic mercurial encephalopathy: in vivo and in vitro effects of methyl mercury on synaptosomal respiration. *J Neurochem*, 25, 759-66.
- WALDRON, K. J., RUTHERFORD, J. C., FORD, D. & ROBINSON, N. J. 2009. Metalloproteins and metal sensing. *Nature*, 460, 823-30.
- WANG, M., WANG, Y., WANG, J., LIN, L., HONG, H. & WANG, D. 2011. Proteome profiles in medaka (*Oryzias melastigma*) liver and brain experimentally exposed to acute inorganic mercury. *Aquat Toxicol*, 103, 129-39.
- WANG, M., WANG, Y., ZHANG, L., WANG, J., HONG, H. & WANG, D. 2013. Quantitative proteomic analysis reveals the mode-of-action for chronic mercury hepatotoxicity to marine medaka (*Oryzias melastigma*). *Aquat Toxicol*, 130-131, 123-31.
- WANG, Y., WANG, D., LIN, L. & WANG, M. 2015. Quantitative proteomic analysis reveals proteins involved in the neurotoxicity of marine medaka *Oryzias melastigma* chronically exposed to inorganic mercury. *Chemosphere*, 119, 1126-33.
- WANG, Z., GERSTEIN, M. & SNYDER, M. 2009. RNA-Seq: a revolutionary tool for transcriptomics. *Nat Rev Genet*, 10, 57-63.
- WARIS, G. & AHSAN, H. 2006. Reactive oxygen species: role in the development of cancer and various chronic conditions. *J Carcinog*, 5, 14.
- WATANABE, C., YIN, K., KASANUMA, Y. & SATOH, H. 1999. In utero exposure to methylmercury and Se deficiency converge on the neurobehavioral outcome in mice. *Neurotoxicol Teratol*, 21, 83-8.



WEED, L. E., E.E. 1931. The Utility of Phenyl-Mercury-Nitrate as a Disinfectant. *The Journal of Infectious Diseases*, 49, 440-449.

WEERAPANA, E., WANG, C., SIMON, G. M., RICHTER, F., KHARE, S., DILLON, M. B., BACHOVCHIN, D. A., MOWEN, K., BAKER, D. & CRAVATT, B. F. 2010. Quantitative reactivity profiling predicts functional cysteines in proteomes. *Nature*, 468, 790-5.

WHO 1991. Environmental Health Criteria 118: Inorganic Mercury.

WHO 2002. Recommendations from the Strategic Advisory Group of Experts. *Weekly Epidemiol. Rec.*, 77, 305-316.

XU, F. F. & IMLAY, J. A. 2012. Silver(I), mercury(II), cadmium(II), and zinc(II) target exposed enzymic iron-sulfur clusters when they toxify *Escherichia coli*. *Appl Environ Microbiol*, 78, 3614-21.

ZHANG, H., FENG, X., LARSEN, T., SHANG, L. & LI, P. 2010. Bioaccumulation of methylmercury versus inorganic mercury in rice (*Oryza sativa* L.) grain. *Environ Sci Technol*, 44, 4499-504.

ZHANG, Y., ROMERO, H., SALINAS, G. & GLADYSHEV, V. N. 2006. Dynamic evolution of selenocysteine utilization in bacteria: a balance between selenoprotein loss and evolution of selenocysteine from redox active cysteine residues. *Genome Biol*, 7, R94.

ZORATTI, M. & SZABO, I. 1995. The mitochondrial permeability transition. *Biochim Biophys Acta*, 1241, 139-76.

**CHAPTER 2**  
**ORGANIC AND INORGANIC MERCURIALS HAVE DISTINCT EFFECTS ON**  
**CELLULAR THIOLS, METAL HOMEOSTASIS, AND FE-BINDING PROTEINS**  
**IN *ESCHERICHIA COLI*<sup>1</sup>**

---

<sup>1</sup>LAVOIE, S.P., MAPOLELO, D.T., COWART, D.M., POLACCO, B.P., JOHNSON, M.K., SCOTT, R.A., MILLER, S.M., SUMMERS, A.O. 2015. Organic and inorganic mercurials have distinct effects on cellular thiols, metal homeostasis, and Fe-binding proteins in *Escherichia coli*. *J Biol Inorg Chem*, 20, 1239-1251; Reprinted with permission of publisher.

## ABSTRACT

The protean chemical properties of the toxic metal mercury (Hg) have made it attractive in diverse applications since antiquity. However, growing public concern has led to an international agreement to decrease its impact on health and the environment. During a recent proteomics study of acute Hg exposure in *E. coli*, we also examined the effects of inorganic and organic Hg compounds on thiol- and metal- homeostases. On brief exposure, lower concentrations of divalent inorganic mercury Hg(II) blocked bulk cellular thiols and protein-associated thiols more completely than higher concentrations of monovalent organomercurials, phenylmercuric acetate (PMA) and merthiolate (MT). Cells bound Hg(II) and PMA in excess of their available thiol ligands; X-ray absorption spectroscopy indicated nitrogens as likely additional ligands. The mercurials released protein bound iron (Fe) more effectively than common organic oxidants and all disturbed the  $\text{Na}^+/\text{K}^+$  electrolyte balance, but none provoked efflux of six essential transition metals including Fe. PMA and MT made stable cysteine monothiol adducts in many Fe-binding proteins, but stable Hg(II) adducts were only seen in CysXxx(n)Cys peptides. We conclude that on acute exposure: (a) the distinct effects of mercurials on thiol- and Fe-homeostases reflected their different uptake and valences; (b) their similar effects on essential metal- and electrolyte-homeostases reflected the energy-dependence of these processes; and (c) peptide phenylmercury-adducts were more stable or detectable in mass spectrometry than Hg(II)-adducts. These first in vivo observations in a well-defined model organism reveal differences upon acute exposure to inorganic and organic mercurials that may underlie their distinct toxicology.

## INTRODUCTION

The toxic metallic element mercury occurs naturally as the insoluble HgS ore (cinnabar), as soluble inorganic complexes of  $\text{Hg}^{+2}$ ,  $\text{Hg}^{+1}$ , or  $(\text{Hg}_2)^{2+}$  with counterions such as acetate, nitrate, and the halides, and as organomercurials generated by microbial and anthropogenic processes (Barkay et al., 2003). Mercury also has a zero valent form ( $\text{Hg}^0$ ), which is stable at standard temperatures and pressures as a dense liquid with a highly volatile monoatomic vapor (Barkay et al., 2003). Approximately 75% of mercury released to the environment comes from anthropogenic sources, primarily emissions from fossil fuels, and urban and industrial waste disposal sites, although natural sources such as volcanoes also contribute mercury to the environment (Mason et al., 1994). Historically, mercury has been used in classical and medieval medicine and alchemy (Norn et al., 2008). Modern uses include batteries, switches, thermostats, electrodes (e.g. in the chlor-alkali process) and medical devices, including the Hg-Ag amalgam of dental restorations, a major source of chronic exposure in humans (Barkay et al., 2003, Crinnion, 2000, Richardson et al., 2011). Two other very direct sources of human exposure are through the use of mercury in artisanal gold mining (Malm, 1998) and consumption of fish containing methyl-mercury (Crinnion, 2000). Chronic and acute mercury exposure in humans can result in neurotoxicity, nephrotoxicity, immunotoxicity, hepatotoxicity, gastrointestinal toxicity, and neonatal development problems (Crinnion, 2000, Bakir et al., 1973, Yorifuji et al., 2008, Davidson et al., 2004). The organomercurials, methylmercury and ethylmercury (a component of the common disinfectant, merthiolate, also known as thimerosal), are considered primarily neurotoxic and both inorganic forms,  $\text{Hg}^0$  and  $\text{Hg}^{2+}$  are considered primarily nephrotoxic (Clarkson and Magos, 2006). The biochemical basis for these differences is unclear.

As with other ubiquitous environmental electrophiles such as arsenic and lead, there is no

single biochemical target of Hg damage. Mercury has a strong affinity for sulfur ligands (Cheesman et al., 1988, Oram et al., 1996), so the expected cellular targets for mercury are low molecular weight thiols (RSH) involved in intracellular redox homeostasis (Valko et al., 2005) and the thiol groups of proteins (Clarkson and Magos, 2006). The major low molecular weight thiol in animals and many bacteria is glutathione (GSH), which acts as an intracellular redox buffer (Schafer and Buettner, 2001). Approximately 92% percent of human proteins have one or more cysteines (Miseta and Csutora, 2000). *In vitro*, mercury damages enzymes with an active site cysteine (Carvalho et al., 2008), displaces metal ion cofactors (O'Connor et al., 1993), disrupts structural stability (Imesch et al., 1992) and forms a stable cross-link between intra- and inter-protein cysteine residues (Carvalho et al., 2008, Soskine et al., 2002). Mercury reacts even more strongly with the selenol (RSeH) of the rare amino acid selenocysteine, found across all domains of life (Khan and Wang, 2009, Gladyshev and Kryukov, 2001).

Cells maintain optimum available concentrations of essential metals homeostatically (Finney and O'Halloran, 2003, Helbig et al., 2008), and disruption of these balances by a toxic metal can damage many processes (Ercal et al., 2001). Approximately half of all enzymes in the six Enzyme Commission (EC) functional classes use metal cofactors (Andreini et al., 2008, Waldron et al., 2009, Cvetkovic et al., 2010). Transition metal cofactors are often coordinated by protein cysteine residues and are vulnerable to displacement by mercury with consequent loss of protein function. Despite many studies on individual enzymes and cellular processes, there has been no comprehensive study of the bulk effects of Hg on the thiol pool and metal homeostasis in any organism. As part of a larger proteomics project to define the mercury exposome (Polacco et al., 2011), we examined the effects of brief, acute exposure of growing cells to inorganic and

organomercurials (Fig. B.S1) on the cellular content of thiols, of essential metals, and of free iron and iron-binding proteins in *E. coli* K-12 MG1655.

## **MATERIALS AND METHODS**

### *Preparation of cells.*

For each experiment *E. coli* K-12 MG1655 was subcultured from cryostorage on Luria-Bertani (LB) agar and grown overnight at 37°C. A half-dozen well-isolated colonies were used to inoculate a 50 ml starter culture of Neidhardt MOPS minimal medium (Neidhardt et al., 1974) supplemented with 20 mg/L uracil and 5 mg/L thiamine, which was then incubated at 37°C with shaking at 250 rpm for 18 hrs. Neidhardt MOPS minimal medium was selected as it is the standard medium for most ‘omics work in *E. coli* using K-12 MG1655 strain. The saturated starter culture was diluted 1:40 to initiate the experimental culture, which was then incubated at 37°C with shaking at 250 rpm. At OD<sub>595</sub> of approximately 0.6, the culture was split into four 450 ml aliquots in Fernbach flasks. For each experiment a defined concentration of each mercurial (i.e. a compound containing mercury) or oxidant was added to all but one culture aliquot (the unexposed control) and all were incubated for 15 min or 30 min at 37°C, with shaking at 250 rpm. All data presented are from 30-min exposures except for proteomics data (Tables 2.2 and B.S3-B.S7) and for BODIPY-protein-thiols data in Figure 2.2, which are from 15-min exposure cultures. Cultures were harvested by centrifugation at 17,700 x g at 4°C. Each cell pellet was suspended in ice-cold MOPS minimal medium at one 100<sup>th</sup> the original culture volume (100X), and then dispensed as 1 ml aliquots. The cells were washed by centrifuging at 10,600 x g for 4 min at 4°C, suspending in 1 ml of ice-cold 20 mM Tris-HCl (pH 7.4), repeating centrifugation, and finally suspended in 500 µl (200X) of 20 mM Tris-HCl (pH 7.4) for cryostorage at -70°C until they were used in specific assays as described below. Where assays required lysates rather

than intact cells, the frozen cell suspensions were thawed on ice, diluted to 50X with 20 mM Tris-HCl (pH 7.4) and lysed 3 times by French Press (10K psi, 4°C).

#### *Quantifying protein.*

The protein concentrations of the crude French Press lysates were quantified by the Bradford method (Bradford, 1976) using Coomassie Plus<sup>TM</sup> reagent (Pierce). The number of cells was estimated based on protein constituting 16% of the cell wet weight and the wet weight of one *E. coli* cell being  $9.5 \times 10^{-13}$  g (Cayley and Record, 2003). Where intracellular concentration is reported, a cell volume of  $6.7 \times 10^{-16}$  L/cell was used for calculations (Cayley and Record, 2003).

#### *Quantifying total cellular thiols.*

Total thiols in French Press cell lysates of cultures exposed to mercurials (or not) for 30 min, were determined by reaction with 5,5'-dithiobis(2-nitro-benzoic acid) (DTNB; Sigma) using the extinction coefficient at 412 nm for thionitrobenzoate (TNB) of  $13,600 \text{ M}^{-1} \text{ cm}^{-1}$  (Ellman, 1959). The total thiol to Hg ratio was determined based on the calculated molecules of thiol per cell in the unexposed control, relative to the total atoms of mercury quantified by ICP-MS per cell in exposed cultures. In order to measure thiols of proteins in the native state available for interaction with the mercurials, urea was not used here.

#### *Detecting protein thiols.*

Protein thiols in fresh French Press lysates of mercurial-exposed cultures were treated (or not) with 10 M urea, and covalently labeled in the dark, at room temperature, by reaction for 60 min with BODIPY<sup>®</sup> iodoacetamide (BODIPY-I, BODIPY<sup>®</sup> FL C1-IA, N-(4,4-Difluoro-5,7-Dimethyl-4-Bora-

3a,4a-Diaza-s-Indacene-3-yl)Methyl)Iodoacetamide) (Invitrogen) using a 2-fold molar excess over total lysate thiol concentration measured in the unexposed control culture (see Table 2.1 footnote). Unreacted BODIPY-I was removed with a Sepharose gel (BioGel P-2, BioRad) spin column and eluted protein was quantified by the Bradford method (Bradford, 1976). The excitation spectrum of BODIPY does not overlap with the Bradford assay and controls were performed to confirm this (data not shown). A constant protein mass of BODIPY-tagged cell lysate was separated by SDS-PAGE on a 12.5% Next-Gel<sup>®</sup> (Amresco) and, after rinsing with deionized water, the protein-associated BODIPY fluorescence was recorded with a GE Typhoon Trio (488 nm excitation, 520 nm bandpass 40 emission filter, 375 V photomultiplier tube (PMT), 200  $\mu$ m resolution, normal sensitivity). Lastly, to measure total protein intensity in each gel lane, the gel was stained with Imperial<sup>™</sup> protein stain (Pierce), destained in deionized water overnight, and imaged with Typhoon (Ex: 633 nm excitation, Em: 670 nm bandpass BP30 emission filter, PMT: 750 V, 200  $\mu$ m resolution, normal sensitivity), which also served as confirmation that an equal mass of protein was loaded in each lane. Using GeneTools (Syngene, Inc), the summed intensity (fluorescence or Coomassie stain) for each lane of a mercurial-exposed lysate was compared to that of the unexposed lysate to estimate the loss of BODIPY reactivity or of bulk protein in each exposure condition. Densitometric protein profiles from exposed and unexposed cultures were also overlaid to look for gain or loss of individual fluorescent or Coomassie-stained bands.

#### *Quantifying free iron by electron paramagnetic resonance (EPR).*

A 1 ml aliquot of 100X intact cells, from 30-min exposure cultures, was treated with 100  $\mu$ l of 100 mM of cell-impermeant diethylene triamine pentaacetic acid (DTPA; Sigma) to block iron uptake from the medium and with 100  $\mu$ l of 200 mM cell-permeant deferoxamine mesylate salt (DF; Sigma).



The iron chelator deferoxamine does not disrupt protein bound iron and will only bind free (i.e. uncomplexed iron that is not bound by proteins) intracellular Fe(III) and Fe(II) that is oxidized in the presence of the iron chelator and molecular oxygen to form the  $S = 5/2$  Fe(III):DF complex, which exhibits an intense EPR signal at  $g = 4.3$  (Woodmansee and Imlay, 2002). An identical aliquot was not treated with DPTA/DF and both were incubated at 37°C, 250 rpm for 15 min and then centrifuged at 10,600 x  $g$  for 4 min at 4°C. The cell pellets were washed with 1 ml of ice-cold 20 mM Tris-HCl (pH 7.4) and each pellet was suspended in 300  $\mu$ l of 20 mM Tris-HCl (pH 7.4) in 10% (vol/vol) glycerol and cryostored at -70°C until EPR analysis. For EPR analysis cell suspensions were thawed on ice and loaded into quartz EPR tubes and re-frozen in liquid nitrogen. EPR standards of the Fe(III):DF complex were generated by reacting 100  $\mu$ M FeCl<sub>3</sub> in 20 mM Tris-HCl (pH 7.4) and 20 mM DF for 15 min at 37°C, 250 rpm. The concentration of the Fe(III):DF chromophore was quantified at 420 nm using an extinction coefficient of 2865 M<sup>-1</sup> cm<sup>-1</sup> (Woodmansee and Imlay, 2002). Dilutions of the Fe(III):DF complex were made in 20 mM Tris-HCl (pH 7.4) in 10% glycerol for 0, 10, 20, 30, 40 and 50  $\mu$ M standards. X-band (~ 9.6 GHz) EPR spectra were recorded at -203°C (70 K) using an ESP-300D spectrometer (Bruker, Billerica, MA), equipped with an ESR 900 helium flow cryostat (Oxford Instruments, Concord, MA). The Fe(III):DF concentration of each sample was determined from the standard curve under non-saturating conditions by using peak-to-trough height of the isotropic EPR signal at  $g = 4.3$ .

#### *Observing mercury adducts of E. coli iron-binding proteins by LC-MS/MS*

Cultures were prepared as above for 15 min exposure to 40  $\mu$ M PMA, 160  $\mu$ M merthiolate or 20  $\mu$ M mercuric acetate, but harvested cells were suspended in ammonium bicarbonate buffer amended with iodoacetamide (IAM) to prevent redistribution of mercury adducts by exchange with

free thiols during preparation for liquid chromatography-coupled mass spectrometry (LC-MS/MS) proteomic analysis (Polacco et al., 2011) (Zink et. al., manuscript in preparation). Gene Ontology (GO) terms in UniProtKB (Huntley et al., 2015) were used to generate a list of all encoded *E. coli* proteins that bind iron alone, in iron-sulfur clusters, or in heme groups (Table B.S1 and B.S2). This list (current as of June 2015) was searched against the results of LC-MS/MS proteomes obtained from cultures exposed to PMA (3 biological replicate proteomes, Table B.S3), merthiolate (MT) (1 proteome, Table B.S4) or mercuric acetate (1 proteome, Table B.S5) (full datasets to be published in Zink et. al., manuscript in preparation) to identify iron-binding proteins whose cysteines formed stable adducts with these compounds. All proteome summaries contain data from corresponding no-mercury control samples, which are included in total spectral counts.

LC-MS/MS peptide hit lists were generated by SEQUEST using the *E. coli* genome sequence (GenBank: U00096.2) and allowing alkylation by IAM or adducts of Hg, phenylHg (PhHg) or ethylHg (EtHg) as modifications of cysteine. SEQUEST results were re-scored by MS-GF (Kim et al., 2008), and SEQUEST matches to Hg and PhHg and EtHg adducts were additionally re-scored by PeptideProphet (Keller et al., 2002) to maximize true identifications of Hg adducts. Filtering criteria were selected based on false discovery rates (FDR) computed from searches against a reversed sequence database as decoys. The primary filter for spectral matches was MS-GF's spectral probability, which we required to score less than  $1.6 \times 10^{-10}$  for acceptance of any peptide match. This threshold yielded a FDR of 0.001 over all spectra. To eliminate false discoveries that are singletons, we further improved accuracy by both requiring more than one spectrum for any peptide and, for proteins with only a single observed peptide, requiring a MS-GF spectrum probability less than  $1 \times 10^{-11}$  and at least one tryptic end (semi or fully tryptic). For matches to peptides modified by Hg, we relaxed the MS-GF spectrum probability threshold to  $5 \times 10^{-7}$ , but required PeptideProphet's probability to be

greater than 0.8 for acceptance. Both thresholds yielded a high FDR when used alone, but when combined and with two additional criteria that peptides be fully tryptic and from proteins passing by the MS-GF spectral probability filter, these criteria produced zero matches to Hg modified decoy sequences (FDR = 0.0). As an alternative estimate of FDR focused on incorrect modifications rather than on incorrect sequences, we used “Hg adducts” detected in the Hg-free samples as a distinct estimate of FDR. This yielded an FDR of 0.009 for spectra identified as Hg-modified. Detailed qualitative (Zink, et al., in preparation) and quantitative (Polacco, et al. in preparation) analyses of mercurial modifications of the complete *E.coli* proteomes are underway and will be submitted elsewhere.

#### *Quantifying bulk cellular inorganic elements.*

One ml cryoarchived aliquots of 100X concentrated intact cells from each exposure condition were thawed on ice and brought to 5 ml total volume with HPLC grade water. They were then diluted with concentrated trace metal grade nitric acid including a 1 ppm gold background and digested by microwave in sealed Teflon containers. Metal concentrations in the digested solutions were determined with a Perkin-Elmer ELAN 9000 ICP-MS using internal standards and intermittent blanks to exceed requirements for EPA Method 3051A ([www.epa.gov/osw/hazard/testmethods/sw846/pdfs/3051a.pdf](http://www.epa.gov/osw/hazard/testmethods/sw846/pdfs/3051a.pdf)) and 6020B (<http://www.epa.gov/wastes/hazard/testmethods/sw846/pdfs/6020b.pdf>). These analyses were carried out at the University of Georgia Laboratory for Environmental Analysis ([www.uga.edu/lea](http://www.uga.edu/lea)).

### *Identifying bulk cellular mercury ligands.*

Mercury was added to a known amount of growing cells and incubation was continued for 30 min followed by harvest, concentration and cryostorage as above. A 500  $\mu$ l aliquot of 200X concentrated cells for each exposure condition was thawed on ice and 8  $\mu$ l was loaded into 5 wells of an XAS microcuvette for each exposure condition examined and flash frozen in liquid nitrogen. Pure standards of mercury compounds mixed with glutathione (or not) were prepared at room temperature and 8  $\mu$ l was loaded into each of 5 wells of an XAS cuvette and flash frozen in liquid nitrogen.

Mercury L<sub>3</sub>-edge data were collected at -263°C (10 K) beamlines 9-3 and 7-3 at the Stanford Synchrotron Radiation Laboratory (SSRL), with the SPEAR storage ring operating in a dedicated mode at 3.0 GeV and 50 to 100 mA. An Si[220] double crystal-monochromator and a 30-element Ge solid state X-ray fluorescence detector were employed for data collection. No photoreduction was observed when comparing the first and last spectra collected for a given sample. The first inflection of a Hg-Sn amalgam standard was used for energy calibration. Extended X-ray absorption fine structure (EXAFS) analysis was performed with EXAFSPAK software (<http://www-ssrl.slac.stanford.edu/exafspak.html>) according to standard procedures (Scott, 2000, George et al., 1996). Fourier transforms (FT) were calculated with sulfur-based phase-shift correction. Theoretical and phase-shift functions employed in simulations were generated with FEFF 8.2 code (Ankudinov et al., 2002, Mustre de Leon et al., 1991). Curve fitting analysis was performed as described previously (Casper et al., 1999).

## **RESULTS**

*HgCl<sub>2</sub> blocked total and protein-associated thiols more effectively than did phenylmercury or merthiolate.*

*Blockage of cellular thiols after 30 min exposure.*

As measured by Ellman's reagent (DTNB), lysed cells from unexposed cultures had an average bulk thiol content of  $3.59\text{E}+06$  molecules/cell  $\pm 1.54\text{E}+05$  (Table 2.1). The two organomercurials examined, PMA and MT, were used as surrogates to methylmercury, but are also of public health interest in their own right. The organomercurial PMA at  $40\text{ }\mu\text{M}$  in the media, accumulated to levels that blocked all DTNB-detectable thiols. Merthiolate at  $160\text{ }\mu\text{M}$  in the media, only blocked approximately 89% of total thiols. In contrast, exposure to as little as  $8\text{ }\mu\text{M}$   $\text{HgCl}_2$  in the media resulted in a 46% loss of reactive thiols and at  $20\text{ }\mu\text{M}$   $\text{HgCl}_2$  or above, cellular thiols were undetectable. Thus, neutral, bivalent,  $\text{HgCl}_2$  is more effective per mole in blocking thiols in intact growing cells than larger lipophilic, monovalent PMA or MT. Note also that PMA and  $\text{Hg(II)}$  accumulated in cells to levels in excess of the measured thiol content of the cells (rightmost column in Table 2.1); this is examined further in the last section of the Results.

The fluorescent thiol-reactive dye, BODIPY-iodoacetamide was used to generate a qualitative SDS-PAGE “fingerprint” of total cell lysate proteins with reactive thiols. The profiles of BODIPY-tagged proteins, not treated with urea, were nearly indistinguishable from each other (Fig. 2.1). Thus, during 30 min each compound was able to enter intact cells and form stable adducts to protein thiols preventing subsequent reaction with the fluorescent probe BODIPY.

*Blockage of protein-bound thiols after 15 min exposure.*

Shorter exposure time revealed differences between the mercurial compounds in BODIPY-iodoacetamide tagged lysate profiles of cells exposed to mercurials for only 15-minutes (Fig. 2.2. Urea treatment of the lysate prior to reacting with BODIPY-I uncovered additional thiols, presumably in the interior of proteins (even numbered lanes). A range of

concentrations for each mercury compound was tested to determine exposure conditions that would result in intracellular accumulation high enough to bind protein thiols and allow for detection of mercury adducts in proteomics analysis. Note that BODIPY-iodoacetamide was chosen over its maleimide derivative for its preference for cysteine thiols (Tyagarajan et al., 2003). Faint gel bands observed in lysates lacking any detectable thiols by Ellman's assay (Table 2.1) likely arose from BODIPY's acetamide's weak reactivity with the more abundant amino acids histidine (Fruchter and Crestfield, 1967), lysine (Boja and Fales, 2001), and tyrosine (Cotner and Claggett, 1973).

The total fluorescence intensity in each lane was compared densitometrically to the corresponding urea-treated or untreated lane for the lysate from the unexposed condition. No unique BODIPY-reactive protein bands appeared or disappeared upon mercury exposure (data not shown). Rather, BODIPY-reactive proteins decreased uniformly with increasing mercury exposure. However, there was no change in intensity of bulk protein band patterns as detected by Coomassie Blue (data not shown) indicating the mercurial-provoked loss of BODIPY-reactivity is not caused by non-specific loss of proteins through precipitation or aggregation.

In lysates of cells exposed to 20  $\mu$ M (lane 3) or 80  $\mu$ M HgCl<sub>2</sub> (lane 5), BODIPY-protein fluorescence decreased by 38% and 39%, respectively, compared to the corresponding unexposed cell lysate (lane 1). Urea treatment of the unexposed lysate (lane 2) increased BODIPY fluorescence (relative to lane 1) by unmasking buried cysteine thiols. In contrast, urea treatment of lysates of Hg-exposed cells yielded very low BODIPY fluorescence (lanes 4 and 6 compared to lanes 3 and 5, respectively), indicating that in the intact cells these nominally buried cysteines had either been blocked directly by Hg(II) or possibly oxidized to disulfides by reactive

oxygen species provoked by Hg(II) inhibition of respiratory proteins (see Fe-release and Fe-binding proteome results below).

Exposure to the larger aromatic, monovalent mercurial, phenylmercury acetate (PMA) blocked BODIPY access to only 24% (20  $\mu$ M, lane 7) and 29 % (40  $\mu$ M, lane 9) of protein thiols in lysates without urea compared to lysates of cells not exposed to mercurials or urea (lane 1). Urea treatment of lysed PMA-exposed cells also showed more modest blockage (greater BODIPY fluorescence) at 20  $\mu$ M PMA (lane 8) than the corresponding urea-treated lysate of cells exposed to 20  $\mu$ M HgCl<sub>2</sub> (lane 4). However, the urea-treated cells exposed to 40  $\mu$ M PMA (lane 10) did suffer a decrease in BODIPY fluorescence equal to the 20  $\mu$ M HgCl<sub>2</sub>-exposed cells, consistent with their respective valences. This suggests that neutral HgCl<sub>2</sub> enters the cell no less rapidly than hydrophobic phenylmercury, which may also be present as the chloride in this minimal medium.

Exposures to the large, negatively charged merthiolate (MT; ethyl-mercury thiosalicylate), did not block protein cysteines from reaction with BODIPY at 40  $\mu$ M (lane 11) or 80  $\mu$ M (lane 13) and blocked only weakly at 160  $\mu$ M (lane 15) (compared to lysates from cells exposed neither to mercurials nor urea, lane 1). Urea treatment showed that just 11%, 14% and 19% (lanes 12, 14, and 16 compared to lane 2) of BODIPY-reactive thiols had been blocked by merthiolate in intact cells. This weak blockade of protein and cellular (Table 2.1) thiols by MT is consistent with its uptake impediments (size and negative charge) and the strength of the S-Hg bond with its thiosalicylate ligand ( $K_{\text{form}}$  of  $10^{38}$ , (Basinger et al., 1981)). Thiosalicylate is thermodynamically less likely to be displaced from ethylmercury by protein or cellular thiols than the more weakly associated acetate of PMA ( $K_{\text{form}}$   $10^8$ , (Khokhlova et al., 1982)) or chloride ( $K_{\text{form}}$   $10^{14}$ , (Powell et al., 2005)) of Hg(II).

Thus, in this bulk qualitative “fingerprint” analysis with BODIPY, these three Hg compounds differed in uptake rate, but did not differ significantly in their ability to react with cellular thiol targets that they ultimately blocked, though whether the blockage was directly by mercurial ligands or indirectly by oxidation of the thiols upon mercurial-provoked generation of reactive oxygen species (ROS) is not distinguishable by these methods.

#### *Mercurials released protein-bound Fe(II)*

Iron is a redox active metal, so the concentration of intracellular uncomplexed iron, i.e. iron that is not bound to proteins, is normally kept low, at 15 – 30  $\mu\text{M}$  by sequestration via storage proteins (Woodmansee and Imlay, 2002). The labile iron pool (i.e. protein-bound but readily releasable Fe(II)) in *E. coli* is approximately 100  $\mu\text{M}$  and is largely comprised of iron-sulfur clusters in proteins of several essential cellular pathways (Johnson et al., 2005). Heme-iron and Fe(III) in storage proteins, such as bacterioferritin, are not considered labile under aerobic conditions (Keyser and Imlay, 1997). In agreement with published values (Woodmansee and Imlay, 2002), using EPR to observe Desferal-complexed Fe(III) we found uncomplexed iron concentrations of 20 - 25  $\mu\text{M}$  in intact cells not exposed to mercurials (Fig. 2.3). Cells exposed to the common oxidants, 4 mM  $\text{H}_2\text{O}_2$  or 8 mM tert-butyl hydroperoxide, had 15 - 25% more free iron (non-protein bound Fe(III)) than unexposed cells. Both organomercurials were more effective on a molar basis at releasing iron than were the common oxidants. MT at 25-fold lower concentration released a similar amount of iron as  $\text{H}_2\text{O}_2$ , and PMA at 100-fold lower concentration than  $\text{H}_2\text{O}_2$  nearly doubled the free iron content. Inorganic mercury,  $\text{HgCl}_2$ , increased free iron more dramatically on a molar basis than both the common oxidants and the organomercurials. As little as 16  $\mu\text{M}$   $\text{HgCl}_2$  caused a 120% increase in free iron and 80  $\mu\text{M}$



HgCl<sub>2</sub> caused an average 220% increase in uncomplexed iron, freeing as much as 80% of the estimated labile iron pool (Fig. B.S2). The increase in free iron in the cell could have generated reactive oxygen species via Fenton chemistry, but mercury interference with the OxyBlot assay precluded determination of oxidative damage to proteins via carbonylation (data not shown).

*Mercurials formed stable adducts with cysteines of iron-sulfur centers.*

Using shotgun LC-MS/MS proteomics modified to detect protein-mercury adducts in mercurial-exposed cultures, we observed 78 of *E.coli*'s 214 encoded Fe-binding proteins based on gene ontology in UniProtKB database (Table B.S2) by one or more peptides each (50,870 total spectra) (Table B.S6). We detected cysteine-containing peptides from 46 iron-binding proteins of the 75 that encode at least one cysteine in 4,571 spectra (9% of the total spectra from Fe-proteins). Thirty-four cysteine sites from 20 different Fe-binding proteins (416 spectra total, 9%) were observed with mercury adducts (Tables B.S6 and B.S7). Some Hg-adducts were observed in PMA exposed cultures which likely arose from spontaneous dephenylation of the PhHg adduct in peptides with multiple cysteines, possibly via a mechanism analogous to MerB (Lafrance-Vanasse et al., 2009, Parks et al., 2009).

We operationally defined a cysteine residue that was modifiable by IAM (yielding the carbamidomethyl- or CAM-adduct) in the no-mercury control condition as one that would also be available for modification in mercury-exposure conditions. Indeed, cysteine sites yielding many CAM-adducts in the no-mercury condition were generally seen with PhHg- or Hg-adducts when exposed to mercurials. At Cys positions showing <10 CAM-adduct spectra mercurial adducts were rarely observed. This could arise from unknown intrinsic differences in the detectability of a given peptide by MS when it bears chemically distinct adducts. Thus, this more

fine grained, but still qualitative, analysis was consistent with the above bulk analyses with DTNB and BODIPY-I (Table 2.1 and Figures 2.1 and 2.2), i.e., cysteines modifiable by IAM, were also available for modification by mercurials (Table B.S6).

Eleven of the 20 Fe-binding proteins observed with RHg and/or Hg adducts had a mercury bound to a cysteine site that is directly involved in coordinating non-heme iron or iron present in an Fe-S cluster (Tables 2.2 and B.S7). Nine of these sites are in Fe-S centers or are involved in cluster assembly, two proteins use an iron ion as a cofactor and one protein has not been structurally characterized. Thus, mercurials can displace Fe from many different proteins as also reported for a specific example, the 4Fe-4S dehydratases (Xu and Imlay, 2012). Our LC-MS/MS identification of Hg adducts reveals for the first time that in vivo mercury compounds make stable adducts with the vacated Fe-S center cysteines, potentially impeding the repair of those Fe-S centers. In addition, the chemistry dictates that once mercury is bound to thiols, ( $\log \beta_2 = 40 - 45$  of  $\text{HgL}_2$  thiol complex (Cheesman et al., 1988, Oram et al., 1996, Stricks and Kolthoff, 1953)), this type of modification is not easily repaired and iron ( $\log \beta_2 = 18.8$  of  $\text{Fe}(\text{cys})_2$  (Güzeloğlu et al., 1998)) cannot simply displace the mercury from the thiol. Observable adducts of inorganic Hg(II) appear to be biased toward two-cysteine peptides that offer the stability of chelation. Three such proteins are conserved in higher organisms, IscU and MsrB in mitochondria specifically (see footnote in Table 2.2).

Proteomics data was also searched for other transition metal binding proteins to determine if mercury can target these proteins (Table B.S8). There were few to no mercury adducts to proteins that bind Co (1), Cu (1), Mn (5) or Ni (0) compared to Zn (27 distinct proteins). This is consistent with Zn being a group 12, soft, divalent metal with thiophilic coordination preferences similar to Hg, whereas the others use N, O, or thioether (i.e.

methionine) sulfur ligands as often or more often than thiol sulfur (i.e. cysteine) that Hg prefers. ROS-induced protein modifications were not searched in the proteomics datasets, due to difficulty in distinguishing true *in vivo* induced modifications versus artifacts arising from sample processing without special considerations (McClintock et al., 2013), which was not a research goal of this proteomics project.

#### *Mercurials disturbed the electrolyte balance*

Of nine essential metals examined by ICP-MS in intact cells (Fig. 2.4) only the bulk alkali metal electrolytes,  $\text{Na}^+$  and  $\text{K}^+$ , changed significantly after exposure to mercurials. In cultures exposed to 80  $\mu\text{M}$   $\text{HgCl}_2$ , the  $\text{K}^+$  content decreased 62% and the  $\text{Na}^+$  content increased 200% relative to unexposed cells. Similar changes were observed in cultures exposed to 40  $\mu\text{M}$  PMA, 16  $\mu\text{M}$   $\text{HgCl}_2$  and 160  $\mu\text{M}$  MT (Fig. 2.4) but with lower magnitude. These  $\text{K}^+$  and  $\text{Na}^+$  changes are consistent with mercurial disruption of thiol homeostasis and consequent  $\text{K}^+$  efflux by the GSH-responsive  $\text{K}^+/\text{H}^+$  antiporter KefC (Roosild et al., 2010), resulting in lower intracellular pH (Ferguson, 1999). The increase in  $\text{Na}^+$  could be a consequence of  $\text{Na}^+$  uptake by the NhaA ( $\text{Na}^+/\text{H}^+$  antiporter) in response to the low intracellular pH provoked by KefC importing  $\text{H}^+$  as it ejects  $\text{K}^+$  (Hunte et al., 2005, Padan, 2011, Taglicht et al., 1991).

Interestingly, although EPR (Fig. 2.3) showed a large increase in uncomplexed iron on exposure to 16 or 80  $\mu\text{M}$   $\text{HgCl}_2$ , total cellular iron content did not change significantly, indicating little or none of the free Fe was lost from the cells. Thus, the putative defensive ferrous ion efflux activity of cation diffusion facilitator FieF (Grass et al., 2005) may be non-functional under acute mercurial exposure, nor were other Fe homeostasis functions including down-regulation of iron uptake (Zheng et al., 1999) and induction of Fe(III) storage proteins (Grass et al., 2005). Transporters for the other metal cations are energy-dependent (Nies, 2003),

so their efflux may have been prevented by immediate inhibition of these processes by the mercurials. No other metals experienced statistically significant changes in intracellular concentration from the unexposed or exposures under experimental conditions used.

*Cells bound mercury compounds in large excess over their total available thiol ligands.*

*Bulk cellular binding of mercury compounds after 30 min exposure.*

The total thiol content of washed cells not exposed to mercurials averaged  $3.59 \times 10^6$  molecules/cell (approximately 9-10 mM, assuming a cytosolic volume of  $6.7 \times 10^{-16}$  L/cell (Cayley and Record, 2003)) (Table 2.1). Experimental conditions used to measure cell-bound metals normally assume both uptake and efflux and therefore derive equilibrium values. However, the nearly covalent nature of Hg-S bonds, especially in bis-coordinated complexes, renders them essentially irreversible, unlike less thiophilic transition metals. Likely owing to slow uptake even at 160  $\mu$ M in the media, the large, monovalent anionic MT bound only 70% of available thiols. However, both PMA and inorganic Hg were stably bound in considerable excess over the total cellular thiol content at much lower exposure concentrations. Cells exposed to just 40  $\mu$ M of the smaller aromatic, monovalent PMA bound almost 1.5-fold more of it than the measured thiol groups available. Even cells exposed to 16  $\mu$ M inorganic  $\text{HgCl}_2$  bound a 1.23:1 molar excess of it over measureable thiols; since Hg is bivalent, these cells accumulated 2.46-fold more Hg than needed to occupy all of their available thiols. At 80  $\mu$ M  $\text{HgCl}_2$  the cells bound a 3.4:1 molar excess of Hg to measured thiols, or 6.8-fold more Hg than needed to saturate all cellular thiols. Thus, even when normal metal uptake systems are likely shut down by the toxic metal, a variety of cellular ligands competed well with weaker ligands in the medium for the two neutral, membrane-permeant compounds,  $\text{HgCl}_2$  and phenylmercury (probably as the chloride

given the medium composition). Intrigued by these findings, we used x-ray absorption fine structure (EXAFS) spectroscopy to learn what additional ligands mercury was taking in *E. coli* cells.

*Excess cell-bound mercury takes nitrogen and/or oxygen ligands in addition to sulfur.*

EXAFS reports the type, number, and distance of elements coordinated to a specific metallic element (Scott, 2000). We exposed actively growing cells for 30 min to a range of  $\text{HgCl}_2$  concentrations from under-saturation to over-saturation of cellular thiols to discern novel ligands arising as Hg binding sites exceeded the cellular thiol pool (Fig. 2.5 and Table B.S9 for fit details). Cells exposed to 10 or 20  $\mu\text{M}$   $\text{HgCl}_2$  fit best to a model of two sulfur ligands at 2.34 Å radius, as expected based on Hg/thiol ratios observed in Table 2.1. At higher  $\text{HgCl}_2$  concentrations, that exceeded the cellular thiol pool, EXAFS heterogeneity increased indicating Hg coordination to other ligands near 2.0 Å, consistent with nitrogen, oxygen, or carbon (low mass elements not distinguishable by EXAFS). Nonetheless, Hg:S coordination remained dominant and was distinguishable from chloride by spectral near edge features (Fig. 2.5A and mercurial complexes with model sulfur (glutathione, Fig. B.S3B and B.S3D and B.S4), oxygen (acetate, Fig. B.S4), or nitrogen (imidazole, Fig. B.S5) compounds). At 40 or 80  $\mu\text{M}$   $\text{HgCl}_2$  exposure, the shorter and broader Fourier transform peaks yielded mixed, non-integral fits (Fig. 2.5D). Although oxygen and carbon gave similar first shell fits to those for nitrogen (data not shown), nitrogen is softer than oxygen and is the more likely biological ligand given mercury's known preferences for bis-coordination with the imino nitrogens of nucleotide bases (Miyake et al., 2006, Tanaka et al., 2007) and histidine (Brooks and Davidson, 1960). A Hg-C signal could have arisen from oxymercuration of unsaturated lipids but this remote possibility was ruled out

by ICP-MS quantification of Hg in cellular fractions prepared by a standard lipid extraction (Bligh and Dyer, 1959)(data not shown).

Cells exposed to 40  $\mu$ M PMA best fit a one carbon (2.05 Å) and one sulfur (2.32 Å) structure, reflecting the carbon of the phenyl group and a sulfur of a cellular thiol group (Fig. B.S6). Although cells exposed to 40 or 80  $\mu$ M PMA bound an almost 1.5-fold molar excess of PhHg (Table 2.1), its native oxygen from acetate and carbon ligand to phenyl group precluded resolution of cellular C, O, or N ligands by EXAFS, but cellular thiol ligands were distinguishable by EXAFS as replacing the phenylmercury's acetate oxygen ligand (Fig. B.S6C). In contrast, cells exposed to 160  $\mu$ M MT fit only to one carbon (2.10 Å) and one sulfur (2.36) Å each, reflecting the ethyl group carbon and sulfur either from MT's thiosalicylate moiety or from the cellular thiol pool (Fig. B.S7). Note that HgCl<sub>2</sub> and PMA reacted with the model compound imidazole to form a Hg-N bond (Fig. B.S5) but no Hg-N bond was observed when merthiolate was mixed with imidazole, indicating that the thiol of merthiolate was not displaced by imidazole. The N3 imino nitrogen of imidazole is not sufficiently nucleophilic to displace the strong S ligand of thiosalicylate and the covalent C-Hg bond of ethylmercury is not exchangeable.

## DISCUSSION

Knowing how mercury compounds differ in their basic biochemical interactions *in vivo* is fundamental to understanding the damage they do to cells, how cells recover – or not – from that damage, and what interventions can prevent or minimize the damage and accelerate recovery. This study is the first to compare the effects of inorganic and organic mercury compounds at the biochemical, physiological, and proteomic levels in any model organism.

### *Relevance to environmental exposures.*

The work described here is part of a larger proteomics study carried out in a multi-user, production-scale, high-throughput proteomics facility and for safety reasons we used two common antiseptics, PMA and merthiolate (MT), as surrogates for the often mentioned neurotoxin, methylmercury, although PMA and MT are also of public health interest in their own right. Inorganic mercury concentrations employed here were within the range that bacteria would experience in the GI tract after installation or removal of dental amalgam fillings (Summers et al., 1993) and in highly contaminated environments, such as mercury mines (Malm, 1998). Natural bacterial exposures to the organomercurials are more difficult to estimate. Methylmercury was long used as a seed grain fungicide and phenylmercury and merthiolate were previously used in contact lens cleaning solutions (Rietschel and Wilson, 1982, Tosti and Tosti, 1988) and vaginal douches (Freed, 1948) and the latter was also used for minor skin wounds and as a surgical scrub (Weed, 1931) but there are no data on the resulting ambient concentrations. The use of thimerosal (the same as MT) in vaccines was questioned in 2001 (Ball et al., 2001) and it has gradually been removed from pediatric vaccines administered in the United States, but is still included in pediatric vaccines administered in developing countries and in adult vaccines worldwide (WHO, 2002).

### *Effects of mercury compounds on bulk properties of the cell*

#### *Blocking total and bulk protein thiols.*

In brief exposures, the relative effectiveness of each compound for blocking cellular thiols on a per mole basis was  $\text{HgCl}_2 > \text{PMA} > \text{MT}$  (Table 2.1, Fig. 2.1 and 2.2). Monovalent PMA was roughly half as effective, short term, as bivalent Hg(II) in blocking bulk cellular or

protein thiols, suggesting that, on short exposure, the relative efficiency of thiol blockage simply reflects the valence of the mercurial. Uptake and accumulation of mercury was aided by the fact that cells were grown in a defined minimal medium. The shaking required for aerobic growth ensured distribution of mercury throughout the culture and the growth medium contains no strong competitive ligands for mercury compounds, apart from chloride, so the cells become a thermodynamic sink for mercury binding due to their abundance of suitable intracellular ligands. Neutral  $\text{HgCl}_2$  (Gutknecht, 1981) and PMA, which is likely phenylmercuric chloride due to the high concentration of chloride in the medium (approximately 55 mM), were likely taken up with similar efficiency by passive diffusion (Barkay et al., 1997). In contrast, despite its generally hydrophobic character, the predominantly negatively charged carboxylate group of merthiolate ( $\text{pK}_a \sim 4.2$ ) under the conditions of these studies (pH 7.4) (Fig. B.S1) is expected to slow its entry into the cell. In longer term exposure (Fig. 2.1) thiol blockage by all three compounds is nearly identical, although some of this may result from mercurial-provoked ROS.

*E. coli* exports glutathione which reaches micromolar concentrations in the periplasm (Owens and Hartman, 1986) where it may function in disulfide bond formation (Eser et al., 2009). However, *E. coli* does not readily take up mercury bound to glutathione (Ndu et al., 2012, Owens and Hartman, 1986) and although cysteine may increase bioavailability of inorganic mercury, it has little effect on organomercurial uptake (Barkay et al., 1997, Ndu et al., 2012), likely because in aerobic culture extracellular thiols will be oxidized to disulfides. Our finding that cells accumulate inorganic mercury and phenylmercury in excess of measured available thiols suggests passive diffusion driven first by intracellular thiols and then by intracellular non-thiol ligands is more probable than active uptake of mercury in MG1655 which does not carry a typically plasmid-borne mercury resistance (*mer*) locus (Barkay et al., 2003). In addition, this



quantitative measurement of accumulation reveals that inorganic mercury continues to accumulate as the concentration increases, while PMA appears to plateau at less than 2 fold excess and much higher concentrations of merthiolate do not saturate the cellular thiol pool within the same exposure time.

Once mercurials enter the cytoplasm 5-10 mM glutathione will readily displace ( $\log K_{\text{form}} = 35 - 40$ ) the weakly associated chloride or acetate counterions and even thiosalicylate, which has a less basic and, thus, lower affinity thiolate (Mah and Jalilehvand, 2008, Ravichandran, 2004). The resulting derivatives of Hg(II), phenylmercury and ethylmercury can readily swap their glutathione ligands (Cheesman et al., 1988) for protein cysteine thiols. Organisms have evolved pathways to repair damage to oxidized protein thiols (Imlay, 2013), but mercury bound to a protein cysteine can only be rapidly and effectively removed by the proteins of the *mer* operon (Barkay et al., 2003, Ledwidge et al., 2005), a defense only available in prokaryotes that have acquired the *mer* locus through horizontal gene transfer.

#### *Releasing protein-bound iron.*

Mercury's high affinity for thiol ligands presents a challenge to enzymes that use iron-sulfur clusters (Jung et al., 1995, Keyer and Imlay, 1997). *E. coli*'s labile iron pool is approximately 100  $\mu\text{M}$  (Keyer and Imlay, 1997) and exposure to  $\text{HgCl}_2$  at a 3.5-fold molar excess over cellular thiols can release as much as 80% of the labile iron pool to the free state. Our EPR data for free iron in the unexposed control culture (Fig. 2.3) were within range of other published data from *E. coli* grown in other minimal media (Finney and O'Halloran, 2003, Woodmansee and Imlay, 2002) and were very reproducible.

Exposure to organic oxidizing compounds only resulted in marginal increases in free iron, indicating that cellular pathways that provide protection and repair from ROS are relatively effective at combating exposure to these chemicals. Merthiolate exposure resulted in a small but not significant increase in free iron. PMA's effectiveness in blocking thiols was reflected in still greater release of free iron, however, inorganic Hg(II) was most effective in releasing Fe. It is important to note that 16  $\mu\text{M}$  inorganic  $\text{HgCl}_2$  resulted in a greater increase in free iron, relative to 40  $\mu\text{M}$  PMA, even though Table 2.1 shows that more mercury was present in the cell in the PMA exposure, and this difference shows that the degree of damage induced is not that same for both inorganic and organic mercury, i.e. they are qualitatively different in their in vivo biochemical effects. Similar ligand preferences of mercury and ferrous iron likely increase mercury's effectiveness in disrupting labile iron centers. Inorganic mercury was only observed in peptides with multiple proximal cysteines (Table B.S7), a motif common among Fe-S cluster proteins (Roche et al., 2013). In addition to direct damage caused by mercury binding, disruption of iron homeostasis can lead to oxidative stress, resulting in further damage to proteins and DNA by ROS (Imlay, 2013).

#### *Disrupting electrolyte balance.*

Mercury also disrupted the cellular electrolyte balance likely via the KefC antiporter, which is inactive when bound to reduced glutathione. Glutathione-S-conjugates induce a conformational change in KefC that activates efflux of  $\text{K}^+$  (Roosild et al., 2010). Bis-coordination of GSH by Hg will deplete the free GSH pool and our results are the first to suggest that mercurials can activate KefC. The resulting rapid efflux of  $\text{K}^+$  ions and concomitant import of  $\text{H}^+$  ions by KefC is believed to protect the cell (Ferguson, 1999) by decreasing the cellular pH,

so as to protonate potential binding sites for electrophiles. The increase in Na<sup>+</sup> content may result from activation of sodium uptake by NhaA (a Na<sup>+</sup>/H<sup>+</sup> antiporter) under low intracellular pH conditions leading to restoration of the electrolyte balance (Hunte et al., 2005, Padan, 2011, Taglicht et al., 1991).

### *Effects of mercury compounds on specific proteins*

Given our observation of Hg-provoked intracellular Fe(III) release, we examined closely the effects of mercurial exposure on the subset of Fe-binding proteins observed in our larger proteomics study. Proteomics analysis detected 20 Fe-binding proteins modified by mercury (Table B.S7) and in many cases the mercury-binding site was a cysteine residue that coordinates an Fe-S cluster and would not be easily repaired without the proteins of the *mer* operon (Hong et al., 2010, Ledwidge et al., 2005). The mercury vulnerable iron-binding proteins we observed play critical roles ranging from Fe-S cluster assembly (IscA & IscU), to redox defense (Fdx, MsrB, SodB, YggX) and amino-acid biosynthesis (GltB & GltD).

Mercurials also formed adducts with proteins that bind other transition metals, primarily zinc (Table B.S8), which like mercury is group 12, soft, divalent metal. However, since Zn is spectroscopically silent and Zn fluorescent probes do not penetrate bacterial cells, we could not assess how much Zn was freed from its natural protein sites by exposure to mercurials. Notably, ribosomal protein L31 which is implicated in Zn storage (Gabriel and Helmann, 2009), was observed with mercurial adducts.

## CONCLUSIONS

Inorganic mercury in short term assays is more effective at blocking total and protein thiols than PMA, and both compounds are more effective in such blockage than merthiolate, likely due to its inefficient uptake. All three mercurials disturb the electrolyte balance, but none of them provokes bulk loss of the alkaline earth metal, Mg, nor of 6 essential transition metals. When Hg(II) exceeds the available cellular thiol pool, non-thiol cellular targets, such as nitrogen ligands in nucleotide bases and protein histidine and amine groups form complexes with it, but this is not seen with PMA. Characteristically cysteine-rich, Fe-binding and Zn-binding proteins formed mass spectrometry stable adducts with organic and inorganic mercurials. Although each mercurial caused similar thiol blockage in 30 minute exposures, inorganic Hg(II) was strikingly more effective in freeing protein-bound iron and bound most stably to peptides capable of chelating it with two or more cysteines. Thus, there are both quantitative and qualitative differences in the biochemical effects of these mercurials in living cells. Our novel findings on cellular Hg(II) biochemistry emphasize that the inorganic forms, Hg(II) and Hg(0) from which it is derived, can damage cells as effectively as the organomercurials, which are commonly referred to by non-specialists as the most toxic forms of Hg. These are the first in vivo observations in a well-defined model organism of the biochemical differences of inorganic and organic mercury exposure that contribute to their distinct toxicological profiles in bacteria and likely also higher organisms. It is also the first to assess the use of mass spectrometry proteomics for qualitative measurement of stable protein-mercurial adducts.

## **ACKNOWLEDGMENTS**

We thank Mary Lipton, Erika Zink and Samuel Purvine (all of the DOE Pacific Northwest National Laboratory) for chemical and biophysical acquisition and SEQUEST analysis of the proteomic data, Tejas Chaudhari and Sagar Tarkhadkar (Department of Computer Sciences, Univ. of Georgia) for assistance with database development and management, and Graham George (University of Saskatchewan and the Canadian Light Source) for mercuric bromide EXAFS data collection. This work was supported by DOE awards ER64408 and ER65286 to AOS and ER64409 and ER65195 to SMM and NIH award GM62524 to MKJ.

## REFERENCES

- ANDREINI, C., BERTINI, I., CAVALLARO, G., HOLLIDAY, G. L. & THORNTON, J. M. 2008. Metal ions in biological catalysis: from enzyme databases to general principles. *J Biol Inorg Chem*, 13, 1205-18.
- ANKUDINOV, A. L., BOULDIN, C. E., REHR, J. J., SIMS, J. & HUNG, H. 2002. Parallel calculation of electron multiple scattering using Lanczos algorithms. *Physical Review B*, 65.
- BAKIR, F., DAMLUJI, S. F., AMIN-ZAKI, L., MURTADHA, M., KHALIDI, A., AL-RAWI, N. Y., TIKRITI, S., DAHAHIR, H. I., CLARKSON, T. W., SMITH, J. C. & DOHERTY, R. A. 1973. Methylmercury poisoning in Iraq. *Science*, 181, 230-41.
- BALL, L. K., BALL, R. & PRATT, R. D. 2001. An assessment of thimerosal use in childhood vaccines. *Pediatrics*, 107, 1147-54.
- BARKAY, T., GILLMAN, M. & TURNER, R. R. 1997. Effects of dissolved organic carbon and salinity on bioavailability of mercury. *Appl Environ Microbiol*, 63, 4267-71.
- BARKAY, T., MILLER, S. M. & SUMMERS, A. O. 2003. Bacterial mercury resistance from atoms to ecosystems. *FEMS Microbiol Rev*, 27, 355-84.
- BASINGER, M. A., CASAS, J., JONES, M. M., WEAVER, A. D. & WEINSTEIN, N. H. 1981. Structural requirements for Hg (II) antidotes. *Journal of Inorganic and Nuclear Chemistry*, 43, 1419-1425.
- BLIGH, E. G. & DYER, W. J. 1959. A rapid method of total lipid extraction and purification. *Can J Biochem Physiol*, 37, 911-7.
- BOJA, E. S. & FALES, H. M. 2001. Overalkylation of a protein digest with iodoacetamide. *Anal Chem*, 73, 3576-82.
- BRADFORD, M. M. 1976. A rapid and sensitive method for the quantitation of microgram quantities of protein utilizing the principle of protein-dye binding. *Anal Biochem*, 72, 248-54.
- BROOKS, P. & DAVIDSON, N. 1960. Mercury(II) Complexes of Imidazole and Histidine. *Journal of the American Chemical Society*, 82, 2118-2123.
- CARVALHO, C. M., CHEW, E. H., HASHEMY, S. I., LU, J. & HOLMGREN, A. 2008. Inhibition of the human thioredoxin system. A molecular mechanism of mercury toxicity. *J Biol Chem*, 283, 11913-23.
- CAYLEY, S. & RECORD, M. T., JR. 2003. Roles of cytoplasmic osmolytes, water, and crowding in the response of *Escherichia coli* to osmotic stress: biophysical basis of osmoprotection by glycine betaine. *Biochemistry*, 42, 12596-609.

- CHEESMAN, B. V., ARNOLD, A. P. & RABENSTEIN, D. L. 1988. Nuclear magnetic resonance studies of the solution chemistry of metal complexes. 25. Hg(thiol)<sub>3</sub> complexes and HG(II)-thiol ligand exchange kinetics. *J. Am. Chem. Soc.*, 110, 6359-6364.
- CLARKSON, T. W. & MAGOS, L. 2006. The toxicology of mercury and its chemical compounds. *Crit Rev Toxicol*, 36, 609-62.
- COSPER, N. J., STALHANDSKE, C. M., SAARI, R. E., HAUSINGER, R. P. & SCOTT, R. A. 1999. X-ray absorption spectroscopic analysis of Fe(II) and Cu(II) forms of a herbicide-degrading alpha-ketoglutarate dioxygenase. *J Biol Inorg Chem*, 4, 122-9.
- COTNER, R. C. & CLAGETT, C. O. 1973. O-carboxamidomethyl tyrosine as a reaction product of the alkylation of proteins with iodoacetamide. *Anal Biochem*, 54, 170-7.
- CRINNION, W. J. 2000. Environmental medicine, part three: long-term effects of chronic low-dose mercury exposure. *Altern Med Rev*, 5, 209-23.
- CVETKOVIC, A., MENON, A. L., THORGERSEN, M. P., SCOTT, J. W., POOLE, F. L. II, JENNEY, F. E. JR, LANCASTER, W. A., PRAISSMAN, J. L., SHANMUKH, S., VACCARO, B. J., TRAUGER, S. A., KALISIAK, E., APON, J. V., SIUZDAK, G., YANNONE, S. M., TAINER, J. A. & ADAMS, M. W. 2010. Microbial metalloproteomes are largely uncharacterized. *Nature*, 466, 779-82.
- DAVIDSON, P. W., MYERS, G. J. & WEISS, B. 2004. Mercury exposure and child development outcomes. *Pediatrics*, 113, 1023-9.
- ELLMAN, G. L. 1959. Tissue sulfhydryl groups. *Arch Biochem Biophys*, 82, 70-7.
- ERCAL, N., GURER-ORHAN, H. & AYKIN-BURNS, N. 2001. Toxic metals and oxidative stress part I: mechanisms involved in metal-induced oxidative damage. *Curr Top Med Chem*, 1, 529-39.
- ESER, M., MASIP, L., KADOKURA, H., GEORGIOU, G. & BECKWITH, J. 2009. Disulfide bond formation by exported glutaredoxin indicates glutathione's presence in the E. coli periplasm. *Proc Natl Acad Sci U S A*, 106, 1572-7.
- FERGUSON, G. P. 1999. Protective mechanisms against toxic electrophiles in Escherischia coli. *Trends Microbiol*, 7, 242-7.
- FINNEY, L. A. & O'HALLORAN, T. V. 2003. Transition metal speciation in the cell: insights from the chemistry of metal ion receptors. *Science*, 300, 931-6.
- FREED, L. F. 1948. Trichomoniasis, the seventh venereal disease. *S Afr Med J*, 22, 223-9.
- FRUCHTER, R. G. & CRESTFIELD, A. M. 1967. The specific alkylation by iodoacetamide of histidine-12 in the active site of ribonuclease. *J Biol Chem*, 242, 5807-12.

GABRIEL, S. E. & HELMANN, J. D. 2009. Contributions of Zur-controlled ribosomal proteins to growth under zinc starvation conditions. *J Bacteriol*, 191, 6116-22.

GEORGE, G. N., GARRETT, R. M., PRINCE, R. C. & RAJAGOPALAN, K. V. 1996. The molybdenum site of sulfite oxidase: A comparison of wild-type and the cysteine 207 to serine mutant using X-ray absorption spectroscopy. *Journal of the American Chemical Society*, 118, 8588-8592.

GLADYSHEV, V. N. & KRYUKOV, G. V. 2001. Evolution of selenocysteine-containing proteins: significance of identification and functional characterization of selenoproteins. *Biofactors*, 14, 87-92.

GRASS, G., OTTO, M., FRICKE, B., HANEY, C. J., RENSING, C., NIES, D. H. & MUNKELT, D. 2005. FieF (YiiP) from *Escherichia coli* mediates decreased cellular accumulation of iron and relieves iron stress. *Arch Microbiol*, 183, 9-18.

GUTKNECHT, J. 1981. Inorganic Mercury (Hg<sup>2+</sup>) Transport through Lipid Bilayer Membranes. *J. Membrane Biol.*, 61, 61-66.

GÜZELOĞLU, Ş., YALÇIN, G. & PEKIN, M. 1998. The determination of stability constants of N-acetyl-L-cysteine chrome, nickel, cobalt and iron complexes by potentiometric method. *Journal of Organometallic Chemistry*, 568, 143-147.

HELBIG, K., BLEUEL, C., KRAUSS, G. J. & NIES, D. H. 2008. Glutathione and transition-metal homeostasis in *Escherichia coli*. *J Bacteriol*, 190, 5431-8.

HONG, B., NAUSS, R., HARWOOD, I. M. & MILLER, S. M. 2010. Direct measurement of mercury(II) removal from organomercurial lyase (MerB) by tryptophan fluorescence: NmerA domain of coevolved gamma-proteobacterial mercuric ion reductase (MerA) is more efficient than MerA catalytic core or glutathione. *Biochemistry*, 49, 8187-96.

HUNTE, C., SCREPANTI, E., VENTURI, M., RIMON, A., PADAN, E. & MICHEL, H. 2005. Structure of a Na<sup>+</sup>/H<sup>+</sup> antiporter and insights into mechanism of action and regulation by pH. *Nature*, 435, 1197-202.

HUNTLEY, R. P., SAWFORD, T., MUTOWO-MEULLENET, P., SHYPITSYNA, A., BONILLA, C., MARTIN, M. J. & O'DONOVAN, C. 2015. The GOA database: gene Ontology annotation updates for 2015. *Nucleic Acids Res*, 43, D1057-63.

IMESCH, E., MOOSMAYER, M. & ANNER, B. M. 1992. Mercury weakens membrane anchoring of Na-K-ATPase. *Am J Physiol*, 262, F837-42.

IMLAY, J. A. 2013. The molecular mechanisms and physiological consequences of oxidative stress: lessons from a model bacterium. *Nat Rev Microbiol*, 11, 443-54.



- JOHNSON, D. C., DEAN, D. R., SMITH, A. D. & JOHNSON, M. K. 2005. Structure, function, and formation of biological iron-sulfur clusters. *Annu Rev Biochem*, 74, 247-81.
- JUNG, Y. S., YU, L. & GOLBECK, J. H. 1995. Reconstitution of iron-sulfur center FB results in complete restoration of NADP (+) photoreduction in Hg-treated Photosystem I complexes from *Synechococcus* sp. PCC 6301. *Photosynth Res*, 46, 249-55.
- KELLER, A., NESVIZHSKII, A. I., KOLKER, E. & AEBERSOLD, R. 2002. Empirical statistical model to estimate the accuracy of peptide identifications made by MS/MS and database search. *Anal Chem*, 74, 5383-92.
- KEYER, K. & IMLAY, J. A. 1997. Inactivation of dehydratase [4Fe-4S] clusters and disruption of iron homeostasis upon cell exposure to peroxynitrite. *J Biol Chem*, 272, 27652-9.
- KHAN, M. A. & WANG, F. 2009. Mercury-selenium compounds and their toxicological significance: toward a molecular understanding of the mercury-selenium antagonism. *Environ Toxicol Chem*, 28, 1567-77.
- KHOKHLOVA, A., CHERNIKOVA, G. & SHISHIN, L. 1982. COMPLEX-FORMATION OF MERCURY (II) IONS WITH ANIONS OF SOME MONOCARBOXYLIC ACIDS. INST OBS NEORG KHMII IM NS KURNAKOVA LENINSKI PROSPEKT 31, 71 MOSCOW, RUSSIA.
- KIM, S., GUPTA, N. & PEVZNER, P. A. 2008. Spectral probabilities and generating functions of tandem mass spectra: a strike against decoy databases. *J Proteome Res*, 7, 3354-63.
- LAFRANCE-VANASSE, J., LEFEBVRE, M., DI LELLO, P., SYGUSCH, J. & OMICHINSKI, J. G. 2009. Crystal structures of the organomercurial lyase MerB in its free and mercury-bound forms: insights into the mechanism of methylmercury degradation. *J Biol Chem*, 284, 938-44.
- LEDWIDGE, R., PATEL, B., DONG, A., FIEDLER, D., FALKOWSKI, M., ZELIKOVA, J., SUMMERS, A. O., PAI, E. F. & MILLER, S. M. 2005. NmerA, the metal binding domain of mercuric ion reductase, removes Hg<sup>2+</sup> from proteins, delivers it to the catalytic core, and protects cells under glutathione-depleted conditions. *Biochemistry*, 44, 11402-16.
- MAH, V. & JALILEHVAND, F. 2008. Mercury(II) complex formation with glutathione in alkaline aqueous solution. *J Biol Inorg Chem*, 13, 541-53.
- MALM, O. 1998. Gold mining as a source of mercury exposure in the Brazilian Amazon. *Environ Res*, 77, 73-8.
- MASON, R. P., FITZGERALD, W. F. & MOREL, F. M. M. 1994. The Biogeochemical Cycling of Elemental Mercury - Anthropogenic Influences. *Geochimica Et Cosmochimica Acta*, 58, 3191-3198.

- MCCLINTOCK, C. S., PARKS, J. M., BERN, M., GHATTYVENKATAKRISHNA, P. K. & HETTICH, R. L. 2013. Comparative informatics analysis to evaluate site-specific protein oxidation in multidimensional LC-MS/MS data. *J Proteome Res*, 12, 3307-16.
- MISETA, A. & CSUTORA, P. 2000. Relationship between the occurrence of cysteine in proteins and the complexity of organisms. *Mol Biol Evol*, 17, 1232-9.
- MIYAKE, Y., TOGASHI, H., TASHIRO, M., YAMAGUCHI, H., ODA, S., KUDO, M., TANAKA, Y., KONDO, Y., SAWA, R., FUJIMOTO, T., MACHINAMI, T. & ONO, A. 2006. MercuryII-mediated formation of thymine-HgII-thymine base pairs in DNA duplexes. *J Am Chem Soc*, 128, 2172-3.
- MUSTRE DE LEON, J., REHR, J. J., ZABINSKY, S. I. & ALBERS, R. C. 1991. Ab initio curved-wave x-ray-absorption fine structure. *Phys Rev B Condens Matter*, 44, 4146-4156.
- NDU, U., MASON, R. P., ZHANG, H., LIN, S. & VISSCHER, P. T. 2012. Effect of inorganic and organic ligands on the bioavailability of methylmercury as determined by using a mer-lux bioreporter. *Appl Environ Microbiol*, 78, 7276-82.
- NEIDHARDT, F. C., BLOCH, P. L. & SMITH, D. F. 1974. Culture medium for enterobacteria. *J Bacteriol*, 119, 736-47.
- NIES, D. H. 2003. Efflux-mediated heavy metal resistance in prokaryotes. *FEMS Microbiol Rev*, 27, 313-39.
- NORN, S., PERMIN, H., KRUSE, E. & KRUSE, P. R. 2008. [Mercury--a major agent in the history of medicine and alchemy]. *Dan Medicinhist Arbog*, 36, 21-40.
- O'CONNOR, T. R., GRAVES, R. J., DE MURCIA, G., CASTAING, B. & LAVAL, J. 1993. Fpg protein of Escherichia coli is a zinc finger protein whose cysteine residues have a structural and/or functional role. *J Biol Chem*, 268, 9063-70.
- ORAM, P. D., FANG, X., FERNANDO, Q., LETKEMAN, P. & LETKEMAN, D. 1996. The formation of constants of mercury(II)--glutathione complexes. *Chem Res Toxicol*, 9, 709-12.
- OWENS, R. A. & HARTMAN, P. E. 1986. Export of glutathione by some widely used Salmonella typhimurium and Escherichia coli strains. *J Bacteriol*, 168, 109-14.
- PADAN, E. 2011. Regulation of NhaA by protons. *Compr Physiol*, 1, 1711-9.
- PARKS, J. M., GUO, H., MOMANY, C., LIANG, L., MILLER, S. M., SUMMERS, A. O. & SMITH, J. C. 2009. Mechanism of Hg-C protonolysis in the organomercurial lyase MerB. *J Am Chem Soc*, 131, 13278-85.

POLACCO, B. J., PURVINE, S. O., ZINK, E. M., LAVOIE, S. P., LIPTON, M. S., SUMMERS, A. O. & MILLER, S. M. 2011. Discovering mercury protein modifications in whole proteomes using natural isotope distributions observed in liquid chromatography-tandem mass spectrometry. *Mol Cell Proteomics*, 10, M110 004853.

POWELL, K. J., BROWN, P. L., BYRNE, R. H., GAJDA, T., HEFTER, G., SJOBERG, S. & WANNER, H. 2005. CHEMICAL SPECIATION OF ENVIRONMENTALLY SIGNIFICANT HEAVY METALS WITH INORGANIC LIGANDS Part 1. *IUPAC, Pure Appl. Chem.*, 77, 739-800.

RAVICHANDRAN, M. 2004. Interactions between mercury and dissolved organic matter--a review. *Chemosphere*, 55, 319-31.

RICHARDSON, G. M., WILSON, R., ALLARD, D., PURTILL, C., DOUMA, S. & GRAVIERE, J. 2011. Mercury exposure and risks from dental amalgam in the US population, post-2000. *Sci Total Environ*, 409, 4257-68.

RIETSCHEL, R. L. & WILSON, L. A. 1982. Ocular inflammation in patients using soft contact lenses. *Arch Dermatol*, 118, 147-9.

ROCHE, B., AUSSEL, L., EZRATY, B., MANDIN, P., PY, B. & BARRAS, F. 2013. Iron/sulfur proteins biogenesis in prokaryotes: formation, regulation and diversity. *Biochim Biophys Acta*, 1827, 455-69.

ROOSILD, T. P., CASTRONOVO, S., HEALY, J., MILLER, S., PLIOTAS, C., RASMUSSEN, T., BARTLETT, W., CONWAY, S. J. & BOOTH, I. R. 2010. Mechanism of ligand-gated potassium efflux in bacterial pathogens. *Proc Natl Acad Sci U S A*, 107, 19784-9.

SCHAFER, F. Q. & BUETTNER, G. R. 2001. Redox environment of the cell as viewed through the redox state of the glutathione disulfide/glutathione couple. *Free Radic Biol Med*, 30, 1191-212.

SCOTT, R. A. 2000. X-ray absorption spectroscopy. *Physical Methods in Bioinorganic Chemistry – Spectroscopy and Magnetism.*: University Science Books.

SOSKINE, M., STEINER-MORDOCH, S. & SCHULDINER, S. 2002. Crosslinking of membrane-embedded cysteines reveals contact points in the EmrE oligomer. *Proc Natl Acad Sci U S A*, 99, 12043-8.

STRICKS, W. & KOLTHOFF, I. M. 1953. Reactions between Mercuric Mercury and Cysteine and Glutathione. Apparent Dissociation Constants, Heats and Entropies of Formation of Various Forms of Mercuric Mercapto-Cysteine and -Glutathione. *Journal of the American Chemical Society*, 75, 5673-5681.

- SUMMERS, A. O., WIREMAN, J., VIMY, M. J., LORSCHIEDER, F. L., MARSHALL, B., LEVY, S. B., BENNETT, S. & BILLARD, L. 1993. Mercury released from dental "silver" fillings provokes an increase in mercury- and antibiotic-resistant bacteria in oral and intestinal floras of primates. *Antimicrob Agents Chemother*, 37, 825-34.
- TAGLICHT, D., PADAN, E. & SCHULDINER, S. 1991. Overproduction and purification of a functional Na<sup>+</sup>/H<sup>+</sup> antiporter coded by nhaA (ant) from Escherichia coli. *J Biol Chem*, 266, 11289-94.
- TANAKA, Y., ODA, S., YAMAGUCHI, H., KONDO, Y., KOJIMA, C. & ONO, A. 2007. 15N-15N J-coupling across Hg(II): direct observation of Hg(II)-mediated T-T base pairs in a DNA duplex. *J Am Chem Soc*, 129, 244-5.
- TOSTI, A. & TOSTI, G. 1988. Thimerosal: a hidden allergen in ophthalmology. *Contact Dermatitis*, 18, 268-73.
- TYAGARAJAN, K., PRETZER, E. & WIKTOROWICZ, J. E. 2003. Thiol-reactive dyes for fluorescence labeling of proteomic samples. *Electrophoresis*, 24, 2348-58.
- VALKO, M., MORRIS, H. & CRONIN, M. T. 2005. Metals, toxicity and oxidative stress. *Curr Med Chem*, 12, 1161-208.
- WALDRON, K. J., RUTHERFORD, J. C., FORD, D. & ROBINSON, N. J. 2009. Metalloproteins and metal sensing. *Nature*, 460, 823-30.
- WEED, L. E., E.E. 1931. The Utility of Phenyl-Mercury-Nitrate as a Disinfectant. *The Journal of Infectious Diseases*, 49, 440-449.
- WHO 2002. Recommendations from the Strategic Advisory Group of Experts. *Weekly Epidemiol. Rec.*, 77, 305-316.
- WOODMANSEE, A. N. & IMLAY, J. A. 2002. Quantitation of intracellular free iron by electron paramagnetic resonance spectroscopy. *Methods Enzymol*, 349, 3-9.
- XU, F. F. & IMLAY, J. A. 2012. Silver(I), mercury(II), cadmium(II), and zinc(II) target exposed enzymic iron-sulfur clusters when they toxify Escherichia coli. *Appl Environ Microbiol*, 78, 3614-21.
- YORIFUJI, T., TSUDA, T., TAKAO, S. & HARADA, M. 2008. Long-term exposure to methylmercury and neurologic signs in Minamata and neighboring communities. *Epidemiology*, 19, 3-9.
- ZHENG, M., DOAN, B., SCHNEIDER, T. D. & STORZ, G. 1999. OxyR and SoxRS regulation of fur. *J Bacteriol*, 181, 4639-43.

**Table 2.1 Effect of mercury binding on detectable cellular thiols.**

<b>Condition <sup>a</sup></b>  <b>(biological replicates)</b>	<b>Total Hg<sup>b</sup></b>  <b>atoms/cell</b> <b>(s.d.)</b>	<b>Total Thiol Groups<sup>c</sup></b>  <b>molecules/ cell</b> <b>(s.d.)</b>	<b>Hg/Thiol<sup>d</sup></b>  <b>(% s.d.)</b>
<b>Unexposed (7)</b>	0.00 (0)	3.59E+06 (1.54E+06)	—
<b>40μM PMA (4)</b>	5.12E+06 (1.44E+06)	0.00E+00 (0.00E+00)	1.43 (47)
<b>80μM PMA (1)</b>	5.91E+06	0.00E+00	1.65
<b>160μM MT (4)</b>	2.51E+06 (8.80E+05)	3.04E+05 (2.35E+05)	0.70 (24)
<b>8μM HgCl<sub>2</sub> (2)</b>	5.19E+05 (4.16E+05)	1.95E+06 (2.70E+05)	0.15 (59)
<b>10μM HgCl<sub>2</sub> (1)</b>	8.44E+05	1.31E+06	0.24
<b>16μM HgCl<sub>2</sub> (3)</b>	4.41E+06 (7.16E+05)	5.32E+03 (9.21E+03)	1.23 (19)
<b>20μM HgCl<sub>2</sub> (1)</b>	3.75E+06	0.00E+00	1.05
<b>40μM HgCl<sub>2</sub> (2)</b>	6.33E+06 (3.70E+05)	0.00E+00 (0.00E+00)	1.76 (17)
<b>80μM HgCl<sub>2</sub> (5)</b>	1.23E+07 (6.86E+05)	0.00E+00 (0.00E+00)	3.43 (17)

<sup>a</sup> 30 min exposure to PMA = phenylmercury acetate, MT = merthiolate, HgCl<sub>2</sub> = mercuric chloride.

<sup>b</sup> Measured by ICP-MS; for replicates >1 all values are averages.

<sup>c</sup> Measured by the Ellman's assay (Ellman, 1959)

<sup>d</sup> The denominator is the thiol concentration of the unexposed cells, 3.59x10<sup>6</sup> thiol groups per cell with an average 1.33x10<sup>9</sup> cells/ml (s.d. = 1.99x10<sup>8</sup>) from 7 biological replicates. The % standard deviation is derived by error propagation.

**Table 2.2 Selected iron-binding cysteine sites observed with mercury adducts<sup>a</sup>.**

<b>Protein</b>	<b>Cys #</b>	<b>Fe site</b>	<b>Adduct<sup>b</sup></b>
AcnB, Aconitate hydratase 2	769 <sup>c</sup> , 772 <sup>c</sup>	4Fe-4S	*Hg
CysL, Sulfite reductase hemoprotein	434, 440	4Fe-4S	Hg
GltB, Glutamate synthase, large chain	1108, 1113	3Fe-4S	Hg
GltD, Glutamate synthase, small chain	94	4Fe-4S	PhHg
GltD, Glutamate synthase, small chain	94, 98	4Fe-4S	Hg
IscA, Fe-S cluster assembly	35	variable	PhHg
IscU, NifU Fe-S cluster assembly scaffold	37 <sup>c</sup> , 106 <sup>c</sup>	variable	PhHg
IspG, GcpE, hydroxy-methylbutenyl diphosphate synthase	305	4Fe-4S	PhHg
LeuC, isopropylmalate dehydratase	347	4Fe-4S	PhHg
LuxS, S-ribosylhomocysteine lyase	128	Fe	PhHg
MsrB, methionine sulfoxide reductase	95 <sup>c</sup> , 98 <sup>c</sup>	Fe or Zn	*Hg
SdhB, Succinate dehydrogenase	75	2Fe-2S	PhHg

<sup>a</sup> See Table B.S7 for detailed data.

<sup>b</sup> \*Hg designates adducts observed in PMA exposure datasets.

<sup>c</sup> Cysteine positions conserved in human (taxid:9606) homologs.

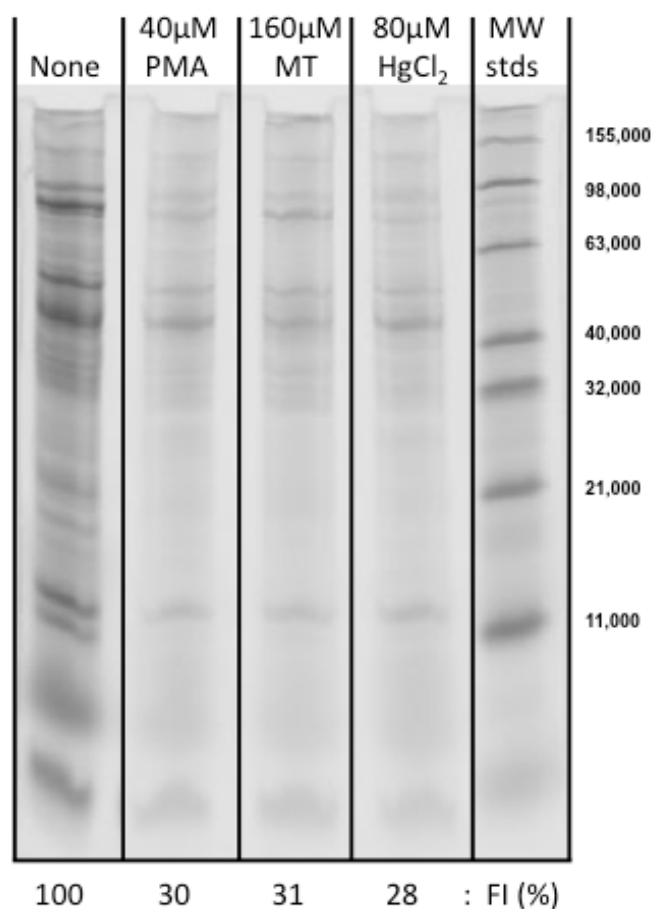


**Figure 2.1 Differential effects of Hg(II), PMA, or merthiolate (MT) on total detectable protein thiols.** Lysates of cells exposed (or not) for 30 minutes during growth to mercurials as indicated were reacted with BODIPY-I. Their proteins were separated by SDS-PAGE and imaged by fluorescence (GE Typhoon: Ex: 633 nm, Em: 670BP30, PMT: 750 V, 200 µm resolution, normal sensitivity). Lanes presented are from a single gel that was trimmed for this figure; lanes not shown were identical to these, confirming that the additional 15 minutes at 37° for DF and DTPA treatment had no effect on BODIPY detection of protein thiols. Fluorescence Intensities (FI) for each condition are normalized to the corresponding unexposed cells (lane 1). See Materials and Methods

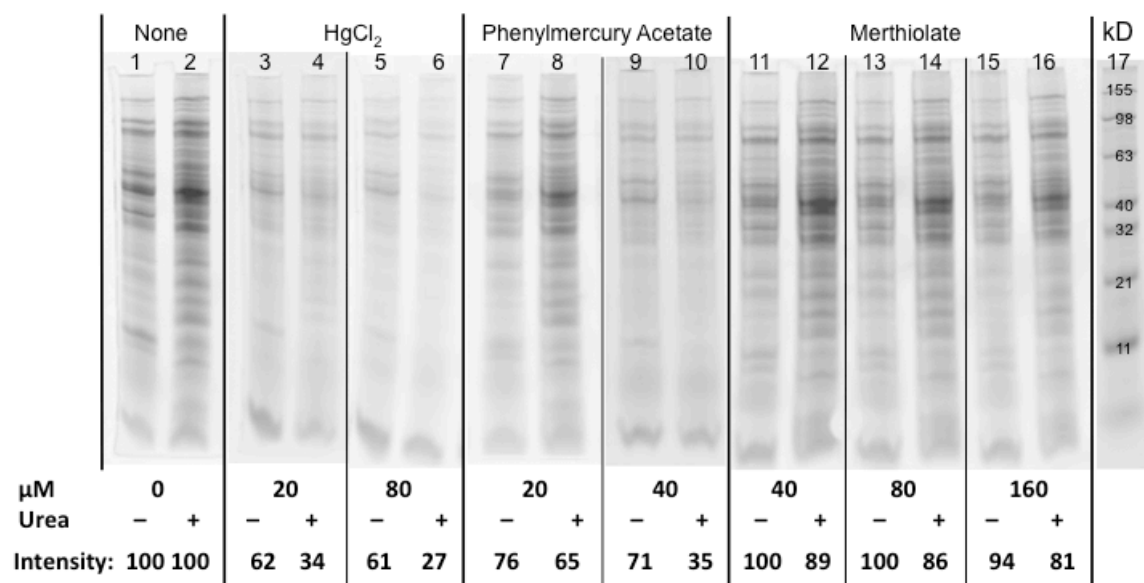


**Figure 2.2 Effects of Hg(II), PMA, or merthiolate (MT) on total detectable protein thiols.**

Lysates of cells exposed (or not) to mercurials as indicated for 15 minutes during growth were reacted (or not) with 10 M urea and then with BODIPY-I. Their proteins were separated by SDS-PAGE and imaged by fluorescence (GE Typhoon: Ex: 633 nm, Em: 670BP30, PMT: 750 V, 200 μm resolution, normal sensitivity). Images from several gels prepared under the same conditions were compiled for this figure. Total densitometric lane intensity of unexposed cultures varied by 17% s.d. without urea (e.g. lane 1) and by 13% s.d. with urea (e.g. lane 2). Total densitometric lane intensity for each condition was normalized to the corresponding lane intensity of unexposed cells. (see Materials and Methods)



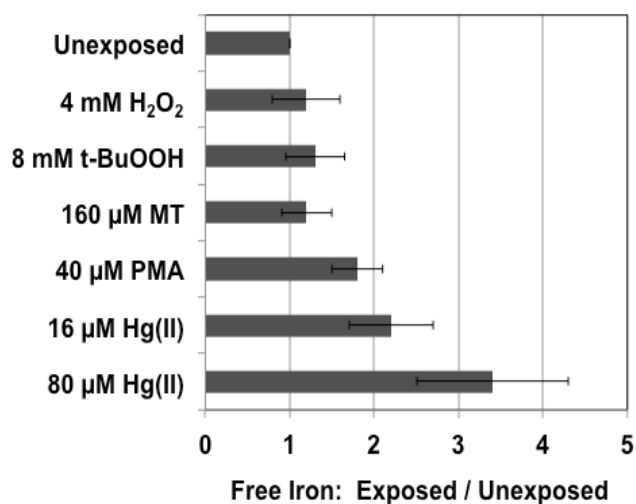


**Figure 2.3 Increases in free intracellular iron levels in cells exposed to mercurials and common organic oxidants.** The increase in intracellular free iron is represented as the average X-fold increase in the Fe(III):DF complex EPR signal at  $g = 4.3$  for each stress condition relative to the unexposed control whose average free iron concentration was  $24.4 \mu\text{M}$  ( $\pm 4.9 \mu\text{M}$ ). Error bars are standard deviation of biological replicates. Replicates for each condition were: Unexposed (6);  $\text{H}_2\text{O}_2$  (2); t-BuOOH (2); MT (3); PMA (3);  $16\mu\text{M HgCl}_2$  (3); and  $80 \mu\text{M HgCl}_2$  (5)

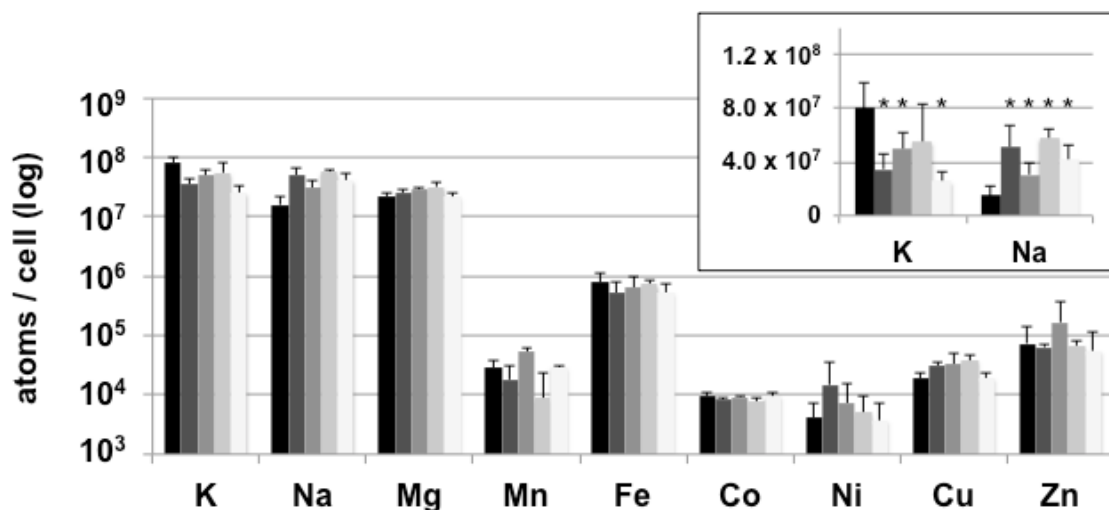


**Figure 2.4 Effect of mercurials on intracellular levels of essential metal ions.**

Exponential phase MG1655 cells were unexposed (black) or exposed to 40  $\mu$ M PMA (dark grey), 160  $\mu$ M MT (medium grey), 16  $\mu$ M HgCl<sub>2</sub> (light grey) or 80  $\mu$ M HgCl<sub>2</sub> (off-white) for 30 minutes, harvested, washed, and assayed for nine essential elements by ICP-MS. Inset: K<sup>+</sup> and Na<sup>+</sup> content on smaller scale. Error bars represent standard deviation of biological replicates: Unexposed (7); PMA (4); MT (4); 16  $\mu$ M HgCl<sub>2</sub> (3); 80  $\mu$ M HgCl<sub>2</sub> (6). Significance (\*) was determined by t-test comparison of the means at the 95% confidence level with two-tailed p-values equal to <0.05.

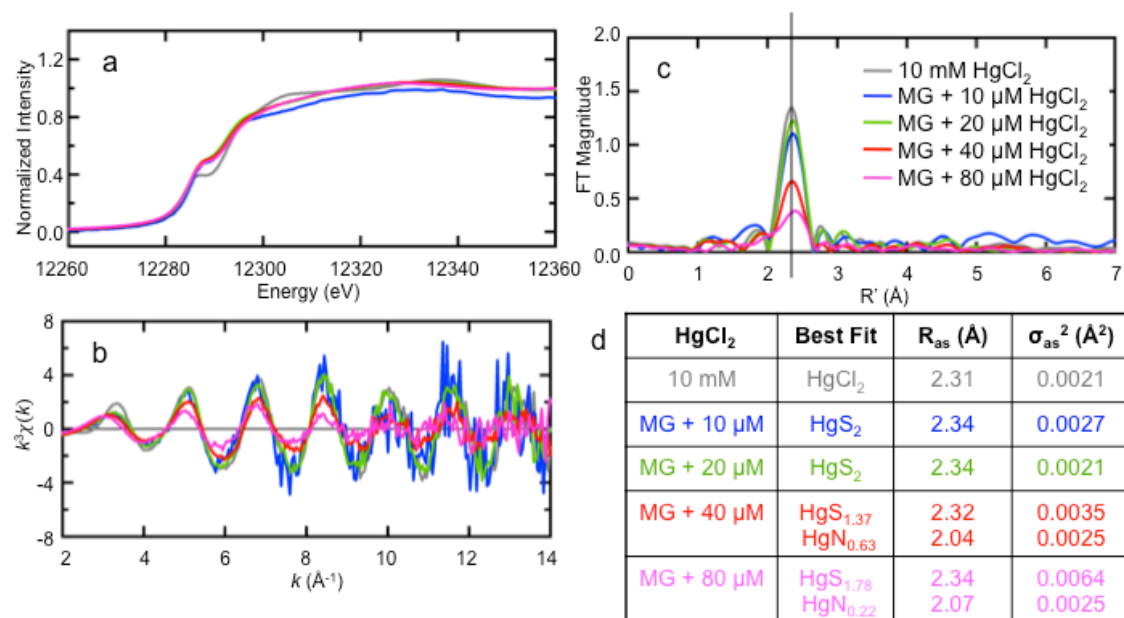


**Figure 2.5 Changes in cellular ligands as Hg concentration is increased.** HgCl<sub>2</sub> (10 mM, gray) was added to a known amount of growing cells at 10 μM (blue), 20 μM (green), 40 μM (red), or 80 μM (pink). Panels are the near edge (A) and EXAFS (B) spectra of the concentrated washed cell suspensions and the HgCl<sub>2</sub> standard. Panel C is the corresponding Fourier transforms of the EXAFS data in (B) and panel D contains the EXAFS fitting results. Best Fit subscripts denote the number of scatterers per metal atom. R<sub>as</sub> is the observed metal-scatterer distance. σ<sub>as</sub><sup>2</sup> is the Debye-Waller or temperature factor.

### CHAPTER 3

#### THE ORGANOMERCURY EXPOSOME OF *ESCHERICHIA COLI*<sup>1</sup>

---

<sup>1</sup>ZINK, E.M., LAVOIE, S.P., POLACCO, B.P., PURVINE, S.O., MILLER, S.M., LIPTON, M.S., SUMMERS, A.O.; Co-first author. To be submitted to *Metallomics*.

## ABSTRACT

Mercury (Hg), the 80th element of the Periodic Table, is chemically and physically versatile. Although in all forms it is long known to be quite toxic, Hg has been widely dispersed beyond its geological deposits as a result of ancient and modern anthropogenic activities. Human exposure can result in neurotoxicity, nephrotoxicity, immunotoxicity and gastrointestinal toxicity with the severity depending on the chemical form and quantity of Hg involved and on yet-to-be fully defined human genetic factors. However, there are several paradoxes in Hg toxicity such as the fact that very low doses can have seemingly beneficial effects (called hormesis) and the fact that Hg is toxic at micromolar levels despite the fact that many bacteria and all vertebrates have millimolar levels of small thiol compounds such as glutathione that can compete with mercury's protein thiol targets. Here we use global proteomics in a simple model organism, *Escherichia coli*, to learn which thiol-containing proteins are most vulnerable to forming stable adducts with the organomercurial (RHg), phenylmercuric acetate. To do this, we adjusted standard bottom-up mass spectrometry proteomics methods to preserve mercurial adducts formed during exposure of intact growing cells. Mass spectrometric detection of peptides bearing mercury adducts was optimized with a recently devised computational filter for identification of the unique stable isotope fingerprint of Hg in a high-throughput proteomic scale. We found (1) that method modifications useful for preserving mercury adducts did not compromise detection/observation of peptides generally, (2) that cysteine-containing peptides predicted in *E. coli* were observed effectively with the modified method, and (3) that the 307 abundant proteins whose cysteines reproducibly formed stable RHg adducts occur in all major metabolic functional groups and include 22 proteins whose targeted peptide has a homolog in humans. We conclude that high-throughput proteomics can reproducibly identify proteins that form stable adducts with RHg

compounds. Thus, global proteomics could facilitate research on mercury intoxication and recovery from it in model eukaryotic systems and enable molecular diagnostics to support epidemiology of sub-clinical effects of mercurial exposure.

## INTRODUCTION

Mercury exists at standard temperatures and pressures as a metallic liquid, as ionic salts, or as a monoatomic vapor (Clarkson and Magos, 2006). This protean and reactive element has been used by humans since antiquity in applications as diverse as cosmetics, disinfectants, electrodes, dental restorations, recovery of precious metals and radionuclides, and religious rituals (Norn et al., 2008). Historically, Hg has been regarded with fascination and fear for its varied useful properties and its well recognized toxicity.

In present times human applications continue to spread Hg throughout our external and internal environments well beyond its natural ore deposits. For economic reasons the commercial utility of Hg has largely overshadowed concerns for its toxicity. However, public awareness late in the last century led to efforts to decrease its dissemination from coal-fired power plants (Mason et al., 1994) and to constrain consumption of fish, the major dietary source of neurotoxic methylmercury (Li et al., 2010). Although industrial synthesis of this fungicide was banned over four decades ago, methylmercury contamination is increasing globally because bacteria in many natural ecosystems synthesize it when exposed to inorganic mercury from acid rain or industrial or dental sources (Hintelmann, 2010, Parks et al., 2013).

Because of its varied natural forms the toxicology of mercury is complex and the toxicokinetics and exact molecular targets of any single form have not been well defined. The only large human exposure datasets come from occupational exposure to Hg(0) in adult chlor-

alkali plant workers (Pranjic et al., 2003), catastrophic methylmercury fungicide exposure events affecting children and adults (Bakir et al., 1973), studies of the effect on children of their mothers' fish consumption (Davidson et al., 2006), and recent studies on exposure of dental practitioners or child dental patients (Richardson et al., 2011). These studies agree that exposure at any age to inorganic or organic mercurials can have varied neurological manifestations, though tight correspondence between apparent dose and signs or symptoms is often not found (Clarkson and Magos, 2006). Thus, public pressure has led worldwide to phasing out the chlor-alkali process, the use of mercury in batteries, antiseptics, and fungicides, and to increasing regulation of Hg emissions from coal-fired power plants (Mackey et al., 2014). Hg use in dentistry is also regulated in the US and Europe as a toxic substance before it is put into the patient's mouth and after it is removed for disposal. Canada and several EU countries are constraining or phasing out the dental application of Hg; in the US dental amalgam is considered completely safe as long as it is in the patient's mouth. A recent risk analysis indicates that exposure to dental mercury restorations results in Hg exposures in excess of EPA guidelines in 30-40% of the US population (Richardson et al., 2011). Artisanal gold recovery in the Amazon and Africa leads to varied exposure to Hg(0) vapor for months or years, but related health effects on the indigene miners have only recently been examined (Malm, 1998).

The widely varying levels of concern and action for such dramatically different potential Hg exposures (i.e. recommending limits on fish consumption to a few micrograms of methylmercury per week (WHO, 1976) but permitting grams of Hg(0) in the mouth for many years (<http://www.fda.gov/MedicalDevices/ProductsandMedicalProcedures/DentalProducts/DentalAmalgam/ucm171094.htm>) highlight the paradoxical nature of mercury's health affects and the

limits of our ability to detect and define them. Chemically, all forms of mercury but Hg(0) are reactive electrophiles and the latter is readily converted into electrophilic Hg(II) by widely found peroxidases in animals, plants and aerobic microbes (Smith et al., 1998). Like organic electrophilic toxicants such as methylglyoxal, Hg(II) bonds avidly with thiol groups on proteins and small molecule redox buffers such as glutathione and cysteine and, when thiol ligands are saturated, RHg and Hg(II) bind with other soft nucleophiles such as imino nitrogens in nucleobases, especially thymine (LaVoie et al., 2015, Miyake et al., 2006). It is widely recognized that protein cysteine thiols vary widely in reactivity with any electrophile as a function of their local molecular environment (Masip et al., 2006). In addition, the potential for forming very stable bis-thiol chelates of bivalent Hg(II) (Table C.S1) will vary among proteins. The rare but very important amino acid selenocysteine also binds mercurials very strongly (Sugiura et al., 1978). Another hallmark of Hg intoxication is that it is a cumulative poison (Clarkson and Magos, 2006), tending to accumulate in certain organs, suggesting that it occupies sites subject to little exchange with other thiols in the same cell. Thus, the above noted paradox of Hg intoxication is also reflected at the level of cell biology, i.e. despite having millimolar levels of small thiol redox buffers such as glutathione, aerobic bacteria are nonetheless sensitive to micromolar mercury compounds (Barkay et al., 2003) and animal cells in tissue culture are sensitive to much less (Podzimek et al., 2005).

These paradoxes of Hg chemistry and biology lead to the hypothesis that there is a range of vulnerability to mercury (organic or inorganic) among proteins. Vulnerability here is operationally defined as easily forming strong, stable ligands with mercury compounds (i.e. a high on-rate and low off-rate) with consequent deleterious effect on the normal activity of the protein; this is the case for some, but has not been tested for all thiol-containing proteins.



To test this hypothesis by identifying such proteins we briefly exposed the model organism *Escherichia coli* MG1655 to phenylmercuric acetate (PMA), formerly used as a preservative in paint and over-the-counter medications, as a surrogate for the neurotoxin, methylmercury. PMA is monovalent and, unlike bivalent inorganic Hg(II), will not crosslink cysteines in different peptides. To optimize visualization of protein-PhHg adducts we used toxic concentrations of each compound. Cellular damage of these acute concentrations of mercurials has been reported elsewhere (LaVoie et al., 2015). Thus, here we are not here looking at a response to a stressor as usually done in descriptive global proteomics; rather the cells are acutely exposed only long enough to accumulate adducts, but are not diluted into mercury-free medium to allow recovery.

Observation of protein-RHg adducts by MS is facilitated by a computational filter we have recently devised (Polacco et al., 2011) that takes advantage of Hg's seven readily visible stable isotopes (Figure 3.1). Fortuitously, Hg's higher mass stable isotopes are more abundant than its lower mass isotopes, a trend exactly opposite the abundances of the low mass components (H, C, N, O, S) of amino acids. Consequently, addition of a single Hg atom to a typical peptide (up to ~5000 Da) imparts a characteristic distortion to the isotope distribution, which can be distinguished in survey spectra (MS1) or in sequencing spectra (MS2). The use of the Hg stable isotope profile has been reported for assessment of the thiol metabolome (Krupp et al., 2008, Rao et al., 2010) and for tryptic fragments of single proteins (Trumpler et al., 2009). Here we report the full functional analysis of the *E.coli* proteome determined with the method reported in Polacco et al (Polacco et al., 2011).

## MATERIALS AND METHODS

### *Culture conditions*

*The bacterial strain used was Escherichia coli K-12 MG1655. E. coli* cells from -70 °C stocks were grown overnight at 37 °C on Luria-Bertani (LB) plate. Six well isolated colonies from overnight plate were inoculated into 30 ml of Neidhardt-MOPS minimal medium (Neidhardt et al., 1974) supplemented with 20 mg/L uracil and 500 µg/L thiamine and grown overnight at 37°C with shaking at 250 rpm. These overnight liquid cultures were subcultured (1:40) into 1700 ml of the same medium, then split into two 2800 ml Fernbach flasks with 850 ml in each and incubated at 37 °C, 250 rpm until culture OD<sub>595</sub> was approximately 0.5 - 0.6. The two cultures were then combined to ensure homogeneity and divided again with 800 ml in each Fernbach flask. Phenylmercuric acetate was added to give 40 µM final concentration in one flask and the other remained untreated. Incubation of both cultures continued for 15 min when they were centrifuged at 17,700 x g, for 10 min at 4 °C. Cell pellets were suspended in 8 ml of 50 mM ammonium bicarbonate (pH 7.8) at 100X the original culture volume. The cell suspensions were dispensed as 1 ml aliquots for future experiments and iodoacetamide (IAM) at 10 or 20 mM was added or not to some aliquots, all aliquots were then stored at -70 °C until being shipped on dry ice to PNNL for proteomic analysis.

### *Cell lysis*

For proteomic analysis thawed 1 ml cell suspensions were diluted to volume in 100 mM ammonium bicarbonate, pH 8.0, with [IAM] appropriate to each experiment and lysed with a PBI Barocycler NEP 3229 (Ringham et al., 2007) for ten cycles, holding at 35, 000 psi with 20 second intervals. Protein concentrations were determined with the Bradford assay and the cell lysates were immediately fractionated as below.

### *Subcellular Fractionation*

Half of cell lysate was used for the global preparation and the other half was centrifuged to produce the soluble and insoluble fractions. Specifically, unbroken cells were removed via centrifugation at 4000 rpm at 4°C for 2 m and the supernatant was removed and further centrifuged at 100,000 rpm for 10 m at 4°C for precipitation of cell walls and ribosomes. The supernatant of the 100K spin (“soluble” fraction) was removed and cryoarchived. The 100K pellet (“insoluble” fraction) was suspended in 100 µl of 100 mM ammonium bicarbonate with [IAM] appropriate to each experiment and centrifuged again. The combined supernatants spins defined the soluble proteins; proteins remaining in the pellet defined the insoluble proteins. The pellet was solubilized in 50 mM ammonium bicarbonate, pH 7.8 with 1% 3-[3-(cholamidopropyl)dimethyl-ammonio]-1-propanesulfonate (CHAPS). Protein concentrations in soluble, insoluble and global fractions were determined by the Bradford assay using BSA as a standard.

### *Protein Denaturation and Trypsinolysis*

The standard proteomic protocol (Callister et al., 2008) calls for denaturation of protein fractions in 7 M urea and 2 M thiourea and reduction with 5 mM dithiothreitol (DTT), for the global and soluble fractions and 10 mM DTT for the insoluble fraction. We expected that high molarity DTT and thiourea would destabilize PhHg adducts and found this was the case in preliminary experiments (data not shown). So, instead, as noted above, harvested cells were suspended in buffered IAM and frozen; the IAM concentration was maintained throughout the pre-LC-MS/MS steps. Global and soluble fractions were then diluted 10-fold with 100 mM ammonium bicarbonate containing IAM as appropriate; the insoluble fractions were diluted with 50 mM ammonium bicarbonate including IAM as appropriate. Calcium chloride was added to 1

mM and the fractions were digested for 3 h at 37°C with sequencing grade modified trypsin (Promega, Madison WI) at a ratio of 1:50 (wt/wt) trypsin-to-protein. Digested proteins were desalted with a C-18 SPE column (Supelco, St. Louis, MO), concentrated by SpeedVac (Thermo Savant, San Jose CA) to 0.1 ml and the peptide content was measured with the BCA assay (Pierce, Rockford IL).

### *Peptide Detection and Identification*

Peptides were observed by mass spectrometry after fractionation of the global, soluble and insoluble preparations from the standard protocol using a previously described method (Callister et al., 2008). Briefly, peptides in each subcellular fraction were separated by reverse-phase liquid chromatography using an established protocol (Kiebel et al., 2006, Monroe et al., 2007, Smith et al., 2002). Triplicate mass spectra of global, soluble and insoluble fractions were obtained on a ThermoScientific Exactive Orbitrap mass spectrometer (Thermo Scientific, San Jose, CA) outfitted with a custom built electrospray ionization (ESI) interface (Callister et al., 2008, Kelly et al., 2006, Livesay et al., 2008). Peptides were identified in MS/MS spectra via SEQUEST based on the Comprehensive Microbial Resource (Peterson et al., 2001) for the genome sequence of *Escherichia coli* K12-MG1655. Cysteine modifications allowed IAM (+57.0215) or PMA (+278.0019).

LC-MS/MS peptide hit lists were generated by SEQUEST using the *E. coli* genome sequence (GenBank: U00096.2) and allowing alkylation by IAM or adducts of Hg and phenylHg (PhHg) as modifications of cysteine. SEQUEST results were re-scored by MS-GF (Kim et al., 2008), and SEQUEST matches to Hg and PhHg adducts were additionally re-scored by PeptideProphet (Keller et al., 2002) to maximize true identifications of Hg adducts. Filtering criteria were selected based on false discovery rates (FDR) computed from searches against a

reversed sequence database as decoys. The primary filter for spectral matches was MS-GF's spectral probability, which we required to score less than  $1.6\text{e-}10$  for acceptance of any peptide match. This threshold yielded a FDR of 0.001 over all spectra. To eliminate false discoveries that are singletons, we further improved accuracy by both requiring more than one spectrum for any peptide and, for proteins with only a single observed peptide, requiring a MS-GF spectrum probability less than  $1\text{e-}11$  and at least one tryptic end (semi or fully tryptic). For matches to peptides modified by Hg, we relaxed the MS-GF spectrum probability threshold to  $5\text{e-}7$ , but required PeptideProphet's probability to be greater than 0.8 for acceptance. Both thresholds yielded a high FDR when used alone, but when combined and with two additional criteria that peptides be fully tryptic and from proteins passing by the MS-GF spectral probability filter, these criteria produced zero matches to Hg modified decoy sequences (FDR = 0.0). As an alternative estimate of FDR focused on incorrect modifications rather than on incorrect sequences, we used “Hg adducts” detected in the Hg-free samples as a distinct estimate of FDR. This yielded an FDR of 0.009 for spectra identified as Hg-modified.

## **RESULTS AND DISCUSSION**

### *Rationale for Modifications of the Standard Global Proteomics Protocol*

In initial experiments (LaVoie et al., 2015) we identified exposure conditions for PMA and MT sufficient to saturate all measureable thiols in cells in the exposure reactions in order to optimize the likelihood of acquiring abundant mercurial adducts. While these concentrations of 40 to 160  $\mu\text{M}$  (8 to 32 ppm) are higher than concentrations allowed in food and water they are comparable to concentrations in Hg mining areas (up to thousands of ppm) (Malm, 1998) and in feces of primates with recently installed amalgam dental restorations (up to 200 ppm) (Summers

et al., 1993) where the mercury resistance locus likely originated and continues to evolve, respectively (Barkay et al., 2003).

Inorganic ionic mercury, Hg(II), forms thermodynamically stable adducts with halide anions and especially strong adducts with the chalcogen anions, sulfide and selenide (Table C.S1). However, Hg(II) is kinetically labile, readily exchanging with different monothiols via trigonal intermediates (Cheesman et al., 1988). Nonetheless, a small molecule or protein that provides two thiol ligands affording the ideal linear, 180 ° geometry for Hg(II) bis-coordination, have a chelation effect increasing the formation constant 5 orders of magnitude above monothiols. The even stronger trigonal coordination provided by the bacterial transcriptional metalloregulator, MerR (Watton et al., 1990, Zeng et al., 1998), inspired our search for other cellular proteins that provide very strong coordination of inorganic or organic mercurials but suffer damage thereby.

In the cell, the small monothiol tripeptide, glutathione (GSH) at 5-10 mM competes with protein cysteine thiols for PhHg and can also move PhHg-adducts among protein cysteine sites. IAM was employed to quench glutathione and to block any buried protein thiols that did not bind PhHg in the intact cell and minimize its re-association to other thiols during protein denaturation. A pilot study also showed that standard post-cell lysis treatment with dithithreitol and use of thiourea eliminated nearly 100% of Hg adducts, so these were removed from our modified proteomics protocol.

The summary of observations and identification criteria are shown in Table 3.1 and consequences of these protocol alterations are depicted in Figure 3.2 and Table C.S2. Without PMA or IAM (bar 1) we observed only 1,833 spectra of cysteine-containing peptides (Cys-peptides), all as free thiols (red). With 10 mM IAM alone (bar 3) we observed nearly 8-fold more

Cys-peptides (13,997 spectra), 91% in the alkylated form, -S-CAM (orange). Doubling the IAM concentration (bar 5) barely increased the Cys-peptide signal (15,476 spectra) and the extent of alkylation (92%, orange). The unmodified (red) Cys-peptides declined slightly from 1,240 in 10 mM IAM to 1,221 in 20 mM IAM. With an average of 24 spectra per unique Cys-peptide site in these no-PMA conditions, bars 3 and 5 represent 98% of the 1,291 unique cysteine sites observed or 8% of the total unique cysteine sites encoded in the *E. coli* genome (Table 3.2). Exposure to PMA decreases the number of observed cysteine sites by half.

Exposure of the cells to PMA alone (bar 2) tripled the Cys-peptide signal compared to IAM alone (bar 1), 65% of which had PhHg or Hg adducts (blue, aqua, green, 3,203 spectra) and rest were unmodified (1,747 spectra). In contrast, when PMA exposure was followed by IAM treatment (bars 4 and 6), the Cys-peptide signal declined dramatically compared to the IAM-treatments alone (bars 3 and 5, respectively). The 10 mM IAM treatment (bar 4) diminished Hg/PhHg-modified peptides (blue, aqua, green) slightly and even greater loss of mercurated peptides occurred in the 20 mM IAM condition (bar 6), suggesting that IAM removed some mercurial adducts. Although alkyl adducts increased (yellow, bars 4 and 6) compared to the no IAM condition (bar 2), they remained but 10% (bar 4) or 20% (bar 6) of the IAM-accessible thiols represented in the no-PMA conditions (bars 3 and 5, respectively), suggesting that PMA also competes with alkylation. The fraction of un-modified (red) Cys-peptides is roughly similar in all PMA-exposure conditions.

The two types of inorganic Hg adducts (green and aqua) may result from some free Hg in the PMA stock. However, peptides with suitably placed cysteine pairs and nearby Asp residues might protonolyze PMA as do Cys95, Cys159, and Asp99 of the organomercurial lyase, MerB (Pitts and Summers, 2002). Lacking an additional cysteine pair like two-cysteine NMerA

domain of MerA, such a fortuitous CXnC... D/E motif would remain stuck with the Hg(II). In a group of Fe-metabolism proteins all of the observed Hg(II) adducts bound to two-cysteine peptides also included D, E or both nearby in the same peptide (LaVoie et al., 2015).

Comparing mercurial adducts in the no-IAM condition (bar 2) with alkyl-adducts in the no-PMA condition (bar 3), indicates that many more Cys-peptides are available for modification by the polar acetamide than by the organomercurial. Although LaVoie et al. (LaVoie et al., 2015) observed exposure to 40  $\mu$ M PMA rendered nearly 100% of their lysate proteins unmodifiable in vitro by BODIPY-iodoacetamide, that could be explained by disulfide formation during the burst of reactive oxygen species (ROS) on PMA-induced collapse of the respiratory pathway. Disulfide formation could also explain the overall decline in all Cys-peptides under all three PMA-exposure conditions in Figure 3.2. Interpeptide and peptide-GSH disulfides are unstable in proteomic mass spectrometry conditions used here and require separate approaches only recently developed for their reliable detection (Switzar et al., 2016).

As anticipated IAM decreased the observed PhHg-adducts, suggesting that some such adducts observed in the absence of IAM (Figure 3.2, bar 2) might have arisen by re-association during protein processing for LC-MS/MS. However, arguing against extensive re-association is the absence of any such modifications in the mini-proteome internal standards, which contains two cysteines in bovine cytochrome C and four cysteines in rabbit GAPDH. An alternative possibility is that IAM destabilizes the PhHg-Cys-peptide adduct. In separate work with the natural Hg-binding metalloregulator, MerR, we have found that Cys-PhHg adducts are unstable to excess IAM in physiological thiol conditions, possibly owing to displacement of the PhHg-S mono-dentate ligand by iodide released during IAM alkylation (Polacco, Wireman, et al., MS in



preparation). Such chemistry has not otherwise been reported, but iodine is a very strong ligand for Hg (Nagypal and Beck, 1982).

Although the use of IAM to prevent PhHg re-association did not work exactly as expected, we consider it likely that the adducts we did observe, having survived IAM exposure and LC-MS/MS conditions, represent stable points of association with Hg in the corresponding proteins. Such sites in the native protein make it vulnerable to PhHg- (or Hg)-mediated inactivation.

Several smaller scale studies of the interaction of mercurials with eukaryotic and prokaryotic proteins have been done with 2D gel electrophoresis followed by mass spectrophotometric identification of modified proteins (Berg et al., 2010, Fanous et al., 2008, Gao et al., 2013, Marsano et al., 2010). More recently, Weerapana et al (Weerapana et al., 2010) employed capture of biotinylated cysteine-containing peptides to define a set of highly reactive cysteines in bacterial and human proteins. A subset of 13 proteins (16 cysteine sites) we observed as modified by Hg or RHg was also reported to be highly reactive *in vivo* with a strongly electrophilic thiol tagging agent Table C.S3.

#### *Functional roles of MG1655 chromosome-encoded proteins*

Protein and peptide identifications were sorted by Clusters of Orthologous Groups (COGs) annotated functional roles (Markowitz et al., 2012, Tatusov et al., 2000) to determine the distribution of these observations across the genome and identify any biases of mercury binding towards particular functions (Figure 3.3, 3.S1, & 3.S2). Protein coverage of each functional category ranged from 26 – 81% (Table C.S4), with intracellular trafficking being the lowest and translation being the highest. Since the proportion of observed COG proteins (green) in each functional category is equal to or greater than their proportion in that category in the genome

(blue), this indicates we are not completely missing any particular category (Figure 3.3). About 40% of observed cysteine-containing proteins (purple) and 50% of PhHg-modified (red) proteins are from just four functional categories: amino acid biosynthesis, energy metabolism, protein synthesis and nucleotide synthesis. The metabolism categories tend to be more cysteine-rich than other functions and account for the greater proportion of cysteine peptides and mercury modification observations. Translation is not a cysteine-rich category, but accounted for the highest proportion of peptide observations (22%) for all categories (Figure C.S1). Mercury-modified proteins were observed in 19 out of 21 functional categories, only RNA processing and intracellular trafficking were not observed to have R/Hg adducts.

Forty-eight percent of observed Cys-containing proteins were modified by PMA. There are 251 cysteine sites from the 307 total proteins that were highly modified by mercury (defined as having >50% of observations for a given Cys site be mercury modified). The corresponding heavily modified proteins serve a variety of essential cell functions. The alpha, beta and delta subunits of the F1 sector of the ATP-synthase were modified and are important for energy production. Other energy-related proteins modified include, glyceraldehyde-3-phosphate dehydrogenase, a key component of glycolysis, and citrate synthase and succinate dehydrogenase are in the TCA cycle. The RNA polymerase  $\alpha$ ,  $\beta$ ,  $\beta'$  subunits were modified, as was the major sigma factor,  $\sigma^{70}$ . Proteins involved in amino acid biosynthesis were highly modified, as were eight tRNA synthetases. Protein synthesis was also vulnerable with mercury modifications observed for fourteen ribosomal proteins and for translation elongation factors, Ef-Tu and Ef-G. The pivotal DNA repair protein RecA bound PhHg. Redox homeostasis enzymes also suffered mercury modification including: thioredoxin 1, glutaredoxin 3, alkyl hydroperoxide reductase, superoxide dismutase B, and lipid hydroperoxide reductase. Cysteines are involved in

the activities of the enzymes among these proteins and R/Hg-modification will likely inactivate them resulting in stasis of cell division and/or cell death. The most prominent of the non-enzyme, structural proteins suffering P/Hg modification were the ribosomal proteins, which may serve as Zn reservoirs in the cell (Hensley et al., 2011).

#### *Human homologs of Hg vulnerable E.coli proteins*

There are 64 proteins encoded by *E. coli* that have a human homolog with  $\geq 50\%$  sequence identity and we observed 20 of these with PhHg or Hg modifications (Table C.S5). The search for homologs was refined to identify conserved domains using 320 mercury modified peptide sequences and identified 22 proteins and 33 distinct cysteine sites that are conserved in a human protein of the same or similar function (Table 3.3 and Table C.S6). Thirteen of these homologous proteins are mitochondrial. There were 8 proteins that contained two cysteine residues, as part of CX<sub>n</sub>C motif, which are capable of chelating divalent mercury. The Comparative Toxicogenomics Database (Davis et al., 2009) was used to identify diseases associated with these conserved proteins that were susceptible to mercury damage. There were five proteins with high disease inference scores to associated diseases (Table 3.3) including various types of cancer, osteoarthritis, and Alzheimer Disease. These conserved cysteine sites could serve as potential biomarkers for specimens collected from mercury-exposed individuals.

## **CONCLUSIONS**

In summary, this work has optimized conditions for observing cysteine thiols in bottom up proteomics, finding that approximately 8% of encoded cysteines can be reproducibly observed as CAM-adducts compared to only 1% without IAM treatment under these conditions. Considering cysteines capable of forming CAM adducts as reflecting those which could be

available for modification by electrophiles of health importance such as mercurials, we found that 48% of these CAM-modifiable proteins were modified by phenylmercury or inorganic mercury in cells exposed during late exponential growth. One hundred percent of peptides forming adducts with another strong electrophile (Weerapana et al., 2010), were also modified by mercurials in our experiments. We did observe 14 proteins modified only by the mercurials and not by IAM, suggesting subtle influences of cellular anatomy or biochemistry.

In addition to identifying adduct-available cysteines, IAM was also intended to limit re-association of mercury adducts to other cysteines during denaturation for proteomic analysis. Indeed, IAM decreased the number of R/Hg adducts observed which is consistent with such protection of unfolding cysteine thiols. However, the large excess of IAM used might also have destabilized the PhHg adducts, a possibility we have confirmed with a purified natural Hg binding protein (MS in preparation).

This work also extends our observation in Fe-binding proteins that under conditions of bottom-up LC-MS/MS proteomics, Hg(II)-cysteine adducts are only stable in peptides providing at least 2 cysteines for chelation of this bivalent metal. In contrast, monovalent phenylmercury and ethylmercury (LaVoie et al., 2015) form stable adducts on many different monothiol peptides.

This work is relevant to metazoan health in two ways. Firstly, stable R/Hg adducts occur in abundant proteins in all but two COG functional categories consistent with the wide variety of disease syndromes from neurological to autoimmune reported to arise from inorganic or organic Hg exposure. Thus, there can be no single disease whose etiology can ascribe to Hg or RHg exposure because these compounds have so many and varied targets inside the cell. Secondly, our work here and previously (LaVoie et al., 2015) strongly suggests the different

pathophysiology of organic and inorganic Hg compounds reflects their valences (i.e. on a molar basis bivalent inorganic Hg is at least 2-fold more damaging to cellular thiols (LaVoie et al., 2015) than monovalent PMA or merthiolate) and also the kinds of protein thiols that make stable ligands with these two types of compounds.

Lastly, with the rapid development of MS capable of robust top-down proteomics, our stable isotope computation filter can be applied directly to native proteins from cells exposed to mercurials without risking artifacts due to IAM-exposure and trypsinolysis. Top-down mercurial proteomics can be used on tissue cultures or metazoan models to examine how cells recover from mercury exposure and identifying interventions that optimize recovery from acute Hg exposure and protection from chronic Hg exposure.

## **ACKNOWLEDGMENTS**

This work was funded by the Department of Energy (Biological Sciences Division). Proteomics work was performed at the Environmental Molecular Sciences Laboratory (a national scientific user facility sponsored by the U.S. DOE Office of Biological and Environmental Research) located at the Pacific Northwest National Laboratory, operated by Battelle for the DOE. Pure protein/peptide and informatic analyses were performed at UCSF with support of DOE grant to Susan M. Miller and cell cultivation, mercury exposure, biochemical analyses, and MySQL database development and implementation were performed at UGA with support of DOE grant to Anne O. Summers. Portions of this work were submitted by Erika M. Zink in partial fulfillment of the requirements of Washington State University for the Master of Science degree and by Stephen P. LaVoie in partial fulfillment of the requirements of the University of Georgia for the Doctor of Philosophy degree in Microbiology.

## REFERENCES

- BAKIR, F., DAMLUJI, S. F., AMIN-ZAKI, L., MURTADHA, M., KHALIDI, A., AL-RAWI, N. Y., TIKRITI, S., DAHAHIR, H. I., CLARKSON, T. W., SMITH, J. C. & DOHERTY, R. A. 1973. Methylmercury poisoning in Iraq. *Science*, 181, 230-41.
- BARKAY, T., MILLER, S. M. & SUMMERS, A. O. 2003. Bacterial mercury resistance from atoms to ecosystems. *FEMS Microbiol Rev*, 27, 355-84.
- BERG, K., PUNTERVOLL, P., VALDERSNES, S. & GOKSOYR, A. 2010. Responses in the brain proteome of Atlantic cod (*Gadus morhua*) exposed to methylmercury. *Aquat Toxicol*, 100, 51-65.
- CALLISTER, S. J., MCCUE, L. A., TURSE, J. E., MONROE, M. E., AUBERRY, K. J., SMITH, R. D., ADKINS, J. N. & LIPTON, M. S. 2008. Comparative bacterial proteomics: analysis of the core genome concept. *PLoS One*, 3, e1542.
- CHEESMAN, B. V., ARNOLD, A. P. & RABENSTEIN, D. L. 1988. Nuclear magnetic resonance studies of the solution chemistry of metal complexes. 25. Hg(thiol)<sub>3</sub> complexes and HG(II)-thiol ligand exchange kinetics. *J. Am. Chem. Soc.*, 110, 6359-6364.
- CHEN, J., HE, Q. Y., YUEN, A. P. & CHIU, J. F. 2004. Proteomics of buccal squamous cell carcinoma: the involvement of multiple pathways in tumorigenesis. *Proteomics*, 4, 2465-75.
- CHEN, X. L., ZHOU, L., YANG, J., SHEN, F. K., ZHAO, S. P. & WANG, Y. L. 2010. Hepatocellular carcinoma-associated protein markers investigated by MALDI-TOF MS. *Mol Med Rep*, 3, 589-96.
- CLARKSON, T. W. & MAGOS, L. 2006. The toxicology of mercury and its chemical compounds. *Crit Rev Toxicol*, 36, 609-62.
- DAVIDSON, P. W., MYERS, G. J., WEISS, B., SHAMLAYE, C. F. & COX, C. 2006. Prenatal methyl mercury exposure from fish consumption and child development: a review of evidence and perspectives from the Seychelles Child Development Study. *Neurotoxicology*, 27, 1106-9.
- DAVIS, A. P., MURPHY, C. G., SARACENI-RICHARDS, C. A., ROSENSTEIN, M. C., WIEGERS, T. C. & MATTINGLY, C. J. 2009. Comparative Toxicogenomics Database: a knowledgebase and discovery tool for chemical-gene-disease networks. *Nucleic Acids Res*, 37, D786-92.
- DENG, F. Y., LIU, Y. Z., LI, L. M., JIANG, C., WU, S., CHEN, Y., JIANG, H., YANG, F., XIONG, J. X., XIAO, P., XIAO, S. M., TAN, L. J., SUN, X., ZHU, X. Z., LIU, M. Y., LEI, S. F., CHEN, X. D., XIE, J. Y., XIAO, G. G., LIANG, S. P. & DENG, H. W. 2008. Proteomic analysis of circulating monocytes in Chinese premenopausal females with extremely discordant bone mineral density. *Proteomics*, 8, 4259-72.
- FANOUS, A., WEISS, W., GORG, A., JACOB, F. & PARLAR, H. 2008. A proteome analysis of the cadmium and mercury response in *Corynebacterium glutamicum*. *Proteomics*, 8, 4976-86.

- GAO, Y., PENG, X., ZHANG, J., ZHAO, J., LI, Y., LI, Y., LI, B., HU, Y. & CHAI, Z. 2013. Cellular response of *E. coli* upon Hg<sup>2+</sup> exposure--a case study of advanced nuclear analytical approach to metalloproteomics. *Metallomics*, 5, 913-9.
- HANCZKO, R., FERNANDEZ, D. R., DOHERTY, E., QIAN, Y., VAS, G., NILAND, B., TELARICO, T., GARBA, A., BANERJEE, S., MIDDLETON, F. A., BARRETT, D., BARCZA, M., BANKI, K., LANDAS, S. K. & PERL, A. 2009. Prevention of hepatocarcinogenesis and increased susceptibility to acetaminophen-induced liver failure in transaldolase-deficient mice by N-acetylcysteine. *J Clin Invest*, 119, 1546-57.
- HENSLEY, M. P., TIERNEY, D. L. & CROWDER, M. W. 2011. Zn(II) binding to *Escherichia coli* 70S ribosomes. *Biochemistry*, 50, 9937-9.
- HINTELMANN, H. 2010. Organomercurials. Their formation and pathways in the environment. *Met Ions Life Sci*, 7, 365-401.
- JIANG, H., LI, F., XIE, Y., HUANG, B., ZHANG, J., ZHANG, J., ZHANG, C., LI, S. & XIANG, J. 2009. Comparative proteomic profiles of the hepatopancreas in *Fenneropenaeus chinensis* response to hypoxic stress. *Proteomics*, 9, 3353-67.
- KELLER, A., NESVIZHISKII, A. I., KOLKER, E. & AEBERSOLD, R. 2002. Empirical statistical model to estimate the accuracy of peptide identifications made by MS/MS and database search. *Anal Chem*, 74, 5383-92.
- KELLY, R. T., PAGE, J. S., LUO, Q., MOORE, R. J., ORTON, D. J., TANG, K. & SMITH, R. D. 2006. Chemically etched open tubular and monolithic emitters for nanoelectrospray ionization mass spectrometry. *Anal Chem*, 78, 7796-801.
- KIEBEL, G. R., AUBERRY, K. J., JAITLEY, N., CLARK, D. A., MONROE, M. E., PETERSON, E. S., TOLIC, N., ANDERSON, G. A. & SMITH, R. D. 2006. PRISM: a data management system for high-throughput proteomics. *Proteomics*, 6, 1783-90.
- KIM, S., GUPTA, N. & PEVZNER, P. A. 2008. Spectral probabilities and generating functions of tandem mass spectra: a strike against decoy databases. *J Proteome Res*, 7, 3354-63.
- KRUPP, E. M., MILNE, B. F., MESTROT, A., MEHARG, A. A. & FELDMANN, J. 2008. Investigation into mercury bound to biothiols: structural identification using ESI-ion-trap MS and introduction of a method for their HPLC separation with simultaneous detection by ICP-MS and ESI-MS. *Anal Bioanal Chem*, 390, 1753-64.
- LAVOIE, S. P., MAPOLELO, D. T., COWART, D. M., POLACCO, B. J., JOHNSON, M. K., SCOTT, R. A., MILLER, S. M. & SUMMERS, A. O. 2015. Organic and inorganic mercurials have distinct effects on cellular thiols, metal homeostasis, and Fe-binding proteins in *Escherichia coli*. *J Biol Inorg Chem*, 20, 1239-51.



- LI, P., FENG, X. & QIU, G. 2010. Methylmercury exposure and health effects from rice and fish consumption: a review. *Int J Environ Res Public Health*, 7, 2666-91.
- LIVESAY, E. A., TANG, K., TAYLOR, B. K., BUSCHBACH, M. A., HOPKINS, D. F., LAMARCHE, B. L., ZHAO, R., SHEN, Y., ORTON, D. J., MOORE, R. J., KELLY, R. T., UDSETH, H. R. & SMITH, R. D. 2008. Fully automated four-column capillary LC-MS system for maximizing throughput in proteomic analyses. *Anal Chem*, 80, 294-302.
- LOPEZ-FARRE, A. J., ZAMORANO-LEON, J. J., AZCONA, L., MODREGO, J., MATEOS-CACERES, P. J., GONZALEZ-ARMENGOL, J., VILLARROEL, P., MORENO-HERRERO, R., RODRIGUEZ-SIERRA, P., SEGURA, A., TAMARGO, J. & MACAYA, C. 2011. Proteomic changes related to "bewildered" circulating platelets in the acute coronary syndrome. *Proteomics*, 11, 3335-48.
- MACKEY, T. K., CONTRERAS, J. T. & LIANG, B. A. 2014. The Minamata Convention on Mercury: attempting to address the global controversy of dental amalgam use and mercury waste disposal. *Sci Total Environ*, 472, 125-9.
- MALM, O. 1998. Gold mining as a source of mercury exposure in the Brazilian Amazon. *Environ Res*, 77, 73-8.
- MARKOWITZ, V. M., CHEN, I. M., PALANIAPPAN, K., CHU, K., SZETO, E., GRECHKIN, Y., RATNER, A., JACOB, B., HUANG, J., WILLIAMS, P., HUNTEMANN, M., ANDERSON, I., MAVROMATIS, K., IVANOVA, N. N. & KYRPIDES, N. C. 2012. IMG: the Integrated Microbial Genomes database and comparative analysis system. *Nucleic Acids Res*, 40, D115-22.
- MARSANO, F., BOATTI, L., RANZATO, E., CAVALETTO, M., MAGNELLI, V., DONDERO, F. & VIARENGO, A. 2010. Effects of mercury on Dictyostelium discoideum: proteomics reveals the molecular mechanisms of physiological adaptation and toxicity. *J Proteome Res*, 9, 2839-54.
- MASIP, L., VEERAVALLI, K. & GEORGIU, G. 2006. The many faces of glutathione in bacteria. *Antioxid Redox Signal*, 8, 753-62.
- MASON, R. P., FITZGERALD, W. F. & MOREL, F. M. M. 1994. The Biogeochemical Cycling of Elemental Mercury - Anthropogenic Influences. *Geochimica Et Cosmochimica Acta*, 58, 3191-3198.
- MIYAKE, Y., TOGASHI, H., TASHIRO, M., YAMAGUCHI, H., ODA, S., KUDO, M., TANAKA, Y., KONDO, Y., SAWA, R., FUJIMOTO, T., MACHINAMI, T. & ONO, A. 2006. MercuryII-mediated formation of thymine-HgII-thymine base pairs in DNA duplexes. *J Am Chem Soc*, 128, 2172-3.
- MONROE, M. E., TOLIC, N., JAITLY, N., SHAW, J. L., ADKINS, J. N. & SMITH, R. D. 2007. VIPER: an advanced software package to support high-throughput LC-MS peptide identification. *Bioinformatics*, 23, 2021-3.

- NAGYPAL, I. & BECK, M. T. 1982. Diagrams for complete representation of binary mononuclear complex systems. *Talanta*, 29, 473-7.
- NEIDHARDT, F. C., BLOCH, P. L. & SMITH, D. F. 1974. Culture medium for enterobacteria. *J Bacteriol*, 119, 736-47.
- NORN, S., PERMIN, H., KRUSE, E. & KRUSE, P. R. 2008. [Mercury--a major agent in the history of medicine and alchemy]. *Dan Medicinhist Arbog*, 36, 21-40.
- PARKS, J. M., JOHS, A., PODAR, M., BRIDOU, R., HURT, R. A., JR., SMITH, S. D., TOMANICEK, S. J., QIAN, Y., BROWN, S. D., BRANDT, C. C., PALUMBO, A. V., SMITH, J. C., WALL, J. D., ELIAS, D. A. & LIANG, L. 2013. The genetic basis for bacterial mercury methylation. *Science*, 339, 1332-5.
- PETERSON, J. D., UMayAM, L. A., DICKINSON, T., HICKEY, E. K. & WHITE, O. 2001. The Comprehensive Microbial Resource. *Nucleic Acids Res*, 29, 123-5.
- PITTS, K. E. & SUMMERS, A. O. 2002. The roles of thiols in the bacterial organomercurial lyase (MerB). *Biochemistry*, 41, 10287-96.
- PODZIMEK, S., PROCHAZKOVA, J., BULTASOVA, L., BARTOVA, J., ULCOVA-GALLOVA, Z., MRKLAS, L. & STEJSKAL, V. D. 2005. Sensitization to inorganic mercury could be a risk factor for infertility. *Neuro Endocrinol Lett*, 26, 277-82.
- POLACCO, B. J., PURVINE, S. O., ZINK, E. M., LAVOIE, S. P., LIPTON, M. S., SUMMERS, A. O. & MILLER, S. M. 2011. Discovering mercury protein modifications in whole proteomes using natural isotope distributions observed in liquid chromatography-tandem mass spectrometry. *Mol Cell Proteomics*, 10, M110 004853.
- PRANJIC, N., SINANOVIC, O. & JAKUBOVIC, R. 2003. Chronic psychological effects of exposure to mercury vapour among chlorine-alkali plant workers. *Med Lav*, 94, 531-41.
- QI, Y., CHIU, J. F., WANG, L., KWONG, D. L. & HE, Q. Y. 2005. Comparative proteomic analysis of esophageal squamous cell carcinoma. *Proteomics*, 5, 2960-71.
- RAO, Y., XIANG, B., BRAMANTI, E., D'ULIVO, A. & MESTER, Z. 2010. Determination of thiols in yeast by HPLC coupled with LTQ-orbitrap mass spectrometry after derivatization with p-(Hydroxymercuri)benzoate. *J Agric Food Chem*, 58, 1462-8.
- REED, T. T., PIERCE, W. M., MARKESBERY, W. R. & BUTTERFIELD, D. A. 2009. Proteomic identification of HNE-bound proteins in early Alzheimer disease: Insights into the role of lipid peroxidation in the progression of AD. *Brain Res*, 1274, 66-76.
- RICHARDSON, G. M., WILSON, R., ALLARD, D., PURTILL, C., DOUMA, S. & GRAVIERE, J. 2011. Mercury exposure and risks from dental amalgam in the US population, post-2000. *Sci Total Environ*, 409, 4257-68.

- RINGHAM, H., BELL, R. L., SMEJKAL, G. B., BEHNKE, J. & WITZMANN, F. A. 2007. Application of pressure cycling technology to tissue sample preparation for 2-DE. *Electrophoresis*, 28, 1022-4.
- RUIZ-ROMERO, C., CALAMIA, V., MATEOS, J., CARREIRA, V., MARTINEZ-GOMARIZ, M., FERNANDEZ, M. & BLANCO, F. J. 2009. Mitochondrial dysregulation of osteoarthritic human articular chondrocytes analyzed by proteomics: a decrease in mitochondrial superoxide dismutase points to a redox imbalance. *Mol Cell Proteomics*, 8, 172-89.
- SMITH, R. D., ANDERSON, G. A., LIPTON, M. S., PASA-TOLIC, L., SHEN, Y., CONRADS, T. P., VEENSTRA, T. D. & UDSETH, H. R. 2002. An accurate mass tag strategy for quantitative and high-throughput proteome measurements. *Proteomics*, 2, 513-23.
- SMITH, T., PITTS, K., MCGARVEY, J. A. & SUMMERS, A. O. 1998. Bacterial oxidation of mercury metal vapor, Hg(0). *Appl Environ Microbiol*, 64, 1328-32.
- SUGIURA, Y., TAMAI, Y. & TANAKA, H. 1978. Selenium protection against mercury toxicity: high binding affinity of methylmercury by selenium-containing ligands in comparison with sulfur-containing ligands. *Bioinorg Chem*, 9, 167-80.
- SUMMERS, A. O., WIREMAN, J., VIMY, M. J., LORSCHIEDER, F. L., MARSHALL, B., LEVY, S. B., BENNETT, S. & BILLARD, L. 1993. Mercury released from dental "silver" fillings provokes an increase in mercury- and antibiotic-resistant bacteria in oral and intestinal floras of primates. *Antimicrob Agents Chemother*, 37, 825-34.
- SWITZAR, L., NICOLARDI, S., RUTTEN, J. W., OBERSTEIN, S. A., AARTSMA-RUS, A. & VAN DER BURGT, Y. E. 2016. In-Depth Characterization of Protein Disulfide Bonds by Online Liquid Chromatography-Electrochemistry-Mass Spectrometry. *J Am Soc Mass Spectrom*, 27, 50-8.
- TAKASHIMA, M., KURAMITSU, Y., YOKOYAMA, Y., IIZUKA, N., HARADA, T., FUJIMOTO, M., SAKAIDA, I., OKITA, K., OKA, M. & NAKAMURA, K. 2006. Proteomic analysis of autoantibodies in patients with hepatocellular carcinoma. *Proteomics*, 6, 3894-900.
- TATUSOV, R. L., GALPERIN, M. Y., NATALE, D. A. & KOONIN, E. V. 2000. The COG database: a tool for genome-scale analysis of protein functions and evolution. *Nucleic Acids Res*, 28, 33-6.
- TRUMPLER, S., LOHMANN, W., MEERMANN, B., BUSCHER, W., SPERLING, M. & KARST, U. 2009. Interaction of thimerosal with proteins-ethylmercury adduct formation of human serum albumin and [small beta]-lactoglobulin A. *Metallomics*, 1, 87-91.
- WATTON, S. P., WRIGHT, J. G., MACDONNELL, F. M., BRYSON, J. W., SABAT, M. & O'HALLORAN, T. V. 1990. Trigonal mercuric complex of an aliphatic thiolate: a spectroscopic and structural model for the receptor site in the mercury(II) biosensor MerR. *Journal of the American Chemical Society*, 112, 2824-2826.

WEERAPANA, E., WANG, C., SIMON, G. M., RICHTER, F., KHARE, S., DILLON, M. B., BACHOVCHIN, D. A., MOWEN, K., BAKER, D. & CRAVATT, B. F. 2010. Quantitative reactivity profiling predicts functional cysteines in proteomes. *Nature*, 468, 790-5.

WHO 1976. Environmental Health Criteria 1: Mercury.

WU, M., BAI, X., XU, G., WEI, J., ZHU, T., ZHANG, Y., LI, Q., LIU, P., SONG, A., ZHAO, L., GANG, C., HAN, Z., WANG, S., ZHOU, J., LU, Y. & MA, D. 2007. Proteome analysis of human androgen-independent prostate cancer cell lines: variable metastatic potentials correlated with vimentin expression. *Proteomics*, 7, 1973-83.

ZENG, Q., STALHANDSKE, C., ANDERSON, M. C., SCOTT, R. A. & SUMMERS, A. O. 1998. The core metal-recognition domain of MerR. *Biochemistry*, 37, 15885-95.

ZHANG, J., WANG, K., ZHANG, J., LIU, S. S., DAI, L. & ZHANG, J. Y. 2011. Using proteomic approach to identify tumor-associated proteins as biomarkers in human esophageal squamous cell carcinoma. *J Proteome Res*, 10, 2863-72.

**Table 3.1. Raw Data Summary**

<b>Category</b>	<b>Criteria to accept SEQUEST ID</b>	<b>Accepted counts</b>	<b>False discovery rate (%)</b>
Proteins: >1 peptide/protein	<ul style="list-style-type: none"> <li>• MSGF &lt; 1.6e-10</li> <li>• Peptide &gt; 1 spectra</li> <li>• Protein &gt; 1 peptide</li> </ul>	Spectra: 765,437 Peptides: 17,070 Proteins: 1301 SUM= 768,327	Spectra: 0.001 Peptides: 0.02 Proteins: 0.08
Proteins: only 1 peptide	<ul style="list-style-type: none"> <li>• MSGF &lt; 1e-11</li> <li>• Peptide &gt; 1 spectrum</li> <li>• Semi- or fully tryptic</li> </ul>	Spectra: 2890 Peptides: 259 Proteins: 259 SUM = 1560	Spectra: 0.4 Peptides: 2 Proteins: 2
Adducts: Cys-PhenylHg or Cys-Hg(II)	<ul style="list-style-type: none"> <li>• Protein ID'd above</li> <li>• MSGF &lt; 5e-7</li> <li>• PeptideProphet &gt; 0.8</li> <li>• Fully tryptic</li> </ul>	Spectra: 8142 Peptides: 646 Proteins: 307	Reversed Decoys: 0.0 Hg-free controls: Spectra: 0.9 Peptides: 0.8 Proteins: 1.6
Total	As indicated above	Spectra: 776,300 Peptides: 17,975 Proteins: 1560	Spectra: 0.003 Peptides: 0.06 Proteins: 0.5

" MS Generating Function (MSGF) generates rigorous p-values (spectral probabilities) of spectral interpretations. Given peptide-spectrum matches as input, MSGF outputs p-values that can be used to discriminate correct and false identifications (Kim et al., 2008). PeptideProphet generates statistical validation of MS/MS search engines' spectra-to-peptide sequence assignments. By employing database search scores, number of tryptic termini, number of missed cleavages, and other information, the method learns to distinguish correctly from incorrectly assigned peptides in the data set and computes for each peptide assigned to an MS/MS spectrum its probability of being correct (Keller et al., 2002).

**Table 3.2. Potentially Modifiable Cysteines vs. PhHg/Hg Modified Cysteines Observed**

<b>Total proteins encoded by genome or in COGs annotation</b>	<b>Observations (spectral counts)</b>
Proteins encoded: 4,321 <sup>a</sup>	1,560 (768,327)
Proteins in COGs: 3,497 <sup>a</sup>	1,474 (764,826)
Cys proteins encoded: 3,594	642 (48,510)
Cys proteins in COGs: 3,037	626 (47,828)
Cys sites encoded in genome: 15,379 <sup>b</sup> Sites in 1,560 observed proteins: 4,954	1,361 (48,510)
PhHg/Hg-modified proteins	307 (8,142) <sup>c</sup>

<sup>a</sup> based on *E. coli* K12 MG1655 from IMG database (<https://img.jgi.doe.gov>)

<sup>b</sup> based on protein sequences from ASAP database(<https://www.genome.wisc.edu/tools/asap.htm>)

<sup>c</sup> only 303 modified proteins (8,074 spectra) are included in COGs annotation.

**Table 3.3. Select human homologs of Hg-vulnerable *E. coli* proteins with high disease inference scores.**

<b><i>E. coli</i> protein description</b>	<b>Homology<sup>a</sup></b>	<b>Human associated disease<sup>b</sup></b>
transaldolase B	94	hepatocellular carcinoma (Hanczko et al., 2009)
alkyl hydroperoxide reductase	55	Hepatocellular (Chen et al., 2010) and squamous cell (Zhang et al., 2011) carcinoma; prostatic (Wu et al., 2007) and esophageal (Zhang et al., 2011) neoplasms
succinate dehydrogenase	73	mitochondrial complex II deficiency; osteoarthritis (Ruiz-Romero et al., 2009)
glyceraldehyde-3-phosphate dehydrogenase (GAPDH)	75	acute coronary syndrome (Lopez-Farre et al., 2011); anoxia (Jiang et al., 2009); hepatocellular (Takashima et al., 2006, Chen et al., 2010) and squamous cell carcinoma (Chen et al., 2004); esophageal (Qi et al., 2005) and mouth (Chen et al., 2004) neoplasms; osteoarthritis (Ruiz-Romero et al., 2009); osteoporosis (Deng et al., 2008)
F1 sector of ATP synthase, alpha subunit	67	Alzheimer disease (Reed et al., 2009)

<sup>a</sup> Homology is percent identity of mercury modified peptide to matching human protein sequence (taxid:9606) from BLASTp (<http://blast.ncbi.nlm.nih.gov/Blast.cgi>) search of nr database. See Table C.S6 for full results and details.

<sup>b</sup> Diseases with double digit inference scores from Comparative Toxicogenomics Database (<http://ctdbase.org/about/dataStatus.go>).

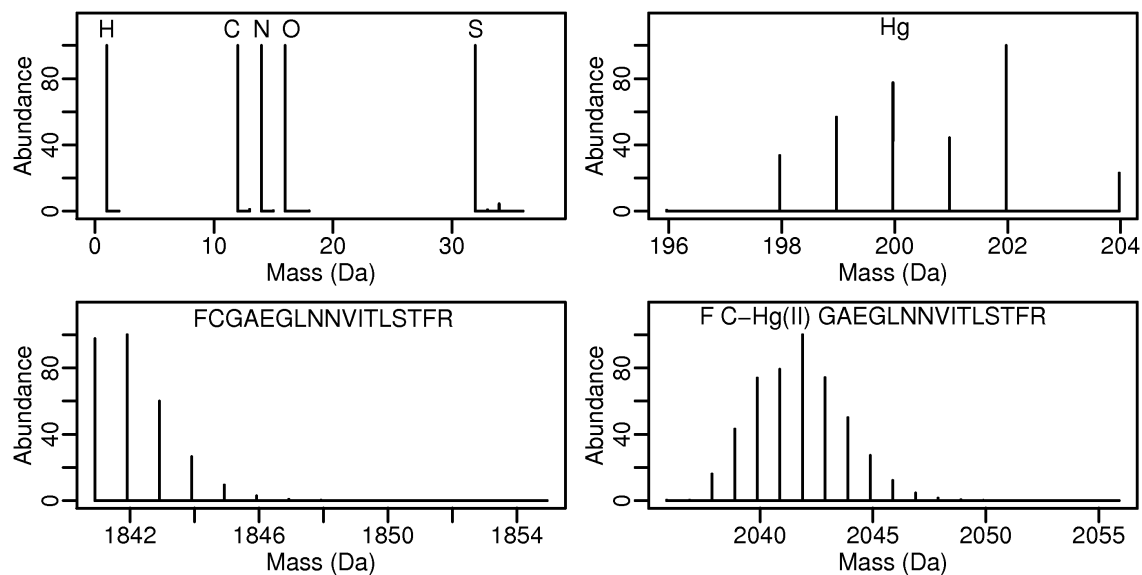


**Figure 3.1. Distinguishing a Hg-containing peptide from its Hg-free form**

**by stable isotope distribution.** *Upper panels:* Stable isotopes of peptide components hydrogen, carbon, nitrogen, oxygen and sulfur (*left*) and of mercury (*right*). *Lower panels:* Stable isotope distribution of a typical peptide without (*left*) and with (*right*) a mercury adduct.



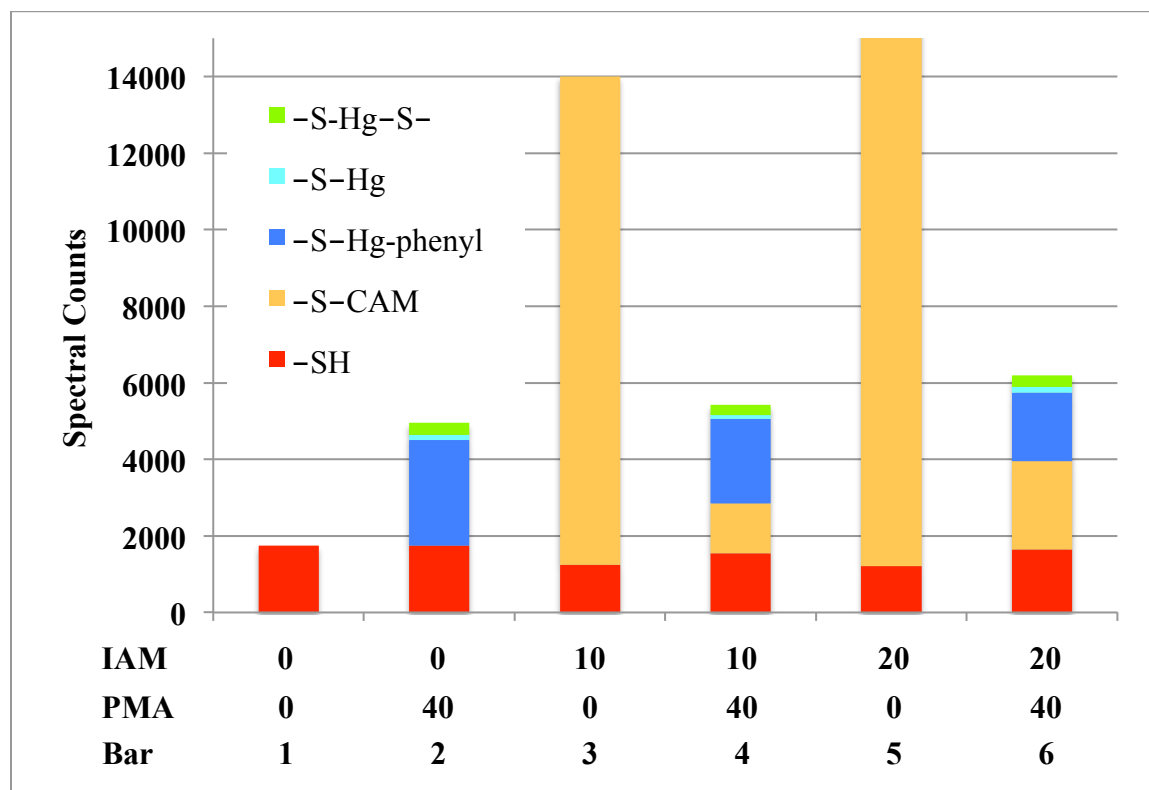


**Figure 3.2. Cysteine modifications differ by treatment condition.** Bar heights are counts of spectra with the cysteine modification indicated by bar color from 3 biological replicates

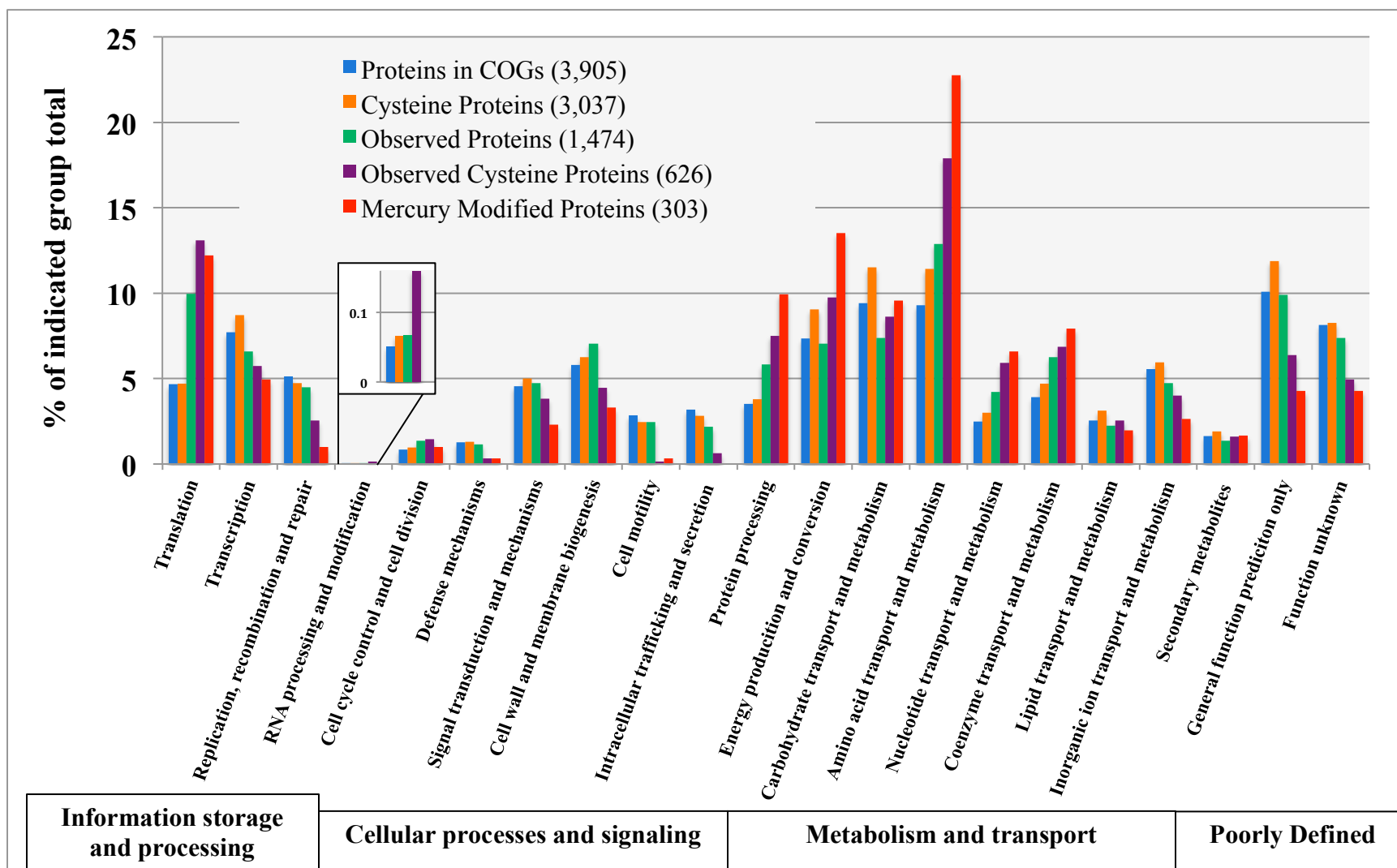


**Figure 3.3. COG functional categories of observed proteins compared to those in the genome.** Distribution of protein observations by function. The Y-axis shows the percent of each category total (indicated by colors). Only 3,905 of the 4,321 genome-encoded proteins (<https://img.jgi.doe.gov>) are included in the COG functional annotation, so totals for each category reflect only proteins included in COGs. The X-axis lists the COG functions.

**CHAPTER 4**

**TRANSCRIPTIONAL RESPONSES OF *ESCHERICHIA COLI* DURING RECOVERY  
FROM INORGANIC OR ORGANIC MERCURY EXPOSURE<sup>1</sup>**

---

<sup>1</sup>LAVOIE, S.P., SUMMERS, A.O.; To be submitted to *BMC Genomics*.

## ABSTRACT

The protean chemical properties of mercury have long made it attractive for various applications, but its toxicity requires that anthropogenic impact on the environment and health be limited. Mercury exists in a multiple chemical forms, but there remains a lack of understanding of how toxicity mechanisms differ between inorganic and organic mercurials at the molecular level. The effects over time on the transcriptome of exponential phase *E. coli* were compared during sub-acute exposure to mercuric chloride (HgCl<sub>2</sub>) and phenylmercuric-acetate (PMA) using RNA-Seq. Bioinformatics analysis of differential gene expression revealed distinct responses to both mercurials throughout recovery. Gene expression was more dynamic over time for HgCl<sub>2</sub>, but PMA altered expression of more genes early in exposure. The down-regulated response was highly conserved between mercurials early in exposure, while up-regulated gene response was more unique to each compound. Energy production, metabolism and most uptake pathways were repressed for both compounds, while nearly all stress response systems were up-regulated by at least one of the compounds during recovery, including: oxidative stress, heat shock, acid stress, metals homeostasis, biofilm regulation, and antibiotic resistance. Only recently has the importance of mercury speciation been recognized in regards to toxicity mechanisms and these results further emphasize that different mercurials have distinct effects. This study provides a highly resolved view of transcriptional response to each mercurial over time in prokaryotic model, which provides insights for animal model studies and how mercury exposure might affect microbial communities.

## INTRODUCTION

Mercury is a metallic element that serves no biological function and is of concern as an environmental toxin. Global mercury emissions are 6500 to 8500 Mg annually and roughly 30 to 50% are from anthropogenic sources (Driscoll et al., 2013, Pirrone et al., 2009), but have previously been estimated to account for up to two-thirds (Mason et al., 1994). Mercury in the environment undergoes a complex biogeochemical cycle and exists in multiple chemical forms that are often microbial mediated transformations (Barkay et al., 2003). Mercury occurs naturally as the insoluble HgS ore (cinnabar), as inorganic complexes of  $\text{Hg}^{+2}$ ,  $\text{Hg}^{+1}$ , or  $(\text{Hg}_2)^{2+}$  of varying solubility depending on ligands, and as organomercurials generated by microbial and anthropogenic processes.

Major sources of chronic mercury exposure in humans are from dental amalgam fillings (Crinnion, 2000, Richardson et al., 2011), consumption of fish containing methylmercury (Diez, 2009), and areas surrounding artisanal gold mining operations (Malm, 1998). Organomercurials, like phenyl-mercury, have historically been used in medical, industrial and agricultural applications as an antimicrobial and fungicide agent (Clarkson and Magos, 2006, Hintelmann et al., 1995, Tchounwou et al., 2003). Toxic effects of mercury exposure in humans are associated with neurological, kidney, liver, gastrointestinal, and developmental disorders (Clarkson and Magos, 2006, Davidson et al., 2004, Valko et al., 2005, Yorifuji et al., 2008, Zahir et al., 2005).

Like other ubiquitous electrophilic metals (Cd, Pb, As), there is no single biochemical target for mercury damage. Mercury has a strong affinity for sulfur and selenium ligands (Cheesman et al., 1988, Oram et al., 1996) and therefore is known to target the cellular thiol pool, composed of glutathione and cysteine thiol groups of proteins (Clarkson and Magos, 2006). This depletion of the cellular thiol pool induces oxidative stress, but mercury does not undergo

Fenton-type chemistry like iron or copper to produce reactive oxygen species (Lund et al., 1991). Previous work using acute exposure in *E. coli* found that mercury targets thiols, metal cofactor binding sites, and disrupts iron homeostasis and the electrolyte balance of the cell (LaVoie et al., 2015).

Studies often generalize the effects of exposure to inorganic and organic mercury compounds as having similar effects, but understanding of distinct toxicity mechanisms for each has remained incomplete. One recent study used a microarray approach to directly compare varying concentrations of mercuric chloride (HgCl<sub>2</sub>) and methylmercury exposure in *C. elegans* and found that the transcriptional response and toxicity was unique for each compound (McElwee et al., 2013). In the present study, RNA-Seq was used to examine the genome wide effects of HgCl<sub>2</sub> and phenylmercuric-acetate (PMA) exposure on *E. coli* K-12 MG1655 over time. This is the first study to examine the transcriptional response to mercury exposure in a microorganism and the only study to directly compare effects of different compounds over time. The changes in gene expression were highly dynamic over time and unique for each compound, which highlights distinct toxicity mechanisms between inorganic and organic mercury exposure.

## **MATERIALS AND METHODS**

### *Cell cultures.*

For each biological RNA-Seq replicate, *E. coli* K-12 MG1655 was subcultured from cryostorage on Luria-Bertani (LB) agar overnight at 37°C. A half-dozen well-isolated colonies were used to inoculate a 20 ml starter culture in Neidhardt MOPS minimal medium (Neidhardt et al., 1974) (0.2% final glucose concentration) with 20 mg/L uracil and 500 µg/L thiamine, which was incubated at 37°C with shaking at 250 rpm overnight (~18 hr). The overnight starter culture

was diluted 1:30 to initiate the experimental culture and divided into three 500 ml flasks with 100 ml in each, which were incubated at 37°C with shaking at 250 rpm. Growth was monitored until  $OD_{595} \approx 0.470$  (~ 200 min), then two of the cultures were exposed to 3  $\mu$ M mercuric chloride ( $HgCl_2$ ) or 3  $\mu$ M phenylmercuric-acetate (PMA) and the third was left as an unexposed control. These mercurial exposures were chosen from prior pilot experiments to find exposure conditions ( $OD_{595}$ , mercurial concentration and sampling times), which displayed a marked decrease in growth rate relative to the unexposed control and subsequent restoration of rapid growth rate (i.e. recovery) within 1 hr after mercury exposure. Duplicate 1 ml aliquots of each culture were collected at 0 (unexposed control only), 10, 30, 60 min after mercury exposure and immediately centrifuged at 21K rpm, for 3 min at 4°C. Spent medium was aspirated and cell pellets were frozen at -70°C in storage freezer within 5 min after collection. Seven biological replicates were prepared following this protocol (average variance across 90 min exposure time points for all cultures ranged from 0.0019 – 0.0073 and the three with the lowest variance between growth curves were prepared for RNA-Seq (avg. variance ranged from 0.0007 – 0.0017).

#### *Purification of mRNA*

One cell pellet from each condition and sampling time was thawed on ice; total RNA was isolated by *RNAsnap*<sup>™</sup> (Stead et al., 2012) and stored at -70°C. DNA contamination was removed by two treatments with Turbo-DNase (Ambion; Life Technologies). RNA concentrations and  $A_{260}/A_{280}$  ratios were determined using Nanodrop<sup>™</sup> 1000 (Thermo Scientific). Ribosomal RNA depletion was performed with the Ribo-Zero<sup>™</sup> rRNA removal kit for Gram-negative bacteria (Epicentre) and concentrated using RNA Clean and Concentrator<sup>™</sup> -5 columns



(Zymo Research) following manufacturer's instructions. Purified mRNA was quantified using Nanodrop<sup>™</sup> and stored at -70°C.

### *Library Preparation and Next-generation Sequencing*

The quality and quantity of rRNA-depleted RNA was assessed on a 2100 Bioanalyzer RNA pico chip (Agilent Technologies) using manufacturer's recommendations. Next generation sequencing libraries were prepared using the Kapa biosystems NGS stranded library prep kit for RNA-Seq with dual indexed Illumina adapters. Library insert size was ~150 bp, as determined by high sensitivity NGS fragment analysis kit for Fragment Analyzer<sup>™</sup> (Advanced Analytical Technologies) using manufacturer's instructions. Quantification of each library was done with a Qubit<sup>®</sup> 2.0 fluorometer (Life Technologies) and all 30 libraries were pooled in equal concentrations. The library preparation, quality analysis, and pooling were performed by the Georgia Genomics Facility (<http://dna.uga.edu>). Paired-end (2 x 50 bp) sequencing of the pooled libraries using the Illumina HiSeq 2000 platform was performed by the HudsonAlpha Institute for Biotechnology Genomic Services Laboratory (<http://gsl.hudsonalpha.org>). See Table D.S1 for index and filename information for data uploaded to NCBI Gene Expression Omnibus database (<http://www.ncbi.nlm.nih.gov/geo/>) with dataset ID: To Be Determined.

### *Data processing and Differential Expression Analysis*

Quality control processing of sequence data was performed using tools in Galaxy (<https://galaxyproject.org>), installed on the Georgia Advanced Computing Resource Center at University of Georgia. The FASTX tools in Galaxy ([http://hannonlab.cshl.edu/fastx\\_toolkit](http://hannonlab.cshl.edu/fastx_toolkit)) were used for filtering by quality (80% of sequence  $\geq$  quality score of 20), then reads were

trimmed at both 5' and 3' ends using a window and step size of 1 with quality score  $\geq 20$ . Forward- and reverse-read mate-pairs were assembled and then aligned to *Escherichia coli* MG1655 K-12 genome using Bowtie2 (Langmead and Salzberg, 2012). SAMtools (Li et al., 2009) was used to convert Bowtie2 output (.bam file) to SAM format. The number of sequence reads that aligned to features in annotation file (Escherichia\_coli\_str\_k\_12\_substr\_mg1655.GCA\_000005845.2.24.gtf from <http://bacteria.ensembl.org>) were tabulated from the resulting SAM alignment files using the HTSeq-count program (Anders et al., 2015) with intersection non-empty mode. Mapped read counts were analyzed for differential expression ( $\text{FDR} \leq 0.01$ , fold-change  $\geq 2$ ) using the baySeq package in R (Hardcastle and Kelly, 2010). Within baySeq, two-way comparisons using quantile normalization were made for all three biological replicate transcriptomes over time for HgCl<sub>2</sub> exposure or PMA exposure versus the unexposed control. We also examined changes over time in the unexposed control culture itself.

## RESULTS

### *Effects of sub-acute mercury exposure on growth of MG1655.*

We defined sub-acute exposure as the concentration of mercury that inhibited growth relative to the unexposed control but allowed cells to resume growth within 1 hour or approximately one generation in this medium (Figure 4.1a, Figure D.S1). Based on pilot experiments the appropriate dose proved to be 3  $\mu\text{M}$  for both mercurials. Exposure to 4 - 5  $\mu\text{M}$  HgCl<sub>2</sub> prevented growth resumption beyond 1 hr and 2.5  $\mu\text{M}$  exposure to either mercurial did not consistently retard growth compared to the unexposed control. Cells were more tolerant to PMA and growth recovery from 5  $\mu\text{M}$  exposure was similar to 3  $\mu\text{M}$  exposure (data not shown).

Mercuric chloride slowed growth from 0 – 10 min, arrested growth between 10 – 30 min, growth recovery began between 30 – 60 min, and close to normal growth rate was achieved beyond 75 min (Figure 4.1a). PMA exposure resulted in a slight decrease in optical density (OD) between 0 – 10 min after exposure consistent with some cell lysis (Schaechter and Santomassino, 1962), but growth recovery began between 10 – 30 min, and a near normal growth rate was achieved after 30 min. The lack of apparent lysis by divalent  $\text{HgCl}_2$  may be due to its ability to cross-link membrane proteins via their cysteines, which is not possible for monovalent PMA.

#### *Transcriptomic analysis of response to inorganic or organic mercury*

##### *Summary of RNA-Seq data:*

Paired-end libraries averaged over 9.5 million reads and mapped reads provided an average of 175X coverage (Figure D.S2). The sequencing data was of high quality, requiring that only 11% low-quality reads be removed. Of the high quality reads, 97% of reads mate-paired, 99.4% of paired reads mapped to the genome and 82% of reads mapped to an annotated genome feature on average from all libraries.

Overall 89% of annotated mapped reads were to coding regions (CDS) and 4% to non-coding RNAs (ncRNA) based on raw un-normalized read counts per gene output from HTseq-count program (Anders et al., 2015)(Figure D.S3, Table D.S2). Mapped reads to rRNA only constituted 0.3% of total reads (std. dev. = 0.425) on average for all libraries (Table D.S2). Pearson correlations of raw read counts confirmed that no strong biases were introduced in biological replicates for each condition (Figure D.S4).

*Summary of differentially expressed genes:*

Differentially expressed genes (DEG) for each condition and time point were determined by pairwise comparisons of mercury exposure conditions relative to unexposed at the corresponding time point and unexposed control alone throughout exposure period (Figure D.S5). At 10 minutes after exposure, expression of 41% or 49% of the 4,472 non-rRNA genes changed significantly for HgCl<sub>2</sub> or PMA-exposed cells respectively, compared to unexposed cells at the same time point. At 30 min, 32% of genes in the HgCl<sub>2</sub>-exposed cells were differentially expressed, while growth remained arrested (Figure 4.1, red). In contrast, PMA-exposed cells at 30 min began to recover their prior growth rate (Figure 4.1, green), but 45% of their genes remained differentially expressed. By 60 min, the PMA-exposed cells were growing at nearly their pre-exposure rate and only 1.5% of genes were differentially expressed, whereas the HgCl<sub>2</sub>-exposed cells were still growing more slowly than pre-exposure with 13% of their genes still differentially expressed compared to the unexposed cells.

*HgCl<sub>2</sub> and PMA transcriptional responses are not the same.*

We anticipated that differential gene expression during each mercury exposure condition, compared to the unexposed cells, would change over time as the cells transitioned from initial growth stasis to recovery of growth. We also expected that some responses would be similar because both mercurials are thiophilic and will bind to glutathione, which acts as the cellular thiol redox buffer, and protein cysteine residues of proteins. However, since there are physiological differences and protein site preferences for each compound in responses to acute Hg- or PMA- exposure (LaVoie et al., 2015 and Zink et. al. in preparation) we aimed here at a

lower exposure using a longitudinal protocol to discern more subtle distinctions between these mercurials as the cells experience stasis and then recover their growth rate.

Exposure to PMA resulted in 1,631 (917 up and 714 down) genes that overlap at both 10 min and 30 min (Figure 4.2), with 529 and 350 unique to 10 min and 30 min, respectively. The culture had recovered normal growth by the 60 min time point and therefore only 19 genes were shared at all times. There were very few unique genes to the 60 min time point and over 50% were unique only because their expression level was a reversal of an earlier time point (i.e. up early and down late or vice-versa), which suggests the cell is simply attempting to restore normal equilibrium of messages for these genes.

HgCl<sub>2</sub> exposure was different from PMA in that more genes overlapped between at all times, but fewer between just 10 and 30 min. This is in part due to a greater percentage of total DEGs being unique to 10 min, 44% for HgCl<sub>2</sub> compared to only 24% in the PMA condition. DEGs unique to 30 min were similar for HgCl<sub>2</sub> and PMA, 20% and 17% respectively. Shared genes made up 23% (734 total, 335 up and 399 down) of differentially expressed genes that overlap at both 10 and 30 min, while 7% (267 total, 117 up and 150 down) of genes were shared over all times in the HgCl<sub>2</sub> exposure. The more gradual decrease in DEGs over time for HgCl<sub>2</sub> (22% decrease for 10-30 min and 61% for 30-60 min) is reflected in the slower recovery of normal growth rate, observed in growth curve, compared to the PMA exposure (8% decrease for 10-30 min and 97% for 30-60 min).

Comparison of differentially expressed genes shared between HgCl<sub>2</sub> and PMA at each time point (Figure 4.3) revealed that the transcriptional responses were not the same. For up-regulated genes, the number of unique genes to PMA was greater than the number of genes in common between the two mercurials. The opposite was true for down-regulated genes, where

both mercurials had more genes in common than genes that were unique, with the exception of the 60 min time point. More than 98% of the down-regulated genes were shared at the 10 min time point and roughly 70% at the 30 min time point for both mercurials. This suggests that the down-regulated responses are more conserved, while the diversity in the up-regulated genes further illustrates how the stress response induced by these two mercurials are distinct.

Heatmap analysis of the log-fold change data (Figure 4.4) for each condition helps to reveal that *E. coli* appears to have a more pre-programmed stress response to PMA exposure, since most of the differentially expressed genes are the same for the first 30 minutes and then gene expression returns to normal as growth is fully recovered by 60 minutes post-exposure. This is in contrast to HgCl<sub>2</sub> exposure, which displays more variability in gene expression over the exposure period examined. This profile suggests that the types of stress and resources needed by the cell to survive and recover growth are distinct and changing over time. This view of the differential expressed genes helps to highlight the numbers presented in Figure 4.2 and Figure 4.3 and shows that expression of individual genes is more dynamic at each time point in the HgCl<sub>2</sub> exposure.

Up-regulated genes with a fold-change  $\geq 32$  ( $\log_2$  fold-change  $\geq 5$ ) in at least one time point are shown in Table 4.1 for HgCl<sub>2</sub> exposure and Table 4.2 for PMA exposure. Even though more DEGs were observed in the PMA exposure, only 20 genes had a  $\geq 32$  fold-change, while HgCl<sub>2</sub> had 39 genes and only 6 of these genes overlap between the two mercurials. The late phase response of genes that had no change at 10 min, but were differentially expressed at 60 min provides a view of changes that occur during recovery phase (Table D.S3). There were 95 genes up-regulated and 140 genes down-regulated for HgCl<sub>2</sub> exposure. Approximately a third of these genes for both up and down were involved in energy production and metabolic pathways.

Roughly 60% of these genes overlap with genes that were differentially expressed during the first 30 min of PMA exposure, but expression changes are delayed until later in the HgCl<sub>2</sub> exposure. In contrast only 6 genes were up and 10 down for late-phase response to PMA exposure (Table D.S3).

We have previously observed mercury bound to proteins by proteomics analysis (Zink et. al. in preparation), and transcriptional response was examined for the 310 proteins observed with mercury modifications (Table D.S4). Over the first 30 minutes of exposure for both mercurials, the transcription of these genes increased for 15-21%, decreased for 31-38%, and remained unchanged from the unexposed control for 45-53%. Therefore mercury binding to proteins does not appear to result in a clear expression response pattern. But despite the lack of a clear correlation between protein binding and gene expression changes, some protein functions were targeted more than others (ATP-synthase, ribosomal proteins, and some amino acid biosynthesis genes) and all of these genes had interesting transcriptional responses to mercury exposure, which are discussed further below.

#### *Differentially expressed genes grouped by functional category.*

The sums of differentially expressed genes for each condition were grouped by Clusters of Orthologous Groups (COGs) to identify differences in cellular response based on functional roles of genes between the two mercurials (Figure 4.5). Overall most categories share some similarities for both mercurials during the first 30 min of exposure, despite clear differences the response pattern to each compound over time in the heatmap (Figure 4.4), but not all categories were effected the same by both mercurials. Across all functional categories, transcriptional response to PMA exposure remains much more static over the first thirty minutes of exposure,

compared to inorganic mercury, which divided into three trend types. First, the number of up-regulated genes decrease and number of down-regulated genes increase from 10 min to 30 min for categories C, E, and G, which suggests a transition or delayed response to down-regulate energy production and metabolism of amino acids and carbohydrates. Second, a decrease in both up and down DEGs from 10 min and 30 min for categories H, I, J, K, L, M, O, P, Q, R, S, T, U, and V. Third, a trend unique to the cell motility category (N) which decreased moderately over time for up-regulated genes, but down-regulated genes remained roughly equal across all times. COGs only provides functional annotations for 3,497 of 4,497 total genes, so functional categories discussed below in more detail are not limited to COGs annotated genes.

#### *DNA replication and repair.*

Genes responsible for replication and repair of DNA responded similarly for both mercurials. DNA polymerase genes capable of translesion synthesis (*polB*, *dinB*, *umuCD*) were up-regulated more in HgCl<sub>2</sub> conditions. A number of DNA repair genes were up-regulated only for HgCl<sub>2</sub>, including *xthA*, *uvrAB* and *mutM* at 10 and 30 min and *recN* at all times. Conversely, *mutH* and *mutY* were only up-regulated for PMA at 10 and 30 min. The *recA* gene serves multiple roles in DNA repair, but is activated by strand breaks and induces SOS response (Kuzminov, 1999, Lusetti and Cox, 2002). It was up-regulated for both mercurials, but 10 fold for Hg at 10 min versus only two fold for PMA at 10 min, while being roughly equal at 30 min and no change at 60 min. Somewhat surprisingly *recBCD* genes, which are needed for strand break repair, showed either no change or negative fold-change. Transcription for a number of other genes involved in repair and methylation (*recG*, *recF*, *nth*, *dam*, *hdsS*, and *mcrC*) were



repressed greater than two-fold for PMA relative to the fold-changes observed in HgCl<sub>2</sub> conditions at 10 min and 30 min.

### *Transcription.*

The transcription function category includes RNA polymerase subunits and regulatory proteins. Even though the number of down-regulated transcription related genes was similar for both mercurials, over 40% of all genes in the category were up-regulated at 10 min for PMA and nearly twice as many up-regulated genes in the PMA exposure relative to HgCl<sub>2</sub> at 30 min. The greater number of up-regulated regulatory proteins might explain why the total number of differentially expressed genes was greater in PMA exposure at 10 and 30 min. RNA polymerase genes (*rpoABC*) were down 2-4 fold for PMA at 10 and 30 min, but *rpoZ* was up 2-3 fold over the same time, while only *rpoA* was down for HgCl<sub>2</sub> at 30 min with no significant changes for other genes. The transcription termination factor, *Rho*, was down only for PMA at 10 min and 30 min, but the anti-Rho factor (*rof*) was up for both HgCl<sub>2</sub> (3 fold) and PMA (10-14 fold). The RNA degradosome complex (*rne*, *eno*, *rhlB*, *pnp*, *ppk*) (Carpousis, 2007) components were all down for PMA, except the helicase (*rhlB*), while only enolase was down for HgCl<sub>2</sub> at 10 and 30 min (lower half of Figure 4.6). Expression of the RNA processing enzyme RNase II (*rnb*) was down (PMA: -25 at 10 min and -15 at 30 min / HgCl<sub>2</sub>: -6 at 10 min and -4 at 30 min); conversely, RNase R (*rnr*) was up 3-5 fold for both mercurials (lower half of Figure 4.6). Changes in expression of these RNA processing enzymes might affect the turnover of some messages, during PMA exposure.

Many transcriptional regulators and sigma factors, annotated in the RegulonDB (Salgado et al., 2012, Salgado et al., 2013), were expressed differently with the two mercurials (Table 4.3

and Tables S9). Six activators (*mhpR*, *glcC*, *gadX*, *soxS*, *mlrA*, *phoB*) and three repressors (*mcbR*, *iscR*, *betI*) were up at all times for HgCl<sub>2</sub>, but only the activator *gadX* was up at all times. *gadX* serves as the transcriptional activator for acid resistance system and multidrug efflux (Nishino et al., 2008, Tucker et al., 2003). Approximately 10-15% more transcription factor genes increased expression after PMA exposure compared to HgCl<sub>2</sub>, but twice as many repressors were down for HgCl<sub>2</sub> over the same time period.

*E. coli* has seven sigma factors that interact with RNA polymerase core to modulate expression of gene sets with varying functions (Ishihama, 2000) (Table 4.3). Sigma 70 (*rpoD*) regulates housekeeping genes expressed during log-phase growth. Even though *rpoD* was only up 3-fold for Hg at 10 min, more  $\sigma^{70}$  regulated genes had increased expression under the PMA condition at 10 and 30 min, but very similar numbers for genes with decreased expression. No significant change in sigma factor expression and similar numbers of DEGs for both mercurials was observed for Sigma 54 (*rpoN*), which controls genes related to nitrogen and sigma 24 (*rpoE*), which controls genes related to heat shock and membrane stress. The motility and flagellar synthesis sigma factor 28 (*fliA*) was down 3-6 fold for Hg at 30 and 60 min, which appears to have decreased the number of up-regulated genes for HgCl<sub>2</sub> compared to PMA, even though the number of down-regulated genes is roughly the same. But these genes remained down over the entire hour only for HgCl<sub>2</sub>. The largest changes in sigma factor expression at 10 and 30 min were observed for sigma 32 (*rpoH*), which responds to heat shock during log-phase growth and the general stress response sigma factor,  $\sigma^{38}$  (*rpoE*), but a similar number of total DEGs were observed for both mercurials within these sigma factor networks.  $\sigma^{32}$  responds to an increase in misfolded proteins (Arsene et al., 2000), so this response is likely reflective of mercury bound to proteins causing misfolding and aggregation, rather than a temperature induced response. The

general stress response regulated by  $\sigma^{38}$  was expected to increase in response to mercury exposure, but would have expected greater than 25-30% of both  $\sigma^{32}$  and  $\sigma^{38}$  genes to be up-regulated.

*E. coli* encodes at least 65 small non-coding RNAs, based on current annotation, and although the RNA purification and library preparation methods used were not optimum for recovery for their yield, we observed differential expression for a number of them. A number of these regulatory genes were up-regulated for both mercurials; *gadY* (increased acid resistance), *gcvB* (repressed amino acid transport), *oxyS* (oxidative stress), *rprA* (*rpoS* translation activator), and *sgrS* (destabilizes *ptsG* mRNA for glucose transport), while *acrZ* (increases *rpoS* translation), *cyaR* (destabilizes *ompX* mRNA, which alters adhesion and motility), and *fnrS* (mediates shift to anaerobic metabolism) were down-regulated. Several ncRNAs were only affected by PMA in at least one time point: up-regulated genes were *dicF* (inhibits *ftsZ*, involved in cell division), *eyeA* (unknown function), *mcaS* (motility and biofilm regulator), *micC* (regulates *ompC* expression), *spf* (catabolite repression), and down-regulated genes were *rybB* (represses *ompC* and *ompW* translation), and *rydB* (unknown function). Genes only affected by  $\text{HgCl}_2$  were *ryjA* (unknown function), which was up-regulated at 10 and 30 min and *sibABD* (antisense regulator of toxic Ibs proteins), which were all down two-fold at 60 min.

### *Translation.*

Expressions of genes involved in translation were similar for both compounds, but a strong bias for down-regulation of ribosomal protein genes was revealed in  $\text{HgCl}_2$  exposure (Figure D.S7 and Table D.S5). Upon  $\text{HgCl}_2$  exposure 83% and 74% of ribosomal proteins were down regulated at 10 min and 30 min respectively, versus only 4% and 41% for PMA at the

corresponding times, while both showed no change from unexposed at 60 min. Transcription of r-proteins is linked to metabolism and regulated by ppGpp and DksA, which binds ppGpp and RNA polymerase to alter expression (Lemke et al., 2011). Even though ppGpp synthase genes, SpoT and RelA, are down or unchanged, DksA is up for both compounds. The decline in r-protein expression may also result from translational feedback due to excess ribosomal proteins binding their own mRNA and inhibiting its translation (Nomura et al., 1984, Wilson and Nierhaus, 2007). Fourteen r-proteins were observed to bind PMA and Hg (Zink et. al. in preparation), which may interfere with their correct assembly and result in free r-proteins that could repress translation and alter mRNA levels. The transcriptional difference here suggests HgCl<sub>2</sub> interferes with ribosome assembly more than PMA does.

Initiation and elongation factors remained largely unchanged, but all three peptide chain release factor genes were down for PMA at 10 min and the ribosome recycling factor (*frr*) was up at 10 and 30 min for PMA. There were 8 tRNA-synthase genes down at 10 min for HgCl<sub>2</sub> and none were up, compared to 4 down and 2 up for PMA at 10 and 30 min (Table D.S5). tRNA gene expression was also repressed for both mercury compounds for most amino acids, but arginine, lysine, methionine, tyrosine, and valine were the most affected.

#### *Energy production.*

Expression of electron transport chain (ETC) genes was down overall and the individual gene responses were more similar for both mercurials than most other functional categories (Figure D.S8). Approximately 30-50% of ETC genes were down for all times for HgCl<sub>2</sub> and 30 min for PMA. Only 5% of genes increased for HgCl<sub>2</sub> at 30 and 60 min and for PMA at 60 min, but roughly 15-18% were up for Hg at 10 min and for PMA at 10 and 30 min. Expression was

down for 85-100% of NADH:ubiquinone oxidoreductase genes for Hg at 10 and 30 min and 77% for PMA at 10 and 30 min. ATP-synthase subunit genes were also strongly effected with 90-100% down with Hg at 10 and 30 min and 70-80% down with PMA at 10 and 30 min. Many of the ATP-synthase subunit genes have been observed with mercury modifications by proteomics (Table D.S4) (Zink et. al. in preparation).

Expression of genes for glucose metabolism also generally decreased, but not all steps were affected equally by both mercurials (Figure D.S6). Overall up-regulated genes declined from 21% at 10 min to 12% at 60 min and down-regulated genes increased from 23% at 10 min to 33% at 30 min and then declined to 10% at 60 min for HgCl<sub>2</sub>. PMA had 10% up-regulated genes and 44-48% down-regulated genes at 10 and 30 min and 98% of genes were expressed at levels equivalent to the unexposed cells by 60 min. Expression of five genes of the pentose-phosphate pathway rose in at least one time point for HgCl<sub>2</sub>, but only *pgl* increased for PMA at 10 min. The ribose-5-phosphate isomerase (*rpiB*) was up 40-fold for Hg at 10 min, and serves as a backup enzyme for *rpiA* (Sorensen and Hove-Jensen, 1996), which did not differ from the unexposed cells for either mercurial at any time. Glycolysis responded similarly to both mercurials, with the greatest number of these genes being down-regulated at 30 min. The expression changes in TCA cycle genes were distinct for Hg and PMA; six genes were up-regulated in at least one time point for HgCl<sub>2</sub> and only one was up-regulated for PMA.

Expression of genes for nicotinamide adenine dinucleotide (NAD) and NAD-phosphate (NADP) synthesis and turnover pathways was repressed by mercury exposure (Figure D.S7). The biosynthesis genes were moderately down-regulated with *nadB* being the only gene down for both mercurials at all times; *nadA* decreased for Hg at 30 and 60 min and for PMA at 30 min. Expression of the *pncABC* salvage pathway did not change. The NAD reduction pathways were

more affected than the NADP reduction pathways, with only *pgi* down for both mercurials and *edd* down only for HgCl<sub>2</sub>. The transhydrogenase (*pntAB*) was down only for PMA at 10 and 30 min. Expression of other genes for NAD to NADH reduction in glycolysis and the TCA cycle were also down for both mercurials.

The *torCAD* genes that make up the trimethylamine N-oxide anaerobic respiratory system were strongly up-regulated by PMA exposure. This could be a side effect of the dimethyl sulfoxide (DMSO) used to dissolve the PMA, but remains unclear since the final concentration in the culture was only 0.015% and anaerobic DMSO reductase genes (*dmsABC*) were down-regulated. The *tor* system can reduce DMSO to generate energy, but TorC is a c-type cytochrome and requires heme to function (Ansaldi et al., 1999). Since heme maturation genes are not up-regulated, the protein is likely in its non-functional apo-protein form (Ansaldi et al., 1999).

Globally, redox metabolism declines immediately after exposure and normal gene expression levels are not restored until growth rate is recovered. KEGG maps created using iPath (Yamada et al., 2011) depict system wide metabolism changes over time (Figure D.S8 for HgCl<sub>2</sub> and Figure D.S9 for PMA).

#### *Amino acid metabolism and transport.*

The two mercurials had distinct effects on expression of genes for biosynthesis of amino acids (Figure 4.9). Since mercury targets cysteine thiol groups and will deplete the reduced cellular thiol pool, we expected an increase in cysteine and glutathione biosynthesis. Surprisingly, most genes for biosynthesis of these biothiols and for general sulfur metabolism were no different from the unexposed cells, with the exception of *cysE*, and sulfur transport was

down-regulated for both mercurials at 10 min and 30 min. The PMA-provoked decline in expression was much greater for some genes than that provoked by HgCl<sub>2</sub>.

Methionine gene expression increased for 7 genes with HgCl<sub>2</sub>, but 11 genes were down-regulated with PMA, especially *metE* dropping 187-fold with PMA at 30 min (Figure 4.9). Expression of genes for histidine synthesis also responded differently to each mercurial, rising dramatically with HgCl<sub>2</sub> from at 30 to 60 min (Figure 4.9). In contrast, all *his* genes expression dropped with PMA from 10 to 30 min. Genes for synthesis of leucine, isoleucine, and valine had the opposite response to histidine, with most going down with HgCl<sub>2</sub> at 10 and 30 min, but increasing with PMA, except for *ilvC* (Figure 4.9). Expression of other amino acids biosynthetic pathways were largely unchanged or declined with both mercurials. Branched-chain, dipeptide and oligopeptide transporters were also down for both mercurials, with greater negative fold-changes for PMA.

#### *Motility and biofilm.*

Expression of motility and chemotaxis genes declined strongly for both mercurials at 10 and 30 min. Nearly all flagellar component genes were down-regulated, with negative changes that were up to 36-times greater for PMA than changes observed in HgCl<sub>2</sub> exposure (Figure 4.10). Only PMA exposure increased expression of fimbriae and curli fiber genes, which alter motility and increase adhesion (Figure 4.11) (Van Houdt and Michiels, 2005). There were 15 genes up-regulated by PMA exposure that were annotated as homologs of FimA with unknown function. FimA is the major structural component of fimbriae, but these genes may serve other functions. Notably, motility genes whose expression dropped remained low until 60 min,

indicating that the structurally and energetically intensive motility systems are very slow to recover.

Hg and PMA exposures also provoked expression of several biofilm-related genes (Figure 4.11). The *bhsA* and *bdcA* loci were among the most highly up-regulated genes during HgCl<sub>2</sub> exposure, with changes 30-40 times higher than observed for PMA (Table 4.1). Both of these genes are not well characterized, but have been shown to decrease biofilm formation and increase resistance to external stressors (Martin and Imlay, 2011, Zhang et al., 2007). Only PMA increased expression of genes for PGA polysaccharide production (Itoh et al., 2008) and biofilm related genes, *ycgZ*, *ymgA*, *ariA*, *ymgC* (Lee et al., 2007). Thus, PMA elicits a broader response that potentially alters the cell surface and increases adhesion, in contrast to Hg, which only inhibits motility and does not activate adhesion pathways.

#### *Cell wall biogenesis, porins, efflux systems and electrolyte balance.*

The transcriptional response of peptidoglycan, membrane biosynthesis, and cell division genes was similar for both mercurials (Figure D.S10). Expression increased for roughly 20% of lipid biosynthesis genes, including cardiolipin, and expression decreased for 20-30% of genes. Transcription of genes for murein synthesis (*murCDEFGIJ*) in particular declined for both mercurials during the first 30 min.

*E. coli* encodes a number of antibiotic resistance efflux systems that are up-regulated by mercury exposure (Figure 4.12). The multiple antibiotic resistance locus (*marRAB*), which decreases porin expression and increases drug efflux (Aleksun and Levy, 1999), was strongly up-regulated at 10 and 30 min, with greater changes observed for PMA. Even though expression of some porin genes was repressed (*ompC*, *ompF*, *ompT*, *ompW*), three non-specific porins



(*ompG*, *ompL*, *ompN*) were up-regulated by PMA. Genes from several TolC dependent antibiotic efflux systems were up-regulated as well, including *acrEF*, *emrD*, *emrKY*, and several *mdt* genes (Nishino et al., 2003). HgCl<sub>2</sub> exposure also up-regulated two-component sensor genes (*phoQP* and *basSR*) that regulate genes involved in modification of the cell surface and increase polymyxin resistance (Raetz et al., 2007).

The response to osmotic stress and maintenance of electrolyte balance are important membrane functions requiring adaptation in an ever-changing environment. During Hg exposure expression of the sodium antiporter, NhaA, increased 4-fold at 10 min and the calcium/potassium antiporter, ChaA, was up 3-fold at 10 and 30 min (Figure 4.13). In contrast, the major electrolyte, potassium, did show moderate changes in some transport subunit genes, but not all, so no clear response pattern emerged. However, transcription of genes for defense against osmotic stress was uniformly up-regulated: betaine genes (*betABIT* and *proP*), *osmBCEFY*, and mechanosensitive channel proteins (*mscL* and *mscS*) increased for both mercurials, as did a putative osmoprotectant ABC permease (*yehYXW*) (Checroun and Gutierrez, 2004) for Hg at 30 and 60 min.

#### *Inorganic ion transport and chaperones.*

Inorganic Hg can displace beneficial thiophilic metals from their native binding sites in proteins, potentially affecting transport and disrupting transition metal homeostasis, which could lead to expression changes for genes of non-ferrous metal transporters (Figure 4.13), iron homeostasis (Figure 4.14) and metal binding proteins and enzymes.

Inorganic mercury exposure releases labile iron, which could itself increase oxidative stress (Imlay, 2013, LaVoie et al., 2015). Most iron uptake pathways declined early for both

mercurials, consistent with increased expression of the Fur repressor. The cytochrome *c* maturation genes involved in heme transport to the periplasm (*ccmABCDE*) were also down for both mercurials. The putative ferrous iron and zinc efflux pump, *fieF* (Grass et al., 2005) increased 2-fold for Hg at 10 min only, suggesting it may have a brief role in restoring homeostasis.

There are two iron-sulfur cluster assembly pathways in *E. coli* (Bandyopadhyay et al., 2008, Johnson et al., 2005). Expression of the primary Isc system (*iscRSUA*, *hscBA*, and *fdx*) increased strongly for both mercurials, but with greater changes for HgCl<sub>2</sub>. The secondary *sufABCDSE* system activated under oxidative stress or iron limiting conditions increased greatly, but only for HgCl<sub>2</sub>. These transcriptional responses confirm and extend biochemical findings (LaVoie et al., 2015) that iron-sulfur clusters are more vulnerable to inorganic mercury than to organomercurials.

Zinc uptake was moderately altered, with expression of *zupT* increasing 3 to 5-fold for both mercurials during the first thirty minutes. In contrast, expression of the P-type ATPase zinc efflux pump, *zntA* (Rensing et al., 1997), increased 20 to 40-fold for both mercurials at 10 and 30 min, as well increasing expression throughout recovery for the periplasmic binding protein ZraP. *E. coli* has two copper/silver efflux systems, Cue and Cus (Outten et al., 2001). Surprisingly, the Cus system (*cusRS*, *cusCFBA*) genes primarily used under anaerobic conditions were among the most down-regulated genes under PMA exposure. The Cue system consists of the multicopper oxidase, CueO, and a P-type ATPase, CopA, both regulated by the MerR homolog, CueR. Expression of both *cueO* and *copA* was up over 20-fold for HgCl<sub>2</sub> at 10 and 30 min, but only 5-fold for PMA briefly at 10 min. The nickel uptake system (Eitinger and Mandrand-Berthelot, 2000)(*nikABCDER*) was also very strongly down-regulated under PMA exposure conditions

over all times although expression of repressor NikR was unchanged, except for a 3-fold increase with Hg at 10 min. Expression of the nickel and cobalt efflux gene, *rcnA*, increased with Hg at 10 and 30 min and with PMA at 30 min. Manganese (*mntH*), and magnesium (*mgtA*, *corA*) uptake genes both increased with both mercurials during the first 30 min of exposure.

Inorganic anions used by *E. coli* include phosphate, sulfate, and molybdate. Expression of the ABC phosphate transport system (*pstSCAB*) genes increased greatly for both mercurials, with PMA-provoked changes as high as 165-fold for the phosphate binding protein, *pstS*. The two-component phosphate regulatory system, PhoBR increased 22-fold for Hg at 30 min and 105-fold for PMA at 30 min for *phoB*. Sulfate and thiosulfate uptake by ABC transporter (*cysPUWA*) was strongly decreased for HgCl<sub>2</sub> at 30 mins and PMA at 10 and 30 min. Expression of molybdate uptake (*modABC*) increased for HgCl<sub>2</sub> at 10 min and decreased at 60 min, but the increase in expression was higher for PMA during the first 30 min of exposure. The arsenate resistance operon was also highly induced by HgCl<sub>2</sub> (Table 4.1).

#### *Oxidative stress response and repair.*

There are two oxidative stress response pathways in *E. coli*, the *oxyRS* and *soxRS* regulons (Imlay, 2013, Seo et al., 2015). OxyR, a LysR-family transcriptional regulator, uses a cysteine pair to sense H<sub>2</sub>O<sub>2</sub> damage and regulates 49 genes when oxidized (Choi et al., 2001). HgCl<sub>2</sub> exposure increased expression of 22 OxyR regulon genes at 10 min, which declined to 13 genes by 60 min. In contrast, PMA provoked expression of 16 genes at 10 and 30 min, but none at 60 min. The *oxyS* gene was among the most highly expressed genes with over a 1,000 fold-change for HgCl<sub>2</sub> at 10 and 30 min, and a more moderate change of  $\leq 10$  for PMA. *oxyS*, is a

small RNA regulated by OxyR, that represses *rpoS*, *fhlACD* and other genes to prevent redundant induction of stress response genes (Altuvia et al., 1998).

The SoxRS regulon is the other primary oxidative stress response system in *E. coli*. SoxR belongs to the MerR family of transcriptional regulators and uses the oxidation state of 2Fe-2S clusters to respond to superoxide ( $O_2^-$ ) stress and induce transcription of *SoxS* (Amabile-Cuevas and Dempse, 1991, Greenberg et al., 1990, Tsaneva and Weiss, 1990, Watanabe et al., 2008). SoxS is a transcriptional activator protein that plays a role in regulation of over 50 genes (Keseler et al., 2013, Seo et al., 2015) (Table D.S6). HgCl<sub>2</sub> exposure up-regulated 24 genes at 10 min, 20 at 30 min and 13 at 60 min up-regulated upon and PMA exposure up-regulated 25 at 10 min, 22 at 30 min and 0 at 60 min.

Key genes with differentially expressed in these oxidative stress regulons upon mercury exposure include the ROS scavengers: catalase (*katG*), alkyl hydroperoxide reductase (*ahpCF*), and superoxide dismutase (*sodA*)(Figure 4.15). Thiol homeostasis genes included *gor*, *grxA*, and *trxC* (Figure 4.15). Iron homeostasis, cluster assembly and repair genes (*fur*, *dps*, *fldA*, *fpr*, *hemH*, *sufABCDE*, and *yggX*) were also up-regulated. PMA induced comparatively lower fold-changes in *grxA*, *trxC*, *ahpC*, *dps*, *fldA*, *hemH*, and *yggx*. The manganese uptake protein, *mntH*, was up 5-7 fold for both mercurials at 10 and 30 min and plays an important role in ROS resistance (Anjem et al., 2009). Oxidation-resistant dehydratase isozymes, *acnA* and *fumC* (Park and Gunsalus, 1995, Varghese et al., 2003), also increased, but only for HgCl<sub>2</sub> exposure.

We expected that regulation of redox homeostasis proteins such as glutaredoxins, thioredoxins and glutathione-related genes would respond to mercury exposure (Figure 4.15). Glutaredoxin 1 (*grxA*) expression was up for both mercurials, but much higher for HgCl<sub>2</sub> at 10 and 30 min than for PMA. Glutaredoxin 2 (*grxB*) was down for both mercurials, but glutaredoxin

3 (*grxC*) was up two-fold for PMA at 10 min only, and glutaredoxin 4 (*grxD*) was up three-fold for PMA at 10 and 30 min only. Thioredoxin reductase (*trxB*) increased two-fold for PMA at 30 min only, but was up 8-fold for Hg at 10 min and 4-fold for Hg at 30 min; in contrast, thioredoxin 1 (*trxA*) expression only increased two-fold for PMA at 10 min. Thioredoxin 2 (*trxC*) expression was more strongly affected by HgCl<sub>2</sub> than PMA, like glutaredoxin. Expression was up 134-fold for Hg at 10 min, 50-fold for Hg at 30 min, and 7-fold for Hg at 60 min, whereas PMA provoked a 24-fold change at both 10 and 30 min. The thiol peroxidase, *tpx*, was also up two-fold for PMA at 10 and 30 min, but did not change for HgCl<sub>2</sub>.

Glutathione (GSH) is important as the cell's redox buffer and as a primary target for mercury, most related genes showed some change in expression (Figure 4.15). Somewhat surprisingly, expression of GSH biosynthesis and utilization genes increased only modestly. The  $\gamma$ -glutamyltranspeptidase (*ggt*) increased 4-fold with Hg at 60 min only; GSH synthase (*gshA*) did not change and *gshB* was up 2-3 fold for both mercurials at 10 min only. GSH reductase (*gor*) increased only with Hg at 10 min. The largest change occurred in the GSH-dependent disulfide oxidoreductase (*yfcG*) that was up 4 to 8-fold for all times with HgCl<sub>2</sub> and 4-fold for PMA at 10 and 30 min. Several GSH S-transferase genes (*gstA*, *gstB*, *yfcF*, *yqiG*, *yibF*, *yncG*) increased expression with both mercurials, while glutathione transporter genes (*gsiABCD* and *cydCD*) decreased for both mercurials during the first 30 minutes.

#### *Heat shock response.*

Expression of genes for the proteases and chaperones of the heat shock response, which degrade or repair of misfolded proteins were increased by both mercurials (Georgopoulos and Welch, 1993) (top half of Figure 4.6). The proteases *lon*, *clpXP* and *ftsH* gene expression

increased 4 to 6-fold at 10 min with HgCl<sub>2</sub> and *lon* and *clpXP* increased 3-fold at 10 and 30 min with PMA. Twelve heat shock proteins (HSP) and chaperones increased at 10 min, four at 30 min and four at 60 min after HgCl<sub>2</sub> exposure, compared to only five that increased at 10 min, six at 30 min and three at 60 min for PMA. IbpAB, which provides resistance to superoxide and to copper-induced oxidative stress (Kitagawa et al., 2000, Matuszewska et al., 2008), had the highest increase for both mercurials across all three times. Up-regulation of these genes might be expected, since divalent inorganic mercury, but not monovalent PMA, can stably crosslink proteins or their subdomains, disrupting tertiary and quaternary structures, and allosteric movements (Soskine et al., 2002, Imesch et al., 1992, Carvalho et al., 2008).

## DISCUSSION

Mercury is an environmental toxin that serves no biologically beneficial role and exposure to this element has a negative impact on the health of all organisms, from microbes to humans. The effects of mercury exposure are often generalized and differences between inorganic and organic mercury species are not well characterized. This study examines the effects of two mercury species on transcription over time in a non-resistant strain of *E. coli* MG1655. PMA was of interest on its own, but also served as a surrogate to the more environmentally abundant organomercurial species, methylmercury, in this study. Cultures exposed to a sub-acute concentration during exponential phase allowed for examination of initial transcriptional response and to monitor changes throughout recovery period for a broader view of cellular resources and defense mechanisms required for survival.

The sub-acute mercury exposure conditions used in this study were determined by identifying a mercury concentration that was high enough to exhibit toxic effects by inhibiting

growth rate, but low enough to allow for recovery of a positive growth rate within one-hour after exposure. Concentrations lower than 3  $\mu\text{M}$  did not consistently inhibit growth rate and higher concentrations of  $\text{HgCl}_2$  did not allow for recovery within the desired time frame. This exposure concentration is within the range that bacteria might experience in the gastrointestinal tract from installation or removal of dental amalgam fillings (Summers et al., 1993) and in highly contaminated environments, such as surrounding artisanal gold mining operations (Malm, 1998).

Even though PMA exposed cultures recovered faster than equimolar exposure to  $\text{HgCl}_2$ , a greater proportion of the genome was differentially expressed during the first 30 min of exposure. These results agree with observations in *C. elegans*, where  $\text{MeHg}$  exposure resulted in greater than four-times as many DEGs than  $\text{HgCl}_2$ , for all concentrations tested (McElwee and Freedman, 2011). But in contrast to *E. coli*, where growth was inhibited more by inorganic exposure, the effective concentration was lower for the organomercurial, methylmercuric chloride, than  $\text{HgCl}_2$  in *C. elegans* (McElwee and Freedman, 2011).

The peak of total DEGs was 10 min after exposure for both compounds. There were more down-regulated genes for  $\text{HgCl}_2$  throughout, in contrast to PMA, which had more up-regulated genes than down throughout exposure period. Even though the  $\text{HgCl}_2$  exposed culture showed no indication of growth recovery from 10 min to 30 min, there was a 22% decrease in DEGs, while PMA over the same period showed a moderate increase in optical density, but only decreased DEGs by 8%. In contrast, microarray analysis of livers from  $\text{HgCl}_2$  exposed zebrafish found an increasing number of differentially expressed genes throughout observed exposure period, as mercury was accumulated by cells (Ung et al., 2010).

Comparison of the DEGs for both compounds at each time point revealed that the down-regulated transcriptional response strongly overlapped for both compounds, especially at 10 min

and the up-regulated response shared fewer genes. These results suggest that the down-regulated response is more conserved and the less conserved up-regulated response highlights distinct differences between each compound, requiring a unique transcriptional response for each. Exposure in *C. elegans* also found that transcriptional response was distinct between inorganic and organic mercury exposure and in many cases had the opposite affect on transcription (McElwee et al., 2013).

A search of the literature did not reveal any studies that examined the transcriptional response of a bacterium to mercury exposure, so it was unknown how the cell would response, but some predictions could be made based on known biochemical induced damage and protein targets. Discussion of gene and functional level transcriptional changes were broken down into predicted changes and changes that were not initially predicted.

*Predicted transcriptional response, based on known toxicity mechanisms:*

Knowing that mercury targets thiols and deplete the glutathione pool, it was expected that cysteine and glutathione biosynthesis pathways would be up-regulated, but surprisingly cysteine biosynthesis was down and GSH biosynthesis remained mostly unchanged for both compounds, which is different from the response to H<sub>2</sub>O<sub>2</sub> exposure (Zheng et al., 2001). Even though thiol biosynthesis did not increase, genes involved in maintaining the thiol and redox balance within the cell did increase. Expression of thioredoxin (*trxC*) and glutaredoxin (*grxA*) were among the most highly up-regulated genes for HgCl<sub>2</sub> exposure. Glutathione reductase is up early for HgCl<sub>2</sub> and oxidoreductase and S-transferase genes, which serve protective roles against oxidative stress and xenobiotics (Kanai et al., 2006), were also up for both compounds.



Mercury becomes less reactive towards other targets when coordinated by glutathione, due to strong binding affinity and is the best defense available for cells without the *mer* operon. But if the GSH pool becomes depleted, and NAD(P)H is not being generated at a sufficient rate to maintain the GSH/GSSG balance while metabolism is repressed, then the cell loses its primary defense mechanism and becomes more reliant on stress response and repair pathways to survive damage and secondary effects caused by mercury binding to macromolecules. Therefore it is likely that a key factor in determining survival and ability to recovery growth is dependent on not exceeding the threshold concentration that overwhelms the reduced glutathione pool.

Inorganic mercury was also expected to disrupt iron homeostasis and target iron-sulfur clusters (LaVoie et al., 2015, Xu and Imlay, 2012). Iron uptake was repressed for both compounds, consistent with oxidative stress, but expression of the uptake repressor (*fur*) was only up for HgCl<sub>2</sub>. Fur is up-regulated as part of the OxyR regulon (Varghese et al., 2007, Zheng et al., 2001) and requires ferrous iron as a co-repressor (Bagg and Neilands, 1987), but has also been shown to respond to other divalent metals (de Lorenzo et al., 1987) and therefore could be directly interacting with Hg<sup>2+</sup>. Even though both compounds increased expression of the primary Fe-S cluster assembly and repair system (*isc*), only HgCl<sub>2</sub> induced the secondary system (*suf*), which is induced under stress conditions (Bandyopadhyay et al., 2008). Also only HgCl<sub>2</sub> exposure increased expression of iron storage proteins: ferritin, bacterioferritin, and Dps. Dps was one of the most highly up-regulated genes in HgCl<sub>2</sub> exposure and serves the dual function of binding free iron and protecting DNA from ROS damage (Zhao et al., 2002).

Oxidative stress is closely linked with iron homeostasis (Imlay, 2013) and inorganic mercury exposure induced much greater fold-changes in genes that respond to oxidative stress. Mercury has previously been shown to induce oxidative damage in rat kidney mitochondria

(Lund et al., 1991), which agrees with observations in *E. coli*. The small RNA *oxyS* was the second most highly up-regulated gene for HgCl<sub>2</sub> exposure and expression was >100 fold over PMA. The ROS scavenger *ahpF* was also highly up-regulated, along with *katG* early phase and *sodA* late phase, but only for HgCl<sub>2</sub>. Alternative oxidative resistant enzymes, aconitase A (Varghese et al., 2003) and fumarase C (Liochev and Fridovich, 1993), were also only up for HgCl<sub>2</sub>, as well much greater fold-changes for the manganese dependent alternative ribonucleotide reductase genes (*nrdHIEF*) (Martin and Imlay, 2011). The glutaredoxin-like protein that functions like thioredoxin, *nrdH* (Jordan et al., 1997), was highly up-regulated by HgCl<sub>2</sub> and might serve an important role in supporting other thioredoxin and glutaredoxin proteins. These results highlight key differences in toxicity mechanisms between mercury compounds and illuminate how inorganic mercury exposed *E. coli* has to modulate transcriptional response over time to not only deal with mercury binding, but also the resulting cascading effects of oxidative stress.

Increased expression of heat shock response was expected as a consequence of mercury binding to proteins (Arsene et al., 2000). Mercury bound to proteins can disrupt protein folding, assembly and cause aggregation through inorganic mercury disulfide cross-links. Increased expression of heat shock chaperonins and protease genes was observed for both compounds, but more genes responded to HgCl<sub>2</sub> exposure at 10 min than PMA. The *ibpA* and *ibpB* genes were two of the most highly up-regulated genes for both compounds, with higher fold-changes for HgCl<sub>2</sub>. These small proteins serve a chaperone-like role and aid in degradation of misfolded proteins by Lon and have been shown to be important in oxidative stress resistance (Bissonnette et al., 2010, Gaubig et al., 2011, Matuszewska et al., 2008).

Fourteen different r-protein subunits were observed with mercury modifications by proteomics analysis, so it was possible that ribosome structure could be affected. Inorganic mercury exposure repressed expression of up to 83% of ribosomal protein genes, consistent with  $\text{Cd}^{2+}$  exposure observations in *E. coli* (Wang and Crowley, 2005). The ability of inorganic mercury to cross-link proteins and potentially bind to rRNA, appears to interfere with ribosome assembly more than monovalent PMA, resulting in greater translational feedback and repression of r-proteins transcription. Disruption of ribosome assembly could also be a key factor that contributes to the slower recovery of growth in inorganic exposure.

Energy production and metabolism were also expected to be targets, but it was surprising how much expression was repressed for these functional categories. Three ATP-synthase subunits had been observed with mercury modifications by proteomics (Zink et. al. in preparation), but expression of all nine subunits was repressed at 10 min for  $\text{HgCl}_2$  and 8 for PMA at 30 min. Cadmium exposure in *E. coli* repressed expression of aerobic energy metabolism genes, but observed a corresponding shift towards anaerobic pathways (Wang and Crowley, 2005). This is in contrast to mercury, where both aerobic and anaerobic energy metabolism was repressed. Even though the oxygen sensors *fnr* (Salmon et al., 2003) and *aer* (Bibikov et al., 1997) that trigger anaerobic shift regulation were up for PMA and unchanged for  $\text{HgCl}_2$ . Expression of glucose metabolism pathway genes are also predominately down for both compounds, but twice as many genes are down under PMA conditions. So it is not surprising that amino acid, carbohydrate and nucleotide metabolism genes are down, as well as energy dependent transport of these molecules, with limited energy available.

Mercury was predicted to disrupt some non-ferrous metals homeostasis, including electrolyte balance (LaVoie et al., 2015). In addition to targeting iron cofactors, mercury can

displace other metals, like zinc. Expression of metal uptake genes was down and increased expression of metal efflux genes for zinc, copper, nickel and cobalt, with generally greater fold-changes for HgCl<sub>2</sub>. Zinc efflux by ZntA is regulated by MerR homolog ZntR, which can respond to Hg(II), but ZntA does not efflux mercury (Anjem et al., 2009). Manganese serves a protective role under oxidative stress conditions, as an alternative metal co-factor to iron, and uptake by *mntH* was up-regulated for both compounds, as part of the OxyR regulon (Anjem et al., 2009). Disruption of the electrolyte balance by potassium efflux and sodium uptake was predicted, but expression of potassium efflux subunit genes were not uniformly up-regulated. The sodium antiporter, *nhaA*, was up for both compounds. So it is more likely that normal levels of these proteins are sufficient to respond to mercury exposure, but a transcriptional change for these genes is not induced.

*Transcriptional changes not initially predicted:*

Flagellar motility and chemotaxis was strongly repressed for both mercury compounds and one of the slowest functions to recovery normal transcription levels. Motility gene expression is regulated by  $\sigma^{28}$  (*fliA*) and FlhDC (Fitzgerald et al., 2014) and expression of these genes was correspondingly down for HgCl<sub>2</sub>, but surprisingly unchanged during PMA exposure. Therefore it remains unclear if there are other regulatory mechanisms are in play under PMA conditions. It is possible repression occurs as a result of FliA competing with increased expression of RpoS (Dong et al., 2011) or repression of FlhDC by small RNAs, like *oxyS* and *gadY* (De Lay and Gottesman, 2012), which are both up-regulated during mercury exposure. Even though mercury exposure had been observed to down-regulated locomotion in *C. elegans*

(McElwee et al., 2013), it was not expected that mercury exposure would so strongly repress motility in *E. coli*.

We expected that mercury might induce changes in biofilm and adhesion related genes as a mechanism to limit permeability, but specific changes could not be predicted. The *bhsA* gene was the most highly up-regulated for HgCl<sub>2</sub> and *bdcA* was the third highest. These genes function are not well characterized, but have been shown to play a role in biofilm dispersal or reduced biofilm formation (Martin and Imlay, 2011, Zhang et al., 2007). BhsA expression is up-regulated by a variety of stressor and may play an important role in decreasing permeability of the cell surface (Mermod et al., 2012, Zhang et al., 2007). PMA exposure increased expression of polysaccharide PGA synthesis, which aids adhesion in biofilm formation (Itoh et al., 2008) and induced greater fold-changes in *ycgZ*, *ymgA*, *ariA*, *ymgC* genes (Lee et al., 2007). Fimbriae and curli fibers are important adhesion surface structures for biofilm formation (Van Houdt and Michiels, 2005) that were up-regulated only by PMA exposure. There are also a number of FimA homologs of unknown function up-regulated by PMA. These are distinct differences between PMA and HgCl<sub>2</sub> response, but it is unclear why only PMA induces biofilm formation pathways and HgCl<sub>2</sub> induces such high changes in dispersal genes.

The phosphate uptake transport system genes constitute many of the most highly up-regulated genes for PMA exposure. The PhoBR two-component system regulates expression of phosphate transport genes, but also regulates a variety of other genes that increase virulence (Crepin et al., 2011). Pho regulon expression might also explain fimbriae and biofilm formation observed for PMA exposure (Crepin et al., 2011). Expression is up-regulated under phosphate limiting conditions (Hsieh and Wanner, 2010), so it appears that PMA inhibits phosphate uptake

by an unknown mechanism that HgCl<sub>2</sub> does not, possibly through direct interaction with periplasmic PstS.

Multiple antibiotic efflux systems and polymyxin resistance surface modifications were up-regulated by mercury exposure, but greater changes for PMA. Chronic mercury exposure has already been shown to contribute to selection of multiple antibiotic resistant species of bacteria, through co-selection of mercury resistance (Pal et al., 2015, Wireman et al., 1997). Increased expression of antibiotic resistance and surface modifications reveal that low-level mercury exposure could increase virulence and prime cells for increased antibiotic resistance.

Amino acid biosynthesis was repressed for most amino acids, but a few of these biosynthetic pathways responded uniquely to each mercury compound. Methionine auxotrophy has been shown to occur under oxidative stress conditions, due to susceptibility of methionine synthase (MetE) (Hondorp and Matthews, 2004). So it is not surprising that methionine biosynthesis genes were up-regulated under HgCl<sub>2</sub> conditions, which exhibited stronger oxidative stress response than PMA. But it is curious that expression of these genes was more strongly down under PMA conditions. Histidine biosynthesis also was up-regulated by HgCl<sub>2</sub> and down-regulated by PMA, but it remains unclear what drives these differences, as well the opposite response for leucine, isoleucine and valine biosynthesis.

Arsenate resistance genes responded strongly to HgCl<sub>2</sub>, but are not expected to efflux mercury and therefore should not serve any beneficial role against mercury. This response is likely induced by mercury interactions with cysteine residues of ArsR (Busenlehner et al., 2003). A number of e14 phage genes were highly up-regulated by HgCl<sub>2</sub> and CPS-53 phage genes for PMA. These vestigial prophage genes are not well characterized, but have been shown to

respond and provide increased resistance to environmental stressors (Mehta et al., 2004, Wang et al., 2010), so their role remains unclear.

## CONCLUSIONS

Toxicity mechanisms of mercury exposure in various organisms have long been studied, but detailed understanding of differences between mercury species remains limited. This study is the first to examine not only the transcriptional response differences between inorganic mercury ( $\text{HgCl}_2$ ) and an organomercurial (phenylmercuric acetate) in a model microorganism, but also to examine the effects throughout recovery. In conjunction with work to identify protein targets (Zink et. al. in preparation) and biochemical damage of acute exposure (LaVoie et al., 2015), the addition of this work provides a system wide examination of the *in vivo* effects of mercury exposure in *E. coli* and highlights distinct differences between compounds. Sub-acute exposure influenced expression of 40-50% of all genes in the genome and the resulting transcriptional response was distinct for each compounds. The unique aspects of the transcriptional response to each mercury compound illuminate which systems are negatively impacted and how the cell allocates available resources, to combat toxicity mechanisms until growth rate can be restored. Energy production, metabolism and most uptake pathways are repressed, while nearly all stress response systems were up-regulated by at least one compound, including oxidative stress, heat shock, acid stress, metals homeostasis, biofilm regulation, and antibiotic resistance. Glutathione is a key factor in defense against mercury exposure and likely dictates the threshold between sub-acute and acute exposure concentrations. Further study will be required to analyze the intracellular mercury concentration in the cell at each time point, to determine if the concentration decreases as growth rate is restored, by an unknown efflux mechanism or is

reduced by some means other than MerA, or if it remains constant, suggesting sequestration by extracellular thiols inhibiting uptake and reactivity. Microbiome studies are rapidly unveiling the importance of commensal bacteria to health of animals, so findings from this well studied model microorganism provides a reference for predicting how chronic mercury exposure might affect complex microbial communities and alter the health of the host.

## REFERENCES

- ALEKSHUN, M. N. & LEVY, S. B. 1999. The mar regulon: multiple resistance to antibiotics and other toxic chemicals. *Trends Microbiol*, 7, 410-3.
- ALTUVIA, S., ZHANG, A., ARGAMAN, L., TIWARI, A. & STORZ, G. 1998. The Escherichia coli OxyS regulatory RNA represses fhlA translation by blocking ribosome binding. *EMBO J*, 17, 6069-75.
- AMABILE-CUEVAS, C. F. & DEMPLE, B. 1991. Molecular characterization of the soxRS genes of Escherichia coli: two genes control a superoxide stress regulon. *Nucleic Acids Res*, 19, 4479-84.
- ANDERS, S., PYL, P. T. & HUBER, W. 2015. HTSeq--a Python framework to work with high-throughput sequencing data. *Bioinformatics*, 31, 166-9.
- ANJEM, A., VARGHESE, S. & IMLAY, J. A. 2009. Manganese import is a key element of the OxyR response to hydrogen peroxide in Escherichia coli. *Mol Microbiol*, 72, 844-58.
- ANSALDI, M., BORDI, C., LEPELLETIER, M. & MEJEAN, V. 1999. TorC apocytochrome negatively autoregulates the trimethylamine N-oxide (TMAO) reductase operon in Escherichia coli. *Mol Microbiol*, 33, 284-95.
- ARSENE, F., TOMOYASU, T. & BUKAU, B. 2000. The heat shock response of Escherichia coli. *Int J Food Microbiol*, 55, 3-9.
- BAGG, A. & NEILANDS, J. B. 1987. Ferric uptake regulation protein acts as a repressor, employing iron (II) as a cofactor to bind the operator of an iron transport operon in Escherichia coli. *Biochemistry*, 26, 5471-7.



BANDYOPADHYAY, S., CHANDRAMOULI, K. & JOHNSON, M. K. 2008. Iron-sulfur cluster biosynthesis. *Biochem Soc Trans*, 36, 1112-9.

BARKAY, T., MILLER, S. M. & SUMMERS, A. O. 2003. Bacterial mercury resistance from atoms to ecosystems. *FEMS Microbiol Rev*, 27, 355-84.

BIBIKOV, S. I., BIRAN, R., RUDD, K. E. & PARKINSON, J. S. 1997. A signal transducer for aerotaxis in *Escherichia coli*. *J Bacteriol*, 179, 4075-9.

BISSONNETTE, S. A., RIVERA-RIVERA, I., SAUER, R. T. & BAKER, T. A. 2010. The IbpA and IbpB small heat-shock proteins are substrates of the AAA+ Lon protease. *Mol Microbiol*, 75, 1539-49.

BUSENLEHNER, L. S., PENNELLA, M. A. & GIEDROC, D. P. 2003. The SmtB/ArsR family of metalloregulatory transcriptional repressors: Structural insights into prokaryotic metal resistance. *FEMS Microbiol Rev*, 27, 131-43.

CARPOUSIS, A. J. 2007. The RNA degradosome of *Escherichia coli*: an mRNA-degrading machine assembled on RNase E. *Annu Rev Microbiol*, 61, 71-87.

CARVALHO, C. M., CHEW, E. H., HASHEMY, S. I., LU, J. & HOLMGREN, A. 2008. Inhibition of the human thioredoxin system. A molecular mechanism of mercury toxicity. *J Biol Chem*, 283, 11913-23.

CHECROUN, C. & GUTIERREZ, C. 2004. Sigma(s)-dependent regulation of yehZYXW, which encodes a putative osmoprotectant ABC transporter of *Escherichia coli*. *FEMS Microbiol Lett*, 236, 221-6.

CHEESMAN, B. V., ARNOLD, A. P. & RABENSTEIN, D. L. 1988. Nuclear magnetic resonance studies of the solution chemistry of metal complexes. 25. Hg(thiol)<sub>3</sub> complexes and HG(II)-thiol ligand exchange kinetics. *J. Am. Chem. Soc.*, 110, 6359-6364.

CHOI, H., KIM, S., MUKHOPADHYAY, P., CHO, S., WOO, J., STORZ, G. & RYU, S. E. 2001. Structural basis of the redox switch in the OxyR transcription factor. *Cell*, 105, 103-13.

CLARKSON, T. W. & MAGOS, L. 2006. The toxicology of mercury and its chemical compounds. *Crit Rev Toxicol*, 36, 609-62.

CREPIN, S., CHEKABAB, S. M., LE BIHAN, G., BERTRAND, N., DOZOIS, C. M. & HAREL, J. 2011. The Pho regulon and the pathogenesis of *Escherichia coli*. *Vet Microbiol*, 153, 82-8.

CRINNION, W. J. 2000. Environmental medicine, part three: long-term effects of chronic low-dose mercury exposure. *Altern Med Rev*, 5, 209-23.

DAVIDSON, P. W., MYERS, G. J. & WEISS, B. 2004. Mercury exposure and child development outcomes. *Pediatrics*, 113, 1023-9.

DE LAY, N. & GOTTESMAN, S. 2012. A complex network of small non-coding RNAs regulate motility in *Escherichia coli*. *Mol Microbiol*, 86, 524-38.

DE LORENZO, V., WEE, S., HERRERO, M. & NEILANDS, J. B. 1987. Operator sequences of the aerobactin operon of plasmid ColV-K30 binding the ferric uptake regulation (fur) repressor. *J Bacteriol*, 169, 2624-30.

DIEZ, S. 2009. Human health effects of methylmercury exposure. *Rev Environ Contam Toxicol*, 198, 111-32.

DONG, T., YU, R. & SCHELLHORN, H. 2011. Antagonistic regulation of motility and transcriptome expression by RpoN and RpoS in *Escherichia coli*. *Mol Microbiol*, 79, 375-86.

DRISCOLL, C. T., MASON, R. P., CHAN, H. M., JACOB, D. J. & PIRRONE, N. 2013. Mercury as a global pollutant: sources, pathways, and effects. *Environ Sci Technol*, 47, 4967-83.

EITINGER, T. & MANDRAND-BERTHELOT, M. A. 2000. Nickel transport systems in microorganisms. *Arch Microbiol*, 173, 1-9.

FITZGERALD, D. M., BONOCORA, R. P. & WADE, J. T. 2014. Comprehensive mapping of the *Escherichia coli* flagellar regulatory network. *PLoS Genet*, 10, e1004649.

GAUBIG, L. C., WALDMINGHAUS, T. & NARBERHAUS, F. 2011. Multiple layers of control govern expression of the *Escherichia coli* *ibpAB* heat-shock operon. *Microbiology*, 157, 66-76.

GEORGOPOULOS, C. & WELCH, W. J. 1993. Role of the major heat shock proteins as molecular chaperones. *Annu Rev Cell Biol*, 9, 601-34.

GRASS, G., OTTO, M., FRICKE, B., HANEY, C. J., RENSING, C., NIES, D. H. & MUNKELT, D. 2005. FieF (YiiP) from *Escherichia coli* mediates decreased cellular accumulation of iron and relieves iron stress. *Arch Microbiol*, 183, 9-18.

GREENBERG, J. T., MONACH, P., CHOU, J. H., JOSEPHY, P. D. & DEMPLE, B. 1990. Positive control of a global antioxidant defense regulon activated by superoxide-generating agents in *Escherichia coli*. *Proc Natl Acad Sci U S A*, 87, 6181-5.

HARDCASTLE, T. J. & KELLY, K. A. 2010. baySeq: empirical Bayesian methods for identifying differential expression in sequence count data. *BMC Bioinformatics*, 11, 422.

HINTELMANN, H., HEMPEL, M. & WILKEN, R. D. 1995. Observation of unusual organic mercury species in soils and sediments of industrially contaminated sites. *Environ Sci Technol*, 29, 1845-50.

HONDORP, E. R. & MATTHEWS, R. G. 2004. Oxidative stress inactivates cobalamin-independent methionine synthase (MetE) in *Escherichia coli*. *PLoS Biol*, 2, e336.

- HSIEH, Y. J. & WANNER, B. L. 2010. Global regulation by the seven-component Pi signaling system. *Curr Opin Microbiol*, 13, 198-203.
- IMESCH, E., MOOSMAYER, M. & ANNER, B. M. 1992. Mercury weakens membrane anchoring of Na-K-ATPase. *Am J Physiol*, 262, F837-42.
- IMLAY, J. A. 2013. The molecular mechanisms and physiological consequences of oxidative stress: lessons from a model bacterium. *Nat Rev Microbiol*, 11, 443-54.
- ISHIHAMA, A. 2000. Functional modulation of Escherichia coli RNA polymerase. *Annu Rev Microbiol*, 54, 499-518.
- ITOH, Y., RICE, J. D., GOLLER, C., PANNURI, A., TAYLOR, J., MEISNER, J., BEVERIDGE, T. J., PRESTON, J. F., 3RD & ROMEO, T. 2008. Roles of pgaABCD genes in synthesis, modification, and export of the Escherichia coli biofilm adhesin poly-beta-1,6-N-acetyl-D-glucosamine. *J Bacteriol*, 190, 3670-80.
- JOHNSON, D. C., DEAN, D. R., SMITH, A. D. & JOHNSON, M. K. 2005. Structure, function, and formation of biological iron-sulfur clusters. *Annu Rev Biochem*, 74, 247-81.
- JORDAN, A., ASLUND, F., PONTIS, E., REICHARD, P. & HOLMGREN, A. 1997. Characterization of Escherichia coli NrdH. A glutaredoxin-like protein with a thioredoxin-like activity profile. *J Biol Chem*, 272, 18044-50.
- KANAI, T., TAKAHASHI, K. & INOUE, H. 2006. Three distinct-type glutathione S-transferases from Escherichia coli important for defense against oxidative stress. *J Biochem*, 140, 703-11.
- KESELER, I. M., MACKIE, A., PERALTA-GIL, M., SANTOS-ZAVALA, A., GAMA-CASTRO, S., BONAVIDES-MARTINEZ, C., FULCHER, C., HUERTA, A. M., KOTHARI, A., KRUMMENACKER, M., LATENDRESSE, M., MUNIZ-RASCADO, L., ONG, Q., PALEY, S., SCHRODER, I., SHEARER, A. G., SUBHRAVETI, P., TRAVERS, M., WEERASINGHE, D., WEISS, V., COLLADO-VIDES, J., GUNSALUS, R. P., PAULSEN, I. & KARP, P. D. 2013. EcoCyc: fusing model organism databases with systems biology. *Nucleic Acids Res*, 41, D605-12.
- KITAGAWA, M., MATSUMURA, Y. & TSUCHIDO, T. 2000. Small heat shock proteins, IbpA and IbpB, are involved in resistances to heat and superoxide stresses in Escherichia coli. *FEMS Microbiol Lett*, 184, 165-71.
- KUZMINOV, A. 1999. Recombinational repair of DNA damage in Escherichia coli and bacteriophage lambda. *Microbiol Mol Biol Rev*, 63, 751-813, table of contents.
- LANGMEAD, B. & SALZBERG, S. L. 2012. Fast gapped-read alignment with Bowtie 2. *Nat Methods*, 9, 357-9.
- LAVOIE, S. P., MAPOLELO, D. T., COWART, D. M., POLACCO, B. J., JOHNSON, M. K., SCOTT, R. A., MILLER, S. M. & SUMMERS, A. O. 2015. Organic and inorganic mercurials have distinct

effects on cellular thiols, metal homeostasis, and Fe-binding proteins in *Escherichia coli*. *J Biol Inorg Chem*, 20, 1239-51.

LEE, J., PAGE, R., GARCIA-CONTRERAS, R., PALERMINO, J. M., ZHANG, X. S., DOSHI, O., WOOD, T. K. & PETI, W. 2007. Structure and function of the *Escherichia coli* protein YmgB: a protein critical for biofilm formation and acid-resistance. *J Mol Biol*, 373, 11-26.

LEMKE, J. J., SANCHEZ-VAZQUEZ, P., BURGOS, H. L., HEDBERG, G., ROSS, W. & GOURSE, R. L. 2011. Direct regulation of *Escherichia coli* ribosomal protein promoters by the transcription factors ppGpp and DksA. *Proc Natl Acad Sci U S A*, 108, 5712-7.

LI, H., HANDSAKER, B., WYSOKER, A., FENNEL, T., RUAN, J., HOMER, N., MARTH, G., ABECASIS, G., DURBIN, R. & GENOME PROJECT DATA PROCESSING, S. 2009. The Sequence Alignment/Map format and SAMtools. *Bioinformatics*, 25, 2078-9.

LIOCHEV, S. I. & FRIDOVICH, I. 1993. Modulation of the fumarases of *Escherichia coli* in response to oxidative stress. *Arch Biochem Biophys*, 301, 379-84.

LUND, B. O., MILLER, D. M. & WOODS, J. S. 1991. Mercury-induced H<sub>2</sub>O<sub>2</sub> production and lipid peroxidation in vitro in rat kidney mitochondria. *Biochem Pharmacol*, 42 Suppl, S181-7.

LUSETTI, S. L. & COX, M. M. 2002. The bacterial RecA protein and the recombinational DNA repair of stalled replication forks. *Annu Rev Biochem*, 71, 71-100.

MALM, O. 1998. Gold mining as a source of mercury exposure in the Brazilian Amazon. *Environ Res*, 77, 73-8.

MARTIN, J. E. & IMLAY, J. A. 2011. The alternative aerobic ribonucleotide reductase of *Escherichia coli*, NrdEF, is a manganese-dependent enzyme that enables cell replication during periods of iron starvation. *Mol Microbiol*, 80, 319-34.

MASON, R. P., FITZGERALD, W. F. & MOREL, F. M. M. 1994. The Biogeochemical Cycling of Elemental Mercury - Anthropogenic Influences. *Geochimica Et Cosmochimica Acta*, 58, 3191-3198.

MATUSZEWSKA, E., KWIATKOWSKA, J., KUCZYNSKA-WISNIK, D. & LASKOWSKA, E. 2008. *Escherichia coli* heat-shock proteins IbpA/B are involved in resistance to oxidative stress induced by copper. *Microbiology*, 154, 1739-47.

MCELWEE, M. K. & FREEDMAN, J. H. 2011. Comparative toxicology of mercurials in *Caenorhabditis elegans*. *Environ Toxicol Chem*, 30, 2135-41.

MCELWEE, M. K., HO, L. A., CHOU, J. W., SMITH, M. V. & FREEDMAN, J. H. 2013. Comparative toxicogenomic responses of mercuric and methyl-mercury. *BMC Genomics*, 14, 698.

- MEHTA, P., CASJENS, S. & KRISHNASWAMY, S. 2004. Analysis of the lambdoid prophage element e14 in the E. coli K-12 genome. *BMC Microbiol*, 4, 4.
- MERMOD, M., MAGNANI, D., SOLIOZ, M. & STOYANOV, J. V. 2012. The copper-inducible ComR (YcfQ) repressor regulates expression of ComC (YcfR), which affects copper permeability of the outer membrane of Escherichia coli. *Biometals*, 25, 33-43.
- NEIDHARDT, F. C., BLOCH, P. L. & SMITH, D. F. 1974. Culture medium for enterobacteria. *J Bacteriol*, 119, 736-47.
- NISHINO, K., SENDA, Y. & YAMAGUCHI, A. 2008. The AraC-family regulator GadX enhances multidrug resistance in Escherichia coli by activating expression of mdtEF multidrug efflux genes. *J Infect Chemother*, 14, 23-9.
- NISHINO, K., YAMADA, J., HIRAKAWA, H., HIRATA, T. & YAMAGUCHI, A. 2003. Roles of TolC-dependent multidrug transporters of Escherichia coli in resistance to beta-lactams. *Antimicrob Agents Chemother*, 47, 3030-3.
- NOMURA, M., GOURSE, R. & BAUGHMAN, G. 1984. Regulation of the synthesis of ribosomes and ribosomal components. *Annu Rev Biochem*, 53, 75-117.
- ORAM, P. D., FANG, X., FERNANDO, Q., LETKEMAN, P. & LETKEMAN, D. 1996. The formation of constants of mercury(II)--glutathione complexes. *Chem Res Toxicol*, 9, 709-12.
- OUTTEN, F. W., HUFFMAN, D. L., HALE, J. A. & O'HALLORAN, T. V. 2001. The independent cue and cus systems confer copper tolerance during aerobic and anaerobic growth in Escherichia coli. *J Biol Chem*, 276, 30670-7.
- PAL, C., BENGTSSON-PALME, J., KRISTIANSSON, E. & LARSSON, D. G. 2015. Co-occurrence of resistance genes to antibiotics, biocides and metals reveals novel insights into their co-selection potential. *BMC Genomics*, 16, 964.
- PARK, S. J. & GUNSALUS, R. P. 1995. Oxygen, iron, carbon, and superoxide control of the fumarase fumA and fumC genes of Escherichia coli: role of the arcA, fnr, and soxR gene products. *J Bacteriol*, 177, 6255-62.
- PIRRONE, N., CINNIRELLA, S., FENG, X., FINKELMAN, R. B., FRIEDLI, H. R., LEANER, J., MASON, R., MUKHERJEE, A. B., STRACHER, G., STREETS, D. G. & TELMER, K. 2009. Global Mercury Emissions to the Atmosphere from Natural and Anthropogenic Sources. In: MASON, R. & PIRRONI, N. (eds.) *Mercury Fate and Transport in the Global Atmosphere: Emissions, Measurements and Models*. Boston, MA: Springer US.
- RAETZ, C. R., REYNOLDS, C. M., TRENT, M. S. & BISHOP, R. E. 2007. Lipid A modification systems in gram-negative bacteria. *Annu Rev Biochem*, 76, 295-329.
- RENSING, C., MITRA, B. & ROSEN, B. P. 1997. The zntA gene of Escherichia coli encodes a Zn(II)-translocating P-type ATPase. *Proc Natl Acad Sci U S A*, 94, 14326-31.

RICHARDSON, G. M., WILSON, R., ALLARD, D., PURTILL, C., DOUMA, S. & GRAVIERE, J. 2011. Mercury exposure and risks from dental amalgam in the US population, post-2000. *Sci Total Environ*, 409, 4257-68.

SALGADO, H., MARTINEZ-FLORES, I., LOPEZ-FUENTES, A., GARCIA-SOTELO, J. S., PORRON-SOTELO, L., SOLANO, H., MUNIZ-RASCADO, L. & COLLADO-VIDES, J. 2012. Extracting regulatory networks of *Escherichia coli* from RegulonDB. *Methods Mol Biol*, 804, 179-95.

SALGADO, H., PERALTA-GIL, M., GAMA-CASTRO, S., SANTOS-ZAVALA, A., MUNIZ-RASCADO, L., GARCIA-SOTELO, J. S., WEISS, V., SOLANO-LIRA, H., MARTINEZ-FLORES, I., MEDINA-RIVERA, A., SALGADO-OSORIO, G., ALQUICIRA-HERNANDEZ, S., ALQUICIRA-HERNANDEZ, K., LOPEZ-FUENTES, A., PORRON-SOTELO, L., HUERTA, A. M., BONAVIDES-MARTINEZ, C., BALDERAS-MARTINEZ, Y. I., PANNIER, L., OLVERA, M., LABASTIDA, A., JIMENEZ-JACINTO, V., VEGA-ALVARADO, L., DEL MORAL-CHAVEZ, V., HERNANDEZ-ALVAREZ, A., MORETT, E. & COLLADO-VIDES, J. 2013. RegulonDB v8.0: omics data sets, evolutionary conservation, regulatory phrases, cross-validated gold standards and more. *Nucleic Acids Res*, 41, D203-13.

SALMON, K., HUNG, S. P., MEKJIAN, K., BALDI, P., HATFIELD, G. W. & GUNSALUS, R. P. 2003. Global gene expression profiling in *Escherichia coli* K12. The effects of oxygen availability and FNR. *J Biol Chem*, 278, 29837-55.

SCHAECHTER, M. & SANTOMASSINO, K. A. 1962. Lysis of *Escherichia coli* by sulfhydryl-binding reagents. *J Bacteriol*, 84, 318-25.

SEO, S. W., KIM, D., SZUBIN, R. & PALSSON, B. O. 2015. Genome-wide Reconstruction of OxyR and SoxRS Transcriptional Regulatory Networks under Oxidative Stress in *Escherichia coli* K-12 MG1655. *Cell Rep*, 12, 1289-99.

SORENSEN, K. I. & HOVE-JENSEN, B. 1996. Ribose catabolism of *Escherichia coli*: characterization of the rpiB gene encoding ribose phosphate isomerase B and of the rpiR gene, which is involved in regulation of rpiB expression. *J Bacteriol*, 178, 1003-11.

SOSKINE, M., STEINER-MORDOCH, S. & SCHULDINER, S. 2002. Crosslinking of membrane-embedded cysteines reveals contact points in the EmrE oligomer. *Proc Natl Acad Sci U S A*, 99, 12043-8.

STEAD, M. B., AGRAWAL, A., BOWDEN, K. E., NASIR, R., MOHANTY, B. K., MEAGHER, R. B. & KUSHNER, S. R. 2012. RNAsnap: a rapid, quantitative and inexpensive, method for isolating total RNA from bacteria. *Nucleic Acids Res*, 40, e156.

SUMMERS, A. O., WIREMAN, J., VIMY, M. J., LORSCHIEDER, F. L., MARSHALL, B., LEVY, S. B., BENNETT, S. & BILLARD, L. 1993. Mercury released from dental "silver" fillings provokes an increase in mercury- and antibiotic-resistant bacteria in oral and intestinal floras of primates. *Antimicrob Agents Chemother*, 37, 825-34.

- TCHOUNWOU, P. B., AYENSU, W. K., NINASHVILI, N. & SUTTON, D. 2003. Environmental exposure to mercury and its toxicopathologic implications for public health. *Environ Toxicol*, 18, 149-75.
- TSANEVA, I. R. & WEISS, B. 1990. *soxR*, a locus governing a superoxide response regulon in *Escherichia coli* K-12. *J Bacteriol*, 172, 4197-205.
- TUCKER, D. L., TUCKER, N., MA, Z., FOSTER, J. W., MIRANDA, R. L., COHEN, P. S. & CONWAY, T. 2003. Genes of the *GadX-GadW* regulon in *Escherichia coli*. *J Bacteriol*, 185, 3190-201.
- UNG, C. Y., LAM, S. H., HLAING, M. M., WINATA, C. L., KORZH, S., MATHAVAN, S. & GONG, Z. 2010. Mercury-induced hepatotoxicity in zebrafish: in vivo mechanistic insights from transcriptome analysis, phenotype anchoring and targeted gene expression validation. *BMC Genomics*, 11, 212.
- VALKO, M., MORRIS, H. & CRONIN, M. T. 2005. Metals, toxicity and oxidative stress. *Curr Med Chem*, 12, 1161-208.
- VAN HOUDT, R. & MICHELIS, C. W. 2005. Role of bacterial cell surface structures in *Escherichia coli* biofilm formation. *Res Microbiol*, 156, 626-33.
- VARGHESE, S., TANG, Y. & IMLAY, J. A. 2003. Contrasting sensitivities of *Escherichia coli* aconitases A and B to oxidation and iron depletion. *J Bacteriol*, 185, 221-30.
- VARGHESE, S., WU, A., PARK, S., IMLAY, K. R. & IMLAY, J. A. 2007. Submicromolar hydrogen peroxide disrupts the ability of Fur protein to control free-iron levels in *Escherichia coli*. *Mol Microbiol*, 64, 822-30.
- WANG, A. & CROWLEY, D. E. 2005. Global gene expression responses to cadmium toxicity in *Escherichia coli*. *J Bacteriol*, 187, 3259-66.
- WANG, X., KIM, Y., MA, Q., HONG, S. H., POKUSAEVA, K., STURINO, J. M. & WOOD, T. K. 2010. Cryptic prophages help bacteria cope with adverse environments. *Nat Commun*, 1, 147.
- WATANABE, S., KITA, A., KOBAYASHI, K. & MIKI, K. 2008. Crystal structure of the [2Fe-2S] oxidative-stress sensor SoxR bound to DNA. *Proc Natl Acad Sci U S A*, 105, 4121-6.
- WILSON, D. N. & NIERHAUS, K. H. 2007. The weird and wonderful world of bacterial ribosome regulation. *Crit Rev Biochem Mol Biol*, 42, 187-219.
- WIREMAN, J., LIEBERT, C. A., SMITH, T. & SUMMERS, A. O. 1997. Association of mercury resistance with antibiotic resistance in the gram-negative fecal bacteria of primates. *Appl Environ Microbiol*, 63, 4494-503.
- XU, F. F. & IMLAY, J. A. 2012. Silver(I), mercury(II), cadmium(II), and zinc(II) target exposed enzymic iron-sulfur clusters when they toxify *Escherichia coli*. *Appl Environ Microbiol*, 78, 3614-21.

- YAMADA, T., LETUNIC, I., OKUDA, S., KANEHISA, M. & BORK, P. 2011. iPath2.0: interactive pathway explorer. *Nucleic Acids Res*, 39, W412-5.
- YORIFUJI, T., TSUDA, T., TAKAO, S. & HARADA, M. 2008. Long-term exposure to methylmercury and neurologic signs in Minamata and neighboring communities. *Epidemiology*, 19, 3-9.
- ZAHIR, F., RIZWI, S. J., HAQ, S. K. & KHAN, R. H. 2005. Low dose mercury toxicity and human health. *Environ Toxicol Pharmacol*, 20, 351-60.
- ZHANG, X. S., GARCIA-CONTRERAS, R. & WOOD, T. K. 2007. YcfR (BhsA) influences Escherichia coli biofilm formation through stress response and surface hydrophobicity. *J Bacteriol*, 189, 3051-62.
- ZHAO, G., CECI, P., ILARI, A., GIANGIACOMO, L., LAUE, T. M., CHIANCONE, E. & CHASTEEN, N. D. 2002. Iron and hydrogen peroxide detoxification properties of DNA-binding protein from starved cells. A ferritin-like DNA-binding protein of Escherichia coli. *J Biol Chem*, 277, 27689-96.
- ZHENG, M., WANG, X., TEMPLETON, L. J., SMULSKI, D. R., LAROSSA, R. A. & STORZ, G. 2001. DNA microarray-mediated transcriptional profiling of the Escherichia coli response to hydrogen peroxide. *J Bacteriol*, 183, 4562-70.



**Table 4.1: Genes with  $\geq 32$  fold-change in at least one time point for HgCl<sub>2</sub> (n=39).**

Gene ID	Gene name	Protein description	Hg t10	Hg t30	Hg t60	PMA t10	PMA t30	PMA t60
b1112	bhsA	Biofilm, cell surface and signaling defects, YhcN family	1949	563	94	46	21	n.s.
b4458	oxyS	OxyS sRNA activates genes that detoxify oxidative damage	1524	1292	150	10	6	n.s.
b4249	bdcA	c-di-GMP-binding biofilm dispersal mediator protein	596	79	7	16	2	n.s.
b3686	ibpB	Chaperone, heat-inducible protein of HSP20 family	402	124	281	37	211	9
b0812	dps	Stress-induced Fe-binding and storage protein	339	52	n.s.	4	2	n.s.
b4248	yjgH	Putative reactive intermediate deaminase	296	24	3	6	2	n.s.
b0849	grxA	Glutaredoxin 1	246	33	n.s.	14	4	n.s.
b1144	ymfJ	Function unknown, e14 prophage	185	39	n.s.	3	3	n.s.
b2582	trxC	Thioredoxin 2, zinc-binding; Trx2	134	50	7	24	24	n.s.
b3501	arsR	Arsenate resistance operon repressor	106	16	n.s.	21	8	n.s.
b1147	ymfL	Function unknown, e14 prophage	95	29	n.s.	n.s.	3	n.s.
b1146	croE	Cro-like repressor, e14 prophage	90	40	n.s.	n.s.	n.s.	n.s.
b3502	arsB	Arsenite pump, inner membrane	86	10	n.s.	12	4	n.s.
b3687	ibpA	Chaperone, heat-inducible protein of HSP20 family	86	19	41	10	28	4
b0606	ahpF	Alkyl hydroperoxide reductase, subunit F	78	11	n.s.	n.s.	n.s.	n.s.
b0475	hemH	Ferrochelatase	72	7	n.s.	2	3	n.s.
b2531	iscR	Transcriptional repressor for isc operon	62	48	9	12	18	n.s.
b4692	oweE	lambda replication protein O homolog; CPS-53/KpLE1 prophage	54	n.s.	n.s.	n.s.	n.s.	n.s.
b2670	alaE	Alanine exporter, inducible; stress-responsive	54	12	n.s.	24	16	n.s.
b1148	ymfM	Function unknown, e14 prophage	49	21	n.s.	n.s.	n.s.	n.s.
b3503	arsC	Arsenate reductase	49	4	n.s.	4	n.s.	n.s.
b1649	nemR	nem operon repressor, NEM-inactivated	43	6	n.s.	3	4	n.s.
b1141	xisE	e14 excisionase, in defective prophage	41	10	n.s.	n.s.	2	n.s.
b3469	zntA	Zn(II), Cd(II), and Pb(II) translocating P-type ATPase	40	19	8	29	22	n.s.
b4090	rpiB	Ribose-5-phosphate isomerase B	40	n.s.	-3	n.s.	n.s.	n.s.
b4599	yneM	membrane-associated, function unknown; regulated by PhoPQ and Mg(2+)	38	36	n.s.	3	3	n.s.
b3828	metR	Positive regulatory gene for metE and metH	36	16	n.s.	-2	4	n.s.
b1140	intE	e14 integrase, in defective prophage	36	11	n.s.	4	4	n.s.
b4030	psiE	Pho regulon, regulated by phoB and cAMP	35	64	17	38	59	n.s.
b2673	nrdH	NrdH-redoxin reducing oxidized NrdEF	35	127	21	7	14	n.s.
b2667	ygaV	Tributyltin-inducible repressor of ygaVP, function unknown	35	n.s.	n.s.	24	11	n.s.
b4060	yjcB	Function unknown	33	11	12	52	35	n.s.
b1684	sufA	Scaffold protein for assembly of iron-sulfur clusters	32	39	5	n.s.	3	n.s.
b2674	nrdI	Flavodoxin required for NrdEF cluster assembly	21	73	22	4	7	n.s.
b1020	phoH	ATP-binding protein, function unknown	8	71	221	61	365	n.s.
b0379	yaiY	Inner membrane protein, function unknown	10	35	6	4	4	n.s.
b0753	ybgS	Function unknown	16	35	18	15	13	n.s.
b4002	zraP	Zn-dependent periplasmic chaperone	3	27	43	n.s.	n.s.	-3
b4663	azuC	Expressed protein, membrane-associated	27	25	36	41	49	n.s.

\* values represent fold-change difference in expression from unexposed control

\* n.s. = not significantly different from unexposed control

**Table 4.2: Genes with  $\geq 32$  fold-change in at least one time point for PMA (n=20).**

Gene ID	Gene name	Protein description	Hg t10	Hg t30	Hg t60	PMA t10	PMA t30	PMA t60
b3728	pstS	Periplasmic phosphate binding protein, high-affinity; ABC phosphate transport system	n.s.	16	8	<b>86</b>	<b>165</b>	n.s.
b1020	phoH	ATP-binding protein, function unknown	8	<b>71</b>	<b>221</b>	<b>61</b>	<b>365</b>	n.s.
b0996	torC	c-Type cytochrome	n.s.	n.s.	n.s.	<b>55</b>	<b>65</b>	<b>77</b>
b4060	yjcB	Function unknown	<b>33</b>	11	12	<b>52</b>	<b>35</b>	n.s.
b0399	phoB	Positive response regulator for pho regulon, two-component system	4	22	3	<b>51</b>	<b>105</b>	n.s.
b1530	marR	Transcription repressor of multiple antibiotic resistance; resistance to tetracycline, chloramphenicol, etc.; dimeric	26	7	n.s.	<b>48</b>	29	n.s.
b1531	marA	Transcriptional activator for multiple antibiotic resistance; AraC family; resistance to tetracycline, chloramphenicol	15	9	n.s.	<b>46</b>	31	n.s.
b1112	bhsA	Biofilm, cell surface and signaling defects, YhcN family	<b>1949</b>	<b>563</b>	<b>94</b>	<b>46</b>	21	n.s.
b1532	marB	Function unknown; probable periplasmic protein in marRAB multiple antibiotic resistance operon	16	8	n.s.	<b>45</b>	27	n.s.
b4663	azuC	Expressed protein, membrane-associated	27	25	<b>36</b>	<b>41</b>	<b>49</b>	n.s.
b4030	psiE	Pho regulon, regulated by phoB and cAMP	<b>35</b>	<b>64</b>	17	<b>38</b>	<b>59</b>	n.s.
b3686	ibpB	Chaperone, heat-inducible protein of HSP20 family	<b>402</b>	<b>124</b>	<b>281</b>	<b>37</b>	<b>211</b>	9
b1748	astC	Succinylornithine transaminase, mutant cannot catabolize arginine, overproduction complements argD mutants; carbon starvation protein	30	31	25	<b>34</b>	<b>36</b>	n.s.
b0241	phoE	Outer membrane phosphoprotein E; trimeric	n.s.	n.s.	n.s.	11	<b>133</b>	n.s.
b1167	yngC	Blue light, low temperature and stress induced, function unknown; BluRF(YcgEF) and RpoS regulons	n.s.	n.s.	7	13	<b>86</b>	n.s.
b4354	yjiY	Predicted transporter, function unknown	n.s.	n.s.	n.s.	20	<b>77</b>	n.s.
b3453	ugpB	sn-Glycerol-3-phosphate transport system, periplasmic binding protein	6	8	9	11	<b>57</b>	n.s.
b1504	ydeS	Function unknown, FimA homolog	n.s.	23	n.s.	n.s.	<b>57</b>	n.s.
b0400	phoR	Sensor histidine kinase/phosphatase for pho regulon; cognate to phoB	2	15	4	14	<b>35</b>	n.s.
b1021	pgaD	Biofilm PGA synthase PgaCD, regulatory subunit; c-di-GMP-stimulated activity and dimerization	n.s.	2	n.s.	12	<b>33</b>	n.s.

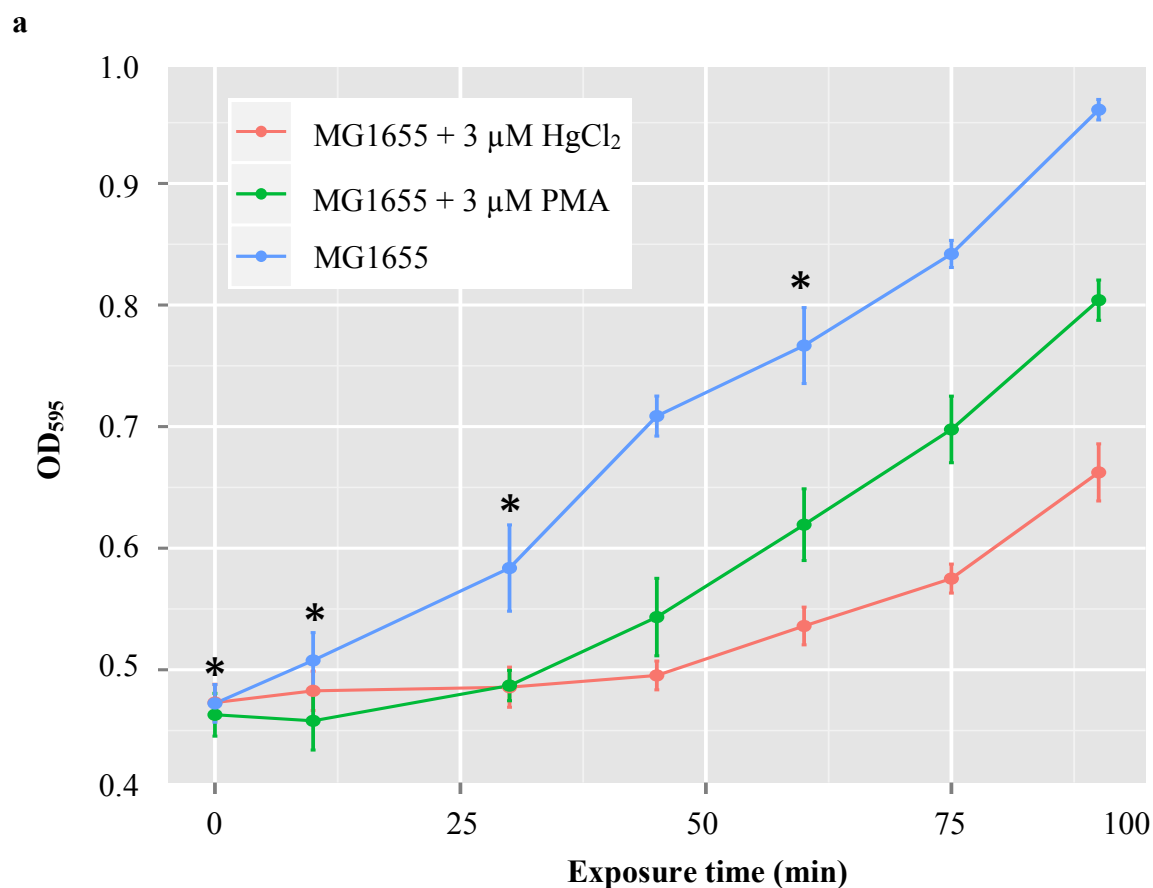
\* values represent fold-change difference in expression from unexposed control

\* n.s. = not significantly different from unexposed control

**Table 4.3: Summary of Sigma Factors and Transcription Factors.**

	Hg_t10	Hg_t30	Hg_t60	PMA_t10	PMA_t30	PMA_t60
<b>Sigma Factors</b>						
<i>fecI</i> , $\sigma^{19}$	-3	n.s.	n.s.	-2	n.s.	n.s.
<i>rpoE</i> , $\sigma^{24}$	n.s.	n.s.	n.s.	n.s.	n.s.	n.s.
<i>fliA</i> , $\sigma^{28}$	n.s.	-3	-6	n.s.	n.s.	n.s.
<i>rpoH</i> , $\sigma^{32}$	2	4	n.s.	6	5	n.s.
<i>rpoS</i> , $\sigma^{38}$	3	3	n.s.	14	10	n.s.
<i>rpoN</i> , $\sigma^{54}$	n.s.	n.s.	n.s.	n.s.	n.s.	n.s.
<i>rpoD</i> , $\sigma^{70}$	3	n.s.	n.s.	n.s.	n.s.	n.s.
<b>Transcription Factors</b>						
up	63 (31%)	46 (23%)	14 (7%)	86 (42%)	78 (38%)	1 (0.5%)
down	28 (14%)	28 (14%)	13 (6%)	22 (11%)	23 (11%)	2 (1%)

Fold-change in expression of sigma factors; with green shading for up-regulated, red shading for down-regulated and n.s. for not significantly different from control. Sum of transcription factor genes either up-regulated or down-regulated and percentage of the total genes (n=203) in parenthesis.



**b**

	t10	t30	t60
3μM HgCl <sub>2</sub>	1,819 (892↑927↓)	1,421 (636↑785↓)	562 (258↑304↓)
3μM PMA	2,179 (1,259↑920↓)	2,006 (1,153↑853↓)	64 (35↑29↓)

**Figure 4.1: Effects of sub-acute mercury exposure on growth of MG1655. (a)** *E. coli* K12 MG1655 in MOPS minimal medium, unexposed (blue) or exposed to 3 μM HgCl<sub>2</sub> (red) or 3 μM PMA (green) during mid-log phase. Asterisks indicate sampling times for RNA-seq. Error bars are standard error (SEM) of 3 biological replicates for each culture condition. See Figure D.S1 for full growth curve. **(b)** Differentially expressed genes (DEG) counts for HgCl<sub>2</sub> and PMA relative to unexposed control culture at each time point.

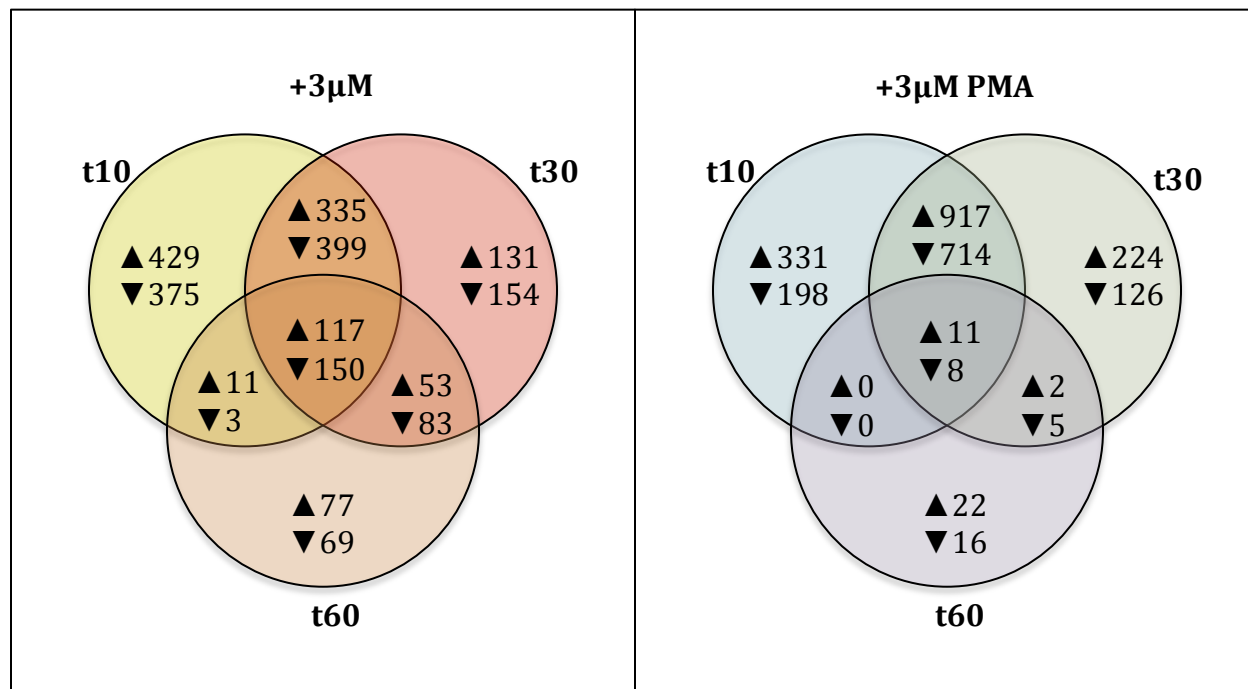


**Figure 4.2:** Shared genes at each sampling time for  $\text{HgCl}_2$  or PMA exposures. DEGs in outer circles represent unique genes not shared between time points.

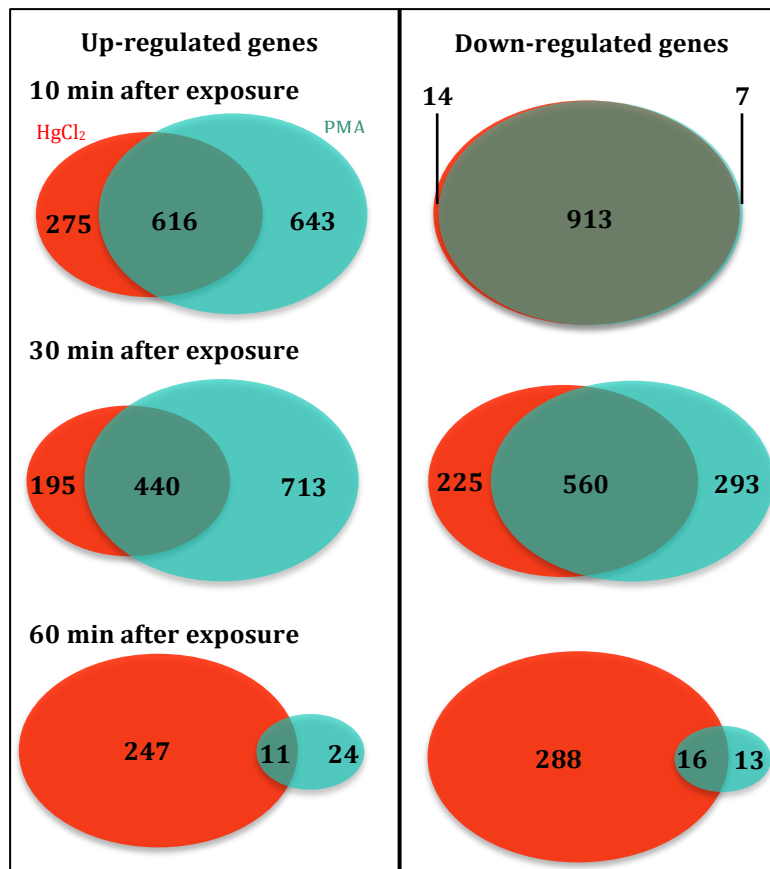


**Figure 4.3: Overlap between differentially expressed genes at each sampling time** The 3  $\mu\text{M}$   $\text{HgCl}_2$  exposure is in red and the 3  $\mu\text{M}$  PMA exposure in green.

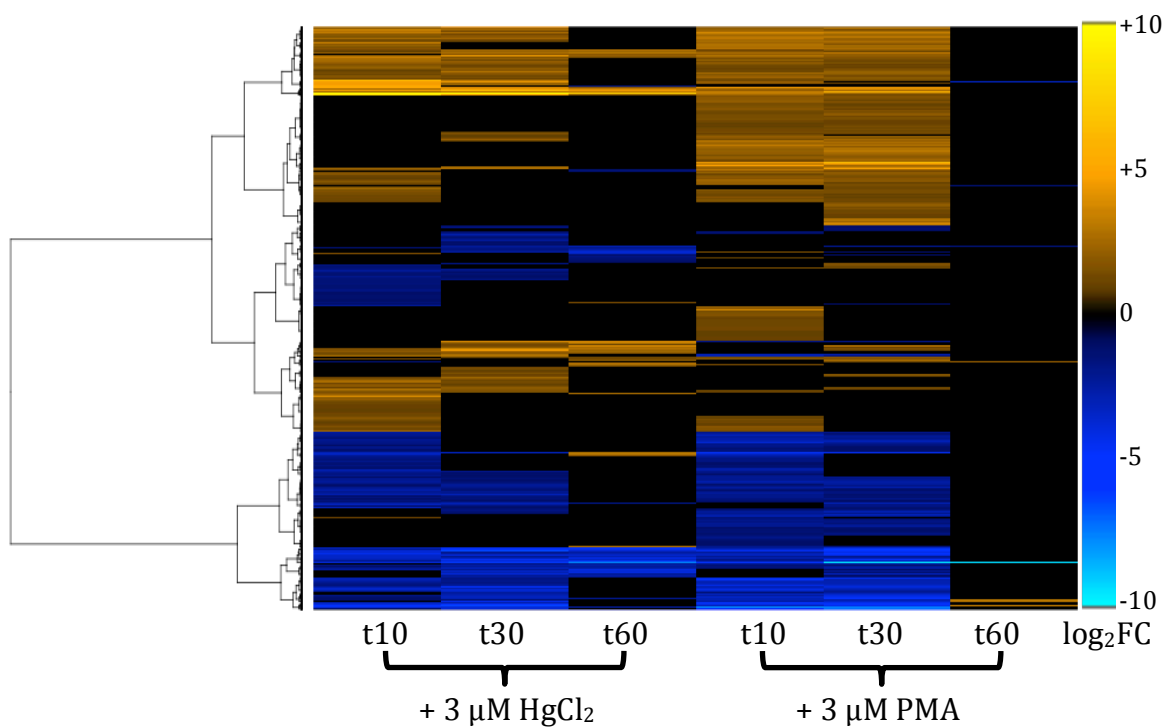


**Figure 4.4: Differentially expressed genes at each sampling time.** Heatmap of all genes that were differentially expressed in at least one mercury exposure condition ( $n = 3,149$ ). Genes were clustered by row using Ward's minimum variance method with non-squared log<sub>2</sub> fold-change input values.

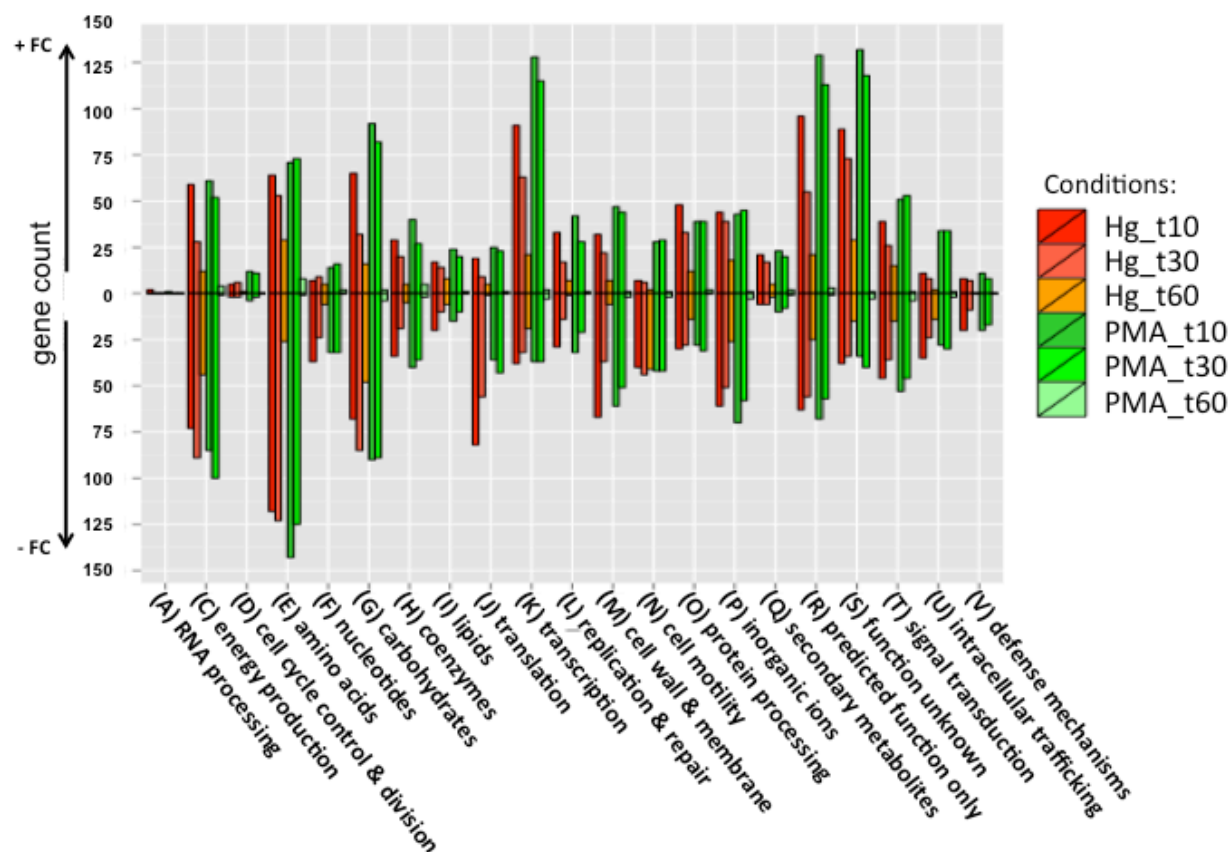


**Figure 4.5: Counts of differentially expressed genes for each condition grouped by COG functional category.** Genes with a  $\log_2$  fold-change  $\geq 1$  for each condition were grouped by COG group. Positive counts represent up-regulated genes and negative counts represent down-regulated genes. COG code, number of proteins encoded by genome and category description: (A, 2) RNA processing and modification; (C, 287) Energy production and conversion; (D, 33) Cell cycle control, cell division, chromosome partitioning; (E, 363) Amino acid transport and metabolism; (F, 97) Nucleotide transport and metabolism; (G, 368) Carbohydrate transport and metabolism; (H, 153) Coenzyme transport and metabolism; (I, 100) Lipid transport and metabolism; (J, 182) Translation, ribosomal structure and biogenesis; (K, 301) Transcription; (L, 200) Replication, recombination and repair; (M, 226) Cell wall, membrane and envelope



biogenesis; (N, 111) Cell motility; (O, 138) Post-translational modification, protein turnover, chaperones; (P, 217) Inorganic ion transport and metabolism; (Q, 64) Secondary metabolites biosynthesis, transport and catabolism; (R, 394) General function prediction only; (S, 318) Function unknown; (T, 178) Signal transduction mechanisms; (U, 124) Intracellular trafficking, secretion, and vesicular transport; (V, 49) Defense mechanisms.

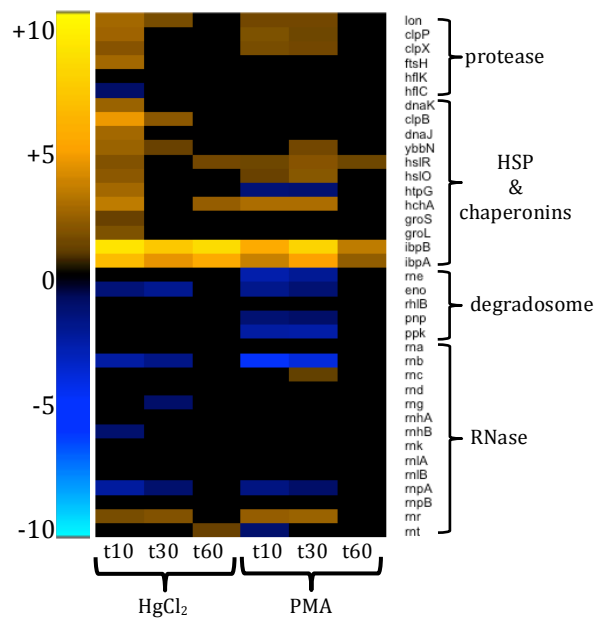


**Figure 4.6: Protease, heat shock proteins, degradosome complex and RNase's.**

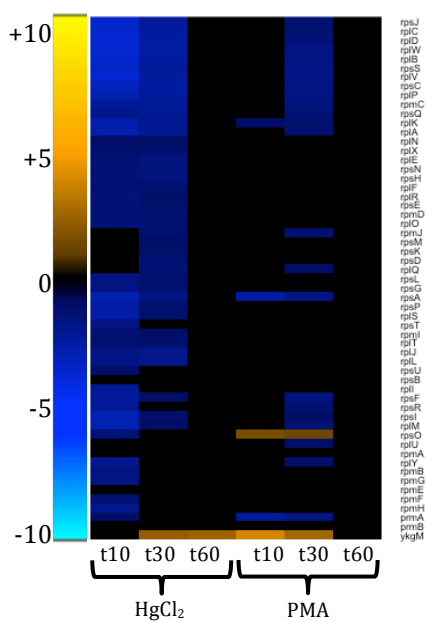


**Figure 4.7: Ribosomal subunit protein genes, grouped by operon (see Table D.S5 for details).**

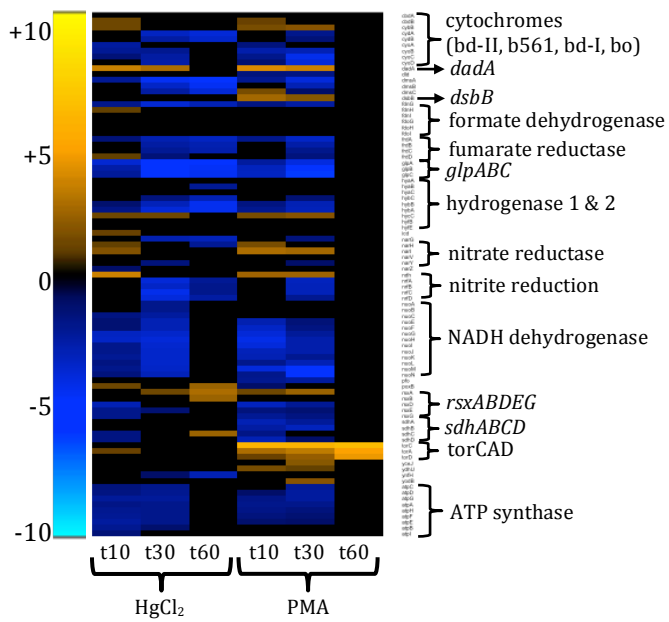


**Figure 4.8: Electron transport chain and ATP-synthase.**

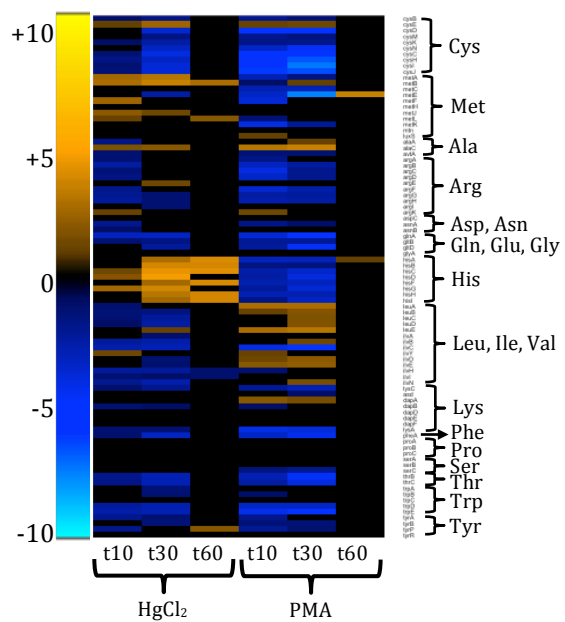


**Figure 4.9: Amino acid biosynthesis.**

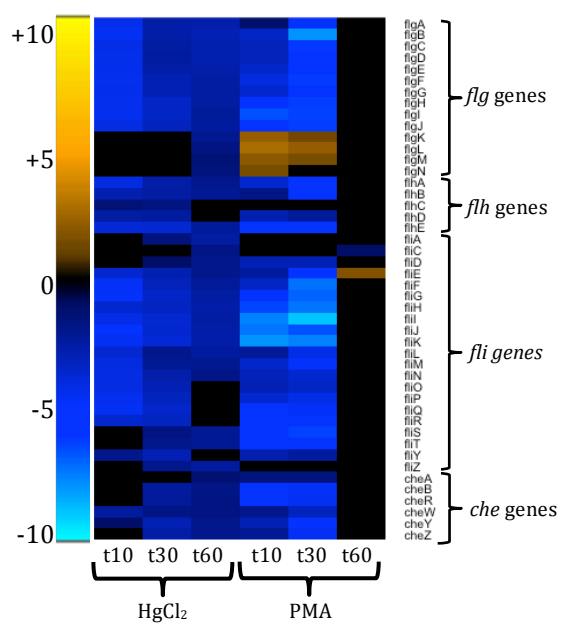


**Figure 4.10: Flagella components and chemotaxis.**

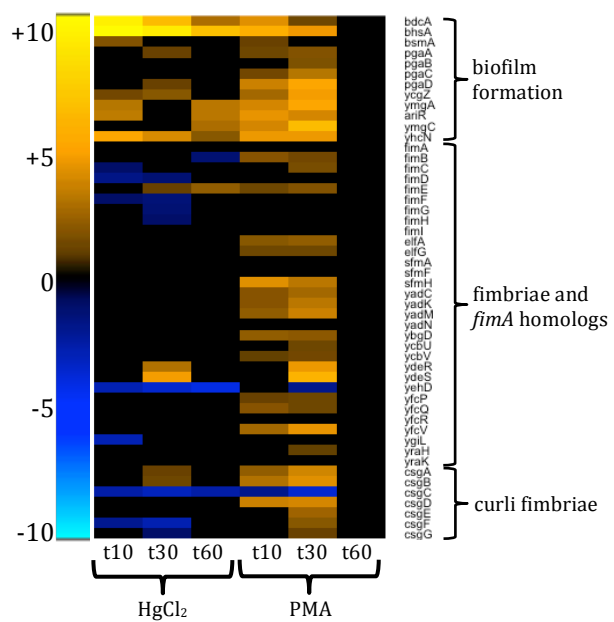


**Figure 4.11: Biofilm formation, fimbriae, and curli fimbriae.**

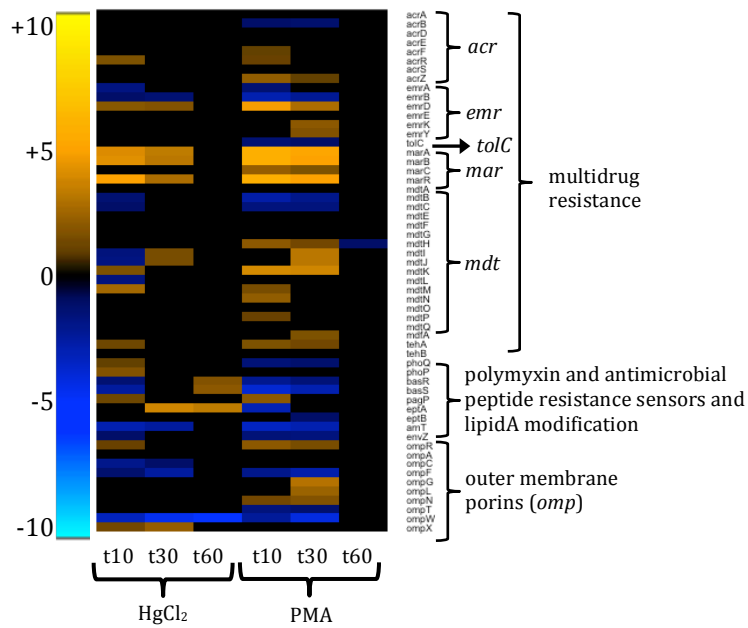


**Figure 4.12: Antibiotic resistance and outer membrane porins.**



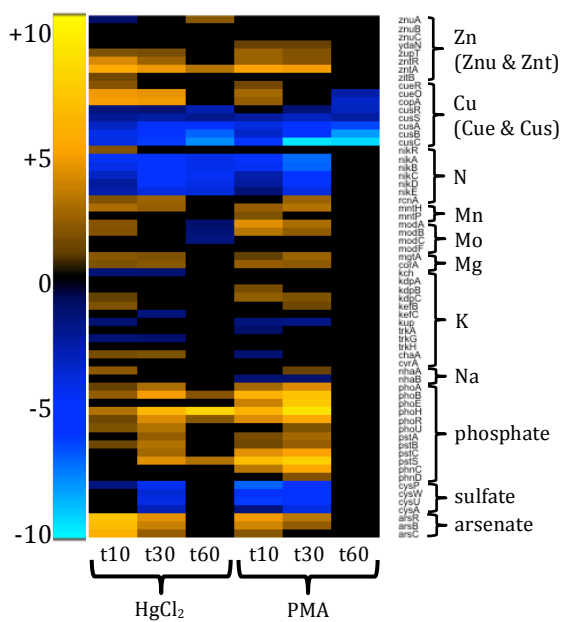


**Figure 4.13: Non-iron inorganic metals transport and regulation.**

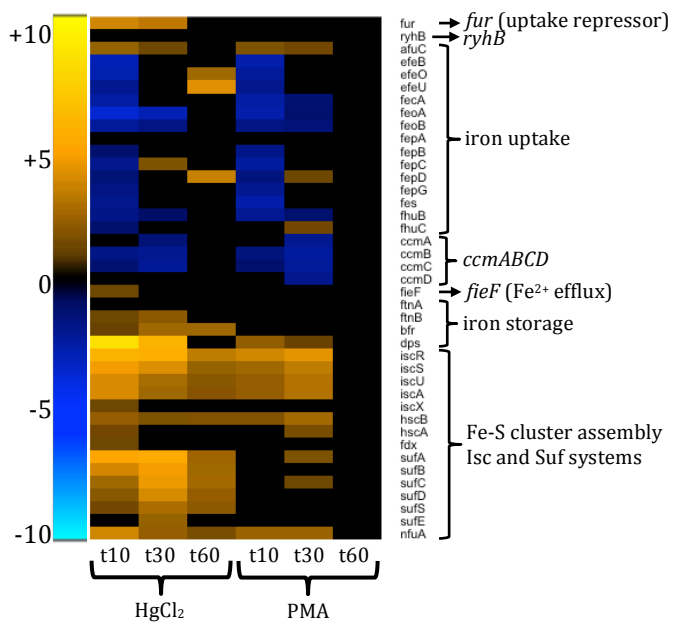


**Figure 4.14: Iron transport, storage, and iron-sulfur cluster assembly.**

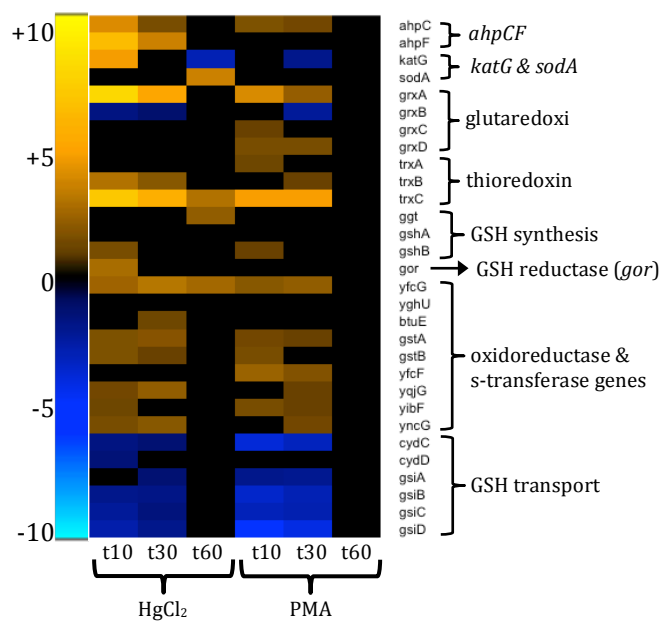


**Figure 4.15: Oxidative stress defense enzymes, glutaredoxin (*grxABCD*), thioredoxin (*trxABC*), and glutathione (GSH) related genes.**

## CHAPTER 5

### SUMMARY

In the preceding chapters, biochemical and molecular methods were used to assess the biochemical effects of mercurials, identify and characterize *in vivo* mercury binding targets, and compare transcriptional responses to inorganic and organic mercury exposure in a model prokaryotic organism.

In Chapter 2, a comparison of the bulk biochemical effects of acute inorganic and organic mercury exposure were examined. Inorganic mercury was more effective in short term exposure at blocking total and proteins thiols than PMA, and both compounds were more effective than merthiolate. All mercurials disrupted the sodium and potassium electrolyte balance of the cell, similar to calcium disruption previously observed in animals. When Hg(II) exceeds the available cellular thiol pool, non-thiol cellular targets such as nitrogen ligands in nucleotide bases and protein histidine and amine groups form complexes with it, but this was not seen with organomercurials. Mercury had previously been shown to disrupt iron-sulfur clusters of dehydratases, but we further showed that Hg(II) was far more effective than organic oxidizers at disrupting iron homeostasis, resulting in an increase in intracellular free iron. Proteomics analysis, discussed in Chapter 3, revealed that mercury not only displaces iron from Fe-S clusters, but also binds to cysteine residues that coordinate iron and zinc cofactors, which prevents repair and restoration of function. These are the first *in vivo* observations in a well defined model organism of the biochemical differences of inorganic and organic mercury

exposure that contribute to their distinct toxicological profiles in bacteria and likely also higher organisms.

In Chapter 3, the *in vivo* protein targets of brief exposure to 40 $\mu$ M PMA were identified using LC-MS/MS proteomics analysis. Sample preparation methods for bottom-up proteomics were optimized to identify cysteine peptides and to preserve *in vivo* mercury binding sites. The *in vitro* addition of iodoacetamide was used to prevent re-association of mercury exchanged between peptides, but the large excess appears to destabilize mercury adducts. A computation filter was developed as part of this project (see Appendix A), which utilizes the isotopic profile of mercury to identify mercury modified peptides from a single protein or within a global proteome. We identified 307 *in vivo* mercury protein targets, which is significant advancement over previous studies using alternative methods. Mercury did not show any bias towards specific functional categories, but rather all functions were observed with adducts. The metabolism categories tend to be more cysteine rich and constituted approximately 40% of cysteine peptide observations and 50% of mercury targets. We identified 22 proteins and 33 cysteine sites conserved in higher organisms that could serve as potential biomarkers. Hg(II) adducts were observed, but only in two cysteine peptides, which suggests that chelation is required to stabilize inorganic mercury adducts for detection by LC-MS/MS. This work provides a new method for using global proteomics to study mercury exposure and further expands knowledge of mercury toxicity mechanisms by identifying protein targets in a model prokaryotic organism.

In Chapter 4, the toxicogenomic effects of sub-acute mercuric chloride and phenylmercuric acetate exposure over time are presented. *E. coli* cultures recovered growth within 30 minutes upon 3  $\mu$ M PMA exposure, but equimolar HgCl<sub>2</sub> exposure required more than 45 minutes to recover a positive growth rate. RNA-Seq data analysis identified toxicity

mechanisms that are shared and unique to each compound. The down-regulated transcriptional response was highly conserved early in exposure, while the up-regulated response was more unique to each compound throughout exposure. Energy production, metabolism and most uptake pathways were repressed for both compounds, while nearly all stress response systems were up-regulated by at least one compound during recovery, including: oxidative stress, heat shock, acid stress, metals homeostasis, biofilm regulation, and antibiotic resistance. Overall, this work builds upon previous studies in animal models that show that inorganic and organic mercury have unique toxicity mechanisms, but in a prokaryotic model organism, and provides a longitudinal view of how cells respond to exposure over time.

In summary, this work provides the most comprehensive view of the effects of mercury exposure in any organism to date. New methods that had not been previously used to study mercury exposure were utilized to compare and identify the biochemical and toxicogenomic effects of exposure to different mercurials. These methods and results could be implemented to study mercury exposure in other organisms. In addition, this work expands knowledge of the effects of mercury on prokaryotes and contributes to understanding how mercury interacts with microbes in the environment and gut of animals.

## **APPENDIX A**

### **DISCOVERING MERCURY PROTEIN MODIFICATIONS IN WHOLE PROTEOMES USING NATURAL ISOTOPE DISTRIBUTIONS OBSERVED IN LIQUID CHROMATOGRAPHY-TANDEM MASS SPECTROMETRY<sup>1</sup>**

---

<sup>1</sup> POLACCO, B. J., PURVINE, S. O., ZINK, E. M., LAVOIE, S. P., LIPTON, M. S., SUMMERS, A. O. & MILLER, S. M. 2011. Discovering mercury protein modifications in whole proteomes using natural isotope distributions observed in liquid chromatography-tandem mass spectrometry. *Mol Cell Proteomics*, 10, M110 004853.; Reprinted with permission of publisher.

## ABSTRACT

The identification of peptides that result from post-translational modifications (PTM) is critical for understanding normal pathways of cellular regulation as well as identifying damage from, or exposures to xenobiotics, i.e. the exposome. However, due to their low abundance in proteomes, effective detection of modified peptides by mass spectrometry (MS) typically requires enrichment to eliminate false identifications. We present a new method for confidently identifying peptides with mercury (Hg)-containing adducts that is based on the influence of mercury's seven stable isotopes on peptide isotope distributions detected by high-resolution MS. Using a pure protein and *E. coli* cultures exposed to phenyl mercuric acetate (PMA), we show the pattern of peak heights in isotope distributions from primary MS single scans efficiently identified Hg adducts in data from chromatographic separation coupled with tandem mass spectrometry (LC-MS/MS) with sensitivity and specificity greater than 90%. Isotope distributions are independent of peptide identifications based on peptide fragmentation (e.g. by SEQUEST), so both methods can be combined to eliminate false positives. Summing peptide isotope distributions across multiple scans improved specificity to 99.4% and sensitivity above 95%, affording identification of an unexpected Hg modification. We also illustrate the theoretical applicability of the method for detection of several less common elements including the essential element, selenium, as selenocysteine in peptides.



## INTRODUCTION

The availability of entire genomic sequences and the development of tandem mass spectrometry and liquid chromatography (LC-MS/MS), has enabled the widespread use of shotgun or bottom-up proteomics over the last decade (Han et al., 2008). Despite imperfect peptide identifications, these techniques effectively catalog even rare proteins present in cells because most proteins are represented by several unique peptides, diminishing the effects of any single false peptide identification. Recent efforts have also enhanced shotgun proteomics to resolve fine scale protein features, such as post-translational modifications (PTM) (Amoresano et al., 2009). However, because many modifications often appear in only a single peptide in typical shotgun proteomics preparations, false peptide identifications can greatly impact the characterization of these modifications.

Preprocessing proteomic preparations to enrich peptides with a PTM of interest is one common strategy used to minimize false identifications. If the modification cannot be enriched, then other independent evidence is needed to increase confidence in PTM identifications. Types of data that have been used for PTM corroboration include characteristic fragmentation such as that for the neutral loss of phosphate (Gesellchen et al., 2006), or modifications observed on overlapping peptides resulting from digestions with different proteases (MacCoss et al., 2002). Here we present a method to discern the anomalous isotope distribution of peptides either post-translationally or co-translationally modified by an element with a distinctive stable isotope “fingerprint” such as the common xenobiotic metal mercury (Hg). This method advances mass spectrometry based proteomics as a possible method for identifying and characterizing the effects of exposures to certain xenobiotics, an area of growing interest recently called the “exposome” (Rappaport, 2011, Wild, 2005).

We first establish theoretically that such perturbations of a peptide's isotope distribution by Hg should be detectable for peptides of unknown sequence, and then demonstrate this experimentally using organomercurial (R<sub>Hg</sub>) modification of a single pure protein and of the entire *E.coli* proteome. Hg is unusual among metals in making nearly covalent bonds with sulfur that survive the LC-MS/MS process (Rubino et al., 2004, Guo et al., 2008), and identifying its most vulnerable protein targets in intact cells is of interest in understanding Hg's pleiotropic toxicity. However, there are no simple preparative procedures with which to extract mercurated proteins from a cell lysate. Thus, we devised a computational filter based on Hg's stable isotope distribution to identify peptides with Hg adducts in the data of an LC-MS/MS proteome.

Because inorganic Hg(II) and organomercurials form very stable bonds with thiols, we have focused on detecting Hg adducts in cysteine-containing peptides. The distinctive isotope distributions of Hg-modified peptides have been qualitatively noted previously (Krupp et al., 2008). Most unmodified peptides have similar isotope distributions. This similarity results from similar ratios of the five peptide elements, C, H, N, O and S in most peptides, and also from the similar isotope distributions of the five elements: each has only two to four stable natural isotopes of which the lightest is substantially more abundant (Figure A.1a). Thus, no single peptide atom, even of sulfur, which has the most complex isotope distribution, can have a very distinctive effect on the peptide isotope distribution. In contrast, Hg has seven detectable stable isotopes with the lightest being the least abundant (Figure A.1b). Thus, the isotope distribution of a peptide with an Hg adduct will be predictably broadened compared to its unmodified version (Figure A.1c-d). We devised a straightforward quantitative scoring function to compare the observed and theoretical isotope distributions of an unidentified peptide that can be used automatically to filter the thousands of spectra produced in typical LC-MS/MS proteomics

experiments. Other tools examine isotope distributions to remove signals of non-peptides or overlapping isotope distributions, e.g., THRASH (Horn et al., 2000) and MaxQuant (Cox and Mann, 2008), but ours is the first case of using isotope distributions as a classifier. We evaluated our scoring function by determining its error rates when thresholds are applied to classify isotope distributions as either an unmodified peptide or a peptide modified with Hg. This technique is independent of peptide sequence identifications, e.g. by SEQUEST (Eng et al., 1994), so it increases the confidence of SEQUEST-identified modifications and eliminates false SEQUEST identifications. Moreover, since analysis of isotope distributions does not require an exact formula for the modification or the peptide, previously unidentified MS features can be highlighted by their anomalous isotope distributions, allowing for the discovery and identification of unexpected modifications through a more focused examination.

## EXPERIMENTAL PROCEDURES

### *Characterizing isotope distributions by fit scores.*

In this study, the isotope distribution characterization is applied to peaks observed in MS<sup>1</sup> scans from an LTQ Orbitrap hybrid Fourier transform mass spectrometer (Thermo Scientific, San Jose, CA) with nominal resolution set to 100,000. All software is implemented in the Python programming language except as noted.

### *Peak identification*

Data files from the MS instrument are first translated to mzXML format in profile mode, which provides a readable list of m/z and intensity data points that define the spectrum. For maximum control over the peak finding and centroiding to aid methods development, we implemented our own procedures, though the software as written can also use pre-centroided

mzXML files. Our peak identification procedure tests each data point in the profile as a candidate peak-top; no peaks are filtered as noise. A window of at most 4 neighboring data points (5 total data points) centered on the candidate data point is checked for the presence of any data points with greater or equal intensity to the candidate data point. This window of five data points, equivalent to four data point intervals, corresponds to the full width at half maximum (FWHM) for most isotope peaks. For example, at  $m/z = 1200$ , the  $m/z$  distance between data points is 0.004, and the FWHM for most observed peaks is near 0.016. If no data points have greater intensity than the peak-top candidate and only adjacent data points have equal intensity, then the candidate is considered a peak-top with intensity set to the intensity of that highest data point. We use peak height, as used by Decon2LS (Jaitly et al., 2009) for example, instead of peak area, as used by MaxQuant (Cox and Mann, 2008) for example, as a measure of abundance to avoid the problem of determining peak boundaries. The  $m/z$  value assigned to the peak is the intensity-weighted average of the  $m/z$  of all five data points within the window examined to determine that the candidate data point is a peak-top. If the rare case occurs where two neighboring data-points are peak-tops and of equal intensity, the  $m/z$  location for this single peak is determined from the weighted average of only four data-points: the two peak top points, and an additional data point on either side.

#### *Clustering peaks in single scans into isotope distributions*

All identified peaks in each individual high-resolution primary MS<sup>1</sup> scan are divided into isotope clusters or distributions of peaks that appear to be isotopic shifts of the same ion. The procedure we use has a similar goal to the deisotoping procedures included in tools such as Decon2LS (Jaitly et al., 2009), but without *a priori* expectations of isotope distributions in order to avoid bias towards modified or unmodified peptides. Starting with the largest peak in the scan,

candidate clusters are made that contain the peak for each charge ( $z$ ) up to charge 6+ by checking  $m/z$  interval steps  $1.002/z$  greater and lower than the main peak (with tolerance of  $\pm 0.015$   $m/z$  units) for compatible peaks. In each step interval, the largest peak is chosen from among all candidates. Because the presence of noise peaks could join two unrelated clusters, or simply make a 2+ cluster appear to be a 4+ cluster, two constraints on pattern shape are applied to stop runaway cluster growth due to small peaks. First, any candidate cluster is trimmed back to the smallest peak between the largest first peak and any secondary peak that is greater than 3 times the smallest intervening peak. Second, any peak with abundance less than 1/100 of the largest first peak halts the stepping in its direction. A charge and final cluster, representing the isotope distribution, is assigned to the starting peak by choosing the charge that produces the cluster with the greatest summed intensity. All peaks assigned to this cluster are removed from subsequent analysis by deleting them from the peak list before starting the cluster search again at the remaining largest peak. A similar algorithm, THRASH (Horn et al., 2000), removes already clustered peaks by subtracting just the heights of the peaks as predicted by an expected shape of the isotope distribution; thus it is able to assign an individual peak to more than one isotope distribution, and de-convolute peaks arising from multiple different peptides. This procedure is not possible for our method where we are searching for different types of isotope distributions.

#### *Calculation of fit scores to theoretical isotopic distributions*

When searching for Hg-modified peptides, each observed isotope distribution is scored for its fit to both a theoretical isotope distribution for an unmodified peptide and one for a peptide modified with a single Hg atom. The procedure would be identical for searching for peptides with Sec, substituting Se for Hg. To compute theoretical isotope distributions, first approximate chemical formulas for the theoretical peptides were produced using average ratios

and procedures (Senko et al., 1995). Isotope distributions based on the theoretical formulas were calculated using the algorithm and source code for emass (Rockwood and Haimi, 2006), modified to work as a module for the Python programming language.

#### *Fit score minimization and calculation*

The alignment and scaling of an observed isotope distribution (**s**) with **m** peaks, with the theoretical isotope distribution (**t**) with **n** peaks is chosen to minimize the deviation of the observed from the theoretical. Keeping consistent with previous nomenclature, as used by Decon2LS (Jaitly et al., 2009), we call this measure of deviation a “Fit” score. Absolute m/z values are ignored, and only positions (first, second, third, etc.) in the isotope distribution are considered. The isotope distribution is then treated as a vector of peak abundances. All possible alignments are considered, fully sliding one isotope distribution over the other, one peak at a time, from where only the extreme left peak of **s** (denoted **s<sub>1</sub>**) aligns with the extreme right of **t** (**t<sub>n</sub>**), to the opposite extreme where only **s<sub>m</sub>** aligns with **t<sub>1</sub>**. For each peak in an isotope distribution that lies beyond the tails of the other, a matching peak of abundance 0 is added to the other distribution. The new aligned isotope distributions are labeled **S** and **T**, each with the new length **L**. The theoretical isotope distribution is normalized to have the abundance of the largest peak set to 1.0. The observed isotope distribution is scaled to optimize the fit, i.e. to minimize **F** in Equation 1, by the use of a scaling factor **k**. The scaling factor **k** used in Equation 1 is computed for each alignment according to Equation 2. Except for the scaling factor **k**, this fit score is identical to the peak fit function used by Decon2LS (Jaitly et al., 2009).

$$(1) \quad F = \frac{\sum_i (kS_i - T_i)^2}{\sum_i T_i^2} \quad (2) \quad k = \frac{\sum_i T_i S_i}{\sum_i S_i^2}$$

### *Multi-scan feature discovery*

We define a multi-scan LC-MS feature as a single chemical species that elutes from the LC column over a period of time and so appears in multiple sequential MS scans. For the purposes of the study described here, these multiple scans provided many replicates from a single LC-MS run for examining isotope distributions, and the individual isotope distributions can be summed to minimize the effects of random noise on any single spectrum. Multi-scan LC-MS features were discovered using the clustering tools in VIPER (Monroe et al., 2007). In brief, all individual scans were first deisotoped using Decon2LS with or without an Hg tag as appropriate. Deisotoped peaks with matching mass and neighboring elution times were grouped using the tool LCMSFeatureFinder, distributed as part of VIPER. To produce a summed isotope distribution for each multi-scan feature, peak heights for each single scan in the feature were collected according to “Clustering peaks in single scans into isotope distributions” above. The single scan isotope distributions were aligned together and the corresponding peak heights summed to give a summed isotope distribution.

### *Rabbit GAPDH pure protein*

Rabbit muscle glyceraldehyde-3-phosphate dehydrogenase (GAPDH) was from Sigma (G2267); all other reagents were of analytical grade. The protein was dissolved in 5 mM potassium phosphate buffer, pH 7.3 to give a stock solution of 10 mg/mL and stored at  $-20^{\circ}\text{C}$  when not in use. An aliquot was used to determine the protein thiol content under denaturing conditions (6 M guanidine hydrochloride) using 5,5'-dithiobis(2-nitrobenzoic acid) (Riddles et al., 1979). For mass spectrometric analysis, an aliquot of the stock was diluted ten-fold with 50 mM  $\text{NH}_4\text{HCO}_3$ , pH  $\sim 8$ . Phenylmercuric acetate (PMA) was added to the dilute protein to give a final ratio of 0.95 equiv PMA/protein thiol. After incubation at  $25^{\circ}\text{C}$  for  $\sim 5$  min, the preparation

was divided into two aliquots; one was placed on ice, and iodoacetamide (20 mM final concentration) was added to the other. After 30 min incubation of the latter in the dark at room temperature, both aliquots were frozen at  $-80^{\circ}\text{C}$  and then sent overnight on dry ice to PNNL for denaturation, trypsinolysis, and LC-MS/MS as described below.

### *Bacterial strains and growth conditions.*

*E. coli* strains K-12 MG1655 and MG1655 containing the NR1 plasmid carrying the Tn21 mer operon, which encodes inorganic mercury resistance (Womble and Rownd, 1988), were used for model organisms. *E. coli* cells from  $-70^{\circ}\text{C}$  stocks were grown overnight at  $37^{\circ}\text{C}$  on Luria-Bertani (LB) plates or LB+25  $\mu\text{g/ml}$  chloramphenicol plates to select for NR1 plasmid. Ten well isolated colonies from each overnight plate were inoculated into Neidhardt MOPS minimal medium (Neidhardt et al., 1974) supplemented with 20 mg/L uracil and 500  $\mu\text{g/L}$  thiamine and grown overnight at  $37^{\circ}\text{C}$  with shaking at 250 rpm. These overnight liquid cultures were subcultured (1:40) into the same medium and incubated at  $37^{\circ}\text{C}$ , 250 rpm until  $\text{OD}_{595} \approx 0.6$  at which time the culture was split evenly and one half was made 40  $\mu\text{M}$  in PMA. Incubation of both culture aliquots continued for 15 min and then both aliquots were harvested by centrifugation at  $17,700 \times g$ , for 10 min at  $4^{\circ}\text{C}$ . Cell pellets were suspended in 50 mM ammonium bicarbonate (pH 7.8) at 0.01 $\times$  the original culture volume, iodoacetamide (IAM) was added, and the suspensions were stored at  $-70^{\circ}\text{C}$  until they were shipped overnight on dry ice to PNNL for final workup and LC-MS/MS analysis.

Data from three separate *E. coli* proteomics experiments were combined in this analysis. Two experiments involved strain MG1655, which does not have a plasmid, and the third experiment used MG1655 carrying the NR1 plasmid encoding the mercury resistance operon. In one experiment on plasmid-free cultures 40 mM IAM was used to preserve Hg-adducts; the other



two experiments used 20 mM IAM. These differences had no significant impact on the detection of Hg adducts in peptides from the PMA-exposed cells. Corresponding unexposed cultures were included in each experiment and their data are also included in the work reported here. Where appropriate, results were pooled across all runs within a single experiment and then averaged across the three experiments. For some statistics, such as counts of PhHg modifications, the counts were too low within individual experiments to treat separately, so all runs were pooled across all three experiments.

## **PROTEOMIC METHODS**

### *Peptide preparations*

Cell suspensions in IAM were diluted as necessary in 100 mM ammonium bicarbonate, pH 8.0, with IAM and lysed with a PBI Barocycler NEP 3229 for ten cycles, holding at 35,000 psi for 20 seconds. A portion of the lysate was fractionated by ultracentrifugation into soluble and insoluble fractions according to described procedures (Callister et al., 2008) except that to avoid interference with protein-phenylmercury bonds, DTT and thiourea were not used. As described (Callister et al., 2008), all samples were digested using sequencing grade modified trypsin (Promega).

### *Peptide detection*

Triplicate aliquots of the unfractionated lysate (“global”), and the soluble and insoluble fractions were analyzed by LC-MS/MS using a ThermoScientific Exactive Orbitrap mass spectrometer (Thermo Scientific, San Jose, CA) outfitted with a custom-built electrospray ionization (ESI) interface that was fabricated in-house (Kelly et al., 2006, Livesay et al., 2008). The HPLC gradient used has been described elsewhere (Callister et al., 2008).

### *Peptide identification*

Peptides from the MS/MS spectra were identified with TurboSEQUEST version 27, revision 12. We generated peak lists as dta files with extract\_msn.exe version 4.0 (ThermoElectron), requiring a minimum of 35 ions per MS/MS spectrum and precursor mass between 200 and 5000 Daltons. We used a custom sequence database combining the peptide translations from the *E. coli* genome sequence, strain K12-MG1655, GenBank accession number U00096.2, GI:48994873, 4331 proteins, together with the sequence of the NR1 plasmid, GenBank accession number DQ364638.1, GI:89033265, 123 proteins. Mass tolerances were 3.0 Daltons for precursor ions and 1.0 Daltons for fragment ions. Variable modifications were allowed at cysteines equal to the mass of alkylation by IAM (+57.0215), adduction by PhHg (+278.0019), or by Hg(II) (+199.9549). We used a modified static cutoff approach (Washburn et al., 2001) for evaluating the significance of SEQUEST identifications. SEQUEST identifications were accepted if they had at least one tryptic end, any number of missed cleavages, and their XCorr values were greater than 1.9, 2.2 or 3.2 for charge states of +1, +2 and  $\geq +3$ , respectively. Also, except in the rare cases where the second-ranked SEQUEST hit was a permutation of cysteine modifications of the first hit, SEQUEST results were required to have a  $\Delta C_n$  of at least 0.1. These score thresholds are in-house standards that aim for a false discovery rate near 1%. Using a decoy approach (Elias and Gygi, 2007) we determined these score thresholds to produce a peptide false discovery rate of 1.44%. To demonstrate the utility of isotope distributions with an alternative peptide identification score, all SEQUEST identifications were rescored by PeptideProphet version 1.0.0.4, downloaded as source on May 9, 2006.

## RESULTS

### *A) Theoretical spectra fit to approximate formulas for Hg peptides*

We began by examining the theoretical best case for our method: identifying Hg-peptide isotope distributions with no instrument noise (Fig. A.2). As noise-free proxies for the observed spectra from an actual experiment, we computed theoretical spectra from exact chemical formulas for the 60,311 cysteine-containing peptides from an *in silico* tryptic digest of the *E. coli* MG1655 proteome. We modeled Hg peptides by *in silico* modification of a single cysteine in each peptide with PhHg.

For each theoretical isotope distribution based on an exact formula of a modified (Fig. A.2a, blue) or unmodified peptide (Fig. A.2a, red), we calculated its fit to isotope distributions based on two different approximate chemical formulas (Fig. A.2a, box 4) computed from the target mass and average ratios of elements in peptides, denoted ‘averagine’ (Senko et al., 1995). The approximate formulas were created for a Hg-modified (purple) and an unmodified (yellow) peptide. Approximate formulas are necessary in a real experiment when the exact formula of an ion detected by MS is unknown. The fit score is a scaled sum of squared deviations in peak heights, with spectra aligned and normalized to produce the best fit score (see Experimental Procedures). A fit score of 0.0 is a perfect match, and a fit score of 1.0 is the asymptotic maximum deviation (i.e. no overlap at all). The theoretical isotope distributions of Hg-modified peptides are detectably distinct from those of unmodified peptides, whether the spectra are fit to an approximate Hg-modified peptide (fitHg, Fig. A.2b), an approximate unmodified peptide (fitAvgn, Fig. A.2c), or the difference of the two,  $\Delta\text{Fit}$  (fitAvgn – fitHg, Fig. A.2d). Note that because a perfect match for a Hg-peptide has a fitHg score of 0.0,  $\Delta\text{Fit}$  scores for Hg-modified peptides have positive values and, conversely,  $\Delta\text{Fit}$  scores for unmodified peptides have negative

values. As peptide mass increases, the modified and unmodified peptides more closely resemble each other. However, there is clear separation at masses up to 5000 Daltons, which exceeds the mass of most peptides commonly detected in proteomic preparations: 99% are < 3000 Daltons according to PepSeeker (McLaughlin et al., 2006), 96% < 4000 Daltons in our own data.

Theoretically, any element with a distinctive natural abundance isotope distribution can give rise to similar distinctions between modified and unmodified peptides depending on the pattern of their isotope distributions (Supplementary Fig. A.S1). Most notably, selenium, which occurs naturally but rarely in proteins as selenocysteine (Sec), may be detectable by this method.

A lower variability of fit values for the modified peptides compared to the unmodified is apparent in Figure A.2 and Supplementary Figure A.S1. This change in variability can be attributed to the homogenizing effect of adding a single atom with a diverse isotope distribution, such as Hg, to the isotope distributions of different peptides (see Supplementary Fig. A.S2).

### *B) Experimental spectra fit to approximate formulas.*

To examine whether this distinction in the shape of isotope distributions is detectable with real-world instrument noise, we analyzed peptides from a Hg-exposed pure protein with high resolution LC-MS/MS. To generate peptides with Hg modifications, we exposed rabbit glyceraldehyde 3-phosphate dehydrogenase (GAPDH) to phenyl mercuric acetate (PMA) and digested it with trypsin. The monovalent organomercurial PMA was used to minimize peptide cross-linking which might occur with bivalent Hg(II). We used SEQUEST to search for a variable modification of mass equal to PhHg at cysteines. In four LC-MS/MS runs, SEQUEST predicted seven different peptides (in 39 MS/MS spectra) as modified by PhHg at one of the four cysteines in a GAPDH monomer. MS/MS spectra (e.g., Fig. A.3) of PhHg-modified and unmodified peptides are highly similar in terms of the presence and relative abundance of

specific y and b ions. However, fragmentation of the PhHg modified peptide appears dominated by a peak consistent with the neutral loss of 78 Daltons, which equals the mass of a phenyl group. Further supporting that this is due to the loss from the PhHg modification, for each of the larger peaks interpreted as y ions that contain a PhHg group, there is a corresponding peak at 78 Daltons less. While these neutral loss peaks appear to be strong indicators of a PhHg modification, we observed no patterns consistent with the neutral loss of the Hg atom. Therefore, detecting neutral loss in MS/MS will not be a general strategy for detecting other types of Hg modifications.

We expanded this initial set of isotope distributions from PhHg-adducts using an LC-MS feature detection tool (see Methods) to identify corresponding isotope distributions in all primary MS scans neighboring (in time) each scan with a SEQUEST identification. This expanded set included many isotope distributions with relatively low intensity (e.g., Fig. A.4e) in addition to the high intensity isotope distributions that preceded the MS<sup>2</sup> scans leading to the initial confident assignments by SEQUEST (e.g., Fig. A.4d). For a comparison set of isotope distributions from unmodified peptides, we chose a subset of the detected unmodified peptides that represents the mass range of all observed peptides (Figs. A.4a and A.4c). Plotting the  $\Delta\text{Fit}$  scores for these experimentally-derived isotope distributions as a function of mass (Fig. A.4b) we found they closely match those observed in the theoretical cases (denoted by the dotted lines in Fig. A.4b), except for isotope distributions with lower-intensity peaks (denoted by the shorter dashes in Fig. A.4b) where separation between modified and unmodified is degraded (Fig. A.4b). There is a slight overlap between the distribution of  $\Delta\text{Fit}$  scores for modified and unmodified peptides, the extent of which is made more visible by histograms of the  $\Delta\text{Fit}$  scores (Fig. A.5a). We used  $\Delta\text{Fit}$  in most subsequent analysis as a summary of both  $\text{fitAvgn}$  and  $\text{fitHg}$ , as we found

it was the best single classifier based on receiver operator characteristic (ROC) analysis of the GAPDH peptides compared to either single fit score alone (shown in Supplementary Fig. A.S3). To be an accurate binary classifier, a  $\Delta$ Fit threshold must lie above the  $\Delta$ Fit of most unmodified peptides and lie below the  $\Delta$ Fit of most modified peptides, thus separating the  $\Delta$ Fit distributions for the two classes (see Fig. A.5a). The proportion of each distribution that is thus accurately classified by  $\Delta$ Fit is called specificity for the unmodified peptides or sensitivity for the modified peptides. The specificity and sensitivity of  $\Delta$ Fit on these peptides from GAPDH, and their relation to the choice of threshold, are shown by the red line in Figure A.5b and the blue line in Figure A.5c, respectively. At a  $\Delta$ Fit threshold of 0.0, specificity is 99.6% and sensitivity is 94%.

### *C) $\Delta$ Fit applied to single scans in *E.coli* proteomic preparations*

#### *$\Delta$ Fit eliminates false positives in SEQUEST identifications*

In typical LC-MS/MS proteomic analysis, fragmentation data obtained in the second MS step are analyzed by software tools such as SEQUEST to identify the peptide sequence, with or without one of a few expected modification types, and the corresponding identity of the protein. The use of these methods alone can lead to unacceptable numbers of falsely identified modifications, especially when numbers of actual modifications are low. In this work, SEQUEST identified 99 spectra as PhHg-modified peptides from three separate proteomic preparations of *E. coli* cells that were not exposed to PMA compared to 377 such spectra in three proteomes of cells that were exposed to PMA, indicating that more than 25% of the total PhHg identifications by SEQUEST from PMA-exposed cells were false. However, each MS<sup>2</sup> scan and its SEQUEST prediction can be assigned an isotope distribution from the precursor MS<sup>1</sup> scan based on the m/z region of the precursor scan that was selected for fragmentation. Using this

MS<sup>1</sup> scan, we can assign a  $\Delta\text{Fit}$  score to each SEQUEST PhHg prediction and accept or reject the SEQUEST prediction.

By comparing the distributions of  $\Delta\text{Fit}$  scores for SEQUEST PhHg predictions from our proteomic analyses of PMA-exposed (Fig. A.6a, purple) and unexposed cells (Fig. A.6a, orange), we find that the distributions have overlapping peaks at  $\Delta\text{Fit} < 0.0$ . This is evidence for similar rates of false positives in both experimental conditions. However, only the histogram for the PMA-exposed samples has a large peak at  $\Delta\text{Fit} > 0.0$ . Applying a  $\Delta\text{Fit}$  threshold to these isotope distributions at 0.0 eliminates most false positives observed in samples from unexposed cells (90 of 99), and eliminates a similar count (102 of 377) in the exposed samples. Of the peptide isotope distributions that pass the  $\Delta\text{Fit}$  filter in the PMA-exposed samples, we deduced that 97% (266.3/275) of them are true positives (precision) by assuming the difference between exposed and unexposed samples is due to true positives alone (computation illustrated in Supplementary Fig. A.S4). Using SEQUEST and a  $\Delta\text{Fit}$  threshold of 0.0 (Fig. A.6a) on these isotope distributions we identified 275 spectra as Hg-modified from 47 peptides and 42 proteins. Example spectra for a PhHg-modified peptide and for the same peptide without PhHg are shown in Supplementary Figure A.S5. Based on our estimated precision, we expect about 9 of the 275 spectra were false positives. A discussion of specific modified peptides and their biological significance will follow in a later publication.

A precision value depends on the ratio of actual modified to unmodified peptides in each preparation; as the proportion of modified peptides increases, so will precision. Other measures of accuracy, specifically sensitivity and specificity, are independent of ratios of modified to unmodified peptides. To enable the evaluation of  $\Delta\text{Fit}$  for use in other preparations with different ratios of modified to unmodified peptides, we computed the sensitivity and specificity of  $\Delta\text{Fit}$

(Fig. A.5 b and c) on those (377 + 99) isotope distributions in the proteomic preparations identified as PhHg-peptides by SEQUEST. Sensitivity was estimated indirectly by comparing both sets of PhHg identifications from the exposed and unexposed conditions and inferring that the differences in both the rates of SEQUEST PhHg identifications and  $\Delta\text{Fit}$  scores  $> 0.0$  are due to Hg-modified peptides (Supplementary Fig. A.S4 outlines the calculation in detail). The comparison of histograms in Figure A.6 provides an alternative illustration: the purple bars that rise above the orange bars show the contribution of Hg-modified peptides. There is a clear decrease in specificity of  $\Delta\text{Fit}$  (from 99.6% to 91%) on these isotope distributions that SEQUEST falsely identifies as PhHg, compared to the pure protein spectra (compare line 'a' in Fig. A.5b with red line). This is partly due to the complexity of proteomic preparations, including lower intensities of some ions, overlapping spectra (where two different ions with similar masses elute at the same time, see Supplementary Figs. A.S6 and A.S7), and non-peptide ions.

Because  $\Delta\text{Fit}$  is independent of  $\text{MS}^2$  data, increasing the accuracy of peptide assignments based on  $\text{MS}^2$  fit, via tools such as PeptideProphet (Keller et al., 2002), does not negate the benefit of  $\Delta\text{Fit}$  and isotope distributions so long as the  $\text{MS}^2$  matching still generates some false predictions of modifications. While rescoring the SEQUEST identifications with PeptideProphet decreases false predictions of PhHg adducts by 87% (13 compared with 99), at a probability threshold of 0.97, these 13 false identifications get reduced to only 2 by requiring  $\Delta\text{Fit} > 0.0$  ( $\Delta\text{Fit}$  specificity = 85%). This PeptideProphet threshold of 0.97 was chosen to produce a similar number of true PhHg identifications as obtained using SEQUEST thresholds in the exposed samples (293 total hits with 280.5 estimated true positives compared with 281.8 true positives using SEQUEST scores alone). Applying a  $\Delta\text{Fit} > 0.0$  filter on the exposed samples results in



257 total identifications of PhHg in the exposed samples ( $\Delta\text{Fit}$  sensitivity = 90%, calculated as in Supplementary Fig. A.S4). If instead we choose a PeptideProphet threshold that results in the same false identification rate as SEQUEST after applying a  $\Delta\text{Fit} > 0.0$  threshold,  $\Delta\text{Fit}$  enables us to lower the PeptideProphet threshold as low as 0.5. An identification made with probability of 0.5 is typically not to be believed as it implies that the assignment is as likely to be wrong as correct. However, by applying the additional  $\Delta\text{Fit} > 0.0$  filter, the number of estimated false positives in the exposed samples is only 10 (compare with 9 using SEQUEST and  $\Delta\text{Fit}$ ) while this relaxed threshold increases the number of PhHg adduct identifications by more than 25% to 350 (from 275 with SEQUEST and  $\Delta\text{Fit}$ ). On this set of modified peptide identifications with PeptideProphet probabilities greater than 0.5, sensitivity and specificity estimates of  $\Delta\text{Fit}$  are comparable when applied to the set of identifications made by SEQUEST (Supplementary Fig. A.S8).

#### *Searching for unexpected modifications*

As the first global proteomic study of the *in vivo* cellular effects of mercury compounds, we cannot be certain of the full range of Hg modifications to expect. SEQUEST or similar programs cannot identify unexpected modifications as these tools only look for a small number of specified modifications. Instead, we would like to reverse the order of analysis to use isotope distributions first to identify those isotope distributions in LC-MS data that are likely Hg-modified peptides, and then examine their mass and  $\text{MS}^2$  fragmentation patterns to identify the peptide and its Hg modification. However, with modifications as rare as the expected PhHg modifications observed when using SEQUEST and  $\Delta\text{Fit}$  together (see previous section), the number of false positive identifications of modified peptides can far exceed the total number of true positive identifications even with the high specificity of  $\Delta\text{Fit}$ . This is made evident in

Figure A.6b by the nearly identical distributions of  $\Delta\text{Fit}$  scores computed for all  $\text{MS}^1$  isotope distributions selected for  $\text{MS}^2$  fragmentation in the three PMA-exposure experiments (purple) versus the three experiments where cells were not exposed (orange). Although the specificity of  $\Delta\text{Fit}$  on these isotope distributions (Fig. A.5b, line b) is greater than the specificity of  $\Delta\text{Fit}$  on the SEQUEST PhHg identifications (Fig. A.5b, line a), the number of isotope distributions with  $\Delta\text{Fit}$  scores above the 0.0 threshold is over 15,000, all necessarily false positives in the unexposed proteomes. A similar number of false positives must be present in the PMA-exposed proteomes, far outnumbering the few hundred true positive PhHg peptides identified by application of  $\Delta\text{Fit}$  to SEQUEST-identified PhHg-adducts above. Thus, use of  $\Delta\text{Fit}$  alone on single scans is not sufficient to identify the relatively rare Hg-modifications.

#### *D) Summed isotope distributions of features appearing in multiple sequential scans*

The LC elution profile for most ions is broad enough that they appear in multiple sequential  $\text{MS}^1$  scans. We took advantage of these ‘multi-scan features’, by summing them to give a more accurate isotope distribution for a given ion (compare Fig. A.7 b & c). One challenge in summing scans is determining the boundaries of the multi-scan feature, i.e. the start and end points of a peptide’s elution, as well as choosing which peaks within successive scans are from the same ion. To address this challenge, we used a clustering algorithm developed for the accurate mass and time tag (AMT) approach for identifying peptides in LC-MS as described in Experimental Procedures (Monroe et al., 2007).

#### *The accuracy of $\Delta\text{Fit}$ on summed isotope distributions from multi-scan features*

The accuracy of  $\Delta\text{Fit}$  on summed isotope distributions from multi-scan features can be measured as for single scans. As with the single scans, we used only the subset of multi-scan

features that SEQUEST predicted were PhHg-modified (Fig A.6c). We computed specificity and sensitivity of  $\Delta\text{Fit}$  for the SEQUEST PhHg identifications as for the single scans, and both specificity and sensitivity improved for summed scans over the single scans (Fig A.5 b and c, compare lines ‘c’ with lines ‘a’). To determine if this increase in accuracy allows the detection of Hg-modifications without SEQUEST, we examined all multi-scan features regardless of any SEQUEST identification. Based on only the results from the unexposed cells, the distribution of  $\Delta\text{Fit}$  scores (Fig. A.6d, orange) gives a specificity of 98.4% at a threshold of 0.0, an improvement over single scans (compare Fig. A.5b, line ‘d’ with line b). However, the number of total positives from the PMA-exposed cells (5362) was only 27% more than the false positives from the unexposed cells at that threshold (4219); i.e. most isotope distributions that pass  $\Delta\text{Fit} > 0$  are false positives (Fig. A.6d).

*Use of  $\Delta\text{Fit}$  and  $\text{fitHg}$  together allows detection of Hg-adducts without SEQUEST pre-filtering*

The lower noise in the summed isotope distributions compared to those from single scans (panel c vs. b in Fig. A.7) improved the match between observed isotope distributions and theoretical Hg-peptide isotope distributions, as measured by  $\text{fitHg}$  (panels e and d in Fig. A.7). Using  $\text{fitHg}$  as an additional filter (i.e.  $\text{fitHg} < 0.05$  AND  $\Delta\text{Fit} > 0.0$ ) eliminated 90% of the unmodified peptides (compare Fig. A.6e with A.6d), sharpening the differences in the  $\Delta\text{Fit}$  distributions for PMA-exposed and unexposed isotope distributions without relying on SEQUEST. Combining  $\Delta\text{Fit}$  and  $\text{fitHg}$  clearly improved specificity (Fig. A.5b, line ‘e’) over  $\Delta\text{Fit}$  alone on summed scans, affording a nearly 10-fold decrease in the false positive rate (1–specificity) from 1.6% to 0.18% (s.d. = 0.06%, n = 3 experiments) at a  $\Delta\text{Fit}$  threshold of 0.0.

As a first step towards investigating modified peptides that may not have been identified by SEQUEST, it is useful to examine the  $\Delta\text{Fit}$  versus mass plots for these Hg-like features in the

PMA exposed samples (Fig. A.8a, or with an expanded view in Supplementary Fig. A.S9a), in comparison with the Hg-like features in the unexposed samples (Fig. A.8b, expanded in Supplementary Fig. A.S9b) to understand patterns of false positives. This comparison makes clear that the PMA-exposed samples have many more Hg-like features in the <3000 Dalton range than appear in the unexposed samples, and also have many repeated observations of the same mass (indicated by vertical clusters of circles) at expected DFit scores. Most of these vertical clusters corresponded to SEQUEST-identified phenyl-Hg adducts, thus confirming that most Hg modifications were detected by SEQUEST. However, some clusters clearly stand out and are at masses not identified by SEQUEST as PhHg adducts. These are likely Hg adducts but remain unidentified without further analysis. We identified one of these using an additional SEQUEST run allowing for the previously unexpected Hg(II)-cysteine modification. This cluster (identified by the red ‘\*’, Fig. A.8) is a peptide with a single Hg(II) chelated by the CTTNC motif in *E. coli* GAPDH (see Supplementary Fig. A.S10 for a labeled MS<sup>2</sup> spectrum), possibly the result of contamination of the PMA stock with Hg(II). Several remaining unidentified clusters appear to be PhHg adducts of tryptic peptides (red lines in Fig. A.8a) based on accurate mass, SEQUEST hits below acceptable thresholds, and observations of other peptides from the same proteins. Relatively few features seen in all three experiments remain completely unidentified, leaving little chance that a major type of Hg-modification remains unidentified.

#### *Examination of false positive Hg-like isotope distributions.*

The set of features with Hg-like isotope distributions from Hg-free *E. coli* proteome preparations displayed in Figure A.8b provide a picture of false positives for our method. In clear contrast with the abundant features in the PMA-exposed preparations, most false positives occur at higher masses, lower intensities and with lower reproducibility between replicate LC-MS/MS

runs and between replicate biological samples. To determine the causes of these false positives, we examined ten features that stand out in this plot because of their high intensities or their reproducibility (highlighted with gray ovals and rectangles in Fig. A.8b). Of these ten, seven cases (gray ovals) were clearly the products of overlapping isotope distributions of co-eluting unmodified peptides of similar mass and abundance, apparent either from the elution profiles of the individual isotope peaks or based on SEQUEST identification of the peptides (Supplementary Figs. A.S11 and A.S12). For the remaining three cases (gray rectangles), the elution profiles and SEQUEST results were inconclusive. Thus, these types of co-elutions are the major cause of the most intense and frequently recurring false positives in the current study.

While the level of these co-elutions in our work was not high enough to have a major impact on identifications, they may present a larger problem for other more complex proteomes. Therefore, efforts to minimize co-elutions through experimental methods such as fractionating the sample, or to computationally detect and exclude them, offer the most promising area for improving false positive rates. Our current method of identifying multiple scan features already excluded many co-elutions by its procedure for joining isotope distributions from different scans into a single multi-scan feature. The method assigns a single mass to every isotope distribution detected in a single scan, equivalent to “deisotoping” to assign a monoisotopic mass. Only the isotope distributions with the same mass from neighboring scans are joined into a multi-scan feature. This eliminates many co-elutions where the relative abundance of the two peptides shifts over the time period of their elutions, thus shifting the assigned mass. The exceptions are features detected in regions of the overlapping elutions where abundances are similar, either in very short time periods between elutions of the two peptides or where the elution of a low abundance peptide overlaps with the elution tail of a higher abundance peptide (Supplementary

Fig. A.S11), as well as those overlapping elutions that have very similar elution times (Supplementary Fig. A.S12). An alternative approach, one used by MaxQuant, is to require the elution profiles of individual isotope peaks to correlate before joining them into a multi-scan feature. This method should exclude those that have significantly different elutions but will not exclude those with similar elutions (see Supplementary Fig. A.S12).

## DISCUSSION

As a tool for the identification of peptides modified by or containing atypical elements, the use of isotope distributions provides an independent method for validating identifications made by SEQUEST or other such algorithms, eliminates the need for additional processing outside of the routine shotgun proteomics pipeline, and does not require peptide fragmentation. Isotope distribution detection requires the use of an MS instrument with enough resolution to resolve individual isotope peaks. We present results on data collected at a nominal FWHM resolution of 100,000, but resolutions as low as 10,000 should be adequate. These resolutions are possible from many currently available systems including the LTQ Orbitrap as used here, Fourier transform ion cyclotron resonance (FTICR) instruments, the latest generation time of flight (TOF) instruments (Domon and Aebersold, 2010), and the latest generation triple quadrupoles (Yang et al., 2002). The only adjustment necessary may be the use of a different peak finding procedure, of which many are available, because the one we used relied on the  $m/z$  spacing of data points as provided by the Orbitrap. As modified peptides are usually present in very low abundances (substoichiometric), they can be passed over for fragmentation in favor of the much more abundant unmodified peptides, especially in complex proteomic preparations. By using isotope distributions, we were able to generate a survey of all MS features with Hg-like isotope

profiles (Fig. A.8) revealing which, if any, Hg-like LC-MS features were missed by MS/MS fragmentation and SEQUEST. Other elements have natural isotope distributions distinct enough to allow for similar detection of their combinations with peptides. This characteristic of selenium is of particular interest because detecting isotope patterns holds promise for the identification of selenocysteine (Sec) peptides and proteins. Isotope distributions could confirm known Sec peptides as well as highlighting LC-MS features that indicate unexpected modifications of Sec peptides. Additionally through construction of a database of alternatively translated protein sequences, by treating the UGA stop codons as Sec codons, the identification of Sec peptides with confirmation by isotope distributions may lead to identification of previously unknown selenoproteins.

Modifications of proteins by bivalent Hg(II) can result in cross-linking of sequentially distant but spatially close cysteines in the folded protein structure. By using the monovalent organomercurial, PMA, we expected to avoid this complicating issue. However, the discovery capability of isotope distributions was demonstrated when their evaluation revealed an ion as a likely Hg-adduct that had failed to be identified by SEQUEST as a PhHg-modification. This peptide proved to be the simplest case of cross-linking by Hg(II), with Hg(II) binding to two cysteines in a single peptide. While SEQUEST was not designed to model the fragmentation patterns caused by this type of internal cross-link, we found that SEQUEST did report significant matches by modeling this bivalent Hg(II) cross-link as a single positively charged modification by Hg(II) at one or the other of the two cysteines in the peptide. This simplification is possible because the main effects on the fragmentation patterns caused by an internal Hg(II) cross-link were simply double peaks for those fragments: i.e., one peak with the added mass of Hg(II) and one without. External cross-links, where two different peptides are joined by a single Hg(II)

present a substantially greater challenge for identification by MS/MS (Chu et al., 2010, Singh et al., 2010).

In summary, the scoring of isotope distributions to detect proteins modified by or including isotopically distinct elements such as Hg is easily and effectively applied to routine shotgun proteomics employing high resolution MS. In its simplest form, isotope distribution scoring can be applied to single precursor spectra and compared to SEQUEST or similar peptide identifications by fragmentation. Especially in complex whole proteome samples, isotope distributions become more powerful, but involve more complex data processing of summed spectra within LC-MS features. Used this way, even on proteomic preparations, isotope distributions are accurate enough to resolve modified peptides without other peptide identifications, enabling identification of unexpected modifications, or to confirm that the expected modifications as identified by other methods are the dominant modification.



## **ACKNOWLEDGEMENTS**

We thank A. Perez for help with GAPDH protein preparations. This work was supported by grants from the Department of Energy, Office of Science, Environmental Remediation Science Program; DE-FG02-07ER64409 (to SMM), DE-FG02-07ER64408 (to AOS). A portion of the research was performed using the Environmental Molecular Sciences Laboratory (EMSL), a national scientific user facility sponsored by the Department of Energy's Office of Biological and Environmental Research and located at Pacific Northwest National Laboratory in Richland, WA.

## REFERENCES

- AMORESANO, A., CARPENTIERI, A., GIANGRANDE, C., PALMESE, A., CHIAPPETTA, G., MARINO, G. & PUCCI, P. 2009. Technical advances in proteomics mass spectrometry: identification of post-translational modifications. *Clinical chemistry and laboratory medicine : CCLM / FESCC*, 47, 647-65.
- CALLISTER, S. J., MCCUE, L. A., TURSE, J. E., MONROE, M. E., AUBERRY, K. J., SMITH, R. D., ADKINS, J. N. & LIPTON, M. S. 2008. Comparative bacterial proteomics: analysis of the core genome concept. *PLoS One*, 3, e1542-e1542.
- CHU, F., BAKER, P. R., BURLINGAME, A. L. & CHALKLEY, R. J. 2010. Finding chimeras: a bioinformatics strategy for identification of cross-linked peptides. *Molecular & cellular proteomics : MCP*, 9, 25-31.
- COX, J. & MANN, M. 2008. MaxQuant enables high peptide identification rates, individualized p.p.b.-range mass accuracies and proteome-wide protein quantification. *Nature Biotechnology*, 26, 1367-1372.
- DOMON, B. & AEBERSOLD, R. 2010. Options and considerations when selecting a quantitative proteomics strategy. *Nature Biotechnology*, 28, 710-21.
- ELIAS, J. E. & GYGI, S. P. 2007. Target-decoy search strategy for increased confidence in large-scale protein identifications by mass spectrometry. *Nature methods*, 4, 207-14.
- ENG, J. K., MCCORMACK, A. L. & YATES, J. R. 1994. An approach to correlate tandem mass spectral data of peptides with amino acid sequences in a protein database. *Journal of the American Society for Mass Spectrometry*, 5, 976-989.
- GESELLCHEN, F., BERTINETTI, O. & HERBERG, F. W. 2006. Analysis of posttranslational modifications exemplified using protein kinase A. *Biochimica et biophysica acta*, 1764, 1788-800.
- GUO, Y., CHEN, L., YANG, L. & WANG, Q. 2008. Counting Sulfhydryls and Disulfide Bonds in Peptides and Proteins Using Mercurial Ions as an MS-Tag. *Journal of the American Society for Mass Spectrometry*, 19, 1108-1113.
- HAN, X., ASLANIAN, A. & YATES, J. R. 2008. Mass spectrometry for proteomics. *Current Opinion in Chemical Biology*, 12, 483-490.
- HORN, D. M., ZUBAREV, R. A. & MCLAFFERTY, F. W. 2000. Automated reduction and interpretation of high resolution electrospray mass spectra of large molecules. *Journal of the American Society for Mass Spectrometry*, 11, 320-332.

JAITLEY, N., MAYAMPURATH, A., LITTLEFIELD, K., ADKINS, J. N., ANDERSON, G. A. & SMITH, R. D. 2009. Decon2LS: An open-source software package for automated processing and visualization of high resolution mass spectrometry data. *BMC Bioinformatics*, 10, 87-87.

KELLER, A., NESVIZHSHII, A. I., KOLKER, E. & AEBERSOLD, R. 2002. Empirical statistical model to estimate the accuracy of peptide identifications made by MS/MS and database search. *Analytical Chemistry*, 74, 5383-5392.

KELLY, R. T., PAGE, J. S., LUO, Q., MOORE, R. J., ORTON, D. J., TANG, K. & SMITH, R. D. 2006. Chemically etched open tubular and monolithic emitters for nanoelectrospray ionization mass spectrometry. *Analytical Chemistry*, 78, 7796-7801.

KRUPP, E. M., MILNE, B. F., MESTROT, A., MEHARG, A. A. & FELDMANN, J. 2008. Investigation into mercury bound to biothiols: structural identification using ESI-ion-trap MS and introduction of a method for their HPLC separation with simultaneous detection by ICP-MS and ESI-MS. *Analytical and bioanalytical chemistry*, 390, 1753-64.

LIVESAY, E. A., TANG, K., TAYLOR, B. K., BUSCHBACH, M. A., HOPKINS, D. F., LAMARCHE, B. L., ZHAO, R., SHEN, Y., ORTON, D. J., MOORE, R. J., KELLY, R. T., UDSETH, H. R. & SMITH, R. D. 2008. Fully automated four-column capillary LC-MS system for maximizing throughput in proteomic analyses. *Analytical Chemistry*, 80, 294-302.

MACCOSS, M. J., MCDONALD, W. H., SARAF, A., SADYGOV, R., CLARK, J. M., TASTO, J. J., GOULD, K. L., WOLTERS, D., WASHBURN, M., WEISS, A., CLARK, J. I. & YATES, J. R., 3RD 2002. Shotgun identification of protein modifications from protein complexes and lens tissue. *Proceedings of the National Academy of Sciences of the United States of America*, 99, 7900-5.

MCLAUGHLIN, T., SIEPEN, J. A., SELLEY, J., LYNCH, J. A., LAU, K. W., YIN, H., GASKELL, S. J. & HUBBARD, S. J. 2006. PepSeeker: a database of proteome peptide identifications for investigating fragmentation patterns. *Nucleic acids research*, 34, D649-54.

MONROE, M. E., TOLIĆ, N., JAITLEY, N., SHAW, J. L., ADKINS, J. N. & SMITH, R. D. 2007. VIPER: an advanced software package to support high-throughput LC-MS peptide identification. *Bioinformatics*, 23, 2021-3.

NEIDHARDT, F. C., BLOCH, P. L. & SMITH, D. F. 1974. Culture medium for enterobacteria. *Journal of Bacteriology*, 119, 736-747.

RAPPAPORT, S. M. 2011. Implications of the exposome for exposure science. *Journal of exposure science & environmental epidemiology*, 21, 5-9.

RIDDLES, P. W., BLAKELEY, R. L. & ZERNER, B. 1979. Ellman's reagent: 5,5'-dithiobis(2-nitrobenzoic acid)--a reexamination. *Analytical Biochemistry*, 94, 75-81.

ROCKWOOD, A. L. & HAIMI, P. 2006. Efficient calculation of accurate masses of isotopic peaks. *Journal of the American Society for Mass Spectrometry*, 17, 415-9.

RUBINO, F. M., VERDUCI, C., GIAMPICCOLO, R., PULVIRENTI, S., BRAMBILLA, G. & COLOMBI, A. 2004. Molecular characterization of homo- and heterodimeric mercury(II)-bis-thiolates of some biologically relevant thiols by electrospray ionization and triple quadrupole tandem mass spectrometry. *Journal of the American Society for Mass Spectrometry*, 15, 288-300.

SENKO, M., BEU, S. & MCLAFFERTY, F. 1995. Determination of monoisotopic masses and ion populations for large biomolecules from resolved isotopic distributions. *Journal of the American Society for Mass Spectrometry*, 6, 229-233.

SINGH, P., PANCHAUD, A. & GOODLETT, D. R. 2010. Chemical cross-linking and mass spectrometry as a low-resolution protein structure determination technique. *Analytical chemistry*, 82, 2636-42.

WASHBURN, M. P., WOLTERS, D. & YATES, J. R. 2001. Large-scale analysis of the yeast proteome by multidimensional protein identification technology. *Nature Biotechnology*, 19, 242-247.

WILD, C. P. 2005. Complementing the genome with an "exposome": the outstanding challenge of environmental exposure measurement in molecular epidemiology. *Cancer epidemiology, biomarkers & prevention : a publication of the American Association for Cancer Research, cosponsored by the American Society of Preventive Oncology*, 14, 1847-50.

WOMBLE, D. D. & ROWND, R. H. 1988. Genetic and physical map of plasmid NR1: comparison with other IncFII antibiotic resistance plasmids. *Microbiological Reviews*, 52, 433-451.

YANG, L., AMAD, M., WINNIK, W. M., SCHOEN, A. E., SCHWEINGRUBER, H., MYLCHREEST, I. & RUDEWICZ, P. J. 2002. Investigation of an enhanced resolution triple quadrupole mass spectrometer for high-throughput liquid chromatography/tandem mass spectrometry assays. *Rapid communications in mass spectrometry : RCM*, 16, 2060-6.

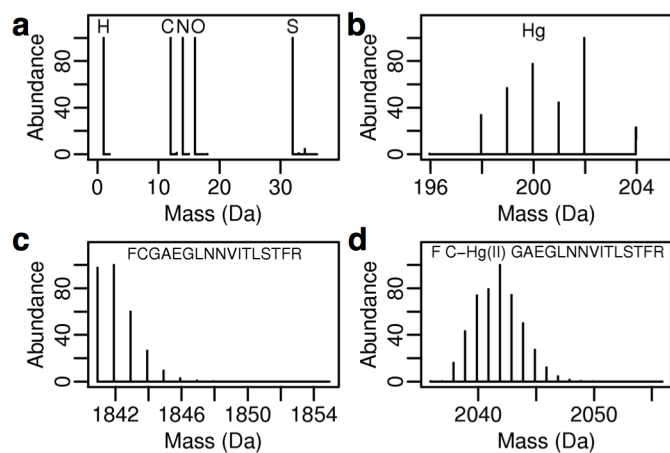


**Figure A.1. Isotope distributions of single atoms and their effects on peptide isotope distributions.** Isotope distributions for single atoms of the five typical peptide elements are shown in (a) and for Hg in (b). Panels (c and d) show computed isotope distributions for the same peptide either unmodified (c) or modified with a single Hg(II) (d).

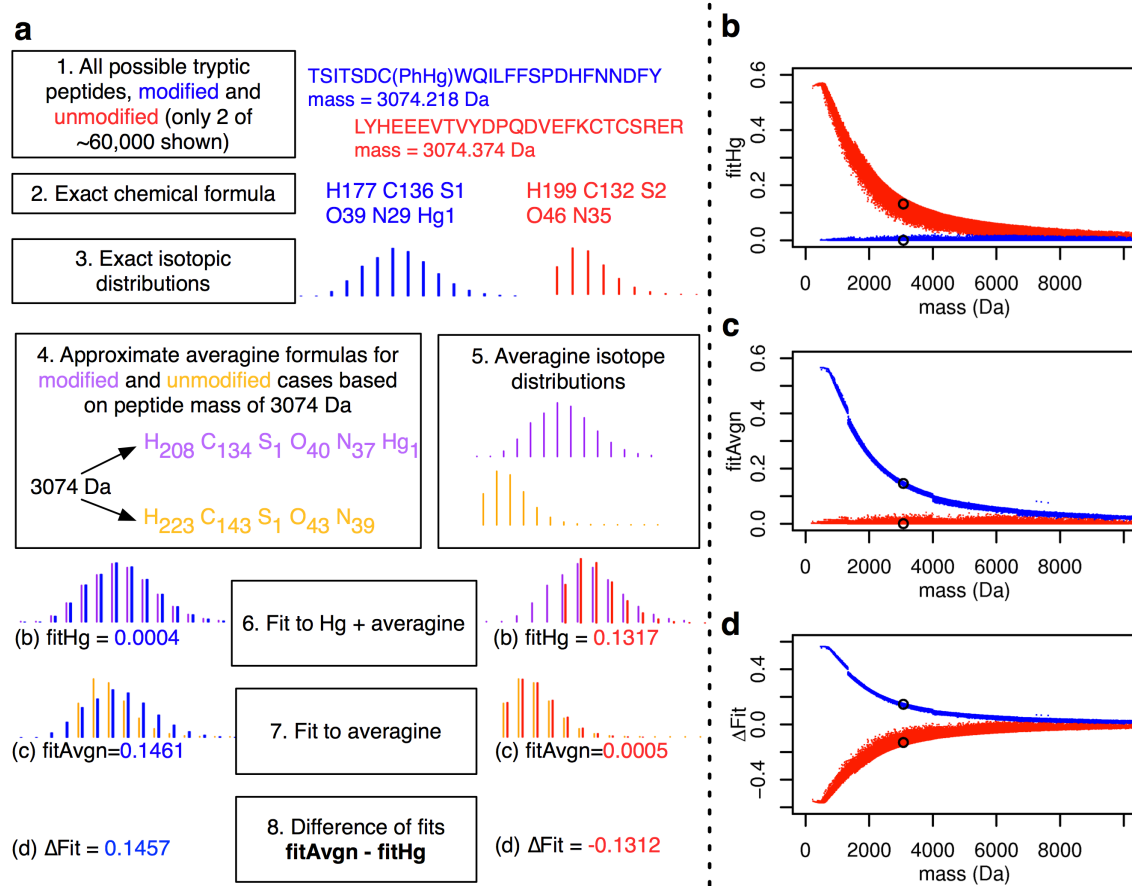


**Figure A.2. Isotope distributions of Hg peptides of unknown sequence are theoretically separable from typical unmodified peptides.** The procedure for generating data for panels (b–d) is outlined in (a). In (a), boxes 1–3 show two examples (blue and red) of the generation of exact isotope distributions of computed *E. coli* tryptic cysteine peptides in Hg-modified and unmodified states (as proxies for observed, unidentified isotope distributions). Boxes 4–5 show the computation of expected isotope distributions based on approximate averagine (14) formulas for these two cases, modified and unmodified. Boxes 6–8 show the fit scores that can be used to classify the unidentified isotope distribution as Hg-modified or unmodified. The relation of these fit scores to the mass of the peptide is shown in panels (b–d) for ~60,000 *E. coli* tryptic peptides

in either modified (blue) or unmodified (red) states. Panel (b) compares the fitHg scores for computed isotope distributions with isotope distributions from averagine+Hg formulas. Panel (c) shows fitAvgn computed by fitting the *E. coli* isotope distributions to isotope distributions from averagine formulas without Hg. Panel (d) shows  $\Delta\text{Fit}$ , the difference between scores in (c) and (b) for each isotope distribution. Points circled in black in (b–d) correspond to the example peptides shown in (a).

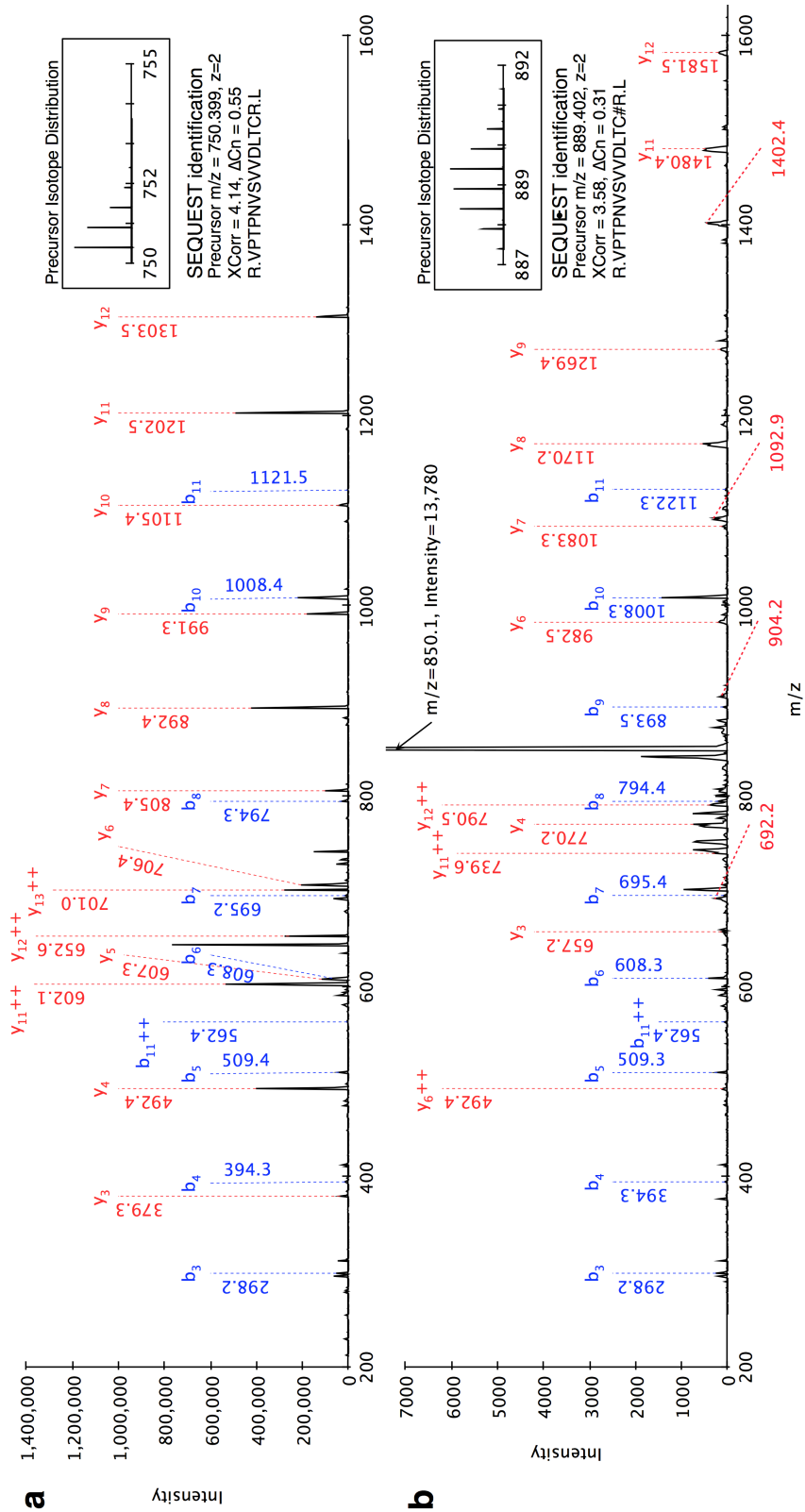




**Figure A.3. MS/MS Spectra of unmodified (a) and PhHg-modified (b) rabbit GAPDH peptide VPTPNVSVVDLTCR.** ‘C#’ denotes a PhHg adduct of cysteine. Inset plots show the isotope distributions of the precursor ions as observed in MS<sup>1</sup>. Peaks that match expected y and b fragmentation ions are labeled with m/z values reported as observed from the spectra. In (b), the top of the tallest peak matches a peak consistent with the neutral loss of 78 Daltons, equal to a phenyl group, from the precursor ion. The full height of this peak is not shown in order to increase the visibility of y and b ions. Red labels under the x-axis in (b) indicate peaks that correspond to a loss of 78 Daltons from a y ion.

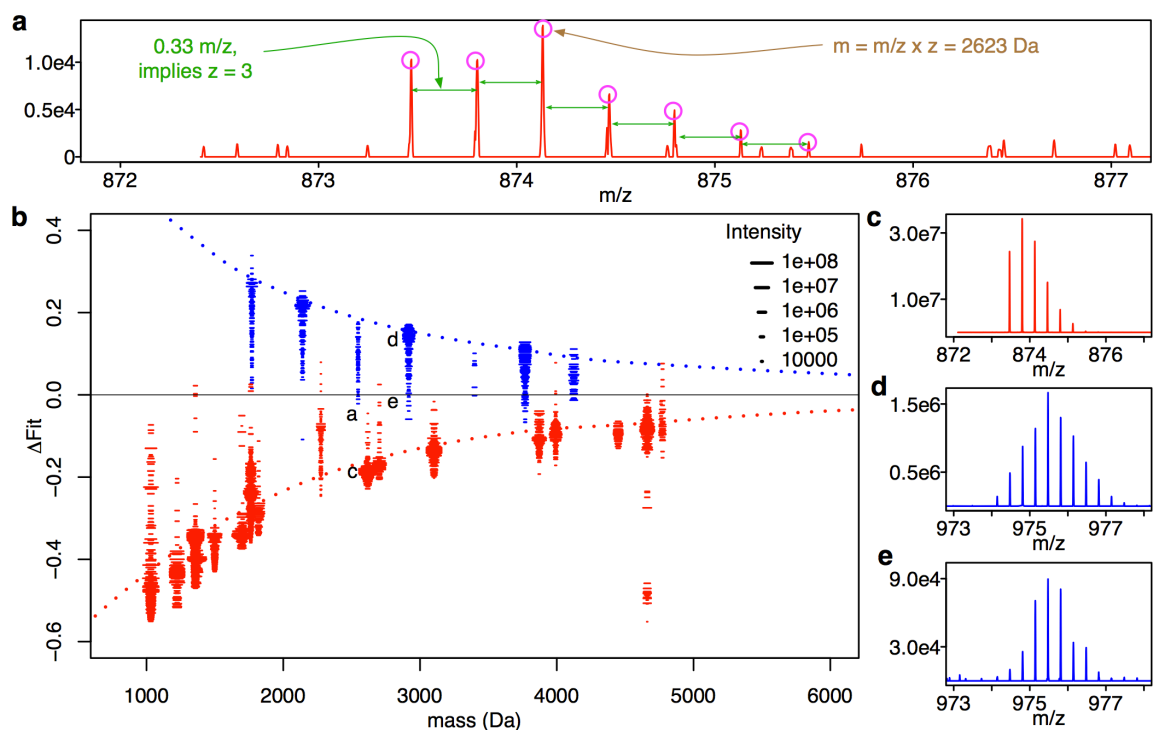


**Figure A.4. Observed isotope distributions of PhHg modified and unmodified rabbit GAPDH peptides are distinct.** The procedure used to generate  $\Delta\text{Fit}$  for observed isotope distributions is identical to that for Figure A.2 except that analysis begins by replacing Figure A.2 boxes 1-3 with observed isotope distributions and observed mass (panels a and c-e). All isotope distributions were collected as described in Experimental Procedures from  $\text{MS}^1$  scans in LC-MS/MS runs of tryptic digests of pure PMA-exposed rabbit GAPDH. Panel (b) plots  $\Delta\text{Fit}$  scores for observed isotope distributions of unmodified (red dashes “-”) and modified peptides (blue dashes “-”) as a function of observed mass. The dotted lines are loess smoothed curves of the values computed on the noise-free isotope distributions shown in Figure A.2(d). Each dash (-) represents the fit score for an individual isotope distribution from a single  $\text{MS}^1$  scan, and the length of the dash indicates the intensity of the tallest peak in that isotope distribution. Labels

“a”, “c”, “d” and “e” identify points corresponding to the example distributions in those panels (a, c, d, and e). The distribution displayed in panel (c) is for the same peptide as in (a) but with a stronger signal. Panels (d) and (e) are examples of relatively strong (d) and weak (e) intensity distributions for another PhHg modified peptide.

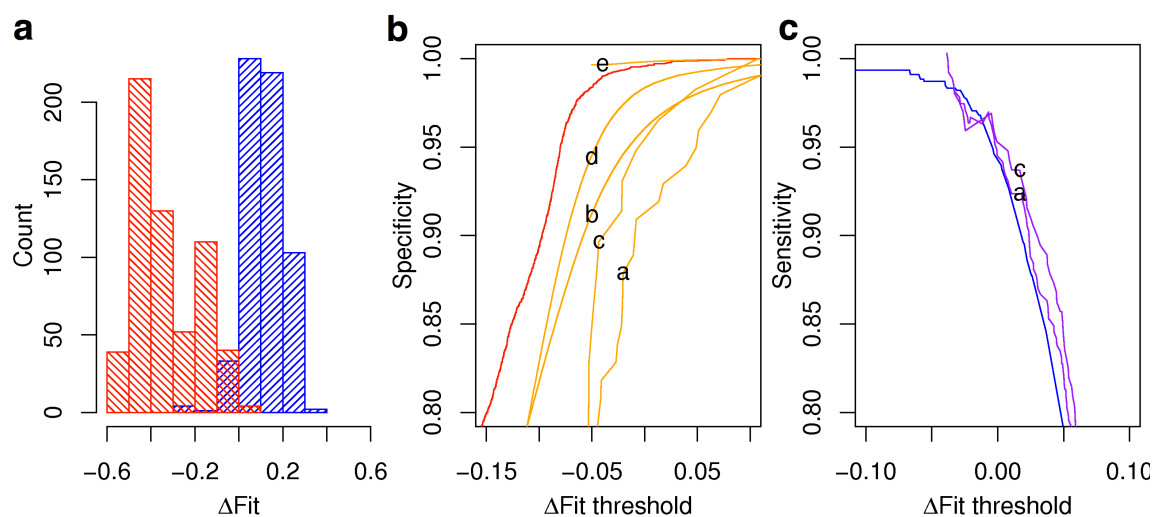


**Figure A.5. Sensitivity and specificity of  $\Delta\text{Fit}$  depends on threshold.** Panel (a) shows the distribution of  $\Delta\text{Fit}$  scores from rabbit GAPDH peptides shown in Figure A.4b. In blue is a histogram of the 590  $\Delta\text{Fit}$  scores from modified peptides. To match the size of the blue distribution, in red is a random sample of 590 out of the 4507 total  $\Delta\text{Fit}$  scores from unmodified peptides. At each  $\Delta\text{Fit}$  threshold, the specificity (panel b, red line) is the fraction of the isotope distributions from unmodified GAPDH peptides (red distribution) that lies to the left of the threshold. The sensitivity (panel c, blue line) is the fraction of the isotope distributions from GAPDH modified peptides (blue distribution) that lies to the right of the threshold. Panels b and c also show sensitivity and specificity of  $\Delta\text{Fit}$  on *E. coli* proteomic preparations for comparison. In panel (b), the specificity shown by orange lines a–d is the fraction of the orange distribution from the same-lettered histogram in Figure A.6 that is less than the threshold. The specificity line labeled “e” shows the fraction of *all* summed features (using the orange distribution in Fig. A.6d) eliminated by both the  $\Delta\text{Fit}$  threshold AND a fitHg threshold of 0.05 to produce the distribution in Figure A.6e. In panel (c) the letters on the purple sensitivity lines refer to the histograms in Figure A.6 that produce the sensitivity estimate.

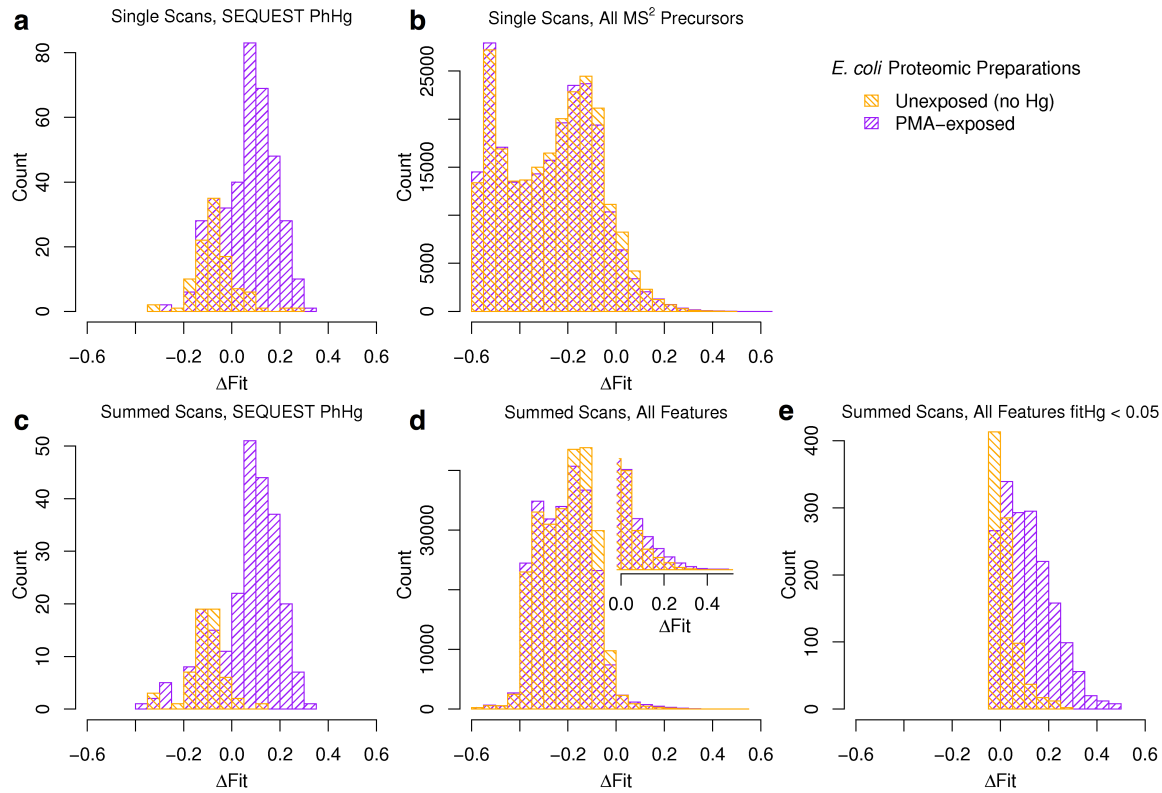


**Figure A.6. Comparisons of  $\Delta\text{Fit}$  distributions from proteomes of PMA-exposed cells with those from unexposed cells show  $\Delta\text{Fit}$  combined with  $\text{fitHg}$  can effectively identify Hg modifications.** In all panels,  $\Delta\text{Fit}$  scores in purple are for peptide isotope distributions from the proteomes of three different *E. coli* cultures exposed to PMA. In orange are  $\Delta\text{Fit}$  scores from the proteomes of three contemporaneous *E. coli* cultures not exposed to PMA. Panel (a) shows  $\Delta\text{Fit}$  scores (of the  $\text{MS}^1$  precursor ion) for all PhHg predictions made by SEQUEST. Panel (b) shows  $\Delta\text{Fit}$  scores for all  $\text{MS}^1$  precursors of  $\text{MS}^2$  scans, regardless of their SEQUEST predictions. Panels (c) and (d) show distributions similar to those in panels (a) and (b), but for isotope distributions summed across all scans of multi-scan features. Panel (d) includes an inset that is an enlargement of the main plot at  $\Delta\text{Fit} > 0$ . In (e) only features with summed isotope distributions that closely match a Hg-modified distribution ( $\text{fitHg} < 0.05$ ) are counted.

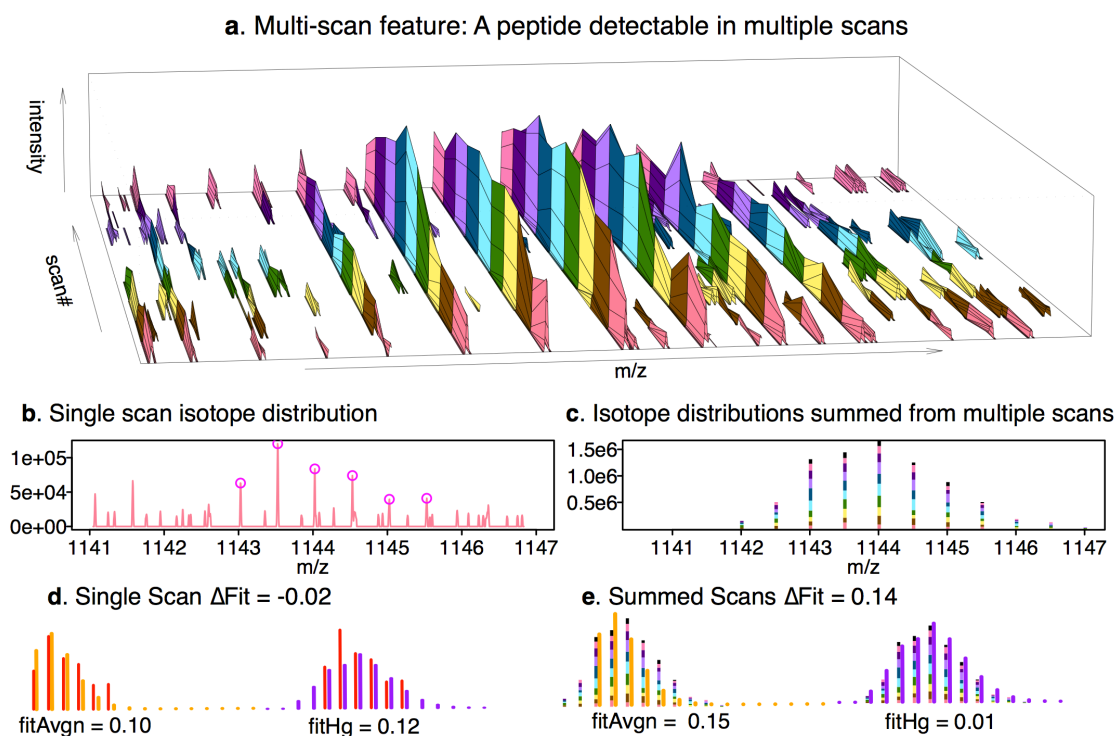


**Figure A.7. Summing isotope distributions over elution profiles decreases noise.** Panel (a) depicts spectra collected in sequential scans of a peptide ion from a proteomic preparation as it elutes from the LC over the time of 10  $\text{MS}^1$  scans. The colored bars serve to visually separate the scans which are represented by the black borders between colors. The earliest scan is in the front with later scans following in back. Panels (b) and (c) show two methods of using these scans to compute isotope distributions. The simplest (b) is to use a single scan whose  $\text{MS}^2$  fragmentation led to SEQUEST identification of this peptide ion as one containing a PhHg-adduct. The scan in (b) is the same scan as the front-most scan in (a). Those peaks that match single mass-unit isotopic shifts and comprise the observed isotope distribution are circled in magenta. In (c) the observed isotope distributions across scans for the same LC-MS feature are summed over all scans included in the feature. The contribution of each scan is drawn with the color that follows

it in panel (a), with the last scan represented by black. Panels (d) and (e) show the alignments and fittings of the observed isotope distributions (b and c) with the averagine-based expected distributions for unmodified (yellow) and modified (purple) cases. In this example, the single scan data (d) give a negative  $\Delta\text{Fit}$  indicating it is not likely a Hg adduct, but the summed multi-scan data (e) give a positive  $\Delta\text{Fit}$  indicating a likely Hg adduct.

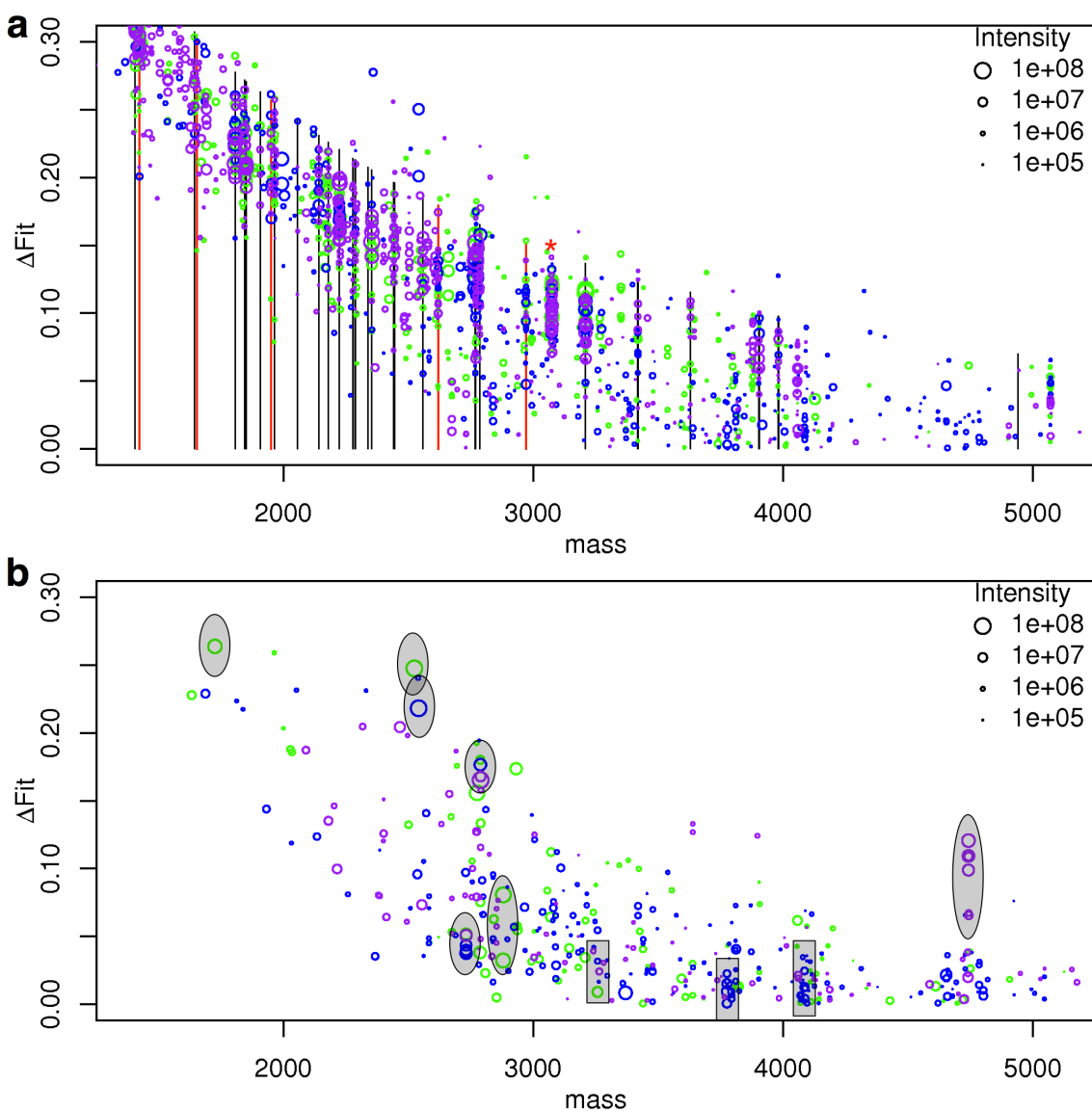


**Figure A.8. All multi-scan features with Hg-adduct-like isotope distributions.** Each circle corresponds to the summed isotope distribution for one multi-scan feature from three different *E. coli* cell cultures, each represented by a different color (green, purple, blue). Only features with  $\Delta\text{Fit} > 0.0$  and  $\text{fitHg} < 0.05$  are plotted. Panel (a) shows data from PMA exposed cultures and panel (b) shows data from the same cultures with no PMA exposure. See Supplementary Figure A.S9 for the same plots with an enlarged x-axis to minimize overlaps. In (a), black vertical lines



show SEQUEST identifications of PhHg adducts in at least one of the LC-MS/MS runs. Clusters marked with red vertical lines were unidentified by SEQUEST because of ambiguous MS<sup>2</sup> fragmentation data but are likely PhHg adducts based on accurate mass, SEQUEST hits below acceptable thresholds, and observations of other peptides from the same proteins. The vertical cluster marked with a red asterisk (\*) is a peptide that coordinates one Hg(II) with its two cysteines in the CTTNC active site motif of *E. coli* GAPDH. In (b), clusters of points highlighted with gray backgrounds were selected for further examination to determine the cause of their Hg-like isotope distributions. Those in gray ovals are the result of co-eluting unmodified peptides that are separated by 2.0 or 3.0 Daltons (see Supplementary Figures A.S11 and A.S12) so that their combined isotope distributions appear as one broad distribution. Those in gray rectangles could not be classified as co-elutions.

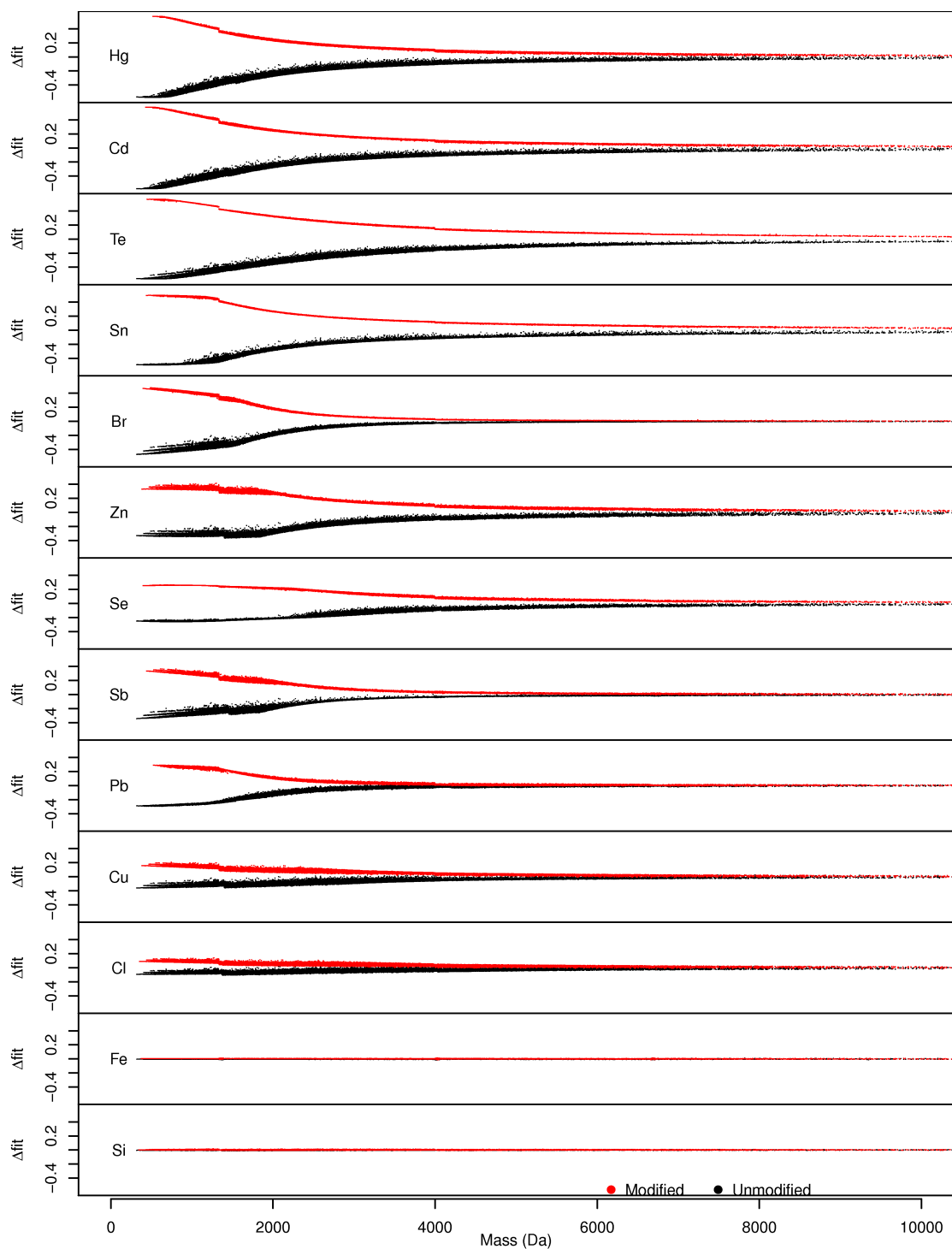


**Figure A.S1. Theoretical  $\Delta\text{Fit}$  for peptides modified with a single atom of the named elements.**  $\Delta\text{Fit}$  was computed as in Figure A.2 except that here a 10% random sampling of all *E. coli* tryptic peptides were used. Red points plot the  $\Delta\text{Fit}$  for a peptide modified with a single

atom of the named element. Black points are  $\Delta\text{Fit}$  values for the unmodified peptides.  $\Delta\text{Fit}$  is computed as the difference between  $\text{fitAvgn}$  and  $\text{fitXx}$ , where 'Xx' is the element named. For example,  $\Delta\text{Fit}$  in the second panel, which assumes a search for a peptide modified with cadmium (Cd), is  $\text{fitAvgn} - \text{fitCd}$  (see Figure A.2.).

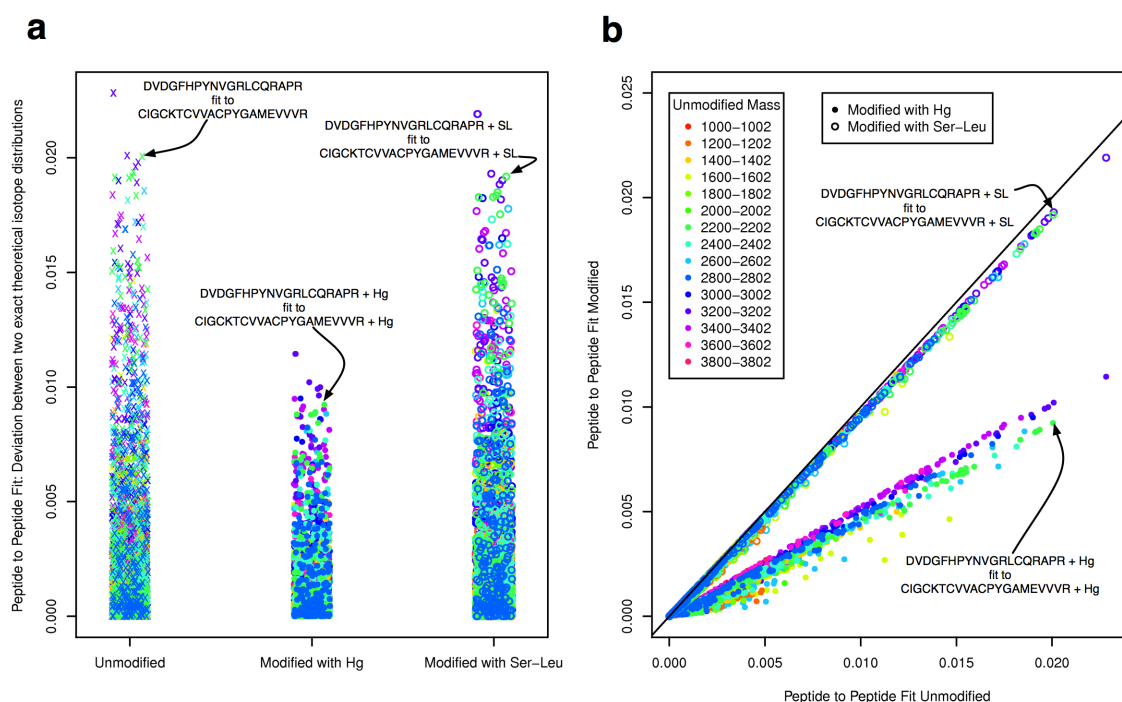


**Figure A.S2. Hg modifications homogenize isotope distributions of different peptides.** To investigate how Hg modifications affect the variability of peptide isotope distributions, we measured the deviation between pairs of theoretical peptide isotope distributions. Our analysis included comparisons for 323 *E. coli* peptides from 15 different 2 Dalton-wide mass ranges, resulting in 3418 pairs of different peptides with similar mass. Panel (a) shows all pair-wise deviations, measured as fit scores according to the procedure described in Experimental Procedures. The first column ('x'es) shows the deviations between unmodified peptides of similar mass on the y-axis. Within each category on the x-axis, the left-to-right placement is assigned randomly in an effort to minimize overlaps. Most peptides have very similar isotope distributions indicated by the large number of fit scores near zero so that it becomes impossible to resolve individual points. Still, many pairs of peptides have fit scores greater than 0.01. For example, the deviation between peptides DVDGFHPYNVGRLCQRAPR and

CIGCKTCVVACPYGAMEVVVR (labeled on plot) gives a fit score of 0.02. This relatively high deviation is due to the effects of the five sulfur atoms in the second peptide compared to only one sulfur atom in the other. The remaining columns in panel (a) show the deviation scores for the same set of peptide pairs where each is modified with the same of two types of modifications. The middle columns shows the effect of an addition of a single Hg atom (filled circles). The smaller range of these fit scores compared with the fit scores for the unmodified peptides indicate that there is about half as much deviation (lower fit scores) between pairs of modified peptides than for the unmodified. The second type of modification, shown in the third column, is a simple insertion of serine and leucine (SL) adding approximately 200 Daltons to the peptide, an equivalent mass to Hg (open circles). These show that the additional mass alone is not sufficient to explain the decrease deviations seen with a Hg modification. Panel (b) shows the same data as in (a) except that the deviation scores for the modified peptide pairs on the y-axis are related to the deviations scores for the same peptide pair, but unmodified, on the x-axis. the black diagonal line is the equivalence line (slope=1, y-intercept=0) where points would lie if the modified and unmodified fit scores were equal. This plot makes clear that the addition of SL has a negligible thought slight effect on decreasing deviations, but the addition of Hg consistently decreases the deviations by about half.

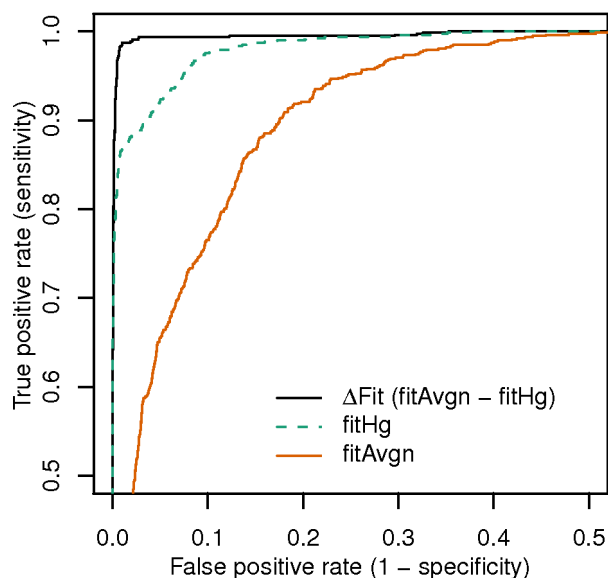


**Figure A.S3. ROC analysis compares the classification ability of different fit scores.** For routine application of this method, we sought a single scoring function that most accurately classifies an observed peptide isotope distribution as one with an Hg adduct or as an Hg-free peptide. The accuracy of such binary classifiers can be described more explicitly by two different components: the true positive and false positive rates. For this work, the true positive rate (TP rate, equivalent to sensitivity) is defined as the fraction of actual Hg-peptide spectra that are identified by our method as Hg-modified. The false positive rate (FP rate, equivalent to 1 - specificity) is defined as the fraction of all Hg-free spectra that are identified as Hg modified. When a binary classifier is based on a continuous scoring function such as our fit scores, both the TP and FP rates depend on the choice of a threshold. However, since thresholds are not directly comparable between different scoring functions, we compared the TP rate at thresholds that produced the same FP rate for each scoring function. To do this we used this receiver-operating characteristic (ROC) graph that plots TP rates on the y-axis against FP rates on the x-axis. To construct such a plot, the threshold is allowed to vary between the most strict where no spectra

pass the threshold (point 0,0 on the plot, not shown), to the most lenient where all spectra pass (point 1,1 on the plot, not shown). At each possible threshold value in between, a TP rate and FP rate can be computed, defining the points of the ROC curve. Typically, the best scoring function is the one that has the 'steepest' ROC curve, or the one with the most area under the curve. When the potential number of false positives is orders of magnitude greater than the potential number of true positives, as it is when most spectra are from unmodified peptides, typically only the region of the curve where the FP rate is near zero is considered. This ROC plot compares three different scoring functions (see Figure A.2 and Experimental Procedures for how they are computed). FitAvgn is the fit of the observed spectrum to an averagine-based theoretical isotope pattern of a peptide of the observed mass. FitHg is the fit of the observed spectrum to a theoretical formula based on averagine with the addition of a single atom of Hg. !Fit is the difference of the individual scores (fitAvgn ! fitHg). The !Fit score gives the highest TP rates at the lowest FP rates outperforming both single fit scores (fitAvgn and fitHg).

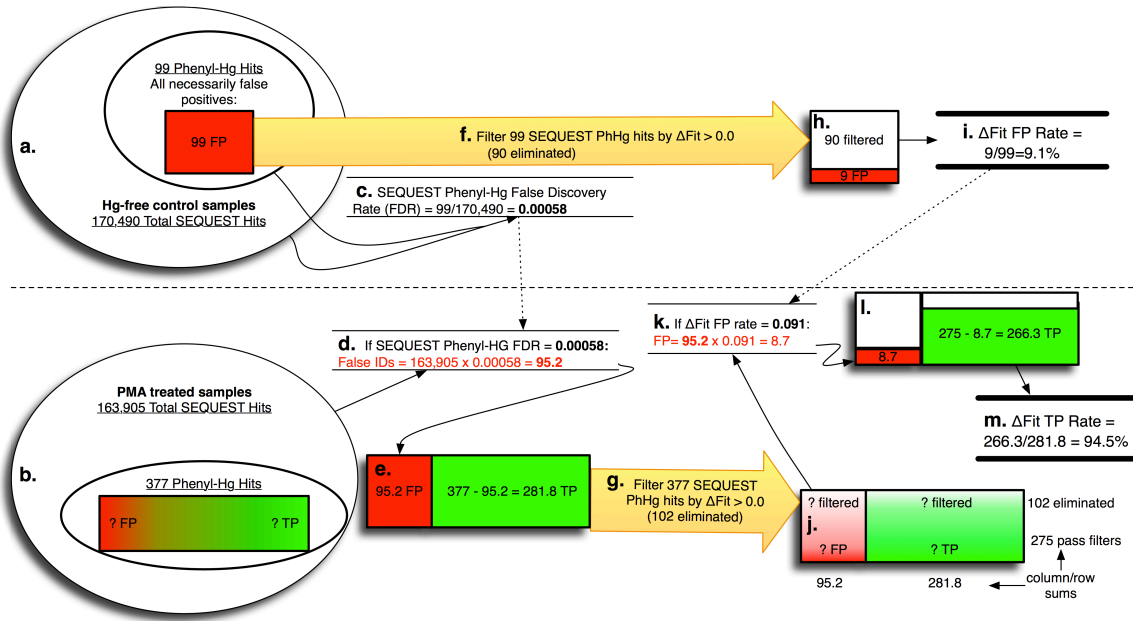


**Figure A.S4. Estimating the sensitivity (TP rate) of !Fit on SEQUEST**

**PhHg predictions.** We estimated error rates by comparing data from cell cultures not exposed to PMA against those from cell cultures exposed to PMA. In brief, the not-exposed proteomic data give false positive (FP) rates from which we infer the additional observations of PhHg-modified peptides from PMA-exposed cells are true positives. In detail, the procedure starts with the total count of all SEQUEST peptide predictions for the un-exposed cells (oval a) and for the PMA-exposed cells (oval b); each has a small subset of peptides predicted by SEQUEST to have one or more PhHg modified cysteines. In (a) all PhHg SEQUEST hits must be FP (solid red bar) as the cells were never exposed to PMA. In (b) the number of FP and TP is unknown (fuzzy boundary between red and green bars). We compute SEQUEST's false discovery rate (FDR) for PhHg modifications in the unexposed proteome to be 0.00058 (c). Applying this PhHg FDR to the total number of SEQUEST identifications in the PMA-treated proteome (d) we estimate the



number of false PhHg identifications (e, solid red box). Note that this only estimates the number of TP and FP, not which SEQUEST identifications are true or false. For this we apply a !Fit filter to each of the SEQUEST PhHg identifications (f and g, yellow block arrows). If !Fit had perfect specificity, it would totally eliminate all PhHg-peptides in f. Instead, nine hits pass the !Fit filter and are marked as FP (h), for a FP rate of 9.1% (i). The effect of the !Fit filter on the PhHg identifications from the PMA-exposed cells (g) is less straightforward. Initially we know how many SEQUEST identifications the filter eliminates but not which are true or false SEQUEST identifications (four question marks and fuzzy colors in panel j). In panel (j) all the row and column sums are known, so assigning a value to one cell determines the value of all other cells. We estimate that there are 8.7 false SEQUEST identifications (k) that pass the !Fit filter using the observed !Fit FP rate of 0.091 (i) for the unexposed cells. Entering this number into panel (j) gives panel (l) and finally an estimate (m) for the sensitivity of !Fit on SEQUEST PhHg identifications (m). This computation was repeated using a range of !Fit thresholds in the filters (yellow arrows f and g) to generate the specificity and sensitivity plots in Figure A.5(panels b and c, lines a and c).

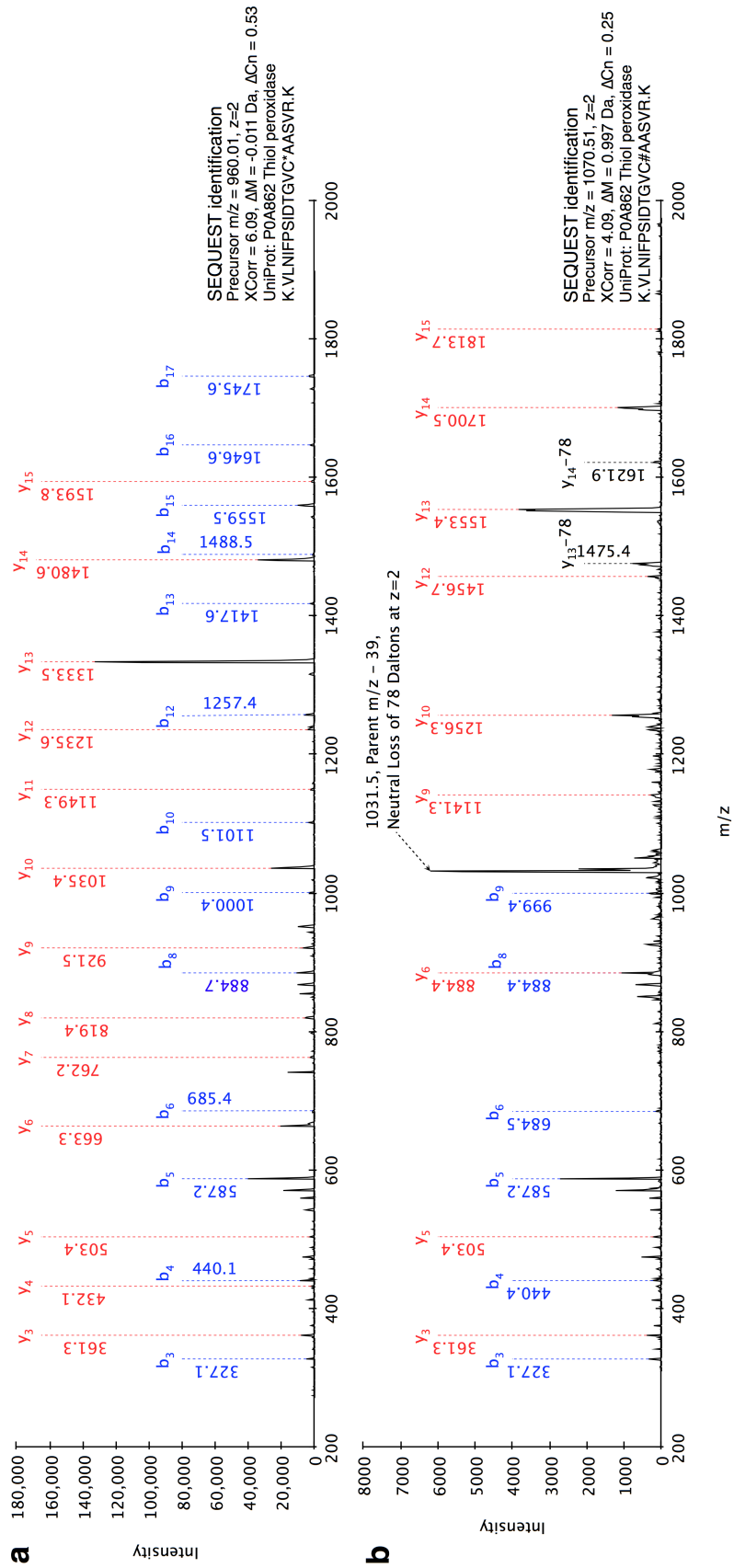


**Figure A.S5. CID fragmentation spectra of a peptide from *E. coli* thiol peroxidase in mercury-free (a) and phenyl-Hg modified (b) forms.** In the Hg-free peptide (a), cysteine was alkylated by iodoacetamide (denoted by C\*). In (b), C# denotes the phenyl-Hg adduct of cysteine. The strong peak apparent at  $m/z = 1031.5$  in (b) is consistent with the neutral loss of phenyl group ( $C_6H_6$ , 78 Daltons). This neutral loss peak is common feature in the fragmentation spectra for PhHg adducts. In (b), the peak at  $m/z = 884.4$  is ambiguous and could signify either or both y6 and b8 ions. Without a clear y6 peak, the peaks for y5 and y9 ions localized the phenyl-Hg modifications to the TGVC subsequence. However, by contrasting with the Hg-free spectrum, the absence in (b) of the peak labeled y6 in (a) indicates the modification is on the cysteine.

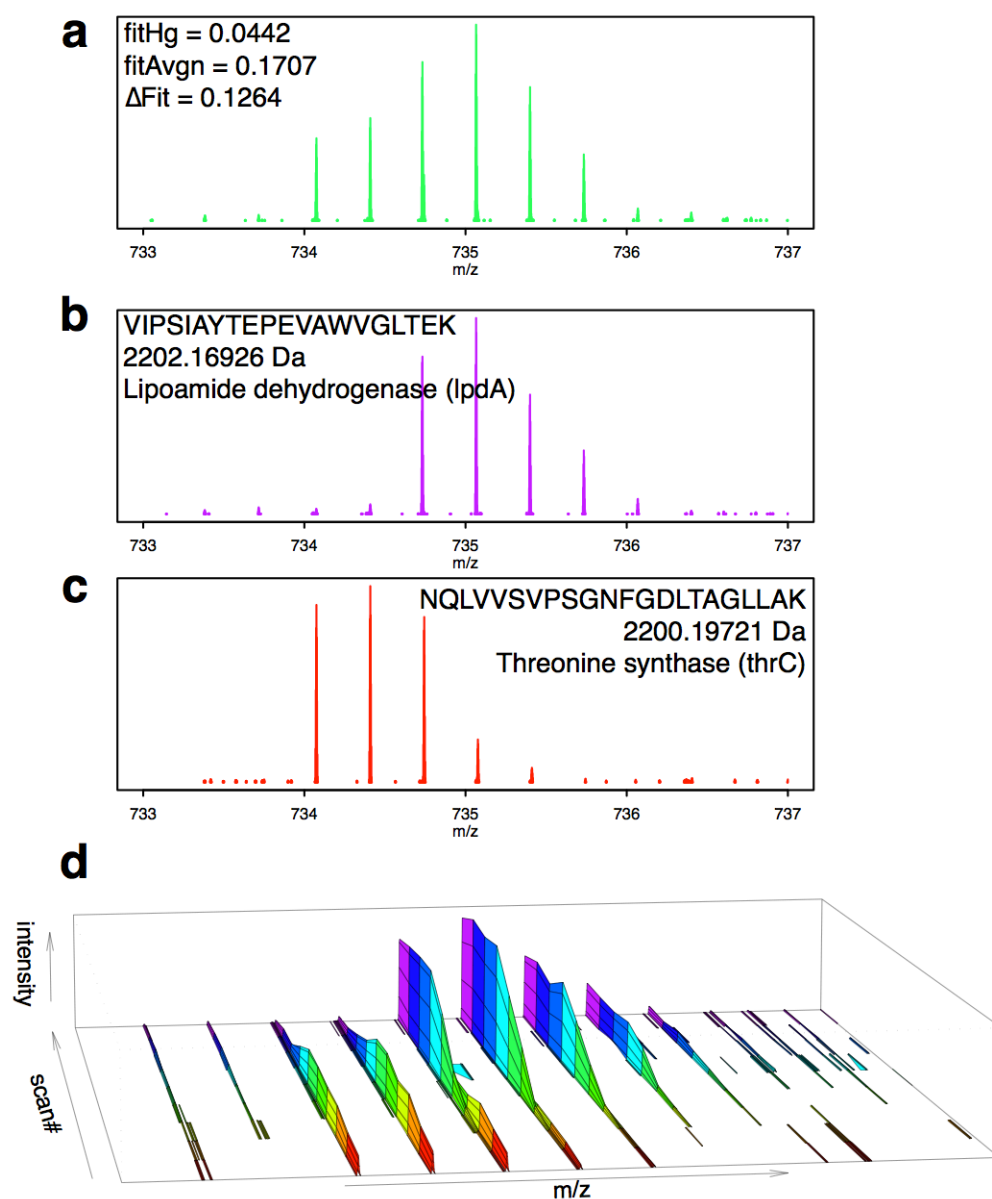


**Figure A.S6. Overlapping isotope distributions of co-eluting unmodified peptides can lead to a Hg-like isotope distribution.** All data are from an LC-MS/MS run of a proteomic preparation from *E. coli* cells not exposed to PMA. Each color on the scan axis indicates a separate sequential scan. Panel (a) shows a region of the  $m/z$  spectrum from the green MS1 scan in panel (d) that appears to be an isotope distribution whose fit scores indicate a single Hg-modified species. Panel (b) shows the same  $m/z$  region from the purple primary

MS1scan later in the LC elution when the two lightest peaks were reduced to insignificant levels. Panel (c) shows the same region of the spectrum from the red scan in panel (d) earlier in the LC elution where the heaviest peaks were missing. Both spectra shown in (b) and (c) were identified by SEQUEST to be the unmodified *E. coli* peptides indicated on their respective plots. Panel (d) shows all MS1 spectra from the same m/z region as in (a-c) over the time of 10 primary MS scans. Colors in (a-c) correspond to the colors in (d). The view in (d) illustrates that the spectra are the result of two peptides with similar masses and overlapping elution profiles. The lighter peptide finishes its elution shortly after the heavier peptide begins its elution.

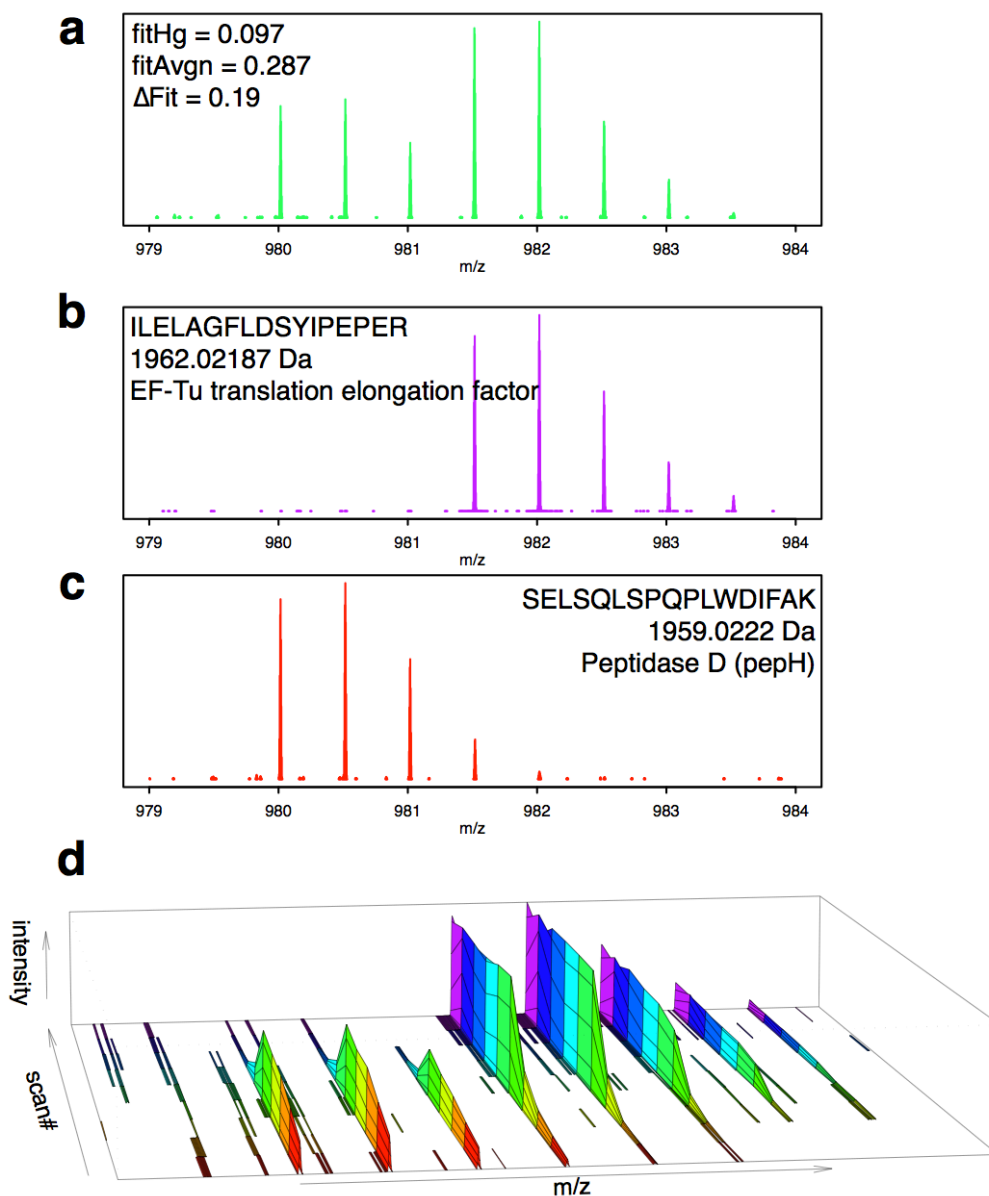


**Figure A.S7. Overlapping isotope distributions of co-eluting unmodified peptides can lead to a Hg-like isotope distribution (example 2).** This figure shows a second example, similar to that shown in Supplementary Figure A.S6. Refer to the legend of Supplementary Figure A.S6 for details.

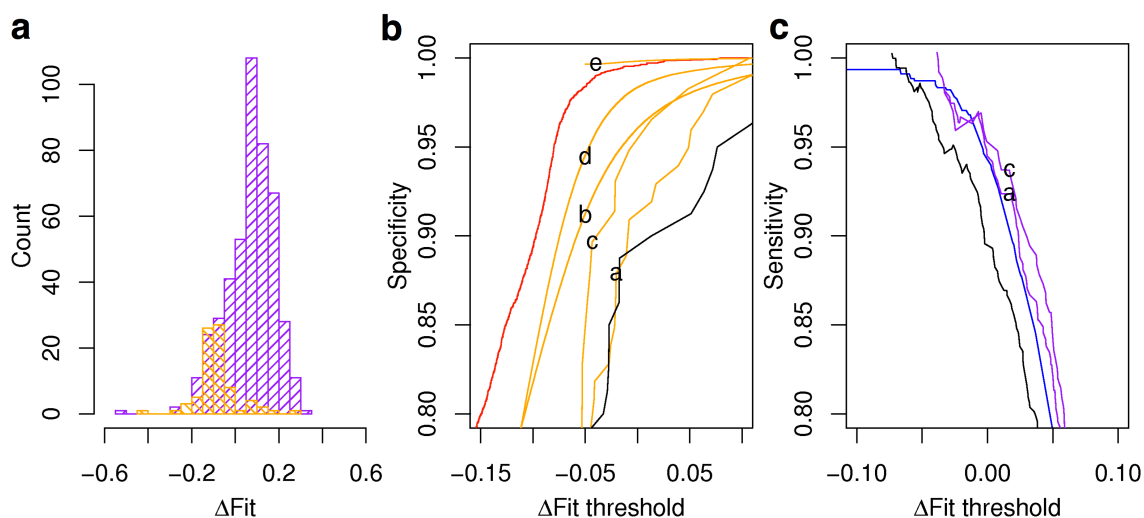


**Figure A.S8. Sensitivity and Specificity of !Fit applied to phenylHg modification**

**predictions scored by PeptideProphet.** Panel (a) shows the distribution of !Fit scores assigned to all isotope distributions that led to SEQUEST identifications of phenyl-Hg adducts and also received a PeptideProphet probability score greater than 0.5. In purple are the phenyl-Hg identifications from PMA exposed samples, and in orange are the phenyl-Hg identifications from unexposed samples. This can be directly compared with Figure A.6a and shows that using PeptideProphet probabilities finds more true identifications in the exposed samples and fewer false identifications in the unexposed samples than using SEQUEST XCorr and !Cn thresholds. On these data there is a particularly large increase in true identifications at !Fit scores between -0.05 and 0.0 when compared with Figure A.6a. Thus PeptideProphet appears more accurate for those MS2 spectra whose isotope distributions in MS1 are more likely to have a !Fit score near 0, which includes low intensity spectra and/or spectra of larger peptides. Panel (b) shows the specificity of !Fit when used to filter spectra identified by SEQUEST as a phenyl-Hg adduct.

This panel is a copy of Figure A.5b except for the addition of the black line that shows the specificity of !Fit on the PeptideProphet data shown in (a). The drop in specificity when compared with the SEQUEST XCorr and !Cn results (line a) that is apparent between thresholds of 0.0 and 0.05 is due to a difference in only 3 identifications (1/80 PeptideProphet and 4/99 SEQUEST PhHg identifications have !Fit between 0 and 0.05), not enough to rule out a difference due to random noise alone. Panel (c) shows the sensitivity of !Fit when used to filter spectra identified by SEQUEST as a PhHg adduct. This panel is a copy of Figure A.5c except for the addition of the black line that shows the sensitivity of !Fit on the PeptideProphet data shown in (a).



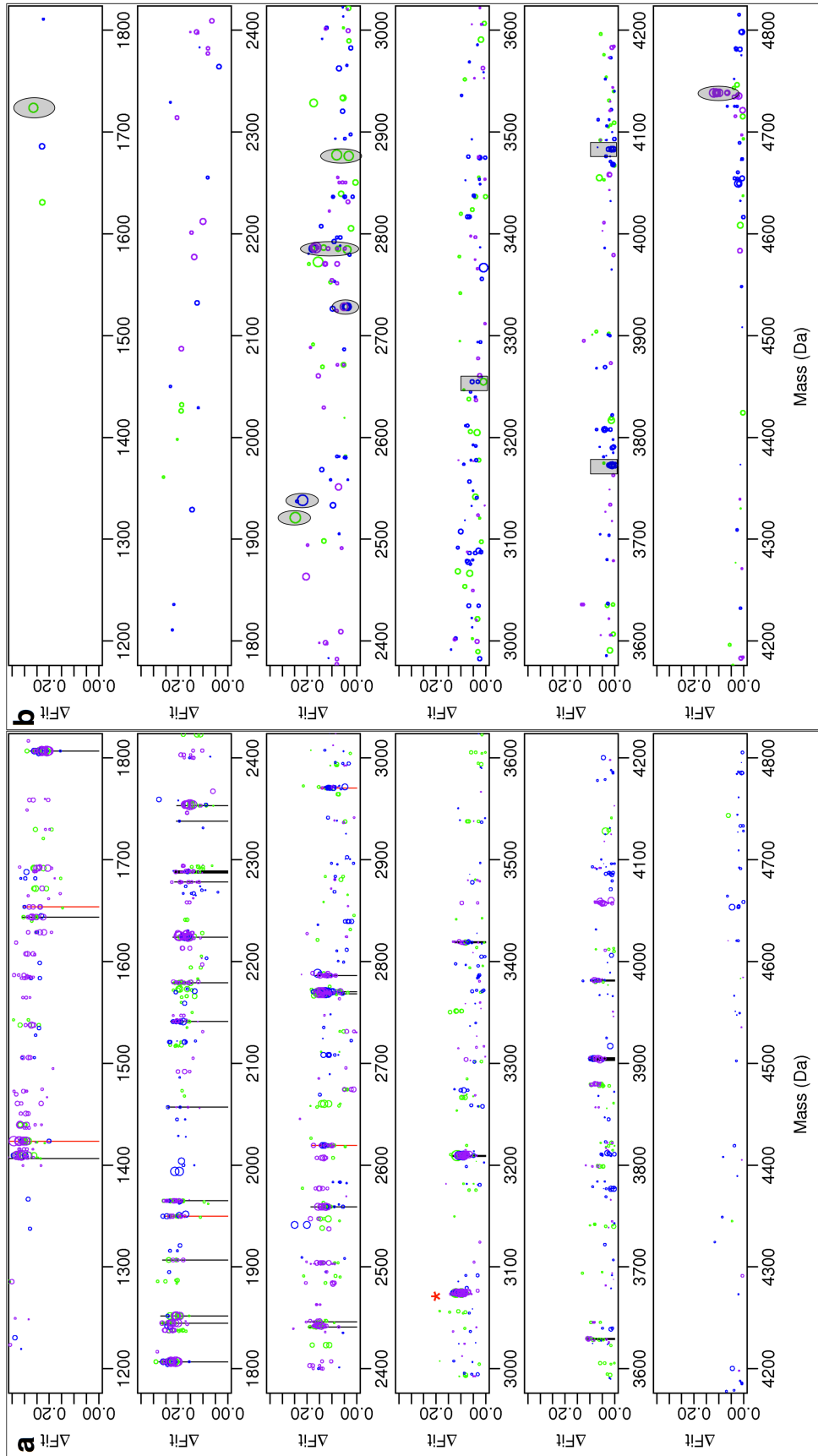


**Figure A.S9. An expanded view of all Hg-adduct-like isotope distributions from summed spectra.** The data and their representations in this plot are identical to those in Figure A.8, but here the length of the x-axis is expanded to better separate LC-MS features with similar mass. Each circle corresponds to the summed isotope distribution of one multi-scan LC-MS feature. Panel (a) shows data from PMA exposed cultures and panel (b) shows data from samples of the same cultures with no PMA exposure. This plot includes data from LC-MS/MS runs of proteomics samples from three different *E. coli* cell cultures, each represented by a different color (green, purple, blue). To minimize false positives, only features with  $\Delta\text{fit} > 0.0$  and  $\text{fitHg} < 0.05$  are plotted. In (a), black vertical lines show identifications by SEQUEST of PhHg adducts in at least one LC-MS/MS run. Clusters marked with red vertical lines were unidentified by SEQUEST because of ambiguous MS<sup>2</sup> fragmentation data but are likely PhHg adducts based on accurate mass, SEQUEST hits below acceptable thresholds, and observations of other peptides from the same proteins. The vertical cluster marked with a red asterisk (\*) is a peptide that binds one Hg(II) with its cysteine pair in the CTTNC active site motif of *E. coli* GAPDH. This unexpected adduct was confirmed by setting SEQUEST to consider Hg(II) as a variable modification of cysteine. In (b), clusters of points highlighted with gray backgrounds were selected for further examination to determine the cause of their Hg-like isotope distributions. Those in gray ovals are the result of co-eluting unmodified peptides that are separated by 2.0 or 3.0 Daltons (see Supplementary Figures A.S11 and A.S12) so that their combined isotope distributions appear as one broad distribution. Those in gray rectangles could not be classified as co-elutions.

# SEQUEST identification

Precursor m/z = 1536.167, z=2  
 UniProt: P0A9B2 Glyceraldehyde-3-phosphate dehydrogenase A

(a) GANFDKYAGQDIVSNASC@TTNCLAPLAK

XCorr = 3.96, ΔM = -0.0196 Da

(b) GANFDKYAGQDIVSNASC@TTNCLAPLAK

XCorr = 3.90, ΔM = -0.0196 Da, ΔCn = 0.25

@ = Hg(II) - 2H = 199.955 Da

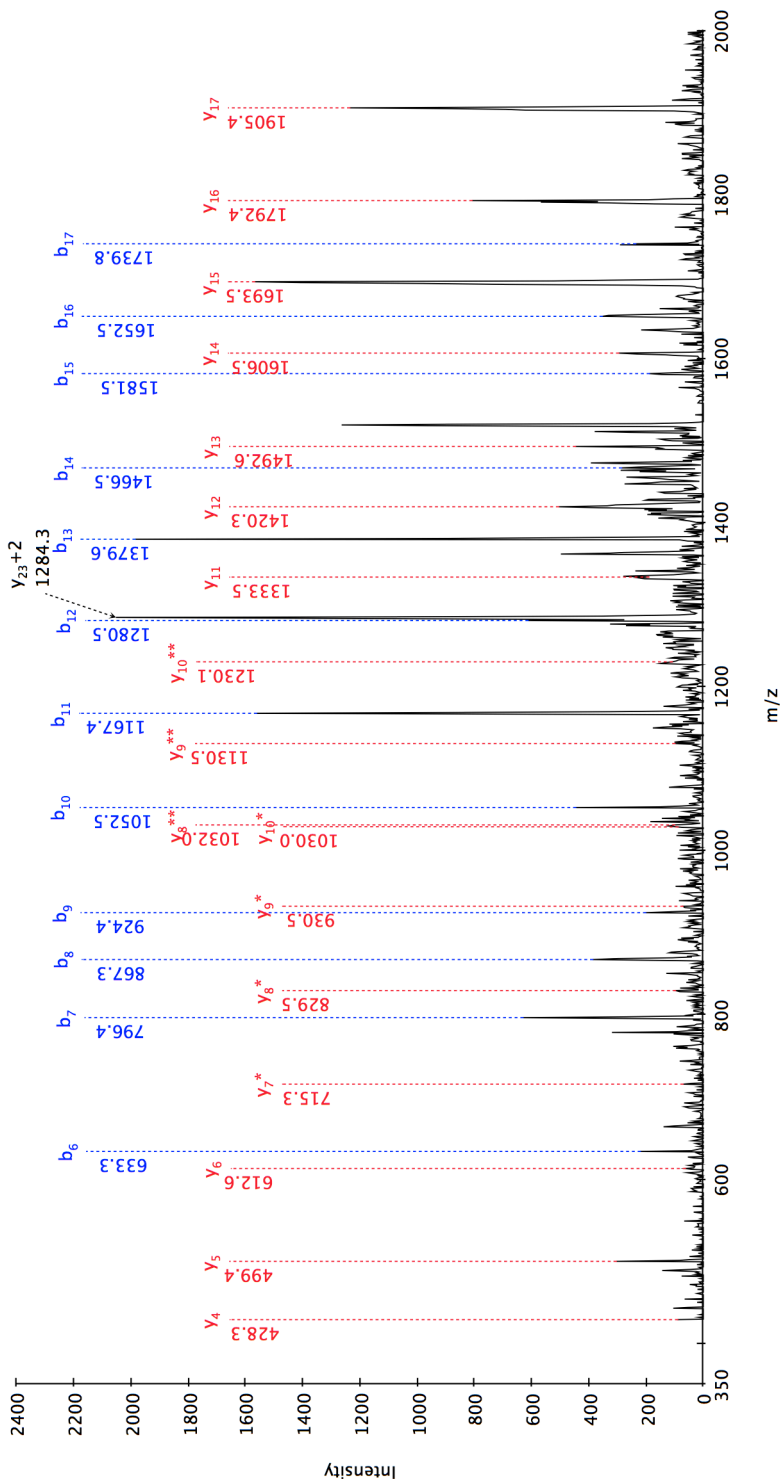
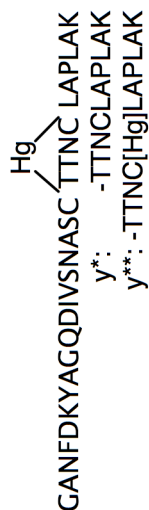


**Figure A.S10. CID fragmentation spectrum of an Hg(II) peptide adduct from *E. coli***

**GAPDH.** This peptide was identified using SEQUEST with a simple variable modification of cysteines equal to the mass of Hg(II) minus the mass of two hydrogens (+199.955 Da). The top two SEQUEST hits are to the same *E. coli* GAPDH peptide with one or the other cysteine modified. This lends strong support to the thiols of both cysteines ligating a single Hg(II). Strong peaks indicate fragments at peptide bonds around the CTTNC motif localized the modification mass to the region of the CTTNC motif, though the relatively low intensity of peaks matching masses of fragmentations within the CTTNC region do not allow for placement of the modification mass on any single residue. Fragments resulting from cleavages of the peptide backbone between the two cysteines that bind Hg can either lose the Hg (labeled y\*, consistent with the (a) ...C@TTNC... identification) or keep the Hg (labeled y\*\*, consistent with the (b) ...CTTNC@... identification).

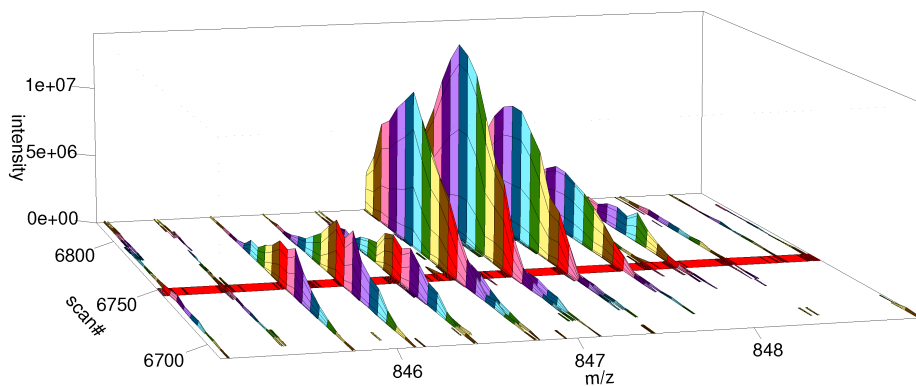


**Figure A.S11. Overlapping isotope distributions of two unmodified peptides produces Hg-like isotope distributions.** As in panel (d) of the Supplemental Figures A.6 and A.7, this plot shows the elution patterns of isotopic peaks for two co-eluting unmodified peptides over the time of 20 MS<sup>1</sup> scans. The LC-MS feature detection collected the two MS<sup>1</sup> scans (scan numbers 6744 and 6751) bordering the red horizontal bar in each peak of the elution profile into a single summed feature with  $\Delta\text{Fit} = 0.25$ . This feature appears as an outlier in Figure A.8 (a and b) and Supplemental Figure A.S9 (a and b) at mass  $\sim 2550$  with  $\Delta\text{Fit}$  even higher than expected for Hg adducts.

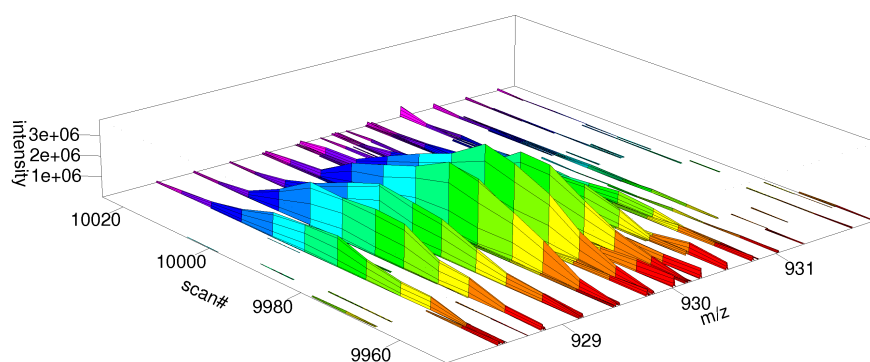


**Figure A.S12. Overlapping isotope distributions of two unmodified peptides produces Hg-like isotope distributions: very similar elution profiles.** As in Supplemental Figure A.S11, this plot shows the elution patterns of isotopic peaks for two co-eluting unmodified peptides over the time of 12 MS<sup>1</sup> scans. The LC-MS feature detection collected ten of these MS<sup>1</sup> scans (scan numbers 9958, 9965, 9971, 9978, 9984, 9991, 9998, 10005, 10012, and 10019) into a single summed feature with  $\Delta\text{Fit} = 0.17$ . This feature appears in a gray oval in Figure A.8(b) and Supplemental Figure A.9(b) at mass  $\sim 2780$ . The elution profiles of individual isotope peaks are similar enough that they do not reveal the pattern of co-elution. Instead we rely on the identification of two unmodified peptides by SEQUEST, see Supplementary Table A.S1.

Peptide (‘ is cleavage site)	UniProt ID	MH (Da.)	XCorr	$\Delta Cn$	$z^*$	$m/z^*$
R.IIMEYLDERFPHPLMPVYPVAR.G	P0ACA3	2783.441	5.53	0.4	2	928.824
R.ILEIEGLPDLKVEQAFELTDASAER.S	P36683	2786.446	5.07	0.37	2	929.493

\*  $z$  and  $m/z$  values are for the precursor ion.

**Table A.S1. SEQUEST identifications of peptides corresponding to elution peaks in Supplementary Figure A.S12.**

## APPENDIX B

### CHAPTER 2 SUPPLEMENTAL MATERIAL<sup>1</sup>

---

<sup>1</sup>LAVOIE, S.P., MAPOLELO, D.T., COWART, D.M., POLACCO, B.P., JOHNSON, M.K., SCOTT, R.A., MILLER, S.M., SUMMERS, A.O. 2015. Organic and inorganic mercurials have distinct effects on cellular thiols, metal homeostasis, and Fe-binding proteins in *Escherichia coli*. *J Biol Inorg Chem*, 20, 1239-1251; Reprinted with permission of publisher.



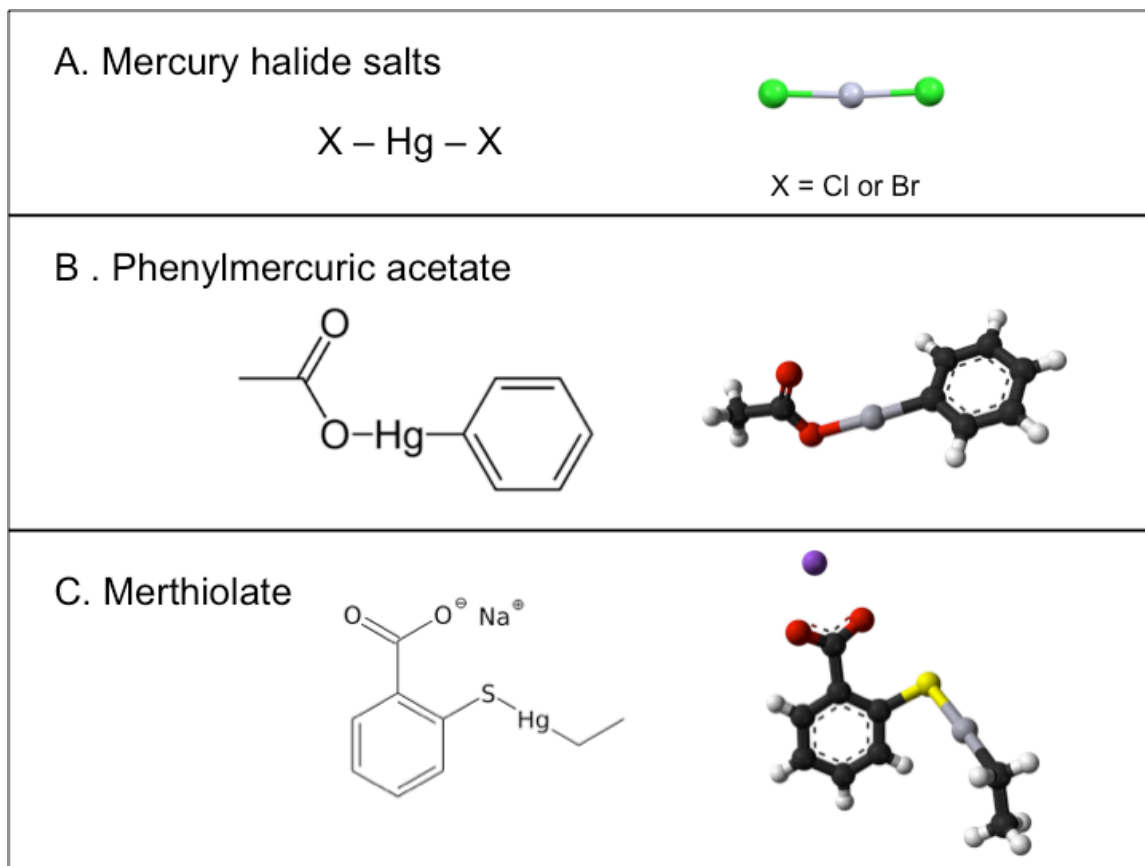


**Figure B.S1. Mercury compounds used in this work.** (A) mercuric chloride,  $\text{HgCl}_2$ ; the structure of  $\text{HgBr}_2$  is similar (B) phenylmercuric acetate,  $\text{C}_8\text{H}_8\text{HgO}_2$  (C) merthiolate (aka: thimerosal or ethylmercury thiosalicylate),  $\text{C}_9\text{H}_9\text{HgNaO}_2\text{S}$

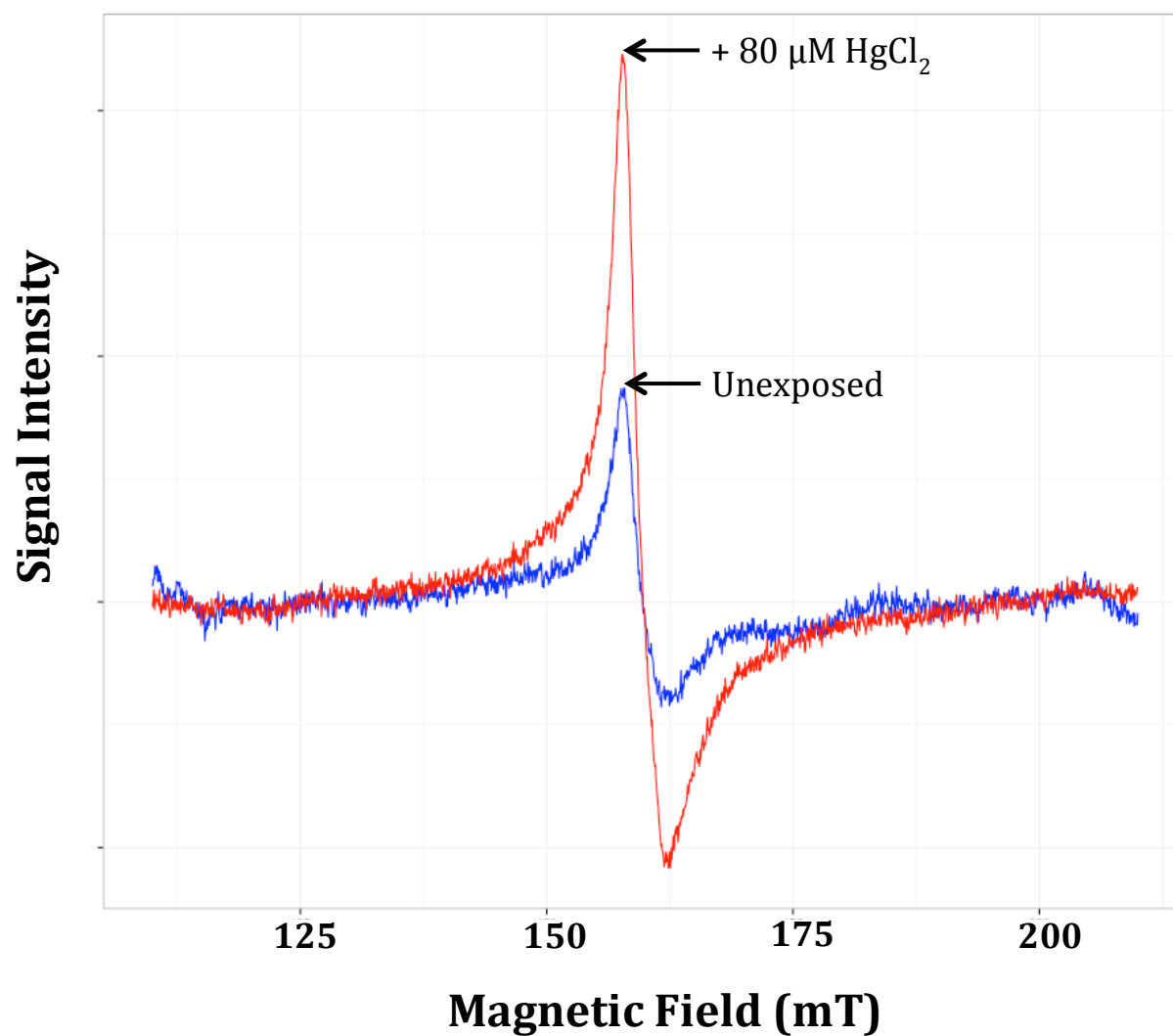


**Figure B.S2. Increase in EPR signal intensity after mercury exposure.** EPR spectra of Fe(III):DF complex at  $g = 4.3$ , unexposed control (blue) and MG + 80  $\mu\text{M}$  HgCl<sub>2</sub> (red). See Materials and Methods for details.

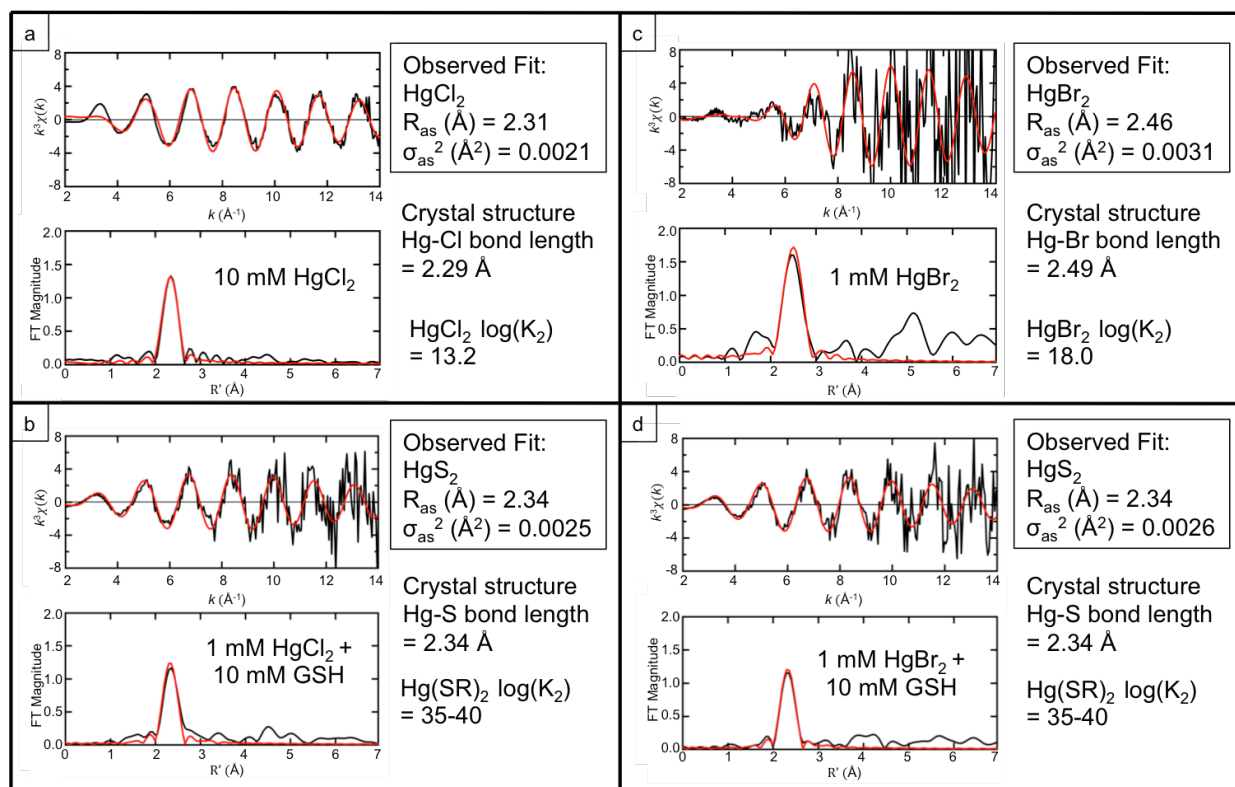


**Figure B.S3. EXAFS of pure chloride or bromide complexes of Hg(II) with or without 10-molar excess of glutathione (GSH).** EXAFS, Fourier transforms and spectral fitting results for (A) 1 mM  $\text{HgCl}_2$ , (B) 1 mM  $\text{HgCl}_2$  + GSH, (C) 1 mM  $\text{HgBr}_2$ , (D) 1 mM  $\text{HgBr}_2$  + GSH.

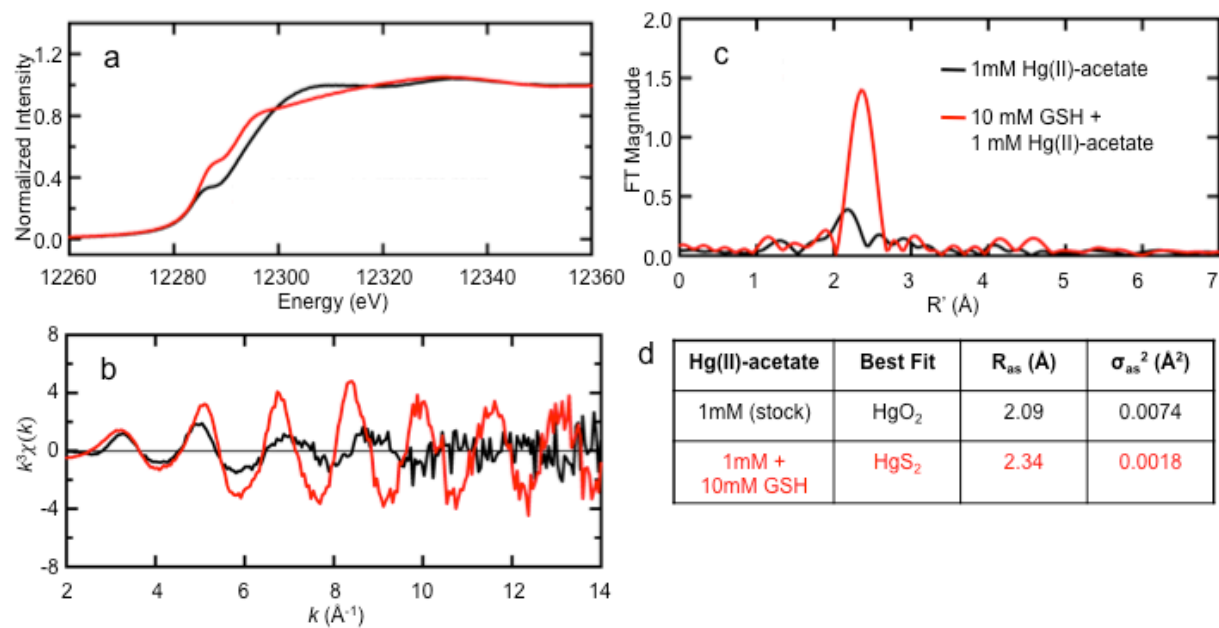


**Figure B.S4.** XANES and EXAFS of pure Hg(II)-acetate (oxygen ligand) with (red) or without (black) 1 mM GSH (sulfur ligand). (A & B) Edge and EXAFS spectra. (C) Fourier transforms of the data in (B). (D) Spectral fitting results.

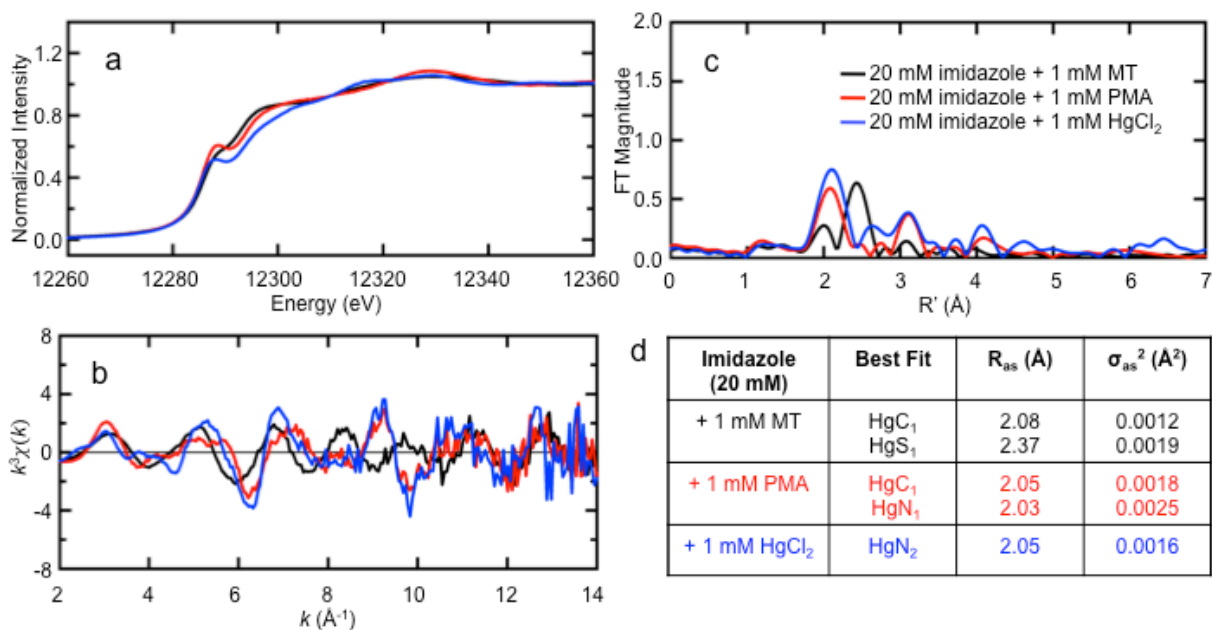


**Figure B.S5. XANES and EXAFS of pure Hg compounds complexed with imidazole. MT, (black) PMA (red) and HgCl<sub>2</sub>, (blue).** (A & B) Edge and EXAFS spectra. (C) Fourier transforms of the data in (B). (D) Spectral fitting results.

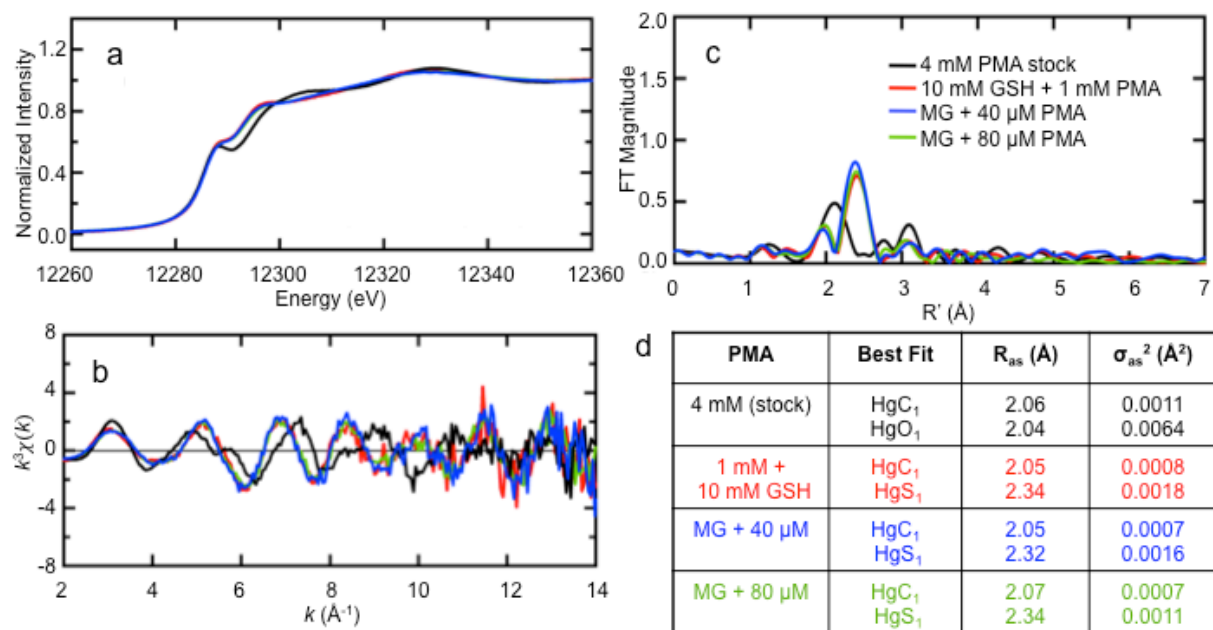


**Figure B.S6. XANES and EXAFS of Hg in intact MG1655 cells exposed to PMA.** Separate late exponential phase cultures were exposed for 30 min to PMA (4 mM stock; black) at concentrations 1.5 - 2.0-fold above the total cellular thiol content in the reaction (40  $\mu$ M, blue, and 80  $\mu$ M, green). The positive control (1 mM PMA + 10 mM GSH; red) was used as standard for fitting. (A & B) Edge and EXAFS spectra of MG1655 cell suspensions and positive control. (C) Fourier transforms of the data in (B). (D) Spectral fitting results.

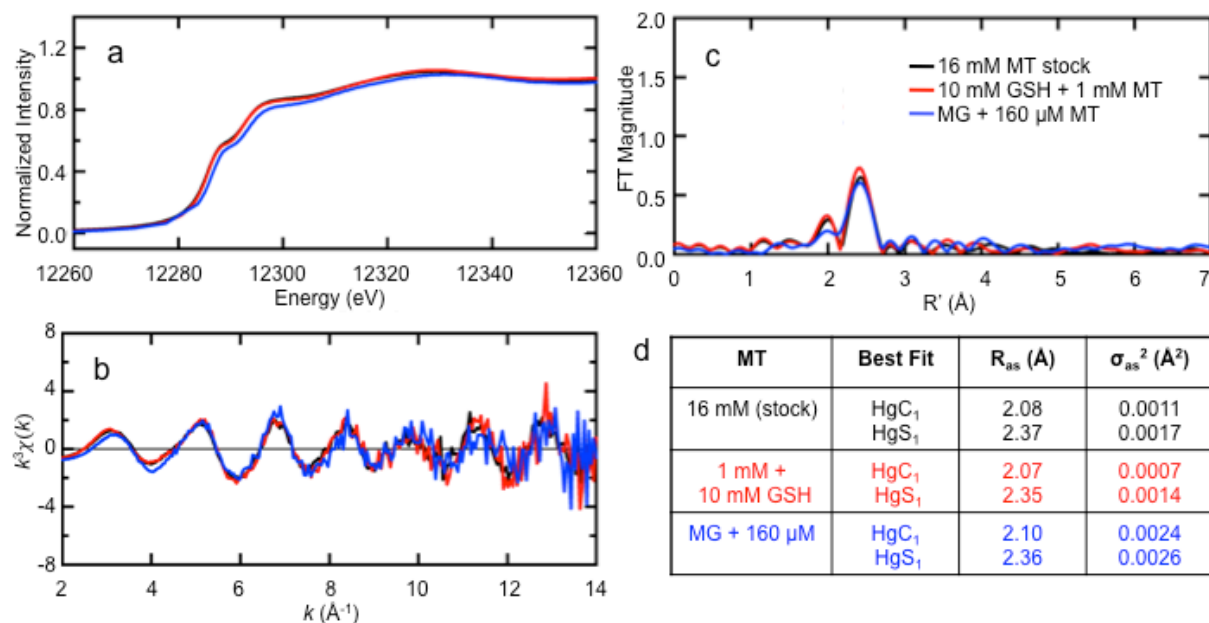


**Figure B.S7. XANES and EXAFS of Hg in intact MG1655 cells exposed to merthiolate**

**(MT).** A late exponential phase culture of MG1655 was exposed for 30 min to MT (black) at 160  $\mu$ M (blue) an 8-fold molar excess over the total cellular thiol content in the reaction, relative to 20  $\mu$ M HgCl<sub>2</sub> being equal molar. The mix of pure chemicals (1 mM MT + 10 mM GSH; red) was used for fitting. (A & B) Edge and EXAFS spectra of MG1655 cell suspension and the positive control. (C) Fourier transforms of the data in (B). (D) Spectral fitting results.

**Table B.S1. Summary of iron binding proteins<sup>a</sup> in *E. coli* based on gene ontology terms in UniProtKB.**

<b>GO term</b>	<b>GO ID</b>	<b>In <i>E. coli</i> MG1655</b>
iron ion binding	0005506	85
ferric iron binding	0008199	6
ferrous iron binding	0008198	18
iron chaperone activity	0034986	1
iron-sulfur cluster binding	0051536	143
2 iron, 2 sulfur cluster binding	0051537	32
3 iron, 4 sulfur cluster binding	0051538	8
4 iron, 4 sulfur cluster binding	0051539	106
heme binding	0020037	28

<sup>a</sup> *E. coli* has 214 proteins defined as interacting with iron; 207 have one or more cysteines. Several are assigned more than one GO term. See Table B.S2 for full list of proteins.



**Table B.S2. Iron binding proteins currently identified in the *E. coli* MG1655 genome.** Retrieved (in June 2015) from UniprotKB database using gene ontology (GO) terms related to iron binding (see Table S1). The total number of encoded cysteine sites based on protein sequences from University of Wisconsin *E. coli* Genome Project ASAP database (version m56) (Column M, *italics*).

UniProt_ID	gene_ID	gene_name	product_description	<i>num_CysSites</i>
P25516	b1276	acnA	Aconitate hydratase A (ACN) (Aconitase) (EC 4.2.1.3) (Iron-responsive protein-like) (IRP-like) (RNA-binding protein) (Stationary phase enzyme)	7
P36683	b0118	acnB	Aconitate hydratase B (ACN) (Aconitase) (EC 4.2.1.3) ((2R,3S)-2-methylisocitrate dehydratase) ((2S,3R)-3-hydroxybutane-1,2,3-tricarboxylate dehydratase) (2-methyl-cis-aconitate hydratase) (EC 4.2.1.99) (Iron-responsive protein-like) (IRP-like) (RNA-binding protein)	10
P31441	b3665	ade	Adenine deaminase (Adenase) (Adenine aminase) (EC 3.5.4.2)	11
P37127	b2468	aegA	Protein AegA	28
P05050	b2212	alkB	Alpha-ketoglutarate-dependent dioxygenase AlkB (EC 1.14.11.33) (Alkylated DNA repair protein AlkB) (DNA oxidative demethylase AlkB)	4
P25550	b3800	aslB	Anaerobic sulfatase-maturing enzyme homolog AslB (AnSME homolog)	14
P0AE56	b3337	bfd	Bacterioferritin-associated ferredoxin	4
P0ABD3	b3336	bfr	Bacterioferritin (BFR) (EC 1.16.3.1) (Cytochrome b-1) (Cytochrome b-557)	0
P12996	b0775	bioB	Biotin synthase (EC 2.8.1.6)	8
P31456	b3690	cbrA	Protein CbrA (CreB-regulated gene A protein)	8
P0ABM1	b2199	ccmC	Heme exporter protein C (Cytochrome c-type biogenesis protein CcmC)	1
P69490	b2197	ccmE	Cytochrome c-type biogenesis protein CcmE (Cytochrome c maturation protein E) (Heme chaperone CcmE)	1
P33927	b2196	ccmF	Cytochrome c-type biogenesis protein CcmF	4
P25524	b0337	codA	Cytosine deaminase (CD) (CDA) (CDase) (EC 3.5.4.1) (Cytosine aminohydrolase) (Isoguanine deaminase) (EC 3.5.4.-)	3
P0AEW4	b3032	cpdA	3',5'-cyclic adenosine monophosphate phosphodiesterase CpdA (3',5'-cyclic AMP phosphodiesterase) (cAMP phosphodiesterase) (EC 3.1.4.17)	5
P76621	b2659	csiD	Protein CsiD	1
P27838	b3807	cyaY	Protein CyaY	2
P0ABE5	b1418	cybB	Cytochrome b561 (Cytochrome b-561)	2
P0ABJ9	b0733	cydA	Cytochrome bd-I ubiquinol oxidase subunit 1 (EC 1.10.3.14) (Cytochrome bd-I oxidase subunit I) (Cytochrome d ubiquinol oxidase subunit I)	3
P0ABK2	b0734	cydB	Cytochrome bd-I ubiquinol oxidase subunit 2 (EC 1.10.3.14) (Cytochrome bd-I oxidase subunit II) (Cytochrome d ubiquinol oxidase subunit II)	3

P0ABI8	b0431	cyoB	Cytochrome bo(3) ubiquinol oxidase subunit 1 (EC 1.10.3.10) (Cytochrome b562-o complex subunit I) (Cytochrome o ubiquinol oxidase subunit 1) (Cytochrome o subunit 1) (Oxidase bo(3) subunit 1) (Ubiquinol oxidase chain A) (Ubiquinol oxidase polypeptide I) (Ubiquinol oxidase subunit 1)	4
P17846	b2763	cysI	Sulfite reductase [NADPH] hemoprotein beta-component (SiR-HP) (SiRHP) (EC 1.8.1.2)	6
P38038	b2764	cysJ	Sulfite reductase [NADPH] flavoprotein alpha-component (SiR-FP) (EC 1.8.1.2)	2
P0A6K3	b3287	def	Peptide deformylase (PDF) (EC 3.5.1.88) (Polypeptide deformylase)	2
P27296	b0799	dinG	Probable ATP-dependent helicase DinG (EC 3.6.4.12) (DNA-damage-inducible protein G)	11
P18775	b0894	dmsA	Dimethyl sulfoxide reductase DmsA (DMSO reductase) (DMSOR) (Me2SO reductase) (EC 1.8.5.3)	15
P18776	b0895	dmsB	Anaerobic dimethyl sulfoxide reductase chain B (DMSO reductase iron-sulfur subunit)	16
P0AA89	b1490	dosC	Diguanylate cyclase DosC (DGC) (EC 2.7.7.65) (Direct oxygen-sensing cyclase)	0
P76129	b1489	dosP	Oxygen sensor protein DosP (EC 3.1.4.52) (Direct oxygen-sensing phosphodiesterase) (Direct oxygen sensor protein) (Ec DOS) (Heme-regulated cyclic di-GMP phosphodiesterase,)	8
P0ABT2	b0812	dps	DNA protection during starvation protein (EC 1.16.-.-)	0
P31545	b1019	efeB	Deferrochelate/oxidase EfeB (EC 1.11.1.-)	4
P39280	b4146	epmB	L-lysine 2,3-aminomutase (LAM) (EC 5.4.3.-) (EF-P post-translational modification enzyme B)	4
P0ACC3	b0156	erpA	Iron-sulfur cluster insertion protein ErpA	3
P42593	b3081	fadH	2,4-dienoyl-CoA reductase [NADPH] (EC 1.3.1.34) (2,4-dienoyl coenzyme A reductase)	10
P13024	b3891	fdhE	Protein FdhE	8
P07658	b4079	fdhF	Formate dehydrogenase H (EC 1.1.99.33) (EC 1.2.1.2) (Formate dehydrogenase-H subunit alpha) (FDH-H) (Formate-hydrogen-lyase-linked, selenocysteine-containing polypeptide)	15
P0AAJ3	b1475	fdnH	Formate dehydrogenase, nitrate-inducible, iron-sulfur subunit (Anaerobic formate dehydrogenase iron-sulfur subunit) (Formate dehydrogenase-N subunit beta) (FDH-N subunit beta)	17
P0AAJ5	b3893	fdoH	Formate dehydrogenase-O iron-sulfur subunit (Aerobic formate dehydrogenase iron-sulfur subunit) (FDH-Z subunit beta) (Formate dehydrogenase-O subunit beta)	16
P0A9R4	b2525	fdx	2Fe-2S ferredoxin	7
P13036	b4291	fecA	Fe(3+) dicitrate transport protein FecA (Iron(III) dicitrate transport protein FecA)	0
P64638	b3410	feoC	Ferrous iron transport protein C	4
P05825	b0584	fepA	Ferrienterobactin receptor (Enterobactin outer-membrane receptor)	2
P13039	b0585	fes	Enterochelin esterase (Ferric enterobactin esterase)	5

P06971	b0150	fhuA	Ferrichrome-iron receptor (Ferric hydroxamate receptor) (Ferric hydroxamate uptake)	4
P16869	b1102	fhuE	FhuE receptor (Outer-membrane receptor for Fe(III)-coprogen, Fe(III)-ferrioxamine B and Fe(III)-rhodotric acid)	1
P39405	b4367	fhuF	Ferric iron reductase protein FhuF	6
P75780	b0805	fiu	Catecholate siderophore receptor Fiu (Ferric iron uptake protein) (TonB-dependent receptor Fiu)	3
P68644	b0043	fixC	Protein FixC	4
P68646	b0044	fixX	Ferredoxin-like protein FixX	4
P0A9E5	b1334	fnr	Fumarate and nitrate reduction regulatory protein	5
P0AC47	b4153	frdB	Fumarate reductase iron-sulfur subunit (EC 1.3.5.1)	11
P0A998	b1905	ftnA	Bacterial non-heme ferritin (EC 1.16.3.2) (Ferritin-1)	1
P0A9A2	b1902	ftnB	Bacterial non-heme ferritin-like protein	2
P0A9S1	b2799	fucO	Lactaldehyde reductase (EC 1.1.1.77) (Propanediol oxidoreductase)	4
P0AC33	b1612	fumA	Fumarate hydratase class I, aerobic (EC 4.2.1.2) (Fumarase A) (Oxaloacetate keto--enol-isomerase) (OAAKE isomerase) (Oxaloacetate tautomerase) (EC 5.3.2.2)	9
P14407	b4122	fumB	Fumarate hydratase class I, anaerobic (EC 4.2.1.2) (D-tartrate dehydratase) (EC 4.2.1.81) (Fumarase B)	9
P09148	b0758	galT	Galactose-1-phosphate uridylyltransferase (Gal-1-P uridylyltransferase) (EC 2.7.7.12) (UDP-glucose--hexose-1-phosphate uridylyltransferase)	6
P52074	b4467	glcF	Glycolate oxidase iron-sulfur subunit	17
P0A996	b2243	glpC	Anaerobic glycerol-3-phosphate dehydrogenase subunit C (G-3-P dehydrogenase)	18
P09831	b3212	gltB	Glutamate synthase [NADPH] large chain (EC 1.4.1.13) (Glutamate synthase subunit alpha) (GLTS alpha chain) (NADPH-GOGAT)	20
P09832	b3213	gltD	Glutamate synthase [NADPH] small chain (EC 1.4.1.13) (Glutamate synthase subunit beta) (GLTS beta chain) (NADPH-GOGAT)	11
P0AC69	b1654	grxD	Glutaredoxin-4 (Grx4) (Monothiol glutaredoxin)	3
P0ABW0	b2540	hcaC	3-phenylpropionate/cinnamic acid dioxygenase ferredoxin subunit	5
P0ABR5	b2538	hcaE	3-phenylpropionate/cinnamic acid dioxygenase subunit alpha (EC 1.14.12.19)	10
P75825	b0873	hcp	Hydroxylamine reductase (EC 1.7.99.1) (Hybrid-cluster protein) (HCP) (Prismane protein)	14
P75824	b0872	hcr	NADH oxidoreductase HCR (EC 1.-.-.-)	11
P32131	b3867	hemN	Oxygen-independent coproporphyrinogen-III oxidase (CPO) (EC 1.3.99.22) (Coproporphyrinogen III dehydrogenase) (CPDH)	9
P24232	b2552	hmp	Flavoheмоprotein (Flavoheмоglobin) (HMP) (Hemoglobin-like protein) (Nitric oxide dioxygenase) (NO oxygenase) (NOD) (EC 1.14.12.17)	2

P69739	b0972	hyaA	Hydrogenase-1 small chain (HYD1) (EC 1.12.99.6) (Membrane-bound hydrogenase 1 small subunit) (NiFe hydrogenase)	14
P0AAM1	b0974	hyaC	Probable Ni/Fe-hydrogenase 1 B-type cytochrome subunit	1
P0AAJ8	b2996	hybA	Hydrogenase-2 operon protein HybA	17
P69741	b2997	hybO	Hydrogenase-2 small chain (HYD2) (EC 1.12.99.6) (Membrane-bound hydrogenase 2 small subunit) (NiFe hydrogenase)	13
P0AAK1	b2724	hycB	Formate hydrogenlyase subunit 2 (FHL subunit 2) (Hydrogenase-3 component B)	16
P16431	b2721	hycE	Formate hydrogenlyase subunit 5 (FHL subunit 5) (Hydrogenase-3 component E)	8
P16432	b2720	hycF	Formate hydrogenlyase subunit 6 (FHL subunit 6) (Hydrogenase-3 component F)	14
P16433	b2719	hycG	Formate hydrogenlyase subunit 7 (FHL subunit 7) (Hydrogenase-3 component G)	7
P0AAK4	b2713	hydN	Electron transport protein HydN	18
P23481	b2481	hyfA	Hydrogenase-4 component A (EC 1.-.-.-)	16
P77329	b2487	hyfG	Hydrogenase-4 component G (EC 1.-.-.-)	7
P77423	b2488	hyfH	Hydrogenase-4 component H	13
P77668	b2489	hyfI	Hydrogenase-4 component I (EC 1.-.-.-)	7
P0AAM3	b2728	hypC	Hydrogenase isoenzymes formation protein HypC	3
P24192	b2729	hypD	Hydrogenase isoenzymes formation protein HypD	13
P05791	b3771	ilvD	Dihydroxy-acid dehydratase (DAD) (EC 4.2.1.9)	12
P0AAC8	b2528	iscA	Iron-binding protein IscA (Iron-sulfur cluster assembly protein)	3
P0AGK8	b2531	iscR	HTH-type transcriptional regulator IscR	3
P0A6B7	b2530	iscS	Cysteine desulfurase IscS (EC 2.8.1.7) (NifS protein homolog) (ThiI transpersulfidase) (TusA transpersulfidase)	3
P0ACD4	b2529	iscU	Iron-sulfur cluster assembly scaffold protein IscU (Sulfur acceptor protein IscU)	3
P0C0L9	b2524	iscX	Protein IscX	1
P62620	b2515	ispG	4-hydroxy-3-methylbut-2-en-1-yl diphosphate synthase (flavodoxin) (EC 1.17.7.3) (1-hydroxy-2-methyl-2-(E)-butenyl 4-diphosphate synthase) (Protein GcpE) (Protein E)	5
P62623	b0029	ispH	4-hydroxy-3-methylbut-2-enyl diphosphate reductase (EC 1.17.1.2)	4
P21179	b1732	katE	Catalase HP11 (EC 1.11.1.6) (Hydroxyperoxidase II)	2
P13029	b3942	katG	Catalase-peroxidase (CP) (EC 1.11.1.21) (Hydroperoxidase I) (HPI) (Peroxidase/catalase)	1
P0AB58	b1280	lapB	Lipopolysaccharide assembly protein B (Lipopolysaccharide regulatory protein)	6
P0A6A6	b0072	leuC	3-isopropylmalate dehydratase large subunit (EC 4.2.1.33) (Alpha-IPM isomerase) (IPMI) (Isopropylmalate isomerase)	9

P60716	b0628	lipA	Lipoyl synthase (EC 2.8.1.8) (Lip-syn) (LS) (Lipoate synthase) (Lipoic acid synthase) (Sulfur insertion protein LipA)	8
P0A725	b0096	lpxC	UDP-3-O-[3-hydroxymyristoyl] N-acetylglucosamine deacetylase (EC 3.5.1.-) (Protein EnvA) (UDP-3-O-acyl-GlcNAc deacetylase)	6
P45578	b2687	luxS	S-ribosylhomocysteine lyase (EC 4.4.1.21) (AI-2 synthesis protein) (Autoinducer-2 production protein LuxS)	3
P0AE18	b0168	map	Methionine aminopeptidase (MAP) (MetAP) (EC 3.4.11.18) (Peptidase M)	7
P0ABR9	b0348	mhpB	2,3-dihydroxyphenylpropionate/2,3-dihydroxycinnamic acid 1,2-dioxygenase (EC 1.13.11.16) (3-carboxyethylcatechol 2,3-dioxygenase)	4
P0AEI1	b0661	miaB	tRNA-2-methylthio-N(6)-dimethylallyl-adenosine synthase (EC 2.8.4.3) ((Dimethylallyl)adenosine tRNA methylthiotransferase MiaB) (tRNA-i(6)A37 methylthiotransferase)	6
P30745	b0781	moaA	Cyclic pyranopterin monophosphate synthase (EC 4.1.99.18) (Molybdenum cofactor biosynthesis protein A)	7
P0A746	b1778	msrB	Peptide methionine sulfoxide reductase MsrB (EC 1.8.4.12) (Peptide-methionine (R)-S-oxide reductase)	6
P17802	b2961	mutY	A/G-specific adenine glycosylase (EC 3.2.2.-)	7
P11458	b0750	nadA	Quinolinate synthase A (EC 2.5.1.72)	9
P33937	b2206	napA	Periplasmic nitrate reductase (EC 1.7.99.4)	12
P0ABL5	b2202	napC	Cytochrome c-type protein NapC	8
P0AAL0	b2208	napF	Ferredoxin-type protein NapF	16
P0AAL3	b2205	napG	Ferredoxin-type protein NapG	16
P33934	b2204	napH	Ferredoxin-type protein NapH	13
P09152	b1224	narG	Respiratory nitrate reductase 1 alpha chain (EC 1.7.99.4) (Nitrate reductase A subunit alpha) (Quinol-nitrate oxidoreductase subunit alpha)	12
P11349	b1225	narH	Respiratory nitrate reductase 1 beta chain (EC 1.7.99.4) (Nitrate reductase A subunit beta) (Quinol-nitrate oxidoreductase subunit beta)	17
P19318	b1467	narY	Respiratory nitrate reductase 2 beta chain (EC 1.7.99.4)	18
P19319	b1468	narZ	Respiratory nitrate reductase 2 alpha chain (EC 1.7.99.4)	17
P63020	b3414	nfuA	Fe/S biogenesis protein NfuA	4
P33590	b3476	nikA	Nickel-binding periplasmic protein	1
P08201	b3365	nirB	Nitrite reductase (NADH) large subunit (EC 1.7.1.15)	21
P0A9I8	b3366	nirD	Nitrite reductase (NADH) small subunit (EC 1.7.1.15)	3
Q46877	b2710	norV	Anaerobic nitric oxide reductase flavorubredoxin (FlrD) (FlavoRb)	8

P69924	b2235	nrdB	Ribonucleoside-diphosphate reductase 1 subunit beta (EC 1.17.4.1) (Protein B2) (Protein R2) (Ribonucleotide reductase 1)	5
P37146	b2676	nrdF	Ribonucleoside-diphosphate reductase 2 subunit beta (EC 1.17.4.1) (R2F protein) (Ribonucleotide reductase 2)	2
P0A9N8	b4237	nrdG	Anaerobic ribonucleoside-triphosphate reductase-activating protein (EC 1.97.1.-) (Class III anaerobic ribonucleotide reductase small component)	5
P0ABK9	b4070	nrfA	Cytochrome c-552 (EC 1.7.2.2) (Ammonia-forming cytochrome c nitrite reductase) (Cytochrome c nitrite reductase)	10
P0ABL1	b4071	nrfB	Cytochrome c-type protein NrfB	10
P0AAK7	b4072	nrfC	Protein NrfC	16
P32710	b4074	nrfE	Cytochrome c-type biogenesis protein NrfE	8
P0AF63	b4178	nsrR	HTH-type transcriptional repressor NsrR	3
P0AB83	b1633	nth	Endonuclease III (EC 4.2.99.18) (DNA-(apurinic or apyrimidinic site) lyase)	7
P0AFC7	b2287	nuoB	NADH-quinone oxidoreductase subunit B (EC 1.6.99.5) (NADH dehydrogenase I subunit B) (NDH-1 subunit B) (NUO2)	5
P0AFD1	b2285	nuoE	NADH-quinone oxidoreductase subunit E (EC 1.6.99.5) (NADH dehydrogenase I subunit E) (NDH-1 subunit E) (NUO5)	5
P31979	b2284	nuoF	NADH-quinone oxidoreductase subunit F (EC 1.6.99.5) (NADH dehydrogenase I subunit F) (NDH-1 subunit F) (NUO6)	9
P33602	b2283	nuoG	NADH-quinone oxidoreductase subunit G (EC 1.6.99.5) (NADH dehydrogenase I subunit G) (NDH-1 subunit G) (NUO7)	16
P0AFD6	b2281	nuoI	NADH-quinone oxidoreductase subunit I (EC 1.6.99.5) (NADH dehydrogenase I subunit I) (NDH-1 subunit I) (NUO9)	9
P76081	b1392	paaE	1,2-phenylacetyl-CoA epoxidase, subunit E (EC 1.-.-.-) (1,2-phenylacetyl-CoA epoxidase, reductase subunit) (1,2-phenylacetyl-CoA monooxygenase, subunit E)	9
P0A9N4	b0902	pflA	Pyruvate formate-lyase 1-activating enzyme (EC 1.97.1.4) (Formate-C-acetyltransferase-activating enzyme 1) (PFL-activating enzyme 1)	6
P32675	b3952	pflC	Pyruvate formate-lyase 2-activating enzyme (EC 1.97.1.4) (Formate-C-acetyltransferase-activating enzyme 2) (PFL-activating enzyme 2)	10
P16688	b4098	phnJ	Alpha-D-ribose 1-methylphosphonate 5-phosphate C-P lyase (PRPn C-P lyase) (EC 4.7.1.1)	4
P25889	b2147	preA	NAD-dependent dihydropyrimidine dehydrogenase subunit PreA (DPD) (EC 1.3.1.1) (Dihydrothymine dehydrogenase) (Dihydrouracil dehydrogenase)	18
P76440	b2146	preT	NAD-dependent dihydropyrimidine dehydrogenase subunit PreT (DPD) (EC 1.3.1.1) (Dihydrothymine dehydrogenase) (Dihydrouracil dehydrogenase)	13
P77243	b0334	prpD	2-methylcitrate dehydratase (2-MC dehydratase) (EC 4.2.1.79) ((2S,3S)-2-methylcitrate dehydratase) (Aconitate hydratase) (ACN) (Aconitase) (EC 4.2.1.3)	7

P64554	b2777	queE	7-carboxy-7-deazaguanine synthase (CDG synthase) (EC 4.3.99.3) (Queuosine biosynthesis protein QueE)	8
P39288	b4166	queG	Epoxymqueuosine reductase (EC 1.17.99.6) (Queuosine biosynthesis protein QueG)	10
P0AEI4	b0835	rimO	Ribosomal protein S12 methylthiotransferase RimO (S12 MTTase) (S12 methylthiotransferase) (EC 2.8.4.4) (Ribosomal protein S12 (aspartate(89)-C(3))-methylthiotransferase) (Ribosome maturation factor RimO)	9
P75817	b0859	rlmC	23S rRNA (uracil(747)-C(5))-methyltransferase RlmC (EC 2.1.1.189) (23S rRNA(m5U747)-methyltransferase)	11
P55135	b2785	rlmD	23S rRNA (uracil(1939)-C(5))-methyltransferase RlmD (EC 2.1.1.190) (23S rRNA(m5U1939)-methyltransferase)	7
P36979	b2517	rlmN	Dual-specificity RNA methyltransferase RlmN (EC 2.1.1.192) (23S rRNA (adenine(2503)-C(2))-methyltransferase) (23S rRNA m2A2503 methyltransferase) (Ribosomal RNA large subunit methyltransferase N) (tRNA (adenine(37)-C(2))-methyltransferase) (tRNA m2A37 methyltransferase)	8
P27431	b1128	roxA	50S ribosomal protein L16 arginine hydroxylase (EC 1.14.11.-) (Ribosomal oxygenase RoxA) (ROX)	1
P0AG07	b3386	rpe	Ribulose-phosphate 3-epimerase (EC 5.1.3.1) (Pentose-5-phosphate 3-epimerase) (PPE) (R5P3E)	1
P77223	b1628	rsxB	Electron transport complex subunit RsxB	14
P77611	b1629	rsxC	Electron transport complex subunit RsxC	14
P16095	b1814	sdaA	L-serine dehydratase 1 (SDH 1) (EC 4.3.1.17) (L-serine deaminase 1) (L-SD1)	9
P30744	b2797	sdaB	L-serine dehydratase 2 (SDH 2) (EC 4.3.1.17) (L-serine deaminase 2) (L-SD2)	10
P07014	b0724	sdhB	Succinate dehydrogenase iron-sulfur subunit (EC 1.3.5.1)	11
P69054	b0721	sdhC	Succinate dehydrogenase cytochrome b556 subunit (Cytochrome b-556)	0
P0AC44	b0722	sdhD	Succinate dehydrogenase hydrophobic membrane anchor subunit	0
P0AGD3	b1656	sodB	Superoxide dismutase [Fe] (EC 1.15.1.1)	1
P0ACS2	b4063	soxR	Redox-sensitive transcriptional activator SoxR	4
P77667	b1684	sufA	Protein SufA	3
P77522	b1683	sufB	FeS cluster assembly protein SufB	13
P42630	b4471	tdcG	L-serine dehydratase TdcG (SDH) (EC 4.3.1.17) (L-serine deaminase)	8
P07913	b3616	tdh	L-threonine 3-dehydrogenase (EC 1.1.1.103)	6
P30136	b3994	thiC	Phosphomethylpyrimidine synthase (EC 4.1.99.17) (Hydroxymethylpyrimidine phosphate synthase) (HMP-P synthase) (HMP-phosphate synthase) (HMPP synthase) (Thiamine biosynthesis protein ThiC)	9
P30140	b3990	thiH	2-iminoacetate synthase (EC 4.1.99.19) (Dehydroglycine synthase) (Tyrosine lyase)	5

P33226	b0996	torC	Cytochrome c-type protein TorC	10
P52005	b1873	torY	Cytochrome c-type protein TorY	10
P05852	b3064	tsaD	tRNA N6-adenosine threonylcarbamoyltransferase (EC 2.3.1.234) (N6-L-threonylcarbamoyladenine synthase) (t(6)A synthase) (t(6)A37 threonylcarbamoyladenine biosynthesis protein TsaD) (tRNA threonylcarbamoyladenine biosynthesis protein TsaD)	3
P05847	b3061	ttdA	L(+)-tartrate dehydratase subunit alpha (L-TTD alpha) (EC 4.2.1.32)	4
P42604	b3091	uxaA	Altronate dehydratase (EC 4.2.1.7) (D-altronate hydro-lyase)	9
P24215	b4322	uxuA	Mannonate dehydratase (EC 4.2.1.8) (D-mannonate hydro-lyase)	3
Q46801	b2868	xdhC	Xanthine dehydrogenase iron-sulfur-binding subunit	11
Q46814	b2881	xdhD	Probable hypoxanthine oxidase XdhD (EC 1.-.-.-)	16
P77165	b0286	yagT	Putative xanthine dehydrogenase YagT iron-sulfur-binding subunit	9
P75764	b0771	ybhJ	Uncharacterized protein YbhJ	12
P75779	b0804	ybiX	PKHD-type hydroxylase YbiX (EC 1.14.11.-)	1
P75794	b0824	ybiY	Putative pyruvate formate-lyase 3-activating enzyme (EC 1.97.1.4) (Formate-C-acetyltransferase-activating enzyme 3) (PFL-activating enzyme 3)	11
P75863	b0947	ycbX	Uncharacterized protein YcbX	9
P52636	b0992	yccM	Putative electron transport protein YccM	13
P52647	b1378	ydbK	Probable pyruvate-flavodoxin oxidoreductase (EC 1.2.7.-)	19
P76134	b1497	ydeM	Anaerobic sulfatase-maturing enzyme homolog YdeM (AnSME homolog)	12
P77561	b1501	ydeP	Protein YdeP	14
P76192	b1673	ydhV	Uncharacterized oxidoreductase YdhV (EC 1.-.-.-)	15
P77375	b1671	ydhX	Uncharacterized ferredoxin-like protein YdhX	16
P0AAL6	b1674	ydhY	Uncharacterized ferredoxin-like protein YdhY	18
P77748	b1687	ydiJ	Uncharacterized protein YdiJ	19
P77714	b1700	ydiT	Ferredoxin-like protein YdiT	5
P76220	b1751	ydjY	Uncharacterized protein YdjY	5
P0ABR7	b1802	yeaW	Putative dioxygenase subunit alpha YeaW (EC 1.14.-.-)	9
P76254	b1803	yeaX	Putative dioxygenase subunit beta YeaX (EC 1.-.-.-)	10
P0A9E9	b2163	yeiL	Regulatory protein YeiL	5
P0ABW3	b2236	yfaE	Uncharacterized ferredoxin-like protein YfaE	7



P76536	b2431	yfeX	Probable deferrochelata se/ peroxidase YfeX (EC 1.11.1.-)	4
P52102	b2562	yfhL	Uncharacterized ferredoxin-like protein YfhL	8
Q46905	b2767	ygcO	Ferredoxin-like protein YgcO	5
Q46811	b2878	ygfK	Uncharacterized protein YgfK	26
Q46819	b2886	ygfS	Putative electron transport protein YgfS	16
Q46820	b2887	ygfT	Uncharacterized protein YgfT	31
P52062	b2955	yggW	Oxygen-independent coproporphyrinogen-III oxidase-like protein YggW (EC 1.3.99.-)	7
P0A8P3	b2962	yggX	Probable Fe(2+)-trafficking protein	1
P24197	b3039	ygiD	4,5-DOPA dioxygenase extradiol (EC 1.13.11.29)	0
Q46861	b4469	ygiQ	UPF0313 protein YgiQ	14
P0ADW6	b3211	yhcC	Uncharacterized protein YhcC	10
P37197	b3518	yhjA	Probable cytochrome c peroxidase (EC 1.11.1.5)	7
P39383	b4334	yjiL	Uncharacterized protein YjiL	6
P39409	b4379	yjjW	Uncharacterized protein YjjW	16
P77536	b0307	ykgF	Uncharacterized electron transport protein YkgF	11
P0AAL9	b0288	ykgJ	Uncharacterized protein YkgJ	10
P76115	b1451	yncD	Probable TonB-dependent receptor YncD	2
P77374	b1587	ynfE	Putative dimethyl sulfoxide reductase chain YnfE (DMSO reductase) (EC 1.8.99.-)	12
P77783	b1588	ynfF	Probable dimethyl sulfoxide reductase chain YnfF (DMSO reductase) (EC 1.8.99.-)	13
P0AAJ1	b1589	ynfG	Probable anaerobic dimethyl sulfoxide reductase chain YnfG (DMSO reductase iron-sulfur subunit YnfG)	16
P64432	b2611	ypjD	Inner membrane protein YpjD	3
P65367	b2790	yqcA	Uncharacterized protein YqcA	1
P45771	b3283	yrdD	Uncharacterized protein YrdD	16
P56256	b3573	ysaA	Putative electron transport protein YsaA	19

**Table B.S3 Observed spectral counts of iron-binding proteins from cultures exposed for 15 minutes to 40  $\mu$ M PMA and unexposed control cultures (3 biological replicates).**

UniProt ID	gene ID	gene name	product description	encoded Cys sites	total peptide spectra	Cys peptide spectra	CAM modified spectra	PMA modified spectra	Hg modified spectra
P25516	Ecoli_b1276	acnA	Aconitate hydratase A (ACN) (Aconitase) (EC 4.2.1.3) (Iron-responsive protein-like) (IRP-like) (RNA-binding protein) (Stationary phase enzyme)	7	153	0	0	0	0
P36683	Ecoli_b0118	acnB	Aconitate hydratase B (ACN) (Aconitase) (EC 4.2.1.3) ((2R,3S)-2-methylisocitrate dehydratase) ((2S,3R)-3-hydroxybutane-1,2,3-tricarboxylate dehydratase) (2-methyl-cis-aconitate hydratase) (EC 4.2.1.99) (Iron-responsive protein-like) (IRP-like) (RNA-binding protein)	10	4155	98	68	0	30
P0ABD3	Ecoli_b3336	bfr	Bacterioferritin (BFR) (EC 1.16.3.1) (Cytochrome b-1) (Cytochrome b-557)	0	151	0	0	0	0
P12996	Ecoli_b0775	bioB	Biotin synthase (EC 2.8.1.6)	8	108	0	0	0	0
P25524	Ecoli_b0337	codA	Cytosine deaminase (CD) (CDA) (CDase) (EC 3.5.4.1) (Cytosine aminohydrolase) (Isoguanine deaminase) (EC 3.5.4.-)	3	27	0	0	0	0
P0AEW4	Ecoli_b3032	cpdA	3',5'-cyclic adenosine monophosphate phosphodiesterase CpdA (3',5'-cyclic AMP phosphodiesterase) (cAMP phosphodiesterase) (EC 3.1.4.17)	5	5	2	0	2	0
P27838	Ecoli_b3807	cyaY	Protein CyaY	2	105	0	0	0	0
P0ABJ9	Ecoli_b0733	cydA	Cytochrome bd-I ubiquinol oxidase subunit 1 (EC 1.10.3.14) (Cytochrome bd-I oxidase subunit I) (Cytochrome d ubiquinol oxidase subunit I)	3	181	0	0	0	0
P0ABK2	Ecoli_b0734	cydB	Cytochrome bd-I ubiquinol oxidase subunit 2 (EC 1.10.3.14) (Cytochrome bd-I oxidase subunit II) (Cytochrome d ubiquinol oxidase subunit II)	3	13	0	0	0	0
P0ABI8	Ecoli_b0431	cyoB	Cytochrome bo(3) ubiquinol oxidase subunit 1 (EC 1.10.3.10) (Cytochrome b562-o complex subunit I) (Cytochrome o ubiquinol oxidase subunit 1) (Cytochrome o subunit 1) (Oxidase bo(3) subunit 1) (Ubiquinol oxidase chain A) (Ubiquinol oxidase polypeptide I) (Ubiquinol oxidase subunit 1)	4	73	0	0	0	0
P17846	Ecoli_b2763	cysI	Sulfite reductase [NADPH] hemoprotein beta-component (SiR-HP) (SiRHP) (EC 1.8.1.2)	6	967	0	0	0	0
P38038	Ecoli_b2764	cysJ	Sulfite reductase [NADPH] flavoprotein alpha-component (SiR-FP) (EC 1.8.1.2)	2	1047	16	16	0	0
P0A6K3	Ecoli_b3287	def	Peptide deformylase (PDF) (EC 3.5.1.88) (Polypeptide deformylase)	2	197	22	18	4	0
P0ABT2	Ecoli_b0812	dps	DNA protection during starvation protein (EC 1.16.-.-)	0	745	0	0	0	0

P0ACC3	Ecoli_b0156	erpA	Iron-sulfur cluster insertion protein ErpA	3	349	3	3	0	0
P13024	Ecoli_b3891	fdhE	Protein FdhE	8	26	0	0	0	0
P0A9R4	Ecoli_b2525	fdx	2Fe-2S ferredoxin	7	161	66	53	13	0
P06971	Ecoli_b0150	fhuA	Ferrichrome-iron receptor (Ferric hydroxamate receptor) (Ferric hydroxamate uptake)	4	2	0	0	0	0
P0A9E5	Ecoli_b1334	fnr	Fumarate and nitrate reduction regulatory protein	5	79	0	0	0	0
P0AC47	Ecoli_b4153	frdB	Fumarate reductase iron-sulfur subunit (EC 1.3.5.1)	11	184	0	0	0	0
P0A998	Ecoli_b1905	ftnA	Bacterial non-heme ferritin (EC 1.16.3.2) (Ferritin-1)	1	626	9	9	0	0
P0AC33	Ecoli_b1612	fumA	Fumarate hydratase class I, aerobic (EC 4.2.1.2) (Fumarase A) (Oxaloacetate keto--enol-isomerase) (OAAKE isomerase) (Oxaloacetate tautomerase) (EC 5.3.2.2)	9	294	39	35	3	1
P0A996	Ecoli_b2243	glpC	Anaerobic glycerol-3-phosphate dehydrogenase subunit C (G-3-P dehydrogenase)	18	35	2	2	0	0
P09831	Ecoli_b3212	gltB	Glutamate synthase [NADPH] large chain (EC 1.4.1.13) (Glutamate synthase subunit alpha) (GLTS alpha chain) (NADPH-GOGAT)	20	4030	292	218	38	0
P09832	Ecoli_b3213	gltD	Glutamate synthase [NADPH] small chain (EC 1.4.1.13) (Glutamate synthase subunit beta) (GLTS beta chain) (NADPH-GOGAT)	11	1569	98	24	51	1
P0AC69	Ecoli_b1654	grxD	Glutaredoxin-4 (Grx4) (Monothiol glutaredoxin)	3	690	236	235	0	1
P32131	Ecoli_b3867	hem N	Oxygen-independent coproporphyrinogen-III oxidase (CPO) (EC 1.3.99.22) (Coproporphyrinogen III dehydrogenase) (CPDH)	9	87	0	0	0	0
P24232	Ecoli_b2552	hmp	Flavo-hemoprotein (Flavo-hemoglobin) (HMP) (Hemoglobin-like protein) (Nitric oxide dioxygenase) (NO oxygenase) (NOD) (EC 1.14.12.17)	2	305	0	0	0	0
P05791	Ecoli_b3771	ilvD	Dihydroxy-acid dehydratase (DAD) (EC 4.2.1.9)	12	401	7	7	0	0
P0AAC8	Ecoli_b2528	iscA	Iron-binding protein IscA (Iron-sulfur cluster assembly protein)	3	146	40	34	6	0
P0AGK8	Ecoli_b2531	iscR	HTH-type transcriptional regulator IscR	3	263	101	5	0	0
P0A6B7	Ecoli_b2530	iscS	Cysteine desulfurase IscS (EC 2.8.1.7) (NifS protein homolog) (ThiI transpersulfidase) (TusA transpersulfidase)	3	914	2	2	0	0
P0ACD4	Ecoli_b2529	iscU	Iron-sulfur cluster assembly scaffold protein IscU (Sulfur acceptor protein IscU)	3	316	109	86	23	0
P0C0L9	Ecoli_b2524	iscX	Protein IscX	1	82	32	20	12	0
P62620	Ecoli_b2515	ispG	4-hydroxy-3-methylbut-2-en-1-yl diphosphate synthase (flavodoxin) (EC 1.17.7.3) (1-hydroxy-2-methyl-2-(E)-butenyl 4-diphosphate synthase) (Protein GcpE) (Protein E)	5	216	11	4	7	0
P62623	Ecoli_b0029	ispH	4-hydroxy-3-methylbut-2-enyl diphosphate reductase (EC 1.17.1.2)	4	60	8	8	0	0

P21179	Ecoli_b1732	katE	Catalase HP11 (EC 1.11.1.6) (Hydroxyperoxidase II)	2	12	0	0	0	0
P13029	Ecoli_b3942	katG	Catalase-peroxidase (CP) (EC 1.11.1.21) (Hydroperoxidase I) (HPI) (Peroxidase/catalase)	1	1425	47	13	0	0
P0AB58	Ecoli_b1280	lapB	Lipopolysaccharide assembly protein B (Lipopolysaccharide regulatory protein)	6	2	0	0	0	0
P0A6A6	Ecoli_b0072	leuC	3-isopropylmalate dehydratase large subunit (EC 4.2.1.33) (Alpha-IPM isomerase) (IPMI) (Isopropylmalate isomerase)	9	1571	217	180	37	0
P60716	Ecoli_b0628	lipA	Lipoyl synthase (EC 2.8.1.8) (Lip-syn) (LS) (Lipoate synthase) (Lipoic acid synthase) (Sulfur insertion protein LipA)	8	55	17	9	0	0
P0A725	Ecoli_b0096	lpxC	UDP-3-O-[3-hydroxymyristoyl] N-acetylglucosamine deacetylase (EC 3.5.1.-) (Protein EnvA) (UDP-3-O-acyl-GlcNAc deacetylase)	6	1	1	1	0	0
P45578	Ecoli_b2687	luxS	S-ribosylhomocysteine lyase (EC 4.4.1.21) (AI-2 synthesis protein) (Autoinducer-2 production protein LuxS)	3	896	115	75	40	0
P0AE18	Ecoli_b0168	map	Methionine aminopeptidase (MAP) (MetAP) (EC 3.4.11.18) (Peptidase M)	7	309	26	26	0	0
P0AE11	Ecoli_b0661	miaB	tRNA-2-methylthio-N(6)-dimethylallyl-adenosine synthase (EC 2.8.4.3) ((Dimethylallyl)adenosine tRNA methylthiotransferase MiaB) (tRNA-i(6)A37 methylthiotransferase)	6	135	13	13	0	0
P0A746	Ecoli_b1778	msrB	Peptide methionine sulfoxide reductase MsrB (EC 1.8.4.12) (Peptide-methionine (R)-S-oxide reductase)	6	208	94	58	5	13
P11458	Ecoli_b0750	nadA	Quinolinate synthase A (EC 2.5.1.72)	9	109	16	5	2	0
P63020	Ecoli_b3414	nfuA	Fe/S biogenesis protein NfuA	4	196	12	12	0	0
P69924	Ecoli_b2235	nrdB	Ribonucleoside-diphosphate reductase I subunit beta (EC 1.17.4.1) (Protein B2) (Protein R2) (Ribonucleotide reductase I)	5	199	32	19	0	13
P0AF63	Ecoli_b4178	nsrR	HTH-type transcriptional repressor NsrR	3	3	0	0	0	0
P0AB83	Ecoli_b1633	nth	Endonuclease III (EC 4.2.99.18) (DNA-(apurinic or apyrimidinic site) lyase)	7	6	0	0	0	0
P0AFC7	Ecoli_b2287	nuoB	NADH-quinone oxidoreductase subunit B (EC 1.6.99.5) (NADH dehydrogenase I subunit B) (NDH-1 subunit B) (NUO2)	5	57	0	0	0	0
P0AFD1	Ecoli_b2285	nuoE	NADH-quinone oxidoreductase subunit E (EC 1.6.99.5) (NADH dehydrogenase I subunit E) (NDH-1 subunit E) (NUO5)	5	417	10	10	0	0
P31979	Ecoli_b2284	nuoF	NADH-quinone oxidoreductase subunit F (EC 1.6.99.5) (NADH dehydrogenase I subunit F) (NDH-1 subunit F) (NUO6)	9	422	9	0	1	0
P33602	Ecoli_b2283	nuoG	NADH-quinone oxidoreductase subunit G (EC 1.6.99.5) (NADH dehydrogenase I subunit G) (NDH-1 subunit G) (NUO7)	16	797	0	0	0	0
P0AFD6	Ecoli_b2281	nuoI	NADH-quinone oxidoreductase subunit I (EC 1.6.99.5) (NADH dehydrogenase I subunit I) (NDH-1 subunit I) (NUO9)	9	44	0	0	0	0
P0A9N4	Ecoli_b0902	pflA	Pyruvate formate-lyase 1-activating enzyme (EC 1.97.1.4) (Formate-C-acetyltransferase-activating enzyme 1) (PFL-activating enzyme 1)	6	174	21	21	0	0
P64554	Ecoli_b2777	queE	7-carboxy-7-deazaguanine synthase (CDG synthase) (EC 4.3.99.3) (Queosine biosynthesis protein QueE)	8	27	5	5	0	0

P0AEI4	Ecoli_b0835	rimO	Ribosomal protein S12 methylthiotransferase RimO (S12 MTTase) (S12 methylthiotransferase) (EC 2.8.4.4) (Ribosomal protein S12 (aspartate(89)-C(3))-methylthiotransferase) (Ribosome maturation factor RimO)	9	113	11	11	0	0
P36979	Ecoli_b2517	rlmN	Dual-specificity RNA methyltransferase RlmN (EC 2.1.1.192) (23S rRNA (adenine(2503)-C(2))-methyltransferase) (23S rRNA m2A2503 methyltransferase) (Ribosomal RNA large subunit methyltransferase N) (tRNA (adenine(37)-C(2))-methyltransferase) (tRNA m2A37 methyltransferase)	8	96	0	0	0	0
P27431	Ecoli_b1128	roxA	50S ribosomal protein L16 arginine hydroxylase (EC 1.14.11.-) (Ribosomal oxygenase RoxA) (ROX)	1	72	0	0	0	0
P0AG07	Ecoli_b3386	rpe	Ribulose-phosphate 3-epimerase (EC 5.1.3.1) (Pentose-5-phosphate 3-epimerase) (PPE) (R5P3E)	1	229	0	0	0	0
P30744	Ecoli_b2797	sdaB	L-serine dehydratase 2 (SDH 2) (EC 4.3.1.17) (L-serine deaminase 2) (L-SD2)	10	4	0	0	0	0
P07014	Ecoli_b0724	sdhB	Succinate dehydrogenase iron-sulfur subunit (EC 1.3.5.1)	11	723	143	20	2	0
P0AC44	Ecoli_b0722	sdhD	Succinate dehydrogenase hydrophobic membrane anchor subunit	0	19	0	0	0	0
P0AGD3	Ecoli_b1656	sodB	Superoxide dismutase [Fe] (EC 1.15.1.1)	1	2551	193	104	83	0
P05852	Ecoli_b3064	tsaD	tRNA N6-adenosine threonylcarbamoyltransferase (EC 2.3.1.234) (N6-L-threonylcarbamoyladenine synthase) (t(6)A synthase) (t(6)A37 threonylcarbamoyladenine biosynthesis protein TsaD) (tRNA threonylcarbamoyladenine biosynthesis protein TsaD)	3	12	0	0	0	0
P75863	Ecoli_b0947	ycbX	Uncharacterized protein YcbX	9	11	0	0	0	0
P52647	Ecoli_b1378	ydbK	Probable pyruvate-flavodoxin oxidoreductase (EC 1.2.7.-)	19	9	0	0	0	0
P77748	Ecoli_b1687	ydiJ	Uncharacterized protein YdiJ	19	765	35	12	5	0
P76536	Ecoli_b2431	yfeX	Probable deferrochelate/oxidase YfeX (EC 1.11.1.-)	4	260	7	7	0	0
P0A8P3	Ecoli_b2962	yggX	Probable Fe(2+)-trafficking protein	1	563	23	21	1	1
P65367	Ecoli_b2790	yqcA	Uncharacterized protein YqcA	1	191	2	2	0	0
P45771	Ecoli_b3283	yrdD	Uncharacterized protein YrdD	16	1	0	0	0	0

**Table B.S4 Observed spectral counts of iron-binding proteins from cultures exposed for 15 minutes to 160  $\mu$ M MT and unexposed control cultures (1 biological replicate).**

UniProt ID	gene ID	gene name	product description	encoded Cys sites	total peptide spectra	Cys peptide spectra	CAM modified spectra	MT modified spectra
P25516	Ecoli_b1276	acnA	Aconitate hydratase A (ACN) (Aconitase) (EC 4.2.1.3) (Iron-responsive protein-like) (IRP-like) (RNA-binding protein) (Stationary phase enzyme)	7	19	0	0	0
P36683	Ecoli_b0118	acnB	Aconitate hydratase B (ACN) (Aconitase) (EC 4.2.1.3) ((2R,3S)-2-methylisocitrate dehydratase) ((2S,3R)-3-hydroxybutane-1,2,3-tricarboxylate dehydratase) (2-methyl-cis-aconitate hydratase) (EC 4.2.1.99) (Iron-responsive protein-like) (IRP-like) (RNA-binding protein)	10	1093	27	27	0
P37127	Ecoli_b2468	aegA	Protein AegA	28	48	48	48	0
P0ABD3	Ecoli_b3336	bfr	Bacterioferritin (BFR) (EC 1.16.3.1) (Cytochrome b-1) (Cytochrome b-557)	0	4	0	0	0
P12996	Ecoli_b0775	bioB	Biotin synthase (EC 2.8.1.6)	8	19	0	0	0
P25524	Ecoli_b0337	codA	Cytosine deaminase (CD) (CDA) (CDase) (EC 3.5.4.1) (Cytosine aminohydrolase) (Isoguanine deaminase) (EC 3.5.4.-)	3	5	0	0	0
P27838	Ecoli_b3807	cyaY	Protein CyaY	2	21	0	0	0
P0ABJ9	Ecoli_b0733	cydA	Cytochrome bd-I ubiquinol oxidase subunit 1 (EC 1.10.3.14) (Cytochrome bd-I oxidase subunit I) (Cytochrome d ubiquinol oxidase subunit I)	3	12	0	0	0
P0ABI8	Ecoli_b0431	cyoB	Cytochrome bo(3) ubiquinol oxidase subunit 1 (EC 1.10.3.10) (Cytochrome b562-o complex subunit I) (Cytochrome o ubiquinol oxidase subunit 1) (Cytochrome o subunit 1) (Oxidase bo(3) subunit 1) (Ubiquinol oxidase chain A) (Ubiquinol oxidase polypeptide I) (Ubiquinol oxidase subunit 1)	4	17	0	0	0
P17846	Ecoli_b2763	cysI	Sulfite reductase [NADPH] hemoprotein beta-component (SiR-HP) (SiRHP) (EC 1.8.1.2)	6	340	8	8	0
P38038	Ecoli_b2764	cysJ	Sulfite reductase [NADPH] flavoprotein alpha-component (SiR-FP) (EC 1.8.1.2)	2	361	4	4	0
P0A6K3	Ecoli_b3287	def	Peptide deformylase (PDF) (EC 3.5.1.88) (Polypeptide deformylase)	2	40	0	0	0
P0ABT2	Ecoli_b0812	dps	DNA protection during starvation protein (EC 1.16.-.-)	0	120	0	0	0
P0ACC3	Ecoli_b0156	erpA	Iron-sulfur cluster insertion protein ErpA	3	67	0	0	0
P0A9R4	Ecoli_b2525	fdx	2Fe-2S ferredoxin	7	47	34	34	0
P0A9E5	Ecoli_b1334	fnr	Fumarate and nitrate reduction regulatory protein	5	18	0	0	0
P0AC47	Ecoli_b4153	frdB	Fumarate reductase iron-sulfur subunit (EC 1.3.5.1)	11	30	0	0	0

P0A998	Ecoli_b1905	ftnA	Bacterial non-heme ferritin (EC 1.16.3.2) (Ferritin-1)	1	119	2	2	0
P0AC33	Ecoli_b1612	fumA	Fumarate hydratase class I, aerobic (EC 4.2.1.2) (Fumarase A) (Oxaloacetate keto--enol-isomerase) (OAAKE isomerase) (Oxaloacetate tautomerase) (EC 5.3.2.2)	9	136	51	51	0
P14407	Ecoli_b4122	fumB	Fumarate hydratase class I, anaerobic (EC 4.2.1.2) (D-tartrate dehydratase) (EC 4.2.1.81) (Fumarase B)	9	23	20	20	0
P0A996	Ecoli_b2243	glpC	Anaerobic glycerol-3-phosphate dehydrogenase subunit C (G-3-P dehydrogenase)	18	5	3	3	0
P09831	Ecoli_b3212	gltB	Glutamate synthase [NADPH] large chain (EC 1.4.1.13) (Glutamate synthase subunit alpha) (GLTS alpha chain) (NADPH-GOGAT)	20	1321	246	230	0
P09832	Ecoli_b3213	gltD	Glutamate synthase [NADPH] small chain (EC 1.4.1.13) (Glutamate synthase subunit beta) (GLTS beta chain) (NADPH-GOGAT)	11	494	112	112	0
P0AC69	Ecoli_b1654	grxD	Glutaredoxin-4 (Grx4) (Monothiol glutaredoxin)	3	99	18	18	0
P32131	Ecoli_b3867	hemN	Oxygen-independent coproporphyrinogen-III oxidase (CPO) (EC 1.3.99.22) (Coproporphyrinogen III dehydrogenase) (CPDH)	9	15	0	0	0
P24232	Ecoli_b2552	hmp	Flavohemoprotein (Flavohemoglobin) (HMP) (Hemoglobin-like protein) (Nitric oxide dioxygenase) (NO oxygenase) (NOD) (EC 1.14.12.17)	2	34	0	0	0
P05791	Ecoli_b3771	ilvD	Dihydroxy-acid dehydratase (DAD) (EC 4.2.1.9)	12	60	4	4	0
P0AAC8	Ecoli_b2528	iscA	Iron-binding protein IscA (Iron-sulfur cluster assembly protein)	3	21	4	4	0
P0AGK8	Ecoli_b2531	iscR	HTH-type transcriptional regulator IscR	3	54	16	0	0
P0A6B7	Ecoli_b2530	iscS	Cysteine desulfurase IscS (EC 2.8.1.7) (NifS protein homolog) (ThiI transpersulfidase) (TusA transpersulfidase)	3	172	0	0	0
P0ACD4	Ecoli_b2529	iscU	Iron-sulfur cluster assembly scaffold protein IscU (Sulfur acceptor protein IscU)	3	73	33	33	0
P0C0L9	Ecoli_b2524	iscX	Protein IscX	1	21	8	8	0
P62620	Ecoli_b2515	ispG	4-hydroxy-3-methylbut-2-en-1-yl diphosphate synthase (flavodoxin) (EC 1.17.7.3) (1-hydroxy-2-methyl-2-(E)-butenyl 4-diphosphate synthase) (Protein GcpE) (Protein E)	5	62	4	4	0
P62623	Ecoli_b0029	ispH	4-hydroxy-3-methylbut-2-enyl diphosphate reductase (EC 1.17.1.2)	4	16	0	0	0
P13029	Ecoli_b3942	katG	Catalase-peroxidase (CP) (EC 1.11.1.21) (Hydroperoxidase I) (HPI) (Peroxidase/catalase)	1	457	35	28	0
P0A6A6	Ecoli_b0072	leuC	3-isopropylmalate dehydratase large subunit (EC 4.2.1.33) (Alpha-IPM isomerase) (IPMI) (Isopropylmalate isomerase)	9	405	115	115	0
P45578	Ecoli_b2687	luxS	S-ribosylhomocysteine lyase (EC 4.4.1.21) (AI-2 synthesis protein) (Autoinducer-2 production protein LuxS)	3	212	17	17	0
P0AE18	Ecoli_b0168	map	Methionine aminopeptidase (MAP) (MetAP) (EC 3.4.11.18) (Peptidase M)	7	72	10	10	0
P0AE11	Ecoli_b0661	miaB	tRNA-2-methylthio-N(6)-dimethylallyl adenosine synthase (EC 2.8.4.3) ((Dimethylallyl)adenosine tRNA methylthiotransferase MiaB) (tRNA-i(6)A37 methylthiotransferase)	6	25	0	0	0

P0A746	Ecoli_b1778	msrB	Peptide methionine sulfoxide reductase MsrB (EC 1.8.4.12) (Peptide-methionine (R)-S-oxide reductase)	6	46	31	29	0
P17802	Ecoli_b2961	mutY	A/G-specific adenine glycosylase (EC 3.2.2.-)	7	2	0	0	0
P11458	Ecoli_b0750	nadA	Quinolinate synthase A (EC 2.5.1.72)	9	5	0	0	0
P63020	Ecoli_b3414	nfuA	Fe/S biogenesis protein NfuA	4	77	11	11	0
P69924	Ecoli_b2235	nrdB	Ribonucleoside-diphosphate reductase 1 subunit beta (EC 1.17.4.1) (Protein B2) (Protein R2) (Ribonucleotide reductase 1)	5	34	2	2	0
P0AB83	Ecoli_b1633	nth	Endonuclease III (EC 4.2.99.18) (DNA-(apurinic or apyrimidinic site) lyase)	7	2	0	0	0
P0AFC7	Ecoli_b2287	nuoB	NADH-quinone oxidoreductase subunit B (EC 1.6.99.5) (NADH dehydrogenase I subunit B) (NDH-1 subunit B) (NUO2)	5	3	0	0	0
P0AFD1	Ecoli_b2285	nuoE	NADH-quinone oxidoreductase subunit E (EC 1.6.99.5) (NADH dehydrogenase I subunit E) (NDH-1 subunit E) (NUO5)	5	105	0	0	0
P31979	Ecoli_b2284	nuoF	NADH-quinone oxidoreductase subunit F (EC 1.6.99.5) (NADH dehydrogenase I subunit F) (NDH-1 subunit F) (NUO6)	9	74	0	0	0
P33602	Ecoli_b2283	nuoG	NADH-quinone oxidoreductase subunit G (EC 1.6.99.5) (NADH dehydrogenase I subunit G) (NDH-1 subunit G) (NUO7)	16	183	0	0	0
P0AFD6	Ecoli_b2281	nuoI	NADH-quinone oxidoreductase subunit I (EC 1.6.99.5) (NADH dehydrogenase I subunit I) (NDH-1 subunit I) (NUO9)	9	7	0	0	0
P0A9N4	Ecoli_b0902	pflA	Pyruvate formate-lyase 1-activating enzyme (EC 1.97.1.4) (Formate-C-acetyltransferase-activating enzyme 1) (PFL-activating enzyme 1)	6	17	3	3	0
P64554	Ecoli_b2777	queE	7-carboxy-7-deazaguanine synthase (CDG synthase) (EC 4.3.99.3) (Queuosine biosynthesis protein QueE)	8	5	0	0	0
P0AEI4	Ecoli_b0835	rimO	Ribosomal protein S12 methylthiotransferase RimO (S12 MTTase) (S12 methylthiotransferase) (EC 2.8.4.4) (Ribosomal protein S12 (aspartate(89)-C(3))-methylthiotransferase) (Ribosome maturation factor RimO)	9	23	4	4	0
P36979	Ecoli_b2517	rlmN	Dual-specificity RNA methyltransferase RlmN (EC 2.1.1.192) (23S rRNA (adenine(2503)-C(2))-methyltransferase) (23S rRNA m2A2503 methyltransferase) (Ribosomal RNA large subunit methyltransferase N) (tRNA (adenine(37)-C(2))-methyltransferase) (tRNA m2A37 methyltransferase)	8	16	3	3	0
P27431	Ecoli_b1128	roxA	50S ribosomal protein L16 arginine hydroxylase (EC 1.14.11.-) (Ribosomal oxygenase RoxA) (ROX)	1	27	0	0	0
P0AG07	Ecoli_b3386	rpe	Ribulose-phosphate 3-epimerase (EC 5.1.3.1) (Pentose-5-phosphate 3-epimerase) (PPE) (R5P3E)	1	18	0	0	0
P07014	Ecoli_b0724	sdhB	Succinate dehydrogenase iron-sulfur subunit (EC 1.3.5.1)	11	147	47	14	0
P0AGD3	Ecoli_b1656	sodB	Superoxide dismutase [Fe] (EC 1.15.1.1)	1	333	34	27	4
P52647	Ecoli_b1378	ydbK	Probable pyruvate-flavodoxin oxidoreductase (EC 1.2.7.-)	19	2	0	0	0
P77748	Ecoli_b1687	ydiJ	Uncharacterized protein YdiJ	19	125	14	14	0



P76536	Ecoli_b2431	yfeX	Probable deferrochelataase/peroxidase YfeX (EC 1.11.1.-)	4	77	3	3	0
P0A8P3	Ecoli_b2962	yggX	Probable Fe(2+)-trafficking protein	1	115	11	11	0
P65367	Ecoli_b2790	yqcA	Uncharacterized protein YqcA	1	21	0	0	0

**Table B.S5 Observed spectral counts of iron-binding proteins from cultures exposed for 15 minutes to 20  $\mu$ M Hg(II)-acetate and unexposed control cultures (1 biological replicates).**

UniProt ID	gene ID	gene name	product description	encoded Cys sites	total peptide spectra	Cys peptide spectra	CAM modified spectra	Hg modified spectra
P25516	Ecoli_b1276	acnA	Aconitate hydratase A (ACN) (Aconitase) (EC 4.2.1.3) (Iron-responsive protein-like) (IRP-like) (RNA-binding protein) (Stationary phase enzyme)	7	61	0	0	0
P36683	Ecoli_b0118	acnB	Aconitate hydratase B (ACN) (Aconitase) (EC 4.2.1.3) ((2R,3S)-2-methylisocitrate dehydratase) ((2S,3R)-3-hydroxybutane-1,2,3-tricarboxylate dehydratase) (2-methyl-cis-aconitate hydratase) (EC 4.2.1.99) (Iron-responsive protein-like) (IRP-like) (RNA-binding protein)	10	1156	39	33	0
P37127	Ecoli_b2468	aegA	Protein AegA	28	46	46	33	0
P0ABD3	Ecoli_b3336	bfr	Bacterioferritin (BFR) (EC 1.16.3.1) (Cytochrome b-1) (Cytochrome b-557)	0	27	0	0	0
P25524	Ecoli_b0337	codA	Cytosine deaminase (CD) (CDA) (CDase) (EC 3.5.4.1) (Cytosine aminohydrolase) (Isoguanine deaminase) (EC 3.5.4.-)	3	155	0	0	0
P27838	Ecoli_b3807	cyaY	Protein CyaY	2	11	0	0	0
P0ABJ9	Ecoli_b0733	cydA	Cytochrome bd-I ubiquinol oxidase subunit 1 (EC 1.10.3.14) (Cytochrome bd-I oxidase subunit I) (Cytochrome d ubiquinol oxidase subunit I)	3	36	0	0	0
P0ABK2	Ecoli_b0734	cydB	Cytochrome bd-I ubiquinol oxidase subunit 2 (EC 1.10.3.14) (Cytochrome bd-I oxidase subunit II) (Cytochrome d ubiquinol oxidase subunit II)	3	6	0	0	0
P0ABI8	Ecoli_b0431	cyoB	Cytochrome bo(3) ubiquinol oxidase subunit 1 (EC 1.10.3.10) (Cytochrome b562-o complex subunit I) (Cytochrome o ubiquinol oxidase subunit 1) (Cytochrome o subunit 1) (Oxidase bo(3) subunit 1) (Ubiquinol oxidase chain A) (Ubiquinol oxidase polypeptide I) (Ubiquinol oxidase subunit 1)	4	28	0	0	0
P17846	Ecoli_b2763	cysI	Sulfite reductase [NADPH] hemoprotein beta-component (SiR-HP) (SiRHP) (EC 1.8.1.2)	6	722	30	14	6
P38038	Ecoli_b2764	cysJ	Sulfite reductase [NADPH] flavoprotein alpha-component (SiR-FP) (EC 1.8.1.2)	2	404	16	16	0
P0A6K3	Ecoli_b3287	def	Peptide deformylase (PDF) (EC 3.5.1.88) (Polypeptide deformylase)	2	34	0	0	0
P0ABT2	Ecoli_b0812	dps	DNA protection during starvation protein (EC 1.16.-.-)	0	163	0	0	0
P0ACC3	Ecoli_b0156	erpA	Iron-sulfur cluster insertion protein ErpA	3	49	0	0	0
P0A9R4	Ecoli_b2525	fdx	2Fe-2S ferredoxin	7	95	30	15	0
P0A9E5	Ecoli_b1334	fnr	Fumarate and nitrate reduction regulatory protein	5	8	0	0	0
P0AC47	Ecoli_b4153	frdB	Fumarate reductase iron-sulfur subunit (EC 1.3.5.1)	11	9	0	0	0

P0A998	Ecoli_b1905	ftnA	Bacterial non-heme ferritin (EC 1.16.3.2) (Ferritin-1)	1	410	0	0	0
P0AC33	Ecoli_b1612	fumA	Fumarate hydratase class I, aerobic (EC 4.2.1.2) (Fumarase A) (Oxaloacetate keto--enol-isomerase) (OAAKE isomerase) (Oxaloacetate tautomerase) (EC 5.3.2.2)	9	179	25	25	0
P14407	Ecoli_b4122	fumB	Fumarate hydratase class I, anaerobic (EC 4.2.1.2) (D-tartrate dehydratase) (EC 4.2.1.81) (Fumarase B)	9	71	25	25	0
P0A996	Ecoli_b2243	glpC	Anaerobic glycerol-3-phosphate dehydrogenase subunit C (G-3-P dehydrogenase)	18	6	3	3	0
P09831	Ecoli_b3212	gltB	Glutamate synthase [NADPH] large chain (EC 1.4.1.13) (Glutamate synthase subunit alpha) (GLTS alpha chain) (NADPH-GOGAT)	20	2935	496	296	7
P09832	Ecoli_b3213	gltD	Glutamate synthase [NADPH] small chain (EC 1.4.1.13) (Glutamate synthase subunit beta) (GLTS beta chain) (NADPH-GOGAT)	11	654	90	53	4
P0AC69	Ecoli_b1654	grxD	Glutaredoxin-4 (Grx4) (Monothiol glutaredoxin)	3	97	32	32	0
P24232	Ecoli_b2552	hmp	Flavo-hemoprotein (Flavo-hemoglobin) (HMP) (Hemoglobin-like protein) (Nitric oxide dioxygenase) (NO oxygenase) (NOD) (EC 1.14.12.17)	2	12	0	0	0
P05791	Ecoli_b3771	ilvD	Dihydroxy-acid dehydratase (DAD) (EC 4.2.1.9)	12	200	12	3	0
P0AAC8	Ecoli_b2528	iscA	Iron-binding protein IscA (Iron-sulfur cluster assembly protein)	3	30	6	6	0
P0AGK8	Ecoli_b2531	iscR	HTH-type transcriptional regulator IscR	3	133	35	4	0
P0A6B7	Ecoli_b2530	iscS	Cysteine desulfurase IscS (EC 2.8.1.7) (NifS protein homolog) (ThiI transpersulfidase) (TusA transpersulfidase)	3	596	0	0	0
P0ACD4	Ecoli_b2529	iscU	Iron-sulfur cluster assembly scaffold protein IscU (Sulfur acceptor protein IscU)	3	124	33	33	0
P0C0L9	Ecoli_b2524	iscX	Protein IscX	1	34	9	9	0
P62620	Ecoli_b2515	ispG	4-hydroxy-3-methylbut-2-en-1-yl diphosphate synthase (flavodoxin) (EC 1.17.7.3) (1-hydroxy-2-methyl-2-(E)-butenyl 4-diphosphate synthase) (Protein GcpE) (Protein E)	5	113	20	8	0
P62623	Ecoli_b0029	ispH	4-hydroxy-3-methylbut-2-enyl diphosphate reductase (EC 1.17.1.2)	4	4	4	4	0
P21179	Ecoli_b1732	katE	Catalase HP II (EC 1.11.1.6) (Hydroxyperoxidase II)	2	2	0	0	0
P13029	Ecoli_b3942	katG	Catalase-peroxidase (CP) (EC 1.11.1.21) (Hydroperoxidase I) (HPI) (Peroxidase/catalase)	1	563	22	15	0
P0A6A6	Ecoli_b0072	leuC	3-isopropylmalate dehydratase large subunit (EC 4.2.1.33) (Alpha-IPM isomerase) (IPMI) (Isopropylmalate isomerase)	9	397	106	101	0
P60716	Ecoli_b0628	lipA	Lipoyl synthase (EC 2.8.1.8) (Lip-syn) (LS) (Lipoate synthase) (Lipoic acid synthase) (Sulfur insertion protein LipA)	8	24	7	7	0
P45578	Ecoli_b2687	luxS	S-ribosylhomocysteine lyase (EC 4.4.1.21) (AI-2 synthesis protein) (Autoinducer-2 production protein LuxS)	3	306	62	28	0
P0AEI8	Ecoli_b0168	map	Methionine aminopeptidase (MAP) (MetAP) (EC 3.4.11.18) (Peptidase M)	7	112	7	0	0
P0AEI1	Ecoli_b0661	miaB	tRNA-2-methylthio-N(6)-dimethylallyl-adenosine synthase (EC	6	113	0	0	0

			2.8.4.3) ((Dimethylallyl)adenosine tRNA methylthiotransferase MiaB) (tRNA-i(6)A37 methylthiotransferase)					
P0A746	Ecoli_b1778	msrB	Peptide methionine sulfoxide reductase MsrB (EC 1.8.4.12) (Peptide-methionine (R)-S-oxide reductase)	6	110	52	31	0
P11458	Ecoli_b0750	nadA	Quinolinate synthase A (EC 2.5.1.72)	9	18	0	0	0
P63020	Ecoli_b3414	nfuA	Fe/S biogenesis protein NfuA	4	53	0	0	0
P69924	Ecoli_b2235	nrdB	Ribonucleoside-diphosphate reductase 1 subunit beta (EC 1.17.4.1) (Protein B2) (Protein R2) (Ribonucleotide reductase 1)	5	82	8	8	0
P0AFC7	Ecoli_b2287	nuoB	NADH-quinone oxidoreductase subunit B (EC 1.6.99.5) (NADH dehydrogenase I subunit B) (NDH-1 subunit B) (NUO2)	5	10	0	0	0
P0AFD1	Ecoli_b2285	nuoE	NADH-quinone oxidoreductase subunit E (EC 1.6.99.5) (NADH dehydrogenase I subunit E) (NDH-1 subunit E) (NUO5)	5	41	0	0	0
P31979	Ecoli_b2284	nuoF	NADH-quinone oxidoreductase subunit F (EC 1.6.99.5) (NADH dehydrogenase I subunit F) (NDH-1 subunit F) (NUO6)	9	88	0	0	0
P33602	Ecoli_b2283	nuoG	NADH-quinone oxidoreductase subunit G (EC 1.6.99.5) (NADH dehydrogenase I subunit G) (NDH-1 subunit G) (NUO7)	16	244	0	0	0
P0AFD6	Ecoli_b2281	nuoI	NADH-quinone oxidoreductase subunit I (EC 1.6.99.5) (NADH dehydrogenase I subunit I) (NDH-1 subunit I) (NUO9)	9	4	0	0	0
P0A9N4	Ecoli_b0902	pflA	Pyruvate formate-lyase 1-activating enzyme (EC 1.97.1.4) (Formate-C-acetyltransferase-activating enzyme 1) (PFL-activating enzyme 1)	6	3	0	0	0
P0AEI4	Ecoli_b0835	rimO	Ribosomal protein S12 methylthiotransferase RimO (S12 MTTase) (S12 methylthiotransferase) (EC 2.8.4.4) (Ribosomal protein S12 (aspartate(89)-C(3))-methylthiotransferase) (Ribosome maturation factor RimO)	9	22	0	0	0
P36979	Ecoli_b2517	rlmN	Dual-specificity RNA methyltransferase RlmN (EC 2.1.1.192) (23S rRNA (adenine(2503)-C(2))-methyltransferase) (23S rRNA m2A2503 methyltransferase) (Ribosomal RNA large subunit methyltransferase N) (tRNA (adenine(37)-C(2))-methyltransferase) (tRNA m2A37 methyltransferase)	8	19	8	8	0
P27431	Ecoli_b1128	roxA	50S ribosomal protein L16 arginine hydroxylase (EC 1.14.11.-) (Ribosomal oxygenase RoxA) (ROX)	1	11	0	0	0
P0AG07	Ecoli_b3386	rpe	Ribulose-phosphate 3-epimerase (EC 5.1.3.1) (Pentose-5-phosphate 3-epimerase) (PPE) (R5P3E)	1	91	0	0	0
P07014	Ecoli_b0724	sdhB	Succinate dehydrogenase iron-sulfur subunit (EC 1.3.5.1)	11	138	52	9	0
P0AGD3	Ecoli_b1656	sodB	Superoxide dismutase [Fe] (EC 1.15.1.1)	1	313	33	23	0
P52647	Ecoli_b1378	ydbK	Probable pyruvate-flavodoxin oxidoreductase (EC 1.2.7.-)	19	10	0	0	0
P77748	Ecoli_b1687	ydiJ	Uncharacterized protein YdiJ	19	100	25	7	0
P76536	Ecoli_b2431	yfeX	Probable deferrochelataase/peroxidase YfeX (EC 1.11.1.-)	4	88	11	11	0
P0A8P3	Ecoli_b2962	yggX	Probable Fe(2+)-trafficking protein	1	233	3	3	0

**Table B.S6. Summary of iron binding proteins observed by LC-MS/MS analysis for all exposure conditions.**

UniProt_ID	gene_ID	gene_name	protein_description	encoded Cys sites	SUM total peptide spectra	SUM Cys peptide spectra	SUM CAM spectra	SUM PhHg spectra	SUM HgII spectra	SUM MT spectra
P25516	Ecoli_b1276	acnA	Aconitate hydratase A (ACN) (Aconitase) (EC 4.2.1.3) (Iron-responsive protein-like) (IRP-like) (RNA-binding protein) (Stationary phase enzyme)	7	233	0	0	0	0	0
P36683	Ecoli_b0118	acnB	Aconitate hydratase B (ACN) (Aconitase) (EC 4.2.1.3) ((2R,3S)-2-methylisocitrate dehydratase) ((2S,3R)-3-hydroxybutane-1,2,3-tricarboxylate dehydratase) (2-methyl-cis-aconitate hydratase) (EC 4.2.1.99) (Iron-responsive protein-like) (IRP-like) (RNA-binding protein)	10	6404	164	128	0	30	0
P37127	Ecoli_b2468	aegA	Protein AegA	28	94	94	81	0	0	0
P0ABD3	Ecoli_b3336	bfr	Bacterioferritin (BFR) (EC 1.16.3.1) (Cytochrome b-1) (Cytochrome b-557)	0	182	0	0	0	0	0
P12996	Ecoli_b0775	bioB	Biotin synthase (EC 2.8.1.6)	8	127	0	0	0	0	0
P25524	Ecoli_b0337	codA	Cytosine deaminase (CD) (CDA) (CDase) (EC 3.5.4.1) (Cytosine aminohydrolase) (Isoguanine deaminase) (EC 3.5.4.-)	3	187	0	0	0	0	0
P0AEW4	Ecoli_b3032	cpdA	3',5'-cyclic adenosine monophosphate phosphodiesterase CpdA (3',5'-cyclic AMP phosphodiesterase) (EC 3.1.4.17)	5	5	2	0	2	0	0
P27838	Ecoli_b3807	cyaY	Protein CyaY	2	137	0	0	0	0	0
P0ABJ9	Ecoli_b0733	cydA	Cytochrome bd-I ubiquinol oxidase subunit 1 (EC 1.10.3.14) (Cytochrome bd-I oxidase subunit I) (Cytochrome d ubiquinol oxidase subunit I)	3	229	0	0	0	0	0
P0ABK2	Ecoli_b0734	cydB	Cytochrome bd-I ubiquinol oxidase subunit 2 (EC 1.10.3.14) (Cytochrome bd-I oxidase subunit II) (Cytochrome d ubiquinol oxidase subunit II)	3	19	0	0	0	0	0
P0ABI8	Ecoli_b0431	cyoB	Cytochrome bo(3) ubiquinol oxidase subunit 1 (EC 1.10.3.10) (Cytochrome b562-o complex subunit I) (Cytochrome o ubiquinol oxidase subunit 1) (Cytochrome o subunit 1) (Oxidase bo(3) subunit 1) (Ubiquinol oxidase chain A) (Ubiquinol oxidase polypeptide I) (Ubiquinol oxidase subunit 1)	4	118	0	0	0	0	0
P17846	Ecoli_b2763	cysI	Sulfite reductase [NADPH] hemoprotein beta-component (SiR-HP) (SiRHP) (EC 1.8.1.2)	6	2029	38	22	0	6	0

P38038	Ecoli_b2764	cysJ	Sulfite reductase [NADPH] flavoprotein alpha-component (SiR-FP) (EC 1.8.1.2)	2	1812	36	36	0	0	0
P0A6K3	Ecoli_b3287	def	Peptide deformylase (PDF) (EC 3.5.1.88) (Polypeptide deformylase)	2	271	22	18	4	0	0
P0ABT2	Ecoli_b0812	dps	DNA protection during starvation protein (EC 1.16.-.-)	0	1028	0	0	0	0	0
P0ACC3	Ecoli_b0156	erpA	Iron-sulfur cluster insertion protein ErpA	3	465	3	3	0	0	0
P13024	Ecoli_b3891	fdhE	Protein FdhE	8	26	0	0	0	0	0
P0A9R4	Ecoli_b2525	fdx	2Fe-2S ferredoxin	7	303	130	102	13	0	0
P06971	Ecoli_b0150	fhuA	Ferrichrome-iron receptor (Ferric hydroxamate receptor) (Ferric hydroxamate uptake)	4	2	0	0	0	0	0
P0A9E5	Ecoli_b1334	fnr	Fumarate and nitrate reduction regulatory protein	5	105	0	0	0	0	0
P0AC47	Ecoli_b4153	frdB	Fumarate reductase iron-sulfur subunit (EC 1.3.5.1)	11	223	0	0	0	0	0
P0A998	Ecoli_b1905	ftnA	Bacterial non-heme ferritin (EC 1.16.3.2) (Ferritin-1)	1	1155	11	11	0	0	0
P0AC33	Ecoli_b1612	fumA	Fumarate hydratase class I, aerobic (EC 4.2.1.2) (Fumarase A) (Oxaloacetate keto--enol-isomerase) (OAAKE isomerase) (Oxaloacetate tautomerase) (EC 5.3.2.2)	9	609	115	111	3	1	0
P14407	Ecoli_b4122	fumB	Fumarate hydratase class I, anaerobic (EC 4.2.1.2) (D-tartrate dehydratase) (EC 4.2.1.81) (Fumarase B)	9	94	45	45	0	0	0
P0A996	Ecoli_b2243	glpC	Anaerobic glycerol-3-phosphate dehydrogenase subunit C (G-3-P dehydrogenase)	18	46	8	8	0	0	0
P09831	Ecoli_b3212	gltB	Glutamate synthase [NADPH] large chain (EC 1.4.1.13) (Glutamate synthase subunit alpha) (GLTS alpha chain) (NADPH-GOGAT)	20	8286	1034	744	38	7	0
P09832	Ecoli_b3213	gltD	Glutamate synthase [NADPH] small chain (EC 1.4.1.13) (Glutamate synthase subunit beta) (GLTS beta chain) (NADPH-GOGAT)	11	2717	300	189	51	5	0
P0AC69	Ecoli_b1654	grxD	Glutaredoxin-4 (Grx4) (Monothiol glutaredoxin)	3	886	286	285	0	1	0
P32131	Ecoli_b3867	hemN	Oxygen-independent coproporphyrinogen-III oxidase (CPO) (EC 1.3.99.22) (Coproporphyrinogen III dehydrogenase) (CPDH)	9	102	0	0	0	0	0
P24232	Ecoli_b2552	hmp	Flavoheмоprotein (Flavoheмоglobin) (HMP) (Hemoglobin-like protein) (Nitric oxide dioxygenase) (NO oxygenase) (NOD) (EC 1.14.12.17)	2	351	0	0	0	0	0
P05791	Ecoli_b3771	ilvD	Dihydroxy-acid dehydratase (DAD) (EC 4.2.1.9)	12	661	23	14	0	0	0
P0AAC8	Ecoli_b2528	iscA	Iron-binding protein IscA (Iron-sulfur cluster	3	197	50	44	6	0	0

			assembly protein)							
P0AGK8	Ecoli_b2531	iscR	HTH-type transcriptional regulator IscR	3	450	152	9	0	0	0
P0A6B7	Ecoli_b2530	iscS	Cysteine desulfurase IscS (EC 2.8.1.7) (NifS protein homolog) (ThiI transpersulfidase) (TusA transpersulfidase)	3	1682	2	2	0	0	0
P0ACD4	Ecoli_b2529	iscU	Iron-sulfur cluster assembly scaffold protein IscU (Sulfur acceptor protein IscU)	3	513	175	152	23	0	0
P0C0L9	Ecoli_b2524	iscX	Protein IscX	1	137	49	37	12	0	0
P62620	Ecoli_b2515	ispG	4-hydroxy-3-methylbut-2-en-1-yl diphosphate synthase (flavodoxin) (EC 1.17.7.3) (1-hydroxy-2-methyl-2-(E)-butenyl 4-diphosphate synthase) (Protein GcpE) (Protein E)	5	391	35	16	7	0	0
P62623	Ecoli_b0029	ispH	4-hydroxy-3-methylbut-2-enyl diphosphate reductase (EC 1.17.1.2)	4	80	12	12	0	0	0
P21179	Ecoli_b1732	katE	Catalase HP11 (EC 1.11.1.6) (Hydroxyperoxidase II)	2	14	0	0	0	0	0
P13029	Ecoli_b3942	katG	Catalase-peroxidase (CP) (EC 1.11.1.21) (Hydroperoxidase I) (HPI) (Peroxidase/catalase)	1	2445	104	56	0	0	0
P0AB58	Ecoli_b1280	lapB	Lipopolysaccharide assembly protein B (Lipopolysaccharide regulatory protein)	6	2	0	0	0	0	0
P0A6A6	Ecoli_b0072	leuC	3-isopropylmalate dehydratase large subunit (EC 4.2.1.33) (Alpha-IPM isomerase) (IPMI) (Isopropylmalate isomerase)	9	2373	438	396	37	0	0
P60716	Ecoli_b0628	lipA	Lipoyl synthase (EC 2.8.1.8) (Lip-syn) (LS) (Lipoate synthase) (Lipoic acid synthase) (Sulfur insertion protein LipA)	8	79	24	16	0	0	0
P0A725	Ecoli_b0096	lpxC	UDP-3-O-[3-hydroxymyristoyl] N-acetylglucosamine deacetylase (EC 3.5.1.-) (Protein EnvA) (UDP-3-O-acyl-GlcNAc deacetylase)	6	1	1	1	0	0	0
P45578	Ecoli_b2687	luxS	S-ribosylhomocysteine lyase (EC 4.4.1.21) (AI-2 synthesis protein) (Autoinducer-2 production protein LuxS)	3	1414	194	120	40	0	0
P0AE18	Ecoli_b0168	map	Methionine aminopeptidase (MAP) (MetAP) (EC 3.4.11.18) (Peptidase M)	7	493	43	36	0	0	0
P0AEI1	Ecoli_b0661	miaB	tRNA-2-methylthio-N(6)-dimethylallyl adenosine synthase (EC 2.8.4.3) ((Dimethylallyl)adenosine tRNA methylthiotransferase MiaB) (tRNA-i(6)A37 methylthiotransferase)	6	273	13	13	0	0	0
P0A746	Ecoli_b1778	msrB	Peptide methionine sulfoxide reductase MsrB (EC 1.8.4.12) (Peptide-methionine (R)-S-oxide reductase)	6	364	177	118	5	13	0

P17802	Ecoli_b2961	mutY	A/G-specific adenine glycosylase (EC 3.2.2.-)	7	2	0	0	0	0	0
P11458	Ecoli_b0750	nadA	Quinolinate synthase A (EC 2.5.1.72)	9	132	16	5	2	0	0
P63020	Ecoli_b3414	nfuA	Fe/S biogenesis protein NfuA	4	326	23	23	0	0	0
P69924	Ecoli_b2235	nrdB	Ribonucleoside-diphosphate reductase 1 subunit beta (EC 1.17.4.1) (Protein B2) (Protein R2) (Ribonucleotide reductase 1)	5	315	42	29	0	13	0
P0AF63	Ecoli_b4178	nsrR	HTH-type transcriptional repressor NsrR	3	3	0	0	0	0	0
P0AB83	Ecoli_b1633	nth	Endonuclease III (EC 4.2.99.18) (DNA-(apurinic or apyrimidinic site) lyase)	7	8	0	0	0	0	0
P0AFC7	Ecoli_b2287	nuoB	NADH-quinone oxidoreductase subunit B (EC 1.6.99.5) (NADH dehydrogenase I subunit B) (NDH-1 subunit B) (NUO2)	5	70	0	0	0	0	0
P0AFD1	Ecoli_b2285	nuoE	NADH-quinone oxidoreductase subunit E (EC 1.6.99.5) (NADH dehydrogenase I subunit E) (NDH-1 subunit E) (NUO5)	5	563	10	10	0	0	0
P31979	Ecoli_b2284	nuoF	NADH-quinone oxidoreductase subunit F (EC 1.6.99.5) (NADH dehydrogenase I subunit F) (NDH-1 subunit F) (NUO6)	9	584	9	0	1	0	0
P33602	Ecoli_b2283	nuoG	NADH-quinone oxidoreductase subunit G (EC 1.6.99.5) (NADH dehydrogenase I subunit G) (NDH-1 subunit G) (NUO7)	16	1224	0	0	0	0	0
P0AFD6	Ecoli_b2281	nuoI	NADH-quinone oxidoreductase subunit I (EC 1.6.99.5) (NADH dehydrogenase I subunit I) (NDH-1 subunit I) (NUO9)	9	55	0	0	0	0	0
P0A9N4	Ecoli_b0902	pflA	Pyruvate formate-lyase 1-activating enzyme (EC 1.97.1.4) (Formate-C-acetyltransferase-activating enzyme 1) (PFL-activating enzyme 1)	6	194	24	24	0	0	0
P64554	Ecoli_b2777	queE	7-carboxy-7-deazaguanine synthase (CDG synthase) (EC 4.3.99.3) (Queuosine biosynthesis protein QueE)	8	32	5	5	0	0	0
P0AEI4	Ecoli_b0835	rimO	Ribosomal protein S12 methylthiotransferase RimO (S12 MTTase) (S12 methylthiotransferase) (EC 2.8.4.4) (Ribosomal protein S12 (aspartate(89)-C(3))-methylthiotransferase) (Ribosome maturation factor RimO)	9	158	15	15	0	0	0
P36979	Ecoli_b2517	rlmN	Dual-specificity RNA methyltransferase RlmN (EC 2.1.1.192) (23S rRNA (adenine(2503)-C(2))-methyltransferase) (23S rRNA m2A2503 methyltransferase) (Ribosomal RNA large subunit methyltransferase N) (tRNA (adenine(37)-C(2))-methyltransferase) (tRNA m2A37 methyltransferase)	8	131	11	11	0	0	0



P27431	Ecoli_b1128	roxA	50S ribosomal protein L16 arginine hydroxylase (EC 1.14.11.-) (Ribosomal oxygenase RoxA) (ROX)	1	110	0	0	0	0	0
P0AG07	Ecoli_b3386	rpe	Ribulose-phosphate 3-epimerase (EC 5.1.3.1) (Pentose-5-phosphate 3-epimerase) (PPE) (R5P3E)	1	338	0	0	0	0	0
P30744	Ecoli_b2797	sdaB	L-serine dehydratase 2 (SDH 2) (EC 4.3.1.17) (L-serine deaminase 2) (L-SD2)	10	4	0	0	0	0	0
P07014	Ecoli_b0724	sdhB	Succinate dehydrogenase iron-sulfur subunit (EC 1.3.5.1)	11	1008	242	43	2	0	0
P0AC44	Ecoli_b0722	sdhD	Succinate dehydrogenase hydrophobic membrane anchor subunit	0	19	0	0	0	0	0
P0AGD3	Ecoli_b1656	sodB	Superoxide dismutase [Fe] (EC 1.15.1.1)	1	3197	260	154	83	0	4
P05852	Ecoli_b3064	tsaD	tRNA N6-adenosine threonylcarbamoyltransferase (EC 2.3.1.234) (N6-L-threonylcarbamoyladenine synthase) (t(6)A synthase) (t(6)A37 threonylcarbamoyladenine biosynthesis protein TsaD) (tRNA threonylcarbamoyladenine biosynthesis protein TsaD)	3	12	0	0	0	0	0
P75863	Ecoli_b0947	ycbX	Uncharacterized protein YcbX	9	11	0	0	0	0	0
P52647	Ecoli_b1378	ydbK	Probable pyruvate-flavodoxin oxidoreductase (EC 1.2.7.-)	19	21	0	0	0	0	0
P77748	Ecoli_b1687	ydiJ	Uncharacterized protein YdiJ	19	990	74	33	5	0	0
P76536	Ecoli_b2431	yfeX	Probable deferrioxalate/peroxidase YfeX (EC 1.11.1.-)	4	425	21	21	0	0	0
P0A8P3	Ecoli_b2962	yggX	Probable Fe(2+)-trafficking protein	1	911	37	35	1	1	0
P65367	Ecoli_b2790	yqcA	Uncharacterized protein YqcA	1	212	2	2	0	0	0
P45771	Ecoli_b3283	yrdD	Uncharacterized protein YrdD	16	1	0	0	0	0	0
				50870	4571	3235	335	77	4	

#### Color key for PhHg, MT and Hg(II) adducts observed

	CAM only
	PhHg and Hg adducts
	Hg adducts only
	PhHg or MT adducts only
	protein lacks cysteine
	protein contains a cysteine, but no cysteine peptides were observed

**Table B.S7. Thirty-four cysteines in 20 different Fe-binding proteins formed stable mercury adducts.**

Column A: UniProtKB identifier, B: gene reference number assigned by *E. coli* genome project, C: gene name, D: Protein Data Bank structure identifier (*italic font indicates homolog structure*), E: cysteine residue position modified by mercury, F: yes or no, if that cysteine binds iron in the protein, as determined by UniProtKB annotation and/or crystal structure data, G: total modified peptide spectra observed, H: AdductType, indicates the type of mercury modification, I: peptide sequence including modification type (@ = Hg; # = PhHg), J: protein description, K: main functional role of protein based on COG categories.

UniProt ID	Reference ID	Gene name	PDB <sup>^</sup>	Cys position	In Fe-binding site?	# SpecObsvd	AdductType*	Cysteine position(s) modified	Protein description	Functional category
P36683	Ecoli_b0118	acnB	1L5J	769, 772	yes (4Fe-4S)	30	*Hg	R.IEIPGC@SLCMGN QAR.V	Aconitate hydratase 2 (Aconitase) (EC 4.2.1.3) (2-methylisocitrate dehydratase) (EC 4.2.1.99)	Energy production and conversion
P0AEW4	Ecoli_b3032	cpdA	<i>IDO5</i>	88	no	2	PhHg	R.APC#VWLPGNHDF QPAMYSALQDAGIS PAK.R	3',5'-cyclic adenosine monophosphate phosphodiesterase CpdA (EC 3.1.4.17)	Nucleotide metabolism
P17846	Ecoli_b2763	cysI	1AOP	434, 440	yes (4Fe-4S)	6	Hg	R.ENSMAC@VSFPTC @PLAMAEAR.F	Sulfite reductase [NADPH] hemoprotein beta-component (SiR-HP) (SiRHP) (EC 1.8.1.2)	Inorganic ion metabolism
P0A6K3	Ecoli_b3287	def	1BS4	130	no	4	PhHg	R.ALDRDGKPFEELEA DGLLAIC#IQHEMDH LVGK.L	Peptide deformylase (PDF) (EC 3.5.1.88) (Polypeptide deformylase)	Post-translational modification
P0A9R4	Ecoli_b2525	fdx	1I7H	13	no	13	PhHg	K.IVILPHQDLC#PDG AVLEANSGETILDAA LR.N	2Fe-2S ferredoxin	Energy production and conversion
P0AC33	Ecoli_b1612	fumA		543	no	3	PhHg	K.IEVEDFPFILVDD KGNDFQIQLTQC# TR.C	Fumarate hydratase class I, aerobic (Fumarase) (EC 4.2.1.2)	Energy production and conversion
P09831	Ecoli_b3212	glbB	<i>IEA0</i>	1074	no	12	PhHg	K.YAGC#PWELGLVE TQQALVANGLR.H	Glutamate synthase [NADPH] large chain (EC 1.4.1.13) (GLTS alpha chain) (NADPH-GOGAT)	Amino acid metabolism
P09831	Ecoli_b3212	glbB		1108, 1113	yes (3Fe-4S)	7	Hg	R.IC@HLNNC@ATG VATQDDKLR.K	Glutamate synthase [NADPH] large chain	Amino acid metabolism

									(EC 1.4.1.13) (GLTS alpha chain) (NADPH-GOGAT)	
P09831	Ecoli_b3212	gltB		1232	no	26	PhHg	K.ALYC#TENNPPFD NGLLNAQLLQQA FVDER.Q	Glutamate synthase [NADPH] large chain (EC 1.4.1.13) (GLTS alpha chain) (NADPH-GOGAT)	Amino acid metabolism
P09832	Ecoli_b3213	gltD	IRSG	94	yes (4Fe-4S)	6	PhHg	R.IFEAAELSHQTNTL PEVC#GR.V	Glutamate synthase [NADPH] small chain (EC 1.4.1.13) (GLTS beta chain) (NADPH-GOGAT)	Amino acid metabolism
P09832	Ecoli_b3213	gltD		94, 98	yes (4Fe-4S)	4	Hg	R.IFEAAELSHQTNTL PEVC@GRVC@PQD R.L	Glutamate synthase [NADPH] small chain (EC 1.4.1.13) (GLTS beta chain) (NADPH-GOGAT)	Amino acid metabolism
P09832	Ecoli_b3213	gltD		161	no	9	PhHg	K.KVAIIGAGPAGLA C#ADVLTR.N	Glutamate synthase [NADPH] small chain (EC 1.4.1.13) (GLTS beta chain) (NADPH-GOGAT)	Amino acid metabolism
P09832	Ecoli_b3213	gltD		161	no	36	PhHg	R.VAIIGAGPAGLA C#ADVLTR.N	Glutamate synthase [NADPH] small chain (EC 1.4.1.13) (GLTS beta chain) (NADPH-GOGAT)	Amino acid metabolism
P0AAC8	Ecoli_b2528	iscA	1R94	35	yes (cluster assembly)	6	PhHg	R.TSGC#SGMAYVLE FVDEPTPEDIVFEDK. G	Iron-binding protein IscA (Iron-sulfur cluster assembly protein)	Energy production and conversion
P0ACD4	Ecoli_b2529	icsU nifU	1R9P	37	yes (cluster assembly)	6	PhHg	R.NVGSFDNNDENV GSGMVGAPAC#GDV MK.L	NifU-like, Iron-sulfur cluster assembly scaffold protein	Energy production and conversion
P0ACD4	Ecoli_b2529	icsU nifU		106	yes (cluster assembly)	17	PhHg	K.IHC#SILAEDAIA	NifU-like, Iron-sulfur cluster assembly scaffold protein	Energy production and conversion
P62620	Ecoli_b2515	ispG	4MWA	305	yes (4Fe-4S)	7	PhHg	R.LEDIITPMDVSIIG C#VVNGPGEALVSTL GVTGGNKK.S	4-hydroxy-3-methylbut-2-en-1-yl diphosphate synthase (EC 1.17.7.1)	Lipid metabolism

									(Protein GcpE)	
P0A6A6	Ecoli_b0072	leuC	4KP2	204	no	23	PhHg	K.TGSAGGTGHVVEF C#GEAIRDLSMEGR. M	3-isopropylmalate dehydratase large subunit (EC 4.2.1.33) (Alpha-IPM isomerase)	Amino acid metabolism
P0A6A6	Ecoli_b0072	leuC		347	yes (4Fe-4S)	12	PhHg	K.ALAYMGLKPGIPL TEVAIDKVFIGSC#T NSR.I	3-isopropylmalate dehydratase large subunit (EC 4.2.1.33) (Alpha-IPM isomerase)	Amino acid metabolism
P0A6A6	Ecoli_b0072	leuC		347	yes (4Fe-4S)	2	PhHg	K.ALAYMGLKPGIPL TEVAIDKVFIGSC#T NSRIEDLR.A	3-isopropylmalate dehydratase large subunit (EC 4.2.1.33) (Alpha-IPM isomerase)	Amino acid metabolism
P45578	Ecoli_b2687	luxS	IJ6W	41	no	2	PhHg	R.FC#VPNKEVMPE. G	S- ribosylhomocysteine lyase (EC 4.4.1.21) (Autoinducer-2 production protein LuxS)	Signal transduction
P45578	Ecoli_b2687	luxS		83	no	19	PhHg	R.NHLNGNGVEIIDIS PMGC#R.T	S- ribosylhomocysteine lyase (EC 4.4.1.21) (Autoinducer-2 production protein LuxS)	Signal transduction
P45578	Ecoli_b2687	luxS		128	yes (Fe ion)	19	PhHg	K.VQDQNIPELNVY QC#GTYQMHSLEA QDIAR.S	S- ribosylhomocysteine lyase (EC 4.4.1.21) (Autoinducer-2 production protein LuxS)	Signal transduction
P0A746	Ecoli_b1778	msrB	3HCJ	64	no	5	PhHg	K.YDSGC#GWPSFYE PVSEESIR.Y	Peptide methionine sulfoxide reductase MsrB (EC 1.8.4.12)	Post- translational modification
P0A746	Ecoli_b1778	msrB		95, 98	yes (Fe or Zn ion)	13	*Hg	R.C#@GNC@DAHLGH VFPDGPQPTGER.Y	Peptide methionine sulfoxide reductase MsrB (EC 1.8.4.12)	Post- translational modification
P11458	Ecoli_b0750	nadA	1WZU	64	no	2	PhHg	R.NAVMVAHYTYDP EIQLAEETGGC#ISD SLEMAR.F	Quinolinate synthase A (EC 2.5.1.72)	Coenzyme metabolism

P69924	Ecoli_b2235	nrdB ftsB	1AV8	269, 273	no	13	*Hg	R.SGADDPEMAEIAE EC@KQEC@YDLFV QAAQQEKDWADYL FR.D	Ribonucleoside- diphosphate reductase 1 subunit beta (EC 1.17.4.1)	Nucleotide metabolism
P07014	Ecoli_b0724	sdhB	1NEK	75	yes (2Fe-2S)	2	PhHg	K.NGLAC#ITPISALN QPGKK.I	Succinate dehydrogenase iron- sulfur subunit (EC 1.3.99.1)	Energy production and conversion
P0AGD3	Ecoli_b1656	sodB	1ISA	80	no	83	PhHg	R.SSEGGVFNNAAQV WNHTFYWNC#LAPN AGGEPTGK.V	Superoxide dismutase [Fe] (EC 1.15.1.1)	Defense mechanisms
P0AGD3	Ecoli_b1656	sodB		80	no	4	EtHg	R.SSEGGVFNNAAQV WNHTFYWNC&LAP NAGGEPTGK.V	Superoxide dismutase [Fe] (EC 1.15.1.1)	Defense mechanisms
P77748	Ecoli_b1687	ydiJ		426	no	5	PhHg	K.GAAKPIPAEDTC# VPPEHLADYIAEFR. A	Uncharacterized protein YdiJ, predicted FAD- linked oxidoreductase	Energy production and conversion
P0A8P3	Ecoli_b2962	yggX	1XS8	7	?	1	PhHg	R.TIFC#TFLQR.E	Probable Fe(2+)- trafficking protein	Defense mechanisms
P0A8P3	Ecoli_b2962	yggX		7	?	1	*Hg	R.TIFC@TFLQR.E	Probable Fe(2+)- trafficking protein	Defense mechanisms

Table is sorted by gene name and cysteine position.

Color code:

	single peptide, same adduct
	single peptide, different adducts
	different peptides and/or different adducts

^PDB: those in italics are homology models; all others are X-ray or NMR structures of the indicated *E.coli* protein.

\* AdductType: Adducts designated simply as Hg are from the mercuric-acetate exposure dataset; adducts designated “\*Hg” were observed in PMA exposure datasets.

**Table B.S8. Observed Spectral Counts for non-iron transition metal binding proteins based on Gene Ontology (GO) annotation in UniProtKB database.**

dataset	metal	UniProt ID	gene_ID	gene_name	product_description	total peptide spectra	Cys peptide spectra	CAM spectra	PhHg spectra	HgII spectra	EtHg spectra
PMA	Zn	P0A9Q5	Ecoli_b2316	accD	Acetyl-coenzyme A carboxylase carboxyl transferase subunit beta (ACCase subunit beta) (Acetyl-CoA carboxylase carboxyltransferase subunit beta) (EC 6.4.1.2)	428	3	0	0	3	0
MT	Zn	P0A9Q5	Ecoli_b2316	accD	Acetyl-coenzyme A carboxylase carboxyl transferase subunit beta (ACCase subunit beta) (Acetyl-CoA carboxylase carboxyltransferase subunit beta) (EC 6.4.1.2)	51	0	0	0	0	0
Hg(II)-acetate	Zn	P0A9Q5	Ecoli_b2316	accD	Acetyl-coenzyme A carboxylase carboxyl transferase subunit beta (ACCase subunit beta) (Acetyl-CoA carboxylase carboxyltransferase subunit beta) (EC 6.4.1.2)	73	10	8	0	0	0
PMA	Zn	P0A6A3	Ecoli_b2296	ackA	Acetate kinase (EC 2.7.2.1) (Acetokinase)	754	159	134	25	0	0
MT	Zn	P0A6A3	Ecoli_b2296	ackA	Acetate kinase (EC 2.7.2.1) (Acetokinase)	195	61	61	0	0	0
Hg(II)-acetate	Zn	P0A6A3	Ecoli_b2296	ackA	Acetate kinase (EC 2.7.2.1) (Acetokinase)	284	67	50	0	0	0
PMA	Zn	P26646	Ecoli_b3253	acuI	Probable acrylyl-CoA reductase AcuI (EC 1.3.1.84) (Acryloyl-coenzyme A reductase AcuI)	55	5	0	0	0	0
MT	Zn	P26646	Ecoli_b3253	acuI	Probable acrylyl-CoA reductase AcuI (EC 1.3.1.84) (Acryloyl-coenzyme A reductase AcuI)	2	0	0	0	0	0
Hg(II)-acetate	Zn	P26646	Ecoli_b3253	acuI	Probable acrylyl-CoA reductase AcuI (EC 1.3.1.84) (Acryloyl-coenzyme A reductase AcuI)	5	0	0	0	0	0
PMA	Zn	P22333	Ecoli_b1623	add	Adenosine deaminase (EC 3.5.4.4) (Adenosine aminohydrolase)	104	2	2	0	0	0
MT	Zn	P22333	Ecoli_b1623	add	Adenosine deaminase (EC 3.5.4.4) (Adenosine aminohydrolase)	6	0	0	0	0	0
PMA	Zn	P00957	Ecoli_b2697	alaS	Alanine--tRNA ligase (EC 6.1.1.7) (Alanyl-tRNA synthetase) (AlaRS)	1106	23	21	2	0	0
MT	Zn	P00957	Ecoli_b2697	alaS	Alanine--tRNA ligase (EC 6.1.1.7) (Alanyl-tRNA synthetase) (AlaRS)	262	0	0	0	0	0
Hg(II)-	Zn	P00957	Ecoli_b2697	alaS	Alanine--tRNA ligase (EC 6.1.1.7) (Alanyl-	516	15	15	0	0	0

acetate					tRNA synthetase) (AlaRS)						
Hg(II)-acetate	Mn	P75713	Ecoli_b0515	allE	(S)-ureidoglycine aminohydrolase (UGHY) (UGlyAH) (EC 3.5.3.26)	2	0	0	0	0	0
PMA	Co	P23908	Ecoli_b3957	argE	Acetylornithine deacetylase (AO) (Acetylornithinase) (EC 3.5.1.16) (N-acetylornithinase) (NAO)	739	17	12	5	0	0
MT	Co	P23908	Ecoli_b3957	argE	Acetylornithine deacetylase (AO) (Acetylornithinase) (EC 3.5.1.16) (N-acetylornithinase) (NAO)	217	33	33	0	0	0
Hg(II)-acetate	Co	P23908	Ecoli_b3957	argE	Acetylornithine deacetylase (AO) (Acetylornithinase) (EC 3.5.1.16) (N-acetylornithinase) (NAO)	123	6	6	0	0	0
PMA	Zn	P23908	Ecoli_b3957	argE	Acetylornithine deacetylase (AO) (Acetylornithinase) (EC 3.5.1.16) (N-acetylornithinase) (NAO)	739	17	12	5	0	0
MT	Zn	P23908	Ecoli_b3957	argE	Acetylornithine deacetylase (AO) (Acetylornithinase) (EC 3.5.1.16) (N-acetylornithinase) (NAO)	217	33	33	0	0	0
Hg(II)-acetate	Zn	P23908	Ecoli_b3957	argE	Acetylornithine deacetylase (AO) (Acetylornithinase) (EC 3.5.1.16) (N-acetylornithinase) (NAO)	123	6	6	0	0	0
PMA	Zn	P07639	Ecoli_b3389	aroB	3-dehydroquinate synthase (EC 4.2.3.4)	165	3	3	0	0	0
MT	Zn	P07639	Ecoli_b3389	aroB	3-dehydroquinate synthase (EC 4.2.3.4)	49	2	2	0	0	0
Hg(II)-acetate	Zn	P07639	Ecoli_b3389	aroB	3-dehydroquinate synthase (EC 4.2.3.4)	100	6	6	0	0	0
PMA	Zn	P66948	Ecoli_b2494	bepA	Beta-barrel assembly-enhancing protease (EC 3.4.-.-)	29	0	0	0	0	0
MT	Zn	P66948	Ecoli_b2494	bepA	Beta-barrel assembly-enhancing protease (EC 3.4.-.-)	10	0	0	0	0	0
Hg(II)-acetate	Zn	P66948	Ecoli_b2494	bepA	Beta-barrel assembly-enhancing protease (EC 3.4.-.-)	13	0	0	0	0	0
PMA	Zn	P61517	Ecoli_b0126	can	Carbonic anhydrase 2 (EC 4.2.1.1) (Carbonate dehydratase 2)	385	62	55	7	0	0
MT	Zn	P61517	Ecoli_b0126	can	Carbonic anhydrase 2 (EC 4.2.1.1) (Carbonate dehydratase 2)	122	32	32	0	0	0
Hg(II)-acetate	Zn	P61517	Ecoli_b0126	can	Carbonic anhydrase 2 (EC 4.2.1.1) (Carbonate dehydratase 2)	221	26	26	0	0	0
PMA	Zn	P0ABF6	Ecoli_b2143	cdd	Cytidine deaminase (EC 3.5.4.5) (Cytidine aminohydrolase) (CDA)	234	15	15	0	0	0
MT	Zn	P0ABF6	Ecoli_b2143	cdd	Cytidine deaminase (EC 3.5.4.5) (Cytidine aminohydrolase) (CDA)	84	0	0	0	0	0
Hg(II)-	Zn	P0ABF6	Ecoli_b2143	cdd	Cytidine deaminase (EC 3.5.4.5) (Cytidine	22	11	11	0	0	0

acetate					aminohydrolase) (CDA)						
PMA	Zn	P0A6H1	Ecoli_b0438	clpX	ATP-dependent Clp protease ATP-binding subunit ClpX (ATP-dependent unfoldase ClpX)	556	14	14	0	0	0
MT	Zn	P0A6H1	Ecoli_b0438	clpX	ATP-dependent Clp protease ATP-binding subunit ClpX (ATP-dependent unfoldase ClpX)	174	19	19	0	0	0
Hg(II)-acetate	Zn	P0A6H1	Ecoli_b0438	clpX	ATP-dependent Clp protease ATP-binding subunit ClpX (ATP-dependent unfoldase ClpX)	183	0	0	0	0	0
PMA	Zn	P75960	Ecoli_b1120	cobB	NAD-dependent protein deacylase (EC 3.5.1.-) (Regulatory protein SIR2 homolog)	59	0	0	0	0	0
PMA	Zn	P25524	Ecoli_b0337	codA	Cytosine deaminase (CD) (CDA) (CDase) (EC 3.5.4.1) (Cytosine aminohydrolase) (Isoguanine deaminase) (EC 3.5.4.-)	27	0	0	0	0	0
MT	Zn	P25524	Ecoli_b0337	codA	Cytosine deaminase (CD) (CDA) (CDase) (EC 3.5.4.1) (Cytosine aminohydrolase) (Isoguanine deaminase) (EC 3.5.4.-)	5	0	0	0	0	0
Hg(II)-acetate	Zn	P25524	Ecoli_b0337	codA	Cytosine deaminase (CD) (CDA) (CDase) (EC 3.5.4.1) (Cytosine aminohydrolase) (Isoguanine deaminase) (EC 3.5.4.-)	155	0	0	0	0	0
PMA	Cu	P36649	Ecoli_b0123	cueO	Blue copper oxidase CueO (Copper efflux oxidase)	942	3	0	3	0	0
MT	Cu	P36649	Ecoli_b0123	cueO	Blue copper oxidase CueO (Copper efflux oxidase)	8	0	0	0	0	0
Hg(II)-acetate	Cu	P36649	Ecoli_b0123	cueO	Blue copper oxidase CueO (Copper efflux oxidase)	91	0	0	0	0	0
PMA	Cu	P0A9G4	Ecoli_b0487	cueR	HTH-type transcriptional regulator CueR (Copper efflux regulator) (Copper export regulator)	3	0	0	0	0	0
PMA	Cu	P69488	Ecoli_b4137	cutA	Divalent-cation tolerance protein CutA (C-type cytochrome biogenesis protein CycY)	14	6	6	0	0	0
PMA	Cu	P67826	Ecoli_b1874	cutC	Copper homeostasis protein CutC	36	30	30	0	0	0
PMA	Cu	P0ABJ1	Ecoli_b0432	cyoA	Cytochrome bo(3) ubiquinol oxidase subunit 2 (Cytochrome b562-o complex subunit II) (Cytochrome o ubiquinol oxidase subunit 2) (Cytochrome o subunit 2) (Oxidase bo(3) subunit 2) (Ubiquinol oxidase chain B) (Ubiquinol oxidase polypeptide II) (Ubiquinol oxidase subunit 2)	267	0	0	0	0	0
MT	Cu	P0ABJ1	Ecoli_b0432	cyoA	Cytochrome bo(3) ubiquinol oxidase subunit 2 (Cytochrome b562-o complex subunit II) (Cytochrome o ubiquinol oxidase subunit 2)	15	0	0	0	0	0



					(Cytochrome o subunit 2) (Oxidase bo(3) subunit 2) (Ubiquinol oxidase chain B) (Ubiquinol oxidase polypeptide II) (Ubiquinol oxidase subunit 2)						
Hg(II)-acetate	Cu	P0ABJ1	Ecoli_b0432	cyoA	Cytochrome bo(3) ubiquinol oxidase subunit 2 (Cytochrome b562-o complex subunit II) (Cytochrome o ubiquinol oxidase subunit 2) (Cytochrome o subunit 2) (Oxidase bo(3) subunit 2) (Ubiquinol oxidase chain B) (Ubiquinol oxidase polypeptide II) (Ubiquinol oxidase subunit 2)	98	0	0	0	0	0
PMA	Cu	P0ABI8	Ecoli_b0431	cyoB	Cytochrome bo(3) ubiquinol oxidase subunit 1 (EC 1.10.3.10) (Cytochrome b562-o complex subunit I) (Cytochrome o ubiquinol oxidase subunit 1) (Cytochrome o subunit 1) (Oxidase bo(3) subunit 1) (Ubiquinol oxidase chain A) (Ubiquinol oxidase polypeptide I) (Ubiquinol oxidase subunit 1)	73	0	0	0	0	0
MT	Cu	P0ABI8	Ecoli_b0431	cyoB	Cytochrome bo(3) ubiquinol oxidase subunit 1 (EC 1.10.3.10) (Cytochrome b562-o complex subunit I) (Cytochrome o ubiquinol oxidase subunit 1) (Cytochrome o subunit 1) (Oxidase bo(3) subunit 1) (Ubiquinol oxidase chain A) (Ubiquinol oxidase polypeptide I) (Ubiquinol oxidase subunit 1)	17	0	0	0	0	0
Hg(II)-acetate	Cu	P0ABI8	Ecoli_b0431	cyoB	Cytochrome bo(3) ubiquinol oxidase subunit 1 (EC 1.10.3.10) (Cytochrome b562-o complex subunit I) (Cytochrome o ubiquinol oxidase subunit 1) (Cytochrome o subunit 1) (Oxidase bo(3) subunit 1) (Ubiquinol oxidase chain A) (Ubiquinol oxidase polypeptide I) (Ubiquinol oxidase subunit 1)	28	0	0	0	0	0
PMA	Zn	P21888	Ecoli_b0526	cysS	Cysteine--tRNA ligase (EC 6.1.1.16) (CysteinyI-tRNA synthetase) (CysRS)	349	0	0	0	0	0
MT	Zn	P21888	Ecoli_b0526	cysS	Cysteine--tRNA ligase (EC 6.1.1.16) (CysteinyI-tRNA synthetase) (CysRS)	28	0	0	0	0	0
Hg(II)-acetate	Zn	P21888	Ecoli_b0526	cysS	Cysteine--tRNA ligase (EC 6.1.1.16) (CysteinyI-tRNA synthetase) (CysRS)	222	0	0	0	0	0
PMA	Co	P0AED7	Ecoli_b2472	dapE	Succinyl-diaminopimelate desuccinylase (SDAP desuccinylase) (EC 3.5.1.18) (N-succinyl-L-2,6-diaminoheptanedioate amidohydrolase)	17	0	0	0	0	0
Hg(II)-acetate	Co	P0AED7	Ecoli_b2472	dapE	Succinyl-diaminopimelate desuccinylase (SDAP desuccinylase) (EC 3.5.1.18) (N-	19	0	0	0	0	0

					succinyl-LL-2,6-diaminoheptanedioate amidohydrolase)						
PMA	Zn	P0AED7	Ecoli_b2472	dapE	Succinyl-diaminopimelate desuccinylase (SDAP desuccinylase) (EC 3.5.1.18) (N-succinyl-LL-2,6-diaminoheptanedioate amidohydrolase)	17	0	0	0	0	0
Hg(II)-acetate	Zn	P0AED7	Ecoli_b2472	dapE	Succinyl-diaminopimelate desuccinylase (SDAP desuccinylase) (EC 3.5.1.18) (N-succinyl-LL-2,6-diaminoheptanedioate amidohydrolase)	19	0	0	0	0	0
PMA	Mn	P0A6J8	Ecoli_b0381	ddlA	D-alanine--D-alanine ligase A (EC 6.3.2.4) (D-Ala-D-Ala ligase A) (D-alanylalanine synthetase A)	38	0	0	0	0	0
Hg(II)-acetate	Mn	P0A6J8	Ecoli_b0381	ddlA	D-alanine--D-alanine ligase A (EC 6.3.2.4) (D-Ala-D-Ala ligase A) (D-alanylalanine synthetase A)	15	0	0	0	0	0
PMA	Mn	P07862	Ecoli_b0092	ddlB	D-alanine--D-alanine ligase B (EC 6.3.2.4) (D-Ala-D-Ala ligase B) (D-alanylalanine synthetase B)	41	0	0	0	0	0
MT	Mn	P07862	Ecoli_b0092	ddlB	D-alanine--D-alanine ligase B (EC 6.3.2.4) (D-Ala-D-Ala ligase B) (D-alanylalanine synthetase B)	2	0	0	0	0	0
Hg(II)-acetate	Mn	P07862	Ecoli_b0092	ddlB	D-alanine--D-alanine ligase B (EC 6.3.2.4) (D-Ala-D-Ala ligase B) (D-alanylalanine synthetase B)	4	0	0	0	0	0
PMA	Zn	P0A6K3	Ecoli_b3287	def	Peptide deformylase (PDF) (EC 3.5.1.88) (Polypeptide deformylase)	197	22	18	4	0	0
MT	Zn	P0A6K3	Ecoli_b3287	def	Peptide deformylase (PDF) (EC 3.5.1.88) (Polypeptide deformylase)	40	0	0	0	0	0
Hg(II)-acetate	Zn	P0A6K3	Ecoli_b3287	def	Peptide deformylase (PDF) (EC 3.5.1.88) (Polypeptide deformylase)	34	0	0	0	0	0
PMA	Mn	P0A6K6	Ecoli_b4383	deoB	Phosphopentomutase (EC 5.4.2.7) (Phosphodeoxyribomutase)	210	63	63	0	0	0
MT	Mn	P0A6K6	Ecoli_b4383	deoB	Phosphopentomutase (EC 5.4.2.7) (Phosphodeoxyribomutase)	35	6	6	0	0	0
Hg(II)-acetate	Mn	P0A6K6	Ecoli_b4383	deoB	Phosphopentomutase (EC 5.4.2.7) (Phosphodeoxyribomutase)	62	2	2	0	0	0
PMA	Co	P15723	Ecoli_b0160	dgt	Deoxyguanosinetriphosphate triphosphohydrolase (dGTP triphosphohydrolase) (dGTPase) (EC 3.1.5.1)	6	1	0	1	0	0
MT	Co	P15723	Ecoli_b0160	dgt	Deoxyguanosinetriphosphate triphosphohydrolase (dGTP triphosphohydrolase) (dGTPase) (EC	8	0	0	0	0	0

					3.1.5.1)						
PMA	Mn	P15723	Ecoli_b0160	dgt	Deoxyguanosinetriphosphate triphosphohydrolase (dGTP triphosphohydrolase) (dGTPase) (EC 3.1.5.1)	6	1	0	1	0	0
MT	Mn	P15723	Ecoli_b0160	dgt	Deoxyguanosinetriphosphate triphosphohydrolase (dGTP triphosphohydrolase) (dGTPase) (EC 3.1.5.1)	8	0	0	0	0	0
PMA	Zn	P0ABS1	Ecoli_b0145	dksA	RNA polymerase-binding transcription factor DksA (DnaK suppressor protein)	300	63	44	0	0	0
MT	Zn	P0ABS1	Ecoli_b0145	dksA	RNA polymerase-binding transcription factor DksA (DnaK suppressor protein)	58	17	17	0	0	0
Hg(II)-acetate	Zn	P0ABS1	Ecoli_b0145	dksA	RNA polymerase-binding transcription factor DksA (DnaK suppressor protein)	130	27	25	0	2	0
PMA	Zn	P0ABS5	Ecoli_b3066	dnaG	DNA primase (EC 2.7.7.-)	2	0	0	0	0	0
MT	Zn	P0ABS5	Ecoli_b3066	dnaG	DNA primase (EC 2.7.7.-)	3	0	0	0	0	0
PMA	Zn	P08622	Ecoli_b0015	dnaJ	Chaperone protein DnaJ (HSP40) (Heat shock protein J)	125	20	12	8	0	0
MT	Zn	P08622	Ecoli_b0015	dnaJ	Chaperone protein DnaJ (HSP40) (Heat shock protein J)	23	0	0	0	0	0
Hg(II)-acetate	Zn	P08622	Ecoli_b0015	dnaJ	Chaperone protein DnaJ (HSP40) (Heat shock protein J)	63	6	6	0	0	0
PMA	Zn	P0A6Y8	Ecoli_b0014	dnaK	Chaperone protein DnaK (HSP70) (Heat shock 70 kDa protein) (Heat shock protein 70)	3749	39	39	0	0	0
MT	Zn	P0A6Y8	Ecoli_b0014	dnaK	Chaperone protein DnaK (HSP70) (Heat shock 70 kDa protein) (Heat shock protein 70)	839	32	32	0	0	0
Hg(II)-acetate	Zn	P0A6Y8	Ecoli_b0014	dnaK	Chaperone protein DnaK (HSP70) (Heat shock 70 kDa protein) (Heat shock protein 70)	1693	24	24	0	0	0
PMA	Mn	P45568	Ecoli_b0173	dxr	1-deoxy-D-xylulose 5-phosphate reductoisomerase (DXP reductoisomerase) (EC 1.1.1.267) (1-deoxyxylulose-5-phosphate reductoisomerase) (2-C-methyl-D-erythritol 4-phosphate synthase)	4	4	4	0	0	0
PMA	Zn	P76541	Ecoli_b2439	eutL	Ethanolamine utilization protein EutL	3	0	0	0	0	0
PMA	Zn	P0AB71	Ecoli_b2925	fbaA	Fructose-bisphosphate aldolase class 2 (FBP aldolase) (FBPA) (EC 4.1.2.13) (Fructose-1,6-bisphosphate aldolase) (Fructose-bisphosphate aldolase class II)	2617	263	162	92	0	0

MT	Zn	P0AB71	Ecoli_b2925	fbaA	Fructose-bisphosphate aldolase class 2 (FBP aldolase) (FBPA) (EC 4.1.2.13) (Fructose-1,6-bisphosphate aldolase) (Fructose-bisphosphate aldolase class II)	926	121	121	0	0	0
Hg(II)-acetate	Zn	P0AB71	Ecoli_b2925	fbaA	Fructose-bisphosphate aldolase class 2 (FBP aldolase) (FBPA) (EC 4.1.2.13) (Fructose-1,6-bisphosphate aldolase) (Fructose-bisphosphate aldolase class II)	981	66	23	0	0	0
PMA	Zn	P0A6T5	Ecoli_b2153	folE	GTP cyclohydrolase 1 (EC 3.5.4.16) (GTP cyclohydrolase I) (GTP-CH-I)	959	2	2	0	0	0
MT	Zn	P0A6T5	Ecoli_b2153	folE	GTP cyclohydrolase 1 (EC 3.5.4.16) (GTP cyclohydrolase I) (GTP-CH-I)	221	9	9	0	0	0
Hg(II)-acetate	Zn	P0A6T5	Ecoli_b2153	folE	GTP cyclohydrolase 1 (EC 3.5.4.16) (GTP cyclohydrolase I) (GTP-CH-I)	349	5	5	0	0	0
PMA	Zn	P25437	Ecoli_b0356	frmA	S-(hydroxymethyl)glutathione dehydrogenase (EC 1.1.1.284) (Alcohol dehydrogenase class-3) (EC 1.1.1.1) (Alcohol dehydrogenase class-III) (Glutathione-dependent formaldehyde dehydrogenase) (FALDH) (FDH) (GSH-FDH) (EC 1.1.1.-)	234	4	0	0	0	0
MT	Zn	P25437	Ecoli_b0356	frmA	S-(hydroxymethyl)glutathione dehydrogenase (EC 1.1.1.284) (Alcohol dehydrogenase class-3) (EC 1.1.1.1) (Alcohol dehydrogenase class-III) (Glutathione-dependent formaldehyde dehydrogenase) (FALDH) (FDH) (GSH-FDH) (EC 1.1.1.-)	22	0	0	0	0	0
Hg(II)-acetate	Zn	P25437	Ecoli_b0356	frmA	S-(hydroxymethyl)glutathione dehydrogenase (EC 1.1.1.284) (Alcohol dehydrogenase class-3) (EC 1.1.1.1) (Alcohol dehydrogenase class-III) (Glutathione-dependent formaldehyde dehydrogenase) (FALDH) (FDH) (GSH-FDH) (EC 1.1.1.-)	38	2	2	0	0	0
PMA	Mn	P0AAI3	Ecoli_b3178	ftsH	ATP-dependent zinc metalloprotease FtsH (EC 3.4.24.-) (Cell division protease FtsH)	816	23	22	1	0	0
MT	Mn	P0AAI3	Ecoli_b3178	ftsH	ATP-dependent zinc metalloprotease FtsH (EC 3.4.24.-) (Cell division protease FtsH)	211	19	19	0	0	0
Hg(II)-acetate	Mn	P0AAI3	Ecoli_b3178	ftsH	ATP-dependent zinc metalloprotease FtsH (EC 3.4.24.-) (Cell division protease FtsH)	280	19	19	0	0	0
PMA	Zn	P0AAI3	Ecoli_b3178	ftsH	ATP-dependent zinc metalloprotease FtsH (EC 3.4.24.-) (Cell division protease FtsH)	816	23	22	1	0	0
MT	Zn	P0AAI3	Ecoli_b3178	ftsH	ATP-dependent zinc metalloprotease FtsH	211	19	19	0	0	0

					(EC 3.4.24.-) (Cell division protease FtsH)						
Hg(II)-acetate	Zn	P0AAI3	Ecoli_b3178	ftsH	ATP-dependent zinc metalloprotease FtsH (EC 3.4.24.-) (Cell division protease FtsH)	280	19	19	0	0	0
PMA	Cu	P26648	Ecoli_b3017	ftsP	Cell division protein FtsP	16	0	0	0	0	0
MT	Cu	P26648	Ecoli_b3017	ftsP	Cell division protein FtsP	7	0	0	0	0	0
PMA	Zn	P0A9A9	Ecoli_b0683	fur	Ferric uptake regulation protein (Ferric uptake regulator)	376	15	4	0	3	0
MT	Zn	P0A9A9	Ecoli_b0683	fur	Ferric uptake regulation protein (Ferric uptake regulator)	59	7	7	0	0	0
Hg(II)-acetate	Zn	P0A9A9	Ecoli_b0683	fur	Ferric uptake regulation protein (Ferric uptake regulator)	65	0	0	0	0	0
PMA	Zn	P0C8J6	Ecoli_b2096	gatY	D-tagatose-1,6-bisphosphate aldolase subunit GatY (TBPA) (TagBP aldolase) (EC 4.1.2.40) (D-tagatose-bisphosphate aldolase class II) (Tagatose-bisphosphate aldolase)	909	56	51	0	5	0
MT	Zn	P0C8J6	Ecoli_b2096	gatY	D-tagatose-1,6-bisphosphate aldolase subunit GatY (TBPA) (TagBP aldolase) (EC 4.1.2.40) (D-tagatose-bisphosphate aldolase class II) (Tagatose-bisphosphate aldolase)	294	78	78	0	0	0
Hg(II)-acetate	Zn	P0C8J6	Ecoli_b2096	gatY	D-tagatose-1,6-bisphosphate aldolase subunit GatY (TBPA) (TagBP aldolase) (EC 4.1.2.40) (D-tagatose-bisphosphate aldolase class II) (Tagatose-bisphosphate aldolase)	373	26	26	0	0	0
PMA	Ni	P0AC81	Ecoli_b1651	gloA	Lactoylglutathione lyase (EC 4.4.1.5) (Aldoketomutase) (Glyoxalase I) (Glx I) (Ketone-aldehyde mutase) (Methylglyoxalase) (S-D-lactoylglutathione methylglyoxal lyase)	46	0	0	0	0	0
MT	Ni	P0AC81	Ecoli_b1651	gloA	Lactoylglutathione lyase (EC 4.4.1.5) (Aldoketomutase) (Glyoxalase I) (Glx I) (Ketone-aldehyde mutase) (Methylglyoxalase) (S-D-lactoylglutathione methylglyoxal lyase)	13	0	0	0	0	0
PMA	Zn	P0AC84	Ecoli_b0212	gloB	Hydroxyacylglutathione hydrolase (EC 3.1.2.6) (Glyoxalase II) (Glx II)	49	0	0	0	0	0
MT	Zn	P0AC84	Ecoli_b0212	gloB	Hydroxyacylglutathione hydrolase (EC 3.1.2.6) (Glyoxalase II) (Glx II)	3	0	0	0	0	0
PMA	Zn	P0A6F3	Ecoli_b3926	glpK	Glycerol kinase (EC 2.7.1.30) (ATP:glycerol 3-phosphotransferase) (Glycerokinase) (GK)	3186	194	168	26	0	0
MT	Zn	P0A6F3	Ecoli_b3926	glpK	Glycerol kinase (EC 2.7.1.30) (ATP:glycerol 3-phosphotransferase) (Glycerokinase) (GK)	966	133	133	0	0	0
Hg(II)-acetate	Zn	P0A6F3	Ecoli_b3926	glpK	Glycerol kinase (EC 2.7.1.30) (ATP:glycerol 3-phosphotransferase) (Glycerokinase) (GK)	1481	118	75	0	0	0

Hg(II)-acetate	Mn	P0A9C9	Ecoli_b3925	glpX	Fructose-1,6-bisphosphatase 1 class 2 (FBPase 1 class 2) (EC 3.1.3.11) (D-fructose-1,6-bisphosphate 1-phosphohydrolase 1 class 2)	11	0	0	0	0	0
PMA	Zn	P04805	Ecoli_b2400	gltX	Glutamate--tRNA ligase (EC 6.1.1.17) (Glutamyl-tRNA synthetase) (GluRS)	852	68	16	2	0	0
MT	Zn	P04805	Ecoli_b2400	gltX	Glutamate--tRNA ligase (EC 6.1.1.17) (Glutamyl-tRNA synthetase) (GluRS)	216	11	6	0	0	0
Hg(II)-acetate	Zn	P04805	Ecoli_b2400	gltX	Glutamate--tRNA ligase (EC 6.1.1.17) (Glutamyl-tRNA synthetase) (GluRS)	509	59	12	0	0	0
PMA	Zn	P0A825	Ecoli_b2551	glyA	Serine hydroxymethyltransferase (SHMT) (Serine methylase) (EC 2.1.2.1)	4145	316	208	108	0	0
MT	Zn	P0A825	Ecoli_b2551	glyA	Serine hydroxymethyltransferase (SHMT) (Serine methylase) (EC 2.1.2.1)	1043	129	129	0	0	0
Hg(II)-acetate	Zn	P0A825	Ecoli_b2551	glyA	Serine hydroxymethyltransferase (SHMT) (Serine methylase) (EC 2.1.2.1)	1434	104	89	0	0	0
PMA	Zn	P63224	Ecoli_b0222	gmhA	Phosphoheptose isomerase (EC 5.3.1.28) (Sedoheptulose 7-phosphate isomerase)	699	28	21	0	0	0
MT	Zn	P63224	Ecoli_b0222	gmhA	Phosphoheptose isomerase (EC 5.3.1.28) (Sedoheptulose 7-phosphate isomerase)	182	28	28	0	0	0
Hg(II)-acetate	Zn	P63224	Ecoli_b0222	gmhA	Phosphoheptose isomerase (EC 5.3.1.28) (Sedoheptulose 7-phosphate isomerase)	274	42	23	0	7	0
PMA	Zn	P63228	Ecoli_b0200	gmhB	D-glycero-beta-D-manno-heptose-1,7-bisphosphate 7-phosphatase (EC 3.1.3.82) (D,D-heptose 1,7-bisphosphate phosphatase) (HBP phosphatase)	207	0	0	0	0	0
MT	Zn	P63228	Ecoli_b0200	gmhB	D-glycero-beta-D-manno-heptose-1,7-bisphosphate 7-phosphatase (EC 3.1.3.82) (D,D-heptose 1,7-bisphosphate phosphatase) (HBP phosphatase)	42	0	0	0	0	0
Hg(II)-acetate	Zn	P63228	Ecoli_b0200	gmhB	D-glycero-beta-D-manno-heptose-1,7-bisphosphate 7-phosphatase (EC 3.1.3.82) (D,D-heptose 1,7-bisphosphate phosphatase) (HBP phosphatase)	26	0	0	0	0	0
PMA	Mn	P37689	Ecoli_b3612	gpmI	2,3-bisphosphoglycerate-independent phosphoglycerate mutase (BPG-independent PGAM) (Phosphoglyceromutase) (iPGM) (EC 5.4.2.12)	1320	42	41	1	0	0
MT	Mn	P37689	Ecoli_b3612	gpmI	2,3-bisphosphoglycerate-independent phosphoglycerate mutase (BPG-independent PGAM) (Phosphoglyceromutase) (iPGM) (EC 5.4.2.12)	328	14	14	0	0	0
Hg(II)-acetate	Mn	P37689	Ecoli_b3612	gpmI	2,3-bisphosphoglycerate-independent phosphoglycerate mutase (BPG-independent	374	24	20	0	0	0

					PGAM) (Phosphoglyceromutase) (iPGM) (EC 5.4.2.12)						
PMA	Mn	P04425	Ecoli_b2947	gshB	Glutathione synthetase (EC 6.3.2.3) (GSH synthetase) (GSH-S) (GSHase) (Glutathione synthase)	339	15	15	0	0	0
MT	Mn	P04425	Ecoli_b2947	gshB	Glutathione synthetase (EC 6.3.2.3) (GSH synthetase) (GSH-S) (GSHase) (Glutathione synthase)	75	2	2	0	0	0
Hg(II)-acetate	Mn	P04425	Ecoli_b2947	gshB	Glutathione synthetase (EC 6.3.2.3) (GSH synthetase) (GSH-S) (GSHase) (Glutathione synthase)	53	2	2	0	0	0
PMA	Zn	P31658	Ecoli_b1967	hchA	Molecular chaperone Hsp31 and glyoxalase 3 (EC 4.2.1.130) (Aminopeptidase HchA) (EC 3.4.11.-) (D-lactate dehydratase) (Glyoxalase III) (Holdase) (Holding molecular chaperone)	12	0	0	0	0	0
PMA	Zn	P0ACB2	Ecoli_b0369	hemB	Delta-aminolevulinic acid dehydratase (ALAD) (ALADH) (EC 4.2.1.24) (Porphobilinogen synthase)	275	3	2	1	0	0
MT	Zn	P0ACB2	Ecoli_b0369	hemB	Delta-aminolevulinic acid dehydratase (ALAD) (ALADH) (EC 4.2.1.24) (Porphobilinogen synthase)	36	2	2	0	0	0
Hg(II)-acetate	Zn	P0ACB2	Ecoli_b0369	hemB	Delta-aminolevulinic acid dehydratase (ALAD) (ALADH) (EC 4.2.1.24) (Porphobilinogen synthase)	48	0	0	0	0	0
PMA	Mn	P06988	Ecoli_b2020	hisD	Histidinol dehydrogenase (HDH) (EC 1.1.1.23)	601	52	35	1	0	0
MT	Mn	P06988	Ecoli_b2020	hisD	Histidinol dehydrogenase (HDH) (EC 1.1.1.23)	138	34	30	0	0	0
Hg(II)-acetate	Mn	P06988	Ecoli_b2020	hisD	Histidinol dehydrogenase (HDH) (EC 1.1.1.23)	113	32	14	0	0	0
PMA	Zn	P06988	Ecoli_b2020	hisD	Histidinol dehydrogenase (HDH) (EC 1.1.1.23)	601	52	35	1	0	0
MT	Zn	P06988	Ecoli_b2020	hisD	Histidinol dehydrogenase (HDH) (EC 1.1.1.23)	138	34	30	0	0	0
Hg(II)-acetate	Zn	P06988	Ecoli_b2020	hisD	Histidinol dehydrogenase (HDH) (EC 1.1.1.23)	113	32	14	0	0	0
PMA	Zn	P23894	Ecoli_b1829	htpX	Protease HtpX (EC 3.4.24.-) (Heat shock protein HtpX)	15	0	0	0	0	0
Hg(II)-acetate	Ni	P0AAN3	Ecoli_b2727	hypB	Hydrogenase isoenzymes nickel incorporation protein HypB	2	0	0	0	0	0
Hg(II)-acetate	Zn	P0AAN3	Ecoli_b2727	hypB	Hydrogenase isoenzymes nickel incorporation protein HypB	2	0	0	0	0	0

PMA	Zn	P39377	Ecoli_b4328	iadA	Isoaspartyl dipeptidase (EC 3.4.19.-)	75	0	0	0	0	0
MT	Zn	P39377	Ecoli_b4328	iadA	Isoaspartyl dipeptidase (EC 3.4.19.-)	34	0	0	0	0	0
Hg(II)-acetate	Zn	P39377	Ecoli_b4328	iadA	Isoaspartyl dipeptidase (EC 3.4.19.-)	29	0	0	0	0	0
PMA	Zn	P00956	Ecoli_b0026	ileS	Isoleucine--tRNA ligase (EC 6.1.1.5) (Isoleucyl-tRNA synthetase) (IleRS)	1139	94	86	8	0	0
MT	Zn	P00956	Ecoli_b0026	ileS	Isoleucine--tRNA ligase (EC 6.1.1.5) (Isoleucyl-tRNA synthetase) (IleRS)	364	68	68	0	0	0
Hg(II)-acetate	Zn	P00956	Ecoli_b0026	ileS	Isoleucine--tRNA ligase (EC 6.1.1.5) (Isoleucyl-tRNA synthetase) (IleRS)	356	105	100	0	0	0
PMA	Mn	P62617	Ecoli_b2746	ispF	2-C-methyl-D-erythritol 2,4-cyclodiphosphate synthase (MECDP-synthase) (MECPP-synthase) (MECPS) (EC 4.6.1.12)	139	3	0	0	0	0
MT	Mn	P62617	Ecoli_b2746	ispF	2-C-methyl-D-erythritol 2,4-cyclodiphosphate synthase (MECDP-synthase) (MECPP-synthase) (MECPS) (EC 4.6.1.12)	2	0	0	0	0	0
PMA	Zn	P62617	Ecoli_b2746	ispF	2-C-methyl-D-erythritol 2,4-cyclodiphosphate synthase (MECDP-synthase) (MECPP-synthase) (MECPS) (EC 4.6.1.12)	139	3	0	0	0	0
MT	Zn	P62617	Ecoli_b2746	ispF	2-C-methyl-D-erythritol 2,4-cyclodiphosphate synthase (MECDP-synthase) (MECPP-synthase) (MECPS) (EC 4.6.1.12)	2	0	0	0	0	0
PMA	Mn	P30125	Ecoli_b0073	leuB	3-isopropylmalate dehydrogenase (EC 1.1.1.85) (3-IPM-DH) (Beta-IPM dehydrogenase) (IMDH)	908	104	94	6	0	0
MT	Mn	P30125	Ecoli_b0073	leuB	3-isopropylmalate dehydrogenase (EC 1.1.1.85) (3-IPM-DH) (Beta-IPM dehydrogenase) (IMDH)	290	65	65	0	0	0
Hg(II)-acetate	Mn	P30125	Ecoli_b0073	leuB	3-isopropylmalate dehydrogenase (EC 1.1.1.85) (3-IPM-DH) (Beta-IPM dehydrogenase) (IMDH)	516	88	49	0	0	0
PMA	Zn	P0A9P0	Ecoli_b0116	lpdA	Dihydrolipoyl dehydrogenase (EC 1.8.1.4) (Dihydrolipoamide dehydrogenase) (E3 component of pyruvate and 2-oxoglutarate dehydrogenases complexes) (Glycine cleavage system L protein)	2488	393	152	7	11	0
MT	Zn	P0A9P0	Ecoli_b0116	lpdA	Dihydrolipoyl dehydrogenase (EC 1.8.1.4) (Dihydrolipoamide dehydrogenase) (E3 component of pyruvate and 2-oxoglutarate	842	168	102	0	0	0



					dehydrogenases complexes) (Glycine cleavage system L protein)						
Hg(II)-acetate	Zn	P0A9P0	Ecoli_b0116	lpdA	Dihydrolipoyl dehydrogenase (EC 1.8.1.4) (Dihydrolipoamide dehydrogenase) (E3 component of pyruvate and 2-oxoglutarate dehydrogenases complexes) (Glycine cleavage system L protein)	1240	188	69	0	3	0
PMA	Zn	P0A725	Ecoli_b0096	lpxC	UDP-3-O-[3-hydroxymyristoyl] N-acetylglucosamine deacetylase (EC 3.5.1.-) (Protein EnvA) (UDP-3-O-acetyl-GlcNAc deacetylase)	1	1	1	0	0	0
PMA	Mn	P76558	Ecoli_b2463	maeB	NADP-dependent malic enzyme (NADP-ME) (EC 1.1.1.40)	788	106	95	11	0	0
MT	Mn	P76558	Ecoli_b2463	maeB	NADP-dependent malic enzyme (NADP-ME) (EC 1.1.1.40)	251	54	54	0	0	0
Hg(II)-acetate	Mn	P76558	Ecoli_b2463	maeB	NADP-dependent malic enzyme (NADP-ME) (EC 1.1.1.40)	316	59	57	0	0	0
PMA	Zn	P00946	Ecoli_b1613	manA	Mannose-6-phosphate isomerase (EC 5.3.1.8) (Phosphohexomutase) (Phosphomannose isomerase) (PMI)	569	6	6	0	0	0
MT	Zn	P00946	Ecoli_b1613	manA	Mannose-6-phosphate isomerase (EC 5.3.1.8) (Phosphohexomutase) (Phosphomannose isomerase) (PMI)	86	0	0	0	0	0
Hg(II)-acetate	Zn	P00946	Ecoli_b1613	manA	Mannose-6-phosphate isomerase (EC 5.3.1.8) (Phosphohexomutase) (Phosphomannose isomerase) (PMI)	156	0	0	0	0	0
PMA	Mn	P17109	Ecoli_b2264	menD	2-succinyl-5-enolpyruvyl-6-hydroxy-3-cyclohexene-1-carboxylate synthase (SEPHCHC synthase) (EC 2.2.1.9) (Menaquinone biosynthesis protein MenD)	4	0	0	0	0	0
PMA	Zn	P25665	Ecoli_b3829	metE	5-methyltetrahydropteroyltriglutamate--homocysteine methyltransferase (EC 2.1.1.14) (Cobalamin-independent methionine synthase) (Methionine synthase, vitamin-B12 independent isozyme)	19471	2415	1105	215	70	0
MT	Zn	P25665	Ecoli_b3829	metE	5-methyltetrahydropteroyltriglutamate--homocysteine methyltransferase (EC 2.1.1.14) (Cobalamin-independent methionine synthase) (Methionine synthase, vitamin-B12 independent isozyme)	5215	771	569	0	0	13
Hg(II)-acetate	Zn	P25665	Ecoli_b3829	metE	5-methyltetrahydropteroyltriglutamate--homocysteine methyltransferase (EC 2.1.1.14) (Cobalamin-independent methionine synthase) (Methionine synthase,	7037	1165	347	0	0	0

					vitamin-B12 independent isozyme)						
PMA	Zn	P13009	Ecoli_b4019	metH	Methionine synthase (EC 2.1.1.13) (5-methyltetrahydrofolate--homocysteine methyltransferase) (Methionine synthase, vitamin-B12-dependent) (MS)	301	5	4	1	0	0
MT	Zn	P13009	Ecoli_b4019	metH	Methionine synthase (EC 2.1.1.13) (5-methyltetrahydrofolate--homocysteine methyltransferase) (Methionine synthase, vitamin-B12-dependent) (MS)	25	0	0	0	0	0
Hg(II)-acetate	Zn	P13009	Ecoli_b4019	metH	Methionine synthase (EC 2.1.1.13) (5-methyltetrahydrofolate--homocysteine methyltransferase) (Methionine synthase, vitamin-B12-dependent) (MS)	149	9	9	0	0	0
MT	Zn	P12282	Ecoli_b0826	moeB	Molybdopterin-synthase adenyllyltransferase (EC 2.7.7.80) (MoaD protein adenylase) (Molybdopterin-converting factor subunit 1 adenylase) (Sulfur carrier protein MoaD adenyllyltransferase)	6	6	6	0	0	0
PMA	Zn	P0A746	Ecoli_b1778	msrB	Peptide methionine sulfoxide reductase MsrB (EC 1.8.4.12) (Peptide-methionine (R)-S-oxide reductase)	208	94	58	5	13	0
MT	Zn	P0A746	Ecoli_b1778	msrB	Peptide methionine sulfoxide reductase MsrB (EC 1.8.4.12) (Peptide-methionine (R)-S-oxide reductase)	46	31	29	0	0	0
Hg(II)-acetate	Zn	P0A746	Ecoli_b1778	msrB	Peptide methionine sulfoxide reductase MsrB (EC 1.8.4.12) (Peptide-methionine (R)-S-oxide reductase)	110	52	31	0	0	0
PMA	Mn	P08337	Ecoli_b0099	mutT	8-oxo-dGTP diphosphatase (8-oxo-dGTPase) (EC 3.6.1.55) (7,8-dihydro-8-oxoguanine-triphosphatase) (Mutator protein MutT) (dGTP pyrophosphohydrolase)	6	0	0	0	0	0
MT	Zn	P0AF18	Ecoli_b0677	nagA	N-acetylglucosamine-6-phosphate deacetylase (EC 3.5.1.25) (GlcNAc 6-P deacetylase)	3	3	3	0	0	0
PMA	Zn	P75959	Ecoli_b1119	nagK	N-acetyl-D-glucosamine kinase (EC 2.7.1.59) (GlcNAc kinase)	7	7	7	0	0	0
PMA	Zn	P0A6C1	Ecoli_b2159	nfo	Endonuclease 4 (EC 3.1.21.2) (Endodeoxyribonuclease IV) (Endonuclease IV)	15	0	0	0	0	0
PMA	Ni	P0A6Z6	Ecoli_b3481	nikR	Nickel-responsive regulator	142	0	0	0	0	0
MT	Ni	P0A6Z6	Ecoli_b3481	nikR	Nickel-responsive regulator	3	0	0	0	0	0
PMA	Zn	P0A8D0	Ecoli_b0413	nrdR	Transcriptional repressor NrdR	11	0	0	0	0	0

Hg(II)-acetate	Zn	P0A8D0	Ecoli_b0413	nrdR	Transcriptional repressor NrdR	7	0	0	0	0	0
PMA	Co	P19624	Ecoli_b0052	pdxA	4-hydroxythreonine-4-phosphate dehydrogenase (EC 1.1.1.262) (4-(phosphohydroxy)-L-threonine dehydrogenase)	7	0	0	0	0	0
MT	Co	P19624	Ecoli_b0052	pdxA	4-hydroxythreonine-4-phosphate dehydrogenase (EC 1.1.1.262) (4-(phosphohydroxy)-L-threonine dehydrogenase)	3	0	0	0	0	0
Hg(II)-acetate	Co	P19624	Ecoli_b0052	pdxA	4-hydroxythreonine-4-phosphate dehydrogenase (EC 1.1.1.262) (4-(phosphohydroxy)-L-threonine dehydrogenase)	2	0	0	0	0	0
PMA	Zn	P19624	Ecoli_b0052	pdxA	4-hydroxythreonine-4-phosphate dehydrogenase (EC 1.1.1.262) (4-(phosphohydroxy)-L-threonine dehydrogenase)	7	0	0	0	0	0
MT	Zn	P19624	Ecoli_b0052	pdxA	4-hydroxythreonine-4-phosphate dehydrogenase (EC 1.1.1.262) (4-(phosphohydroxy)-L-threonine dehydrogenase)	3	0	0	0	0	0
Hg(II)-acetate	Zn	P19624	Ecoli_b0052	pdxA	4-hydroxythreonine-4-phosphate dehydrogenase (EC 1.1.1.262) (4-(phosphohydroxy)-L-threonine dehydrogenase)	2	0	0	0	0	0
PMA	Zn	P40191	Ecoli_b2418	pdxK	Pyridoxine kinase (EC 2.7.1.35) (PN/PL/PM kinase) (Pyridoxal kinase) (Pyridoxamine kinase) (Vitamin B6 kinase)	141	28	23	5	0	0
MT	Zn	P40191	Ecoli_b2418	pdxK	Pyridoxine kinase (EC 2.7.1.35) (PN/PL/PM kinase) (Pyridoxal kinase) (Pyridoxamine kinase) (Vitamin B6 kinase)	47	12	12	0	0	0
Hg(II)-acetate	Zn	P40191	Ecoli_b2418	pdxK	Pyridoxine kinase (EC 2.7.1.35) (PN/PL/PM kinase) (Pyridoxal kinase) (Pyridoxamine kinase) (Vitamin B6 kinase)	46	9	9	0	0	0
PMA	Zn	P77150	Ecoli_b1636	pdxY	Pyridoxamine kinase (PM kinase) (EC 2.7.1.35)	241	56	51	3	2	0
MT	Zn	P77150	Ecoli_b1636	pdxY	Pyridoxamine kinase (PM kinase) (EC 2.7.1.35)	34	16	16	0	0	0
Hg(II)-acetate	Zn	P77150	Ecoli_b1636	pdxY	Pyridoxamine kinase (PM kinase) (EC 2.7.1.35)	55	4	4	0	0	0
PMA	Mn	P68767	Ecoli_b4260	pepA	Cytosol aminopeptidase (EC 3.4.11.1) (Aminopeptidase A/I) (Leucine aminopeptidase) (LAP) (EC 3.4.11.10)	261	26	24	2	0	0

					(Leucyl aminopeptidase)						
MT	Mn	P68767	Ecoli b4260	pepA	Cytosol aminopeptidase (EC 3.4.11.1) (Aminopeptidase A/I) (Leucine aminopeptidase) (LAP) (EC 3.4.11.10) (Leucyl aminopeptidase)	75	15	15	0	0	0
Hg(II)-acetate	Mn	P68767	Ecoli b4260	pepA	Cytosol aminopeptidase (EC 3.4.11.1) (Aminopeptidase A/I) (Leucine aminopeptidase) (LAP) (EC 3.4.11.10) (Leucyl aminopeptidase)	110	13	13	0	0	0
PMA	Mn	P37095	Ecoli b2523	pepB	Peptidase B (EC 3.4.11.23) (Aminopeptidase B)	172	21	21	0	0	0
MT	Mn	P37095	Ecoli b2523	pepB	Peptidase B (EC 3.4.11.23) (Aminopeptidase B)	32	6	6	0	0	0
Hg(II)-acetate	Mn	P37095	Ecoli b2523	pepB	Peptidase B (EC 3.4.11.23) (Aminopeptidase B)	186	32	17	0	0	0
PMA	Zn	P15288	Ecoli b0237	pepD	Cytosol non-specific dipeptidase (EC 3.4.13.18) (Aminoacyl-histidine dipeptidase) (Beta-alanyl-histidine dipeptidase) (Carnosinase) (Cysteinylglycinase) (Peptidase D) (Xaa-His dipeptidase) (X-His dipeptidase)	680	33	33	0	0	0
MT	Zn	P15288	Ecoli b0237	pepD	Cytosol non-specific dipeptidase (EC 3.4.13.18) (Aminoacyl-histidine dipeptidase) (Beta-alanyl-histidine dipeptidase) (Carnosinase) (Cysteinylglycinase) (Peptidase D) (Xaa-His dipeptidase) (X-His dipeptidase)	249	46	46	0	0	0
Hg(II)-acetate	Zn	P15288	Ecoli b0237	pepD	Cytosol non-specific dipeptidase (EC 3.4.13.18) (Aminoacyl-histidine dipeptidase) (Beta-alanyl-histidine dipeptidase) (Carnosinase) (Cysteinylglycinase) (Peptidase D) (Xaa-His dipeptidase) (X-His dipeptidase)	312	33	28	0	0	0
PMA	Zn	P04825	Ecoli b0932	pepN	Aminopeptidase N (EC 3.4.11.2) (Alpha-aminoacylpeptide hydrolase)	496	45	24	11	0	0
MT	Zn	P04825	Ecoli b0932	pepN	Aminopeptidase N (EC 3.4.11.2) (Alpha-aminoacylpeptide hydrolase)	138	24	24	0	0	0
Hg(II)-acetate	Zn	P04825	Ecoli b0932	pepN	Aminopeptidase N (EC 3.4.11.2) (Alpha-aminoacylpeptide hydrolase)	97	0	0	0	0	0
PMA	Mn	P15034	Ecoli b2908	pepP	Xaa-Pro aminopeptidase (EC 3.4.11.9) (Aminoacylproline aminopeptidase) (Aminopeptidase P II) (APP-II) (X-Pro aminopeptidase)	117	0	0	0	0	0

MT	Mn	P15034	Ecoli_b2908	pepP	Xaa-Pro aminopeptidase (EC 3.4.11.9) (Aminoacylproline aminopeptidase) (Aminopeptidase P II) (APP-II) (X-Pro aminopeptidase)	33	0	0	0	0	0
Hg(II)-acetate	Mn	P15034	Ecoli_b2908	pepP	Xaa-Pro aminopeptidase (EC 3.4.11.9) (Aminoacylproline aminopeptidase) (Aminopeptidase P II) (APP-II) (X-Pro aminopeptidase)	64	0	0	0	0	0
PMA	Mn	P21165	Ecoli_b3847	pepQ	Xaa-Pro dipeptidase (X-Pro dipeptidase) (EC 3.4.13.9) (Imidodipeptidase) (Proline dipeptidase) (Prolidase)	417	4	4	0	0	0
MT	Mn	P21165	Ecoli_b3847	pepQ	Xaa-Pro dipeptidase (X-Pro dipeptidase) (EC 3.4.13.9) (Imidodipeptidase) (Proline dipeptidase) (Prolidase)	155	6	6	0	0	0
Hg(II)-acetate	Mn	P21165	Ecoli_b3847	pepQ	Xaa-Pro dipeptidase (X-Pro dipeptidase) (EC 3.4.13.9) (Imidodipeptidase) (Proline dipeptidase) (Prolidase)	210	7	5	0	0	0
PMA	Zn	P29745	Ecoli_b1127	pepT	Peptidase T (EC 3.4.11.4) (Aminotripeptidase) (Tripeptidase) (Tripeptide aminopeptidase)	140	0	0	0	0	0
MT	Zn	P29745	Ecoli_b1127	pepT	Peptidase T (EC 3.4.11.4) (Aminotripeptidase) (Tripeptidase) (Tripeptide aminopeptidase)	45	0	0	0	0	0
Hg(II)-acetate	Zn	P29745	Ecoli_b1127	pepT	Peptidase T (EC 3.4.11.4) (Aminotripeptidase) (Tripeptidase) (Tripeptide aminopeptidase)	28	0	0	0	0	0
PMA	Mn	P0A9K7	Ecoli_b3724	phoU	Phosphate-specific transport system accessory protein PhoU (Pst system accessory protein PhoU) (Negative regulator of Pho regulon)	71	12	12	0	0	0
Hg(II)-acetate	Mn	P0A9K7	Ecoli_b3724	phoU	Phosphate-specific transport system accessory protein PhoU (Pst system accessory protein PhoU) (Negative regulator of Pho regulon)	40	4	4	0	0	0
PMA	Zn	P0A7A9	Ecoli_b4226	ppa	Inorganic pyrophosphatase (EC 3.6.1.1) (Pyrophosphate phospho-hydrolase) (PPase)	1047	63	46	0	0	0
MT	Zn	P0A7A9	Ecoli_b4226	ppa	Inorganic pyrophosphatase (EC 3.6.1.1) (Pyrophosphate phospho-hydrolase) (PPase)	383	33	33	0	0	0
Hg(II)-acetate	Zn	P0A7A9	Ecoli_b4226	ppa	Inorganic pyrophosphatase (EC 3.6.1.1) (Pyrophosphate phospho-hydrolase) (PPase)	449	0	0	0	0	0
PMA	Zn	P0A9M8	Ecoli_b2297	pta	Phosphate acetyltransferase (EC 2.3.1.8) (Phosphotransacetylase)	980	54	42	12	0	0
MT	Zn	P0A9M8	Ecoli_b2297	pta	Phosphate acetyltransferase (EC 2.3.1.8) (Phosphotransacetylase)	191	18	18	0	0	0

Hg(II)-acetate	Zn	P0A9M8	Ecoli_b2297	pta	Phosphate acetyltransferase (EC 2.3.1.8) (Phosphotransacetylase)	376	15	12	0	0	0
PMA	Zn	P05458	Ecoli_b2821	ptrA	Protease 3 (EC 3.4.24.55) (Pitrilysin) (Protease III) (Protease pi)	4	0	0	0	0	0
Hg(II)-acetate	Zn	P05458	Ecoli_b2821	ptrA	Protease 3 (EC 3.4.24.55) (Pitrilysin) (Protease III) (Protease pi)	12	0	0	0	0	0
PMA	Mn	P15640	Ecoli_b4005	purD	Phosphoribosylamine--glycine ligase (EC 6.3.4.13) (GARS) (Glycinamide ribonucleotide synthetase) (Phosphoribosylglycinamide synthetase)	608	11	11	0	0	0
MT	Mn	P15640	Ecoli_b4005	purD	Phosphoribosylamine--glycine ligase (EC 6.3.4.13) (GARS) (Glycinamide ribonucleotide synthetase) (Phosphoribosylglycinamide synthetase)	116	5	5	0	0	0
Hg(II)-acetate	Mn	P15640	Ecoli_b4005	purD	Phosphoribosylamine--glycine ligase (EC 6.3.4.13) (GARS) (Glycinamide ribonucleotide synthetase) (Phosphoribosylglycinamide synthetase)	164	6	6	0	0	0
PMA	Zn	P05020	Ecoli_b1062	pyrC	Dihydroorotase (DHOase) (EC 3.5.2.3)	544	55	26	29	0	0
MT	Zn	P05020	Ecoli_b1062	pyrC	Dihydroorotase (DHOase) (EC 3.5.2.3)	90	10	10	0	0	0
Hg(II)-acetate	Zn	P05020	Ecoli_b1062	pyrC	Dihydroorotase (DHOase) (EC 3.5.2.3)	182	23	15	0	0	0
PMA	Zn	P0A7F3	Ecoli_b4244	pyrI	Aspartate carbamoyltransferase regulatory chain	60	0	0	0	0	0
Hg(II)-acetate	Zn	P0A7F3	Ecoli_b4244	pyrI	Aspartate carbamoyltransferase regulatory chain	5	0	0	0	0	0
PMA	Zn	P28304	Ecoli_b4051	qorA	Quinone oxidoreductase 1 (EC 1.6.5.5) (NADPH:quinone reductase 1) (Zeta-crystallin homolog protein)	26	0	0	0	0	0
MT	Zn	P28304	Ecoli_b4051	qorA	Quinone oxidoreductase 1 (EC 1.6.5.5) (NADPH:quinone reductase 1) (Zeta-crystallin homolog protein)	9	0	0	0	0	0
Hg(II)-acetate	Zn	P28304	Ecoli_b4051	qorA	Quinone oxidoreductase 1 (EC 1.6.5.5) (NADPH:quinone reductase 1) (Zeta-crystallin homolog protein)	8	0	0	0	0	0
PMA	Zn	P77756	Ecoli_b0444	queC	7-cyano-7-deazaguanine synthase (EC 6.3.4.20) (7-cyano-7-carbaguanine synthase) (PreQ(0) synthase) (Queuosine biosynthesis protein QueC)	34	0	0	0	0	0
Hg(II)-acetate	Zn	P77756	Ecoli_b0444	queC	7-cyano-7-deazaguanine synthase (EC 6.3.4.20) (7-cyano-7-carbaguanine synthase) (PreQ(0) synthase) (Queuosine biosynthesis protein QueC)	2	0	0	0	0	0

PMA	Zn	P0A8V0	Ecoli_b2268	rnb	Ribonuclease BN (RNase BN) (EC 3.1.-.-) (Ribonuclease Z homolog) (RNase Z homolog)	3	0	0	0	0	0
Hg(II)-acetate	Zn	P0A8V0	Ecoli_b2268	rnb	Ribonuclease BN (RNase BN) (EC 3.1.-.-) (Ribonuclease Z homolog) (RNase Z homolog)	11	0	0	0	0	0
PMA	Zn	P0A7I7	Ecoli_b1277	ribA	GTP cyclohydrolase-2 (EC 3.5.4.25) (GTP cyclohydrolase II)	76	6	6	0	0	0
MT	Zn	P0A7I7	Ecoli_b1277	ribA	GTP cyclohydrolase-2 (EC 3.5.4.25) (GTP cyclohydrolase II)	5	0	0	0	0	0
PMA	Mn	P0A7J0	Ecoli_b3041	ribB	3,4-dihydroxy-2-butanone 4-phosphate synthase (DHBP synthase) (EC 4.1.99.12)	380	68	50	18	0	0
MT	Mn	P0A7J0	Ecoli_b3041	ribB	3,4-dihydroxy-2-butanone 4-phosphate synthase (DHBP synthase) (EC 4.1.99.12)	50	11	11	0	0	0
Hg(II)-acetate	Mn	P0A7J0	Ecoli_b3041	ribB	3,4-dihydroxy-2-butanone 4-phosphate synthase (DHBP synthase) (EC 4.1.99.12)	60	2	2	0	0	0
PMA	Zn	P25539	Ecoli_b0414	ribD	Riboflavin biosynthesis protein RibD [Includes: Diaminohydroxyphosphoribosylaminopyrimidine deaminase (DRAP deaminase) (EC 3.5.4.26) (Riboflavin-specific deaminase); 5-amino-6-(5-phosphoribosylamino)uracil reductase (EC 1.1.1.193) (HTP reductase)]	2	0	0	0	0	0
Hg(II)-acetate	Zn	P25539	Ecoli_b0414	ribD	Riboflavin biosynthesis protein RibD [Includes: Diaminohydroxyphosphoribosylaminopyrimidine deaminase (DRAP deaminase) (EC 3.5.4.26) (Riboflavin-specific deaminase); 5-amino-6-(5-phosphoribosylamino)uracil reductase (EC 1.1.1.193) (HTP reductase)]	11	0	0	0	0	0
PMA	Zn	P21513	Ecoli_b1084	rne	Ribonuclease E (RNase E) (EC 3.1.26.12)	611	6	6	0	0	0
MT	Zn	P21513	Ecoli_b1084	rne	Ribonuclease E (RNase E) (EC 3.1.26.12)	155	0	0	0	0	0
Hg(II)-acetate	Zn	P21513	Ecoli_b1084	rne	Ribonuclease E (RNase E) (EC 3.1.26.12)	460	0	0	0	0	0
PMA	Zn	P60422	Ecoli_b3317	rplB	50S ribosomal protein L2	2140	26	25	0	1	0
MT	Zn	P60422	Ecoli_b3317	rplB	50S ribosomal protein L2	479	13	13	0	0	0
Hg(II)-acetate	Zn	P60422	Ecoli_b3317	rplB	50S ribosomal protein L2	1880	0	0	0	0	0
PMA	Zn	P0AA10	Ecoli_b3231	rplM	50S ribosomal protein L13	1154	0	0	0	0	0
MT	Zn	P0AA10	Ecoli_b3231	rplM	50S ribosomal protein L13	321	0	0	0	0	0
Hg(II)-	Zn	P0AA10	Ecoli_b3231	rplM	50S ribosomal protein L13	1040	0	0	0	0	0

acetate											
PMA	Zn	P0A7M9	Ecoli_b3936	rpmE	50S ribosomal protein L31	440	405	237	1	99	0
MT	Zn	P0A7M9	Ecoli_b3936	rpmE	50S ribosomal protein L31	82	74	74	0	0	0
Hg(II)-acetate	Zn	P0A7M9	Ecoli_b3936	rpmE	50S ribosomal protein L31	124	120	57	0	12	0
PMA	Zn	P0A7Z4	Ecoli_b3295	rpoA	DNA-directed RNA polymerase subunit alpha (RNAP subunit alpha) (EC 2.7.7.6) (RNA polymerase subunit alpha) (Transcriptase subunit alpha)	2629	313	218	88	0	0
MT	Zn	P0A7Z4	Ecoli_b3295	rpoA	DNA-directed RNA polymerase subunit alpha (RNAP subunit alpha) (EC 2.7.7.6) (RNA polymerase subunit alpha) (Transcriptase subunit alpha)	738	115	111	0	0	2
Hg(II)-acetate	Zn	P0A7Z4	Ecoli_b3295	rpoA	DNA-directed RNA polymerase subunit alpha (RNAP subunit alpha) (EC 2.7.7.6) (RNA polymerase subunit alpha) (Transcriptase subunit alpha)	1409	162	134	0	0	0
PMA	Zn	P0A7V0	Ecoli_b0169	rpsB	30S ribosomal protein S2	2922	309	173	127	0	0
MT	Zn	P0A7V0	Ecoli_b0169	rpsB	30S ribosomal protein S2	742	121	116	0	0	5
Hg(II)-acetate	Zn	P0A7V0	Ecoli_b0169	rpsB	30S ribosomal protein S2	1604	172	108	0	0	0
PMA	Co	P0A9K9	Ecoli_b3349	slyD	FKBP-type peptidyl-prolyl cis-trans isomerase SlyD (PPIase) (EC 5.2.1.8) (Histidine-rich protein) (Metallochaperone SlyD) (Rotamase) (Sensitivity to lysis protein D) (WHP)	374	0	0	0	0	0
MT	Co	P0A9K9	Ecoli_b3349	slyD	FKBP-type peptidyl-prolyl cis-trans isomerase SlyD (PPIase) (EC 5.2.1.8) (Histidine-rich protein) (Metallochaperone SlyD) (Rotamase) (Sensitivity to lysis protein D) (WHP)	112	0	0	0	0	0
Hg(II)-acetate	Co	P0A9K9	Ecoli_b3349	slyD	FKBP-type peptidyl-prolyl cis-trans isomerase SlyD (PPIase) (EC 5.2.1.8) (Histidine-rich protein) (Metallochaperone SlyD) (Rotamase) (Sensitivity to lysis protein D) (WHP)	176	0	0	0	0	0
PMA	Cu	P0A9K9	Ecoli_b3349	slyD	FKBP-type peptidyl-prolyl cis-trans isomerase SlyD (PPIase) (EC 5.2.1.8) (Histidine-rich protein) (Metallochaperone SlyD) (Rotamase) (Sensitivity to lysis protein D) (WHP)	374	0	0	0	0	0



MT	Cu	P0A9K9	Ecoli_b3349	slyD	FKBP-type peptidyl-prolyl cis-trans isomerase SlyD (PPIase) (EC 5.2.1.8) (Histidine-rich protein) (Metallochaperone SlyD) (Rotamase) (Sensitivity to lysis protein D) (WHP)	112	0	0	0	0	0
Hg(II)-acetate	Cu	P0A9K9	Ecoli_b3349	slyD	FKBP-type peptidyl-prolyl cis-trans isomerase SlyD (PPIase) (EC 5.2.1.8) (Histidine-rich protein) (Metallochaperone SlyD) (Rotamase) (Sensitivity to lysis protein D) (WHP)	176	0	0	0	0	0
PMA	Ni	P0A9K9	Ecoli_b3349	slyD	FKBP-type peptidyl-prolyl cis-trans isomerase SlyD (PPIase) (EC 5.2.1.8) (Histidine-rich protein) (Metallochaperone SlyD) (Rotamase) (Sensitivity to lysis protein D) (WHP)	374	0	0	0	0	0
MT	Ni	P0A9K9	Ecoli_b3349	slyD	FKBP-type peptidyl-prolyl cis-trans isomerase SlyD (PPIase) (EC 5.2.1.8) (Histidine-rich protein) (Metallochaperone SlyD) (Rotamase) (Sensitivity to lysis protein D) (WHP)	112	0	0	0	0	0
Hg(II)-acetate	Ni	P0A9K9	Ecoli_b3349	slyD	FKBP-type peptidyl-prolyl cis-trans isomerase SlyD (PPIase) (EC 5.2.1.8) (Histidine-rich protein) (Metallochaperone SlyD) (Rotamase) (Sensitivity to lysis protein D) (WHP)	176	0	0	0	0	0
PMA	Zn	P0A9K9	Ecoli_b3349	slyD	FKBP-type peptidyl-prolyl cis-trans isomerase SlyD (PPIase) (EC 5.2.1.8) (Histidine-rich protein) (Metallochaperone SlyD) (Rotamase) (Sensitivity to lysis protein D) (WHP)	374	0	0	0	0	0
MT	Zn	P0A9K9	Ecoli_b3349	slyD	FKBP-type peptidyl-prolyl cis-trans isomerase SlyD (PPIase) (EC 5.2.1.8) (Histidine-rich protein) (Metallochaperone SlyD) (Rotamase) (Sensitivity to lysis protein D) (WHP)	112	0	0	0	0	0
Hg(II)-acetate	Zn	P0A9K9	Ecoli_b3349	slyD	FKBP-type peptidyl-prolyl cis-trans isomerase SlyD (PPIase) (EC 5.2.1.8) (Histidine-rich protein) (Metallochaperone SlyD) (Rotamase) (Sensitivity to lysis protein D) (WHP)	176	0	0	0	0	0
PMA	Mn	P00448	Ecoli_b3908	sodA	Superoxide dismutase [Mn] (EC 1.15.1.1) (MnSOD)	1271	0	0	0	0	0
MT	Mn	P00448	Ecoli_b3908	sodA	Superoxide dismutase [Mn] (EC 1.15.1.1) (MnSOD)	159	0	0	0	0	0

Hg(II)-acetate	Mn	P00448	Ecoli_b3908	sodA	Superoxide dismutase [Mn] (EC 1.15.1.1) (MnSOD)	284	0	0	0	0	0
PMA	Mn	P60651	Ecoli_b2937	speB	Agmatinase (EC 3.5.3.11) (Agmatine ureohydrolase) (AUH)	118	2	2	0	0	0
MT	Mn	P60651	Ecoli_b2937	speB	Agmatinase (EC 3.5.3.11) (Agmatine ureohydrolase) (AUH)	20	0	0	0	0	0
Hg(II)-acetate	Mn	P60651	Ecoli_b2937	speB	Agmatinase (EC 3.5.3.11) (Agmatine ureohydrolase) (AUH)	14	0	0	0	0	0
PMA	Mn	P0A836	Ecoli_b0728	sucC	Succinyl-CoA ligase [ADP-forming] subunit beta (EC 6.2.1.5) (Succinyl-CoA synthetase subunit beta) (SCS-beta)	2371	381	163	29	7	0
MT	Mn	P0A836	Ecoli_b0728	sucC	Succinyl-CoA ligase [ADP-forming] subunit beta (EC 6.2.1.5) (Succinyl-CoA synthetase subunit beta) (SCS-beta)	639	124	70	0	0	0
Hg(II)-acetate	Mn	P0A836	Ecoli_b0728	sucC	Succinyl-CoA ligase [ADP-forming] subunit beta (EC 6.2.1.5) (Succinyl-CoA synthetase subunit beta) (SCS-beta)	699	185	147	0	0	0
PMA	Mn	P0A840	Ecoli_b2744	surE	5'/3'-nucleotidase SurE (EC 3.1.3.5) (EC 3.1.3.6) (Exopolyphosphatase) (EC 3.6.1.11) (Nucleoside monophosphate phosphohydrolase) (Stationary-phase survival protein SurE)	4	0	0	0	0	0
PMA	Zn	P0A8M3	Ecoli_b1719	thrS	Threonine--tRNA ligase (EC 6.1.1.3) (Threonyl-tRNA synthetase) (ThrRS)	737	131	86	27	0	0
MT	Zn	P0A8M3	Ecoli_b1719	thrS	Threonine--tRNA ligase (EC 6.1.1.3) (Threonyl-tRNA synthetase) (ThrRS)	108	51	49	0	0	0
Hg(II)-acetate	Zn	P0A8M3	Ecoli_b1719	thrS	Threonine--tRNA ligase (EC 6.1.1.3) (Threonyl-tRNA synthetase) (ThrRS)	310	74	74	0	0	0
PMA	Mn	P27302	Ecoli_b2935	tktA	Transketolase 1 (TK 1) (EC 2.2.1.1)	2431	90	73	0	0	0
MT	Mn	P27302	Ecoli_b2935	tktA	Transketolase 1 (TK 1) (EC 2.2.1.1)	563	38	38	0	0	0
Hg(II)-acetate	Mn	P27302	Ecoli_b2935	tktA	Transketolase 1 (TK 1) (EC 2.2.1.1)	1155	92	52	0	0	0
PMA	Zn	P0AGG4	Ecoli_b2582	trxC	Thioredoxin-2 (Trx-2) (EC 1.8.1.8) (Protein-disulfide reductase)	25	9	2	0	0	0
MT	Zn	P0AGG4	Ecoli_b2582	trxC	Thioredoxin-2 (Trx-2) (EC 1.8.1.8) (Protein-disulfide reductase)	3	3	3	0	0	0
Hg(II)-acetate	Zn	P0AGG4	Ecoli_b2582	trxC	Thioredoxin-2 (Trx-2) (EC 1.8.1.8) (Protein-disulfide reductase)	2	0	0	0	0	0
PMA	Zn	P0A6P1	Ecoli_b0170	tsf	Elongation factor Ts (EF-Ts) (Bacteriophage Q beta RNA-directed RNA polymerase subunit IV)	4318	91	79	0	0	0
MT	Zn	P0A6P1	Ecoli_b0170	tsf	Elongation factor Ts (EF-Ts) (Bacteriophage Q beta RNA-directed RNA polymerase	937	22	22	0	0	0

					subunit IV)						
Hg(II)-acetate	Zn	P0A6P1	Ecoli_b0170	tsf	Elongation factor Ts (EF-Ts) (Bacteriophage Q beta RNA-directed RNA polymerase subunit IV)	2073	97	49	0	0	0
PMA	Zn	P0A698	Ecoli_b4058	uvrA	UvrABC system protein A (UvrA protein) (Excinuclease ABC subunit A)	21	2	2	0	0	0
MT	Zn	P0A698	Ecoli_b4058	uvrA	UvrABC system protein A (UvrA protein) (Excinuclease ABC subunit A)	7	0	0	0	0	0
Hg(II)-acetate	Zn	P0A698	Ecoli_b4058	uvrA	UvrABC system protein A (UvrA protein) (Excinuclease ABC subunit A)	7	0	0	0	0	0
PMA	Zn	P0A8H8	Ecoli_b0101	yacG	DNA gyrase inhibitor YacG	28	28	23	5	0	0
MT	Zn	P0A8H8	Ecoli_b0101	yacG	DNA gyrase inhibitor YacG	9	9	9	0	0	0
PMA	Zn	P75691	Ecoli_b0325	yahK	Aldehyde reductase YahK (EC 1.1.1.2) (Zinc-dependent alcohol dehydrogenase YahK)	77	0	0	0	0	0
MT	Zn	P75691	Ecoli_b0325	yahK	Aldehyde reductase YahK (EC 1.1.1.2) (Zinc-dependent alcohol dehydrogenase YahK)	11	0	0	0	0	0
Hg(II)-acetate	Zn	P75691	Ecoli_b0325	yahK	Aldehyde reductase YahK (EC 1.1.1.2) (Zinc-dependent alcohol dehydrogenase YahK)	27	0	0	0	0	0
PMA	Ni	P0A898	Ecoli_b0659	ybeY	Endoribonuclease YbeY (EC 3.1.-.-)	37	23	23	0	0	0
PMA	Zn	P0A898	Ecoli_b0659	ybeY	Endoribonuclease YbeY (EC 3.1.-.-)	37	23	23	0	0	0
PMA	Zn	P75914	Ecoli_b1034	ycdX	Probable phosphatase YcdX (EC 3.1.3.-)	55	0	0	0	0	0
MT	Zn	P75914	Ecoli_b1034	ycdX	Probable phosphatase YcdX (EC 3.1.3.-)	4	0	0	0	0	0
Hg(II)-acetate	Zn	P75914	Ecoli_b1034	ycdX	Probable phosphatase YcdX (EC 3.1.3.-)	6	0	0	0	0	0
PMA	Zn	P33030	Ecoli_b2173	yeiR	Uncharacterized protein YeiR	1	0	0	0	0	0
PMA	Co	P76491	Ecoli_b2291	yfbR	5'-deoxynucleotidase YfbR (EC 3.1.3.89) (5'-deoxyribonucleotidase) (Nucleoside 5'-monophosphate phosphohydrolase)	42	0	0	0	0	0
PMA	Co	P77625	Ecoli_b2293	yfbT	Sugar phosphatase YfbT (EC 3.1.3.23)	111	0	0	0	0	0
MT	Co	P77625	Ecoli_b2293	yfbT	Sugar phosphatase YfbT (EC 3.1.3.23)	6	0	0	0	0	0
Hg(II)-acetate	Co	P77625	Ecoli_b2293	yfbT	Sugar phosphatase YfbT (EC 3.1.3.23)	4	0	0	0	0	0
PMA	Mn	P77625	Ecoli_b2293	yfbT	Sugar phosphatase YfbT (EC 3.1.3.23)	111	0	0	0	0	0
MT	Mn	P77625	Ecoli_b2293	yfbT	Sugar phosphatase YfbT (EC 3.1.3.23)	6	0	0	0	0	0
Hg(II)-	Mn	P77625	Ecoli_b2293	yfbT	Sugar phosphatase YfbT (EC 3.1.3.23)	4	0	0	0	0	0

acetate											
PMA	Zn	P67095	Ecoli_b2300	yfcE	Phosphodiesterase YfcE (EC 3.1.4.-)	71	14	12	2	0	0
MT	Zn	P67095	Ecoli_b2300	yfcE	Phosphodiesterase YfcE (EC 3.1.4.-)	35	6	6	0	0	0
Hg(II)-acetate	Zn	P67095	Ecoli_b2300	yfcE	Phosphodiesterase YfcE (EC 3.1.4.-)	17	15	15	0	0	0
PMA	Cu	P33644	Ecoli_b2593	yfiH	Laccase domain protein YfiH	24	7	0	0	0	0
PMA	Mn	P31467	Ecoli_b3715	yieH	6-phosphogluconate phosphatase (EC 3.1.3.-)	2	2	2	0	0	0
PMA	Mn	P0A8Y3	Ecoli_b3885	yihX	Alpha-D-glucose 1-phosphate phosphatase YihX (Alpha-D-glucose-1-P phosphatase) (EC 3.1.3.10) (Alpha-D-glucose-1-phosphatase) (Haloacid dehalogenase-like phosphatase 4) (HAD4)	55	0	0	0	0	0
MT	Mn	P0A8Y3	Ecoli_b3885	yihX	Alpha-D-glucose 1-phosphate phosphatase YihX (Alpha-D-glucose-1-P phosphatase) (EC 3.1.3.10) (Alpha-D-glucose-1-phosphatase) (Haloacid dehalogenase-like phosphatase 4) (HAD4)	5	0	0	0	0	0
Hg(II)-acetate	Mn	P0A8Y3	Ecoli_b3885	yihX	Alpha-D-glucose 1-phosphate phosphatase YihX (Alpha-D-glucose-1-P phosphatase) (EC 3.1.3.10) (Alpha-D-glucose-1-phosphatase) (Haloacid dehalogenase-like phosphatase 4) (HAD4)	2	0	0	0	0	0
PMA	Mn	P0A8Y1	Ecoli_b4374	yjjG	Pyrimidine 5'-nucleotidase YjjG (EC 3.1.3.5) (House-cleaning nucleotidase) (Non-canonical pyrimidine nucleotide phosphatase) (Nucleoside 5'-monophosphate phosphohydrolase) (dUMP phosphatase)	5	2	2	0	0	0
PMA	Cu	P0AA57	Ecoli_b1841	yobA	Protein YobA	101	0	0	0	0	0
MT	Cu	P0AA57	Ecoli_b1841	yobA	Protein YobA	19	0	0	0	0	0
Hg(II)-acetate	Cu	P0AA57	Ecoli_b1841	yobA	Protein YobA	43	0	0	0	0	0
PMA	Zn	Q46856	Ecoli_b3011	yqhD	Alcohol dehydrogenase YqhD (EC 1.1.1.-)	82	0	0	0	0	0
MT	Zn	Q46856	Ecoli_b3011	yqhD	Alcohol dehydrogenase YqhD (EC 1.1.1.-)	29	0	0	0	0	0
Hg(II)-acetate	Zn	Q46856	Ecoli_b3011	yqhD	Alcohol dehydrogenase YqhD (EC 1.1.1.-)	71	0	0	0	0	0
PMA	Zn	P0A9W9	Ecoli_b3279	yrdA	Protein YrdA	135	0	0	0	0	0
MT	Zn	P0A9W9	Ecoli_b3279	yrdA	Protein YrdA	10	0	0	0	0	0
Hg(II)-	Zn	P0A9W9	Ecoli_b3279	yrdA	Protein YrdA	13	0	0	0	0	0

acetate											
PMA	Zn	P45771	Ecoli_b3283	yrdD	Uncharacterized protein YrdD	1	0	0	0	0	0
PMA	Zn	P76344	Ecoli_b1973	zinT	Metal-binding protein ZinT (Cadmium-induced protein ZinT)	714	0	0	0	0	0
Hg(II)-acetate	Zn	P76344	Ecoli_b1973	zinT	Metal-binding protein ZinT (Cadmium-induced protein ZinT)	310	0	0	0	0	0

\* data in table sorted by gene\_name and grouped by mercury exposure condition dataset

\* bold colored rows indicate mercury modification of cysteine residue(s) within protein and lighter colors cells color code the dataset (PMA=red, Merthiolate(MT)=purple, and Hg(II)-acetate=blue)

\* gene names highlighted in green are proteins that GO annotated to bind more than one metal

\* cells highlighted in orange show mercury modified peptides with only a single observed spectrum

### Summary:

Cobalt (Co) binding proteins (GO:0050897): observed 8 of 9 (89%) and 1 had PhHg adducts with  $\geq 2$  spectra (14.3%)

Copper (Cu) binding proteins (GO:0005507): observed 10 of 16 (63%) and 1 had PhHg adducts with  $\geq 2$  spectra (10%)

Manganese (Mn) binding proteins (GO:0030145): observed 32 of 56 (57%) and 5 unique proteins had PhHg adducts with  $\geq 2$  spectra (15.6%)

Nickel (Ni) binding proteins (GO:0016151): observed 5 of 17 (29%) and none had mercurial adducts (0%)

Zinc (Zn) binding proteins (GO:0008270): observed 91 of 152 (60%). 25 had PhHg adducts, 3 had EtHg adducts, and 4 had Hg(II) adducts with  $\geq 2$  spectra (27 unique proteins = 35.2%)

**Table B.S9. EXAFS fit data summary.**

Column 1, Figure number in this work. Column 2, Sample Description. Column 3, Shell is the chemical unit defined for the multiple scattering calculation; subscripts denote the number of scatterers per metal atom. Column 4,  $R_{as}$  is the metal-scatterer distance. Column 5,  $\sigma_{as}^2$ , is the mean square deviation in  $R_{as}$  aka Debye-Waller factor. Column 6,  $f$ , is a normalized error (chi-squared) as follows:

$$f = \frac{\left\{ \sum_i \left[ k^3 (\chi_i^{obs} - \chi_i^{calc}) \right]^2 / N \right\}^{1/2}}{\left[ (k^3 \chi^{obs})_{max} - (k^3 \chi^{obs})_{min} \right]}$$

Figure #	Sample Description	Shell	$R_{as}$ (Å)	$\sigma_{as}^2$ (Å <sup>2</sup> )	$f$
4	1mM HgCl <sub>2</sub>	Hg-Cl <sub>2</sub>	2.31	0.0021	0.064
4	MG + 10μM HgCl <sub>2</sub>	Hg-S <sub>2</sub>	2.34	0.0027	0.122
4	MG + 20μM HgCl <sub>2</sub>	Hg-S <sub>2</sub>	2.34	0.0021	0.072
4	MG + 40μM HgCl <sub>2</sub>	Hg-S 1.37 Hg-N 0.63	2.32 2.04	0.0035 0.0025	0.079
4	MG + 80μM HgCl <sub>2</sub>	Hg-S 1.78 Hg-N 0.22	2.34 2.07	0.0064 0.0025	0.106

Figure #	Sample Description	Shell	$R_{as}$ (Å)	$\sigma_{as}^2$ (Å <sup>2</sup> )	$f$
S3	1mM HgCl <sub>2</sub>	Hg-Cl <sub>2</sub>	2.31	0.0021	0.064
S3	1mM HgCl <sub>2</sub> + 10mM GSH	Hg-S <sub>2</sub>	2.34	0.0025	0.099
S3	1mM HgBr <sub>2</sub>	Hg-Br <sub>2</sub>	2.46	0.0031	0.110
S3	1mM HgBr <sub>2</sub> + 10mM GSH	Hg-S <sub>2</sub>	2.34	0.0026	0.101

Figure #	Sample Description	Shell	$R_{as}$ (Å)	$\sigma_{as}^2$ (Å <sup>2</sup> )	$f$
S4	1mM Hg(II)-acetate	Hg-O <sub>2</sub>	2.09	0.0074	0.130
S4	1mM Hg(II)-acetate + 10mM GSH	Hg-S <sub>2</sub>	2.34	0.0018	0.065

Figure #	Sample Description	Shell	$R_{as}$ (Å)	$\sigma_{as}^2$ (Å <sup>2</sup> )	$f$
S5	1mM MT + 20mM imidazole	Hg-S <sub>1</sub> Hg-C <sub>1</sub>	2.37 2.08	0.0019 0.0012	0.085
S5	1mM PMA + 20mM imidazole	Hg-C <sub>1</sub> Hg-N <sub>1</sub>	2.05 2.03	0.0018 0.0025	0.122
S5	1mM HgCl <sub>2</sub> + 20mM imidazole	Hg-N <sub>2</sub>	2.05	0.0016	0.134

Figure #	Sample Description	Shell	$R_{as}$ (Å)	$\sigma_{as}^2$ (Å <sup>2</sup> )	$f$
S6	4mM PMA	Hg-C1	2.06	0.0011	0.108
		Hg-O1	2.04	0.0064	
S6	1mM PMA + 10mM GSH	Hg-C1	2.05	0.0008	0.089
		Hg-S1	2.34	0.0018	
S6	MG + 40μM PMA	Hg-C1	2.05	0.0007	0.080
		Hg-S1	2.32	0.0016	
S6	MG + 80μM PMA	Hg-C1	2.07	0.0007	0.094
		Hg-S1	2.34	0.0011	

Figure #	Sample Description	Shell	$R_{as}$ (Å)	$\sigma_{as}^2$ (Å <sup>2</sup> )	$f$
S7	16mM MT	Hg-C1	2.07	0.0011	0.100
		Hg-S1	2.37	0.0017	
S7	1mM MT + 10mM GSH	Hg-C1	2.07	0.0007	0.070
		Hg-S1	2.35	0.0014	
S7	MG + 160μM MT	Hg-C1	2.10	0.0024	0.094
		Hg-S1	2.36	0.0026	

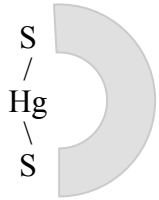
**APPENDIX C**  
**CHAPTER 3 SUPPLEMENTAL MATERIAL<sup>1</sup>**

---

<sup>1</sup>ZINK, E.M., LAVOIE, S.P., POLACCO, B.P., PURVINE, S.O., MILLER, S.M., LIPTON, M.S., SUMMERS, A.O.; Co-first author. To be submitted to *Metallomics*.



**Table C.S1. Formation constants of mercurial complexes**

Compound	Formation Constant	Reference
$\text{Hg}(\text{NO}_3)_2$	1.6	(Waki and Fritz, 1966)
$\text{Hg}(\text{OAc})_2$	8.4	(Ravichandran, 2004)
$\text{HgCl}_2$	14	(Ravichandran, 2004)
$\text{HgBr}_2$	17.3	(Ravichandran, 2004)
$\text{HgI}_2$	23.8	(Nagypal and Beck, 1982)
$\text{Hg}(\text{SR})_2$	35-40	(Van Der Linden and Beers, 1974, Oram et al., 1996)
MethylHgCl	5.25	(Baughman et al., 1973)
EthylHgCl	5.43	(Sugimoto et al., 1984)
PhenylHgCl	5.77	(Starý et al., 1978)
MethylHg-cysteine	15.7	(Baughman et al., 1973)
EthylHg-cysteine EthylHg-thiosalicylate	None published	None published
PhenylHg-glutathione PhenylHg-cysteine	7.09 4.77	(Hojo et al., 1976)
$\text{Hg}(\text{SeR})_2$	45	(Dyrssen and Wedborg, 1991)
 Bis-thiol Chelate	35-44	(Casas and Jones, 1980)

**Table C.S2. Data summary of cysteine modifications by condition for Figure 2.** Values in table represent spectral count observations for each modification type from *in vivo* phenylmercuric-acetate (PMA) exposure or no-mercury conditions and *in vitro* iodoacetamide (IAM) conditions.

Adducts by Condition	-SH	-S-CAM	-S-Hg-phenyl	-S-Hg	-S-Hg-S-
0 IAM, 0 PMA	1,737	0	0	0	0
0 IAM, 40 $\mu$ M PMA	1,747	0	2,764	133	306
10 $\mu$ M IAM, 0 $\mu$ M PMA	1,240	12,757	0	0	0
10 $\mu$ M IAM, 40 $\mu$ M PMA	1,552	1,302	2,195	108	261
20 $\mu$ M IAM, 0 $\mu$ M PMA	1,211	14,255	0	0	0
20 $\mu$ M IAM, 40 $\mu$ M PMA	1,652	2,305	1,778	160	300

**Table C.S3. Reactive Cysteine Sites in *E. coli* from Weerapana et al 2010 observed with Mercury Modifications.**

Weerapana Ratio	Reference	Cys Site	Gene Name	IAM condition	Total count	CAM count	PMA count	HgII count	Chelate count	Description
6.22	Ecoli_b2779	247	eno	0	91	null	61	8	null	Enolase; phosphoprotein; component of RNA degradosome
6.22	Ecoli_b2779	247	eno	10mM	90	20	49	7	null	Enolase; phosphoprotein; component of RNA degradosome
6.22	Ecoli_b2779	247	eno	20mM	96	38	35	8	null	Enolase; phosphoprotein; component of RNA degradosome
5.98	Ecoli_b3251	113	mreB	0	3	null	3	null	null	Cell wall structural actin-like protein in MreBCD complex
5.98	Ecoli_b3251	113	mreB	10mM	3	1	2	null	null	Cell wall structural actin-like protein in MreBCD complex
5.59	<a href="#">Ecoli_b3339</a>	138	tufA	0	108	null	99	null	null	EF-Tu, Elongation Factor-Translation
5.59	<a href="#">Ecoli_b3339</a>	138	tufA	10mM	64	30	31	1	null	EF-Tu, Elongation Factor-Translation
5.59	<a href="#">Ecoli_b3339</a>	138	tufA	20mM	78	32	37	3	null	EF-Tu, Elongation Factor-Translation
5.58	Ecoli_b1779	150	gapA	0	88	null	null	68	75	Glyceraldehyde 3-P dehydrogenase A
5.58	Ecoli_b1779	150	gapA	10mM	88	21	2	54	60	Glyceraldehyde 3-P dehydrogenase A
5.58	Ecoli_b1779	150	gapA	20mM	77	26	4	36	43	Glyceraldehyde 3-P dehydrogenase A
5.03	Ecoli_b3251	324	mreB	0	10	null	10	null	null	Cell wall structural actin-like protein in MreBCD complex
5.03	Ecoli_b3251	324	mreB	10mM	11	1	9	1	null	Cell wall structural actin-like protein in MreBCD complex
5.03	Ecoli_b3251	324	mreB	20mM	8	3	4	null	null	Cell wall structural actin-like protein in MreBCD complex
4.95	Ecoli_b3310	84	rplN	0	11	null	10	null	null	50S ribosomal subunit protein L14
4.95	Ecoli_b3310	84	rplN	10mM	14	1	12	null	null	50S ribosomal subunit protein L14
4.95	Ecoli_b3310	84	rplN	20mM	14	null	12	null	null	50S ribosomal subunit protein L14
4.94	<a href="#">Ecoli_b4015</a>	245	aceA	0	12	null	12	null	null	Isocitrate lyase, acetate utilization, glyoxylate shunt; tetrameric
4.94	<a href="#">Ecoli_b4015</a>	245	aceA	10mM	11	null	11	null	null	Isocitrate lyase, acetate utilization, glyoxylate shunt; tetrameric
4.94	<a href="#">Ecoli_b4015</a>	245	aceA	20mM	18	3	15	null	null	Isocitrate lyase, acetate utilization, glyoxylate shunt; tetrameric
4.68	Ecoli_b3342	27	rpsL	0	8	null	8	null	null	30S ribosomal subunit protein S12; RNA chaperone

4.68	Ecoli_b3342	27	rpsL	10mM	18	6	9	null	null	30S ribosomal subunit protein S12; RNA chaperone
4.68	Ecoli_b3342	27	rpsL	20mM	9	8	1	null	null	30S ribosomal subunit protein S12; RNA chaperone
4.64	Ecoli_b2752	251	cysD	0	6	null	6	null	null	Sulfate adenylyltransferase subunit 2
4.64	Ecoli_b2752	251	cysD	10mM	11	8	2	null	null	Sulfate adenylyltransferase subunit 2
4.64	Ecoli_b2752	251	cysD	20mM	20	18	1	1	null	Sulfate adenylyltransferase subunit 2
4.57	Ecoli_b3985	71	rplJ	0	82	null	73	null	null	50S ribosomal subunit protein L10; streptomycin resistance
4.57	Ecoli_b3985	71	rplJ	10mM	102	55	43	null	null	50S ribosomal subunit protein L10; streptomycin resistance
4.57	Ecoli_b3985	71	rplJ	20mM	94	54	30	null	null	50S ribosomal subunit protein L10; streptomycin resistance
4.18	<a href="#">Ecoli_b4015</a>	43	aceA	0	5	null	4	null	null	Isocitrate lyase, acetate utilization, glyoxylate shunt; tetrameric
4.18	<a href="#">Ecoli_b4015</a>	43	aceA	10mM	18	11	6	null	null	Isocitrate lyase, acetate utilization, glyoxylate shunt; tetrameric
4.18	<a href="#">Ecoli_b4015</a>	43	aceA	20mM	9	8	1	null	null	Isocitrate lyase, acetate utilization, glyoxylate shunt; tetrameric
4.01	<a href="#">Ecoli_b0720</a>	207	gltA	0	14	null	11	1	null	Citrate synthase; hexameric
4.01	<a href="#">Ecoli_b0720</a>	207	gltA	10mM	28	14	9	null	null	Citrate synthase; hexameric
4.01	<a href="#">Ecoli_b0720</a>	207	gltA	20mM	42	22	5	2	null	Citrate synthase; hexameric
4.00	Ecoli_b0169	87	rpsB	0	53	1	50	null	null	30S ribosomal subunit protein S2; binds Zn(II)
4.00	Ecoli_b0169	87	rpsB	10mM	44	9	35	null	null	30S ribosomal subunit protein S2; binds Zn(II)
4.00	Ecoli_b0169	87	rpsB	20mM	59	10	42	null	null	30S ribosomal subunit protein S2; binds Zn(II)
3.37	<a href="#">Ecoli_b4015</a>	288	aceA	0	23	null	22	null	null	Isocitrate lyase, acetate utilization, glyoxylate shunt; tetrameric
3.37	<a href="#">Ecoli_b4015</a>	288	aceA	10mM	24	null	22	null	null	Isocitrate lyase, acetate utilization, glyoxylate shunt; tetrameric
3.37	<a href="#">Ecoli_b4015</a>	288	aceA	20mM	22	null	21	null	null	Isocitrate lyase, acetate utilization, glyoxylate shunt; tetrameric
2.15	Ecoli_b1324	61	tpx	0	122	null	77	6	null	Lipid hydroperoxide peroxidase; thiol peroxidase
2.15	Ecoli_b1324	61	tpx	10mM	176	52	83	3	null	Lipid hydroperoxide peroxidase; thiol

										peroxidase
2.15	Ecoli_b1324	61	tpx	20mM	166	60	61	5	null	Lipid hydroperoxide peroxidase; thiol peroxidase
1.52	Ecoli_b3781	33	trxA	0	14	null	null	13	14	Thioredoxin 1; Trx; with TrxB
1.52	Ecoli_b3781	33	trxA	10mM	7	null	null	6	7	Thioredoxin 1; Trx; with TrxB
1.52	Ecoli_b3781	33	trxA	20mM	4	null	null	4	4	Thioredoxin 1; Trx; with TrxB

- 13 distinct proteins and 16 cysteine sites sorted by Weerapana et al 2010 reactivity ratio
- gene Reference numbers in blue are proteins with more than one cysteine site observed
- cell colors have no meaning, just alternating colors serve to group each gene as a visual aid

**Table C.S4. Observed *E. coli* proteins for each COG category.**

Encoded Proteins	Observed Proteins <sup>a</sup>	% coverage	COG Code	COG Functional Categories
<b>Information storage and processing</b>				
182	147	80.8	J	Translation, ribosome structure and biogenesis
301	97	32.2	K	Transcription
200	66	33	L	Replication, recombination and repair
2	1	50	A	RNA processing and modification
<b>Cellular processing and signaling</b>				
33	20	60.6	D	Cell cycle control, cell division, chromosome partitioning
49	17	34.7	V	Defense mechanisms
178	70	39.3	T	Signal transduction and mechanisms
226	104	46	M	Cell wall/membrane/envelope biogenesis
111	36	32.4	N	Cell motility
124	32	25.8	U	Intracellular trafficking, secretion, and vesicular transport
138	86	62.3	O	Posttranslational modification, protein turnover, chaperones
<b>Metabolism</b>				
287	104	36.2	C	Energy production and conversion
368	109	29.6	G	Carbohydrate transport and metabolism
363	190	52.3	E	Amino acid transport and metabolism
97	62	63.9	F	Nucleotide transport and metabolism
153	92	60.1	H	Coenzyme transport and metabolism
100	33	33	I	Lipid transport and metabolism
217	70	32.3	P	Inorganic ion transport and metabolism
64	20	31.3	Q	Secondary metabolites biosynthesis, transport and metabolism
<b>Poorly characterized</b>				
394	146	37.1	R	General function prediction only
318	109	34.3	S	Function unknown

<sup>a</sup> Observed proteins based on 1,560 total proteins from all conditions, but note that COGs contains 3,905 annotations for only 3,497 proteins, so 408 have more than one function.

**Table C.S5. *E. coli* protein homologs to human proteins with sequence identity > 50%<sup>a</sup>.**

IMG Reference ID	Reference Gene Name	Reference Gene ID	Reference Coordinates	Reference Genome	Query Gene ID	Query Gene Name	Query Locus Tag	Query Coordinates	Query Genome	% Identity	Bit Score	E-value
646311907	transaldolase B	b0008	1, 313	Escherichia coli K-12, MG1655	639360175	transaldolase 1	TALD O1	11, 326	Homo sapiens	60	372.9	0
646311912	chaperone Hsp70, co-chaperone with DnaJ	b0014	2, 624	Escherichia coli K-12, MG1655	639343228	heat shock 70kDa protein 9 (mortalin)	HSPA 9	53, 673	Homo sapiens	60.2	743.8	0
646311913	chaperone Hsp40, co-chaperone with DnaK	b0015	7, 70	Escherichia coli K-12, MG1655	639368774	DnaJ (Hsp40) homolog, subfamily C, member 5 beta	DNAJ C5B	21, 84	Homo sapiens	54.7	79	4.50 E-13
646312002	GMP reductase	b0104	3, 345	Escherichia coli K-12, MG1655	639350589	guanosine monophosphate reductase 2	GMP R2	22, 363	Homo sapiens	69.1	492.7	0
646312131	DNA polymerase IV	b0231	4, 110	Escherichia coli K-12, MG1655	639350692	polymerase (DNA directed) kappa	POLK	103, 205	Homo sapiens	51.4	118.2	6.30 E-25
646312222	betaine aldehyde dehydrogenase, NAD-dependent	b0312	4, 490	Escherichia coli K-12, MG1655	639337879	aldehyde dehydrogenase 9 family, member A1	ALDH 9A1	31, 518	Homo sapiens	51.7	498	0
646312228	ankyrin repeat protein	b0318	159, 200	Escherichia coli K-12, MG1655	639339490	HECT domain containing 1	HECT D1	442, 483	Homo sapiens	50	47	0.001
646312264	alcohol dehydrogenase class III/glutathione-dependent	b0356	1, 368	Escherichia coli K-12, MG1655	639334389	alcohol dehydrogenase 5 (class III), chi polypeptide	ADH5	6, 373	Homo sapiens	62.5	488	0

	formaldehyde dehydrogenase											
646312341	proteolytic subunit of ClpA-ClpP and ClpX-ClpP ATP-dependent serine proteases	b0437	14, 205	Escherichia coli K-12, MG1655	639367556	ClpP caseinolytic peptidase, ATP-dependent, proteolytic subunit homolog (E. coli)	CLPP	56, 247	Homo sapiens	56.2	232.3	0
646312378	adenylate kinase	b0474	1, 184	Escherichia coli K-12, MG1655	639337370	adenylate kinase 2	AK2	16, 203	Homo sapiens	53.7	204.9	0
646312587	glucosamine-6-phosphate deaminase	b0678	1, 258	Escherichia coli K-12, MG1655	639332113	glucosamine-6-phosphate deaminase 1	GNPD A1	1, 258	Homo sapiens	59.7	324.7	0
646312635	succinate dehydrogenase, flavoprotein subunit	b0723	7, 551	Escherichia coli K-12, MG1655	639354912	succinate dehydrogenase complex, subunit A, flavoprotein (Fp)	SDHA	61, 603	Homo sapiens	55.9	578.9	0
646312636	succinate dehydrogenase, FeS subunit	b0724	4, 233	Escherichia coli K-12, MG1655	639354922	succinate dehydrogenase complex, subunit B, iron sulfur (Ip)	SDHB	41, 270	Homo sapiens	55.6	261.5	0
646312638	dihydrolipoyl transsuccinase	b0727	154, 405	Escherichia coli K-12, MG1655	639336774	dihydrolipoamide S-succinyltransferase (E2 component of 2-oxoglutarate complex)	DLST	198, 453	Homo sapiens	57	287.7	0



646312640	succinyl-CoA synthetase, NAD(P)-binding, alpha subunit	b0729	3, 284	Escherichia coli K-12, MG1655	639369029	succinate-CoA ligase, GDP-forming, alpha subunit	SUCLG1	50, 336	Homo sapiens	66.9	387.5	0
646312667	phosphoglyceromutase 1	b0755	1, 250	Escherichia coli K-12, MG1655	639355570	similar to Phosphoglycerate mutase 1 (Phosphoglycerate mutase isozyme B) (PGAM-B) (BPG-dependent PGAM 1)	LOC642969	1, 253	Homo sapiens	58.5	308.1	0
646312670	galactose-1-phosphate uridylyltransferase	b0758	4, 343	Escherichia coli K-12, MG1655	639339563	galactose-1-phosphate uridylyltransferase	GALT	24, 366	Homo sapiens	56.6	422.5	0
646312671	UDP-galactose-4-epimerase	b0759	2, 336	Escherichia coli K-12, MG1655	639339477	UDP-galactose-4-epimerase	GALE	4, 344	Homo sapiens	52.8	369.4	0
646312829	fused lipid transporter subunits of ABC superfamily: membrane component/ATP-binding component	b0914	401, 575	Escherichia coli K-12, MG1655	639343660	ATP-binding cassette, subfamily B (MDR/TAP), member 5	ABCB5	1, 174	Homo sapiens	50.3	173.3	2.70 E-41
646313202	aconitate hydratase 1	b1276	37, 891	Escherichia coli K-12, MG1655	639349745	aconitase 1, soluble	ACO1	34, 889	Homo sapiens	52.9	898.7	0
646313265	O-6-alkylguanine-DNA:cysteine-protein	b1335	89, 170	Escherichia coli K-12, MG1655	639348153	O-6-methylguanine-DNA methyltransferase	RP11-109A6.1	94, 176	Homo sapiens	50.6	89.4	1.50 E-16

	methyltransferase					rase						
646313386	predicted NADP-dependent, Zn-dependent oxidoreductase	b1449	252, 329	Escherichia coli K-12, MG1655	639359201	hypothetical protein LOC652825	LOC652825	15, 92	Homo sapiens	51.3	89.7	2.30 E-16
646313542	pyridine nucleotide transhydrogenase, beta subunit	b1602	10, 458	Escherichia coli K-12, MG1655	639338608	nicotinamide nucleotide transhydrogenase	NNT	624, 1076	Homo sapiens	52	454.5	0
646313543	pyridine nucleotide transhydrogenase, alpha subunit	b1603	1, 509	Escherichia coli K-12, MG1655	639338608	nicotinamide nucleotide transhydrogenase	NNT	57, 587	Homo sapiens	50.9	485	0
646313551	fumarate hydratase (fumarase C), aerobic Class II	b1611	237, 460	Escherichia coli K-12, MG1655	639343776	similar to Fumarate hydratase, mitochondrial precursor (Fumarase)	LOC341651	14, 237	Homo sapiens	61.2	270.8	0
646313624	component of SufBCD complex, ATP-binding component of ABC superfamily	b1682	13, 60	Escherichia coli K-12, MG1655	639360179	transporter 2, ATP-binding cassette, sub-family B (MDR/TAP)	DAQB-69D7.2	482, 527	Homo sapiens	52.1	52.8	2.30 E-05
646313722	methionine sulfoxide reductase B	b1778	6, 137	Escherichia coli K-12, MG1655	639339168	methionine sulfoxide reductase B3	MSRB3	46, 177	Homo sapiens	50	160.6	4.30 E-38
646313723	glyceraldehyde-3-phosphate dehydrogenase A	b1779	3, 330	Escherichia coli K-12, MG1655	639339628	glyceraldehyde-3-phosphate dehydrogenase	GAPDH	4, 332	Homo sapiens	66.1	444.5	0

646313982	6-phosphoglucose dehydrogenase, decarboxylating	b2029	1,466	Escherichia coli K-12, MG1655	639350979	phosphoglucose dehydrogenase	PGD	1,469	Homo sapiens	54.2	503.1	0
646314006	GDP-D-mannose dehydratase, NAD(P)-binding	b2053	4,352	Escherichia coli K-12, MG1655	639340628	GDP-mannose 4,6-dehydratase	RP1-118B18.1	25,364	Homo sapiens	60	428.3	0
646314110	S-formylglutathione hydrolase	b2154	1,276	Escherichia coli K-12, MG1655	639337457	esterase D/formylglutathione hydrolase	ESD	3,280	Homo sapiens	52.7	303.1	0
646314182	acetyl-CoA acetyltransferase	b2224	5,392	Escherichia coli K-12, MG1655	639345877	acetyl-Coenzyme A acetyltransferase 2 (acetoacetyl Coenzyme A thiolase)	ACAT2	9,396	Homo sapiens	53.6	390.2	0
646314247	NADH:ubiquinone oxidoreductase, chain B	b2287	39,185	Escherichia coli K-12, MG1655	639344770	NADH dehydrogenase (ubiquinone) Fe-S protein 7, 20kDa (NADH-coenzyme Q reductase)	NDUF S7	64,210	Homo sapiens	54.1	176	1.60 E-42
646314333	predicted CoA-transferase, NAD(P)-binding	b2371	9,80	Escherichia coli K-12, MG1655	639366670	chromosome 7 open reading frame 10	C7orf10	47,119	Homo sapiens	50.7	79.7	2.70 E-13
646314427	transaldolase A	b2464	4,316	Escherichia coli K-12,	639360175	transaldolase 1	TALD O1	15,330	Homo sapiens	59.3	358.2	0

				MG1655								
64631449 5	iron-sulfur cluster assembly scaffold protein	b2529	3, 128	Escherichi a coli K- 12, MG1655	6393385 64	IscU iron- sulfur cluster scaffold homolog (E. coli)	ISCU	35, 160	Homo sapiens	75.4	200.7	0
64631449 6	cysteine desulfurase (tRNA sulfurtransfer ase), PLP- dependent	b2530	4, 404	Escherichi a coli K- 12, MG1655	6393693 85	NFS1 nitrogen fixation 1 homolog (S. cerevisiae)	NFS1	58, 457	Homo sapiens	60.2	514.2	0
64631454 9	uracil-DNA- glycosylase	b2580	6, 220	Escherichi a coli K- 12, MG1655	6393655 78	uracil-DNA glycosylase	UNG	97, 310	Homo sapiens	57.7	260.4	0
64631462 3	succinate- semialdehyde dehydrogenas e I, NADP- dependent	b2661	8, 481	Escherichi a coli K- 12, MG1655	6393663 06	aldehyde dehydrogenas e 5 family, member A1 (succinate- semialdehyde dehydrogenas e)	ALDH 5A1	58, 546	Homo sapiens	54.2	533.1	0
64631471 2	adenosine 5'- phosphosulfat e kinase	b2750	7, 199	Escherichi a coli K- 12, MG1655	6393694 00	3'- phosphoadeno sine 5'- phosphosulfat e synthase 1	PAPS S1	27, 226	Homo sapiens	51.2	194.1	0
64631474 2	enolase	b2779	6, 426	Escherichi a coli K- 12, MG1655	6393373 12	enolase 3 (beta, muscle)	ENO3	5, 427	Homo sapiens	56.1	440.3	0
64631479 2	thymidylate synthetase	b2827	3, 264	Escherichi a coli K- 12, MG1655	6393629 08	thymidylate synthetase	TYMS	32, 313	Homo sapiens	51.4	287	0
64631486 9	glycine decarboxylase	b2903	14, 957	Escherichi a coli K-	6393405 48	glycine dehydrogenas	GLDC	63, 1009	Homo sapiens	53.4	1003. 4	0

	, PLP-dependent, subunit (protein P) of glycine cleavage complex			12, MG1655		e (decarboxylating)						
646314885	methylmalonyl-CoA mutase	b2917	6, 711	Escherichia coli K-12, MG1655	639349383	methylmalonyl Coenzyme A mutase	MUT	42, 741	Homo sapiens	59.3	835.9	0
646314908	S-adenosylmethionine synthetase	b2942	5, 369	Escherichia coli K-12, MG1655	639347984	methionine adenosyltransferase I, alpha	MAT1A	19, 388	Homo sapiens	58.5	426.4	0
646315143	protease, ATP-dependent zinc-metallo	b3178	146, 589	Escherichia coli K-12, MG1655	639332811	YME1-like 1 (S. cerevisiae)	YME1L1	332, 761	Homo sapiens	50.8	434.9	0
646315202	malate dehydrogenase, NAD(P)-binding	b3236	2, 310	Escherichia coli K-12, MG1655	639348093	malate dehydrogenase 2, NAD (mitochondrial)	MDH2	26, 334	Homo sapiens	58.5	338.6	0
646315305	protein chain elongation factor EF-Tu (duplicate of tufB)	b3339	2, 393	Escherichia coli K-12, MG1655	639361520	Tu translation elongation factor, mitochondrial	TUFM	50, 443	Homo sapiens	56.3	469.5	0
646315393	glycogen phosphorylase	b3428	13, 812	Escherichia coli K-12, MG1655	639354018	phosphorylase, glycogen; liver (Hers disease, glycogen storage disease type VI)	PYGL	24, 830	Homo sapiens	50.1	827	0
646315421	leucine/isoleucine/valine transporter	b3455	32, 70	Escherichia coli K-12,	639338550	ATP-binding cassette, sub-family A	ABCA5	1327, 1365	Homo sapiens	51.3	45.4	0.0037

	subunit			MG1655		(ABC1), member 5						
646315466	glutathione oxidoreductase	b3500	5, 450	Escherichia coli K-12, MG1655	639342484	glutathione reductase	GSR	65, 522	Homo sapiens	54.8	485.7	0
646315598	glycine C-acetyltransferase	b3617	9, 397	Escherichia coli K-12, MG1655	639338553	glycine C-acetyltransferase (2-amino-3-ketobutyrate coenzyme A ligase)	GCAT	31, 418	Homo sapiens	55.2	420.2	0
646315717	F1 sector of membrane-bound ATP synthase, beta subunit	b3732	2, 460	Escherichia coli K-12, MG1655	639350183	ATP synthase, H <sup>+</sup> transporting, mitochondrial F1 complex, beta polypeptide	ATP5B	59, 523	Homo sapiens	71.7	641.3	0
646315719	F1 sector of membrane-bound ATP synthase, alpha subunit	b3734	5, 509	Escherichia coli K-12, MG1655	639350028	ATP synthase, H <sup>+</sup> transporting, mitochondrial F1 complex, alpha subunit 1, cardiac muscle	ATP5A1	48, 549	Homo sapiens	56.3	542.7	0
646315726	5-methylamino methyl-2-thiouridine modification at tRNA U34	b3741	7, 339	Escherichia coli K-12, MG1655	639339479	mitochondrial translation optimization 1 homolog (S. cerevisiae)	MTO1	37, 376	Homo sapiens	50.6	332	0
646315816	bifunctional 2-octaprenyl-6-methoxy-1,4-benzoquinone methylase/ S-	b3833	90, 250	Escherichia coli K-12, MG1655	639368119	coenzyme Q5 homolog, methyltransferase (S. cerevisiae)	COQ5	166, 326	Homo sapiens	51.2	164.9	4.20 E-39

	adenosylmethionine:2-DMK methyltransferase											
646315961	protein chain elongation factor EF-Tu (duplicate of tufA)	b3980	2, 394	Escherichia coli K-12, MG1655	639361520	Tu translation elongation factor, mitochondrial	TUFM	50, 444	Homo sapiens	56.2	469.9	0
646315988	phosphoribosylglycinamide synthetase phosphoribosylamine-glycine ligase	b4005	2, 424	Escherichia coli K-12, MG1655	639339828	phosphoribosylglycinamide formyltransferase, phosphoribosylglycinamide synthetase, phosphoribosylaminoimidazole synthetase	GART	4, 426	Homo sapiens	51.1	406.8	0
646315989	fused IMP cyclohydrolase/phosphoribosylaminoimidazolecarboxamide formyltransferase	b4006	472, 529	Escherichia coli K-12, MG1655	639349502	5-aminoimidazole-4-carboxamide ribonucleotide formyltransferase/IMP cyclohydrolase	ATIC	535, 592	Homo sapiens	50	60.8	1.80 E-07
646316002	homocysteine-N5-methyltetrahydrofolate transmethylation, B12-dependent	b4019	6, 1227	Escherichia coli K-12, MG1655	639349342	5-methyltetrahydrofolate-homocysteine methyltransferase	MTR	20, 1265	Homo sapiens	54.2	1285.4	0
646316008	glucosephosphate isomerase	b4025	7, 548	Escherichia coli K-12,	639340705	glucose phosphate isomerase	GPI	5, 553	Homo sapiens	64.8	725.3	0

				MG1655								
64631605	acetyl-CoA synthetase	b4069	226, 645	Escherichia coli K-12, MG1655	639352844	acyl-CoA synthetase short-chain family member 2	RP5-1161H23.2	278, 696	Homo sapiens	60	555.4	0
646316131	Cpn60 chaperonin GroEL, large subunit of GroESL	b4143	3, 548	Escherichia coli K-12, MG1655	639343243	heat shock 60kDa protein 1 (chaperonin)	HSPD1	27, 572	Homo sapiens	50.9	552.7	0
646316210	methionine sulfoxide reductase A	b4219	8, 209	Escherichia coli K-12, MG1655	639349228	methionine sulfoxide reductase A	MSR A	29, 230	Homo sapiens	60.6	260	0

<sup>a</sup> based on *E. coli* K12 MG1655 and *Homo sapiens* sequences and BLAST results from IMG database (<https://img.jgi.doe.gov>)

\* There are 64 proteins in *E. coli* that have a human homolog protein match of >50% sequence identity and 20 of these proteins (rows highlighted in Red) were observed with mercury adducts.



**Table C.S6. Conserved cysteine sites in *Homo sapiens* based on sequence homology to mercury modified peptides from *E. coli* and diseases associated with protein from the Comparative Toxicogenomics Database.**

Gene ID	Cys site	Ecoli product	E.coli Query peptide	Human Blast Hit peptide	E-value	% Identity	NCBI GI #	NCBI gene #	Human Gene name	NCBI BlastHit Description	PDB ID	GO Cellular Component	Mercury-associated disease genes with inference score by compound
<a href="#">Ecoli_b0008</a>	167	<a href="#">transaldolase B</a>	ACAEAGV FLISPFVGR	ACAEAG VTLISPFVGR	0.1	0.938	6648092	6888	TALDO	TALDO1 transaldolase 1 [ <i>Homo sapiens</i> ]	1FO5	cytoplasm, cytosol	drug-induced liver damage (HgCl2/5.15), <a href="#">hepatocellular carcinoma</a> (HgCl2/31.84), transaldolase deficiency (HgCl2/5.05)
<a href="#">Ecoli_b0116</a>	45	lipoamide dehydrogenase, E3 component is part of three enzyme complexes	YNTLGGV CLNVGCI PSK	TLGGTC LNVGCIP SK	0.12	0.933	194390238	1738	DLD	DLD dihydrolipoamide dehydrogenase [ <i>Homo sapiens</i> ]	3RNM	acrosomal matrix, flagellum, <a href="#">mitochondrial matrix</a> , <a href="#">mitochondrion</a> , oxoglutarate dehydrogenase complex, pyruvate dehydrogenase complex	
	50		YNTLGGV CLNVGCI PSK	TLGGTC LNVGCIP SK									
<a href="#">Ecoli_b0605</a>	166	<a href="#">alkyl hydroperoxide reductase, C22 subunit</a>	AAQYVAS HPGEVCP AKWKEG EATLAPS LDLVGKI	AFQYTD EH- GEVCPA GWKPGS DTIKPNVD	0.032	0.552	1617118	7001	PRDX2	PRDX2 peroxiredoxin 2 [ <i>Homo sapiens</i> ]	1QMV	cytoplasm, <a href="#">mitochondrion</a>	<a href="#">hepatocellular carcinoma</a> (Hg/49.93), <a href="#">prostatic neoplasms</a> (Hg/38.33), melanoma(Hg/6.53), <a href="#">esophageal neoplasms</a> (Hg/28.89), keloid (Hg/4.11), <a href="#">down syndrome</a> (Hg/10.09), myeloid leukemia (Hg/4.52)

	47		WSVFFFY PADFTFV CPT <sup>EL</sup> GD VADHYEE LQK	YVVFFF YPLDFTF VC <sup>PT</sup> EII AFSDRA EEFKK	0.00 01	0.613	559598 87	5052	PRDX1	peroxiredoxin 1 [Homo sapiens]	3HY2	cytoplasm, melanosome, mitochondrio n, nucleus	squamous cell carcinoma (CH3CIHg/20.50), esophageal neoplasms (CH3CIHg/13.50), non- small-cell lung carcinoma (CH3CIHg/18.26), schistosomiasis (CH3CIHg/4.54), keloid (CH3CIHg/5.14)
Ecoli_ b0723	257	succinate dehydrogenas e, flavoprotein subunit	AGVPVQD MEMWQF HPTGIAG AGVLVTE GCR	AGLPCQ DLEFVQF HPTGIYG AGCLITE GCR	5.00 E-07	0.733	194381 536	6389	SDHA	SDHA succinate dehydrogenase complex, subunit A, flavoprotein (Fp) [ Homo sapiens ]		mitochondrial inner membrane, mitochondrial respiratory chain complex II, mitochondrio n	cardiomyopathy (HgCl2/3.67), Leigh disease (HgCl2/8.90), mitochondrial complex II deficiency (HgCl2/4.59), osteoarthritis (HgCl2/24.52)
Ecoli_ b0726	165	2-oxoglutarate decarboxylase , thiamin- requiring	LGELLEA LKQTYCG PIGAEYM HITSTEER	LREIRRL ENTYCFQ HIGLEFM FINDVEQ	9.2	0.429	160419 019	55753	OGDHL	2-oxoglutarate dehydrogenase -like, mitochondrial		mitochondrial matrix	
Ecoli_ b0729	124	succinyl-CoA synthetase, NAD(P)- binding, alpha subunit	MIGPNC <sup>P</sup> GVITPGE CK	LIGPNC <sup>P</sup> GVINPGE CK	0.09 5	0.875	940979 4	8802	SUCLG1	succinyl-CoA synthetase alpha subunit [Homo sapiens]		cytoplasm, mitochondrial inner membrane, mitochondrial matrix, mitochondrio n, plasma membrane, succinate- CoA ligase complex (GDP- forming)	
	133		MIGPNC <sup>P</sup> GVITPGE CK	LIGPNC <sup>P</sup> GVINPGE CK									
Ecoli_ b1203	35	predicted GTP-binding protein	AGIEAAN FPFCTIEP NTGVVP MPDPR	AENFPFC TIDPNES RVPVPD ER	0.01 5	0.682	119631 554	29789	OLA1	OLA1 Obg- like ATPase 1 [ Homo sapiens ]		cytoplasm	
Ecoli_ b1637	38	tyrosyl-tRNA synthetase	LAQGPIA LYCGFDP TADSLHL GHLVPLL CLKR	ASFPQTI YCGFDP TADS	1.7	0.706	468064 9	51067	YARS2	YARS2 tyrosyl-tRNA synthetase 2, mitochondrial [ Homo sapiens ]	3ZXI	mitochondrial matrix, mitochondrio n	

Ecoli_b1778	95	methionine sulfoxide reductase B	CGNCDA HLGHVFP DGPQPTG ER	CKQCEA HLGHVF PDGPGP NGQR	0.003	0.727	71051456	22921	MSRB2	MSRB2 methionine sulfoxide reductase B2, mitochondrial [ Homo sapiens ]		mitochondrion	
	98		CGNCDA HLGHVFP DGPQPTG ER	CKQCEA HLGHVF PDGPGP NGQR									
Ecoli_b1779	150	glyceraldehyde-3-phosphate dehydrogenase A	GANFDKY AGQDIVS NASCTTN CLAPLAK	GVNHFK YANSLKI ISNASCT TNCLAPLAK	0.001	0.75	53734502	2597	GAPDH	GAPDH glyceraldehyde-3-phosphate dehydrogenase [ Homo sapiens ]	3GPD	cytoplasm, cytosol, lipid particle, membrane, microtubule cytoskeleton, nucleus, perinuclear region of cytoplasm	acute coronary syndrome (Hg/18.66), anoxia (CH3HgX/4.55), hepatocellular carcinoma (Hg/49.93), squamous cell carcinoma (Hg/45.17), esophageal neoplasms (Hg/28.89), mouth neoplasms (Hg/13.60), osteoarthritis (CH3HgX/14.20), osteoporosis (CH3HgX/14.96)
	154		GANFDKY AGQDIVS NASCTTN CLAPLAK	GVNHFK YANSLKI ISNASCT TNCLAPLAK									
Ecoli_b1852	245	glucose-6-phosphate 1-dehydrogenase	DMIQNHL LQILCMIA MSPPSDL SADSIRDEK	DVMQNH LLQMLC LVAMEK PASTNSD DVRDEK	2.00E-05	0.548	116242483	2539	G6PD	Glucose-6-phosphate 1-dehydrogenase ; G6PD	1QKI	centrosome, cytoplasm, cytosol, internal side of plasma membrane, intracellular membrane-bounded organelle	acute kidney damage (Hg/5.27), hemolytic anemia (CH3HgX/3.65), congenital nonspherocytic hemolytic anemia (CH3HgX/4.32), favism (CH3HgX/4.86), glucosephosphate dehydrogenase deficiency (CH3HgX/4.52), chronic granulomatous disease (CH3HgX/4.32), phagocyte bactericidal dysfunctionhemolysis (CH3HgX/4.86)
Ecoli_b2508	305	IMP dehydrogenase	VGIGPGSI CTTR	VGIGPGS VCTTR	4.8	0.917	33150542	51292	GMPr2	GMP dehydrogenase [Homo sapiens]	2A7R	cytosol	

Ecoli_b2529	37	FeS cluster assembly scaffold	NVGSFDN NDENVGS GMVGAP ACGDVMK	NVGSLD KTSKNV GTGLVG APACGD VMK	6.00 E-06	0.741	313104 118	23479	ISCU	Iron-sulfur cluster assembly enzyme ISCU, mitochondrial		cytoplasm, cytosol, mitochondrion, nucleus	
Ecoli_b3213	161	glutamate synthase, 4Fe-4S protein, small subunit	KVAIIGA GPAGLAC ADVLR	KIALFGA GPASISC ASFLAR	9.3	0.55	559629 06	1806	DPYD	dihydropyrimidine dehydrogenase [Homo sapiens]		cytoplasm, cytosol	
Ecoli_b3236	109	malate dehydrogenase, NAD(P)-binding	TCPKACI GIITNPVN TTVAIAA EVLKK	CPEAMIC VIANPVN STIPITAE VFKE	0.11	0.615	932792 35	4191	MDH2	MDH2 malate dehydrogenase 2, NAD (mitochondrial) [ Homo sapiens ]	2DFD	mitochondrial inner membrane, mitochondrial matrix, mitochondrion, NOT nucleolus, nucleus, plasma membrane	
	113		TCPKACI GIITNPVN TTVAIAA EVLKK	CPEAMIC VIANPVN STIPITAE VFKE									
Ecoli_b3297	121	30S ribosomal subunit protein S11	ITNITDVT PIPHNGC RPPKKR	VISITDN TPIPHNG CRPRKAR	0.06 5	0.714	144956 81	64963	MRPS11	MRPS11 mitochondrial ribosomal protein S11 [ Homo sapiens ]		mitochondrial small ribosomal subunit	
Ecoli_b3339	82	protein chain elongation factor EF-Tu (duplicate of tufB)	HYAHVD CPGHADY VK	HYAHTD CPGHADY VK	0.00 3	0.933	341476 30	7284	TUFM	elongation factor Tu, mitochondrial precursor [Homo sapiens]		mitochondrial nucleoid, mitochondrion	
Ecoli_b3734	193	F1 sector of membrane-bound ATP synthase, alpha subunit	DSGIKCIY VAIGQKA STISNVVR	CIYVAIG QKRSTV AQLVK	3.7	0.667	139383 39	498	ATP5A1	ATP5A1 ATP synthase, H+ transporting, mitochondrial F1 complex		mitochondrial inner membrane, mitochondrial matrix,	Alzheimer disease (HgCl2/23.91), endotoxemia (HgCl2/8.45)

	243		KLEEHGA LANTIVV VATASES AALQYLA PYAGCA MGEYFR	RLTDAD AMKYTI VVSATA SDAAPL QYLAPY SGCSMG EYFR	1.00 E-08	0.65	131119 01	498	ATP5A1	ATP5A1 ATP synthase, H+ transporting, mitochondrial F1 complex		mitochondrio n, mitochondrial proton- transporting ATP synthase complex catalytic core F1, plasma membrane, colocalizes with signalosome	
Ecoli_ b3781	33	thioredoxin 1	IIHLTDDS FDTDVLK ADGAILV DFWAEW CGPCK	VIELTDD SFDKNV LDSEDV WMVEFY APWCGH CK	9.00 E-05	0.545	193785 970	10130	PDIA6	PDIA6 protein disulfide isomerase family A, member 6 [ Homo sapiens ]	1X5D	endoplasmic reticulum, endoplasmic reticulum lumen, endoplasmic reticulum membrane, endoplasmic reticulum- Golgi intermediate compartment, melanosome, plasma membrane	
	36		IIHLTDDS FDTDVLK ADGAILV DFWAEW CGPCK	VIELTDD SFDKNV LDSEDV WMVEFY APWCGH CK									
Ecoli_ b3926	256	glycerol kinase	GGTRIPIS GIAGDQQ AALFGQL CVKEGM AK	VPISGCL GDQCAA LVGQMC FQEGQA K	0.00 6	0.654	212286 188	2712	GK2	GK2 glycerol kinase 2 [ Homo sapiens ]		cytoplasm, mitochondrial outer membrane	
	270		NTYGTGC FMLMNT GEK	NTYGTG CFLLCNT GHK	0.15	0.812	119619 459	2710	GK	GK glycerol kinase [ Homo sapiens ]		cytoplasm, cytosol, mitochondrial outer membrane	
Ecoli_ b3960	121	argininosuccin ate lyase	SRNDQVA TDLKLWC KDTVSEL LTANR	SRNDQV VTDLRL WMRQTC STL	1.1	0.667	28878	435	ASL	ASL argininosuccin ate lyase [ Homo sapiens ]	1AOS	cytoplasm, cytosol	

Ecoli_b3988	454	RNA polymerase, beta prime subunit	AIQLHPL VCAAYN ADFDGDQ MAVHVP LTLEAQL EAR	VCTPYN ADFDGD EMNLHL PQTEEA KAEA	0.00 02	0.643	246020 8	11128	POLR3A	RNA polymerase III largest subunit [Homo sapiens]		DNA-directed RNA polymerase III complex, NOT nucleolus, nucleoplasm, nucleus	
-------------	-----	------------------------------------	--	--	------------	-------	-------------	-------	--------	---	--	--	--

#### Table Summary

- 22 *E. coli* proteins have 33 distinct cysteine-containing peptides with high homology to one or more such human tryptic peptides from 25 human proteins.
- The cysteine site hit in *E. coli* is in **red** and additional cysteines in the human protein sequence are in **green** as are the corresponding non-cysteine residues in the homologous *E. coli* peptide.
- These additional cysteines in the human proteins have replaced large, aliphatic residues in 4 cases (V, V, I, M) and a large polar residue (Q) in the fifth.
- Eight of the 33 cysteine sites are in CXnC peptides where both cysteines were observed as Ph/Hg adducts in *E. coli*.

#### Functional and disease associations

- All of the human proteins have well defined functions that are the same as or closely related to the function in *E. coli*
- Fourteen *E. coli* proteins are homologs of human proteins that function in or affect the mitochondria (shown in **orange**).
- Genes inferred to have some association with syndromes resulting from Hg exposure per the Comparative Toxicogenomics Database (<http://ctdbase.org/about/dataStatus.go>).
- Those with double-digit inference scores are highlighted in **blue** as are the corresponding *E. coli* proteins.
- CTD database Inference Score Information (references on webpage): <http://ctdbase.org/help/diseaseGeneDetailHelp.jsp>

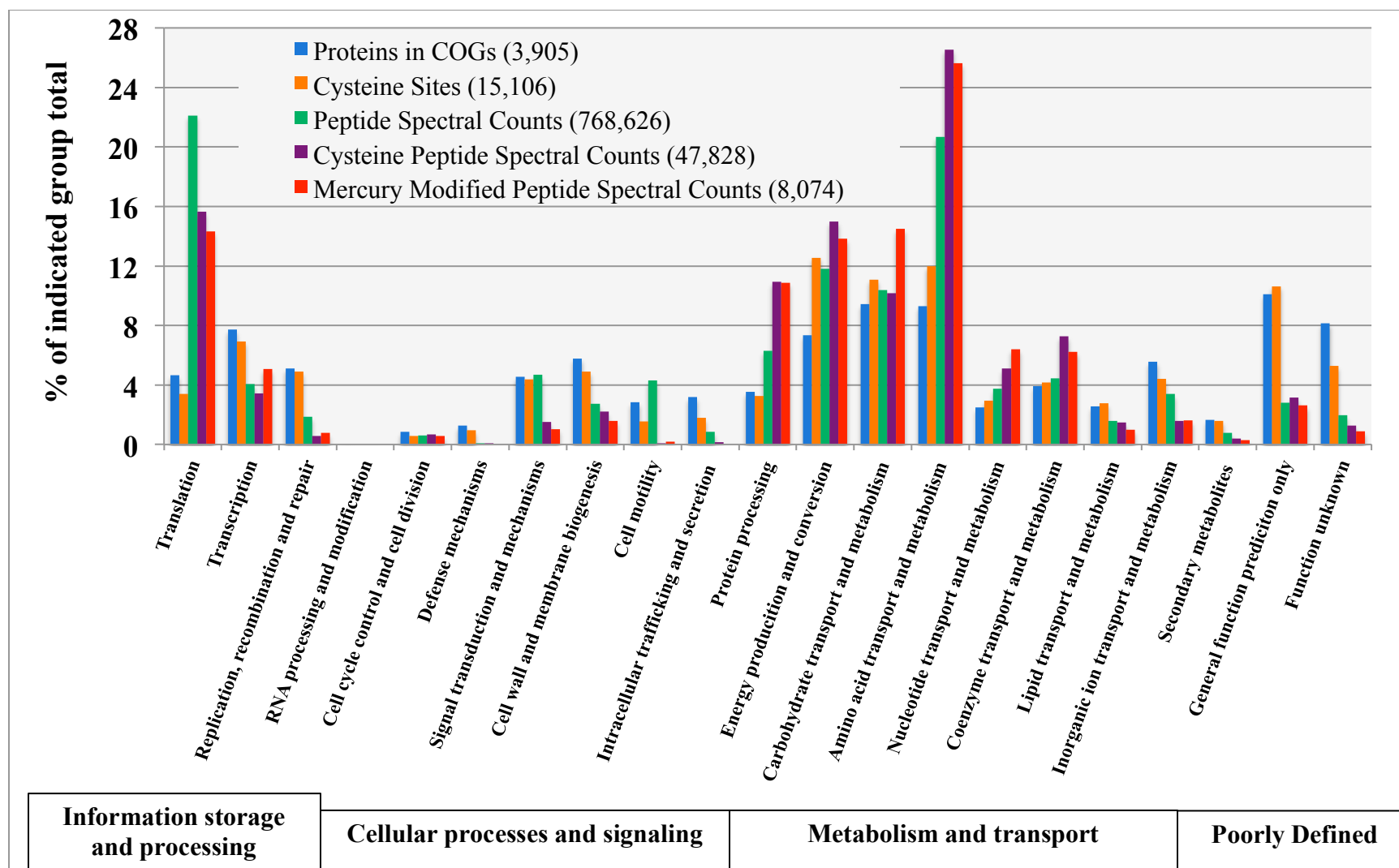


**Figure C.S1. COG functional categories of observed peptides compared to those in the genome.** Distribution of peptide spectral counts observations. The Y-axis shows the percent of each category total (indicated by colors). Only 3,905 of the 4,321 genome-encoded proteins (<https://img.jgi.doe.gov>) are included in the COG functional annotation, so totals for each category reflect only proteins included in COGs. The X-axis lists the COG functions.

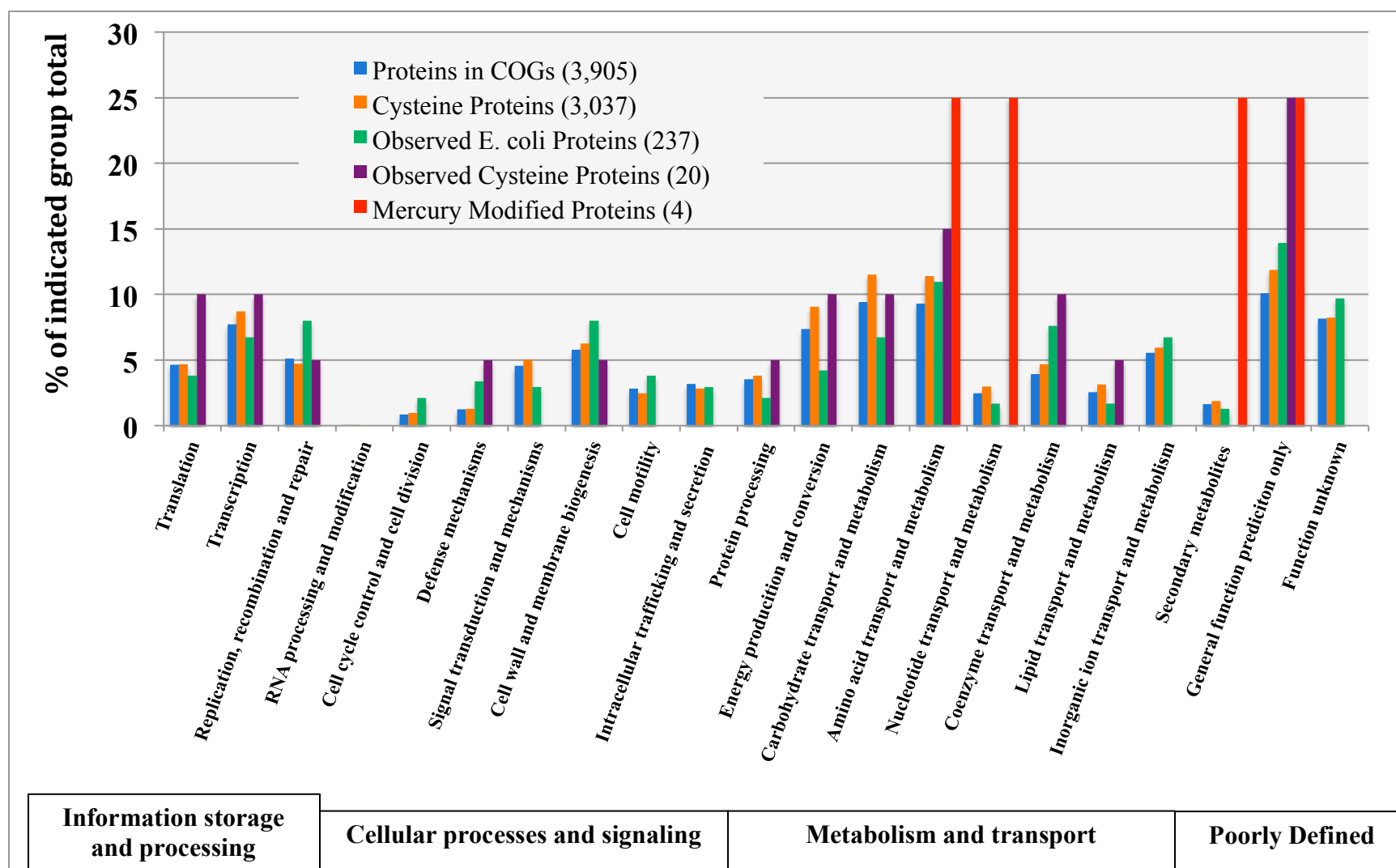


**Figure C.S2. Observed COG Single Peptide Proteins by Functional Categories.** Distribution of peptides with only a single peptide observed for each protein, rather than >1 peptide-per-protein cutoff used for other plots. The Y-axis shows the percent of each category total (indicated by colors). Only 3,905 of the 4,321 genome-encoded proteins (<https://img.jgi.doe.gov>) are included in the COG functional annotation, so totals for each category reflect only proteins included in COGs. The X-axis lists the COG functions.



## REFERENCES

- BAUGHMAN, G. L., GORDON, J. A., WOLFE, N. L. & ZEPP, R. G. 1973. Chemistry of Organomercurials in Aquatic Systems. *In*: CENTER, N. E. R. (ed.).
- CASAS, J. S. & JONES, M. M. 1980. Mercury(II) complexes with sulfhydryl containing chelating agents: Stability constant inconsistencies and their resolution. *Journal of Inorganic and Nuclear Chemistry*, 42, 99-102.
- DYRSSEN, D. & WEDBORG, M. 1991. The sulphur-mercury(II) system in natural waters. *Water Air & Soil Pollution*, 56, 507-519.
- HOJO, Y., SUGIURA, Y. & TANAKA, H. 1976. Organomercury complexes of penicillamine and some other sulfur-containing ligands. *Journal of Inorganic and Nuclear Chemistry*, 38, 641-644.
- NAGYPAL, I. & BECK, M. T. 1982. Diagrams for complete representation of binary mononuclear complex systems. *Talanta*, 29, 473-7.
- ORAM, P. D., FANG, X., FERNANDO, Q., LETKEMAN, P. & LETKEMAN, D. 1996. The formation of constants of mercury(II)--glutathione complexes. *Chem Res Toxicol*, 9, 709-12.
- RAVICHANDRAN, M. 2004. Interactions between mercury and dissolved organic matter--a review. *Chemosphere*, 55, 319-31.
- STARÝ, J., KRATZER, K. & PRÁŠILOVÁ, J. 1978. Dithizone extraction of methylmercury, ethylmercury and phenylmercury. 100, 627-633.
- SUGIMOTO, T., NAITO, K. & TAKEI, S. 1984. The extraction of organomercury with 8-quinolinol into benzene. *Bull. Chem. Soc. Jpn.*, 57, 2271-2275.
- VAN DER LINDEN, W. E. & BEERS, C. 1974. Determination of the composition and the stability constants of complexes of mercury(II) with amino acids. *Analytica Chimica Acta*, 68, 143-154.
- WAKI, H. & FRITZ, J. S. 1966. The effect of organic solvents on complexes and ion exchange—II nitrate complexes of some divalent metals in isopropyl alcohol. *Journal of Inorganic and Nuclear Chemistry*, 28, 577-589.

**APPENDIX D**  
**SUPPLEMENTAL MATERIAL FOR CHAPTER 4<sup>1</sup>**

---

<sup>1</sup>LAVOIE, S.P., SUMMERS, A.O.; To be submitted to *BMC Genomics*.

## SUPPORTING METHODS

### *RNAsnap<sup>TM</sup> method details*

Resuspend cell pellet in 100µl of RNAsnap extraction solution (95% formamide (RNA grade), 18mM EDTA (pH 8), 0.025% SDS, 1% βME) by vortex vigorously. Then lysed cells by heating at 95°C in a sand bath for 7 min. Pelleted cell debris by centrifuging warm sample at 16,000 g for 5 min at room temperature. Transferred 90 µl of supernatant to a fresh tube, without disturbing clear gelatinous pellet. Quantified RNA with Nanodrop<sup>TM</sup> using RNAsnap solution for blank. Then performed phenol/chloroform extraction, by adding 340 µl of RNase free H<sub>2</sub>O and 430 µl of acidic phenol/chloroform (Ambion, 5:1 solution, pH 4.5) and vortex vigorously for 30 sec. Centrifuged at 21,000 g for 15 min at 4°C, then transfer 350 µl of aqueous phase to a fresh tube. Added 40 µl of sodium acetate (3 M, pH 5.5) and 1 ml of 100% ethanol (~2.5x volume), then mixed by inverting several times. Then precipitated for 1 hr at -70°C and moved to -20°C to continue precipitation overnight. Centrifuged precipitated samples at 21,000 g for 15 min at 4°C to pellet, carefully removed supernatant by aspiration, washed pellet with 300 µl of 70% ethanol and repeated centrifugation. Supernatant was carefully removed by aspiration, air dried pellet completely, and allowed at least 30 min to suspend in RNase free H<sub>2</sub>O. Then quantify using Nanodrop to determine RNA recovery and stored at -70°C until DNase treatment. RNA quality was assessed after DNase treatment by running 500 ng of RNA on 1% agarose – 0.5 X TBE gel with 0.5 µg/ml ethidium bromide, run at 50V for 2 hr. RNA was denatured prior to loading by suspension in Gel Loading Buffer II (Ambion; Life Technologies) and heating for 5 min. at 95°C.

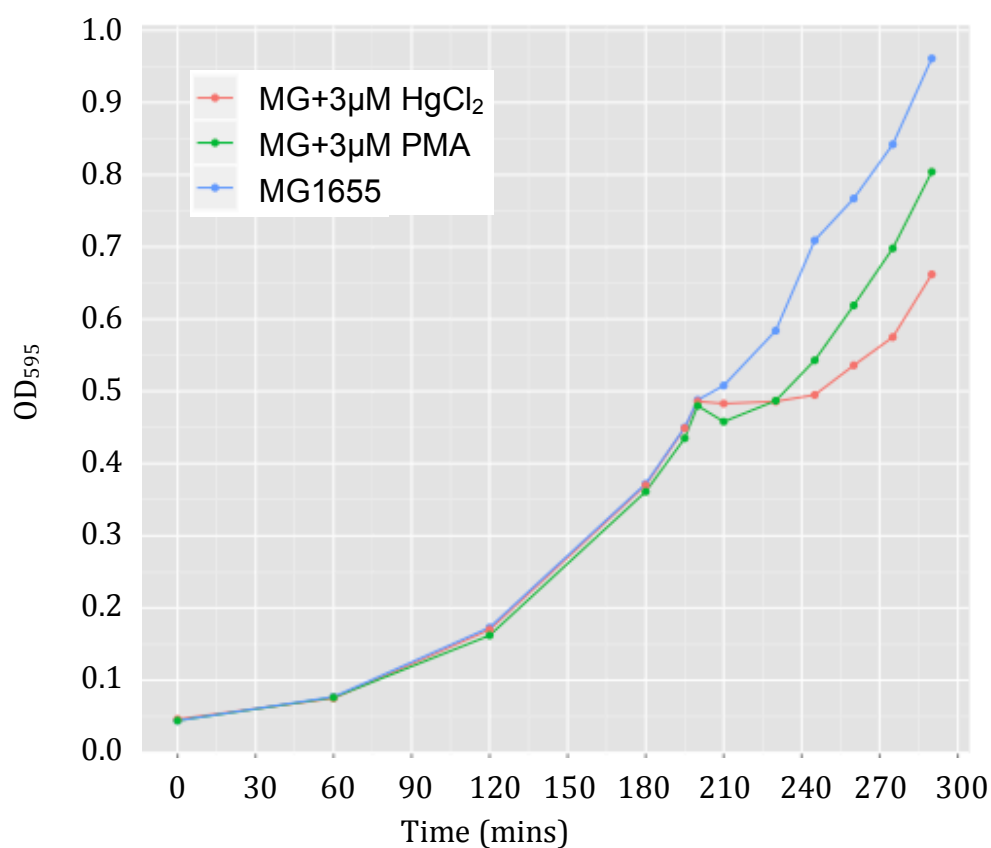


**Figure D.S1: Complete growth curves for all conditions.** Average optical density values from 3 biological replicate cultures for each condition: MG1655 unexposed culture (blue), MG + 3μM HgCl<sub>2</sub> (red), and MG + 3μM PMA (green). Samples for RNA-seq were collected at 200 (t<sub>0</sub>), 210 (t<sub>10</sub>), 230 (t<sub>30</sub>), and 260 (t<sub>60</sub>) minute time points following exposure to mercury.

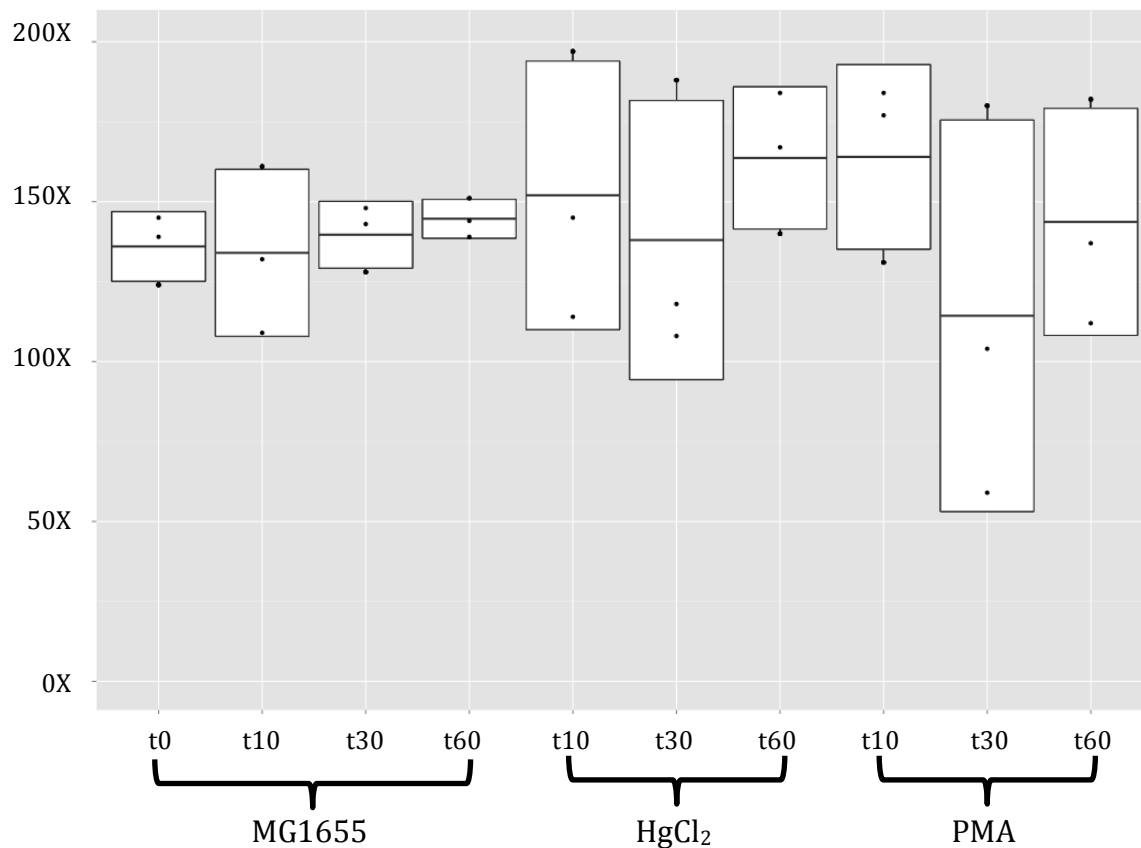


**Figure D.S2: Genome coverage for each condition.** The y-axis is the Mapped Reads Genome Coverage for 3 biological replicate libraries at each condition based on the formula: (number of paired-end reads mapped to genome by Bowtie2) x (read length, 50 bp x 2 for paired-end = 100 bp total) / (genome size, 4.64 Mb). Each box represents upper and lower quantiles with the internal horizontal bar as the median and dots indicate data points.

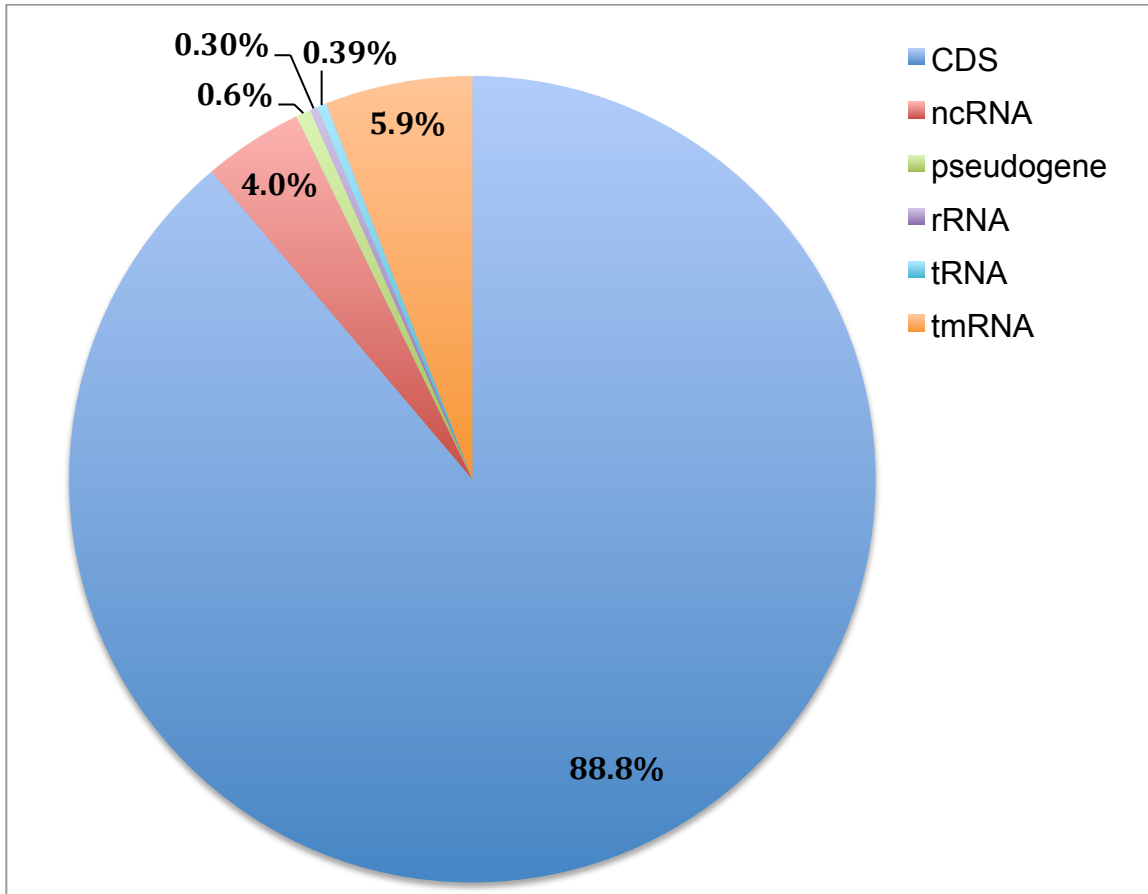


**Figure D.S3: Mapped read counts by feature-type for the unexposed control culture averaged across all time points.** Percentages were calculated based average raw read counts from 3 biological replicates, by taking the sum of counts for each feature type, divided by the total counts for all features, then taking the average across all time points (0,10,30 and 60 min) for the unexposed control culture. See data in Table D.S2 for details for each condition.

Figure D.S4a

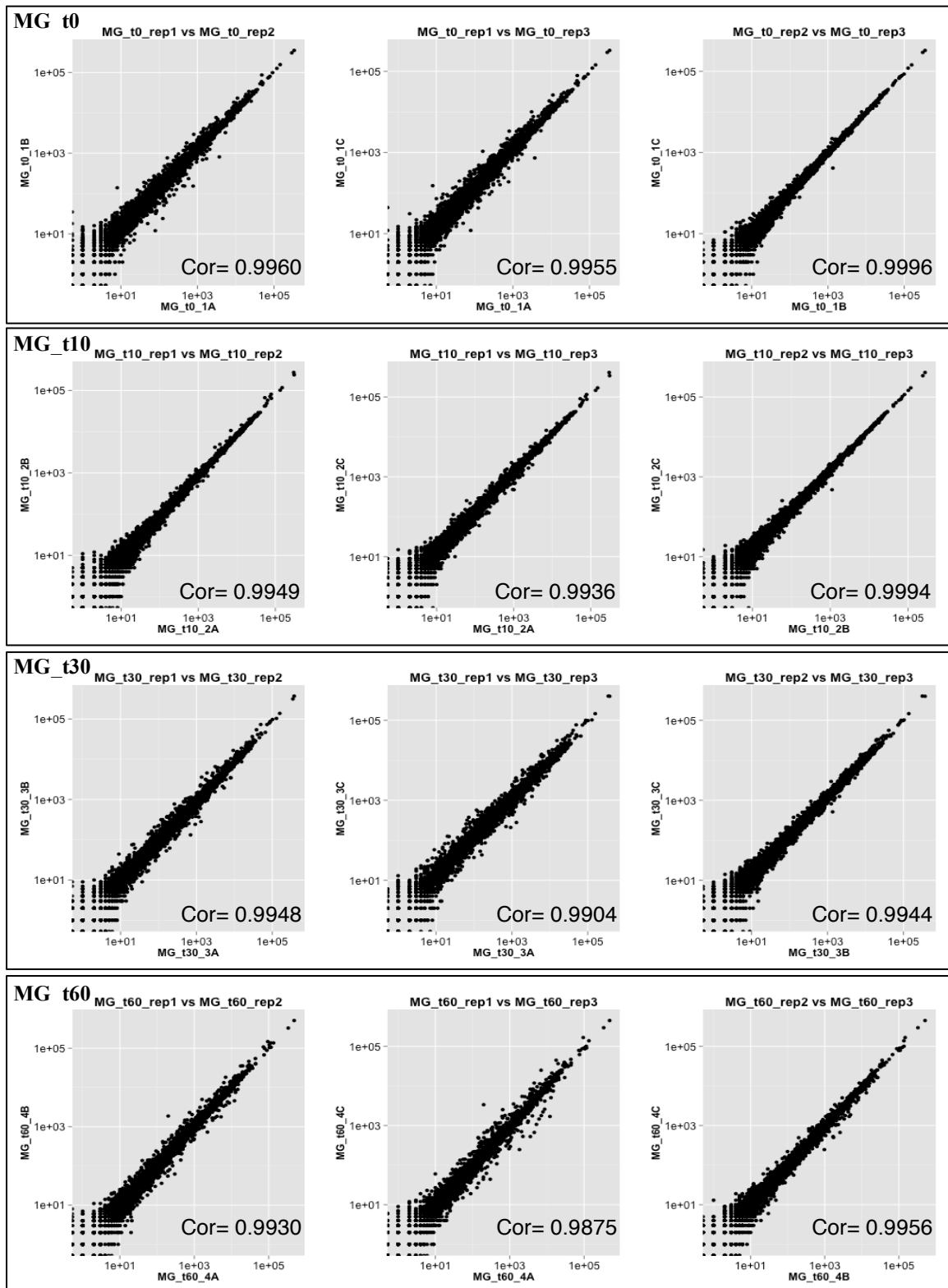
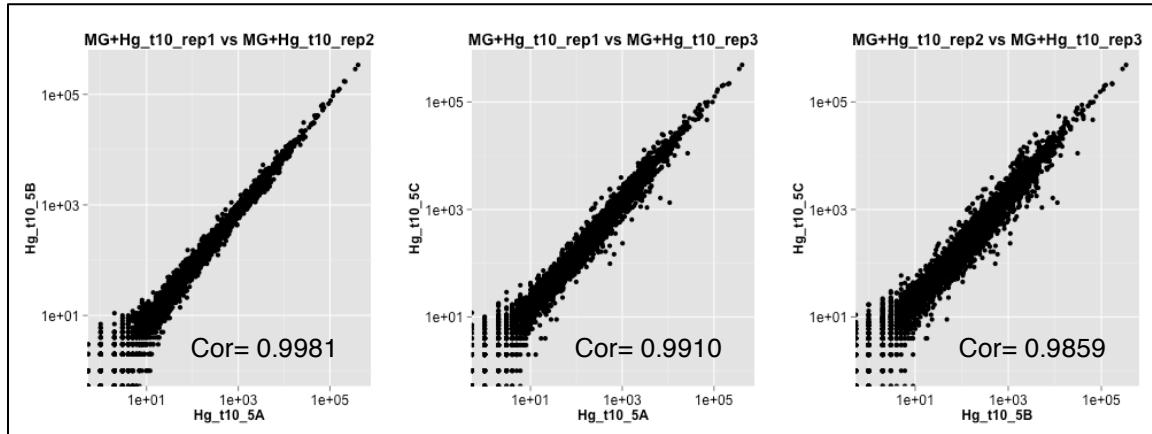
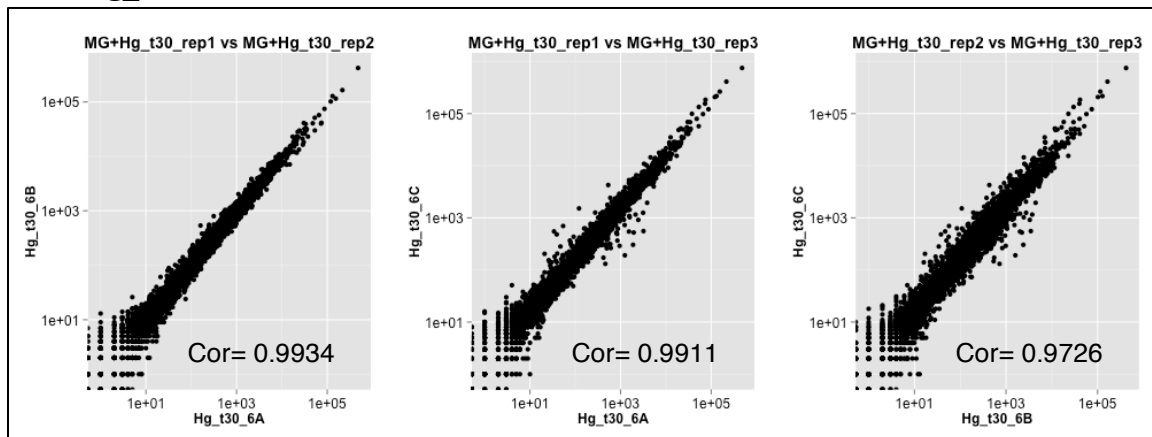


Figure D.S4b

MG+Hg\_t10



MG+Hg\_t30



MG+Hg\_t60

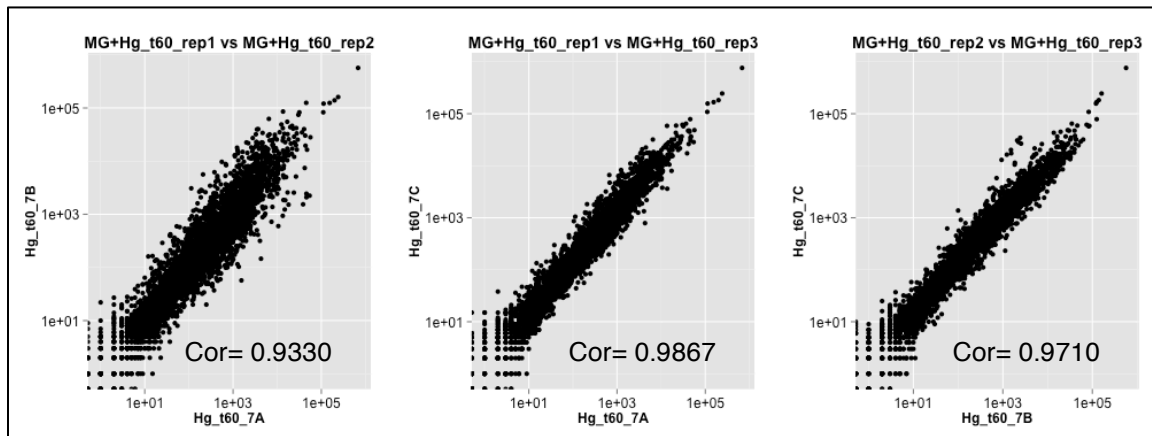
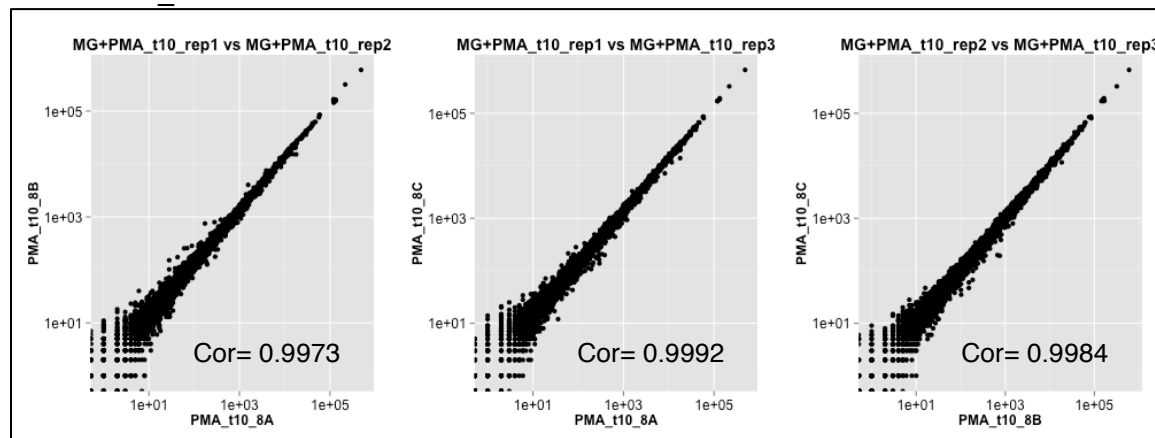


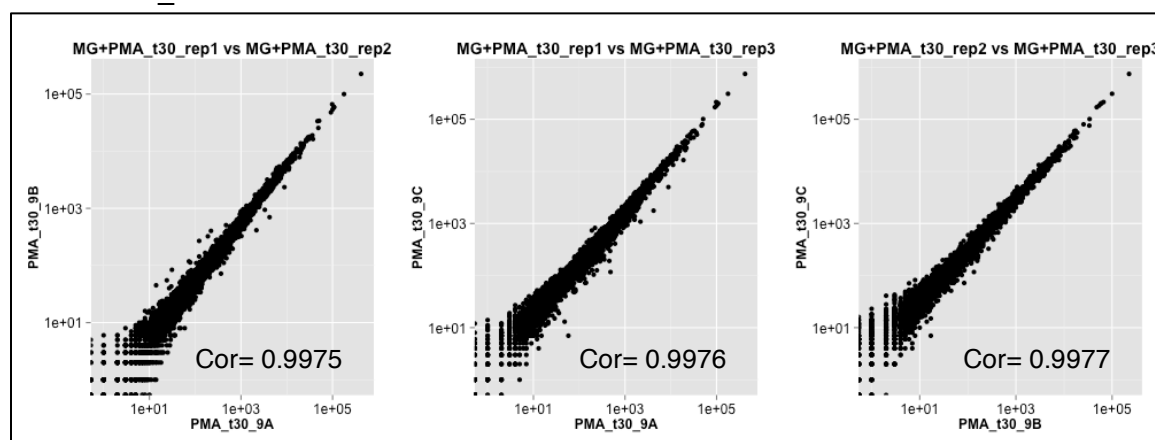


Figure D.S4c

### MG+PMA\_t10



### MG+PMA\_t30



### MG+PMA\_t60

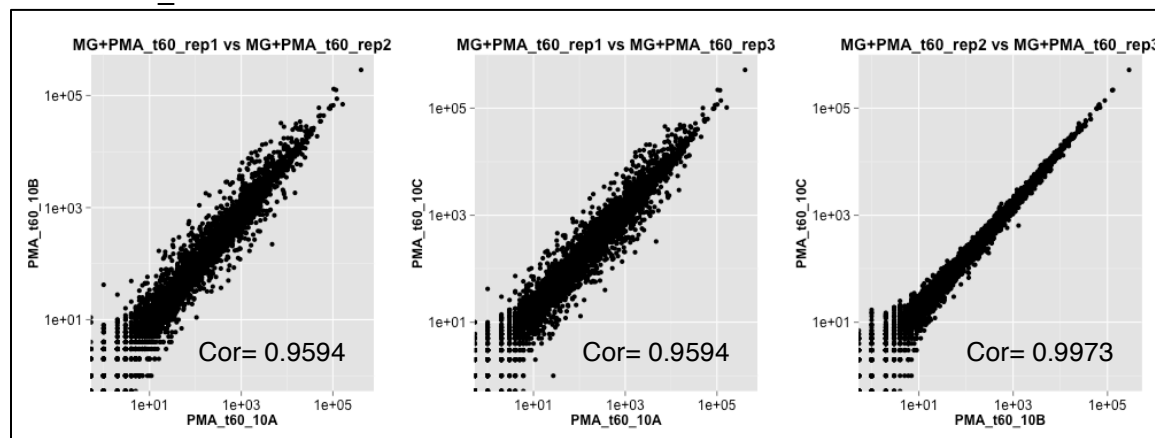


**Figure D.S4: Pearson correlation plots of gene counts in biological replicates for each condition.** Untreated (a), HgCl<sub>2</sub> (b), and PMA (c). Pearson correlations were determined by pairwise comparisons of biological replicates (rep1 vs rep2, rep1 vs rep3, rep2 vs rep3) using raw (unnormalized) read counts per gene (with rRNA counts removed) for each condition examined.

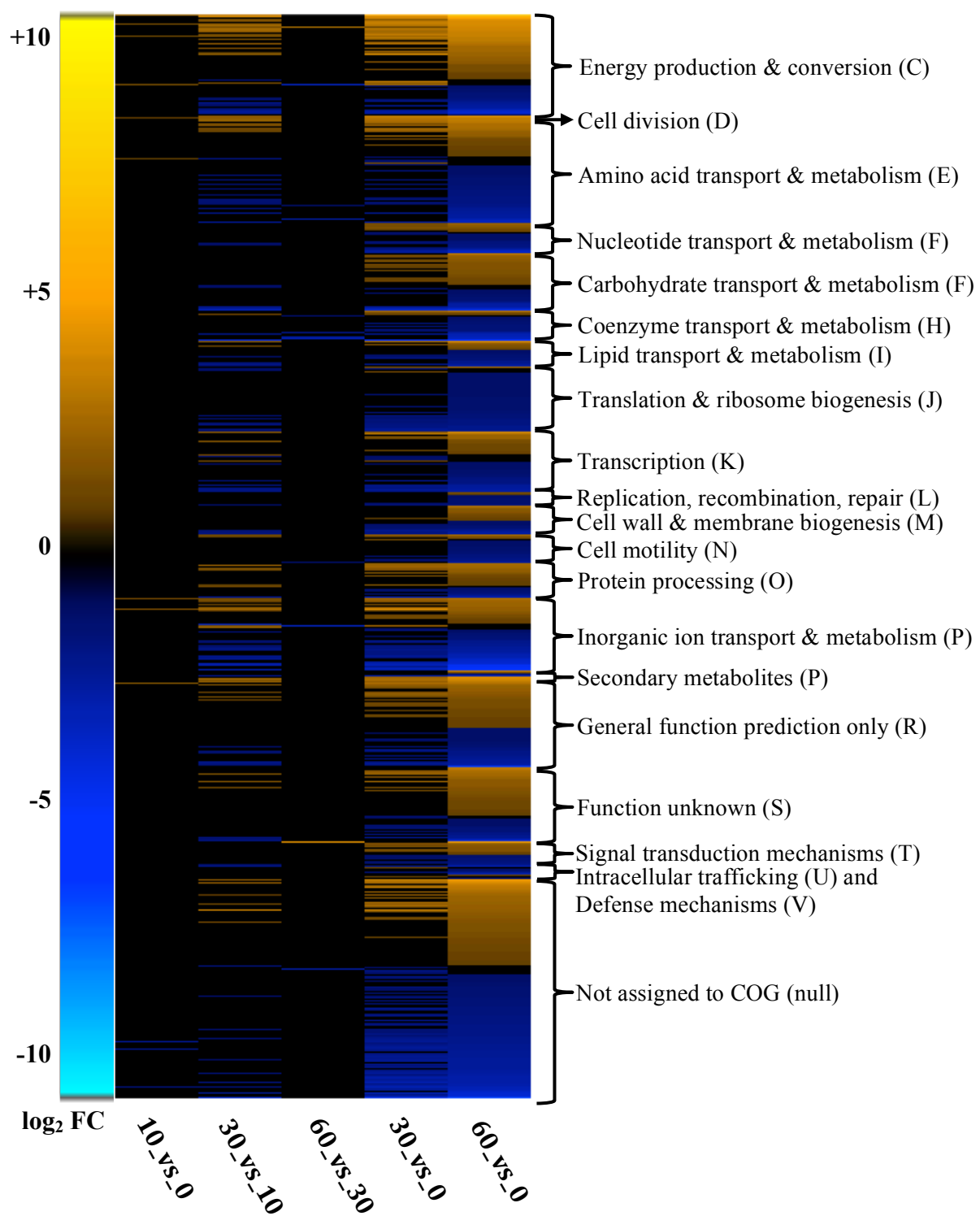


**Figure D.S5: Heatmap of differentially expressed genes over time in unexposed control culture.** Genes are sorted highest to lowest for “60\_vs\_0” column and grouped by COG category. Genes with  $\log_2$  fold-change  $\geq 1$  in at least one condition were included and grouped alphabetically by COG category. Conditions: t10\_vs\_t0 (n=15), t30\_vs\_t10 (n=195), t60\_vs\_t30 (n= 16), t30\_vs\_t0 (n=422), t60\_vs\_t0 (n=815). Total genes for all conditions = 864 (C=79, D=1, E=86, F=24, G=46, H=24, I=21, J=51, K=49, L=10, M=23, N=23, O=28, P=58, Q=5, R=72, S=59, T=20, U=6, V=4, null=175).

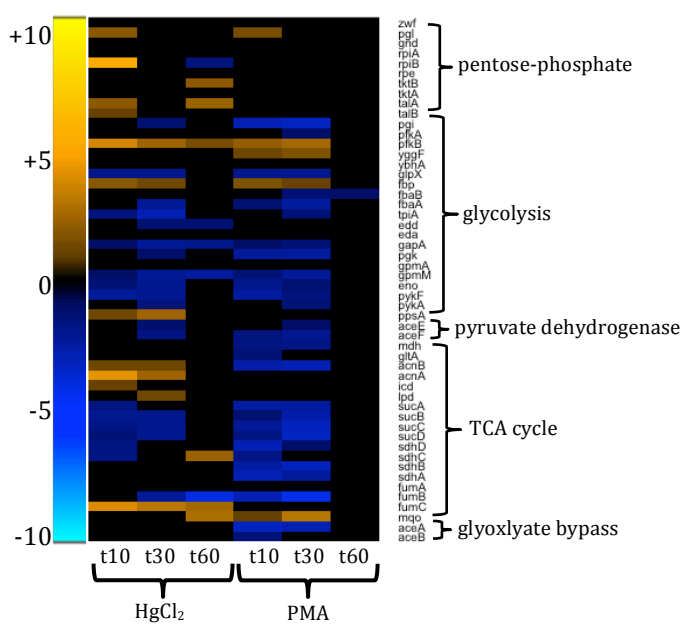


**Figure D.S6: Glucose metabolism**

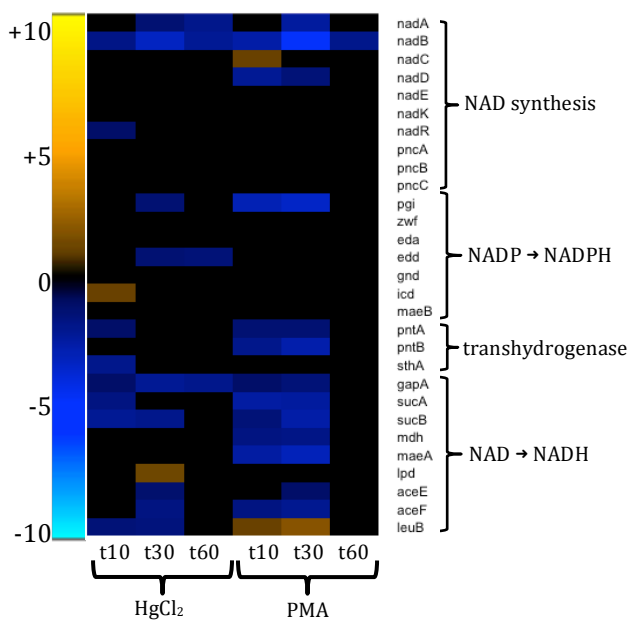
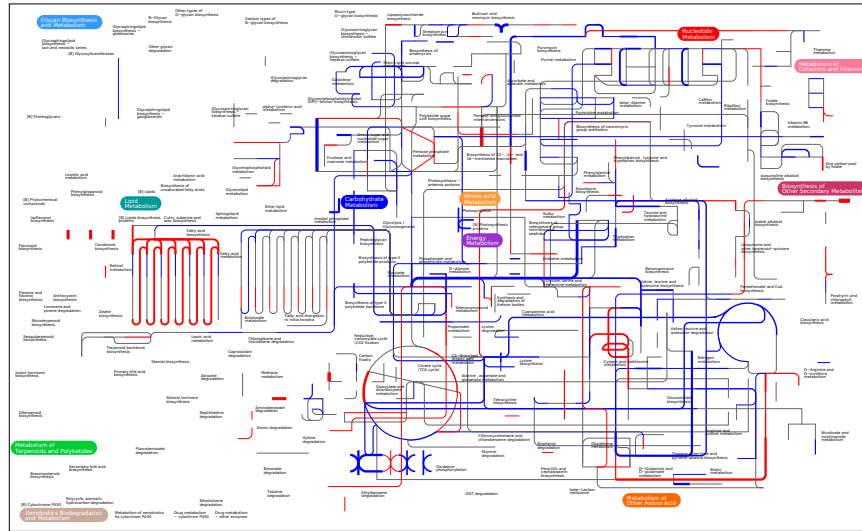
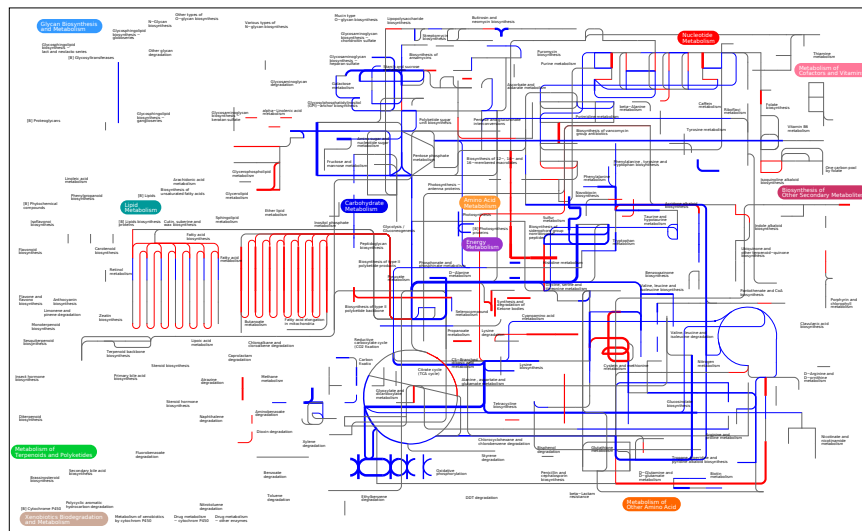


**Figure D.S7: NAD(P)H synthesis and reduction pathways.**

Hg\_t10



Hg\_t30



Hg\_t60

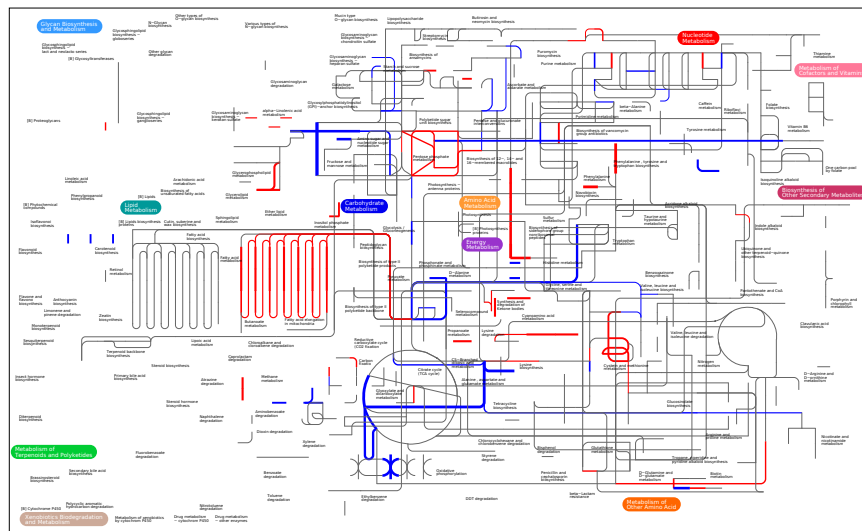
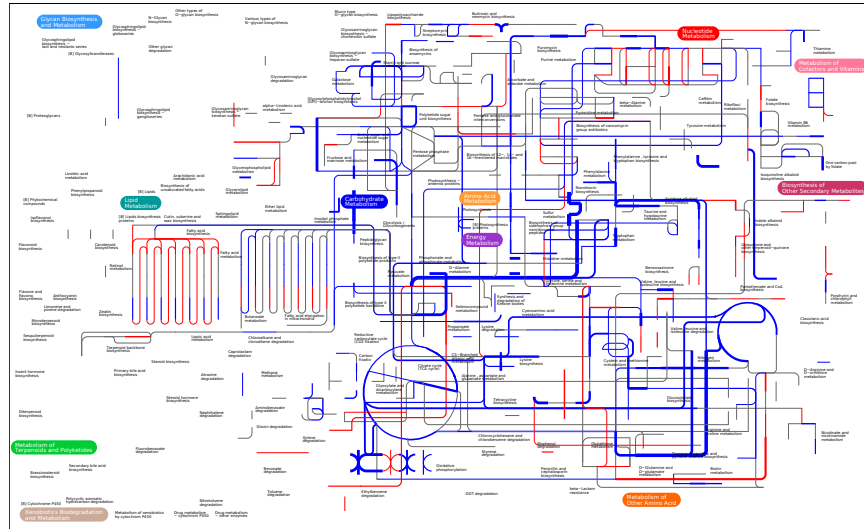


**Figure D.S8: iPath of *E. coli* K12 MG1655 metabolic KEGG map during HgCl<sub>2</sub> exposure.**

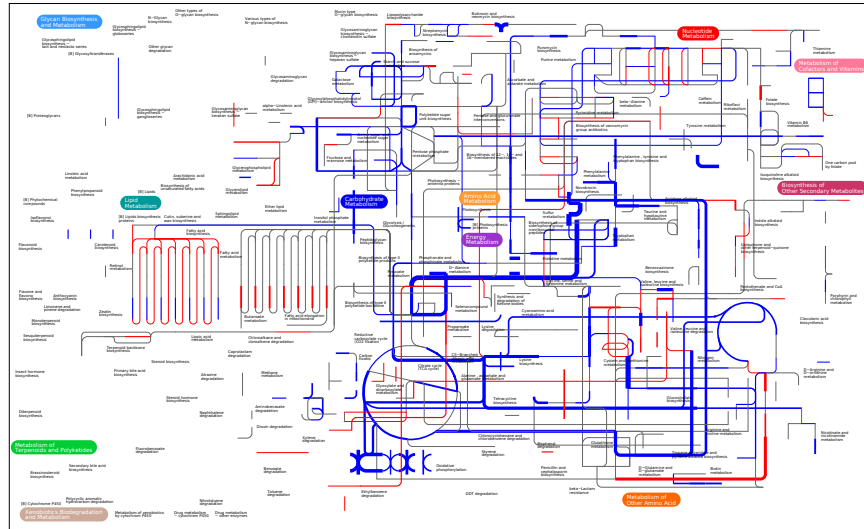
Up-regulated genes are red; Down-regulated genes are blue.

(<http://pathways.embl.de/iPath2.cgi#>)

PMA\_t10



PMA\_t30



PMA\_t60

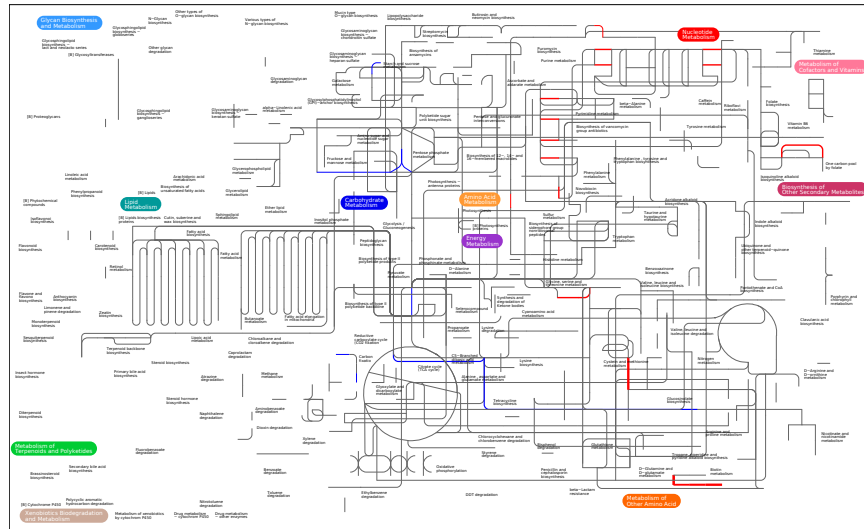




**Figure D.S9: iPath of *E. coli* K12 MG1655 metabolic KEGG map during PMA exposure.**

Up-regulated genes are red; Down-regulated genes are blue.

(<http://pathways.embl.de/iPath2.cgi#>)

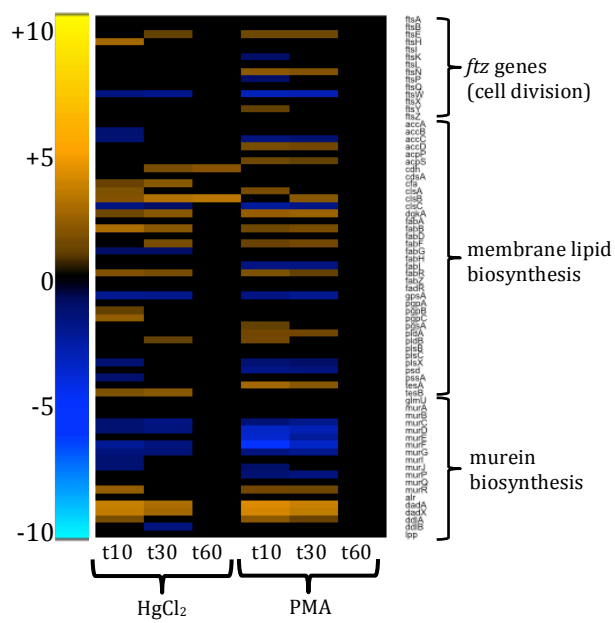


**Figure D.S10: Cell division and cell wall biosynthesis.**

**Table D.S1: Sequencing index tag for each sample library.**

<b>Sample ID</b>	<b>index</b>	<b>sequence</b>
1A (MG_t0)	701-501	ATTACTCG-TATAGCCT
2A (MG_t10)	701-502	ATTACTCG-ATAGAGGC
3A (MG_t30)	701-503	ATTACTCG-CCTATCCT
4A (MG_t60)	701-504	ATTACTCG-GGCTCTGA
5A (MG+Hg_t10)	701-505	ATTACTCG-AGGCGAAG
6A (MG+Hg_t30)	701-506	ATTACTCG-TAATCTTA
7A (MG+Hg_t60)	701-507	ATTACTCG-CAGGACGT
8A (MG+PMA_t10)	701-508	ATTACTCG-GTACTGAC
9A (MG+PMA_t30)	702-501	TCCGGAGA-TATAGCCT
10A (MG+PMA_t60)	702-502	TCCGGAGA-ATAGAGGC
1B (MG_t0)	702-503	TCCGGAGA-CCTATCCT
2B (MG_t10)	702-504	TCCGGAGA-GGCTCTGA
3B (MG_t30)	702-505	TCCGGAGA-AGGCGAAG
4B (MG_t60)	702-506	TCCGGAGA-TAATCTTA
5B (MG+Hg_t10)	702-507	TCCGGAGA-CAGGACGT
6B (MG+Hg_t30)	702-508	TCCGGAGA-GTACTGAC
7B (MG+Hg_t60)	703-501	CGCTCATT-TATAGCCT
8B (MG+PMA_t10)	703-502	CGCTCATT-ATAGAGGC
9B (MG+PMA_t30)	703-503	CGCTCATT-CCTATCCT
10B (MG+PMA_t60)	703-504	CGCTCATT-GGCTCTGA
1C (MG_t0)	703-505	CGCTCATT-AGGCGAAG
2C (MG_t10)	703-506	CGCTCATT-TAATCTTA
3C (MG_t30)	703-507	CGCTCATT-CAGGACGT
4C (MG_t60)	703-508	CGCTCATT-GTACTGAC
5C (MG+Hg_t10)	704-501	GAGATTCC-TATAGCCT
6C (MG+Hg_t30)	704-502	GAGATTCC-ATAGAGGC
7C (MG+Hg_t60)	704-503	GAGATTCC-CCTATCCT
8C (MG+PMA_t10)	704-504	GAGATTCC-GGCTCTGA
9C (MG+PMA_t30)	704-505	GAGATTCC-AGGCGAAG
10C (MG+PMA_t60)	704-506	GAGATTCC-TAATCTTA

**Table D.S2: Average sum of mapped read counts by feature type from 3 biological replicates for each condition.**

	<b>MG_t0</b>	<b>MG_t10</b>	<b>MG_t30</b>	<b>MG_t60</b>	<b>Hg_t10</b>	<b>Hg_t30</b>	<b>Hg_t60</b>	<b>PMA_t10</b>	<b>PMA_t30</b>	<b>PMA_t60</b>
<b>sum of counts for all feature types (4,495 total)</b>	6304455	6216680	6471741	6708912	7060100	6407018	7594243	7617725	5306298	6674420
<b>sum of CDS features (4,140 total)</b>	5637398 (89%)	5600499 (90%)	5756229 (89%)	5824959 (87%)	6264405 (89%)	5362239 (84%)	6377199 (84%)	6535950 (86%)	4446307 (84%)	5940351 (89%)
<b>sum of ncRNA features (63 total)</b>	226511 (3.6%)	219188 (3.5%)	259520 (4.0%)	326701 (4.9%)	350434 (5.0%)	436892 (6.8%)	484101 (6.4%)	420290 (5.5%)	313073 (5.9%)	248544 (3.7%)
<b>sum of pseudogene features (178 total)</b>	34727 (0.6%)	32490 (0.5%)	38669 (0.6%)	39796 (0.6%)	16693 (0.2%)	15572 (0.2%)	24078 (0.3%)	54826 (0.7%)	41601 (0.8%)	36088 (0.5%)
<b>sum of rRNA features (22 total)</b>	24956 (0.40%)	14601 (0.23%)	17620 (0.27%)	18935 (0.28%)	1510 (0.02%)	25925 (0.40%)	364 (0.01%)	4010 (0.05%)	29871 (0.56%)	23752 (0.36%)
<b>sum of tRNA features (86 total)</b>	42271 (0.67%)	21539 (0.35%)	17451 (0.27%)	17998 (0.27%)	13814 (0.20%)	16077 (0.25%)	39166 (0.52%)	17836 (0.23%)	13134 (0.25%)	20339 (0.30%)
<b>sum of tmRNA features (2 total)</b>	338581 (5%)	328355 (5%)	382239 (6%)	480511 (7%)	413212 (6%)	550291 (9%)	669320 (9%)	584792 (8%)	462282 (9%)	405337 (6%)
<b>sum of tRNA-pseudogene features (3 total)</b>	11 (<0.1%)	7 (<0.1%)	13 (<0.1%)	11 (<0.1%)	31 (<0.1%)	22 (<0.1%)	15 (<0.1%)	22 (<0.1%)	30 (<0.1%)	9 (<0.1%)

\* (%) represents the percent of the total read counts for each category divided by the total reads for all features per condition.

**Table D.S3: Late phase response to HgCl<sub>2</sub> and PMA exposure.**

Late phase response to HgCl <sub>2</sub>									
Gene ID	Gene name	COG code	Protein description	Hg t10	Hg t30	Hg t60	PMA t10	PMA t30	PMA t60
b3603	lldP	C	L-lactate permease; also involved in glycolate uptake	n.s.	8	12	n.s.	6	n.s.
b1627	rsxA	C	Required for the reduction of SoxR; inner membrane protein	n.s.	3	7	2	5	n.s.
b1628	rsxB	C	Required for the reduction of SoxR; predicted iron-sulfur protein	n.s.	n.s.	5	n.s.	n.s.	n.s.
b2979	glcD	C	Glycolate oxidase subunit	n.s.	6	5	2	4	n.s.
b2975	glcA	C	Glycolate permease; also recognizes lactate	n.s.	n.s.	3	n.s.	n.s.	n.s.
b3742	mioC	C	Required for biotin synthase activity in vitro; flavodoxin-like FMN-binding protein; transcription of mioC through oriC may have physiological significance in suboptimal conditions	n.s.	n.s.	2	n.s.	n.s.	n.s.
b2866	xdhA	C	Xanthine dehydrogenase molybdenum-binding subunit; involved in limited purine catabolism; mutation confers adenine sensitivity	n.s.	n.s.	-2	n.s.	-2	n.s.
b3253	acuI	C	Putative acryloyl-CoA reductase	n.s.	n.s.	-3	n.s.	n.s.	n.s.
b2993	hybD	C	Maturation endoprotease for Ni-containing hydrogenase 2	n.s.	n.s.	-3	n.s.	n.s.	n.s.
b2296	ackA	C	Acetate kinase, produces acetyl phosphate; mutants are fluoroacetate resistant; creBC regulon; binds Zn(II)	n.s.	-3	-3	n.s.	n.s.	n.s.
b4072	nrfC	C	Formate-dependent nitrite reduction; nonheme FE-S protein, ferredoxin-like	n.s.	-20	-4	n.s.	-9	n.s.
b3062	ttdB	C	L-Tartrate dehydratase beta subunit	n.s.	n.s.	-4	n.s.	n.s.	n.s.
b3573	ysaA	C	Ferredoxin-like protein, function unknown	n.s.	-3	-4	n.s.	n.s.	n.s.
b0973	hyaB	C	Hydrogenase 1 large subunit [NiFe], periplasmic	n.s.	n.s.	-4	n.s.	n.s.	n.s.
b3061	ttdA	C	L-Tartrate dehydratase alpha subunit	n.s.	n.s.	-5	5	2	n.s.
b4152	frdC	C	Fumarate reductase membrane anchor polypeptide	n.s.	-5	-7	n.s.	-4	n.s.
b4153	frdB	C	Fumarate reductase iron-sulfur protein subunit	n.s.	-6	-7	n.s.	-6	n.s.
b0992	yccM	C	Putative polyferredoxin, function unknown	n.s.	-5	-7	n.s.	-3	n.s.
b2994	hybC	C	Hydrogenase 2 [Ni Fe] large subunit, periplasmic	n.s.	-3	-8	n.s.	-3	n.s.
b1224	narG	C	Nitrate reductase I (NRA), alpha subunit	n.s.	-7	-9	n.s.	-3	n.s.
b0306	ykgE	C	Cysteine-rich protein, predicted lactate-related catabolism; function unknown	n.s.	-3	-9	n.s.	n.s.	n.s.
b0734	cydB	C	Cytochrome d (bd-I) terminal oxidase subunit II; upregulated in biofilms and microaerobic conditions; aerobically repressed by H-NS; anaerobically repressed	n.s.	-6	-12	n.s.	-3	n.s.

			by Fnr							
b0872	hcr	C	Hydrid-cluster protein oxidoreductase; FAD and [2Fe-2S] cofactors, NADH as electron donor	n.s.	-7	-13	n.s.	n.s.	n.s.	
b0733	cydA	C	Cytochrome d (bd-I) terminal oxidase subunit I; upregulated in biofilms and microaerobic conditions; aerobically repressed by H-NS; anaerobically repressed by Fnr	n.s.	-10	-14	n.s.	-4	n.s.	
b3945	gldA	C	Glycerol dehydrogenase, NAD <sup>+</sup> dependent; 1,2-propanediol (and derivatives) oxidoreductase; D-1-amino-2-propanol:NAD <sup>+</sup> oxidoreductase	n.s.	-5	-16	n.s.	-4	n.s.	
b4122	fumB	C	Fumarase B, anaerobic	n.s.	-5	-17	-7	-20	n.s.	
b1589	ynfG	C	S- and N-oxide reductase, apparent Fe-S binding subunit; required for swarming phenotype	n.s.	-5	-17	n.s.	-3	n.s.	
b0895	dmsB	C	DMSO reductase subunit B; apparent Fe-S binding subunit; anaerobic	n.s.	-10	-23	n.s.	-7	n.s.	
b1673	ydhV	C	Predicted oxidoreductase, function unknown; FNR, NarL and NarP regulons	n.s.	-10	-42	n.s.	-9	n.s.	
b2024	hisA	E	Phosphoribosylformimino-5-aminoimidazole carboxamide ribotide isomerase; 1-(5'-phosphoribosyl)-5-[(5'-phosphoribosylamino)methylideneamino] imidazole-4-carboxamide isomerase	n.s.	7	14	-9	-9	2	
b2025	hisF	E	Imidazole glycerol phosphate (IGP) synthase, cyclase subunit	n.s.	6	14	-7	-9	n.s.	
b2023	hisH	E	Imidazole glycerol phosphate (IGP) synthase, amidotransferase	n.s.	8	13	-8	-7	n.s.	
b2026	hisI	E	PR-ATP pyrophosphatase/PR-AMP cyclohydrolase, bifunctional	n.s.	6	13	-4	-10	n.s.	
b2022	hisB	E	Imidazoleglycerolphosphate dehydratase/histidinol phosphatase; bifunctional enzyme; HAD21	n.s.	13	13	-3	-3	n.s.	
b1744	astE	E	Succinylglutamate desuccinylase, arginine catabolism	n.s.	n.s.	9	n.s.	n.s.	n.s.	
b1745	astB	E	Succinylarginine dihydrolase, arginine catabolism	n.s.	3	6	n.s.	2	n.s.	
b2130	yehY	E	Putative ABC permease, function unknown; osmotically and stationary phase inducible; part of putative ABC transporter; membrane protein	n.s.	3	5	n.s.	n.s.	n.s.	
b2845	yqeG	E	Putative amino acid:H <sup>+</sup> symport permease, function unknown	n.s.	3	4	3	6	n.s.	
b3447	ggt	E	gamma-Glutamyltranspeptidase, glutathione metabolism; Ntn hydrolase; autocatalytic processing into two subunits; periplasmic	n.s.	n.s.	4	n.s.	n.s.	n.s.	
b2677	proV	E	High-affinity transport for glycine; glycine betaine-binding protein	n.s.	n.s.	4	n.s.	6	n.s.	
b2129	yehX	E	Putative ATP-binding protein, function unknown; osmotically and stationary phase inducible; part of putative ABC transporter	n.s.	3	4	2	n.s.	n.s.	
b2128	yehW	E	Putative ABC permease, function unknown; osmotically and stationary phase inducible; part of putative ABC transporter; membrane protein	n.s.	n.s.	3	n.s.	n.s.	n.s.	
b0854	potF	E	Putrescine ABC transporter periplasmic binding protein	n.s.	n.s.	3	-6	-2	n.s.	
b1851	edd	E	Phosphogluconate dehydratase; growth on gluconate	n.s.	-3	-3	n.s.	n.s.	n.s.	

b3540	dppF	E	Dipeptide/heme transport, ATP-binding protein; also transports 5-aminolevulinic acid	n.s.	-3	-3	-3	-42	n.s.
b0007	yaaJ	E	Predicted transporter, sodium:alanine (SAF) symporter family; function unknown	n.s.	-3	-4	-3	-5	n.s.
b3110	yhaO	E	Putative amino acid:H <sup>+</sup> symport permease, function unknown	n.s.	n.s.	-4	2	n.s.	n.s.
b3415	gntT	E	High-affinity gluconate transport	n.s.	-4	-5	-2	-7	n.s.
b2146	preT	E	Dihydropyrimidine dehydrogenase, NADH-dependent, subunit N; pyrimidine metabolism; upregulated in biofilms	n.s.	-4	-9	n.s.	n.s.	n.s.
b2957	ansB	E	L-Asparaginase II	n.s.	-4	-18	n.s.	-6	n.s.
b4213	cpdB	F	2',3'-cyclic nucleotide 2'-phosphodiesterase, periplasmic	n.s.	n.s.	-2	n.s.	n.s.	n.s.
b3831	udp	F	Uridine phosphorylase	n.s.	-3	-4	n.s.	-3	n.s.
b1623	add	F	Adenosine deaminase	n.s.	-5	-5	n.s.	-3	n.s.
b2147	preA	F	Dihydropyrimidine dehydrogenase, NADH-dependent, subunit C; pyrimidine metabolism; required for swarming phenotype	n.s.	-2	-5	n.s.	n.s.	n.s.
b4238	nrdD	F	Ribonucleoside-triphosphate reductase; class III anaerobic ribonucleotide reductase	n.s.	-2	-5	n.s.	-3	n.s.
b3452	ugpA	G	sn-Glycerol-3-phosphate transport system, integral membrane protein	n.s.	3	15	n.s.	12	n.s.
b3364	tsgA	G	Putative transporter, tellurite-inducible, function unknown; also induced by selenite	n.s.	8	13	2	6	n.s.
b3451	ugpE	G	sn-Glycerol-3-P transport system; membrane protein	n.s.	n.s.	8	n.s.	n.s.	n.s.
b1896	otsA	G	Trehalose phosphate synthase; cold- and heat- induced; required for viability at 4C; rpoS regulon	n.s.	3	7	-2	-2	n.s.
b2587	kgtP	G	alpha-Ketoglutarate permease	n.s.	3	4	n.s.	2	n.s.
b2465	tktB	G	Transketolase B; binds Zn(II)	n.s.	n.s.	4	n.s.	n.s.	n.s.
b1197	treA	G	Trehalase, periplasmic	n.s.	n.s.	3	n.s.	n.s.	n.s.
b0963	mgsA	G	Methylglyoxal synthase	n.s.	n.s.	-2	n.s.	n.s.	n.s.
b4211	qorB	G	Quinone oxidoreductase B, NADPH dependent; QOR2	n.s.	n.s.	-2	n.s.	n.s.	n.s.
b3599	mtlA	G	Mannitol-specific Enzyme IIABC of PTS transport system	n.s.	n.s.	-2	n.s.	n.s.	n.s.
b0837	ylil	G	Soluble aldose sugar dehydrogenase; Asd; binds PQQ; outer membrane protein	n.s.	n.s.	-2	n.s.	n.s.	n.s.
b0679	nagE	G	PTS system EIIABC(Nag) component; N-acetylglucosamine transport	n.s.	n.s.	-3	-3	-3	n.s.
b3526	kdgK	G	Ketodeoxygluconokinase	n.s.	n.s.	-3	2	n.s.	n.s.
b1594	mlc	G	Global transcriptional repressor; regulates pts operon expression at P0; required for anaerobic growth on glucosamine, binds nagC promoters; regulates manX and malT; makes large colonies; autorepressor	n.s.	-2	-3	n.s.	n.s.	n.s.
b1521	uxaB	G	D-Altronate oxidoreductase, NAD-dependent; galacturonate branch of hexuronate	n.s.	-3	-3	n.s.	n.s.	n.s.

			pathway							
b3881	yihT	G	Function unknown, LacD sugar aldolase family	n.s.	n.s.	-3	n.s.	n.s.	n.s.	n.s.
b3883	yihV	G	Predicted sugar kinase, function unknown	n.s.	n.s.	-3	n.s.	n.s.	n.s.	n.s.
b2388	glk	G	Glucokinase	n.s.	n.s.	-4	-2	-2	n.s.	n.s.
b3132	kbaZ	G	Ketose bisphosphate aldolase KbaYZ subunit; required for full activity and stability of KbaY	n.s.	-3	-5	n.s.	n.s.	n.s.	n.s.
b0129	yadI	G	Predicted PTS Enzyme IIA, sugar specificity unknown	n.s.	-3	-5	-5	-6	n.s.	n.s.
b0994	torT	G	Periplasmic TMAO binding protein; required for ToSR response to TMAO	n.s.	-2	-5	n.s.	n.s.	n.s.	n.s.
b2167	fruA	G	Fructose permease, PTS Enzyme IIBC component	n.s.	n.s.	-5	n.s.	-2	n.s.	n.s.
b1200	dhaK	G	Dihydroxyacetone kinase, PTS-dependent, dihydroxyacetone-binding subunit; DhaK(2):DhaL:DhaM(2) complex	n.s.	-4	-6	-2	-3	n.s.	n.s.
b3128	garD	G	D-galactarate dehydratase; uxaA paralog; contains conserved CxxS redox motif	n.s.	-3	-6	n.s.	n.s.	n.s.	n.s.
b2703	srlE	G	Glucitol/sorbitol-specific enzyme IIB component of PTS	n.s.	-15	-9	-4	-40	n.s.	n.s.
b2702	srlA	G	D-glucitol-specific enzyme II of phosphotransferase system	n.s.	-9	-25	-3	-44	n.s.	n.s.
b0774	bioA	H	7,8-diaminopelargonic acid aminotransferase	n.s.	n.s.	5	-7	-9	9	9
b0775	bioB	H	Biotin synthase; dethiobiotin to biotin pathway; iron-sulfur enzyme	n.s.	n.s.	5	-2	-4	15	15
b2311	ubiX	H	3-octaprenyl-4-hydroxybenzoate carboxylase; UbiD isozyme	n.s.	3	2	n.s.	n.s.	n.s.	n.s.
b0751	pnuC	H	Nicotinamide riboside uptake permease	n.s.	-3	-3	n.s.	-2	-4	-4
b0750	nadA	H	Quinolate synthase, [4Fe-4S] cluster subunit, A protein	n.s.	-3	-4	n.s.	-5	n.s.	n.s.
b3846	fadB	I	Multifunctional fatty acid oxidation complex subunit alpha; four enzyme activities: L-3-hydroxyacyl-CoA dehydrogenase, 3-hydroxyacyl-CoA epimerase, dodecenoyl-CoA-delta-isomerase, and small-chain-length enoyl-CoA hydratase (crotase)	n.s.	6	9	n.s.	n.s.	n.s.	n.s.
b3845	fadA	I	3-ketoacyl-CoA thiolase, fatty acid oxidation complex subunit beta	n.s.	3	4	n.s.	n.s.	n.s.	n.s.
b3918	cdh	I	CDP-diglyceride hydrolase; Salmonella ortholog has both UDP sugar hydrolase (UshB) and NAD pyrophosphatase (PnuE) activities	n.s.	3	3	n.s.	n.s.	n.s.	n.s.
b0039	caiA	I	Crotonobetaine reductase, CII component	n.s.	n.s.	-2	n.s.	n.s.	n.s.	n.s.
b2426	ucpA	I	Furfural resistance, predicted oxidoreductase, COG1028 family	n.s.	n.s.	-3	n.s.	n.s.	n.s.	n.s.
b3157	yhbT	I	Function unknown, COG3154 family of putative lipid carrier proteins	n.s.	n.s.	-3	2	n.s.	n.s.	n.s.
b2705	srlD	I	Sorbitol-6-phosphate dehydrogenase	n.s.	-5	-6	n.s.	-6	n.s.	n.s.
b3882	yihU	I	gamma-Hydroxybutyrate dehydrogenase, NADH-dependent	n.s.	n.s.	-6	n.s.	n.s.	n.s.	n.s.
b0296	ykgM	J	50S ribosomal protein L31 type B; alternative L31 utilized during zinc limitation	n.s.	4	5	13	6	n.s.	n.s.



b0330	prpR	K	Transcriptional regulator of prp operon; propionate catabolism via 2-methylcitrate cycle, characterized primarily in Salmonella	n.s.	4	12	n.s.	n.s.	n.s.
b3604	lldR	K	Dual role activator/repressor for lldPRD operon	n.s.	4	5	-6	n.s.	n.s.
b0059	rapA	K	RNA polymerase binding protein; mutants are UV-S; mutant biofilms have less polysaccharide and are antibiotic sensitive; ATPase and putative helicase	n.s.	n.s.	3	-3	n.s.	n.s.
b0345	lacI	K	Transcriptional repressor of lac operon	n.s.	2	2	2	2	n.s.
b1916	sdiA	K	Quorum-sensing ftsQAZ-P2, acrABCDE transcriptional activator; fluoroquinolone resistance; overproduction confers drug resistance by stimulating the acr genes; SdiA senses exogenous N-acyl homoserine lactones	n.s.	n.s.	2	n.s.	3	n.s.
b0080	cra	K	Catabolite repressor-activator	n.s.	n.s.	-2	n.s.	n.s.	n.s.
b1620	malI	K	Maltose regulon regulatory protein	n.s.	n.s.	-2	n.s.	n.s.	n.s.
b1799	dmlR	K	Transcriptional activator for dmlA, autorepressor	n.s.	n.s.	-3	n.s.	n.s.	n.s.
b1071	flgM	K	Anti-sigma 28 (FlhA) factor; regulator of FlhD	n.s.	n.s.	-3	4	3	n.s.
b3118	tdcA	K	Transcriptional activator of tdc operon	n.s.	-5	-6	3	n.s.	n.s.
b1922	fliA	K	Transcription factor sigma 28 for class III flagellar operons	n.s.	-3	-6	n.s.	n.s.	n.s.
b2869	ygeV	K	Putative RpoN-dependent transcriptional activator, function unknown; induced by AI-2 pheromone	n.s.	-3	-6	n.s.	n.s.	n.s.
b3906	rhaR	K	Transcriptional activator for rhaSR, AraC family	n.s.	n.s.	-7	n.s.	n.s.	n.s.
b4116	adiY	K	Transcriptional activator for adiA, AraC family	n.s.	-7	-11	n.s.	-3	-5
b4313	fimE	L	Site-specific recombinase, fimA promoter inversion; biased towards the ON to OFF fimbriae phase switching direction	n.s.	2	4	3	3	n.s.
b0708	phr	L	Deoxyribodipyrimidine photolyase; DNA photolyase; monomeric	n.s.	n.s.	3	n.s.	n.s.	n.s.
b1652	rnt	L	RNase T; RNA processing	n.s.	n.s.	2	-2	n.s.	n.s.
b4312	fimB	L	Site-specific recombinase, fimA promoter inversion; mediates fimbriae phase switching, along with FimE	n.s.	n.s.	-2	3	3	n.s.
b2028	ugd	M	UDP-glucose 6-dehydrogenase	n.s.	5	8	n.s.	8	n.s.
b2253	arnB	M	UDP-4-amino-4-deoxy-L-arabinose synthase; UDP-4-ketopentose aminotransferase; L-glutamate is the amine donor	n.s.	6	7	4	8	n.s.
b2131	osmF	M	Predicted periplasmic binding protein, function unknown; osmotically and stationary phase inducible; part of putative ABC transporter	n.s.	5	4	n.s.	n.s.	n.s.
b3047	yqiH	N	Predicted periplasmic pilus chaperone, function unknown	n.s.	n.s.	5	n.s.	n.s.	n.s.
b1888	cheA	N	Histidine protein kinase sensor of chemotactic response; CheY is cognate response regulator; autophosphorylating; CheAS is a short form produced by an internal start at codon 98	n.s.	n.s.	-3	-3	-3	n.s.

b1890	motA	N	H <sup>+</sup> -driven stator protein of flagellar rotation	n.s.	n.s.	-3	3	3	n.s.
b1889	motB	N	H <sup>+</sup> -driven stator protein of flagellar rotation	n.s.	n.s.	-3	n.s.	n.s.	n.s.
b1070	flgN	N	Initiation of flagellar filament assembly	n.s.	n.s.	-3	3	n.s.	n.s.
b1884	cheR	N	Chemotaxis MCP protein methyltransferase, SAM-dependent; binds C-terminus of chemoreceptors; makes glutamate methyl esters	n.s.	-5	-3	-60	-22	n.s.
b1083	flgL	N	Flagellar synthesis, hook-associated protein	n.s.	n.s.	-3	6	4	n.s.
b1883	cheB	N	Chemotaxis MCP protein-glutamate methylesterase; reverses CheR methylation at specific MCP glutamates	n.s.	-5	-3	-28	-24	n.s.
b1923	fliC	N	Flagellin, structural gene, H-antigen	n.s.	n.s.	-3	n.s.	n.s.	-2
b1924	fliD	N	Hook-associated protein 2, axial family	n.s.	-2	-4	-7	-8	n.s.
b1881	cheZ	N	CheY-P phosphatase	n.s.	-6	-4	-5	-22	n.s.
b1082	flgK	N	Flagellar synthesis, hook-associated protein	n.s.	n.s.	-4	4	2	n.s.
b1885	tap	N	Dipeptide chemoreceptor, methyl-accepting; MCP IV; flagellar regulon	n.s.	-5	-4	-33	-15	n.s.
b1925	fliS	N	Flagellar chaperone, inhibits premature FliC assembly; cytosolic	n.s.	-3	-4	-43	-80	n.s.
b1886	tar	N	Aspartate, maltose chemoreceptor, methyl-accepting; MCP II; also senses repellents cobalt and nickel; flagellar regulon	n.s.	-3	-5	n.s.	n.s.	n.s.
b2110	yehC	N	Predicted periplasmic pilus chaperone, function unknown	n.s.	-14	-13	n.s.	-8	n.s.
b3064	tsaD	O	tRNA(NNU) t(6)A37 threonylcarbamoyladenine modification; glycation binding protein	n.s.	3	2	3	3	n.s.
b4237	nrdG	O	Ribonucleotide reductase activase, generating glycyl radical; contains iron; binds NrdD tightly	n.s.	-5	-4	n.s.	-3	n.s.
b2730	hypE	O	Hydrogenases 1,2,3 accessory protein, carbamoyl dehydratase; required for CN ligand synthesis at the metallocenter; converts thiocarbamate at its C-terminal Cys to a thiocyanate	n.s.	-5	-6	n.s.	-3	n.s.
b3908	sodA	P	Superoxide dismutase, Mn	n.s.	n.s.	11	n.s.	n.s.	n.s.
b1797	yeaR	P	Stress-induced protein, function unknown; DUF1971 family; involved in cadmium and peroxide resistance	n.s.	5	11	3	9	n.s.
b3070	yqjH	P	Ferric-chelate reductase, NADPH-dependent; siderophore-interacting protein (SIP); nickel-resistance	n.s.	4	11	n.s.	n.s.	n.s.
b3728	pstS	P	Periplasmic phosphate binding protein, high-affinity; ABC phosphate transport system	n.s.	16	8	86	165	n.s.
b1469	narU	P	Nitrite extrusion protein 2	n.s.	n.s.	6	3	n.s.	n.s.
b1732	katE	P	Catalase HPII, heme d-containing; hydroperoxidase II; response to oxidative stress; chromate resistance	n.s.	-3	3	n.s.	-2	n.s.

b1308	pspE	P	Rhodanese, thiosulfate:cyanide sulfurtransferase; expressed in response to stress as part of psp operon, but also transcribed independently	n.s.	n.s.	-2	n.s.	n.s.	n.s.
b4046	zur	P	Repressor for znuABC, the zinc high-affinity transport genes; dimer; binds two Zn(II) ions per monomer	n.s.	n.s.	-2	n.s.	n.s.	n.s.
b0765	modC	P	Molybdate uptake; chlorate resistance	n.s.	n.s.	-3	n.s.	n.s.	n.s.
b2431	yfeX	P	Porphyrinogen oxidase, cytoplasmic; binds heme and protoporphyrin IX (PPIX)	n.s.	-3	-3	n.s.	n.s.	n.s.
b3367	nirC	P	Nitrite uptake transporter; membrane protein	n.s.	-6	-4	n.s.	-4	n.s.
b4070	nrfA	P	Cytochrome c nitrite reductase, cytochrome c552, periplasmic; formate-dependent; required for NO synthesis	n.s.	-14	-5	n.s.	-9	n.s.
b2292	yfbS	P	Putative transporter, function unknown	n.s.	-3	-6	n.s.	-3	n.s.
b4073	nrfD	P	Formate-dependent nitrite reduction; transmembrane protein similar to QOR	n.s.	-15	-6	n.s.	-4	n.s.
b1656	sodB	P	Superoxide dismutase, Fe; response to oxidative stress; chromate resistance; negatively regulated by ryhB RNA as part of indirect positive regulation by Fur; acid-inducible	n.s.	-3	-6	-8	-17	n.s.
b3518	yhjA	P	Probable cytochrome c peroxidase; mutants are sensitive to peroxide during anaerobic growth	n.s.	-5	-6	n.s.	-2	n.s.
b1223	narK	P	Nitrate/nitrite antiporter; promotes nitrite extrusion and uptake	n.s.	-8	-7	n.s.	-5	n.s.
b3366	nirD	P	Nitrite reductase [NAD(P)H] subunit	n.s.	-29	-14	-3	-19	n.s.
b4114	eptA	R	Lipid A phosphoethanolamine transferase, associated with polymyxin resistance	n.s.	12	10	-8	n.s.	n.s.
b1055	yceA	R	Predicted rhodanese, function unknown	n.s.	5	7	-2	n.s.	n.s.
b2210	mgo	R	Malate oxidoreductase; possibly previously described FAD-dependent phospholipid-activated malate oxidase	n.s.	n.s.	7	2	8	n.s.
b1973	zinT	R	Periplasmic zinc and cadmium binding protein; induced by zinc, cadmium or peroxide; Zur, SoxS and Fur regulated	n.s.	n.s.	5	4	n.s.	n.s.
b2660	lhgO	R	L-2-hydroxyglutarate oxidase; second gene in csiD-lhgO-gabDTP-csiR operon	n.s.	2	4	n.s.	n.s.	n.s.
b3819	rarD	R	Chloramphenicol resistance	n.s.	3	3	2	4	n.s.
b3399	yrfG	R	GMP/IMP nucleotidase; physiological role unknown; HAD8	n.s.	n.s.	2	n.s.	n.s.	n.s.
b1539	ydfG	R	Malonic semialdehyde reductase, NADPH-dependent; L-allo-threonine dehydrogenase, NADP+-dependent, other in vitro substrates include L-serine, D-serine, D-threonine and 3-hydroxyisobutyrate	n.s.	n.s.	-2	n.s.	n.s.	n.s.
b2991	hybF	R	Accessory protein required for the maturation of hydrogenases 1 and 2; may be involved in nickel incorporation	n.s.	n.s.	-3	2	n.s.	n.s.
b1601	tqsA	R	Pheromone AI-2 transporter; mutants have increased intracellular AI-2 and decreased extracellular AI-2; controls biofilm formation	n.s.	n.s.	-3	n.s.	n.s.	n.s.
b4055	aphA	R	Acid phosphatase, periplasmic, class B, nucleotidase; active on 3'- and 5'-	n.s.	n.s.	-3	n.s.	n.s.	n.s.

			mononucleotides and monodeoxynucleotides; glucose-repressed; monomeric						
b2877	mocA	R	CTP:molybdopterin cytidyltransferase; converts Mo-molybdopterin (Mo-MPT) cofactor (Moco) to the molybdopterin cytosine dinucleotide (MCD) cofactor (a Moco form)	n.s.	n.s.	-4	2	n.s.	-9
b4079	fdhF	R	Formate dehydrogenase H, selenopeptide; molybdate-dependent, sulfur-dependent; part of FHL-1 and FHL-2 (formate hydrogenlyase) complexes	n.s.	-5	-6	n.s.	-3	n.s.
b1590	ynfH	R	S- and N-oxide reductase, membrane bound anchor	n.s.	-2	-8	n.s.	n.s.	n.s.
b2579	grcA	R	Autonomous glycine radical cofactor; can reactivate pyruvate formate lyase after oxidative stress; induced by low pH or propionate; pyruvate formate lyase homolog, spare part for PFL	n.s.	-6	-8	n.s.	n.s.	n.s.
b0896	dmsC	R	DMSO reductase subunit C, periplasmic; has a membrane bound anchor	n.s.	-6	-14	3	-2	n.s.
b0788	ybhN	S	Function unknown	n.s.	n.s.	7	n.s.	n.s.	n.s.
b1706	ydiU	S	Function unknown, UPF0061 family	n.s.	4	6	n.s.	2	n.s.
b1520	yneE	S	Predicted inner membrane protein, bestrophin family; possible chloride channel; required for swarming phenotype	n.s.	n.s.	6	n.s.	2	n.s.
b0707	ybgA	S	Function unknown, DUF1722 family	n.s.	n.s.	6	-4	-3	n.s.
b0456	ybaA	S	Function unknown, DUF1428 family	n.s.	n.s.	6	2	n.s.	n.s.
b4045	yjbJ	S	Stress-induced protein, UPF0337 family, function unknown	n.s.	7	6	n.s.	3	n.s.
b1784	yeaH	S	UPF0229 family protein, function unknown	n.s.	n.s.	6	n.s.	n.s.	n.s.
b1536	ydeI	S	Predicted secreted protein, function unknown	n.s.	3	4	n.s.	6	n.s.
b0404	acpH	S	Acyl carrier protein (ACP) phosphodiesterase; ACP hydrolyase	n.s.	2	3	2	n.s.	n.s.
b3099	yqjE	S	Inner membrane protein, DUF1469 family, function unknown	n.s.	n.s.	3	2	2	n.s.
b0195	tsaA	S	tRNA-Thr(GGU) m(6)t(6)A37 methyltransferase, SAM-dependent	n.s.	n.s.	2	-4	-2	n.s.
b3858	yihD	S	Function unknown, DUF1040 family	n.s.	n.s.	-3	n.s.	n.s.	n.s.
b4329	yjiG	S	Inner membrane protein, SpmB family, function unknown	n.s.	n.s.	-3	n.s.	n.s.	n.s.
b2298	yfcC	S	Putative transporter, function unknown	n.s.	-4	-4	n.s.	-3	n.s.
b1976	mtfA	S	Mlc anti-repressor; binds Mlc and blocks its repression of ptsG; cytoplasmic	n.s.	n.s.	-4	n.s.	-2	n.s.
b4363	yjjB	S	Function unknown; expressed P14 protein upstream of dnaTC; putative membrane protein with 4 TM helices	n.s.	-8	-4	n.s.	-6	n.s.
b1753	ynjA	S	Function unknown	n.s.	-2	-4	n.s.	n.s.	n.s.
b0735	ybgE	S	Function unknown, cydAB operon, expressed in minicells	n.s.	-5	-7	n.s.	-2	n.s.
b1752	ydjZ	S	Inner membrane protein, TVP38/TMEM64 family, function unknown	n.s.	-5	-8	n.s.	-5	n.s.

b4515	cydX	S	Expressed protein, membrane-associated, function unknown	n.s.	-3	-11	n.s.	n.s.	n.s.
b1163	bluF	T	Anti-repressor for BluR(YcgE), blue light-responsive; cold shock gene, binds FAD; photoinduced dimerization	n.s.	3	9	n.s.	3	n.s.
b1783	yeaG	T	Protein kinase, function unknown; autokinase	n.s.	5	6	-3	n.s.	n.s.
b1786	yeaJ	T	Predicted membrane-anchored diguanylate cyclase	n.s.	n.s.	3	3	3	n.s.
b2469	narQ	T	Nitrate/nitrite sensor-transmitter protein; anaerobic respiratory path; cognate regulator is NarP; function redundant with narX	n.s.	n.s.	-2	n.s.	n.s.	n.s.
b0993	torS	T	Sensor kinase for torCAD operon	n.s.	-3	-3	n.s.	n.s.	n.s.
b4679	yohP	#N/A	Expressed protein, membrane-associated, function unknown	n.s.	9	18	6	19	n.s.
b1481	bdm	#N/A	Osmoresponsive gene with reduced expression in biofilms; function unknown	n.s.	12	8	n.s.	n.s.	n.s.
b1989	asnV	#N/A	Asparagine tRNA(GUU)	n.s.	n.s.	8	n.s.	n.s.	n.s.
b2252	ais	#N/A	Predicted LPS core heptose(II)-phosphate phosphatase; aluminum-inducible protein; Salmonella ortholog is regulated by PmrAB(BasRS)	n.s.	11	8	7	14	n.s.
b1167	ymgC	#N/A	Blue light, low temperature and stress induced, function unknown; BluRF(YcgEF) and RpoS regulons	n.s.	n.s.	7	13	86	n.s.
b1259	yciG	#N/A	Required for swarming phenotype, function unknown	n.s.	n.s.	6	n.s.	n.s.	n.s.
b1836	yebV	#N/A	Function unknown	n.s.	2	5	n.s.	3	n.s.
b0971	serT	#N/A	Serine tRNA(UGA) 1	n.s.	2	4	n.s.	n.s.	n.s.
b2659	csiD	#N/A	Carbon starvation induced gene, function unknown; first gene in csiD-lhgO-gabDTP operon; tetrameric; structural homolog of 2-oxoglutarate Fe(II)-dependent oxygenases	n.s.	4	4	n.s.	n.s.	n.s.
b4431	rprA	#N/A	Positive regulatory antisense sRNA for rpoS translation	n.s.	4	4	4	4	n.s.
b0458	ylaC	#N/A	Inner membrane protein, DUF1449 family, function unknown	n.s.	5	3	4	8	n.s.
b0234	yafP	#N/A	Predicted acetyltransferase; antimutator activity towards 4-nitroquinoline-1-oxide; lexA regulon	n.s.	-2	3	n.s.	n.s.	n.s.
b2939	yqgB	#N/A	Soluble expressed protein, function unknown	n.s.	n.s.	3	n.s.	n.s.	n.s.
b4542	yohO	#N/A	Expressed protein, function unknown	n.s.	n.s.	3	3	3	n.s.
b1626	ydgK	#N/A	Inner membrane protein, DUF2569 family, function unknown	n.s.	4	3	5	10	n.s.
b1445	ydcX	#N/A	Required for swarming phenotype, DUF2566 family, function unknown	n.s.	n.s.	3	n.s.	n.s.	n.s.
b3046	yqiG	#N/A	Pseudogene reconstruction, FimD family, interrupted by IS2I; outer membrane fimbrial subunit export usher protein family	n.s.	n.s.	3	n.s.	3	n.s.
b4134	pheU	#N/A	Phenylalanine tRNA(GAA)	n.s.	3	3	n.s.	n.s.	n.s.
b3100	yqiK	#N/A	Function unknown	n.s.	n.s.	3	2	2	n.s.

b4537	yecJ	#N/A	Function unknown	n.s.	n.s.	3	n.s.	2	n.s.
b1332	ynaJ	#N/A	Predicted inner membrane protein, DUF2534 family, function unknown	n.s.	2	2	3	4	n.s.
b4696	yneO	#N/A	Pseudogene reconstruction, putative OM autotransporter adhesin; AidA homolog	n.s.	n.s.	-2	n.s.	n.s.	n.s.
b4447	sibD	#N/A	Antisense sRNA regulator of toxic IbsD protein; in SIBd repeat	n.s.	n.s.	-2	n.s.	n.s.	n.s.
b4436	sibA	#N/A	Antisense sRNA regulator of toxic IbsA protein; in SIBa repeat	n.s.	n.s.	-2	n.s.	n.s.	n.s.
b2598	pheL	#N/A	pheA gene regulatory leader peptide	n.s.	n.s.	-2	n.s.	n.s.	n.s.
b3410	feoC	#N/A	Ferrous iron uptake, required for full FeoB activity; putative Fe <sup>2+</sup> S cluster redox or iron sensing transcriptional regulator	n.s.	n.s.	-2	-4	-6	n.s.
b4437	sibB	#N/A	Antisense sRNA regulator of toxic IbsB protein; in SIBb repeat	n.s.	n.s.	-2	n.s.	n.s.	n.s.
b2399	yfeD	#N/A	Conserved protein, DUF1323 family, function unknown; N-terminal HTH domain of the MerR superfamily	n.s.	n.s.	-3	n.s.	n.s.	n.s.
b2992	hybE	#N/A	Hydrogenase 2-specific chaperone	n.s.	n.s.	-3	n.s.	n.s.	n.s.
b4602	ynhF	#N/A	Stress response membrane protein, function unknown	n.s.	n.s.	-3	2	2	n.s.
b2205	napG	#N/A	Quinol dehydrogenase, periplasmic protein; mediates electron transfer from ubiquinol/naphthoquinone to NapAB, via NapC; non-haem, iron-sulfur protein	n.s.	-31	-4	-7	-20	7
b4071	nrfB	#N/A	Cytochrome c nitrite reductase, pentaheme cytochrome, periplasmic; formate-dependent; required for NO synthesis	n.s.	-11	-4	n.s.	-9	n.s.
b1926	fliT	#N/A	Flagellar synthesis, predicted chaperone, role unknown	n.s.	-4	-5	-56	-61	n.s.
b1921	fliZ	#N/A	DNA-binding RpoS antagonist; transiently inhibits RpoS in post-exponential phase; timing factor allowing motility to continue for a while during starvation; not required for normal motility	n.s.	-4	-5	n.s.	n.s.	n.s.
b0848	ybjM	#N/A	Inner membrane protein, function unknown	n.s.	n.s.	-5	6	4	-3
b4606	ypfM	#N/A	Soluble expressed protein, function unknown	n.s.	-2	-6	2	n.s.	n.s.
b1265	trpL	#N/A	Regulatory leader peptide for trp operon	n.s.	-5	-7	n.s.	-4	-3
b0375	yaiV	#N/A	Predicted transcriptional regulator, function unknown	n.s.	-8	-8	n.s.	n.s.	n.s.
b4697	yrdF	#N/A	Pseudogene, N-terminal fragment	n.s.	n.s.	-8	n.s.	n.s.	n.s.
b2876	yqeC	#N/A	Function unknown	n.s.	-7	-12	2	n.s.	n.s.
b0919	ycbJ	#N/A	Function unknown	n.s.	-8	-16	n.s.	-3	n.s.

Late phase response to PMA									
Gene ID	Gene name	COG code	Protein description	Hg t10	Hg t30	Hg t60	PMA t10	PMA t30	PMA t60
b2905	gcvT	E	Aminomethyltransferase, tetrahydrofolate dependent; T-protein of the glycine cleavage system	n.s.	n.s.	n.s.	n.s.	n.s.	5
b2518	ndk	F	Nucleoside diphosphate kinase; NDP kinase	-3	n.s.	n.s.	n.s.	2	4
b0523	purE	F	N5-carboxyaminoimidazole ribonucleotide (N-CAIR) mutase; purine synthesis	-7	n.s.	5	n.s.	n.s.	3
b3635	mutM	L	Formamidopyrimidine-DNA glycosylase/AP lyase; 5'-terminal deoxyribophosphodiesterase; DNA repair; GC to TA; binds Zn(II)	4	3	n.s.	n.s.	n.s.	3
b3024	ygiW	S	Stress-induced protein, function unknown; involved in cadmium and peroxide resistance; secreted protein; binds CsrB sRNA	5	4	n.s.	n.s.	3	3
b1320	ycjW	K	Hyperlethality gene, required for swarming phenotype	-2	n.s.	n.s.	n.s.	n.s.	2
b1969	yedW	K	Putative response regulator, function unknown	n.s.	n.s.	n.s.	n.s.	2	-2
b2097	fbaB	G	Fructose 1,6-bisphosphate aldolase, class I	n.s.	n.s.	n.s.	n.s.	-3	-2
b1923	fliC	N	Flagellin, structural gene, H-antigen	n.s.	n.s.	-3	n.s.	n.s.	-2
b1440	ydcS	E	Polyhydroxybutyrate (PHB) synthase; ABC transporter periplasmic binding protein homolog; upregulated during glucose-limitation	n.s.	n.s.	n.s.	n.s.	3	-3
b1265	trpL	#N/A	Regulatory leader peptide for trp operon	n.s.	-5	-7	n.s.	-4	-3
b4002	zraP	N	Zn-dependent periplasmic chaperone	3	27	43	n.s.	n.s.	-3
b4441	glmY	#N/A	sRNA activator of glmS mRNA, glmZ processing antagonist	n.s.	n.s.	n.s.	n.s.	n.s.	-3
b0751	pnuC	H	Nicotinamide riboside uptake permease	n.s.	-3	-3	n.s.	-2	-4
b4116	adiY	K	Transcriptional activator for adiA, AraC family	n.s.	-7	-11	n.s.	-3	-5
b0571	cusR	K	Response regulator of the cusCFBA-cusRS divergon; cusS sensor and cusR mediate copper induction	-3	-2	-7	n.s.	-3	-9

Table shows all genes that were not differentially expressed at 10 min, but were differentially expressed at 60 min time point.

Values represent fold-change in expression relative to unexposed condition. (green = up-regulated, red = down-regulated, and n.s. = not significantly different from unexposed control)

HgCl<sub>2</sub> response genes are grouped by up-regulated, then down-regulated for each COG category.  
PMA response is grouped by highest to lowest fold-change.

**Table D.S4: Transcriptional response of mercury modified proteins from proteomics analysis (Zink et al.)**

Gene ID	Gene name	protein_description	PMA spectra count	HgII spectra count	Hg t10	Hg t30	Hg t60	PMA t10	PMA t30	PMA t60
b2316	accD	Acetyl-CoA carboxylase, carboxyltransferase beta subunit	0	3	n.s.	n.s.	n.s.	3	3	n.s.
b4015	aceA	Isocitrate lyase, acetate utilization, glyoxylate shunt; tetrameric	143	0	n.s.	n.s.	n.s.	-10	-7	n.s.
b4014	aceB	Malate synthase A; glyoxylate shunt enzyme	10	0	n.s.	n.s.	n.s.	-3	n.s.	n.s.
b0114	aceE	Pyruvate dehydrogenase, decarboxylase component E1; acetate requirement	5	0	n.s.	-2	n.s.	n.s.	-2	n.s.
b0115	aceF	Pyruvate dehydrogenase, dihydrolipoamide acetyltransferase E2; acetate requirement	14	0	n.s.	-3	n.s.	-3	-4	n.s.
b2296	ackA	Acetate kinase, produces acetyl phosphate; mutants are fluoroacetate resistant; creBC regulon; binds Zn(II)	25	0	n.s.	-3	-3	n.s.	n.s.	n.s.
b0118	acnB	Aconitase B; 2-methylaconitate hydratase; apo-enzyme binds mRNA for negative translational autoregulation; iron-sulfur cluster; monomeric	0	30	2	2	n.s.	-6	-7	n.s.
b1241	adhE	Alcohol dehydrogenase, largely anaerobic; aerobic antioxidant; acetaldehyde-CoA dehydrogenase, CoA-linked; allyl alcohol resistance	28	11	-5	-9	-9	-20	-33	n.s.
b0605	ahpC	Alkyl hydroperoxide reductase, subunit C; reduced by the AhpF subunit	102	8	15	3	n.s.	3	2	n.s.
b2697	alaS	Alanine--tRNA ligase	2	0	-3	-3	n.s.	n.s.	n.s.	n.s.
b1415	aldA	Aldehyde dehydrogenase, NAD-dependent; active on lactaldehyde, glycolaldehyde, and other aldehydes	0	8	-5	-2	n.s.	-15	-7	n.s.
b3959	argB	N-acetylglutamate kinase	3	0	-6	n.s.	n.s.	-10	-5	n.s.
b3359	argD	Acetylornithine aminotransferase; succinyldiaminopimelate aminotransferase, PLP-dependent	22	0	-3	n.s.	n.s.	-11	-4	n.s.
b3957	argE	Acetylornithine deacetylase	5	0	n.s.	2	n.s.	n.s.	n.s.	n.s.
b0273	argF	Ornithine carbamoyltransferase; ornithine transcarbamylase; OTCase; CP4-6 putative prophage remnant	11	0	-4	n.s.	n.s.	-12	-6	n.s.
b3172	argG	Argininosuccinate synthase	4	0	-4	-3	n.s.	-6	-5	n.s.
b3960	argH	Argininosuccinate lyase	50	0	-5	-2	n.s.	-7	-6	n.s.
b4254	argI	Ornithine carbamoyltransferase; ornithine transcarbamylase; OTCase	12	11	n.s.	-2	n.s.	n.s.	n.s.	n.s.
b2310	argT	Lys-, Arg-, and Orn-binding protein, periplasmic	5	0	2	2	n.s.	n.s.	2	n.s.
b2255	arnA	UDP-glucuronate dehydrogenase and UDP-ara4N formyltransferase	1	0	-7	-5	n.s.	-17	-12	n.s.
b0754	aroG	3-deoxy-D-arabino-heptulosonate-7-phosphate (DAHP) synthase; phenylalanine repressible; TyrR regulon	130	17	n.s.	n.s.	n.s.	n.s.	n.s.	n.s.



b3433	asd	Aspartate semialdehyde dehydrogenase	60	0	n.s.	n.s.	n.s.	n.s.	-2	n.s.
b0674	asnB	Asparagine synthase B [glutamine-hydrolyzing]	5	5	-2	n.s.	n.s.	n.s.	n.s.	n.s.
b0930	asnS	Asparagine--tRNA ligase	1	0	n.s.	n.s.	n.s.	2	3	n.s.
b3734	atpA	ATP synthase subunit alpha, membrane-bound, F1 sector	86	16	-4	-4	n.s.	-4	-4	n.s.
b3732	atpD	ATP synthase subunit beta, membrane-bound, F1 sector	5	8	-3	-4	n.s.	-2	-5	n.s.
b3735	atpH	ATP synthase subunit delta, membrane-bound, F1 sector	5	0	-4	-4	n.s.	-3	-3	n.s.
b2480	bcp	Peroxiredoxin, thioredoxin-dependent thiol peroxidase; peroxide hypersensitivity; Prx	22	4	n.s.	4	n.s.	4	4	n.s.
b0126	can	Carbonic anhydrase, beta class	7	0	2	4	3	n.s.	n.s.	n.s.
b0032	carA	Carbamoyl phosphate synthase, small subunit; glutamine-hydrolyzing, tetramer of heterodimers	0	1	-5	n.s.	n.s.	-35	-16	n.s.
b1888	cheA	Histidine protein kinase sensor of chemotactic response; CheY is cognate response regulator; autophosphorylating; CheAS is a short form produced by an internal start at codon 98	13	0	n.s.	n.s.	-3	-3	-3	n.s.
b2592	clpB	Bichaperone with DnaK for protein disaggregation; disaggregase; protein-dependent ATPase; role in de novo protein folding under mild stress conditions	9	0	19	4	n.s.	n.s.	n.s.	n.s.
b3032	cpdA	3',5' cAMP phosphodiesterase; mutants have elevated cAMP levels	2	0	n.s.	n.s.	n.s.	n.s.	n.s.	n.s.
b0123	cueO	Multicopper oxidase (laccase), confers copper tolerance; oxidizes model substrate dimethoxyphenol; in vitro ferroxidase and phenoloxidase activities; regulated by copper-responsive CueR activator	3	0	21	18	n.s.	5	n.s.	-6
b1275	cysB	Transcriptional activator for the Cys regulon; N-acetylserine induced; autorepressor	10	5	-2	-3	n.s.	-4	-2	n.s.
b2752	cysD	Sulfate adenylyltransferase subunit 2	14	1	n.s.	-12	n.s.	-51	-47	n.s.
b2763	cysI	Sulfite reductase [NADPH] hemoprotein beta-component; has 4Fe-4S iron-sulfur center	0	6	-2	-14	n.s.	-40	-166	n.s.
b4214	cysQ	3'-phosphoadenosine 5'-phosphate (pAp) phosphatase; converts pAp to AMP; inhibited by lithium and calcium, leading to pAP accumulation; probable PAPS (adenosine 3'-phosphate 5'-phosphosulfate) 3'(2'),5'-bisphosphate nucleotidase: probably converts PAPS to	3	0	3	3	n.s.	4	3	n.s.
b0632	dacA	D-alanine D-alanine carboxypeptidase PBP5, cell morphology; penicillin-binding protein 5; beta-lactamase activity	2	0	-3	n.s.	n.s.	n.s.	n.s.	n.s.
b2478	dapA	Dihydrodipicolinate synthase	5	0	n.s.	n.s.	n.s.	4	3	n.s.
b0031	dapB	Dihydrodipicolinate reductase	21	1	-2	-2	n.s.	-2	n.s.	n.s.
b0166	dapD	2,3,4,5-tetrahydropyridine-2-carboxylate N-succinyltransferase; mutations suppress growth defects of strains lacking superoxide	34	0	n.s.	n.s.	n.s.	n.s.	n.s.	n.s.

		dismutase								
b1919	dcyD	D-cysteine desulfhydrase; needed for protection from, and utilization of, D-cysteine	12	0	n.s.	-3	n.s.	-3	-3	n.s.
b3162	deaD	ATP-dependent RNA helicase, 50S ribosomal subunit biogenesis; translation factor W2; factor X; facilitates translation of mRNAs with 5' secondary structures; multicopy suppressor of rpsB(Ts) mutations	1	0	n.s.	n.s.	n.s.	n.s.	n.s.	n.s.
b3287	def	Peptide deformylase; N-formylmethionylaminoacyl-tRNA deformylase	4	0	8	2	n.s.	3	2	n.s.
b4381	deoC	2-deoxy-D-ribose 5-phosphate aldolase (DERA); deoxyriboaldolase	19	0	n.s.	n.s.	n.s.	-2	-3	n.s.
b0160	dgt	Deoxyguanosine 5'-triphosphate triphosphohydrolase; dGTPase	1	0	n.s.	n.s.	n.s.	3	n.s.	n.s.
b1198	dhaM	Multidomain dihydroxyacetone-specific PTS protein; phosphoryl donor for dihydroxyacetone kinase; DhaK(2):DhaL:DhaM(2) complex	1	0	-3	-4	n.s.	-4	-4	n.s.
b0145	dksA	RNAP-binding protein modulating ppGpp and iNTP regulation; reduces open complex half-life on rRNA promoters; removes transcriptional roadblocks to replication	0	2	2	4	n.s.	4	5	n.s.
b1591	dmsD	Redox enzyme maturation protein (REMP) for DmsA; twin-arginine leader-binding protein; binds DmsA and TorA TAT signal peptides; required for anaerobic growth on glycerol-DMSO medium; stimulates growth on glycerol-fumarate	1	0	n.s.	n.s.	n.s.	2	n.s.	n.s.
b0015	dnaJ	DnaK co-chaperone HSP40; DNA-binding protein; stress-related DNA biosynthesis, responsive to heat shock; binds Zn(II)	8	0	6	n.s.	n.s.	n.s.	n.s.	n.s.
b3860	dsbA	Thiol:disulfide interchange protein, periplasmic; alkali-inducible	3	23	n.s.	n.s.	n.s.	n.s.	n.s.	n.s.
b3640	dut	dUTP pyrophosphatase; dUTPase	29	0	n.s.	2	n.s.	2	2	n.s.
b1850	eda	KHG/KDPG aldolase; 2-keto-4-hydroxyglutarate aldolase and 2-keto-3-deoxy-6-phosphogluconate aldolase activities; homotrimeric; 2-keto-4-hydroxyglutarate aldolase is also known as 4-hydroxy-2-oxoglutarate aldolase. 2-keto-3-deoxy-6-phosphogluconate aldolase	37	0	n.s.	n.s.	n.s.	n.s.	n.s.	n.s.
b3209	elbB	Involved in isoprenoid biosynthesis; also known as sigma cross-reacting protein 27A	16	0	2	n.s.	n.s.	n.s.	-2	n.s.
b2779	eno	Enolase; phosphoprotein; component of RNA degradosome	145	23	-3	-4	n.s.	-4	-3	n.s.
b4391	ettA	Predicted ABC transporter, ATP-binding protein; low abundance protein	4	0	n.s.	n.s.	n.s.	n.s.	n.s.	n.s.
b1092	fabD	Malonyl-CoA-acyl carrier protein transacylase	57	0	n.s.	n.s.	n.s.	n.s.	n.s.	n.s.
b1288	fabI	Enoyl-ACP reductase, NADH dependent	3	0	n.s.	n.s.	n.s.	-3	-3	n.s.
b0180	fabZ	3R-hydroxymyristoyl acyl carrier protein (ACP) dehydratase	1	0	n.s.	n.s.	n.s.	n.s.	n.s.	n.s.
b2925	fbaA	Fructose 1,6-bisphosphate aldolase, class II; binds Zn(II); homodimeric	92	0	n.s.	-5	n.s.	-3	-5	n.s.
b4232	fbp	Fructose-1,6-bisphosphatase; allosteric: inhibited by AMP	21	0	4	2	n.s.	3	2	n.s.

b2525	fdx	Ferredoxin, an iron-sulfur protein; involved in assembly of other Fe-S clusters	13	0	2	n.s.	n.s.	n.s.	n.s.	n.s.
b0684	fldA	Flavodoxin I	0	6	3	n.s.	n.s.	2	n.s.	n.s.
b3288	fmt	Methionyl-tRNA formyltransferase	1	0	7	n.s.	n.s.	n.s.	2	n.s.
b0529	folD	Methenyltetrahydrofolate dehydrogenase/cyclohydrolase	9	4	n.s.	n.s.	n.s.	n.s.	2	n.s.
b3178	ftsH	ATP-dependent membrane protease, complexed with HflCK; regulates lysogeny; mutants are defective in cell growth, septum formation and phage lambda development; mutants rescued by divalent cations; binds Zn(II); hexameric	1	0	6	n.s.	n.s.	n.s.	n.s.	n.s.
b1612	fumA	Fumarase A, aerobic; negatively regulated by ryhB RNA as part of indirect positive regulation by Fur	3	1	n.s.	n.s.	n.s.	n.s.	n.s.	n.s.
b0683	fur	Ferric iron uptake global transcriptional repressor; activated by Fe+2; zinc metalloprotein	0	3	13	9	n.s.	n.s.	n.s.	n.s.
b3340	fusA	Elongation Factor EF-G; GTPase required for translocation from the A-site to the P-site in the ribosome; fusidic acid resistance	63	9	-2	-3	n.s.	n.s.	n.s.	n.s.
b0756	galM	Galactose mutarotase, aldose-1-epimerase; monomeric	4	0	3	2	n.s.	3	2	n.s.
b1236	galU	Glucose-1-P uridylyltransferase; also called UDP-glucose pyrophosphorylase	32	0	n.s.	n.s.	n.s.	n.s.	n.s.	n.s.
b1779	gapA	Glyceraldehyde 3-P dehydrogenase A	43	178	-2	-4	-4	-2	-3	n.s.
b2094	gatA	Galactitol-specific PTS system EIIA component	20	0	-13	-26	n.s.	-19	-46	n.s.
b2093	gatB	Galactitol-specific PTS system EIIB component	64	0	-13	-21	n.s.	-13	-76	n.s.
b2096	gatY	D-Tagatose-1,6-bisphosphate aldolase, class II; requires GatZ subunit for full activity and stability	0	5	-5	-10	-13	-8	-10	n.s.
b2095	gatZ	Tagatose bisphosphate aldolase GatYZ subunit; required for full activity and stability of GatY	4	2	-12	-18	n.s.	-13	-15	n.s.
b2905	gecT	Aminomethyltransferase, tetrahydrofolate dependent; T-protein of the glycine cleavage system	1	0	n.s.	n.s.	n.s.	n.s.	n.s.	5
b1761	gdhA	Glutamate dehydrogenase	97	19	n.s.	-3	n.s.	-5	-5	n.s.
b3553	ghrB	Glyoxylate/hydroxypyruvate reductase B; 2-ketogluconate reductase; activity higher on hydroxypyruvate than glyoxylate	15	15	2	n.s.	n.s.	n.s.	n.s.	n.s.
b3429	glgA	Glycogen synthase	1	0	-2	-3	n.s.	-3	-3	n.s.
b3176	glmM	Phosphoglucosamine mutase; UDP-GlcNAc pathway, peptidoglycan, lipopolysaccharide synthesis; mRNA stability effects	11	0	2	n.s.	n.s.	n.s.	n.s.	n.s.
b3729	glmS	Glucosamine-6-phosphate synthase; glucosamine--fructose-6-phosphate aminotransferase; C-terminal F6P-binding domain has isomerase activity	10	0	-2	n.s.	n.s.	n.s.	n.s.	n.s.

b3870	glnA	Glutamine synthase	25	1	-9	-10	n.s.	-14	-27	n.s.
b2553	glnB	PII regulatory protein for glutamine synthase; potent activator of NRII/GlnL/NtrB phosphatase and inhibitor of NRII autophosphorylation; activates adenylation of GlnA by GlnE	9	0	n.s.	n.s.	n.s.	n.s.	n.s.	n.s.
b3426	glpD	sn-Glycerol-3-phosphate dehydrogenase (aerobic); membrane-anchored	22	0	6	2	n.s.	n.s.	n.s.	n.s.
b3926	glpK	Glycerol kinase	26	0	-4	-4	n.s.	-7	-7	n.s.
b0720	gltA	Citrate synthase; hexameric	178	8	n.s.	n.s.	n.s.	-3	n.s.	n.s.
b3212	gltB	Glutamate synthase, large subunit	38	0	-2	-3	n.s.	-4	-4	n.s.
b3213	gltD	Glutamate synthase, small subunit	51	1	n.s.	-5	n.s.	-5	-25	n.s.
b2400	gltX	Glutamate--tRNA ligase	2	0	-2	n.s.	n.s.	n.s.	n.s.	n.s.
b2551	glyA	Serine hydroxymethyltransferase; binds Zn(II)	108	0	n.s.	n.s.	n.s.	n.s.	n.s.	n.s.
b3559	glyS	Glycine--tRNA ligase, beta-subunit	26	0	-3	n.s.	n.s.	n.s.	n.s.	n.s.
b0222	gmhA	Phosphoheptose isomerase; D-sedoheptulose 7-phosphate isomerase; GDP-heptose biosynthesis; T-phage resistance	0	7	2	n.s.	n.s.	n.s.	n.s.	n.s.
b2029	gnd	6-phosphogluconate dehydrogenase, decarboxylating	16	0	n.s.	n.s.	n.s.	n.s.	n.s.	n.s.
b3612	gpmM	Phosphoglycerate mutase, Mn-dependent, cofactor-independent; iPGM; monomeric	1	0	-2	-5	-5	-3	-5	n.s.
b3608	gpsA	sn-Glycerol-3-phosphate dehydrogenase [NAD(P)+]	3	0	-4	-4	n.s.	-3	-4	n.s.
b4143	groL	Chaperonin Cpn60; phage morphogenesis; GroESL large subunit GroEL, weak ATPase; binds Ap4A	117	1	3	n.s.	n.s.	n.s.	n.s.	n.s.
b3610	grxC	Glutaredoxin 3	42	0	n.s.	n.s.	n.s.	2	n.s.	n.s.
b1654	grxD	Monothiol glutaredoxin Grx4 with CGFS motif; substrate for thioredoxin reductase; mutants are hypersensitive to iron depletion	0	1	n.s.	n.s.	n.s.	3	3	n.s.
b2688	gshA	Glutamate--cysteine ligase; gamma-Glutamylcysteine synthase	0	1	n.s.	n.s.	n.s.	n.s.	n.s.	n.s.
b0838	gstB	Glutathione transferase, iodoacetate-, bromoacetate-specific; natural substrate unknown	0	1	3	2	n.s.	3	n.s.	n.s.
b2507	guaA	GMP synthase	12	0	-2	-5	n.s.	-3	-4	n.s.
b2508	guaB	Inosine-5'-monophosphate (IMP) dehydrogenase	2	22	-3	-3	n.s.	-11	-11	n.s.
b0369	hemB	5-Aminolevulinate dehydratase; also known as porphobilinogen synthase; binds Zn(II)	1	0	3	n.s.	n.s.	n.s.	n.s.	n.s.
b0154	hemL	Glutamate-1-semialdehyde aminomutase	3	1	3	n.s.	n.s.	3	3	n.s.
b2022	hisB	Imidazoleglycerolphosphate dehydratase/histidinol phosphatase; bifunctional enzyme; HAD21	3	0	n.s.	13	13	-3	-3	n.s.
b2021	hisC	Histidinol-phosphate aminotransferase	2	0	2	19	16	-6	-12	n.s.

b2020	hisD	Histidinol dehydrogenase	1	0	4	22	n.s.	-6	-15	n.s.
b2025	hisF	Imidazole glycerol phosphate (IGP) synthase, cyclase subunit	32	0	n.s.	6	14	-7	-9	n.s.
b2019	hisG	ATP-phosphoribosyltransferase	3	0	6	12	n.s.	-5	-13	n.s.
b2023	hisH	Imidazole glycerol phosphate (IGP) synthase, amidotransferase	4	2	n.s.	8	13	-8	-7	n.s.
b2026	hisI	PR-ATP pyrophosphatase/PR-AMP cyclohydrolase, bifunctional	7	0	n.s.	6	13	-4	-10	n.s.
b2309	hisJ	Histidine-binding periplasmic protein; part of HisJMPQ ABC transporter	2	0	-3	n.s.	n.s.	-5	-3	2
		DNA-binding global regulator H-NS; diverse mutant phenotypes affecting transcription, transposition, inversion, cryptic-gene expression; involved in chromosome organization; preferentially binds bent DNA; has N-terminal dimerization domain								
b1237	hns		88	16	n.s.	n.s.	n.s.	3	5	n.s.
b4349	hsdM	DNA methyltransferase M, host modification of foreign DNA	3	0	-3	n.s.	n.s.	-4	-3	n.s.
b3401	hslO	Hsp33, oxidative stress-induced heat shock chaperone; C-terminal zinc-binding motif regulates Hsp33 activity	2	0	4	n.s.	n.s.	2	4	n.s.
		Heat-inducible ATP-dependent protease HslVU, ATPase subunit; involved in the degradation of misfolded proteins; heat shock protein D48.5								
b3931	hslU		3	0	5	n.s.	n.s.	n.s.	n.s.	n.s.
b1136	icd	Isocitrate dehydrogenase, NADP(+)-specific; e14 attachment site	2	5	2	n.s.	n.s.	n.s.	n.s.	n.s.
b0026	ileS	Isoleucine--tRNA ligase	8	0	n.s.	n.s.	n.s.	n.s.	n.s.	n.s.
b3671	ilvB	Acetohydroxy acid synthase I (AHAS-I); acetolactate synthase I (ALS-I); valine sensitive; large subunit	1	1	-5	-6	n.s.	n.s.	2	n.s.
b3774	ilvC	Ketol-acid reductoisomerase	121	147	-7	-7	n.s.	-17	-30	n.s.
		Acetohydroxy acid synthase III (AHAS-III); acetolactate synthase III (ALS-III); valine sensitive; large subunit								
b0077	ilvI		3	0	-2	-2	-2	n.s.	n.s.	n.s.
		Acetohydroxy acid synthase I (AHAS-I) regulatory subunit; acetolactate synthase I (ALS-I); valine sensitive; small subunit								
b3670	ilvN		6	0	-4	-6	n.s.	n.s.	3	n.s.
b3168	infB	Protein chain initiation factor IF2	2	0	n.s.	n.s.	n.s.	n.s.	n.s.	n.s.
b1718	infC	Protein chain initiation factor IF3; unusual AUU start codon	21	0	n.s.	n.s.	n.s.	n.s.	n.s.	n.s.
		Anti-RssB factor, RpoS stabilizer during Pi starvation; anti-adaptor protein								
b0382	iraP		24	0	2	n.s.	n.s.	9	8	n.s.
		Recruit and deliver Fe for Fe-S cluster assembly in IscU; possibly an alternative scaffold for Fe-S cluster assembly								
b2528	iscA		6	0	14	5	3	4	7	n.s.
b2529	iscU	Iron-sulfur cluster assembly scaffold protein	23	0	14	6	4	4	8	n.s.
		Iron binding protein associated with IscS; putative molecular adaptor of IscS function; monomeric								
b2524	iscX		12	0	2	n.s.	n.s.	n.s.	n.s.	n.s.

b2515	ispG	1-hydroxy-2-methyl-2-(E)-butenyl 4-diphosphate synthase; alternative nonmevalonate (DXP) pathway for terpenoid biosynthesis; [4Fe-4S] protein	7	0	n.s.	n.s.	n.s.	n.s.	n.s.	n.s.
b1215	kdsA	3-deoxy-D-manno-octulosonate 8-phosphate (KDO8-P) synthase; LPS biosynthesis	10	0	n.s.	n.s.	n.s.	2	2	n.s.
b0074	leuA	alpha-Isopropylmalate synthase	4	0	-2	n.s.	n.s.	7	7	n.s.
b0073	leuB	3-isopropylmalate dehydrogenase, NAD(+)-dependent	6	0	-3	-3	n.s.	2	3	n.s.
b0072	leuC	3-isopropylmalate dehydratase large subunit; also called alpha-isopropylmalate isomerase	37	0	-3	-5	n.s.	n.s.	3	n.s.
b0071	leuD	3-isopropylmalate dehydratase small subunit; also called alpha-Isopropylmalate isomerase	4	0	-2	-6	n.s.	n.s.	3	n.s.
b0642	leuS	Leucine--tRNA ligase	15	0	n.s.	n.s.	n.s.	n.s.	n.s.	n.s.
b3454	livF	Branched-chain amino acid ABC transporter, ATP-binding membrane protein, high-affinity	1	0	-5	-2	n.s.	-6	-7	n.s.
b3460	livJ	Leu/Ile/Val-binding protein, periplasmic, high-affinity transport; LIV-I system; also involved in phenylalanine accumulation	4	83	-10	-6	n.s.	-30	-21	n.s.
b0439	lon	DNA-binding, ATP-dependent protease LA; lon mutants form long cells	7	0	6	3	n.s.	3	3	n.s.
b0116	lpd	Lipoamide dehydrogenase, NADH-dependent; E3 component of pyruvate and 2-oxoglutarate dehydrogenase complexes; also functions as glycine cleavage system L protein; binds Zn(II)	7	11	n.s.	2	n.s.	n.s.	n.s.	n.s.
b0889	lrp	Global regulatory protein, Leu responsive; regulator of high-affinity branched-chain amino acid transport system; octameric or hexadecameric functional state	38	0	n.s.	n.s.	n.s.	n.s.	n.s.	n.s.
b2687	luxS	S-ribosylhomocysteine lyase, autoinducer 2 (AI-2) synthesis; functions in quorum sensing; acid-inducible	40	0	n.s.	n.s.	n.s.	2	n.s.	n.s.
b4024	lysC	Aspartokinase III	0	1	-2	-4	n.s.	-5	-8	n.s.
b2463	maeB	Malic enzyme, NADP-dependent; NADP-ME	11	0	n.s.	n.s.	n.s.	n.s.	n.s.	n.s.
b3236	mdh	Malate dehydrogenase, NAD-dependent	66	33	n.s.	n.s.	n.s.	-3	-3	n.s.
b1686	menI	Acyl-CoA esterase in vitro	2	0	n.s.	n.s.	n.s.	-3	-6	n.s.
b3939	metB	Cystathionine gamma-synthase; homotetrameric	6	0	7	11	7	-2	2	n.s.
b3829	metE	Methionine synthase, cobalamin-independent; 5-methyltetrahydropteroyltriglutamate-homocysteine methyltransferase; binds Zn(II)	215	70	n.s.	-6	n.s.	-10	-187	11
b3941	metF	5,10-Methylenetetrahydrofolate reductase	8	0	5	n.s.	n.s.	-14	n.s.	n.s.
b4019	metH	Methionine synthase, cobalamin-dependent; 5-methyltetrahydrofolate-homocysteine methyltransferase; binds Zn(II)	1	0	n.s.	n.s.	n.s.	n.s.	n.s.	n.s.

b3938	metJ	Methionine regulon repressor, SAM co-repressor; sulfoximine and methylmethionine sensitivity	52	0	4	3	n.s.	n.s.	n.s.	n.s.
b2942	metK	S-adenosylmethionine synthase; methionine adenosyltransferase; ethionine sensitivity; essential gene	8	0	n.s.	n.s.	n.s.	-17	-5	n.s.
b3940	metL	Aspartokinase II-homoserine dehydrogenase II	3	0	2	n.s.	4	-3	n.s.	n.s.
b0199	metN	ABC transporter ATPase, L,D-methionine uptake; methionine sulfoximine sensitivity	19	0	5	6	n.s.	-6	n.s.	n.s.
b1176	minC	Inhibition of FtsZ ring polymerization; forms membrane-associated coiled arrays, more concentrated at the poles	1	0	n.s.	n.s.	n.s.	n.s.	n.s.	n.s.
b3742	mioC	Required for biotin synthase activity in vitro; flavodoxin-like FMN-binding protein; transcription of mioC through oriC may have physiological significance in suboptimal conditions	2	0	n.s.	n.s.	2	n.s.	n.s.	n.s.
b3195	miaF	Probable ABC phospholipid transporter ATP-binding protein; MlaFEDB phospholipid ABC transporter; maintains OM lipid asymmetry	1	0	4	4	n.s.	4	4	n.s.
b2684	mprA	emrAB repressor, also regulates microcin synthesis; binds uncouplers DNP, CCCP, FCCP	46	0	3	2	n.s.	3	3	n.s.
b3251	mreB	Cell wall structural actin-like protein in MreBCD complex; mecillinam resistance protein	28	1	n.s.	n.s.	n.s.	n.s.	n.s.	n.s.
b1778	msrB	Methionine sulfoxide reductase B; specific for met-R-(o) diastereoisomers within proteins; mutant is cadmium sensitive; free met-R-(o) is inefficiently reduced by MsrB	5	13	3	3	n.s.	n.s.	2	n.s.
b1832	msrC	Free methionine-(R)-sulfoxide reductase	1	0	n.s.	n.s.	n.s.	3	3	n.s.
b0159	mtn	5'-Methylthioadenosine nucleosidase; S-adenosylhomocysteine and 5'-deoxyadenosine are also substrates	13	0	n.s.	n.s.	n.s.	n.s.	n.s.	n.s.
b0750	nadA	Quinolinate synthase, [4Fe-4S] cluster subunit, A protein	2	0	n.s.	-3	-4	n.s.	-5	n.s.
b0639	nadD	Nicotinate mononucleotide adenylyltransferase, NAD(P) biosynthesis	4	0	n.s.	n.s.	n.s.	-4	-3	n.s.
b1740	nadE	NAD synthase, ammonia dependent	8	0	n.s.	n.s.	n.s.	n.s.	n.s.	n.s.
b2518	ndk	Nucleoside diphosphate kinase; NDP kinase	9	0	-3	n.s.	n.s.	n.s.	2	4
b0578	nfsB	Nitroreductase B, oxygen-insensitive, NAD(P)H, FMN-dependent; minor; reduces a variety of nitroaromatics, e.g. dihydropteridine, nitrofurantoin, nitrofurazone, quinones; monomeric or homodimeric	1	0	n.s.	n.s.	n.s.	n.s.	n.s.	n.s.
b2235	nrdB	Ribonucleoside-diphosphate reductase 1, beta subunit; class Ia aerobic ribonucleotide reductase; B2 protein, R2 subunit	0	13	n.s.	n.s.	n.s.	n.s.	n.s.	n.s.
b2284	nuoF	NADH:ubiquinone oxidoreductase subunit F, complex I; NADH dehydrogenase I	1	0	-3	-8	n.s.	-10	-3	n.s.
b3169	nusA	Transcription termination/antitermination L factor; mutant survives lambda induction	39	0	-2	n.s.	n.s.	n.s.	n.s.	n.s.

b0957	ompA	Outer membrane protein A; Outer membrane porin A; T-even phage receptor; weak porin; homodimer, abundant cell surface protein	6	0	n.s.	n.s.	n.s.	n.s.	n.s.	n.s.
b1243	oppA	Oligopeptide-binding protein, periplasmic	2	0	n.s.	-7	n.s.	-13	-15	n.s.
b1247	oppF	Oligopeptide transport, ATP-binding protein	20	0	-2	-9	n.s.	-5	-36	n.s.
b0134	panB	Ketopantoate hydroxymethyltransferase	45	0	n.s.	n.s.	n.s.	n.s.	n.s.	n.s.
b0133	panC	Pantothenate synthase, dimeric	3	0	n.s.	n.s.	n.s.	n.s.	n.s.	n.s.
b0131	panD	Aspartate 1-decarboxylase; pantothenate biosynthesis; residues 1-24 constitute the beta chain; C-terminal 102 residues constitute the alpha chain	4	0	n.s.	3	n.s.	3	3	n.s.
b3403	pck	Phosphoenolpyruvate carboxykinase [ATP]	1	0	n.s.	n.s.	n.s.	n.s.	n.s.	n.s.
b2564	pdxJ	Pyridoxine 5'-phosphate (PNP) synthase; homo-octamer	0	2	2	n.s.	n.s.	3	2	n.s.
b2418	pdxK	B6-vitamer kinase; pyridoxine (PN)/pyridoxal (PL)/pyridoxamine (PM) kinase	5	0	2	n.s.	n.s.	n.s.	n.s.	n.s.
b1636	pdxY	Pyridoxamine kinase	3	2	-3	n.s.	n.s.	-3	-5	n.s.
b4260	pepA	Multifunctional Aminopeptidase A; transcriptional regulator of carAB; DNA-binding role in site-specific recombination mediating ColE1 plasmid multimer resolution; homohexameric	2	0	n.s.	n.s.	n.s.	n.s.	n.s.	n.s.
b0932	pepN	Aminopeptidase N	11	0	n.s.	n.s.	n.s.	n.s.	n.s.	n.s.
b3916	pfkA	6-phosphofructokinase-1; allosteric: activated by MgNDPs, inhibited by PEP; homotetrameric	17	0	n.s.	n.s.	n.s.	n.s.	-2	n.s.
b0903	pflB	Formate acetyltransferase 1; pyruvate formate lyase I; induced anaerobically; radical activated by PflA; deactivated by AdhE	0	2	-2	-7	-7	-5	-22	-2
b2926	pgk	Phosphoglycerate kinase	277	39	n.s.	-2	n.s.	-5	-5	n.s.
b0767	pgl	6-phosphogluconolactonase, pentose phosphate shunt	25	0	4	n.s.	n.s.	3	n.s.	n.s.
b0688	pgm	Phosphoglucomutase	1	0	n.s.	3	n.s.	2	2	n.s.
b1714	pheS	Phenylalanine--tRNA ligase, alpha-subunit	2	0	-4	-3	n.s.	-5	-3	n.s.
b1713	pheT	Phenylalanine--tRNA ligase, beta-subunit	2	5	n.s.	-4	n.s.	-2	n.s.	n.s.
b4041	plsB	Glycerol-3-phosphate acyltransferase	9	0	n.s.	n.s.	n.s.	n.s.	n.s.	n.s.
b4235	pmbA	Probable peptidase required for the maturation and secretion of the antibiotic peptide MccB17; involved in CcdA antidote degradation; tolerance for effects on DNA gyrase by sex factor F gene letD	3	0	n.s.	n.s.	n.s.	n.s.	n.s.	n.s.
b3164	pnp	Polynucleotide phosphorylase; exoribonuclease; PNPase component of RNA degradosome; cold shock protein required for growth at low temperatures	8	0	n.s.	n.s.	n.s.	-3	-2	n.s.
b1603	pntA	Proton-translocating NAD(P) transhydrogenase, alpha subunit;	7	0	-2	n.s.	n.s.	-2	-3	n.s.



		membrane protein								
b3956	ppc	Phosphoenolpyruvate carboxylase; monomeric	1	0	-2	-2	n.s.	-4	-6	n.s.
b0525	ppiB	Periplasmic peptidylprolyl-cis-trans-isomerase B, rotamase	10	0	n.s.	-3	n.s.	n.s.	n.s.	n.s.
b1702	ppsA	Phosphoenolpyruvate synthase; PEP synthase	1	0	2	5	n.s.	n.s.	n.s.	n.s.
b4375	prfC	Peptide chain release factor 3, RF-3; stimulates activity of RF-1 and RF-2	2	0	-3	n.s.	n.s.	-3	n.s.	n.s.
b3498	prlC	Oligopeptidase A, zinc metalloprotease; involved in the degradation of cleaved signal peptides; suppressor allele of LamB signal sequence mutations; heat shock regulon; proteinase In, multifunctional protease	2	0	4	2	n.s.	n.s.	n.s.	n.s.
b0243	proA	gamma-Glutamyl phosphate reductase, proline biosynthesis	1	0	n.s.	n.s.	n.s.	n.s.	n.s.	n.s.
b0386	proC	Pyrroline-5-carboxylate reductase, proline biosynthesis	1	0	n.s.	n.s.	n.s.	n.s.	n.s.	n.s.
b1207	prs	Phosphoribosylpyrophosphate synthase	15	0	n.s.	n.s.	n.s.	-4	-2	n.s.
b2297	pta	Phosphate acetyltransferase, produces acetyl phosphate; creBC regulon; alkali-inducible; binds Zn(II)	12	0	n.s.	-3	n.s.	n.s.	-3	n.s.
b1101	ptsG	Glucose phosphotransferase Enzyme IIBC(Glc); glucose permease; dimeric	3	0	-6	-13	n.s.	-3	-12	n.s.
b2416	ptsI	Phosphotransferase system enzyme I	8	0	-3	-3	n.s.	-3	-3	n.s.
b4177	purA	Adenylosuccinate synthase, purine synthesis	141	33	n.s.	-2	n.s.	-4	-3	n.s.
b1131	purB	Adenylosuccinate lyase, purine synthesis	36	1	-7	n.s.	n.s.	-12	-8	n.s.
b2476	purC	Phosphoribosyl-aminoimidazole-succinocarboxamide synthase; purine synthesis	22	0	-3	n.s.	n.s.	n.s.	n.s.	n.s.
b2312	purF	Amidophosphoribosyltransferase, purine synthesis; also known as glutamine 5'-phosphoribosylpyrophosphate amidotransferase, GPATase	1	0	-10	n.s.	n.s.	-7	-4	n.s.
b4006	purH	Phosphoribosylaminoimidazolecarboxamide formyltransferase; purine synthesis	16	1	-4	n.s.	n.s.	-6	-2	n.s.
b2557	purL	Phosphoribosylformylglycinamide synthase; contains a synthase domain (N) and a glutamine amidotransferase domain (C)	39	0	-4	n.s.	n.s.	-24	-14	n.s.
b2499	purM	Phosphoribosyl-aminoimidazole (AIR) synthase; homodimeric	7	0	-5	n.s.	3	-7	n.s.	n.s.
b1658	purR	Purine regulon repressor	2	0	n.s.	n.s.	n.s.	n.s.	3	n.s.
b1676	pykF	Pyruvate kinase I, fructose 1,6-bisphosphate-activated	31	0	-5	-4	n.s.	-5	-3	n.s.
b1062	pyrC	Dihydroorotase, the third step in pyrimidine biosynthesis; dimeric; Zn(II) metalloenzyme, binuclear metal center	29	0	n.s.	n.s.	n.s.	-2	n.s.	n.s.
b2780	pyrG	CTP synthase; CtpS	29	0	-3	n.s.	n.s.	-3	-2	n.s.
b2699	recA	General recombination and DNA repair; pairing and strand exchange; role in cleavage of LexA repressor, SOS mutagenesis	41	4	10	3	n.s.	2	2	n.s.

b2039	rfbA	Glucose-1-phosphate thymidyltransferase 1; TDP-glucose pyrophosphorylase; needed for dTDP-L-rhamnose synthesis	9	0	n.s.	n.s.	n.s.	-2	n.s.	n.s.
b2040	rfbD	dTDP-L-rhamnose synthase	11	0	-3	n.s.	n.s.	-2	n.s.	n.s.
b3780	rhlB	ATP-dependent RNA helicase; unwinds dsRNA; component of RNA degradosome; also binds PNPase directly; DEAD box family	16	0	n.s.	n.s.	n.s.	n.s.	n.s.	n.s.
b3783	rho	Transcription termination factor Rho; hexameric; RNA-dependent ATPase; ATP-dependent RNA helicase; bicyclomycin target	12	1	n.s.	n.s.	n.s.	-6	-4	n.s.
b3041	ribB	3,4-dihydroxy-2-butanone 4-phosphate synthase; riboflavin biosynthesis; acid-inducible; homodimeric	18	0	n.s.	-3	n.s.	n.s.	n.s.	n.s.
b1286	rnb	RNase II; mRNA degradation	3	0	-6	-4	n.s.	-25	-15	n.s.
b2914	rpiA	Ribose-5-phosphate isomerase A, alkali-inducible	0	3	n.s.	n.s.	n.s.	n.s.	n.s.	n.s.
b3317	rplB	50S ribosomal subunit protein L2; binds Zn(II)	0	1	-12	-5	n.s.	n.s.	-3	n.s.
b3305	rplF	50S ribosomal subunit protein L6; gentamicin sensitivity	57	1	-3	-3	n.s.	n.s.	n.s.	n.s.
b3985	rplJ	50S ribosomal subunit protein L10; streptomycin resistance	146	0	-3	-4	n.s.	n.s.	n.s.	n.s.
b3310	rplN	50S ribosomal subunit protein L14	34	0	-2	-2	n.s.	n.s.	n.s.	n.s.
b3185	rpmA	50S ribosomal subunit protein L27	4	0	n.s.	n.s.	n.s.	n.s.	n.s.	n.s.
b3936	rpmE	50S ribosomal subunit protein L31	1	99	n.s.	n.s.	n.s.	n.s.	n.s.	n.s.
b1717	rpmI	50S ribosomal subunit protein A (L35)	5	0	-2	-2	n.s.	n.s.	n.s.	n.s.
b3295	rpoA	RNA polymerase, alpha subunit; binds Zn(II)	88	0	n.s.	-3	n.s.	n.s.	-2	n.s.
b3987	rpoB	RNA polymerase, beta subunit; binds Zn(II)	28	0	n.s.	n.s.	n.s.	-3	-2	n.s.
b3988	rpoC	RNA polymerase, beta' subunit; binds Zn(II)	47	11	n.s.	n.s.	n.s.	-3	-4	n.s.
b3067	rpoD	RNA polymerase subunit, sigma 70, initiates transcription; housekeeping sigma	2	0	3	n.s.	n.s.	n.s.	n.s.	n.s.
b0911	rpsA	30S ribosomal subunit protein S1; subunit of RNA phage Q beta replicase; binds and stimulates RNAP	26	5	-7	-4	n.s.	-5	-3	n.s.
b0169	rpsB	30S ribosomal subunit protein S2; binds Zn(II)	127	0	n.s.	n.s.	n.s.	n.s.	n.s.	n.s.
b3296	rpsD	30S ribosomal subunit protein S4; NusA-like antitermination factor	0	14	n.s.	-2	n.s.	n.s.	n.s.	n.s.
b3306	rpsH	30S ribosomal subunit protein S8	0	1	-3	-3	n.s.	n.s.	n.s.	n.s.
b3297	rpsK	30S ribosomal subunit protein S11	40	0	n.s.	-2	n.s.	n.s.	n.s.	n.s.
b3342	rpsL	30S ribosomal subunit protein S12; RNA chaperone	18	0	-3	-2	n.s.	n.s.	n.s.	n.s.
b3311	rpsQ	30S ribosomal subunit protein S17	40	0	-4	-4	n.s.	n.s.	-3	n.s.
b3929	rraA	Protein inhibitor of RNase E, modulates global mRNA abundance; trimeric	23	0	3	n.s.	n.s.	2	n.s.	n.s.

b1540	rspR	Predicted DNA-binding transcriptional regulator, function unknown	1	0	n.s.	n.s.	n.s.	n.s.	n.s.	n.s.
b0723	sdhA	Succinate dehydrogenase (SQR) flavoprotein subunit; succinate:ubiquinone oxidoreductase (SQR); complex II of aerobic respiration	145	1	n.s.	n.s.	n.s.	-8	-5	n.s.
b0724	sdhB	Succinate dehydrogenase (SQR) iron-sulfur protein; succinate:ubiquinone oxidoreductase (SQR); complex II of aerobic respiration	2	0	n.s.	n.s.	n.s.	-6	-9	n.s.
b2897	sdhE	Antitoxin of CptAB toxin-antitoxin pair	4	0	n.s.	n.s.	n.s.	2	n.s.	n.s.
b1764	selD	Selenophosphate synthase, ATP-dependent; reduced selenium donor for selenocysteic tRNA synthesis and for the modification of several tRNAs to contain 5-methylaminomethyl-2-selenouridine	0	1	n.s.	n.s.	n.s.	n.s.	n.s.	n.s.
b2913	serA	D-3-Phosphoglycerate dehydrogenase	32	2	n.s.	n.s.	n.s.	n.s.	n.s.	n.s.
b1656	sodB	Superoxide dismutase, Fe; response to oxidative stress; chromate resistance; negatively regulated by ryhB RNA as part of indirect positive regulation by Fur; acid-inducible	83	0	n.s.	-3	-6	-8	-17	n.s.
b2938	speA	Biosynthetic decarboxylase	1	0	n.s.	2	n.s.	n.s.	n.s.	n.s.
b0726	sucA	2-oxoglutarate dehydrogenase, E1 component; yields succinyl-CoA and CO(2); also known as alpha-ketoglutarate dehydrogenase	3	0	-3	n.s.	n.s.	-6	-5	n.s.
b0728	sucC	Succinyl CoA synthase beta-subunit; acid-inducible	29	7	-4	-4	n.s.	-5	-9	n.s.
b0729	sucD	Succinyl CoA synthase alpha-subunit	3	14	-3	-4	n.s.	-3	-10	n.s.
b2464	talA	Transaldolase A; creBC regulon	10	0	4	n.s.	5	n.s.	n.s.	n.s.
b0008	talB	Transaldolase B	13	10	2	n.s.	n.s.	n.s.	n.s.	n.s.
b0406	tgt	tRNA-guanine transglycosylase; queuosine biosynthesis; zinc metalloprotein	1	0	-3	n.s.	n.s.	n.s.	n.s.	n.s.
b0002	thrA	Aspartokinase I and homoserine dehydrogenase I, bifunctional	89	0	-5	-8	n.s.	-11	-25	n.s.
b0003	thrB	Homoserine kinase	33	17	-4	-8	n.s.	-8	-24	n.s.
b0004	thrC	Threonine synthase	37	0	-3	-8	n.s.	-6	-16	n.s.
b1719	thrS	Threonine--tRNA ligase, autogenously regulated; binds Zn(II)	27	0	n.s.	n.s.	n.s.	n.s.	n.s.	n.s.
b3919	tpiA	Triosephosphate isomerase	15	22	-3	-7	n.s.	n.s.	-3	n.s.
b1324	tpx	Lipid hydroperoxide peroxidase; thiol peroxidase, antioxidant, thioredoxin-dependent; peroxiredoxin; scavengase P20; induced by acid or base	401	31	n.s.	n.s.	n.s.	2	2	n.s.
b1260	trpA	Tryptophan synthase, alpha subunit	155	11	n.s.	-3	n.s.	n.s.	n.s.	n.s.
b1261	trpB	Tryptophan synthase, beta subunit	1	0	n.s.	-3	n.s.	-2	n.s.	n.s.

b1262	trpC	Tryptophan synthesis, bifunctional: N-(5-phosphoribosyl)anthranilate isomerase and indole-3-glycerolphosphate synthase	9	0	n.s.	n.s.	n.s.	n.s.	n.s.	n.s.
b1263	trpD	Anthranilate synthase component II, bifunctional; glutamine amidotransferase and phosphoribosyl anthranilate transferase; tryptophan biosynthesis	16	0	-5	-7	n.s.	-10	-11	n.s.
b1264	trpE	Anthranilate synthase component I	1	0	-6	-8	n.s.	-20	-28	n.s.
b3781	trxA	Thioredoxin 1; Trx; with TrxB, also has general chaperone activity; processivity factor for phage T7 gene 5 DNA polymerase	0	25	n.s.	n.s.	n.s.	2	n.s.	n.s.
b0888	trxB	Thioredoxin reductase, NADP+, FAD-binding; with TrxA, also has general chaperone activity; dimeric	1	0	8	4	n.s.	n.s.	2	n.s.
b1807	tsaB	tRNA(NNU) t(6)A37 threonylcarbamoyladenine modification; binding partner and protease for TsaD	7	0	-4	n.s.	n.s.	n.s.	n.s.	n.s.
b1344	ttcA	Required for the formation of 2-thiocytidine s(2)C32 in tRNA	16	0	n.s.	n.s.	n.s.	3	3	n.s.
b3339	tufA	EF-Tu, Elongation Factor-Translation, unstable; GTP-dependent binding of aa-tRNA to the A-site of ribosomes; has intrinsic GTPase activity when bound to kirromycin	223	15	n.s.	-3	n.s.	-2	-4	n.s.
b1637	tyrS	Tyrosine--tRNA ligase	5	18	n.s.	n.s.	n.s.	n.s.	n.s.	n.s.
b2232	ubiG	SAM:OMHMB methyltransferase; Reactions: 2-octaprenyl-6-hydroxylphenol to 2-octaprenyl-6-methoxyphenol; 2-octaprenyl-3-methyl-5-hydroxy-6-methoxy-1,4-benzoquinone to ubiquinone 8	2	0	n.s.	n.s.	n.s.	3	2	n.s.
b3831	udp	Uridine phosphorylase	24	0	n.s.	-3	-4	n.s.	-3	n.s.
b0675	umpH	UMP phosphatase; HAD23	24	0	n.s.	n.s.	n.s.	n.s.	n.s.	n.s.
b3495	uspA	Global regulatory gene for stress response; mutants are UV-S	2	0	5	3	n.s.	3	n.s.	n.s.
b2042	wcaN	Putative regulatory subunit for GalU	36	0	n.s.	n.s.	n.s.	n.s.	n.s.	n.s.
b3787	wecC	UDP-ManNAcA dehydrogenase; needed for ECA (enterobacterial common antigen) synthesis	8	0	-4	n.s.	n.s.	-9	-6	n.s.
b0101	yacG	DNA gyrase inhibitor; Zn(2+)-binding protein	5	0	n.s.	-2	n.s.	-3	-2	n.s.
b0163	yaeH	Function unknown, UPF0325 family	3	0	5	3	n.s.	6	4	n.s.
b4406	yaeP	Function unknown	15	0	5	4	n.s.	9	5	n.s.
b0287	yagU	Required for acid resistance, inner membrane protein, DUF1440 family	4	0	-3	n.s.	n.s.	2	4	-2
b0471	ybaB	DNA-binding protein, function unknown; homodimer; in recR operon; may be involved in DNA repair	0	1	-2	-2	n.s.	-3	-3	n.s.
b0528	ybcJ	Ribosome-associated protein, function unknown; predicted RNA binding protein	4	0	n.s.	n.s.	n.s.	n.s.	n.s.	n.s.
b0711	ybgJ	Predicted allophanate hydrolase, subunit 1	1	0	2	2	n.s.	3	2	n.s.

b0773	ybhB	Raf kinase inhibitor RKIP homolog, function unknown; UPF0098 family; cytoplasmic protein	1	0	n.s.	n.s.	n.s.	n.s.	n.s.	n.s.
b0801	ybiC	Function unknown, lactate, malate dehydrogenase family	29	0	n.s.	-3	n.s.	n.s.	n.s.	n.s.
b0917	ycaR	Function unknown, UPF0434 family; low abundance protein	0	9	n.s.	n.s.	n.s.	n.s.	n.s.	n.s.
b1180	ycgM	Function unknown	1	0	5	3	n.s.	10	7	n.s.
b1203	ychF	Catalase inhibitor protein; ATPase, K <sup>+</sup> -dependent, ribosome-associated; monomeric	46	4	n.s.	n.s.	n.s.	n.s.	n.s.	n.s.
b1287	yciW	Function unknown, CMD superfamily	3	0	-4	-11	n.s.	-30	-20	n.s.
b1539	ydfG	Malonic semialdehyde reductase, NADPH-dependent; L-allo-threonine dehydrogenase, NADP <sup>+</sup> -dependent, other in vitro substrates include L-serine, D-serine, D-threonine and 3-hydroxyisobutyrate	0	2	n.s.	n.s.	-2	n.s.	n.s.	n.s.
b1687	ydiJ	Predicted FAD-linked oxidoreductase, function unknown	5	0	-2	n.s.	n.s.	-6	-5	n.s.
b1864	yebC	Function unknown, expressed protein, UPF0082 family	4	0	-3	-4	n.s.	-3	n.s.	n.s.
b1930	yedF	Predicted sulfurtransferase, function unknown; TusA family	13	0	-2	-5	n.s.	n.s.	n.s.	n.s.
b2012	yeeD	Predicted sulfurtransferase, function unknown; TusA family	42	0	5	-5	n.s.	-6	-16	n.s.
b2300	yfcE	Phosphodiesterase, function unknown; has activity on model substrate bis-pNPP	2	0	2	2	n.s.	6	5	n.s.
b2471	yffB	Predicted reductase, function unknown, ArsC family; low abundance protein	5	0	2	n.s.	n.s.	2	2	n.s.
b2898	ygfZ	Iron-sulfur cluster repair protein; plumbagin resistance protein; hda mutational suppressor; folate and tetrahydrofolate binding protein	3	0	3	n.s.	n.s.	2	n.s.	n.s.
b2959	yggL	Conserved protein, DUF469 family, function unknown	0	1	n.s.	n.s.	n.s.	n.s.	n.s.	n.s.
b2962	yggX	Confers protection of iron-sulfur proteins against oxidative damage; paraquat resistance	1	1	n.s.	2	n.s.	4	3	n.s.
b3205	yhbJ	Senses glucosamine-6-phosphate and inactivates glmZ sRNA; NTPase	3	0	n.s.	n.s.	n.s.	-4	-4	n.s.
b3346	yheO	Function unknown	2	0	n.s.	n.s.	n.s.	n.s.	n.s.	n.s.
b3764	yifE	Function unknown, expressed protein, UPF0438 family	17	0	n.s.	n.s.	n.s.	n.s.	n.s.	n.s.
b1727	yniC	2-deoxyglucose-6-P phosphatase; mutants are hypersensitive to 2-deoxyglucose; overproduction confers 2-deoxyglucose resistance; additional in vitro substrates: mannose-6-P phosphate, 2-deoxyribose-5-P, ribose-5-P, glucose-6-P; HAD1	3	0	2	2	n.s.	4	4	n.s.
b3070	yqjH	Ferric-chelate reductase, NADPH-dependent; siderophore-interacting protein (SIP); nickel-resistance	1	0	n.s.	4	11	n.s.	n.s.	n.s.
b1857	znuA	Zinc periplasmic binding protein, ABC transporter	7	1	-2	n.s.	4	n.s.	n.s.	n.s.
b1852	zwf	Glucose-6-phosphate 1-dehydrogenase	3	0	n.s.	n.s.	n.s.	n.s.	n.s.	n.s.

**Table D.S5: Ribosomal proteins transcriptional response and mercury modifications observed by proteomics.**

Operon	Hg(II) adduct	PMA adduct	Gene ID	Gene name	Protein description	Hg t10	Hg t30	Hg t60	PMA t10	PMA t30	PMA t60
rpsJ(S10)-1			b3321	rpsJ	30S ribosomal subunit protein S10	-11	-5	n.s.	n.s.	-3	n.s.
rpsJ(S10)-2			b3320	rplC	50S ribosomal subunit protein L3	-12	-5	n.s.	n.s.	-3	n.s.
rpsJ(S10)-3			b3319	rplD	50S ribosomal subunit protein L4;	-13	-5	n.s.	n.s.	-3	n.s.
rpsJ(S10)-4			b3318	rplW	50S ribosomal subunit protein L23	-13	-6	n.s.	n.s.	-3	n.s.
rpsJ(S10)-5	1	0	b3317	rplB	50S ribosomal subunit protein L2; binds Zn(II)	-12	-5	n.s.	n.s.	-3	n.s.
rpsJ(S10)-6			b3316	rpsS	30S ribosomal subunit protein S19	-10	-5	n.s.	n.s.	-3	n.s.
rpsJ(S10)-7			b3315	rplV	50S ribosomal subunit protein L22;	-12	-6	n.s.	n.s.	-3	n.s.
rpsJ(S10)-8			b3314	rpsC	30S ribosomal subunit protein S3	-9	-5	n.s.	n.s.	-3	n.s.
rpsJ(S10)-9			b3313	rplP	50S ribosomal subunit protein L16	-8	-5	n.s.	n.s.	-3	n.s.
rpsJ(S10)-10			b3312	rpmC	50S ribosomal subunit protein L29	-5	-5	n.s.	n.s.	-3	n.s.
rpsJ(S10)-11	0	40	b3311	rpsQ	30S ribosomal subunit protein S17	-4	-4	n.s.	n.s.	-3	n.s.
rplK(L11-L1)-1			b3983	rplK	50S ribosomal subunit protein L11;	-6	-4	n.s.	-2	-2	n.s.
rplK(L11-L1)-2			b3984	rplA	50S ribosomal subunit protein L1	-7	-4	n.s.	n.s.	-2	n.s.
rplN(spc)-1	0	34	b3310	rplN	50S ribosomal subunit protein L14	-2	-2	n.s.	n.s.	n.s.	n.s.
rplN(spc)-2			b3309	rplX	50S ribosomal subunit protein L24	-2	-2	n.s.	n.s.	n.s.	n.s.
rplN(spc)-3			b3308	rplE	50S ribosomal subunit protein L5;	-2	-3	n.s.	n.s.	n.s.	n.s.
rplN(spc)-4			b3307	rpsN	30S ribosomal subunit protein S14	-3	-3	n.s.	n.s.	n.s.	n.s.
rplN(spc)-5	1	0	b3306	rpsH	30S ribosomal subunit protein S8	-3	-3	n.s.	n.s.	n.s.	n.s.
rplN(spc)-6	57	1	b3305	rplF	50S ribosomal subunit protein L6;	-3	-3	n.s.	n.s.	n.s.	n.s.
rplN(spc)-7			b3304	rplR	50S ribosomal subunit protein L18;	-3	-2	n.s.	n.s.	n.s.	n.s.
rplN(spc)-8			b3303	rpsE	30S ribosomal subunit protein S5	-3	-2	n.s.	n.s.	n.s.	n.s.
rplN(spc)-9			b3302	rpmD	50S ribosomal subunit protein L30	-3	-2	n.s.	n.s.	n.s.	n.s.
rplN(spc)-10			b3301	rplO	50S ribosomal subunit protein L15	-3	-2	n.s.	n.s.	n.s.	n.s.
rplN(spc)-12			b3299	rpmJ	50S ribosomal subunit protein X (L36)	n.s.	-2	n.s.	n.s.	-2	n.s.
rpsM( $\alpha$ )-1			b3298	rpsM	30S ribosomal subunit protein S13	n.s.	-2	n.s.	n.s.	n.s.	n.s.
rpsM( $\alpha$ )-2	0	40	b3297	rpsK	30S ribosomal subunit protein S11	n.s.	-2	n.s.	n.s.	n.s.	n.s.
rpsM( $\alpha$ )-3	14	0	b3296	rpsD	30S ribosomal subunit protein S4;	n.s.	-2	n.s.	n.s.	n.s.	n.s.

rpsM( $\alpha$ )-4			b3294	rplQ	50S ribosomal subunit protein L17	n.s.	-3	n.s.	n.s.	-2	n.s.
rpsL(str)-1	0	18	b3342	rpsL	30S ribosomal subunit protein S12;	-3	-2	n.s.	n.s.	n.s.	n.s.
rpsL(str)-2			b3341	rpsG	30S ribosomal subunit protein S7,	-3	-2	n.s.	n.s.	n.s.	n.s.
rpsA-1	5	26	b0911	rpsA	30S ribosomal subunit protein S1;	-7	-4	n.s.	-5	-3	n.s.
rpsP(S16)-1			b2609	rpsP	30S ribosomal subunit protein S16;	-6	-2	n.s.	n.s.	n.s.	n.s.
rpsP(S16)-4			b2606	rplS	50S ribosomal subunit protein L19	-6	-2	n.s.	n.s.	n.s.	n.s.
rpsT(S20)			b0023	rpsT	30S ribosomal subunit protein S20	-3	n.s.	n.s.	n.s.	n.s.	n.s.
thrS-3	0	5	b1717	rpmI	50S ribosomal subunit protein A (L35)	-2	-2	n.s.	n.s.	n.s.	n.s.
thrS-4			b1716	rplT	50S ribosomal subunit protein L20	-2	-2	n.s.	n.s.	n.s.	n.s.
rplJ( $\beta\beta'$ )-1	0	146	b3985	rplJ	50S ribosomal subunit protein L10;	-3	-4	n.s.	n.s.	n.s.	n.s.
rplJ( $\beta\beta'$ )-2			b3986	rplL	50S ribosomal subunit protein L7/L12	-4	-4	n.s.	n.s.	n.s.	n.s.
rpsU(S21)			b3065	rpsU	30S ribosomal subunit protein S21	-2	n.s.	n.s.	n.s.	n.s.	n.s.
*S2,tsf(EF-T's)	0	127	b0169	rpsB	30S ribosomal subunit protein S2; binds Zn(II)	n.s.	n.s.	n.s.	n.s.	n.s.	n.s.
*S6,pirB,S18,L9			b4203	rplI	50S ribosomal subunit protein L9	-5	n.s.	n.s.	n.s.	n.s.	n.s.
*S6,pirB,S18,L9			b4200	rpsF	30S ribosomal subunit protein S6;	-5	-2	n.s.	n.s.	-3	n.s.
*S6,pirB,S18,L9			b4202	rpsR	30S ribosomal subunit protein S18	-5	n.s.	n.s.	n.s.	-3	n.s.
*S9-L13			b3230	rpsI	30S ribosomal subunit protein S9	-8	-2	n.s.	n.s.	-2	n.s.
*S9-L13			b3231	rplM	50S ribosomal subunit protein L13; binds Zn(II)	-7	-2	n.s.	n.s.	-2	n.s.
*S15			b3165	rpsO	30S ribosomal subunit protein S15	-3	n.s.	n.s.	3	2	n.s.
*L21-L27			b3186	rplU	50S ribosomal subunit protein L21	n.s.	n.s.	n.s.	n.s.	-2	n.s.
*L21-L27	0	4	b3185	rpmA	50S ribosomal subunit protein L27	n.s.	n.s.	n.s.	n.s.	n.s.	n.s.
*L25			b2185	rplY	50S ribosomal subunit protein L25	-4	n.s.	n.s.	n.s.	-2	n.s.
*L28-L33			b3637	rpmB	50S ribosomal subunit protein L28	-3	n.s.	n.s.	n.s.	n.s.	n.s.
*L28-L33			b3636	rpmG	50S ribosomal subunit protein L33	-3	n.s.	n.s.	n.s.	n.s.	n.s.
*L31	99	1	b3936	rpmE	50S ribosomal subunit protein L31	n.s.	n.s.	n.s.	n.s.	n.s.	n.s.
*L32			b1089	rpmF	50S ribosomal subunit protein L32	-3	n.s.	n.s.	n.s.	n.s.	n.s.
*L34			b3703	rpmH	50S ribosomal subunit protein L34	-4	n.s.	n.s.	n.s.	n.s.	n.s.

**Table D.S6: Oxidative stress response regulons (OxyR, *oxyS*, SoxRS) response to mercury exposure.**

Gene ID	Gene name	product	regulator	regulon	Hg t10	Hg t30	Hg t60	PMA t10	PMA t30	PMA t60
b3961	<b>oxyR</b>	OxyR DNA-binding transcriptional dual regulator	<b>oxyR</b>	oxyRS	n.s.	n.s.	n.s.	n.s.	n.s.	n.s.
b0605	ahpC	alkyl hydroperoxide reductase, AhpC component	oxyR	oxyRS	15	3	n.s.	3	2	n.s.
b0606	ahpF	alkyl hydroperoxide reductase, AhpF component	oxyR	oxyRS	78	11	n.s.	n.s.	n.s.	n.s.
b0881	clpS	Substrate modulator for ClpAP; directs protease activity towards aggregated proteins	oxyR	oxyRS	8	2	n.s.	2	n.s.	n.s.
b0812	dps	stationary phase nucleoid component that sequesters iron and protects DNA from damage	oxyR	oxyRS	339	52	n.s.	4	2	n.s.
b0604	dsbG	thiol:disulfide interchange protein DsbG	oxyR	oxyRS	n.s.	n.s.	n.s.	n.s.	n.s.	n.s.
b4367	fhuF	ferric iron reductase protein	oxyR	oxyRS	-11	n.s.	10	-10	n.s.	n.s.
b2000	flu	antigen 43 (Ag43) phase-variable biofilm formation autotransporter	oxyR	oxyRS	n.s.	-9	n.s.	n.s.	-8	n.s.
b0683	fur	ferric uptake regulation protein	oxyR	oxyRS	13	9	n.s.	n.s.	n.s.	n.s.
b4321	gntP	gluconate / fructuronate transporter	oxyR	oxyRS	-3	-3	n.s.	-2	-3	n.s.
b3500	gor	glutathione reductase	oxyR	oxyRS	6	n.s.	n.s.	n.s.	n.s.	n.s.
b0849	grxA	glutaredoxin 1	oxyR	oxyRS	246	33	n.s.	14	4	n.s.
b0104	guaC	GMP reductase	oxyR	oxyRS	2	4	n.s.	n.s.	n.s.	n.s.
b0873	hcp	hybrid cluster protein (HCP) exhibits hydroxylamine reductase activity	oxyR	oxyRS	-3	-9	-8	-2	-5	n.s.
b0872	hcr	NADH oxidoreductase that catalyzes the reduction of the hybrid-cluster protein (HCP)	oxyR	oxyRS	n.s.	-7	-13	n.s.	n.s.	n.s.
b0475	hemH	ferrochelataase	oxyR	oxyRS	72	7	n.s.	2	3	n.s.
b4435	isrC	IsrC small RNA, not clear whether IsrC simply represents the attenuated UTR of flu or whether it has an independent function	oxyR	oxyRS	n.s.	n.s.	n.s.	n.s.	n.s.	n.s.
b3942	katG	hydroperoxidase I, with both catalase and peroxidase activity	oxyR	oxyRS	24	n.s.	-8	n.s.	-4	n.s.
b1856	mepM	Septation protein, ampicillin sensitivity	oxyR	oxyRS	-3	n.s.	2	n.s.	n.s.	n.s.
b3829	metE	Methionine synthase, cobalamin-independent; 5-methyltetrahydropteroyltriglutamate-homocysteine methyltransferase; binds Zn(II)	oxyR	oxyRS	n.s.	-6	n.s.	-10	-187	11
b3828	metR	Positive regulatory gene for metE and metH; autogenous regulation	oxyR	oxyRS	36	16	n.s.	-2	4	n.s.
b2392	mnhH	Mn <sup>2+</sup> / Fe <sup>2+</sup> H <sup>+</sup> symporter	oxyR	oxyRS	6	5	n.s.	5	7	n.s.
b0851	nfsA	NADPH nitroreductase	oxyR	oxyRS	-3	-2	n.s.	n.s.	n.s.	n.s.



b4458	oxyS	OxyS small regulatory RNA	oxyR	oxyRS	1524	1292	150	10	6	n.s.
b0852	rimK	ribosomal protein S6 modification protein, L-glutamate ligase that catalyzes post-translational addition of up to four C-terminal glutamate residues	oxyR	oxyRS	-2	n.s.	n.s.	n.s.	n.s.	n.s.
b3908	sodA	Superoxide dismutase, Mn	oxyR	oxyRS	n.s.	n.s.	11	n.s.	n.s.	n.s.
b4063	soxR	SoxR, superoxide response protein, DNA-binding transcriptional dual regulator of SoxRS regulon	oxyR	oxyRS	23	5	n.s.	5	2	n.s.
b4062	soxS	SoxS, DNA-binding dual transcriptional activator	oxyR	oxyRS	6	21	4	8	4	n.s.
b1684	sufA	Fe-S transport protein in Fe-S cluster assembly, SufA accepts Fe-S clusters formed by the SufBCD complex	oxyR	oxyRS	32	39	5	n.s.	3	n.s.
b1683	sufB	SufB component of SufBCD Fe-S cluster scaffold complex	oxyR	oxyRS	13	22	5	n.s.	n.s.	n.s.
b1682	sufC	SufC component of SufBCD Fe-S cluster scaffold complex	oxyR	oxyRS	5	21	6	n.s.	2	n.s.
b1681	sufD	SufD component of SufBCD Fe-S cluster scaffold complex	oxyR	oxyRS	4	13	5	n.s.	n.s.	n.s.
b1679	sufE	sulfur acceptor for SufS cysteine desulfurase, SufS-SufE is less susceptible to oxidative modification than IscS-IscU	oxyR	oxyRS	n.s.	5	n.s.	n.s.	n.s.	n.s.
b1680	sufS	L-cysteine desulfurase, SufS-SufE is less susceptible to oxidative modification than IscS-IscU	oxyR	oxyRS	3	7	4	n.s.	n.s.	n.s.
b2582	trxC	thioredoxin 2	oxyR	oxyRS	134	50	7	24	24	n.s.
b4637	uof	RyhB-regulated fur leader peptide	oxyR	oxyRS	11	7	n.s.	2	2	n.s.
b4322	uxuA	D-mannonate dehydratase	oxyR	oxyRS	n.s.	n.s.	n.s.	n.s.	n.s.	n.s.
b4323	uxuB	D-mannonate oxidoreductase	oxyR	oxyRS	n.s.	n.s.	n.s.	n.s.	n.s.	n.s.
b0850	ybjC	predicted inner membrane protein	oxyR	oxyRS	-2	n.s.	n.s.	3	3	n.s.
b0848	ybjM	Inner membrane protein, function unknown	oxyR	oxyRS	n.s.	n.s.	-5	6	4	-3
b0853	ybjN	predicted oxidoreductase	oxyR	oxyRS	n.s.	n.s.	n.s.	n.s.	n.s.	n.s.
b1203	ychF	ribosome-binding ATPase, inhibitor of catalase activity	oxyR	oxyRS	n.s.	n.s.	n.s.	n.s.	n.s.	n.s.
b3518	yhjA	predicted cytochrome C peroxidase	oxyR	oxyRS	n.s.	-5	-6	n.s.	-2	n.s.
b3520	yhjB	Predicted two-component system response regulator, function unknown; CheY-like receiver domain, LuxR-like HTH domain; cognate sensor protein is unknown	oxyR	oxyRS	n.s.	n.s.	n.s.	4	6	n.s.
b4567	yjjZ	Function unknown; Fur regulon	oxyR	oxyRS	n.s.	n.s.	n.s.	4	n.s.	n.s.
b1973	zinT	Periplasmic zinc and cadmium binding protein; induced by zinc, cadmium or peroxide; Zur, SoxS and Fur regulated	oxyR	oxyRS	n.s.	n.s.	5	4	n.s.	n.s.
b1857	znuA	Zinc periplasmic binding protein, ABC transporter	oxyR	oxyRS	-2	n.s.	4	n.s.	n.s.	n.s.
b1859	znuB	High-affinity ABC transport system for zinc	oxyR	oxyRS	n.s.	n.s.	n.s.	n.s.	n.s.	n.s.

b1858	znuC	High-affinity ABC transport system for zinc	oxyR	oxyRS	n.s.	n.s.	n.s.	n.s.	n.s.	n.s.
b4458	<b>oxyS</b>	OxyS small regulatory RNA	<b>oxyS</b>	oxyRS	1524	1292	150	10	6	n.s.
b2731	fhIA	formate hydrogen-lyase transcriptional activator for fdhF, hyc and hyp operons	oxyS	oxyRS	-2	-3	n.s.	n.s.	-2	n.s.
b1891	flhC	flagellar transcriptional regulator, FlhC	oxyS	oxyRS	-3	-3	n.s.	n.s.	n.s.	n.s.
b1892	flhD	flagellar transcriptional regulator, FlhD	oxyS	oxyRS	-6	-5	n.s.	-7	-5	n.s.
b2741	rpoS	sigma factor S, oxyS inhibits translations of rpoS	oxyS	oxyRS	3	3	n.s.	14	10	n.s.
b4063	<b>soxR</b>	SoxR, superoxide response protein, DNA-binding transcriptional dual regulator of SoxRS regulon	<b>soxR</b>	soxRS	23	5	n.s.	5	2	n.s.
b0606	ahpF	Alkyl hydroperoxide reductase, subunit F; NAD(P)H:peroxiredoxin oxidoreductase, reduces AhpC; contains one FAD/monomer	soxR	soxRS	78	11	n.s.	n.s.	n.s.	n.s.
b2601	aroF	3-deoxy-D-arabino-heptulosonate 7-phosphate (DAHP) synthase; tyrosine repressible; TyrR regulon	soxR	soxRS	-4	-2	n.s.	-4	n.s.	n.s.
b0096	lpxC	Lipid A synthesis, UDP-3-O-(R-3-hydroxymyristoyl)-N-acetylglucosamine deacetylase; zinc metalloamidase; cell envelope and cell separation	soxR	soxRS	6	3	n.s.	6	5	n.s.
b4242	mgtA	Magnesium transporter, ATP-dependent; mutant has cobalt resistance; mediates Mg(2+) influx	soxR	soxRS	4	3	n.s.	2	5	n.s.
b3908	sodA	superoxide dismutase (Mn)	soxR	soxRS	n.s.	n.s.	11	n.s.	n.s.	n.s.
b4062	soxS	SoxS, DNA-binding dual transcriptional activator	soxR	soxRS	6	21	4	8	4	n.s.
b2600	tyrA	Tyrosine synthesis: chorismate mutase/prephenate dehydrogenase	soxR	soxRS	-4	-2	n.s.	-4	n.s.	n.s.
b3211	yhcC	Function unknown, Radical SAM superfamily	soxR	soxRS	-4	-5	-6	-3	-3	n.s.
b4060	yjcB	Function unknown	soxR	soxRS	33	11	12	52	35	n.s.
b3207	yrbL	Mg(2+)-starvation-stimulated gene, function unknown	soxR	soxRS	7	n.s.	n.s.	3	n.s.	n.s.
b4062	<b>soxS</b>	SoxS, DNA-binding dual transcriptional activator	<b>soxS</b>	soxRS	6	21	4	8	4	n.s.
b1276	acnA	aconitase, aconitate hydratase 1	soxS	soxRS	17	5	n.s.	n.s.	n.s.	n.s.
b0463	acrA	AcrAB-TolC multidrug efflux system - membrane fusion protein	soxS	soxRS	n.s.	n.s.	n.s.	n.s.	n.s.	n.s.
b0462	acrB	AcrAB-TolC multidrug efflux system - permease subunit	soxS	soxRS	n.s.	n.s.	n.s.	-2	-2	n.s.
b0762	acrZ	small membrane protein that interacts with the AcrAB-TolC multidrug efflux pump, by affecting substrate specificity	soxS	soxRS	n.s.	n.s.	n.s.	4	2	n.s.
b1166	ariR	Connector protein for RcsB regulation of biofilm and acid-resistance	soxS	soxRS	9	n.s.	9	18	13	n.s.
b2601	aroF	3-deoxy-D-arabino-heptulosonate 7-phosphate (DAHP) synthase; tyrosine repressible; TyrR regulon	soxS	soxRS	-4	-2	n.s.	-4	n.s.	n.s.

b0684	fldA	flavodoxin 1	soxS	soxRS	3	n.s.	n.s.	2	n.s.	n.s.
b2895	fldB	flavodoxin 2	soxS	soxRS	n.s.	n.s.	n.s.	3	n.s.	n.s.
b3924	fpr	flavodoxin NADP+ reductase	soxS	soxRS	3	3	n.s.	4	3	n.s.
b1611	fumC	fumarase C	soxS	soxRS	15	8	6	n.s.	n.s.	n.s.
b0683	fur	ferric uptake regulation protein	soxS	soxRS	13	9	n.s.	n.s.	n.s.	n.s.
b2237	inaA	pH-inducible protein involved in stress response	soxS	soxRS	6	2	n.s.	4	3	n.s.
b0096	lpxC	Lipid A synthesis, UDP-3-O-(R-3-hydroxymyristoyl)-N-acetylglucosamine deacetylase; zinc metalloamidase; cell envelope and cell separation	soxS	soxRS	6	3	n.s.	6	5	n.s.
b1531	marA	MarA, multiple antibiotic resistance, DNA-binding transcriptional repressor, soxS paralog	soxS	soxRS	15	9	n.s.	46	31	n.s.
b1532	marB	multiple antibiotic resistance protein	soxS	soxRS	16	8	n.s.	45	27	n.s.
b1530	marR	MarR, multiple antibiotic resistance, DNA-binding transcriptional repressor	soxS	soxRS	26	7	n.s.	48	29	n.s.
b0448	mdlA	ABC exporter permease-ATPase, function unknown	soxS	soxRS	n.s.	2	n.s.	n.s.	2	n.s.
b0449	mdlB	ABC exporter permease-ATPase, function unknown	soxS	soxRS	n.s.	n.s.	n.s.	n.s.	n.s.	n.s.
b4439	micF	MicF small regulatory RNA, regulates translation of the OmpF porin and the stability of OmpF mRNA	soxS	soxRS	n.s.	n.s.	n.s.	n.s.	n.s.	n.s.
b3662	nepl	Purine ribonucleoside exporter; 6-mercaptopurine resistance	soxS	soxRS	3	2	3	6	6	n.s.
b2159	nfo	endonuclease IV, DNA base excision repair	soxS	soxRS	2	2	n.s.	n.s.	n.s.	n.s.
b0851	nfsA	NADPH nitroreductase	soxS	soxRS	-3	-2	n.s.	n.s.	n.s.	n.s.
b0578	nfsB	NAD(P)H nitroreductase NfsB	soxS	soxRS	n.s.	n.s.	n.s.	n.s.	n.s.	n.s.
b1463	nhoA	N-hydroxyarylamine O-acetyltransferase	soxS	soxRS	3	2	n.s.	2	n.s.	n.s.
b1377	ompN	outer membrane pore protein N	soxS	soxRS	n.s.	n.s.	n.s.	3	3	n.s.
b4025	pgi	phosphoglucose isomerase	soxS	soxRS	n.s.	-3	n.s.	-8	-10	n.s.
b0871	poxB	pyruvate oxidase	soxS	soxRS	2	n.s.	5	-2	n.s.	n.s.
b0950	pqiA	paraquat-inducible protein A	soxS	soxRS	-2	n.s.	n.s.	n.s.	n.s.	n.s.
b0951	pqiB	paraquat-inducible protein B	soxS	soxRS	-2	n.s.	n.s.	n.s.	2	n.s.
b1101	ptsG	glucose phosphotransferase system (PTS) permease - PtsG subunit	soxS	soxRS	-6	-13	n.s.	-3	-12	n.s.
b1277	ribA	GTP cyclohydrolase II, catalyzes the opening of the imidazole ring of GTP and removal of pyrophosphate, the first committed step in riboflavin biosynthesis	soxS	soxRS	n.s.	n.s.	n.s.	n.s.	n.s.	n.s.
b0852	rimK	ribosomal protein S6 modification protein, L-glutamate ligase that	soxS	soxRS	-2	n.s.	n.s.	n.s.	n.s.	n.s.

		catalyzes post-translational addition of up to four C-terminal glutamate residues								
b4396	rob	Rob DNA-binding transcriptional activator	soxS	soxRS	n.s.	n.s.	n.s.	n.s.	n.s.	n.s.
b3908	sodA	superoxide dismutase (Mn)	soxS	soxRS	n.s.	n.s.	11	n.s.	n.s.	n.s.
b3035	tolC	TolC outer membrane channel	soxS	soxRS	n.s.	n.s.	n.s.	-2	-2	n.s.
b2600	tyrA	Tyrosine synthesis: chorismate mutase/prephenate dehydrogenase	soxS	soxRS	-4	-2	n.s.	-4	n.s.	n.s.
b4637	uof	RyhB-regulated fur leader peptide	soxS	soxRS	11	7	n.s.	2	2	n.s.
b3625	waaY	lipopolysaccharide core heptose (II) kinase	soxS	soxRS	n.s.	n.s.	n.s.	n.s.	n.s.	n.s.
b3624	waaZ	protein involved in KdoIII attachment during lipopolysaccharide core biosynthesis	soxS	soxRS	n.s.	n.s.	n.s.	n.s.	n.s.	n.s.
b0447	ybaO	Function unknown, predicted transcriptional regulator; Lrp family	soxS	soxRS	4	n.s.	2	3	2	n.s.
b0850	ybjC	predicted inner membrane protein	soxS	soxRS	-2	n.s.	n.s.	3	3	n.s.
b0853	ybjN	predicted oxidoreductase	soxS	soxRS	n.s.	n.s.	n.s.	n.s.	n.s.	n.s.
b1164	ycgZ	Connector protein for RcsB regulation of biofilm and acid-resistance; blue light, low temperature and stress induction, BluRF(YcgEF) and RpoS regulons	soxS	soxRS	3	4	n.s.	6	23	n.s.
b1378	ydbK	pyruvate:flavodoxin oxidoreductase	soxS	soxRS	n.s.	n.s.	n.s.	-4	-5	n.s.
b2962	yggX	Confers protection of iron-sulfur proteins against oxidative damage; paraquat resistance	soxS	soxRS	n.s.	2	n.s.	4	3	n.s.
b3037	ygiB	conserved outer membrane protein	soxS	soxRS	n.s.	n.s.	n.s.	n.s.	n.s.	n.s.
b3038	ygiC	predicted enzyme with ATPase activity, similarity to the glutathionylspermidine synthetase	soxS	soxRS	n.s.	n.s.	n.s.	n.s.	n.s.	n.s.
b1165	ymgA	Connector protein for RcsB regulation of biofilm; blue light, low temperature and stress induction, BluRF(YcgEF) and RpoS regulons	soxS	soxRS	8	n.s.	9	13	29	n.s.
b1167	ymgC	Blue light, low temperature and stress induced, function unknown; BluRF(YcgEF) and RpoS regulons	soxS	soxRS	n.s.	n.s.	7	13	86	n.s.
b2390	ypeC	Predicted secreted protein, function unknown	soxS	soxRS	4	11	4	3	2	n.s.
b3207	yrbL	Mg(2+)-starvation-stimulated gene, function unknown	soxS	soxRS	7	n.s.	n.s.	3	n.s.	n.s.
b1973	zinT	divalent metal binding protein, cadmium, zinc, and nickel	soxS	soxRS	n.s.	n.s.	5	4	n.s.	n.s.
b1852	zwf	glucose 6-phosphate-1-dehydrogenase, G6PDH	soxS	soxRS	n.s.	n.s.	n.s.	n.s.	n.s.	n.s.

\* genes duplicated in both operons are highlighted in blue

\* values represent fold-change (green = up-regulated, red = down-regulated, and n.s. = not significant)